



**rev2021** | Resource Efficient  
Vehicles Conference  
14 – 16 June 2021

Proceedings



**BOMBARDIER**



**VOLVO vti**



*Marström*



ISBN 978-91-8040-047-3

<https://doi.org/10.30746/978-91-8040-047-3>



# Contents

<b>Preface</b>	<b>iii</b>
<b>Supporters</b>	<b>v</b>
<b>Programme Overview</b>	<b>1</b>
<b>Invited speakers</b>	<b>3</b>
<b>Workshops, networking and panel discussion</b>	<b>9</b>
<b>Structured sessions and proceedings</b>	<b>13</b>
Day 1: P01 – Human-Vehicle Interaction I . . . . .	13
Day 1: P02 – Human-Vehicle Interaction II . . . . .	35
Day 1: P03 – Component Design . . . . .	59
Day 1: P04 – Driveline Aspects . . . . .	81
Day 1: P05 – Energy Consumption I . . . . .	106
Day 2: P06 – Energy Consumption II . . . . .	131
Day 2: P07 – Life Cycle Aspects I . . . . .	151
Day 2: P08 – Life Cycle Aspects II . . . . .	171
Day 3: P09 – Materials and Modelling I . . . . .	196
Day 3: P10 – Materials and Modelling II / Early Design I . . . . .	216
Day 3: P11 – Early Design II . . . . .	243
Day 3: P12 – Systems Aspects I . . . . .	268
Day 3: P13 – Systems Aspects II . . . . .	291



# Preface

*rev2021* was the first edition of the conference on Resource Efficient Vehicles, held online on 14-16 June 2021. This vehicle-centric conference aims to bring together participants from academia, industry and public agencies to discuss research from all relevant fields connected to resource efficiency in all motorised modes of transport and interdependent surrounding systems.

The theme of this multidisciplinary conference is *Resolving Functional Conflicts in Vehicle Design*, a theme explored through topics including modelling for multifunctional design; making trade-offs; efficient use of materials and space; integrating new solutions; transforming the product system; transforming the vehicle-transport system; sustainable design; and early-stage design.

The 2021 edition of the conference consisted of 40 selected papers for presentation at the conference, complemented with four workshops, five keynote lectures from invited speakers, and a concluding panel discussion with four invited participants. It was organised by the Centre for ECO<sup>2</sup> Vehicle Design at KTH Royal Institute of Technology in Stockholm.

Thank you for making this first edition a success!

**The Organising Committee**

**Organising Committee** (Centre for ECO<sup>2</sup> Vehicle Design):

*Ciarán O'Reilly,*  
*Carlos Casanueva Perez,*  
*Jenny Jerrelind,*  
*Malte Rothhämel,*  
*Mathilda Karlsson Hagnell,*  
*Per Wennhage,*  
*Peter Göransson,*  
*Romain Rumpler,*  
*Susann Boij.*

**Scientific Committee:**

<i>Lele Zhang,</i>	Beijing Jiaotong University, China
<i>Lewis M. Fulton,</i>	UC Davis, USA
<i>Marco Pierini,</i>	University of Florence, Italy
<i>Marzia Traverso,</i>	RWTH Aachen, Germany
<i>Rupert Baumgartner,</i>	University of Graz, Austria
<i>Thilo Bein,</i>	TU Darmstadt, Germany
<i>Tracy Bhamra,</i>	Loughborough University, UK

# Supporters

*rev2021* would like to sincerely thank all supporters for their contributions and help in organising this conference.

**BOMBARDIER**

,<http://www.bombardier.com>



<http://www.scania.com>



<http://www.trafikverket.se>

**VOLVO**

<http://www.volvogroup.se>



<http://www.volvocars.com>

**vti**

<http://www.vti.se>



<http://www.creodynamics.com>



<http://www.fkg.se>

*Marström*

<http://www.marstrom.com>



<http://www.modularmanagement.com>



<http://www.yovinn.se>



<http://www.vinnova.se>



<http://www.eco2vehicledesign.kth.se>



<http://www.kth.se>

# Programme Overview

rev2021	Day 1	Day 2	Day 3
	14-Jun	15-Jun	16-Jun
09:00	[OP1] Opening	[OP2] Opening	[OP3] Opening
09:10		[KN2] Keynote II	[KN4] Keynote IV
09:20	[ADD] Opening Address		
09:30			
09:40			
09:50	Break	Break	Break
10:00	[P01] Human-Vehicle Interaction I	[P06] Energy Consumption II	[P09] Materials and Modelling I
10:10			
10:20			
10:30			
10:40	Break	Break	Break
10:50			
11:00	[P02] Human-Vehicle Interaction II	[P07] Life Cycle Aspects I	[B16] Materials and Modelling II / Early Design I
11:10			
11:20			
11:30			
11:40	Break		Break
11:50	[P03] Component Design	[P08] Life Cycle Aspects II	[P11] Early Design II
12:00			
12:10			
12:20			
12:30	Lunch	Lunch	Lunch
12:40			
12:50			
13:00			
13:10			
13:20			
13:30	[MDS] Mingle Discussions	[WS1] Workshops	[P12] Systems Aspects I
13:40			
13:50			
14:00			
14:10	Break		Break
14:20	[P04] Driveline Aspects		[P13] Systems Aspects II
14:30		Break	
14:40			
14:50		[WS2] Workshops	
15:00	Break		Break
15:10			
15:20	[P05] Energy Consumption I		[PPD] Pre Panel Discussion
15:30			
15:40			
15:50		Break	
16:00	Break		Break
16:10	[KN1] Keynote I	[KN3] Keynote III	[PND] Panel Discussion
16:20			
16:30			
16:40			[CL3] Closing
16:50	[CL1] Closing	[CL2] Closing	
17:00	End	End	End





# Invited speakers

Overview of plenary lectures – *rev2021*

---

## Monday 14 June

- 09:20-09:50 **Opening Address**  
Staffan Berglund, Scania Group  
*Research and development strategies for resource efficient vehicles*
- 16:10-16:50 **Keynote 1**  
Marzia Traverso, RWTH Aachen  
*A sustainable transport sector: Opportunities and challenges in the European Green Deal context*
- 

## Tuesday 15 June

- 09:10-09:50 **Keynote 2**  
Margriet Van Schijndel-de Nooij, Eindhoven University of Technology  
*Resource efficient mobility: What does it take?*
- 16:10-16:50 **Keynote 3**  
Lewis Fulton, UC Davis  
*Driving toward zero in California: How steep a hill must we climb?*
- 

## Wednesday 16 June

- 09:10-09:50 **Keynote 4**  
Sebastian Stichel, KTH Royal Institute of Technology  
*Resource efficient rail transport systems: A railways perspective to REV*
-



**Opening Address: Research and development strategies for resource efficient vehicles**

*Staffan Berglund*

Director of Engineering at Scania Group and Chairman of the Board of the Centre for ECO<sup>2</sup> Vehicle Design

**Abstract:** The transport industry has always worked to develop resource efficiency in vehicles to meet the customers' demands. Now in the context of sustainability, the transport industry must improve their strategies to support even faster problem solving with an even better holistic view. This presentation looks at how the ECO2 strategies – of taking a cross-scalar view, solving cross-functional conflicts, and promoting cross-fertilisation of ideas – contribute to resource efficient vehicles.

**Keynote 1: A sustainable transport sector: Opportunities and challenges in the European Green Deal context***Marzia Traverso*

Full Professor and Head of the Institute of Sustainability in Civil Engineering, RWTH Aachen, Germany

*Prof. Dr. Marzia Traverso, full professor and head of Institute of Sustainability in Civil Engineering in RWTH Aachen since 1 June 2017. PhD of Environmental Technical Physics of University of Palermo, and environmental engineer, working in the field of Life Cycle Assessment and sustainability performance of building and transport sector and strategic environmental assessment to the transportation urban systems. In 2020, nominated Rapporteur of the Technical Working Group of the European Commission's Platform on Sustainable Finance and member of Technical Advisory Board on Environmental Footprint' (Expert group E03710), PEF EU. In April 2021 Project leader for the development of the ISO standard on Social LCA.*

*Her knowledge on LCSA is built in 20 years of experience in academic and insustrial context. From Nov. 2011 to March 2016, she was project manager at the research and innovation centre of BMW Group. From May 2016 to April 2017 Scientific Officer at European Commission, JRC Seville in Product Bureau, responsible of the development of criteria for GPP on Street Lighting and Traffic signals, GPP of Transport and Framework for Building Sector, Level(s).*

*Author and co-author of several scientific papers in journal such as Sustainability, Int. Journal of Life Cycle Assessment, Industrial Ecology. Subject editor in Social life cycle Assessment in the Int. Journal of LCA. Member of several editorial board such as: Int. Journal of LCA, Sustainable Development, Resources. Founder of a Non-Profit Organization "iSuD – Information for Sustainable Development" for disseminating sustainability concept among Italian consumers. President of Director board of the Forum for Sustainability through Life Cycle Innovation – FSLCI, and Chair of (Technical Listening) Global Listening Centre. Member of the Advisory Board of Madaster Foundation.*

**Abstract:** After the Paris Agreement the European Union has developed the European Green Deal which represents the response to the challenges the world and Europe are facing in reducing its impact to the climate change. It is a growth strategy proposed by the von der Leyen Commission to make Europe the first climate neutral continent by 2050. The main idea is to transform the economy into a clean and circular system, while cutting pollution and restoring biodiversity (A European Green Deal).

According to the European Commission (EC), to reach this 2050 target the following actions are needed: investments in eco-friendly technologies, clean public and private transport, support for research and innovation, decarbonisation of the energy sector, more efficient buildings, and environmental recovery.

**Keynote 2: Resource efficient mobility: What does it take?***Margriet Van Schijndel-de Nooij*

Program Director of Smart Mobility, Eindhoven University of Technology, The Netherlands.

*Margriet van Schijndel has about 20 years of experience working with research programs and coordination. She is currently the Program Director Responsible Mobility within the Eindhoven Artificial Intelligence Systems Institute (EAISI) at Eindhoven University of Technology. She has also been serving as the EARPA Secretary General for 7 years, representing some 53 member organisations performing R&D activities in the field of road mobility research. Within EARPA, she now is Foresight Group leader on Connectivity, Automation and Safety. Furthermore, she is Cluster leader Key Enabling Technologies within the CCAM Partnership.*

*She has been managing or coordinating several large national and European research projects such as UDRIVE, APROSYS, and several EU tender projects, with focus on e.g. large naturalistic driving study, evaluation and validation methodologies, large scale Field Testing, safety in automotive, vulnerable road user protection, ITS solutions for safer intersections, prevention of truck accidents and human modelling in automotive applications.*

**Abstract:** In striving for zero emission mobility, a large focus is on electric vehicles; development, testing and implementation. Needless to say that these vehicles still do create emissions, though less on the time and location of its use. We also do have other modes of mobility which are quite resource efficient. What about them? And what about AI; it often is seen as enabler for automated mobility. Yet, in resource efficiency it can play an essential role as well.



### Keynote 3: Driving toward zero in California: How steep a hill must we climb?

*Lewis M. Fulton*

Ph.D., Director of STEPS+, Institute of Transportation Studies at the UC Davis, USA.

*Lewis Fulton has worked internationally in the field of transport/energy/environment analysis and policy development for 30 years. He is Director of the Sustainable Transportation Energy Pathways (STEPS+) program within the Institute of Transportation Studies at the University of California, Davis. There he leads a range of research activities around new vehicle technologies and new fuels. He was a lead author on the IPCC 5th Assessment Report, Mitigation (“Climate Change 2014: Mitigation of Climate Change”, transport chapter). Current projects include analyses of electric vehicles, shared mobility, automation, and other drivers of transportation futures. He investigates the costs, energy, GHG, employment and other aspects of changing transportation trends and alternative futures.*

*From 2007-2012 he was a Senior Transport Specialist with the International Energy Agency, Paris, as well as Division Head for Energy Technology Policy during 2011-2012. He returned to the IEA in 2007 after working there originally from 1999-2005. At the IEA he led the development of the Mobility Model and directed transport-related analysis connected with the Energy Technology Perspectives series of publications. During 2006-2007 he worked in Kenya with the UN Environment Program, developing and implementing GEF-funded sustainable transport projects around the world. During the 1990s he also worked at the US Department of Energy for 4 years, and taught at the Independent University of Bangladesh and the University of Maryland. He received his Ph.D. in Energy Management and Environmental Policy from the University of Pennsylvania in the United States in 1994.*

**Abstract:** California has set a state-level target of net zero CO<sub>2</sub> emissions economy wide by 2045. The transportation sector must play its part and needs to reach as close to zero emissions by that date as possible. This talk covers the potential strategies for deep cuts in in-state CO<sub>2</sub>, primarily focusing on the light- and heavy-duty road vehicle sectors. It reports on a new state-wide study that finds that very rapid transitions to near-zero vehicle technologies, coupled with very low carbon fuels, will be needed. Policies will be needed that challenge political acceptability boundaries. It presents scenarios and considers the transitional and policy challenges for the state, and implications for states and countries around the world.

**Keynote 4: Resource efficient rail transport systems:  
A railways perspective to REV***Sebastian Stichel*

Professor in Rail Vehicle Dynamics at KTH Royal Institute of Technology and Director of the KTH Railway Group.

*Professor in Rail Vehicle Dynamics at KTH since 2010. Director of the KTH Railway Group since 2011 and Deputy Head of the Department of Engineering Mechanics since 2020. Board member SWEDTRAIN – Swedish Association of Railway Industries – since 2019. Vice-Chair Academia of the European Rail Research Advisory Council (ERRAC) since 2017. Head of Department of Aeronautical and Vehicle Engineering from 2017 to 2019. Chairman of the Shift2Rail Scientific Committee from 2016 to 2018. Worked more than 10 years at Bombardier Transportation. From 2003 to 2010 Manager Vehicle Dynamics with responsibility in Sweden, Germany, UK and France. Master and PhD. degree in Vehicle Technology at Technische Universität Berlin. Supervisor Prof. Klaus Knothe. Adjunct Professor at Beijing Jiaotong University since 2017. Member of the International Advisory Board of the National International Science and Technology Cooperation base on Railway Vehicle Operation Engineering of BJTU. Visiting Professor at University of Illinois at Urbana Champaign in 2013, at Southwest Jiaotong University in 2017 and 2019 and at Indian Institute of Technology, Roorkee in 2019. Current research interests are wheel and rail wear and rolling contact fatigue, freight vehicle dynamics, ride comfort and active suspension, dynamic pantograph-catenary interaction (cf. Rail Vehicle Research Group).*

**Abstract:** Railway Transport is already today in several aspects a resource efficient transport system. It is very energy efficient, has low CO<sub>2</sub> emissions since it is easily electrified, has a high transport capacity in relation to the land use, and it is very safe. Nevertheless, researchers and vehicle manufacturers are working on further reducing energy consumption and emissions from rail vehicles with e.g., lightweight designs, reduced air drag or novel and optimized propulsion systems. Also, the infrastructure, is a very important an integral part of the system, where construction of new railway lines leads to substantial CO<sub>2</sub> emissions in the building phase. Ongoing developments will be shown in the presentation. Another possible contribution to a more sustainable transport system is to change the modal split, i.e., to increase the share of rail transport as part of the whole transport volume, which is propagated for example by the EU. To increase the share of railway transport, it must be made as attractive and cost efficient as possible. Thus, in the presentation aspects of a more attractive railway system will be discussed as well.

# Workshops, networking and panel discussion

Overview of workshops, networking & panel discussion – *rev2021*

---

## Monday 14 June

13:30-14:10 **rev2021 Networking Forum**  
Networking and Mingle Discussions, *Virtual meeting space Gather.Town*

---

## Tuesday 15 June

13:30-14:30 **Parallel Workshops – Part 1**

<b>Workshop A</b>	<b>Workshop B</b>	<b>Workshop C</b>
<i>Making good decisions</i>	<i>Reimagining a more circular transport system</i>	<i>Electrification strategy for road vehicles</i>

14:50-15:50 **Parallel Workshops – Part 2**

<b>Workshop A</b>	<b>Workshop B</b>	<b>Workshop D</b>
<i>Making good decisions</i>	<i>Reimagining a more circular transport system</i>	<i>Innovation modelling for system impact calculations</i>

---

## Wednesday 16 June

15:20-16:00 **Presentation of panelists**  
*Annika Stensson Trigell (Chair, KTH), Jonas Eliasson (Trafikverket), Elisabeth Hörnfeldt (Scania Group), David Wennberg (WMC Consulting)*

15:20-16:00 **Panel discussion**  
*Annika Stensson Trigell (Chair, KTH), Jonas Eliasson (Trafikverket), Elisabeth Hörnfeldt (Scania Group), David Wennberg (WMC Consulting)*  
*Research and development for future resource efficient vehicles*

---

## Workshop A

### **Making good decisions – Managing sustainability issues on heavy-duty powertrain systems during the early design stage**

*Vassiliki Theodoridou, Josef-Peter Schögggl, Katharina Berger, Rupert J. Baumgartner*

Trucks, buses and coaches are responsible for about a quarter of CO<sub>2</sub> emissions from road transport in the EU and despite some improvements in fuel consumption efficiency in recent years, these emissions are still rising. In order to fulfil the need for a more sustainable transportation the EU adopted in 2019 the CO<sub>2</sub> emission standards for heavy-duty vehicles, by setting targets for reducing the average emissions from new lorries for 2025 and 2030. Since eighty percent of the product-related environmental burdens are determined within the early stage of design, it is obvious that managing sustainability issues on this stage will be a key success factor.

Using proper tools and methods as well as the deeper understanding of all these issues from people involved in the product design can make this goal a reality. This workshop presents the most promising concepts to tackle this challenge. The advantages and possible weakness of the various methods will be briefly presented. Furthermore, by highlighting the main drivers for sustainability issues product designer and engineers will gain an overview of “what truly matters” to be considered when picking the best path forward. The interactive session included aims to explore and discuss in detail the special topics of:

- data availability,
- sustainability awareness – awareness of the main drivers for sustainability issues
- tools and methods used and their bottlenecks

## Workshop B

### **Reimagining a more circular transport system**

*Lili-Ann Laan*

Even before the Covid crisis, the E-commerce industry was on the rise, but due to recommendations to stay at home and keeping distance, it has been an absolute e-commerce boom. People order groceries, pharmacy goods, clothes, and technical devices online as never before, and demand for new solutions focusing on receiving the goods has never been higher. Thus, the role as a consumer is well facilitated. But how about the role as a producer of waste and discontinued products?

During this workshop, we will highlight the returning flow and shift the focus from package to waste. Can we design a more circular transport system by considering behaviors, vehicle concepts, and services? Welcome to a workshop where we together try to reimagine a more sustainable future.



## Workshop C

### **Electrification strategy for road vehicles**

*Malte Rothhämel*

Electrification of road traffic is seen as the best actual known strategy to make this mode of transportation more sustainable. It enables higher efficiency, specifically on short distances, low local emissions and moves the focus on efficiency in total as well as life cycle analysis.

Anyhow, there are several thresholds, and the success of electric mobility will not only be a question of technology but also a question of policy. The organisation of establishing charging infrastructure is only one of them.

In this workshop an electrification strategy will be presented as subject of discussion. The goal is to collect different perspectives on that and to discuss them. Even variants and alternatives can be picked out. The expected outcome is a broader view on this topic for all participants and in the best-case new ideas and inspiration for future research.

## Workshop D

### **Innovation modelling for system impact calculations**

*Jordi Vinolas*

When studying innovations in vehicle components it is usually straightforward its influence on the vehicle, but it can be hard to predict what their system-wide impact would be, as the interfaces are usually unclear, the subsystems belong to different stakeholders, and the stakeholder interactions are not necessarily governed by rational decisions.

In this workshop, participants in the EU project NEXTGEAR will be present and discuss this from a cost modelling perspective, showcasing the possibilities and allowing you to apply the methods and techniques for analysing the impact of selected vehicle innovations on the specific vehicle system context, in order to enable the complete understanding of the cascading effects generated by specific subsystem changes.

## Panel Discussion

### Research and development for future resource efficient vehicles

Future resource efficient vehicles need to fulfill different engineering and sustainability challenges. How can research help meet these challenges? Annika Stensson Trigell, KTH Royal Institute of Technology's Vice-Rector for Research, is joined by Jonas Eliasson, Elisabeth Hörnfeldt and David Wennberg to discuss this topic.



#### Chair of the panel discussion

*Annika Stensson Trigell*

Vice-President for Research and Professor in Vehicle Dynamics, KTH Royal Institute of Technology.



#### Panelist

*Jonas Eliasson*

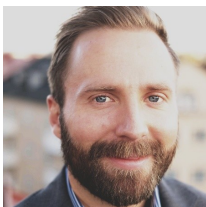
Director of Transport Accessibility at Trafikverket (The Swedish Transport Administration).



#### Panelist

*Elisabeth Hörnfeldt*

Head of Innovation at Scania Group.



#### Panelist

*David Wennberg*

Rail Systems Specialist and Co-Founder of WMC Consulting.

# Structured sessions and proceedings

## Day 1: P01 – Human-Vehicle Interaction I

Session P01 – Human-Vehicle Interaction I, Monday 14 June

---

**Session chairs:** Mikael Nybacka and Jenny Jerrelind

- |             |   |
|-------------|---|
| 10:00-10:10 | <b>P01.A</b><br><i>Autonomous driving and motion sickness – an outlook on causes, evaluation methods and solutions</i><br>Ilhan Yunus, Jenny Jerrelind and Lars Drugge                      |
| 10:10-10:20 | <b>P01.B</b><br><i>Assessing indicators to testing human-AI interaction in autonomous vehicles: A pilot study with Omnipresent AI</i><br>Peer Sathikh, Tan Guan Yi and Fang Zong Rui Dexter |
| 10:20-10:30 | <b>P01.C</b><br><i>Psychoacoustic perspectives on electric truck</i><br>Maria Rådsten Ekman and Karl Bolin  |
| 10:30-10:40 | <b><i>Questions and Answers</i></b>   |
-

---

# Autonomous driving and motion sickness – an outlook on causes, evaluation methods and solutions

Ilhan Yunus<sup>1,2,3\*</sup>, Jenny Jerrelind<sup>2,3</sup> and Lars Drugge<sup>2,3</sup>

<sup>1</sup>Volvo Car Corporation, Gothenburg, Sweden

<sup>2</sup>Engineering Mechanics, KTH Royal Institute of Technology, Stockholm, Sweden

<sup>3</sup>The Centre for ECO<sup>2</sup> Vehicle Design, KTH Royal Institute of Technology, Stockholm, Sweden

\*Corresponding author. Email: [ilhan.yunus@volvocars.com](mailto:ilhan.yunus@volvocars.com)

---

The development of autonomous vehicles is rapidly moving forward through significant efforts from the automotive industry and researchers. The design and the usage of the vehicles can drastically change, leading to a transformation of the vehicle-transport system. One key enabler for the complete success of autonomous vehicles is to design and control the vehicle so that the passengers do not become motion sick. There is therefore a need to investigate what causes motion sickness and how motion sickness can be evaluated. This includes the medical understanding of what is causing motion sickness to understand the human aspects of a range of motion-related parameters such as accelerations, vibrations, etc. Furthermore, with the help of modelling detect and predict motion sickness. There exist today different models to predict and evaluate motion sickness, but they are often rather limited and not directly usable as tools in the vehicle development process. There are both empirical and theoretical approaches used in the modelling of motion sickness, which have different advantages and disadvantages to each other. In this paper, the causes of motion sickness and some existing motion sickness models will be discussed. With the help of identified motion sickness prediction models, new technical innovations needed within vehicle dynamics control and motion planning control can be developed to minimise the risk of motion sickness in autonomous vehicles. Motion sickness prediction models are important tools in the early design stage of development on how to control and design autonomous vehicles so that the functional conflict between safety, comfort and performance is handled for the complete success of autonomous vehicles when it comes to economic and social benefits.

© 2021 by the authors. Published by the Resource Efficient Vehicles Conference.  
This is an open access article under the CC BY license (<http://creativecommons.org/licenses/by/4.0/>).

---

## 1. Introduction

The development of autonomous vehicles is rapidly moving forward through significant efforts from the automotive industry and researchers. The design and the usage of the vehicles can drastically change, leading to a transformation of the vehicle-transport system. One key enabler for the complete success of autonomous vehicles is to design and control the vehicle so that the passengers do not become motion sick. Potentially motion sickness in autonomous vehicles can be a problem which has been highlighted in for example “Will autonomous cars make us sick?” by Diels [1] and “From car sickness to autonomous car sickness” by Iskander et al. [2]. It is quite seldom that drivers become

motion sick, but in autonomous vehicles, all people in the vehicle become passengers which has shown to have an increased tendency to become motion sick. Factors that contribute to motion sickness, but which are different when you are a driver and a passenger, are controllability, perceived control, activity, visual information, and predictability [3]. Since comfort is one of the main drivers for autonomous driving (AD), an important factor that affects the acceptance of autonomous vehicles is the capability of passengers to perform non-driving tasks like reading, relaxing, and/or socialising in a comfortable style with no or limited motion sickness symptoms. So the overall research question is *how shall autonomous vehicles be built and controlled in order to reduce or avoid motion sickness?*

One example of previous activities in the field is the University of Michigan Transportation Research Institute (UMTRI) that has published some interesting reports regarding motion sickness in self-driving vehicles [4]. Furthermore, OEMs like Daimler has developed measures to predict and prevent car sickness with a laying seat [5], JLR promotes a system that mitigates the feeling of motion sickness by adapting the driving style of future autonomous vehicles [6], Citroën has presented SEETROËN, the glasses to eliminate motion sickness [7] and suppliers like ZF [8] and Ricardo [9] are also working on minimising motion sickness in autonomous vehicles. It can be concluded that it is still not well known how to control the vehicle in order to minimise the risk of motion sickness.

The first step towards answering the above research question is to investigate what causes motion sickness and how motion sickness can be evaluated. To be able to predict motion sickness and identify important human and vehicle parameters affecting motion sickness, the first task is to investigate theories in the literature about what causes motion sickness and the current state-of-the-art regarding the usage of human biomedical-based mathematical models to predict motion sickness. The second task is to investigate how different vehicle motion control strategies such as active suspension, active anti-roll bars, rear-wheel steering, etc. could be developed and combined to minimise motion sickness and maintain driving stability. The final task is to identify how self-driving vehicles shall be controlled (steering, braking, and acceleration) to reduce or avoid motion sickness. This includes the development of trajectory planning and tracking algorithms that minimise motion sickness. In the final choice, any influential conflicts with performance and safety need to be taken into account. The three tasks that have been identified to answer the research question are illustrated in Figure 1.

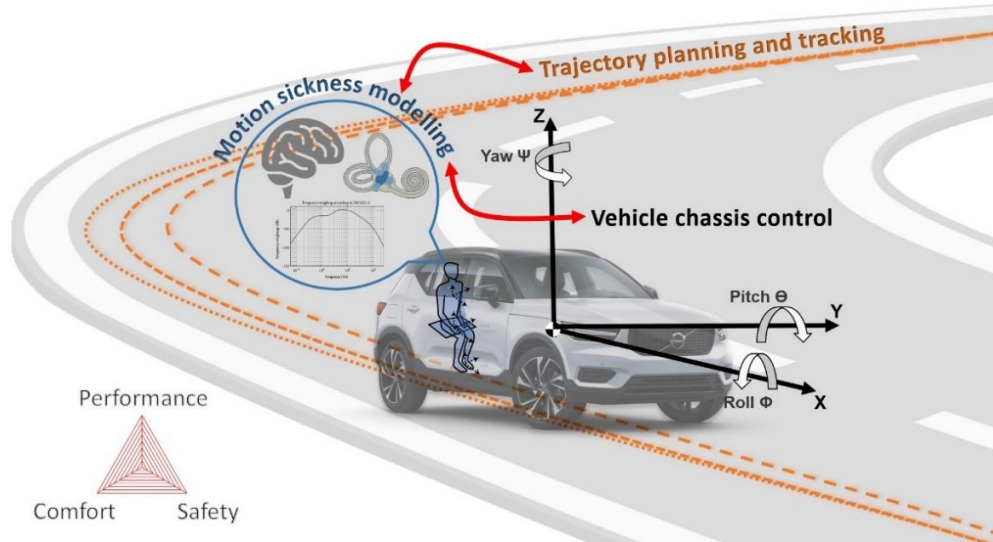


Figure 1. Identified tasks to assess and mitigate motion sickness in autonomous vehicles.

The paper is organised by starting with an introductory section which is stating the motion sickness problem in general and potential negative effects on autonomous driving. In Section 2 existing motion sickness severity prediction models are discussed briefly. This is followed by Section 3.1 that reviews vehicle chassis control techniques to minimise motion sickness for AD platforms and Section 3.2 focuses on recent research on trajectory planning and tracking for autonomous cars to minimise motion sickness. Finally, the paper ends with a concluding section.

## 2. Motion sickness

Motion sickness, based on the Cambridge dictionary, is “*a feeling of being ill, especially of needing to vomit, that some people get in a moving vehicle*”. The “feeling of being ill” can in other words be called “nausea” and “dizziness”. The referred “moving vehicle” can be a car, plane, train, etc. Motion sickness is a very old problem dating back to BC and was initially referred to as “seasickness” by ancient Greeks and Romans [10]. Intensive historical research has been done by Huppert et al. [10] showing the chronological overview of the knowledge about the problem. However, motion sickness has been stated as a more complex problem than just nausea and vomiting and is not completely understood yet [11].

In this part of the paper, the focus is on understanding the human aspects of a range of motion-related parameters such as accelerations, vibrations, etc., and giving an outlook on motion sickness models in the literature. Human biomedical modelling techniques can be used to identify the comfort zone for AD, i.e. to understand the customer expectations and draw the limits of the motion comfort and sickness. To evaluate motion sickness both objective methods (based on measurements) and subjective methods (for example based on personal feelings) are used, which are further described in the two following sections.

### 2.1 Objective methods

There exist today different models to assess motion sickness, but they are often somewhat limited and not always directly usable as tools in the vehicle development process. Here research is needed to develop or combine the models. Objective methods for motion sickness have historically been researched and many motion sickness scales are available in the literature [12] like the Motion Sickness Dose Value (MSDV) from ISO 2631-1 [13]. There are both empirical and theoretical approaches used in the modelling of human motion sickness, which have different advantages and disadvantages to each other [14]. The HFR model (1974) from Human Factors Research (HFR) Inc. California, USA is an experimental-based model that predicts the Motion Sickness Incidence (MSI) which is given in percentage. In Figure 2 the HFR model for the vertical direction ( $z$ ) has been re-generated in MATLAB.

The ISO 2631-1 standard provides the limited weighting filters for the calculation of motion dose values for the assessment of motion comfort and sickness. Figure 3 shows the ISO 2631-1 weighting filters for comfort assessment ( $W_k$  is for the  $z$ -axis and  $W_d$  is for the  $x$  and  $y$ -axis) and the weighting filter for motion sickness assessment ( $W_f$  for the  $z$ -axis). Moreover, a lateral frequency weighting filter ( $W_f$  for the  $y$ -axis) for motion sickness evaluation proposed by Donohew and Griffin [15] has also been added in Figure 3.

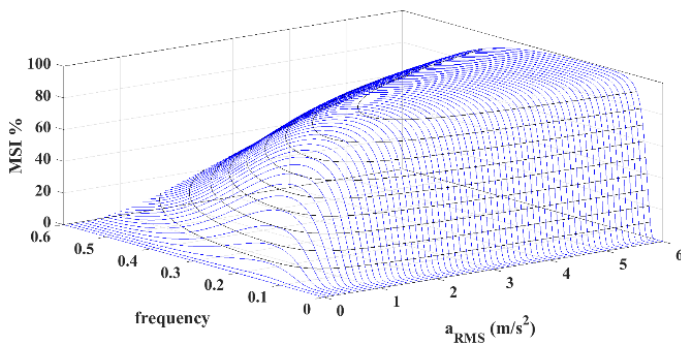


Figure 2. HFR (Human Factors Research) Model

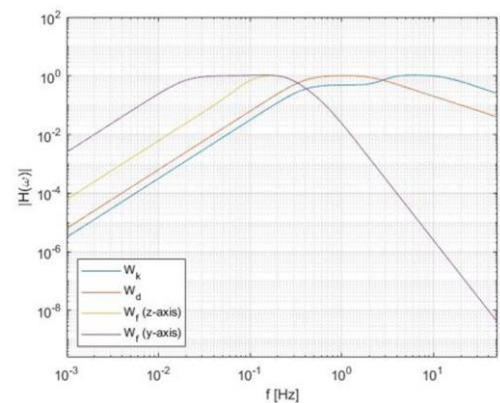


Figure 3. Weighting filters for comfort and motion sickness assessment

The Motion Sickness Dose Value (MSDV) is defined in ISO 2631-1 as:

$$MSDV = \left\{ \int_0^T [a_w(t)]^2 dt \right\}^{\frac{1}{2}} \text{ ms}^{-1.5} \quad (1)$$

where  $a_w(t)$  is the frequency weighted acceleration. The ISO 2631-1 standard needs to be re-visited to enhance the models for AD and may also be extended for a more accurate 3D dimensional model which can be run in real-time.

A widely recognised theory is that motion sickness is caused by a signal mismatch between the internal model in the brain and received signals from the vestibular system and visual stimuli. The sensory conflict theory-based models are focused on the mechanism of motion sickness and motion sickness adaptation which uses a modelled vestibular system and Central Neural System (CNS). The neural mismatch model was proposed by Reason [16] and after that modelled mathematically by Oman [17]. Oman's proposed model is based on sensory conflict theory using two parallel (slow and fast averaging dynamics) filters that take the conflict as input and predict motion sickness incidence.

Bos and Bles [18] extended Oman's model and proposed the Subjective Vertical Conflict (SVC) theory model called 1D-SVC. This is a promising theoretical model which is based on the sensory conflict theory developed by Bos and Bles and validated by using the HFR model. Braccisi and Cianetti [19] proposed an extended version of the 1D-SVC model to a 3D-SVC model called vestibular 3D model (UNIPG) and visual-vestibular models (UNIPG<sub>SeMo</sub>) which are experimentally validated and expanded with a 6-DOF motion model proposed by Wada et al. [20]. Recently, the 6-DOF mathematical model of motion sickness severity prediction has been extended by considering visual inputs by Wada et al. [21].

## 2.2 Subjective methods

Motion sickness can change constantly and individually depending on the movements but also due to non-motion causes. Therefore the level of motion sickness is alternating during the drive which makes it difficult to assess objectively. In addition to objective methods, there are also different questionnaires (measuring scales) available to evaluate motion sickness before, during and/or after the experiment. Subjective questionnaires can also be used for validating the developed motion sickness prediction models (objective evaluation methods). These benefits make motion sickness questionnaires a useful tool to assess and evaluate motion sickness during the development process of autonomous vehicles. Some of the differently structured (based on the susceptibility, assessment, or type of usage) motion sickness questionnaires in the literature are presented as follows. One of the early examples of motion sickness questionnaires is the Pensacola Motion Sickness Questionnaire (MSQ) proposed by Kennedy and Graybiel [22] in 1965. Then, the Simulator Sickness Questionnaire (SSQ) was developed and derived from the MSQ in 1993 by Kennedy et al. [23] to measure simulator sickness (visually induced motion sickness).

To understand how susceptible a participant is to motion sickness, the Motion Sickness Susceptibility Questionnaire (MSSQ) was created and developed by Reason and Brand in 1975, which was revised in 1998 by Golding [24] to improve the relationship of sickness from other non-motion causes (migraine, chemotherapy, etc.). The MSSQ can be used to detect individual differences and gives an advantage of the participant selection process for motion sickness experiments (different motion types e.g boats, cars, planes, trains). Then a shorter version of the questionnaire was developed by Golding [25] in 2006 which maintains the accuracy and is more time-efficient.

To assess overall (using total scores) and multiple dimensions (using GI: Gastrointestinal; C: Central; P: Peripheral; SR: Sopite-related subscale scores) of motion sickness, Gianaros et al. [26] have developed the Motion Sickness Assessment Questionnaire (MSAQ) in 2001. The Misery Scale (MISC) was developed by Bos et al. in 2005 [27] and it is characterised by its simplified rating system for evaluating motion sickness level. The MISC is one of the most commonly used methods during experiments by directly asking the participant for a rating (from score 0: no problem to score 10: vomiting) [27]. Similarly, the Fast Motion Sickness Scale (FMS) is a verbal rating (from 0 to 20) to



grade the participant's motion sickness feeling and was developed by Keshavarz and Hecht [28] in 2011. The main advantage of the scale is to provide a fast and valid classification method for assessing motion sickness during the experiments.

### 3. Solutions for mitigating motion sickness

Technological innovations in the vehicle development process such as vehicle chassis control and motion planning could be used for mitigating motion sickness which will be addressed in this section.

#### 3.1 Vehicle chassis control strategies/techniques to improve ride comfort

Active chassis control systems provide great opportunities for enhancing the comfort of autonomous vehicle platforms. Some examples of techniques that could potentially be used to improve comfort and minimising motion sickness are:

- *Torque vectoring*. The ability to individually control the drive/brake torque of each wheel or axle of the vehicle enables the customisation of the handling/comfort response of the vehicle according to the subjective preferences of different passengers.
- *Rear-wheel steering*. The rear-wheel steering system can reduce the turning radius and is used for vehicles moving in narrow spaces at low speeds. At high speeds, the rear wheels normally steer in the same direction as the front wheels. This can help the vehicle movement in the lateral direction with or without reduced yaw motion.
- *Active suspensions*. The main aim of the active suspension system is to eliminate the vehicle's body motion due to road disturbances. The active suspension system can also affect the roll motion during cornering and the pitch motion during accelerating or braking.
- *Active anti-roll bars*. An active anti-roll bar is designed to reduce the roll motion of the vehicle body during cornering, and it can change the load transfer behaviour between left and right wheels and create a suitable steering characteristic. The main aim of active anti-roll bar systems is to improve the ride comfort, handling, and performance of the vehicle.

There already are a few studies [29], [30], [31] and [32] that have shown that vehicle/chassis control strategies/techniques (torque vectoring, rear-wheel steering, active suspension, active anti-roll bars, etc.) can help to improve motion comfort and have a potential to mitigate motion sickness for AD platforms.

Tavernini et al. [29] have proposed a Model Predictive Control (MPC)-based control algorithm to control and minimise the pitch angle of a vehicle by actively varying the brake force distribution during braking events. Simulation results showed that the proposed optimal distribution of brake forces between the front and rear axles has proved a smooth stop of the vehicle to improve driver comfort without affecting the braking distance. The acceleration peaks at the driver's head are shown to be reduced that can help to improve the driver's comfort feeling during braking which indicates that this research can potentially also be extended to reduce motion sickness.

Utbult [30] has developed feedforward and feedback control algorithms for rear-wheel steering systems and evaluated the controller performance under sinus steer and overtaking scenarios for comfort and motion sickness during highway driving in a simulation environment. It was shown that rear-wheel steering systems can improve comfort and reduce motion sickness. Furthermore, rear-wheel steering can improve maneuverability in low-speeds and improve safety by improving yaw stability.

DiZio et al. [31] experimentally showed that using an active suspension system vibrations from 0.8 to 8 Hz can be reduced for mitigating motion sickness when the passengers were performing a reading activity.

Agrawal and Gustafsson [32] have developed sliding mode, feedforward and PI-based combined control strategies for active anti-roll bars to increase roll damping and reducing the effect of low-frequency road disturbances. Simulation results show that active anti-roll bar systems have a



significant ability to improve both ride and handling performance (changing the understeer characteristic and thereby improve the stability) of the vehicle compared to passive anti-roll bars.

The combination of different chassis control strategies can be called integrated chassis control which can help to enhance safety and comfort by providing high dimensional possibilities to control the vehicle. A short review about integrated chassis control has been given by Lopez et al. [33] which points out how researchers combine the different control systems to improve multi-conflicting objectives such as safety, comfort and performance. Developing active chassis control strategies and algorithms and evaluate them for different test scenarios will help to evaluate the comfort enhancement for future AD vehicle platforms.

### **3.2 Trajectory planning and tracking algorithms considering ride comfort**

Trajectory (motion) planning is one of the challenging and critical functional layers for autonomous vehicles [34]. The trajectory planning and tracking of autonomous vehicles can create subjectively aggressive driving that might deteriorate passenger ride comfort. Therefore, planning the motion of the vehicle plays an important role to provide a pleasant autonomous driving experience. Previous studies like Claussmann et al. [35] and Gonzalez et al. [36] have pointed out the importance of trajectory planning and tracking algorithm development for ride comfort in AD.

The optimisation problem for trajectory planning can be designed to minimise the motion sickness level as an objective function, subject to vehicle dynamics, path, time, distance bounds, energy efficiency, CO<sub>2</sub> emissions, power characteristics, torque, speed, steering limit boundaries, etc. Therefore, the research question could be similarly designed as a trajectory optimisation problem as proposed by Htike et al. [37], where they have evaluated different cost functions considering both motion sickness and journey time and tested their performance under different driving scenarios in a simulation environment. The results show that there is a tradeoff between motion sickness level and journey time. To enhance the autonomous driving experience, the solution to the designed optimisation problem should provide a safe and pleasant journey within preferred spent time while minimising motion sickness.

The study of Bae et al. [38] proposed an optimal velocity planning method for public transport vehicles while keeping the acceleration and jerk limits within the acceleration comfort envelope in a given reference path while solving the nonlinear optimisation problem. Certosini et al. [39] have proposed Non-linear Model Predictive Control (NMPC) based speed planning algorithms by integrating the 3-D extension of the Bos and Bles model called UNIPG model to reduce motion sickness incidence.

Recent publications focusing on finding the optimal solution of path tracking algorithms to minimise motion sickness are for example [40], [41] and [42]. Zengin et al. [40] have proposed an augmented road-vehicle model with a vestibular system model to investigate the effect of look-ahead distance for path tracking algorithms. Sever et al. [41] proposed to tune a gain-scheduled LQR based path following controller to reduce the motion sickness dose value defined in ISO 2631-1 also integrating the dynamics of the human vestibular system similar to Zengin et al. [40]. A fuzzy-PID based path tracking algorithm is proposed by Saruchi et al. [43] that is controlling the wheel angle to reduce the lateral acceleration and the roll angle of the head of the driver and the passengers aiming for reducing motion sickness incidence which is calculated with the help of using the 6-DOF SVC model.

A further review of the design of advanced trajectory planning and tracking algorithms considering comfort metrics (ISO standards, sensory-conflict theory models etc.) is needed. Literature shows that optimisation based advanced control methods could be beneficial to achieve a low discomfort level. There is also a need to take into account that trajectory planning and tracking algorithms are required to be run in real-time for autonomous vehicles to minimise motion sickness.

## 4. Conclusions

Motion sickness in autonomous vehicles is a very multidisciplinary question and could cover many research fields. This paper has briefly investigated the potential risk of the motion sickness problem for autonomous vehicles, assessment methods of the motion sickness problem, and ways of integrating motion sickness models in the autonomous vehicle development process. Furthermore, it has provided an outlook on motion sickness mitigation strategies that focus on increasing passenger comfort. The motion sickness prediction methods can be used to develop and tune technical innovations to minimise the risk of motion sickness in autonomous vehicles and optimise vehicle control tactics. These are important tools in the early design stage of autonomous vehicles so that the functional conflict between safety, comfort, and performance is handled for the complete success of autonomous vehicles when it comes to economic and social benefits. For future studies, there is still a need to further investigate objective methods and models to assess motion sickness accurately to be able to develop and integrate motion sickness mitigation strategies for autonomous vehicles.

## References

- [1] C. Diels, “Will autonomous vehicles make us sick?,” *Contemp. Ergon. Hum. Factors* 2014, pp. 301–307, 2014.
- [2] J. Iskander *et al.*, “From car sickness to autonomous car sickness: A review,” *Transp. Res. Part F Traffic Psychol. Behav.*, vol. 62, pp. 716–726, 2019.
- [3] R. E. Rolnick, A. & Lubow, “Why is the driver rarely motion sick? The role of controllability in motion sickness,” *Ergonomics*, vol. 34, no. 7, pp. 867–879, 1991.
- [4] B. Sivak, Micheal, Schoettle, “Motion Sickness in Self-Driving Vehicles,” *Rep. No. UMTRI-2015-12*, no. April, 2015.
- [5] Daimler, “Kinetosis - nausea when travelling by vehicle,” 2019. <https://www.daimler.com/magazine/mobility/motion-sickness-kinetosis-product-development.html> (accessed Oct. 23, 2020).
- [6] JLR, “Preventing motion sickness - JLR Corporate Website,” 2020. <https://www.jaguarlandrover.com/2018/preventing-motion-sickness> (accessed Oct. 23, 2020).
- [7] Citroën, “Seetroën Glasses - Solution to travel sickness,” 2020. <https://www.citroen.co.uk/about-citroen/citroen-inspired-by-you/seetroen-glasses> (accessed Oct. 23, 2020).
- [8] ZF, “Counteract Motion Sickness - ZF,” 2019. [https://www.zf.com/mobile/en/stories\\_20160.html](https://www.zf.com/mobile/en/stories_20160.html) (accessed Oct. 23, 2020).
- [9] Ricardo, “Ricardo develops technology to avoid motion sickness in autonomous vehicles,” 2019. <https://ricardo.com/news-and-media/news-and-press/ricardo-develops-technology-to-avoid-motion-sickness-in-autonomous-vehicles> (accessed Oct. 23, 2020).
- [10] D. Huppert, J. Benson, and T. Brandt, “A historical view of motion sickness-A plague at sea and on land, also with military impact,” *Front. Neurol.*, vol. 8, no. April, pp. 1–15, 2017.
- [11] J. R. Lackner, “Motion sickness: More than nausea and vomiting,” *Exp. Brain Res.*, vol. 232, no. 8, pp. 2493–2510, 2014.
- [12] S. Salter, C. Diels, P. Herriotts, S. Kanarachos, and D. Thake, “Model to predict motion sickness within autonomous vehicles,” *Proc. Inst. Mech. Eng. Part D J. Automob. Eng.*, vol. 234, no. 5, pp. 1330–1345, 2020.
- [13] ISO, “SVENSK STANDARD SS-ISO 2631-1,” pp. 8–30, 1997.
- [14] R. Lewkowicz, “Modeling Motion Sickness,” *Polish J. Aviat. Med. Bioeng. Psychol.*, vol. 22, no. 3, pp. 32–42, 2017.
- [15] B. E. Donohew and M. J. Griffin, “Motion sickness: Effect of the frequency of lateral oscillation,” *Aviat. Sp. Environ. Med.*, vol. 75, no. 8, pp. 649–656, 2004.
- [16] J. T. Reason, “Motion sickness adaptation: A neural mismatch model,” *J. R. Soc. Med.*, vol. 71, no. 11, pp. 819–829, 1978.
- [17] C. M. Oman, “Motion sickness: A synthesis and evaluation of the sensory conflict theory,” *Can. J. Physiol. Pharmacol.*, vol. 68, no. 2, pp. 294–303, 1990.
- [18] J. E. Bos and W. Bles, “Modelling motion sickness and subjective vertical mismatch detailed for vertical motions,” *Brain Res. Bull.*, vol. 47, no. 5, pp. 537–542, 1998.

- 
- [19] C. Braccresi and F. Cianetti, "Motion sickness. Part I: development of a model for predicting motion sickness incidence," *Int. J. Hum. Factors Model. Simul.*, vol. 2, no. 3, p. 163, 2011.
  - [20] T. Wada, N. Kamij, and S. Doi, "A Mathematical Model of Motion Sickness in 6DOF Motion and Its Application to Vehicle Passengers," *arXiv Neurons Cogn.*, 2015.
  - [21] T. Wada, J. Kawano, Y. Okafuji, A. Takamatsu, and M. Makita, "A Computational Model of Motion Sickness Considering Visual and Vestibular Information," *IEEE Int. Conf. Syst. Man, Cybern.*, 2020.
  - [22] R. S. Kennedy and A. Graybiel, "The Dial test: A standardized procedure for the experimental production of canal sickness symptomatology in a rotating environment," *Nav. Sch. Aviat. Med. Pensacola FL*, no. June, 1965.
  - [23] R. S. Kennedy, N. E. Lane, K. S. Berbaum, and M. G. Lilienthal, "Simulator Sickness Questionnaire: An Enhanced Method for Quantifying Simulator Sickness," *Int. J. Aviat. Psychol.*, vol. 3, no. 3, pp. 203–220, 1993.
  - [24] J. F. Golding, "Motion sickness susceptibility questionnaire revised and its relationship to other forms of sickness," *Brain Res. Bull.*, vol. 47, no. 5, pp. 507–516, 1998.
  - [25] J. F. Golding, "Predicting individual differences in motion sickness susceptibility by questionnaire," *Pers. Individ. Dif.*, vol. 41, no. 2, pp. 237–248, 2006.
  - [26] S. R. Gianaros PJ, Muth ER, Mordkoff JT, Levine ME, "A questionnaire for the assessment of the multiple dimensions of motion sickness," *Aviat Sp. Env. Med.*, vol. 72, no. 2, pp. 115–119, 2001.
  - [27] J. E. Bos, S. N. MacKinnon, and A. Patterson, "Motion sickness symptoms in a ship motion simulator: Effects of inside, outside, and no view," *Aviat. Sp. Environ. Med.*, vol. 76, no. 12, pp. 1111–1118, 2005.
  - [28] B. Keshavarz and H. Hecht, "Validating an efficient method to quantify motion sickness," *Hum. Factors*, vol. 53, no. 4, pp. 415–426, 2011.
  - [29] D. Tavernini, E. Velenis, and S. Longo, "Feedback brake distribution control for minimum pitch," *Veh. Syst. Dyn.*, vol. 55, no. 6, pp. 902–923, 2017.
  - [30] J. Utbult, "A Study on Low-Speed Maneuverability and Highway Lateral Comfort," *Master Thesis, Chalmers Univ. Technol.*, 2017.
  - [31] P. DiZio *et al.*, "An active suspension system for mitigating motion sickness and enabling reading in a car," *Aerosp. Med. Hum. Perform.*, vol. 89, no. 9, pp. 822–829, 2018.
  - [32] H. Agrawal and J. Gustafsson, "Investigation of active anti-roll bars and development of control algorithm," *Master Thesis, Chalmers Univ. Technol.*, 2017.
  - [33] C. A. Vivas-López, D. Hernandez-Alcantara, J. C. Tudón-Martínez, and R. Morales-Menendez, "Review on global chassis control," *IFAC Proc. Vol.*, vol. 46, no. 2, pp. 875–880, 2013.
  - [34] C. Badue *et al.*, "Self-driving cars: A survey," *Expert Syst. Appl.*, vol. 165, no. September 2019, p. 113816, 2021.
  - [35] L. Claussmann, M. Revilloud, D. Gruyer, and S. Glaser, "A Review of Motion Planning for Highway Autonomous Driving," *IEEE Trans. Intell. Transp. Syst.*, vol. 21, no. 5, pp. 1826–1848, 2020.
  - [36] D. González, J. Pérez, V. Milanés, and F. Nashashibi, "A Review of Motion Planning Techniques for Automated Vehicles," *IEEE Trans. Intell. Transp. Syst.*, vol. 17, no. 4, pp. 1135–1145, 2016.
  - [37] Z. Htike, G. Papaioannou, E. Velenis, and S. Longo, "Motion Planning of Self-driving Vehicles for Motion Sickness Minimisation," *Eur. Control Conf. 2020, ECC 2020*, pp. 1719–1724, 2020.
  - [38] I. Bae, J. Moon, and J. Seo, "Toward a comfortable driving experience for a self-driving shuttle bus," *Electron.*, vol. 8, no. 9, pp. 1–13, 2019.
  - [39] C. Certosini, L. Papini, R. Capitani, and C. Annicchiarico, "Preliminary study for motion sickness reduction in autonomous vehicles: An MPC approach," *Procedia Struct. Integr.*, vol. 24, no. 2019, pp. 127–136, 2019.
  - [40] N. Zengin, M. Sever, A. Kirli, and M. S. Arslan, "Analyzing motion sickness level in autonomous vehicles according to look-ahead distance," *2018 6th Int. Conf. Control Eng. Inf. Technol. CEIT 2018*, no. October, pp. 25–27, 2018.
  - [41] M. Sever, N. Zengin, A. Kirli, and M. S. Arslan, "Carsickness-based design and development of a controller for autonomous vehicles to improve the comfort of occupants," *Proc. Inst. Mech. Eng. Part D J. Automob. Eng.*, vol. 235, no. 1, pp. 162–176, 2020.
  - [42] S. 'Atifah Saruchi *et al.*, "Lateral control strategy based on head movement responses for motion sickness mitigation in autonomous vehicle," *J. Brazilian Soc. Mech. Sci. Eng.*, vol. 42, no. 5, 2020.
  - [43] S. A. Saruchi *et al.*, "Novel motion sickness minimization control via fuzzy-PID controller for autonomous vehicle," *Appl. Sci.*, vol. 10, no. 14, 2020.
-

# Assessing indicators to testing human-AI interaction in autonomous vehicles: A pilot study with Omnipresent AI

Peer M. Sathikh<sup>1,\*</sup>, Tan Guan Yi<sup>1</sup> and Fang Zong Rui Dexter<sup>1</sup>

<sup>1</sup>Nanyang Technological University, 50 Nanyang Avenue, Singapore 639798, Singapore

\*Corresponding author. Email: [peersathikh@ntu.edu.sg](mailto:peersathikh@ntu.edu.sg)

---

In present ride-hailing contexts, passengers are used to communicating with a driver during a ride. However, the introduction of Autonomous Vehicles (AVs) presents an interesting scenario, as the AV has no physical driver on board. Yet a level of fear still exists, as the public is unable to fully predict or understand its intentions. The concept of an Omnipresent AI was introduced, allowing for the AI to achieve a sense of presence through 3 postulates previously developed. A simulated roadtrip scenario experiment was done to ascertain the indicators towards further testing these 3 postulates. This paper outlines these indicators obtained from the experiment could form an important part of future research.

© 2021 by the authors. Published by the Resource Efficient Vehicles Conference.  
This is an open access article under the CC BY license (<http://creativecommons.org/licenses/by/4.0/>).

---

## 1. Introduction

Autonomous Vehicles (AVs) are currently being developed for widespread use in transportation in the near future. Progress in this area of mobility ranges from solving technical hurdles like battery capacity, to improving vehicle AI for safer navigation of unexpected events on the road. Yet a gap in development appears to pervade in the form of its social interaction with passengers. In other words, the question asked was how an AI can provide assurance and comfort during interactions with new passengers in ride hailing situations - as a response to a review of earlier findings where passengers experienced anxiety or distrust of the AI driver's behaviour. This paper presents the research, results and analysis from this experiment that could provide useful indicators for future research in this area.

To this aim, a category for this new form of AI was proposed called an Omnipresent AI. From previous work done by the authors, an Omnipresent AI is defined by 3 Postulates based on existing communication theories that describe natural forms of communication in human conversation. [33] These are: 1) That such an AI should adopt a persona to be perceived as a presence, 2) It should be able to manage information in a manner that leads to appropriate responses and 3) It should be able to communicate naturally with users despite not having a physical form. A pilot simulation experiment was set up to first define the qualitative indicators of this new approach to Human-AI interactions in an AV based on the 3 Postulates. This was done to ascertain the validity and the measurable criteria of this new form of AI intervention, allowing it to be further tested using more rigorous quantitative methods. In this paper, the preliminary findings of the pilot study will be discussed in more detail.

## 2. Background

The approach to this research draws from a need to ascertain the effectiveness of an AI intervention from a social interaction standpoint. As the technical, logistical and policy challenges

for Autonomous Vehicles (AVs) are overcome, AVs will be expected to ferry passengers as human drivers of today would do. Yet a certain level of anxiety still exists amongst the public surveyed, due to a perceived lack of control during the ride [30][1]. A review by Rosenzweig and Bartl showed that 91.2% of research paths in AV development are related to the user acceptance of the technology [7], and not much progress appears to have been done in terms of social interactions to address it. This pervading gap in social interactions is seen to exist in the space where humans and AI interact [14] [15] [16]. In what ways can passenger anxiety be alleviated in this AV interaction context?

## **2.1 Approach**

A survey of recent simulation studies focusing on passenger reactions in different forms of AVs [3] [4] [5] [6] show a lack of mediation in terms of user experience, providing an opportunity for further improvement. These simulation studies focused on the acceptance of autonomy “as is”, due to a lack of understanding of the AI’s possibilities in interaction. [20] The authors want to address this research gap to introduce better user acceptance of AVs, with the core belief that the perception or display of underlying intelligence can positively affect the level of trust the passenger can have in the system. This assumption of course is only valid in future scenarios when AI beings have matured to a level of intelligence and competence that approach near equal to humans. In the context of AVs, it would be classified as having an autonomy level of 4 or higher. [31] One AV simulation study in the direction of improving social interactions reported that participants would trust a vehicle more when several anthropomorphic features were assigned to it - the features in the experiment being a pre-recorded human voice, a name, and a gender. [2] In this sense, attaching human-like characteristics and motivations to nonhuman agents increases the ability to make sense, reduce uncertainty, and increase confidence in the agent’s future actions. [8] This suggests incorporating human-like behavior being a possible pathway to bring out the AI being’s inherent intelligence towards fostering trust.

Beyond the scope of research in AVs, research in the direction of according human-like interaction also shows promise. The incorporation of not just performative but also social aspects of human-to-human communication need to be explored, which include mutual agency in conversation [13] [23], the awareness of one’s social role in conversation [34] [24], the consistency of identity and past interactions [22], and different modes of human expression [25] [26] [27]. When combined in practice, it can provide sufficient evidence to believe that the system can comprehend the situation at hand and complement the user’s needs. [11] [12]. To this aim of displaying evidence of cognition and intelligence, these approaches can be said to center around the AI being recognized as a social presence [9] [21]. While these are not the only factors affecting trust in nonhuman agents [10], its contribution is significant and should be explored. For one to achieve a presence involves a discussion of one being a social actor in an interaction environment. In an AI context, social presence can also be described as a condition when part or all of a person’s perception cannot accurately acknowledge the role of technology such that they appear to communicate with one or more other people or entities [17]. To bring about this immersion of sensory input to achieve presence [19], new ways of displaying social presence need to be developed for AI interaction.

## **3. Methodology**

In this research the authors delve deeper, testing a different approach to incorporate a social presence to AV AI interactions based on existing communication principles. Towards fostering trust, the authors chose to develop a theoretical framework to visibly externalize the AI’s mental processes, akin to how a human’s body language and facial expressions when accompanying speech, function as additional social signals to strengthen the meaning of speech very efficiently. In an AI context, this approach may provide more expressive capabilities to display its intelligence in social interactions. This visual identity, or ‘grammar’ to interaction was explored and discussed in our previous work. In

the future it's hoped that this framework can be used by the AI themselves to develop their unique visual expressions to aid in individuality and increasing its social presence.

To unify both the visual and audio aspects of this AI intervention in AVs, it is important to consider the 3 Postulates of an Omnipresent AI which are:

1. *Omnipresent AI should adopt a persona to be perceived as a presence.*
2. *Omnipresent AI should be able to manage information in a manner that leads to appropriate responses.*
3. *Omnipresent AI should be able to communicate naturally with users despite not having a physical form.*

To begin testing these postulates, it is assumed that the testing environment required 1) a simulation environment, 2) an AI Agent with the cognitive capability near equal to a human being, and 3) a relevant interaction scenario. Being a pilot study, a design research methodology was used to perform usability testing of a simulation prototype to fulfill these conditions. This ensured that the feedback provided by participants was genuine as they can feel a sufficient level of immersion to elicit truthful reactions and bring about any emergent behavior or phenomena in this AV context [28].

## 4. Methodology

### 4.1 Apparatus

To test the postulates, the experiment was conducted in a controlled lab setting using 2 different test platforms, one in Virtual Reality (VR) and the other in a physical mock-up of a car. The 3 postulates are hoped to be validated using these platforms, as both versions are planned to bring about different reactions and anticipations during the simulation.

The VR platform was developed using a combination of Unreal Engine by Epic Games to render the vehicle cabin and Touchdesigner by Derivative to display the added visuals.

The physical platform involves a 6m x 2.5m interior of an MPV-sized vehicle set in front of 3 curved projector screens, and an additional flat projector screen on the roof of the mock-up vehicle. This physical version uses 2 instances of Touchdesigner to display the road trip scenario and visual patterns.

In both versions, a Wizard of Oz experiment is performed in which one researcher who is hidden from view of the participant pretends to be the AI in the simulation. [29] This is to simulate a Level 5 AV capable of full autonomy and human-like social interactions required to test the conditions of the 3 Postulates. This was tested by explicitly displaying the AI's intentions using both sound and visuals to bring about a social presence. It was intentionally decided that the roof of the AV serves as the canvas for the 'visual' presence of the AI. For the audio component, speakers were placed in four corners of the simulation space in both test platforms to allow the AI to converse with the passenger. Both versions also play the same pre-recorded 12-minute-long road trip scenario from a housing estate in Singapore to the zoo.



Figure 1: the two experimental setups used. The physical mock-up setup on the left, and the VR setup on the right. Both versions showed the same travel scenario for consistency.

## 4.2 Participants

Being a pilot study, 10 participants each were chosen from the public to test the two platforms. They were then grouped in age ranges of 21-35, 36-55 and 56-70 years to ensure a balanced and diverse range of responses. Participants were screened for inclusion criteria including driver license status and motion sickness. Participants were also paid a token amount for joining the study. The research was approved by the Institutional Review Board in Nanyang Technological University.

Table 1: Participants by age group and gender

Age Groups	21-35	36-55	56-70	Total by Gender
Male (Physical)	2	2	1	5
Male (VR)	2	2	1	5
Female (Physical)	3	1	1	5
Female (VR)	1	2	2	5
Total Participants				20

## 4.3 Experimental Design

In both versions of the experiment, participants were briefed about the experiment being a road trip where they were asked to roleplay a passenger traveling from their home in a nearby housing estate to Singapore Zoo to meet their family members who are already there. They were also briefed that the driver is an AI who will be fetching them, but it was not disclosed that the AI is played by a researcher hidden from view. A researcher who knows about the entire experiment setup also sat with the participant as a co-passenger in the simulation. In both versions, a pre-recorded zoo trip video plays in the front of the simulated vehicle. As the trip progresses, the ‘AI’ will start its audio-visual interaction in the experiment in the form of light conversation, with added visual patterns on the roof that accompany the AI’s speech. To ensure data consistency, the co-passenger and AI take turns to ask a series of scripted questions regarding the trip and the participant’s travel experiences. Any other questions or topics that were elicited by the participant in the experiment were entertained and regarded as continuing the natural flow of conversation to maintain the perception of natural human-like interaction. At the end of the road trip, each participant completed an open-ended questionnaire that assessed initial reactions, anxiety, and effectiveness of the AI interventions. Using both the scripted travel questions and post-simulation questionnaire, the indicators eligible for further testing of the 3 postulates were derived.

## 5. Results

Referring to the previous work of the authors, these 3 postulates can be hypothesized as maintaining the consistency of several qualities, shown in Table 1. To establish parameters, the postulates can be separated into distinct categories. These qualities are first interpreted in the context of AVs, then separated into hypothesized indicators to test the validity of the postulates shown. The hypothesized indicators are then indirectly tested through a semi-formal design questionnaire as part of the usability testing method. Responses are recorded, then coded into categories in Table 2 to Table 4 along with the frequency of occurrence.

Table 1: Hypothesized Indicators for the 3 Postulates

Postulate		Hypothesized Indicator
1	Displaying a presence to be perceived as a trusted presence	1a) Consistency of Personality
		1b) Consistency of Social Role
2	Managing information that leads to appropriate responses	2a) Consistency of Contextual Cues
		2b) Consistency of Passenger Emotional State
3	Communicate naturally even without a physical form	3a) Consistency of Immersion in Conversation
		3b) Consistency in Use of Space

## 5.1 Postulate 1

Postulate 1 is indirectly tested through 2 questions asked in the design questionnaire. The indicators point towards features of interaction that aid in bringing about a consistent personality and social role. The questions that pertain to the indicators for Postulate 1 are:

1. *Were the graphics presented (in terms of the color, shapes, and animation) sufficient to convey what the driver wanted to say?*
2. *How did you feel when entering a vehicle without a driver present?*

Table 2: Occurrence of Indicators for Postulate 1

Hypothesized Indicators	Group	Resultant Indicators	Occurrence
Personality	AI Visual Presentation	Shape	60%
		Animation	25%
		Color	20%
		Visual Engagement	20%
		Spatial Arrangement	15%
Social Role	AI as Driver	Understanding of Technology	35%
		Social Engagement (Enjoying Company)	20%
		Safety Concerns	5%
Personality, Social Role	User Related	Initial Novelty of Experience	40%
		User Agency	10%
		Task Comfort	5%

From the responses given, participants mention the shape of the animated graphics affecting the AI's visual presentation the most. In terms of the AI's social role, participants mention their understanding of the technology being an important factor. For user related indicators, the initial experience of entering an AV, whether positive or negative also was mentioned the most. These indicators point toward further progress needed in briefing or explaining the user on how the technology works to increase passenger comfort.

## 5.2 Postulate 2

Postulate 2 is indirectly tested in 2 simple yes or no questions asked by the AI in the roadtrip travel simulation. The indicators are more task based and focus on the range of responses possible in an interaction. The questions that pertain to the indicators for Postulate 2 are:

- 1) *“There are two options to go to the zoo, Woodlands Rd and the BKE. Do you happen to have a preference?”*
- 2) *(after weather question prompt) ...” Do you guys happen to have an umbrella?”*



Table 3: Occurrence of Indicators for Postulate 2

Hypothesized Indicators	Group	Resultant Indicators	Occurrence
Contextual Cues	Participant Response	Response Given within Context	100%
		User Initiated Question	23.5%
		Follow-up Question	17.6%
		Unexpected Reply	14.7%
		Change in Topic	11.7%
Passenger Emotional State	Participant Response	Uncertain Reply	11.7%
	AI Response	Error Handling	11.7%

From the responses given, the AI in an AV should have the contextual knowledge available to handle not only indirect follow-up replies, but also improvise when the user initiates these questions. As the ‘AI’ was played by a researcher, the recommended testing criteria for chatbots such as Understanding, Navigation, Intelligence and Error Management were excluded as the ‘AI’ was able to perform these to a ‘human level of capacity’ [32]. This is shown in the *Response Given within Context* rate of 100%. This may also explain why passenger emotional state was not found to be as critical a testing criterion, as the ‘AI’ was able to handle misunderstandings or misheard questions well. In the simulation, the only signs of a disturbance in emotional state appeared to happen when 1 participant quickly changed the topic abruptly after answering the question.

### 5.3 Postulate 3

Postulate 3 is indirectly tested through 2 questions asked in the design questionnaire. The indicators point towards features of interaction that aid in bringing about consistency in immersion and use of space. The questions that pertain to the indicators for Postulate 2 are:

- 1) *Was there a moment in the trip that made you feel uncomfortable?*
- 2) *Did the actions of the driver make you feel less anxious?*

Table 4: Occurrence of Indicators for Postulate 3

Hypothesized Indicators	Group	Resultant Indicators	Occurrence
Immersion in Interaction	AI Related	Natural Conversation	35%
		Positive Presence (Calm, Confident)	27.5%
		Accurate Response	17.5%
		Voice Quality	15%
		Initiated Conversation	7.5%
	Scenario Related	Driving Performance	25%
Use of Space	User Related	Trust	2.5%
		Familiarity	2.5%
	AI Related	Visuals	15%

In terms of immersion, the ability to engage in natural conversation, the ability to display a positive presence and provide accurate responses were the most recorded. This points towards further work needed in enhancing the AI’s conversational ability through other sensory experiences to bring about a consistent social presence. The *Use of Space* in natural communication also appears to be less effective than the immersive aspect. This may be attributed to the first-time experience of the

participants in such an environment, and more work needs to be done to make the communicative aspects of the AI more identifiable in future experiments.

## 6. Discussion

The simulated scenario format described was done to obtain indicators to use as testable criteria for future research of the 3 postulates for Omnipresent AI. This approach started with an idea to address AI-human interaction in a different manner. As there is a need for a different kind of intelligence to handle the navigation and socializing tasks of vehicle drivers, the concept of an Omnipresent AI was developed from which the 3 postulates were derived to describe Omnipresent AI. The indicators obtained through this pilot study sufficiently validates the postulates, and points towards implementations that need to be improved, for example in the display of visuals. Due to the complex research premise, the experiment was performed in this present manner described to test the aspects of universal communication principles found in the 3 postulates. One limitation of this experiment is the lack of group interactions in a travel scenario. Another limitation is the lack of different travel scenarios, which limited the responses to only casual trip contexts. Further testing can be performed with other scenarios such as traffic jams and emergencies to ascertain all the communicative abilities needed by the AI towards increasing passenger acceptance.

## 7. Conclusion

This paper indicates that the 3 postulates proposed for an Omnipresent AI are significant in developing AI-Human social interaction, based on universal communication principles. Indicators recorded from participant responses in a simulation experiment point towards the premise for further validation of the 3 postulates. The authors intend to continue utilizing the simulation platforms, and building on the different interaction modes to incorporate the postulates, in order to bring about near human interactions in an autonomous vehicle.

## 8. Acknowledgements

This paper is the result of a grant given by the National Research Foundation of Singapore to NTU-TUMCREATE, a collaboration between Nanyang Technological University and Technical University of Munich.

## References

1. K. Arai, S. Kapoor and R. Bhatia, *Intelligent Systems and Applications*, 1st ed. Springer, Cham, 2021.
2. E. Edmonds, "Self-Driving Cars Stuck in Neutral on the Road to Acceptance", 2020. [Online]. Available: [https://newsroom.aaa.com/2020/03/self-driving-cars-stuck-in-neutral-on-the-road-to-acceptance/#:~:text=\(Mar.,in%20a%20self%2Ddriving%20car.&text=Six%20in%20ten%20\(57%25\),with%20a%20self%2Ddriving%20vehicle.](https://newsroom.aaa.com/2020/03/self-driving-cars-stuck-in-neutral-on-the-road-to-acceptance/#:~:text=(Mar.,in%20a%20self%2Ddriving%20car.&text=Six%20in%20ten%20(57%25),with%20a%20self%2Ddriving%20vehicle.) [Accessed: 23- Apr- 2021].
3. In: *Transportation Research Board 93rd Annual Meeting*. 2014. Public Perceptions of Self-Driving Cars: The Case of Berkeley, California. [online] Transportation Research Board, pp.10-17. Available at: <<https://trid.trb.org/view/1289421>> [Accessed 13 April 2021].
4. Rosenzweig, J., & Bartl, M., 2015. A review and analysis of literature on autonomous driving. *E-Journal Making-of Innovation*, 1-57.
5. Abraham, Hillary, et al. "Autonomous vehicles, trust, and driving alternatives: A survey of consumer preferences." *Massachusetts Inst. Technol, AgeLab, Cambridge* 1 (2016): 16.
6. Tschopp, Marisa & Ruef, Marc. (2020). AI & Trust -Stop asking how to increase trust in AI.
7. Bartneck, Christoph & Lyons, Michael & Saerbeck, Martin. (2017). The Relationship Between Emotion Models and Artificial Intelligence
8. Vinkhuyzen, Erik, and Melissa Cefkin., 2016. "Developing socially acceptable autonomous vehicles." In *Ethnographic Praxis in Industry Conference Proceedings*, vol. 2016, no. 1, pp. 522-534.

9. Stayton, E., Cefkin, M., & Zhang, J., 2017, November. Autonomous Individuals in Autonomous Vehicles: The Multiple Autonomies of Self-Driving Cars. In *Ethnographic Praxis in Industry Conference Proceedings* Vol. 2017, No. 1, pp. 92-110.
10. Cho, Y., Park, J., Park, S. and Jung, E., 2021. *Technology Acceptance Modeling based on User Experience for Autonomous Vehicles*. [online] Dx.doi.org. Available at: <<http://dx.doi.org/10.5143/JESK.2017.36.2.87>> [Accessed 13 April 2021].
11. Morris, D., Erno, J. and Pilcher, J., 2017. Electrodermal Response and Automation Trust during Simulated Self-Driving Car Use. *Proceedings of the Human Factors and Ergonomics Society Annual Meeting*, 61(1), pp.1759-1762.
12. Hewitt, C., Politis, I., Amanatidis, T., & Sarkar, A. (2019, March). Assessing public perception of self-driving cars: The autonomous vehicle acceptance model. In *Proceedings of the 24th international conference on intelligent user interfaces* (pp. 518-527).
13. "SAE International Releases Updated Visual Chart for Its "Levels of Driving Automation" Standard for Self-Driving Vehicles", *Sae.org*, 2021. [Online]. Available: <https://www.sae.org/news/press-room/2018/12/sae-international-releases-updated-visual-chart-for-its-%E2%80%9Clevels-of-driving-automation%E2%80%9D-standard-for-self-driving-vehicles>. [Accessed: 23- Apr- 2021].
14. Waytz, A., Heafner, J. and Epley, N., 2014. The mind in the machine: Anthropomorphism increases trust in an autonomous vehicle. *Journal of Experimental Social Psychology*, 52, pp.113-117.
15. Epley, N., Waytz, A., & Cacioppo, J. T. (2007). On seeing human: a three-factor theory of anthropomorphism. *Psychological review*, 114(4), 864.
16. S. Sundar, "Rise of Machine Agency: A Framework for Studying the Psychology of Human–AI Interaction (HAI)", *Journal of Computer-Mediated Communication*, vol. 25, no. 1, pp. 74-88, 2020. Available: 10.1093/jcmc/zmz026 [Accessed 15 April 2021].
17. H. Dubberly and P. Pangaro, "What is conversation? How can we design for effective conversation?", *Dubberly.com*, 2009. [Online]. Available: <http://www.dubberly.com/articles/what-is-conversation.html>. [Accessed: 16- Apr- 2021].
18. Turner, J. 1988. A theory of social interaction. Stanford University Press, Stanford, Calif.
19. Castelfranchi, C. (1998). Modelling social action for AI agents. *Artificial intelligence*, 103(1-2), 157-182.
20. Tejwani, R., Moreno, F., Jeong, S., Park, H. W., & Breazeal, C. (2020). Migratable AI. *arXiv preprint arXiv:2007.05801*.
21. Goldin-Meadow, S., & Alibali, M. W. (2013). Gesture's role in speaking, learning, and creating language. *Annual review of psychology*, 64, 257-283.
22. Pentland, A. (2010). *Honest signals: how they shape our world*. MIT press.
23. Thompson, R., Vinson, D. and Vigliocco, G., 2009. The link between form and meaning in American Sign Language: Lexical processing effects. *Journal of Experimental Psychology: Learning, Memory, and Cognition*, 35(2), pp.550-557.
24. Bishop, M. Computer Security: Art and Science. Addition-Wesley Press, 2003
25. Marcus, G., and Davis, E. Rebooting AI: Building artificial intelligence we can trust. Vintage, 2019.
26. J. Lee, K. Kim, S. Lee and D. Shin, "Can Autonomous Vehicles Be Safe and Trustworthy? Effects of Appearance and Autonomy of Unmanned Driving Systems", *International Journal of Human-Computer Interaction*, vol. 31, no. 10, pp. 682-691, 2015. Available: 10.1080/10447318.2015.1070547 [Accessed 14 April 2021].
27. C. Oh, J. Bailenson and G. Welch, "A Systematic Review of Social Presence: Definition, Antecedents, and Implications", *Frontiers in Robotics and AI*, vol. 5, 2018. Available: 10.3389/frobt.2018.00114 [Accessed 16 April 2021].
28. P. Hancock, D. Billings, K. Schaefer, J. Chen, E. de Visser and R. Parasuraman, "A Meta-Analysis of Factors Affecting Trust in Human-Robot Interaction", *Human Factors: The Journal of the Human Factors and Ergonomics Society*, vol. 53, no. 5, pp. 517-527, 2011. Available: 10.1177/0018720811417254 [Accessed 15 April 2021].
29. K. Xu and T. Liao, "Explicating Cues: A Typology for Understanding Emerging Media Technologies", 2021.
30. Zeltzer, D. (1992). Autonomy, interaction, and presence. *Presence: Teleoperators & Virtual Environments*, 1(1), 127-132.
31. Dumas, J. S., & Fox, J. E. (2009). Usability testing: Current practice and future directions. *Human-Computer Interaction: Development Process*, 231.
32. Hanington, B., & Martin, B. (2019). *Universal methods of design expanded and revised: 125 Ways to research complex problems, develop innovative ideas, and design effective solutions*. Rockport publishers.
33. N. Abalos, "chatbottest-com/guide", *GitHub*, 2017. [Online]. Available: <https://github.com/chatbottest-com/guide/wiki>. [Accessed: 23- Apr- 2021].

---

# Psychoacoustic perspectives on electric truck

Maria Rådsten Ekman<sup>1,\*</sup>, Karl Bolin<sup>2</sup>

<sup>1</sup> The Centre for ECO<sup>2</sup> Vehicle Design, Teknikringen 8, 100 44 Stockholm, Sweden

<sup>2</sup> The Marcus Wallenberg Laboratory for Sound and Vibration Research, KTH Royal Institute of Technology, Teknikringen 8, 100 44 Stockholm, Sweden

\*Corresponding author. Email: mariare2@kth.se

---

The soundscape is constantly changing, and new sounds are added to the soundscape. To localize sources, we rely both on binaural and monaural cues [1], and the auditory system also provides distance to sound sources [2]. This paper gives an outline of the planned work of determining the interior sound quality within electric heavy vehicles.

© 2021 by the authors. Published by the Resource Efficient Vehicles Conference.  
This is an open access article under the CC BY license (<http://creativecommons.org/licenses/by/4.0/>).

---

## 1. Introduction

Due to global warming and the Paris agreement we need to lower our dependence on fossil fuels for the transport sector and at the same time keep up the increased demand of transport capacity of both persons and goods. One important of many measures is to migrate to electric drive instead of combustion engines in trucks. Apart from the global benefits for the climate of such a transition, the transition will also affect the air quality and sound situation for both drivers and persons living close to traffic. The exterior noise from a truck with a diesel-powered combustion engine is usually dominated by motor noise at low speeds and when increasing the velocity tyre-road noise increases and also aerodynamic noise [3] and the sound situation inside the driver compartment follows a similar pattern. Therefore, the largest impact of the shift towards using electric engines on heavy vehicles will probably occur when driving at slow speeds and thus urban environments are especially interesting.

Numerous sound sources in urban areas, which we are familiar with, will change and new unfamiliar sound sources will be added to the soundscape. Road traffic noise has been a problem for residents near busy roads within cities, but the change from fossil fuel to electric driven vehicles may change this. [4,5] The goal of this project is to suggest measures that can have a positive impact on the internal sound environment in the cabin of electrically driven heavy vehicles and analyse these proposals from a cost perspective. To achieve these objectives the project has started with a survey to professional drivers in order to better understand the internal environment and the importance of different factors for these and this investigation is given in the present paper along with an outline of future work.

## 2. Method

In order to assess the current internal environment for truck drivers and their experience as well as their attitude towards electric or hybrid vehicles. A questionnaire was distributed to the drivers working at the Swedish postal service company PostNord in the spring of 2021. The questionnaire

was distributed at the coffee room for the drivers and in total 47 questionnaires were filled in by the drivers on papers. The respondent's rate was at 94% so no analysis of dropouts was considered necessary. A cross-sectional study design was used in which only one specific group from the population is examined at one time.

## **2.1 Questionnaire setup**

A paper and pencil version of the questionnaire was chosen in order to facilitate for the drivers to complete the task in their coffee breaks. The specific questions for the drivers were asked are stated below:

1. What is important to you as a driver within the truck?
2. Do you notice that the engine noise in the cockpit is disturbing?
3. Is there any sound besides motor sound that you consider as annoying?
4. Have you driven a hybrid?
5. Could you consider driving a hybrid?
6. Have you driven an electric truck?
7. Could you consider an electric truck?
8. If you have driven an electric truck, how did you experience the sound environment?
9. Open comments, please write any additional thoughts on the sound environment in both combustion and electric drives for trucks.

For the first two questions grading with the scale 1-10 (not at all- extremely) were chosen as this is widely spread in noise studies and are considered easily understood by the respondents.

## **2.2 Demographics**

All the drivers were male and most of them had more than 10 years as professional truck drivers, thus the study group is considered to have a high degree of truck experience. Mean age among the drivers was 45 years.

## **3. Results from the survey**

### **3.1 Important factors for driver environment**

The first question in the questionnaire was: "What is important to you as a driver within the truck?", that is about the internal environment within the cockpit and the results are shown in table 1 below. The result from the survey shows that most of the drivers considered all aspects as important when it comes to the driver's internal environment. Ergonomics and ventilation were considered slightly more important than sound and fragrance. As can be seen the reported standard deviations show that there are somewhat higher degrees of unit regarding the importance of ergonomics and ventilation while sound and fragrance shows higher standard deviations indicating diverging opinions amongst the drivers.

Factor	Mean value (1-10)	Standard deviation
Sound	7.7	2.2
Ergonomics	8.4	1.6
Ventilation	8.4	1.5
Fragrance	7.2	2.2

### 3.2 Engine noise annoyance

The second question in the questionnaire was: “Do you notice that the engine noise in the cockpit is disturbing?”. When it comes to the perceived noise annoyance within the cockpit, showed that on the graded scale of one to ten not any driver graded this higher than three. The vast majority 30 of 47 graded the engine noise as not annoying at all (1 on the 10-graded scale) and 12 graded it as “2” and two graded it as “3”. Thus, the internal noise from the combustion engine seems to be a very small factor of disturbance and as later seen in the open question (number 9) some drivers enjoy the sound from the motor and a migration to hybrid or electric drive may be problematic from a perspective of internal sound in the cockpit.

### 3.3 Attitude towards hybrid and electrical trucks

For the fourth and sixth question: “Have you driven a hybrid/electric truck?”, two of the drivers had tested driving an electric truck at Scania. Besides the fact that none of the remaining drivers have any experience driving a hybrid truck or a fully-electric truck. Regarding the fifth and seventh question “Could you consider driving a hybrid/electric truck?” the respondents were mainly positive to drive both hybrid and fully electric vehicles with 67% positive for hybrid vehicles and 83% positive for fully electric vehicles. Why the attitude to drive fully electric is higher than to drive hybrid trucks is unknown to the authors.

### 3.4 Open questions

The drivers had also the possibility to add their point of views concerning the survey, some of the comments are added below for a general overview of the respondents' opinions on noise in the cockpit:

“Electric trucks don’t do anything for the environment, on the contrary they harm the environment.”

“Diesel is better than hybrid and electric trucks.”

“I like to hear the engine so I can hear if something is wrong.”

“I like to hear the horsepower; it is an enjoyment.”

“Sounds that do not belong in the truck i.e., rattling”

“Wind noise”

As can be seen from the quotes many of the drivers that seem sceptical in driving electric vehicles chose to word their opinions. Some of the reasons seem to be correlated to adverse opinions of climate change whereas others are concerned that the acoustic feedback from the combustion engine will disappear and other noise sources, that may not provide as much information, may become dominant. Thus, a minority of the drivers will have to be addressed with different actions in order to be positive to a potential change of driveline.

## 4. Discussion and conclusion

A probable migration to electric driven trucks from combustion engines is probable within a decade. The attitude of professional truck drivers of this change has been examined in this paper by a questionnaire study of truck drivers at the Swedish postal service Postnord in Stockholm, Sweden. The response from the drivers indicates that the sound is an important factor for the working environment and a generally positive attitude towards using both hybrid and fully electrical trucks are observed. Some concerns regarding the new sound environment can also be anecdotally reported which indicates there can be a potential concern for some drivers changing from combustion engines to electrically driven trucks and that the sound environment within the cockpit may not provide feedback from the combustion engine.

As the work on the sound environment recently has started and has been severely hampered by the pandemic this paper also gives an outline of the planned work of determining the interior sound quality within electric heavy vehicles. The work will be conducted by using psychoacoustic measures of sound character, or sound quality, that have been developed for predicting the perceived auditory quality of products, for instance, electric household appliances, and interior car sounds. These measures are typically based on perceptual models first developed by Zwicker in Ref. [6]. It is supposed by the authors that the most important sound quality measures will be:

- Loudness
- Sharpness
- Fluctuation strength
- Roughness:
- Tonality

For further description of these quantities the reader is referred to Ref. [7]. Apart from the sound quality processing and associations of the sounds is naturally also important to study in this context and habituation to a new sound environment is also considered by the authors to be a significant factor. In conclusion the present paper suggests that truck drivers are generally positive to start driving hybrid and electrical vehicles and that the sound in these must be considered one important factor for driver comfort.

## References

1. Moore, D. R., & King, A. J. (2004). Plasticity of binaural systems. In *Plasticity of the Auditory System* (pp. 96-172). Springer, New York, NY.
2. Zahorik, P. (2002). Assessing auditory distance perception using virtual acoustics. *The Journal of the Acoustical Society of America*, 111(4), 1832-1846.
3. Kephelopoulou, S., Paviotti, M., & Anfosso-Lédée, F. (2012). Common noise assessment methods in Europe (CNOSSOS-EU). *Common noise assessment methods in Europe (CNOSSOS-EU)*, 180-p.

4. Nilsson, M. E., & Berglund, B. (2006). Soundscape quality in suburban green areas and city parks. *Acta Acustica united with Acustica*, 92(6), 903-911.
5. Yang, W., & Kang, J. (2005). Acoustic comfort evaluation in urban open public spaces. *Applied acoustics*, 66(2), 211-229.
6. Zwicker, E. (1956). On the loudness of continuous noises. *The Journal of the Acoustical Society of America*, 28(4), 764-764.
7. Zwicker, E., & Fastl, H. (2013). *Psychoacoustics: Facts and models* (Vol. 22). Springer Science & Business Media.



## Day 1: P02 – Human-Vehicle Interaction II

Session P02 – Human-Vehicle Interaction II, Monday 14 June

---

**Session chairs:** Margriet Van Schijndel-de Nooij and Carlos Casanueva Perez

- 11:00-11:10    **P02.A**  
*Optimising tyre wear and exploring its conflict with comfort*  
Georgios Papaioannou, Jenny Jerrelind and Lars Drugge
- 11:10-11:20    **P02.B**  
*Human Machine Interface: A review for future applications in train driving*  
Simon Enjalbert, Livia Maria Gandini, Alexandre Pereda-Baños, Stefano Ricci and Frederic Vanderhaegen
- 11:20-11:30    **P02.C**  
*Objective development in driving simulator motion control: Evaluation of motion cueing using a linearised driving simulator model*  
Henrik Hvitfeldt, Jenny Jerrelind and Lars Drugge
- 11:30-11:40    *Questions and Answers*
-

---

# Optimising tyre wear and exploring its conflict with comfort

Georgios Papaioannou<sup>1,2\*</sup>, Jenny Jerrelind<sup>1,2</sup> and Lars Drugge<sup>1,2</sup>

<sup>1</sup>*Engineering Mechanics, KTH Royal Institute of Technology, Stockholm, Sweden*

<sup>2</sup>*The Centre for ECO<sup>2</sup> Vehicle Design, KTH Royal Institute of Technology, Stockholm, Sweden*

\*Corresponding author. Email: [papaioa@kth.se](mailto:papaioa@kth.se)

---

The automotive industry is shifting its focus on energy efficient driving to tackle rising environmental issues. In this direction, as exhaust particle emissions continuously decrease, the attention is turned on non-exhaust traffic related sources in ground vehicles, such as the interaction between tyre and roads and the tyre wear. Given that the tyres are costly for the vehicle owner and wear creates large waste of old tyres, the modelling and the minimisation of tyre wear have been of great interest recently. The tyre wear is mainly caused by inner (tyre structure and shape) and external (suspension configuration, speed, road surface, etc.) factors. So, this work presents a sensitivity analysis of both inner and external factors, and then explores the optimisation of tyre and suspension parameters for minimising tyre wear and enhancing comfort. More specifically, initially the inner factors are investigated regarding their impact on tyre wear, while external factors, i.e., vehicle loading, velocity and road type, which can be different daily regarding the purpose of the ride, are studied regarding both comfort and tyre wear outlining the conflicting relation between these two objectives. Finally, informed by the results, the optimum tyre and suspension design for a passenger vehicle are sought to both minimise tyre wear, enhance comfort and improve vehicle stability in normal loading conditions while the vehicle drives in a city road (Road Class A) with normal speed.

© 2021 by the authors. Published by the Resource Efficient Vehicles Conference.  
This is an open access article under the CC BY license (<http://creativecommons.org/licenses/by/4.0/>).

---

## 1. Introduction

The automotive industry is shifting its focus on energy efficient driving hoping to tackle rising environmental issues. In this direction, as exhaust particle emissions continuously decrease, the attention is turned on non-exhaust traffic related sources in ground vehicles, such as the interaction between tyre and roads and the tyre wear. Regarding the latter, where this work focuses, it was estimated around 300,000 tonnes in few European countries in 2013 [1]. A significant percentage of these are within PM<sub>10</sub> fraction [2], ending up in air, water, soils etc. and leading to increasing environmental pollution. Hence, the need to develop more environmentally friendly vehicle systems that can decrease tyre wear has risen.

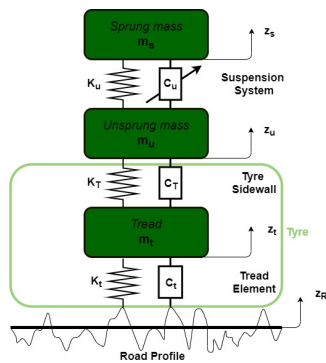
Tyre wear is categorised, according to Huang et al. [3], into two types normal and abnormal. The normal wear is responsible for uniform wear along the tyre circumference and over its width, while the abnormal is defined by uneven and irregular wear. Uneven wear mostly describes the non-uniform wear distribution over the tyre width, whereas the irregular wear mainly considers the circumferential wear. The total amount of wear is mainly caused because of inner (tyre design and manufacturing) and external (vehicle, road, driving condition and circumstances) factors. Considering these, this work investigates the sensitivity of tyre wear with regards to the majority of these factors, and also

the relation of tyre wear with occupants comfort. Even though the modeling of tyre wear has been studied extensively both analytically [4, 5] and experimentally [6, 7], very few works have considered the optimisation towards tyre wear minimisation. This has led to a non clear understanding so far regarding the trade-off between important vehicle performance aspects and wear. Recently Anderson et al. [8] investigated the trade-off between wear performance and handling. However, to the authors' knowledge no emphasis has been given with regards to comfort and wear relation. In this direction, this work considers the optimisation of both tyre and suspension parameters for minimising wear and enhancing comfort on a passenger vehicle. Significant conclusions regarding how tyre wear behaves with regards to important tyre parameters and to passenger comfort are extracted.

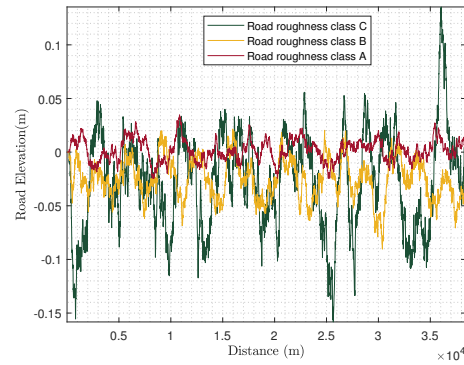
To sum up, this paper is organised as follows: firstly, all the models (vehicle, tread and wear) are described, and the road excitations used are displayed; secondly, the sensitivity analysis is presented; thirdly, the formulation of the multi-objective optimisation and its results are displayed; and finally, conclusions are extracted.

## 2. Methods and materials

The simulation model (Fig. 1a) considers four basic subsystems of the vehicle: the chassis, the suspension systems, the unsprung mass and the tyres. The chassis is considered as a rigid body of mass ( $m_s = 1301/4$  kg), and it is connected with the unsprung mass ( $m_u = 43$  kg) through the suspension system, which is modelled as spring and damper ( $K_u = 25000$  N/m and  $C_u = 2500$  Nm/s). Regarding the tyres, a more detailed modelling is applied compared to the common quarter car model. Firstly, the tyre sidewall is modelled as spring and damper ( $K_T = 0.8 * K_t$  and  $C_T = 508$  Nm/s) and connects the unsprung mass with the tyre tread ( $m_t$ ), whose mass is varying dynamically according to analytical equations. Finally, the tread element consists of linear springs and dampers ( $K_t$  and  $C_t = 2508$  Nm/s), which receive the unevenness of the road profile ( $z_R$ ) as an excitation (Fig. 1b). The tread element stiffness ( $K_t$ ) is evaluated according to the tread model and is described in the following sections. The detailed governing equations of the vehicle model can be found in the literature [9].



(a) Quarter Car Model



(b) Class A, B and C profiles.

### 2.1 Tread model

This model considers the tread as a cuboid element with  $a$ ,  $b$  and  $h$  being its length, width and height respectively. Regarding the first two, they are evaluated according to empirical equations (Eq. (1)) extracted from the literature [10, 11], which consider tyre dimensions, i.e. the outside radius ( $d$  [m]) and the crown thickness ( $b_0$  [m]), and the tyre deformation ( $\delta$  [m]):

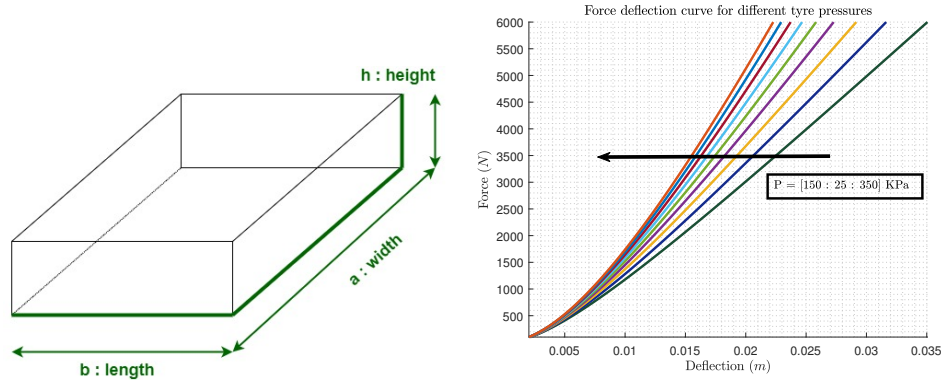
$$a = 4d \left( \frac{\delta}{2d} \right)^s, \quad b = b_0(1 - e^{-\psi}), \quad \delta = \frac{\alpha_1 F_z}{2P} + \sqrt{\left( \frac{\alpha_1 F_z}{2P} \right)^2 + \alpha_2 F_z} \quad (1)$$

where  $\psi$  ( $=115$ ) and  $s$  ( $=0.67$ ) are empirical coefficients,  $\alpha_1$  is  $1/2\pi dr_w$ , with  $r_w$  (m) being the tyre chordwise curvature radius;  $\alpha_2$  ( $=3.70 \times 10^{-8}$ ) is a constant for car tyre;  $P$  (kPa) is the tyre pressure. Finally, the mass of the tread element can be derived by Eq. (2), where  $\rho$  ( $=1156 \text{ kg/m}^3$ ) is density:

$$m_t = abh\rho \quad (2)$$

while  $F_z$  is the wheel load, and when the wear model is coupled with the vehicle model it is evaluated according to Eq. (3), where  $F_{Z_0}$  is the static load applied.

$$F_z = F_{Z_0} + C_t(\dot{z}_t - \dot{z}_R) + K_t(z_t - z_R) \quad (3)$$



(a) Tread element modeled as a cuboid (b) Force-deformation for varying pressures.

Figure 2: The modeling of the tread element ( $m_t$ ) and the force-deflection curves according Eq. (1).

According to the tyre deformation ( $\delta$ -Eq. (1)), the tread deformation is related with the pressure- $P$  (Fig. 2b), the tyre radius- $d$  and chordwise radius- $r_w$ . Therefore, during the sensitivity analysis and the optimisation studied in this work,  $K_t$  is evaluated according to these values. More specifically, the force-deflection curve is evaluated based on Eq. (1) for each potential combination of  $P$ ,  $d$  and  $r_w$  with  $F_z$  varying from 500 N to 7000 N. Then, having obtained the force-deflection curve, the  $K_t$  is evaluated as the slope at the linear region, while the sidewall stiffness ( $K_T$ ) is evaluated by  $0.8 * K_t$ .

## 2.2 Tyre wear quantity

The frictional or wear energy,  $E_w$  [Nm/m<sup>2</sup>] per unit area is evaluated according to Eq. (4), while the wear energy per contact area can be related with the mass loss according to Eq. (5), which is derived by Lupker et al. [12] from experiments:

$$E_y^w = \frac{a}{2} C_x \tan^2 \phi b^2 (1 - q)^2 + \frac{\mu a \tan \phi}{2} F_z [3(1 - q)^4 - 4(1 - q)^3 + 1] \quad (4)$$

$$\Delta m = f_1 E^{f_2} \quad (5)$$

where  $C_x$  ( $=3.57 \cdot 10^7$ ) is the transverse tread elastic coefficient;  $\phi$  the sideslip angle;  $\mu$  ( $=1$ ) is the friction coefficient;  $q = \frac{C_x b a^2}{6 \mu F_z} \phi$ ;  $f_1$  and  $f_2$  ( $=1.5106$ ) are constants at a given temperature. The mass loss ( $\Delta m$ ) evaluated at each time step is used to calculate the  $m_t$  dynamically. As an extension of Eq. (5), Yong et al. [9], incorporated in these two constants the effect of temperature according to Eq. (6), where  $f_0$  ( $=2.0 \cdot 10^{-10}$ ) is  $f_1$  at  $T_0$  ( $=60^\circ$ ) and  $T_t$  is defined as the steady state tread temperature according to Eq. (7) where  $V$  [m/s] is the vehicle velocity;  $r$  ( $=0.229$  m) is the rim radius;  $c$  ( $=0.235$  m) is the tyre width;  $\gamma$  ( $=0.12$ ) is the tyre hysteresis coefficient;  $\beta$  ( $=1.40$ ) is the correction coefficient;  $T_\infty$  is the ambient temperature.

$$\Delta m = f_0 1.02^{T_t - T_0} E^{f_2} \quad (6)$$

$$T_t = \frac{0.0447\gamma (3.6 * V)^{0.16} F_z d^{-0.5} \delta^{0.5}}{\pi\beta [2dc + 0.4(d^2 - r^2) + 0.4(d^2 + dr + r^2) - 0.6r(d + r)]} + T_\infty \quad (7)$$

where the velocity ( $V$ ) and the slip angle ( $\phi$ ) are extracted from simulations from IPG CARMAKER 8.0, while the vehicle drives over an S-path (Fig. 3) on which the various roads are assigned (Fig. 1b).

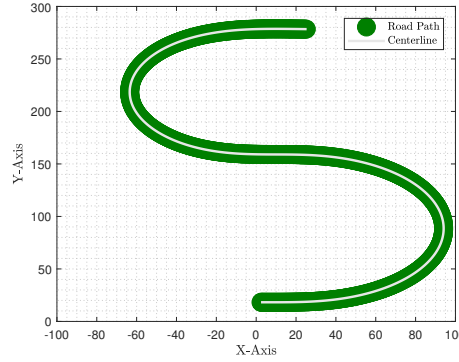


Figure 3: Road path.

The total wear quantity caused by the mass loss (Eq. (6)), is defined as the height change ( $\Delta h$ ):

$$\Delta h = \frac{\Delta m}{\rho ab} \quad (8)$$

Finally, the total wear is defined:

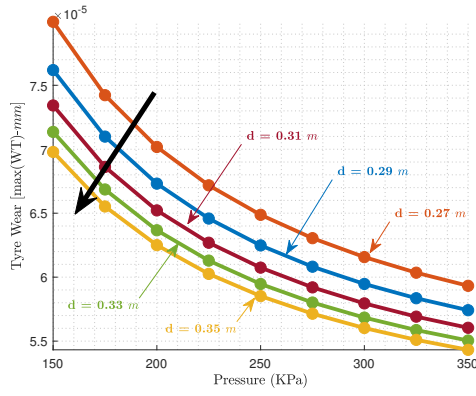
$$W(t) = W(t - t_0) + \Delta h \quad (9)$$

where  $W(t - t_0)$  is the total tread wear before the first tyre revolution;  $t_0 (=2\pi r_r/V)$  is the rotating period and  $r_r$  the rolling radius. In this work, the maximum value of  $W(t)$  ( $\max(W(t))$ ) is considered as the index of wear levels.

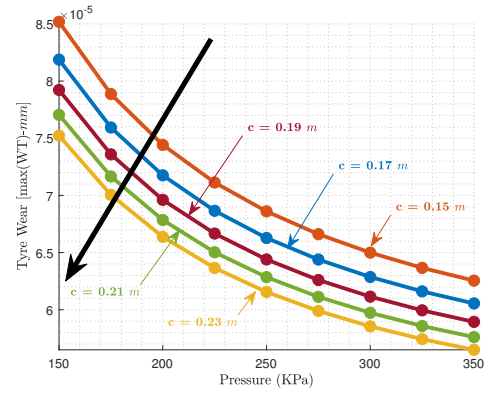
### 3. Sensitivity analysis

As mentioned previously, this work illustrates initially a sensitivity analysis of both inner and external factors. More specifically, the inner factors are investigated regarding their impact on tyre wear, while external factors, which can be different daily regarding the purpose of the ride, are studied regarding both comfort and tyre wear. Regarding the comfort, it is assessed by using the root mean square value of vertical acceleration measurements at the vehicle sprung mass ( $\ddot{z}_s$ ). The sensitivity analysis conducted with regards to various inner factors is displayed in Fig. 4, while with regards to the external factors in Fig. 5.

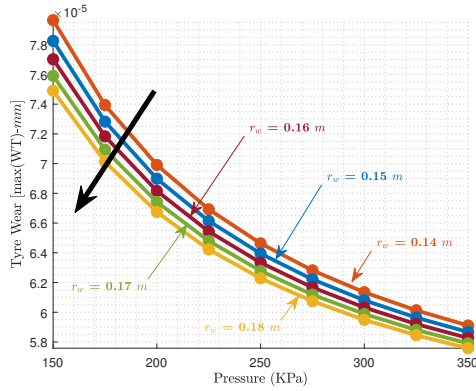
Regarding the inner factors, four case studies are considered. In each of the case studies, both the tyre pressure ( $P$ ) and one inner factor ( $d$ ,  $c$ ,  $r_w$  and  $b_0$ ) are varied in order to capture their relation with tyre wear ( $TW$ ). Their values are presented in the corresponding plots for each case study (Fig. 4a-4d). Regarding the results, according to Fig. 4, the relation of  $TW$  with  $P$  is clear and as  $P$  increases the  $TW$  is decreased. Similar behaviour is illustrated in the rest of the inner factors ( $d$ ,  $c$  and  $r_w$ ) except the crown thickness ( $b_0$ ), where its increase leads to an increase in  $TW$ . Moreover, the most dominant impact on  $TW$  is identified on  $b_0$ , which reaches up to  $\sim 40\%$  increase when it changes from 0.15 to 0.23 m. The next is the impact of  $P$  being  $\sim 25\%$  when  $P$  varies from 150 to 350 kPa, while this change is consistent whatever inner factor is varied. At the same time,  $d$ ,  $c$  and  $r_w$  illustrate the smallest impact being  $\sim 2\%$ ,  $\sim 3\%$ ,  $\sim 1\%$  for changes from 0.27 to 0.35 m, 0.19 to 0.23 m and 0.14 to 0.18 m, respectively.



(a) Tyre pressure with regards to tyre radius



(b) Tyre pressure with regards to tyre width.



(c) Tyre pressure with regards to tyre chordwise radius. (d) Tyre pressure with regards to tyre crown thickness.

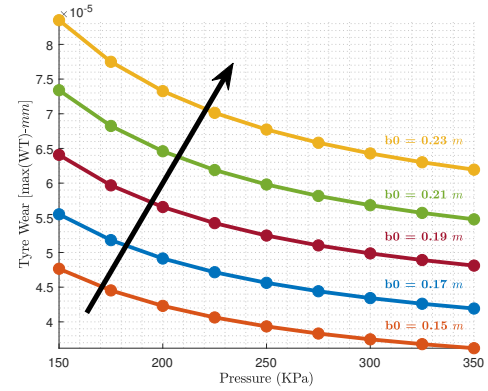


Figure 4: Sensitivity analysis of tyre wear with regards to inner factors related with the tyre structure.

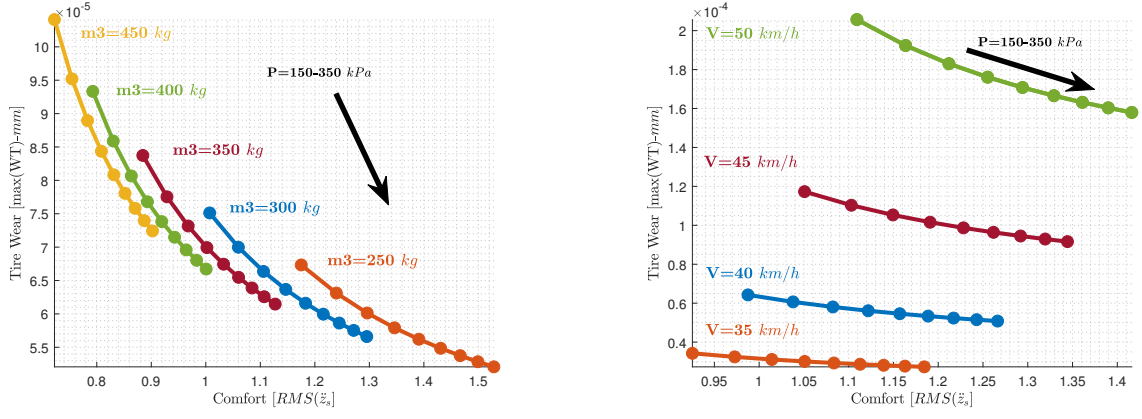
As far as the external factors are concerned, three case studies are considered. In each of the case studies, both the tyre pressure ( $P$  varying from [150,350] kPa) and one external factor (road classes, masses and velocities) are varied in order to capture their relation with tyre wear ( $TW$ ). In Fig. 5c-5b, the tyre wear and comfort levels are presented, displaying the conflicting relations of wear with comfort. Regarding the wear behaviour, according to Fig. 5, the relation of  $TW$  with the external factors is less consistent compared to the previous analysis. At the same time, the different pressures outline for each external factor highlight the conflicting relation between wear and comfort. More specifically for each external factor, the mass analysis (Fig. 5a) presents uniformity with regards to the  $TW$  increase at each mass increase, illustrating an overall change  $\sim 30\%$  when varying from 250 to 450 kg. Similarly, the analysis with regards to the velocity (Fig. 5b) presents an increase  $\sim 80\%$  in  $TW$  whenever the vehicle velocity is increased by 5 km/h. This is also depicted in the slip angles as expected (Fig. 6a), which have a constant increase with every velocity increase. On the other hand, the  $TW$  variations for different road classes are not consistent, where greater  $TW$  increases are identified when the class changes from B to C. This is because of the impact that the different road classes has on the slip angles, as illustrated in Fig. 6. According to Fig. 6, the vibration in the slip angles from class B to C are increasing significantly. However, this might be because of the power spectral densities selected to design the random road classes, leading to a bad class C profile.

## 4. Optimisation

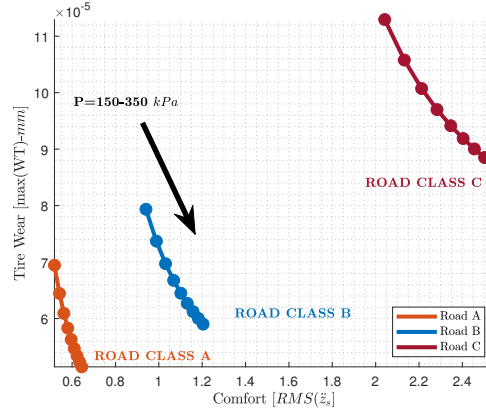
### 4.1 Configuration

As mentioned previously, the second part of this work considers the optimisation of tyre and suspension parameters for minimising tyre wear, but also enhancing comfort and improving vehicle



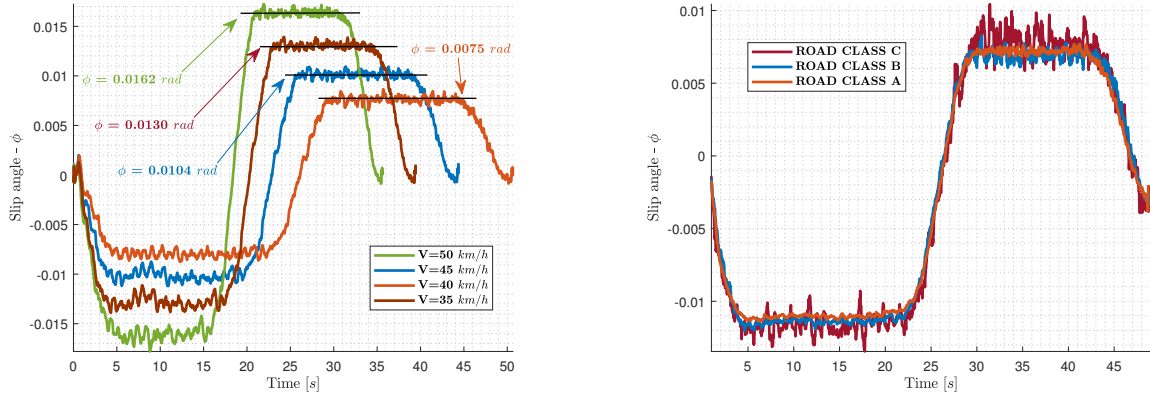


(a) Tyre wear vs. comfort for different sprung masses. (b) Tyre wear vs. comfort for different velocities.



(c) Tyre wear vs. comfort for different road classes

Figure 5: Sensitivity analysis of tyre wear vs. comfort with regards to external factors.



(a) Slip angles for the different velocities (Fig. 5b). (b) Slip angles for the different road classes (Fig. 5c)

Figure 6: The slip angles used in the sensitivity analysis for different road classes and velocities.

stability. Therefore, the appropriate metrics to represent these objectives are the maximum wear quantity ( $F_1 = \max(W(t))$ ), described in Section 2.2, the root mean square value of the sprung mass accelerations ( $F_2 = rms(\ddot{z}_s)$ ) and the root mean square value of the tyre deflections ( $F_3 = rms(z_u - z_R)$ ), respectively. The design variables selected are  $C_3$ ,  $K_3$ ,  $P$ ,  $c$ ,  $d$ ,  $b_0$  and  $r_w$ , while the upper and lower bounds selected for them are illustrated in Table 1 and are according to the sensitivity analysis. Also,  $K_t$  and  $K_T$  are considered indirect design variables as they are evaluated based on the design variables according to Section 2.1. The optimisation is conducted for the vehicle model being

excited by a Class A random road profile. The MATLAB 2017b GAMULTIOBJ toolbox is used.

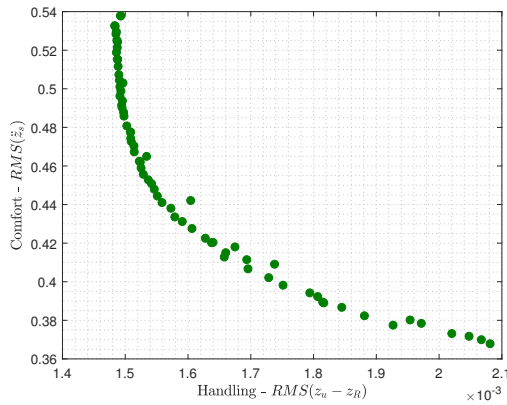
Table 1: Lower and upper bounds for the design variables.

Design Variables	Bounds		
	Lower	Upper	
$C_3$ [N/m]	500	5000	Suspension Parameters
$K_3$ [N/m]	15000	60000	
$P$ [KPa]	150	350	Tyre Parameters
$c$ [m]	0.14	0.22	
$d$ [m]	0.27	0.35	
$b_0$ [m]	0.12	0.19	
$r_w$ [m]	0.12	0.20	

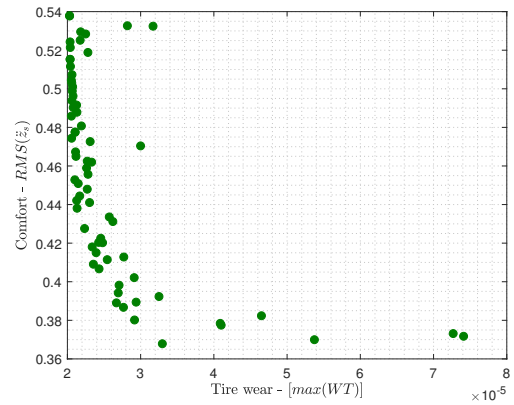
## 4.2 Results

Regarding the optimisation results, they are illustrated in Fig. 7, where the objectives of the optimal solution are plotted. More specifically, Fig. 7a is illustrating the relation between comfort and handling for the optimal solutions provided by the optimisation process, while Fig. 7b presents their relation with regards to their comfort and tyre wear objectives.

According to Fig. 7, the conflicting relation between comfort and handling are accurately captured, which proves the validity of the optimisation results. Also, the optimisation has converged to a well-shaped pareto front (Fig. 7a) due to the correct optimisation configuration for the given problem (i.e. population size at 200, elite count at 5) and also due to the simple excitation studied (class A road profile). As far as comfort and tyre wear are concerned, they display the same conflicting relation with comfort and handling (Fig. 7a) according to Fig. 7b. However, most of the solutions have converged to the same area of tyre wear values ( $\sim 2-3 \times 10^{-5}$ ). The solutions at the lower part of pareto front, which are the ones providing the most comfortable suspension and tyre design ( $RMS(\ddot{z}_s)=[0.36, 0.38]$ ), increase wear more than  $\sim 100\%$ .



(a) Comfort vs. Vehicle handling.



(b) Comfort vs. Tyre wear.

Figure 7: The pareto fronts obtained for the optimisation problem described in Section 4.1.



## 5. Conclusions

To sum up, this work illustrated initially a sensitivity analysis of both inner and external factors, and then explored the optimisation of tyre and suspension parameters for minimising tyre wear and enhancing comfort. The results outlined the conflicting relation between wear and comfort both through the sensitivity analysis and the optimisation. At the same time, handling illustrates a linear relation with wear, i.e the increasing tyre deflections increase wear. Regarding the inner factors, tyre pressure and crown thickness were highlighted as the most dominant with regards their impact towards wear levels providing 25% and 40% changes within the range of study. As far as the external factors are concerned, all the ones studied (vehicle mass and velocity, and road class) illustrated great impact on wear levels, affecting comfort significantly at the same time.

## 6. Acknowledgements

The authors would like to thank the Centre for ECO2 Vehicle Design, funded by the Swedish Innovation Agency Vinnova (Grant Number 2016-05195), for financial support.

## References

1. Jan Kole P, Löhr AJ, Van Belleghem FG, et al. Wear and tear of tyres: A stealthy source of microplastics in the environment. *International Journal of Environmental Research and Public Health*. 2017.
2. Grigoratos T, Gustafsson M, Eriksson O, et al. Experimental investigation of tread wear and particle emission from tyres with different treadwear marking. *Atmospheric Environment*. 2018;182:200–212.
3. Huang H, Chiu Y, Wang C, et al. Three-dimensional global pattern prediction for tyre tread wear. *Proceedings of the Institution of Mechanical Engineers, Part D: Journal of Automobile Engineering*. 2015; 229(2):197–213.
4. da Silva MM, Cunha RH, Neto AC. A simplified model for evaluating tire wear during conceptual design. *International Journal of Automotive Technology*. 2012;13(6):915–922.
5. Ma B, Xu Hg, Chen Y, et al. Evaluating the tire wear quantity and differences based on vehicle and road coupling method. *Advances in Mechanical Engineering*. 2017;9(5):168781401770006.
6. Tandy DF, Pascarella RJ, Neal JW, et al. Effect of Tire Wear on Tire Force and Moment Characteristics. *Tire Science and Technology, TSTCA*. 2010;38(1).
7. Tamada R, Shiraishi M. Prediction of Uneven Tire Wear Using Wear Progress Simulation. *Tire Science and Technology, TSTCA*. 2017;45(2):87–100.
8. Anderson JR, McPillan E. Simulation of the Wear and Handling Performance Trade-off by Using Multi-objective Optimization and TameTire. *Tire Science and Technology, TSTCA*. 2016;44(4):280–290.
9. Li Y, Zuo S, Lei L, et al. Analysis of impact factors of tire wear. *Journal of Vibration and Control*. 2011; 18(6):833–840.
10. Nakajima Y. *Advanced tire mechanics*. Springer Singapore; 2019.
11. Li Y, Zuo S, Duan X, et al. Theory analysis of the steady-state surface temperature on rolling tire. *Proceedings of the Institution of Mechanical Engineers, Part C: Journal of Mechanical Engineering Science*. 2012; 226(5):1278–1289.
12. Lupker H, Cheli F, Braghin F, et al. Numerical prediction of car tire wear. *Tire Science and Technology, TSTCA*. 2004;32(3):164–186.

---

# Human Machine Interface: A review for future applications in train driving

Simon Enjalbert<sup>1</sup>, Livia Maria Gandini<sup>2</sup>, Alexander Pereda Baños<sup>3</sup>, Stefano Ricci<sup>2,\*</sup> and Frederic Vanderhaegen<sup>1</sup>

<sup>1</sup> *Université Polytechnique Hauts-de-France, LAMIH, CNRS, UMR 8201, 59313 Valenciennes, France*

<sup>2</sup> *Sapienza Università di Roma, DICEA, Via Eudossiana 18, 00184 Roma, Italy*

<sup>3</sup> *Eurecat, Centro Tecnológico de Cataluña, 08290 Cerdanyola del Vallès, Spain*

\* *Corresponding author. Email: stefano.ricci@uniroma1.it*

---

The paper deals with the description of preliminary research work based on extended investigation focused on categorized Human Machines Interface (HMI), describing their technical approaches and emerging operational issues. The study aims at reviewing and analysing HMI, their design and control systems currently on the market or in experimental operation. The analysis acts as a review manual on HMI technologies to design customized HMI and analyse the technologies used or tested in the present technological scenario. The paper starts by addressing the systems developed by manufacturers of surface vehicles outside railway field: trucks, cars and ships. It follows with the performances of simulators developed for various transport systems: rail, cars, aviation and integrated solutions. Finally, the focus is on the comparative analysis of the performances of supporting tools for train driver's assistance, a synthetic analysis of results and the organization of the survey among drivers to check expectations and acceptance of potential solutions.

© 2021 by the authors. Published by the Resource Efficient Vehicles Conference.  
This is an open access article under the CC BY license (<http://creativecommons.org/licenses/by/4.0/>).

---

## 1. Introduction

The field of automation is gaining increasing interest from research in various application fields, along a path began in the 1920s, with the first radio-controlled vehicle. Today, there is an increasing interest of companies to invest towards large-scale adoption of self-driving vehicles. Studies on the user experience aboard autonomous or semi-autonomous vehicles are in close connection with the question of trust in the Human Machine Interface (HMI). In particular, in a semi-automatic vehicle, the design of HMI must give awareness of driving situation, to regain effectively the control, whenever called upon to intervene. Within the CARBODIN research project, co-funded under the Shift2Rail Programme, the aim is meeting the expectations of train drivers and staffs with HMI automatic functions to arrive to progress towards their introduction. The focus is on the identification of required inputs and available outputs of various systems and operator preferences, further investigated by dedicated surveys on potential HMI configurations to design new drivers' cabins and build a virtual mock-up with immersive technology using specific banks of sounds and gestures.

## 2. Path towards the future train drivers cabin







The railway transport systems in general are historically less sensible than others are to the pilot application of disruptive technologies. This is firstly due to the combination of the rigorous intrinsic safety requirements qualifying it and the general longer technical life of its components and the system itself. Therefore, in view of the progressive introduction of the innovations supporting the train driving functions, the CARBODIN project [1] aims at joining the identification of the most promising technological driving supports with the expectations of train drivers or other railway operator staffs about HMI in future cabins. The basis of this are 360° surveys about potentially applicable mature technologies on one side as well as preferences and efficiencies of possible new innovative configurations on the other side, by taking into account the key role of human factors, particularly in the design of input and output sensors, gestures and supporting acoustic and visual signals.

## 3. State-of-the-art in driving automation

Within the framework of what discussed above, the progressive introduction of the innovations supporting the train driving functions, started from the analysis of systems developed by manufacturers of surface vehicles, namely trucks, cars and ships. The reasoning behind this choice is that for the application in railway operational environment, almost mono-dimensional due to the guidance of rails, the applications in other surface transport systems have a higher applicability potential than those tested or applied in typical three-dimensional operational environments, such as aviation and the same is for the speed ranges. Nevertheless, aeronautical applications remains in the scope of the study as potential sources of solutions for specific interfaces, such as sensors, sounds and gestures used in real driving systems and simulators.

A systematic review of potentially promising systems is in [2]. Table 1 provides with an overview of the automation functions performed by some systems on the market, in view of a potential use in the trains driving functions.












Table 1. Overview of investigated systems implemented in various typologies of vehicles

Name	Developer	Operating features	Vehicle
<b>MAN PLATOONING</b>		Driver assistance and control with hand always on the wheel	Trucks
<b>HIGHWAY PILOT</b>		Full autopilot with manual selection	Trucks
<b>AUTOPILOT 2.5</b>		Autopilot's assistance and control with hand always on the wheel	Cars
<b>iNEXT-COPILOT</b>		Co-pilot switchable to autonomous driving manually or by voice	Cars
<b>DRIVE PILOT</b>		Fall-back-ready user resuming manual driving by steering, braking, accelerating or switching off manually	Cars
<b>THE FALCO</b>		Full automation with ergonomic HMI, control levers and touch screens for call up and control	Ships

## 4. State-of-the-art in driving simulation

Another important source of technological solutions applicable to rail cabins comes from the professional simulators. Also in this field, surveys and analysis focuses on the surface transport systems and covers purely rail vehicles applications, road vehicles and integrated systems [3] [4] [5], as summarised in Table 2.

Table 2: Overview of investigated simulators

Name	Developer	Operating features	Vehicle
<b>PSCHITT-RAIL</b>	 	Movements capture by eyes trackers and physiological measurement sensors	Trains
<b>SPICA RAIL</b>		Increasing disturbances to evaluate human behaviours and supervision platform	Trains
<b>OKTAL SYDAC</b>		Replicas of the cab to ensure realistic driving experiences	Trains
<b>IFFSTAR-RAIL</b>		Reproduction of driving and rail traffic supervision	Trains
<b>IFFSTAR TS2</b>		Impact of internal and external factors on driver behaviours and fixed-base cab HMI	Cars
<b>NDIVIA DRIVE</b>		Interface among environment, vehicles and traffic scenario by open platform sensors	Cars
<b>VRX-2019</b>	 	Autonomous vehicle experiencing feelings of cockpit's HMI by advanced sensors	Cars
<b>MISSRAIL</b>	 	Automated driving assistance combining accident scenarios including pedestrians, trains and cars with human factor control	Integrated

Simulators represent a key starting point for the design of innovative driving functions, as well as for the safety of traffic supervision within railway systems [6] [7] [8] and interactions with other transport networks [9] [10]. Their benefits are the possibility to test, in advance, applicability and capability to generate improvements of operational performances, to obtain information about the future design and reduce the deployment costs.

## 5. Emerging gesture technologies

From the analysis on driving automation and simulation systems, as well as from a dedicated literature review, emerged a large set of technologies available on the market to control devices by gestures. A not comprehensive list of them is in Table 3.

Starting from analyses developed in a similar study [11], Table 4 summarize the results of a comparative Strength, Weaknesses, Opportunities and Threats (SWOT) analysis focused on the most relevant features differentiating three of the most promising gesture control devices: *KINECT* (by *Microsoft*), *LEAP MOTION* (by *Ultrahaptics*) and *MYO BRACELET* (by *Thalmic Labs*). Due to the recurrence for all systems, the table does not include general threats, such as the

lack of definition of a process for the recovery of gesture control intrusion. Moreover, all the investigated systems investigated have reached, in their respective fields, Technology Readiness Levels (TRL) variable among TRL7 (System prototype demonstration in operational environment), TRL8 (System complete and qualified) and TRL 9 (Actual system proven in operational environment).

Table 3: Overview of control devices by gesture











Name	Developer	Operating features
<b>DEPTHENSE CARLIB</b>	<b>SONY</b>	Controlling movements of infotainments by hand
<b>EYEDRIVE GESTURE CONTROL</b>		Recognizing hand gestures while driving to control devices by infrared sensors
<b>HAPTIX</b>		Recognizing classical hand movements and building a virtual mouse to control screen interface by webcams
<b>KINECT</b>		Capturing body or hand movements to control devices by webcams
<b>LEAP MOTION</b>	ultrahaptics 	Recognizing hands or objects movements for virtual reality by infrared light, 3D micro-cameras
<b>MYO BRACELET</b>	 <b>THALMICLABS™</b>	Detecting hands or fingers movements to control interfaces with electrical activation of muscles
<b>SOLI</b>		Identification of movements of fingers or body by mini-radar
<b>SWIPE</b>	 <b>FIBARO®</b>	Reading hand motions in front of a small contactless tablet for home automation purposes
<b>XPERIA TOUCH DEVICE</b>	<b>SONY</b>	Tracking proximate hand gesture via the smartphone camera

Table 4: Differential items in SWOT analysis of selected control devices by gesture

Name	Developer	Strengths	Weaknesses	Opportunities	Threats
<b>KINECT</b>		1) Identification of body motions	1) Operational difficulties in restricted space 2) Interference movements-sensor	1) Combination of gesture control with facial/voice recognition	-
<b>LEAP MOTION</b>	ultrahaptics 	1) Identification of hands/fingers movements 2) Low price 3) Light weight	1) Deep training need 2) Interference movements-sensor	1) Combination of infrared light and cameras	-
<b>MYO BRACELET</b>	 <b>THALMICLABS™</b>	1) Gesture detection of bracelet wearer 2) Light weight	1) Deep training need 2) Few identified movements	1) Combination of physiological detection with gesture control	-

## 6. Survey on train drivers acceptance

The eminent role of the human behaviour in the field requires integrating the ongoing activity on the promising technologies and solutions with a survey directly involving drivers about their expectations and acceptance of potential solutions.

The objective of this first survey is to select the key targets of the train cab of the future and the interactions should be possible in this driver's cab by involving the drivers themselves from the earliest stages of the creation of these new systems. The envisaged automation is willing to assist the driver in providing the best possible user experience, adapted to the constraints of the job and integrating the latest technologies for more comfort of use and efficiency.

The investigated technologies are applicable to various means of Action (A) and Information (I) that would enable the driver to keep informed of the state of the train, such as:

- **AUDIO:** Voice control of the system (A) and audible notification (I);
- **TOUCH SCREEN:** Use of touch screens (smartphone, tablet, etc.) for entering commands (A) and reading information (I);
- **GESTURE:** Gestures recognition to act on the system without contact (A);
- **VISUAL:** Projection of information into the driver's field of vision and accessible through a Head-Up Display (HUD), without leaving the lane of sight (I).
- **HAPTICAL:** Use of manipulator to add force feedback functions, assist the driver, accompanying or resisting the driver's movements for actions control (A) and information on speed (I).

Table 5 summarizes the potentially covered drivers' tasks included into the survey.

Table 5: Drivers' tasks potentially affected by the use of the selected innovative technologies

Key elements		Auxiliary systems		Additional devices	
Groups	Tasks	Group	Task	Group	Task
Situation awareness	Dead Man's Switch	Station stop	movement authorization	Lighting	Instrument brightness
	Signalling		Stopping		Cabin lighting
Speed regulation	Train Protection & Warning System		Reverser	Comfort systems	Sanitary
	Cruise control	Accessories	Sand spraying		Audio Announcement
	Engine Throttle		Windshield cleaner		Passenger's energy
	Brake		Wiper		Climate control
Flow Management	Door / Bridging plate		Headlight		Lighting
Alarms systems	Whistle		Defrosting		Sound system
	Emergency brake	Management power	Change traction mode	Configuration	Start / Stop
	Emergency stop button		Change voltage		Train settings
	Alarm systems		Pantograph		
	Pantograph				
	Passenger alarm signal				

The survey, carried out in the first months of 2021, involved 1689 drivers from 15 different European countries.

Statistical analyses will follow, developed by means of the following techniques:

- *Boxplot* graphically depicting groups of numerical data through their quartiles, based on Action (A) / Information (I) and group of tasks depending on technologies);
- *Multiple Correspondence Analysis* (MCA) to detect and represent underlying structures in a data set (Age, Profession, Gender, Nationality, Country Network, Train Type).
- *Hierarchical Clustering Analysis* (HCA) to build a hierarchy of clusters.

## 7. Conclusions

All the investigated systems have reached in the respective application fields TRL7, TRL8 or TRL9. Therefore, they appear highly reliable in view of potential applications in the design of future trains' drivers' cabin. The experience matured in the analysis and selection process and in the survey with drivers demonstrated that many of them are well in line with the expectation setup within the CARBODIN and the related PIVOT2 Shift2Rail funded projects. They aim at reaching Technology Readiness Levels variable among TRL5 (Technology validated in relevant environment), TRL6 (Technology demonstrated in relevant environment) and TRL7 (System prototype demonstration in operational environment) [1].

The next research developments, based on the results from the first round of surveys, are progressive refinements that will allow at: 1) eliminating systems and technologies not adapted for innovative driving cabin and selection, based on the needs from operators, 2) implementing promising HMI in virtual mock-up demonstrator for further testing by professional drivers on a simulator.

## Acknowledgments

The CARBODIN project has received funding from the Shift2Rail Joint Undertaking under the European Union's Horizon 2020 research and innovation programme under grant agreement No 881814.

## References

1. CARBODIN - Car Body Shells, Doors and Interiors. H2020 - Shift2Rail Joint Undertaking. Grant Agreement n. 881814, 2019.
2. Enjalbert S., Gandini L.M., Pereda Baños A., Ricci S., Vanderhaegen F. – Human-Machine Interface in Transport Systems: An Industrial Overview for More Extended Rail Applications - Machines, 9, 36, 2021.
3. Vanderhaegen F., Richard P. - MissRail: a platform dedicated to training and research in railway systems - Proceedings of the international conference HCII - Heraklion, Crete, 2014.
4. Vanderhaegen F. - MissRail® and Innorail - <http://www.missrail.org>, 2015.
5. Vanderhaegen F. - Pedagogical learning supports based on human-systems inclusion applied to rail flow control. Cognition - Technology & Work, 2019.
6. Malavasi G., Ricci S. - Simulation of stochastic elements in railway systems using self-learning processes - European Journal of Operational Research, 131, 2001.

7. Ricci S., Tieri A. - Check and forecasting of railway traffic regularity by a Petri Nets based simulation model - Ingegneria Ferroviaria, 9, 2009.
8. Ricci S., Capodilupo L., Tombesi E. - Discrete Events Simulation of Intermodal Terminals Operation: Modelling Techniques and Achievable Results - Civil Comp Proceeding, 2016
9. Fang J., Yan D., Qiao J., Xue J. - DADA: A Large-scale Benchmark and Model for Driver Attention Prediction in Accidental Scenarios. J. – LATEX, 2019
10. Lin S., Wang K., Yang K., Cheng R. - KrNet: A kinetic real-time convolutional neural network for navigational assistance - Lecture Notes on Computer Science, 2018
11. Zhao L. - Gesture Control Technology: An investigation on the potential use in Higher Education - University of Birmingham, IT Innovation Centre, 2016



---

# Objective development in driving simulator motion control: Evaluation of motion cueing using a linearised driving simulator model

Henrik Hvitfeldt<sup>1,2</sup>, Lars Drugge<sup>1,2</sup> and Jenny Jerrelind<sup>1,2</sup>

<sup>1</sup>Engineering Mechanics, KTH Royal Institute of Technology, Stockholm, Sweden

<sup>2</sup>The Centre for ECO<sup>2</sup> Vehicle Design, KTH Royal Institute of Technology, Stockholm, Sweden

\*Corresponding author. Email: hhv@kth.se

---

Even though the automotive industry is heading towards a more objective approach to vehicle testing, subjective evaluation is still an important part of the development process. Subjective evaluation in physical testing has environmental implications and is a function of ambient settings. A more repeatable, faster, safer, and more cost-effective tool for subjective evaluation is to use moving base driving simulators (MBDS). The increasing usage of MBDS in the automotive industry is due to an increasing demand of rapid development and usage of virtual prototyping. The motion cueing algorithms (MCA) maps the movement of the vehicle into the limited space of the simulator. The MBDS could potentially enable a "human in the loop" in the virtual development process, enabling early phase subjective testing. This research aims to develop an objective framework for the validation of MCAs to close the loop on virtual development. The state-of-the-art MCAs are commonly developed and validated subjectively. This causes a tendency to false ques, limited assurance of MCA fidelity and demands physical vehicles for validation, which hinders early phase development. This paper presents a linear driving simulator model based on existing linear models for planar vehicle dynamics, classic motion cueing and human vestibular response. The model can capture important characteristics of the specific forces and rotations that are fed to the driver, through the motion cueing algorithms and offering a method to objectively analyse and potentially tune the motion cueing. The method is applied to the choice of reference point of acceleration in the vehicle to feed the motion cueing, and results indicate that a reference point at the driver's head has a clear advantage compared to a reference point in the chassis over the full frequency range.

© 2021 by the authors. Published by the Resource Efficient Vehicles Conference.  
This is an open access article under the CC BY license (<http://creativecommons.org/licenses/by/4.0/>).

---

## 1. Introduction

The automotive industry is heading towards an objective virtual approach for vehicle development, however, subjective evaluation is still a key aspect [1]. Vehicle manufacturers are targeting rapid development, but there is a conflict between subjective evaluation and rapid development due to the necessity to develop resource demanding and costly physical prototypes. To enable rapid development in the vehicle development phase, moving base driving simulators (MBDS) could enable subjective evaluation within the virtual development loop. The advantages for resource efficiency are two-fold. First, rapid development would be possible and hence, more resource efficient vehicles could be developed in a higher rate and disruptive vehicle concepts could be tested

in early phase development. Second, resource demanding physical testing could potentially be minimised, avoiding the need to waste resources on costly prototypes and physical testing.

MBDS uses motion cueing algorithms (MCA) to map the inertial forces of the vehicle into the motion space of the simulator, which is small compared to the full motion space of a vehicle. The MCAs are commonly developed subjectively and back-to-back tested with an existing vehicle to verify the MCA. The subjective tuning of the MCA causes a need for physical vehicles for validation which hinders early phase development. This is resource inefficient and development of MCA using subjective feedback is limiting the assurance of MCA fidelity. Therefore, objective methods to evaluate MCAs are necessary. An objective framework for MCA evaluation could potentially help vehicle manufacturers to validate the MCA before a physical prototype is built, decreasing the cost, time, and effort.

The usage of MBDS has grown in the automotive industry, mainly due to an increasing demand of rapid development coupled to an increasing usage of virtual prototyping and its effectiveness in development of advanced driver-assistance systems (ADAS) and medical studies [1]. Motion cueing tuning has been investigated in several studies, e.g. [2], [3], [4], targeting for instance every day driving within the linear region, as well as urban driving and performance driving. The tuning is commonly done based on heuristics and subjective evaluation, rather than objective measures. Rather than studying the full system, commonly the tuning done is considering one direction of motion (e.g., lateral acceleration) however the coupling in between states is often disregarded.

Model predictive control (MPC) has been applied to MBDS, where the optimisation problem is setup trying to exploit the full motion space while limiting the motion perception tracking error, minimising the error in all directions [5] [6]. Since the states in planar dynamics of a vehicle are coupled, the relationship between for example yaw rate and lateral acceleration is directly dependent on how the vehicle moves. The coupled states pose a challenge. What vehicle motion should be fed to the driver and/or passenger? How should for example lateral acceleration be scaled and filtered compared to yaw rate? To shed some light of how the states should be scaled to each other versus the utilisation of motion space, and to the general understanding of the human response to MCA tuning, the need for a simplified simulator model is apparent. The model needs to capture the coupling in the planar dynamics and show how the human perception of motion changes due to different motion cueing algorithms.

## 2. Motion cueing modelling for vehicle testing

### 2.1 Linear driving simulator model

Several models of driving simulators already exist, e.g., M. Bruschetta et al. in [5] and [7] uses models of a Stewart platform together with motion cueing to perform optimal control of the motion cueing. The optimal control models use models of the vestibular system to minimise the difference between a driver situated in the vehicle itself and the driver in the simulator. While these models are useful for optimisation, they are advanced and complicated to grasp, and do not include the vehicle. To get a fundamental understanding of how the driver perceives the vehicle dynamics of a vehicle, compared to a driver situated in a simulator with motions filtered through a classic motion cueing, a linear model of a driving simulator was developed, and the modelling is described in this section.

#### 2.1.1 Lateral dynamics

For the lateral dynamics, the linear one-track vehicle model was chosen to keep model complexity low. The one-track model in this case has two degrees of freedom, yaw rate  $\dot{\psi}$  and lateral velocity  $v_y$ . The model can be written as a state-space with the form in eq. (1), or more compactly as in eq. (2):

$$\begin{bmatrix} \dot{v}_y \\ \ddot{\psi} \end{bmatrix} = \begin{bmatrix} -\frac{C_{12}+C_{34}}{mv_x} & \frac{C_{34}b-C_{12}f}{mv_x} - v_x \\ \frac{C_{34}b-C_{12}f}{J_z v_x} & -\frac{C_{34}b^2+C_{12}f^2}{J_z v_x} \end{bmatrix} \begin{bmatrix} v_y \\ \dot{\psi} \end{bmatrix} + \begin{bmatrix} \frac{C_{12}}{m} \\ \frac{fC_{12}}{J_z} \end{bmatrix} \delta \quad (1)$$

$$\dot{\bar{x}}_{ot} = A_{ot}\bar{x}_{ot} + B_{ot}\delta \quad (2)$$

where  $C_{12}, C_{34}$  is the cornering stiffness for front and rear axle,  $J_z$  is the vehicle inertia around the vertical axis,  $m$  is the vehicle mass and  $f, b$  defines the front and rear axle distance from the centre of gravity. From this, lateral acceleration  $a_y$  could be written as a function of the states as in eq. (3) and from the elements of the state-space as in eq. (4):

$$a_y = \dot{v}_y + \dot{\psi}v_x \quad (3)$$

$$a_y = A_{ot}(1)x_{ot}(1) + A_{ot}(2)x_{ot}(2) + B_{ot}(1)\delta + x_{ot}(2)v_x \quad (4)$$

### 2.1.2 Roll model

As the classic motion cueing algorithms uses tilting of the simulator cabin partly to feedback body roll  $\theta_{roll}$  and partly to create sustained lateral acceleration  $a_{y,sim}$ , the roll degree of freedom should be included in the vehicle model as the roll angle will add to this tilt. The roll angle will be included in the motion cueing with a simple gain filtering  $K_{roll}$ . A roll-pendulum model is used:

$$J_x \ddot{\theta}_{roll} = a_y h_{roll} m - \theta_{roll} K_{roll} + m g h_{roll} - C_{roll} \dot{\theta}_{roll} \quad (5)$$

where  $m$  is the sprung mass,  $J_x$  is the roll inertia,  $h_{roll}$  is the roll moment arm,  $K_{roll}$  the roll stiffness and  $C_{roll}$  is the roll damping. The tilt coordination in the classical algorithm is done using a first or second order low-pass filter. A second order low pass filter for the tilt angle  $\theta_{tilt}$  is used in this case and can be formulated as:

$$\ddot{\theta}_{tilt} = K_{tilt} a_y - 2\omega_{tilt} \zeta \dot{\theta}_{tilt} - \omega_{tilt}^2 \theta_{tilt} \quad (6)$$

where  $K_{tilt}$  is the filter gain,  $\omega_{tilt}$  is the filter frequency and  $\zeta$  is the damping coefficient of the filter.

### 2.1.3 Onset motion cueing model

In the classic MCA, the onset feedback is realised through translating the simulator, this is done for lateral (sway) and longitudinal (surge) acceleration. To create the onset-signal the input signal is scaled, and a first order band pass filter is used in combination with a second order high pass filter. The scaling is done to ensure that the motion system does not reach an end stop during operation [9]. The first order band pass filter is used to filter out the low frequency components of the signal and mainly output the onset part of the signal. Further, the filter low passes signals above the bandwidth of the simulator rig. The second order band pass filter is used in order to create a "wash-out effect". The practical effect of this filter is that the second order filter gives a signal that returns the motion platform to its neutral position. The signal is then integrated from an acceleration to a position and a soft limiter is applied to avoid hitting end stops [4]. For the linear model, the onset filter's soft limiter is linearised as a unity gain and is therefore implicit in the equations. The first order band pass filter transfer functions are the following:

$$\begin{aligned}
G &= f_{c,hp} 2\pi \\
D &= f_{c,lp} 2\pi \\
Y &= \frac{Gs}{Gs+1} \frac{D}{Ds+1} G_{input} U
\end{aligned} \tag{7}$$

where  $G_{input}$  is the gain of the onset filter in either  $\dot{\psi}$  or  $a_y$  and  $f_{c,hp}$  and  $f_{c,lp}$  are high respectively low pass cut off frequencies,  $U$  is the input of yaw rate  $\dot{\psi}$  or acceleration from the reference point  $a_{y,j}$ . To include the filters in the model, they need to be written on state-space form. Rewriting the filter in observable canonical form is necessary due to derivative in the input and renders the following:

$$\begin{aligned}
K_1 &= \frac{1+DG}{G} \\
K_2 &= \frac{D}{G} \\
C &= DG_{input} \\
\begin{bmatrix} \dot{q}_1 \\ \dot{q}_2 \end{bmatrix} &= \begin{bmatrix} -K_1 & 1 \\ -K_2 & 0 \end{bmatrix} \begin{bmatrix} q_1 \\ q_2 \end{bmatrix} + \begin{bmatrix} C \\ 0 \end{bmatrix} u
\end{aligned} \tag{8}$$

This will form the input to the second order filter, giving the washout part:

$$\begin{aligned}
q_3 &= \frac{s}{s+K_{hp}} q_1 \\
q_4 &= \frac{s^2}{s^2+a_1s+a_2} q_3
\end{aligned} \tag{9}$$

where  $q_4$  is the output state of the motion cueing, i.e., motion platform  $\dot{\psi}_{mc}$  or  $a_{mc}$ . The coefficients  $a_1, a_2$  are filter parameters for damping and cut-off frequency, respectively, and  $K_{hp}$  defines the high pass cut off frequency. The filter equations can be rewritten to suit the state-space formulation in observable canonical form as in eq. (6).

### 2.1.4 Human model

The vestibular sensory system of the human body consists of the otolithic organs, to sense the specific forces acting on the organ, and semi-circular channels, to sense rotation. The otolithic organs can be modelled as a second order system, with the transfer function from the specific force  $f$  to the perceived specific force  $\hat{f}$  as presented in eq. (10) [8]. The semi-circular channel transfer function from a rotation  $\omega$  to a perceived rotation  $\hat{\omega}$  is presented in eq. (11) [8]. The organs can sense specific forces and rotation in all directions, while in this linear model, only the rotation in yaw and the specific forces in lateral directions are considered.

$$\hat{f} = K_{oto} \frac{\tau_a s + 1}{(\tau_L s + 1)(\tau_b s + 1)} f \tag{10}$$

$$\hat{\omega} = \frac{K_C \omega s}{(\tau_1 s + 1)(\tau_2 s + 1)} \tag{11}$$

where  $\tau_a, \tau_b, \tau_L, \tau_1$  and  $\tau_2$  are time constants and  $K_{oto}, K_C$  are the model gains.

The lateral specific force  $f_y$  in the linear model can be defined as:

$$\begin{aligned} f_y &= \ddot{\theta}_{cabin} h_{rc,sim} + a_{MC} + g \theta_{cabin} \\ \theta_{cabin} &= G_{roll} \theta_{roll} + \theta_{tilt} \end{aligned} \quad (12)$$

where  $\theta_{cabin}$  is the tilt angle of the cabin and  $G_{roll}$  is the scale factor for the cabin roll angle. The rotational velocity input in yaw is simply  $\omega_z = \dot{\psi}_{MC}$ . The perceived inertial forces could be combined with visual inputs to get the full frequency spectrum of perceived movement but is not included at this stage.

### 2.1.5 Complete state space

The full vehicle-driving simulator-human model could be summed up in a state-space model:

$$\dot{\bar{x}}_{sim} = A_{sim} \bar{x}_{sim} + B_{sim} \delta \quad (13)$$

which is a convenient formulation as it only depends on the steering input  $\delta$  in the one-track model. This formulation enables the usage of standard system dynamics analysis methods. It is also possible to omit the motion cueing parts of the state-space presented in eq. (13) and define a vehicle-human system with the perceived inertial forces and motions stemming directly from the one-track model. In this article it is considered as the reference responses for the simulated vehicle:

$$\dot{\bar{x}}_{ref} = A_{ref} \bar{x}_{ref} + B_{ref} \delta \quad (14)$$

Using this, it is possible to compare the vestibular and motion perception response of the human in the simulator compared to the reference, a human situated in the simulated vehicle. To understand how the transfer functions between the vestibular response for acceleration  $\hat{a}_{y,sim}$  and rotation  $\hat{\psi}_{sim}$  are mapped through the frequency range compared to the vestibular responses  $\hat{a}_{y,ref}$  and  $\hat{\psi}_{ref}$  of the reference vehicles, the following transfer functions are defined, which describes the relationship between the vehicle input,  $\delta$ , and the vestibular response for rotation and specific force. To get the transfer function between two of the states the transfer function between the input  $\delta$  and the vestibular response is given as an example:

$$\begin{aligned} \hat{\psi}_{sim} &= G_{\delta}^{\hat{\psi}_{sim}} \delta \\ \hat{a}_{y,sim} &= G_{\delta}^{\hat{a}_{y,sim}} \delta \end{aligned} \quad (15)$$

and from this the relationship between the vestibular response in the frequency domain is:

$$G_{\hat{\psi}_{sim}}^{\hat{a}_{y,sim}} = \frac{G_{\delta}^{\hat{a}_{y,sim}}}{G_{\delta}^{\hat{\psi}_{sim}}} \quad (16)$$

which is the transfer function between the perceived yaw state and the perceived lateral acceleration state. This transfer function is useful to define as the two states are coupled through the one-track model as described in eq. (3), in steady-state the ratio between them will be simply coupled through

the longitudinal velocity. During transient conditions, the relationship between them will be coupled through the lateral velocity acceleration  $\dot{v}_y$  and the longitudinal velocity  $v_x$ .

### 2.1.6 Motion cueing reference point

The motion cueing reference point defined in this article, is the point on the vehicle that is used as input for the motion cueing. Due to the roll, yaw and pitch of a vehicle body, the global acceleration of the points on the body is not uniform. Further, translation and rotation are not necessarily filtered with the same filter in the MCA. This difference in filtering distorts the coupling between lateral acceleration and rotation in the vehicle compared to the coupling in the simulator. To understand how this affects the driver experience, two settings of acceleration reference point, point A (at chassis roll axis) and point B (at driver's head) are evaluated, and illustrated in Figure 1. These two points are considered coupled through the roll acceleration  $\ddot{\theta}$  as  $a_{y,B} = a_{y,A} + h_{rc,d}\ddot{\theta}_{roll}$ . The roll rotation in the MCA is set around each respective point in the cabin.

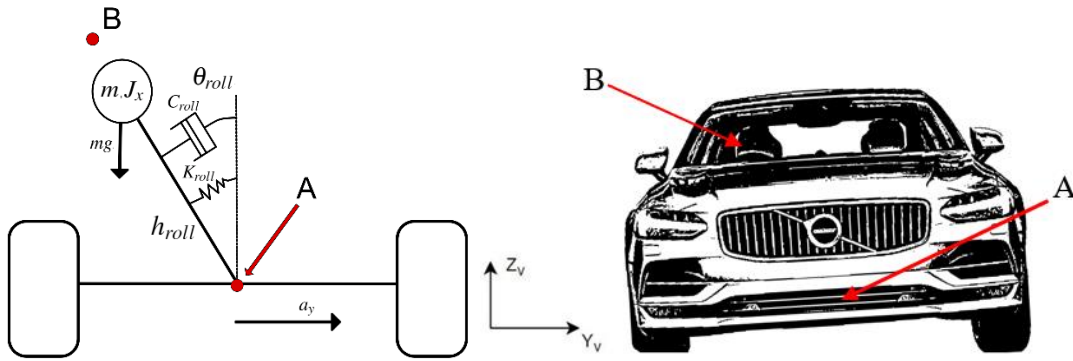


Figure 1: Roll pendulum model and vehicle model indicating the two acceleration reference points.

### 2.1.7 Motion cueing settings

The linear model was applied to the evaluation of two different settings of reference points for the lateral cueing. The first reference point was the roll axis, ref. A, the second was the drivers head acceleration, ref. B. To evaluate the two different reference points for different motion cueing settings, both the reference points were evaluated with added roll and tilt feedback and the tuning parameters are presented in Table 1 together with the onset filter gains. The cut-off frequency  $f_{c,hp}$  and  $f_{c,lp}$  for both yaw and lateral acceleration were 0.55 Hz for high pass and 30 Hz for low pass respectively.

Table 1: Motion cuing settings for onset filters, roll feedback and tilt coordination.

Settings	$G_{input,\psi}$	$G_{input,a_y}$	$G_{roll}$	$K_{tilt}$
S1	1	1	0	0
S2	1	1	0.8	0
S3	1	1	0.8	0.3

## 3. Results

To show the effect of different motion cueing settings, the transfer function between vehicle lateral acceleration  $a_y$  to perceived acceleration  $\hat{a}_y$  is plotted in Figure 2 in a Bode plot. Ref. A shows significant discrepancies in the magnitude for frequencies above 1.0 Hz. For setting S1 with no tilt or roll feedback, there is no isolation of lateral acceleration above the roll mode (1.5-2 Hz). For S2 and

S3 the magnitude is close around the roll mode however, above this the magnitude gain is higher than the reference. Below 0.1 Hz, the tilting effect from the roll feedback and the tilt coordination is clear, and the effect for both the ref. point A and ref. point B is similar. Further, it shows that the tilt effect from the roll feedback comes with significant phase delay, due to damping of the roll.

For ref. B, it shows that for all settings, the magnitude of the transfer function is close to the reference from 1 Hz up to 10 Hz. For frequencies above 10 Hz the magnitude of the feedback is decreasing with frequency, and the phase delay is increasing. This is due to the band pass filter of the motion cueing onset filter. As both the added acceleration due to roll and the chassis acceleration are filtered through the onset filter, the filter has only minor changes in magnitude above 1.0 Hz due to the tilt effect of the roll and coordinated tilt. For frequencies below 1 Hz, the behaviour of the transfer function is very similar to ref. A.

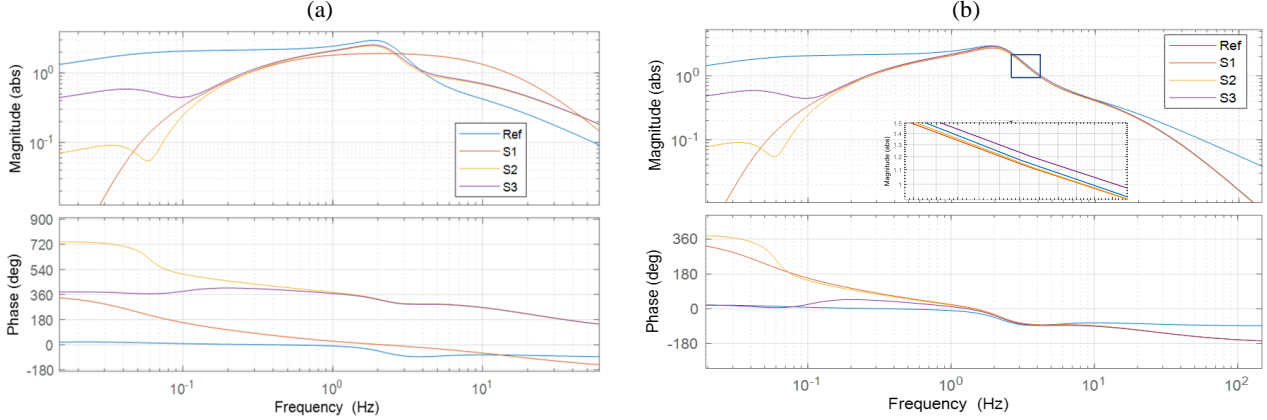


Figure 2: Bode plot of vehicle lateral acceleration  $a_y$  to perceived lateral acceleration  $\hat{a}_y$  for reference and the settings S1-S3 for reference point A (a) and reference point B (b).

The transfer function from perceived  $\hat{\psi}$  to perceived  $\hat{a}_y$  is presented in Figure 3. The behaviour of the transfer function above 1.0 Hz indicates that ref. B has significantly better performance than ref. A compared to the reference vehicle function. This is true for all motion cueing settings.

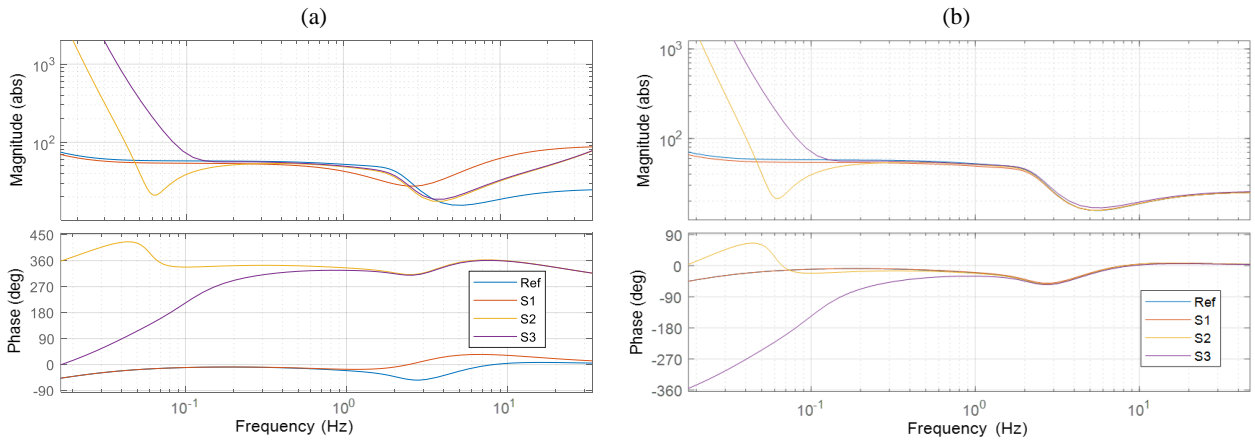


Figure 3: Bode plot of perceived  $\hat{\psi}$  to perceived lateral acceleration  $\hat{a}_y$  for reference and the simulator settings S1-S3 for reference point A (a) and reference point B (b).

For frequencies below 1 Hz, the behaviour of the transfer function for both ref. A and ref. B is similar. S2 and S3 indicates that the ratio between  $\hat{a}_y$  and  $\hat{\psi}_{sim}$  goes up significantly. This is reasonable as the roll and tilt coordination gives frequency content down to 0 Hz for  $\hat{a}_y$ , while the onset/washout filter for  $\hat{\psi}_{sim}$  causes the low frequency parts to be attenuated. Hence, the low frequency ratio in the transfer function grows significantly as the amplitude for  $\hat{\psi}_{sim}$  becomes smaller when the frequency decreases.

## 4. Discussion and conclusion

A linear model of the combination of vehicle, driver and driving simulator model has been developed with the classic motion cueing algorithm. The driving simulator model feedback yaw onset, lateral acceleration onset, roll and coordinated tilt feedback. The model enables estimation of the transfer functions between steering input, simulator states and human vestibular responses, thereby offering a method on estimating human motion perception response based on both simulator and vehicle parametrisation. The model is applied to the evaluation of acceleration reference points A (reference point in the chassis and B, reference point at the driver's head position).

The linear model indicates that a reference point B at the driver's head is advantageous in terms of vehicle input to perceived acceleration output and perceived yaw to perceived acceleration. It shows advantages in both phase lag and magnitude for frequencies close and above the vehicle roll natural frequency (1.5-2.0 Hz) for both metrics. For frequencies below the roll eigenfrequency, no significant differences are evident between the reference point B compared to A. The performance of the two settings is similar in this frequency range and indicates a mismatch in vestibular response between perceived yaw rate and perceived lateral acceleration due to the steady state feedback of tilt coordination and roll, compared to the high-pass filtered yaw feedback.

The linear model is proposed to be used as a method to evaluate motion cueing settings objectively which is a key aspect to enable objective motion cueing for virtual prototypes in early stages, enabling a more resource efficient development and a faster development cycle. The results show that the model can be used to select the reference point of the motion cueing objectively based on the performance over the frequency range of interest, taking in consideration vehicle parameters and human perception of motion.

The presented metrics is a subset of the states that could be evaluated from the linear model. Additional metrics, such as perceived slip angle, could be used to evaluate the motion cueing. Further, it could be extended with longitudinal dynamics, and vestibular-visual motion perception models.

## 5. Acknowledgements

The authors would like to thank the Centre for ECO2 Vehicle Design, funded by the Swedish Innovation Agency Vinnova (Grant Number 2016-05195), for financial support.

## 6. Bibliography

- [1] D. Fisher et al., *Handbook of Driving Simulation for Engineering, Medicine and Psychology*, CRC Press, Apr 2011.
- [2] M. Mooij et al., "Adaptation of the Classic Cueing Algorithm for Automotive Applications," *AIAA Scitech Forum*, Jan. 2019.
- [3] W. Brems et al., "New Motion Cueing Algorithm for Improved Evaluation of Vehicle Dynamics on a Driving Simulator," *SAE 2017-01-1566*, Mar. 2017.
- [4] A. Jamson, "Motion cueing in driving simulators for research applications," *PhD Thesis, University of Leeds*, 2010.
- [5] M. Bruschetta et al., "Nonlinear, MPC-Based Motion Cueing Algorithm for a High-Performance, 9-DOF Dynamic Simulator Platform," *IEEE Transactions on Control Systems Technology*, p. 1–9, May 2016.
- [6] M. Baseggio et al., "An MPC approach to the design of motion cueing algorithms for driving simulators," *14th International IEEE Conference on Intelligent Transportation Systems (ITSC)*, pp. 692-697, 2011.
- [7] M. Bruschetta et al., "A fast implementation of MPC-based motion cueing algorithms for mid-size road vehicle motion simulators," *Vehicle System Dynamics*, vol. 55, no. 6, p. 802–826, 2017.
- [8] J. Houck et al., "Motion Cueing Algorithm Development: Human-Centered Linear and Nonlinear Approaches," *NASA Dissertation*, June 2005.



## Day 1: P03 – Component Design

Session P03 – Component Design, Monday 14 June

---

Session chairs: Giuseppe Petrone and Per Wennhage

- 11:50-12:00    **P03.A**  
*Structural analysis of vehicle frames using higher-order beams*  
Jaeyong Kim, Gang-Won Jang and Yoon Young Kim
- 12:00-12:10    **P03.B**  
*Topological core design of multifunctional sandwich structures*  
Johan Larsson, Peter Göransson and Per Wennhage
- 12:10-12:20    **P03.C**  
*Redesign and structural optimization for lightweighting of a truck door*  
Jan Stroobants, Freek de Bruijn, Saïcha Gerbinet, Jean Pierre Heijster, Carlos López, Reginald Diltoer, Jasper Mols, Johan Potargent, Angélique Léonard, Elke Deckers, Bert Pluymers and Philip Eyckens
- 12:20-12:30    *Questions and Answers*
-

# Structural analysis of vehicle frames using higher-order beams

Jaeyong Kim<sup>1</sup>, Gang-Won Jang<sup>2</sup> and Yoon Young Kim<sup>1,\*</sup>

<sup>1</sup> Seoul National University, Gwanak-ro 1, Gwanak-gu, Seoul 08826, Republic of Korea

<sup>2</sup> Sejong University, Neungdong-ro 209, Gwangjin-gu, Seoul 05006, Republic of Korea

\* Corresponding author. Email: yykim@snu.ac.kr

Using one-dimensional analysis models such as a beam-based model can be efficient in the early-stage design because of their simplicity and analysis efficiency. Despite these advantages, they have not been much explored in the vehicle industry because of their poor accuracy. This is mainly because conventional one-dimensional models using the Euler-Bernoulli or Timoshenko beams considering only six sectional rigid-body modes are incapable to represent stiffness weakening caused by complex deformations due to distortion and warping which cannot be ignored in thin-walled beam members forming a vehicle frame. To account for these complex deformations, a beam model should be capable to represent higher-order sectional modes in addition to the sectional rigid-body modes. In the case of straight beams, the resulting higher-order beam analysis is found to predict nearly as accurate results as obtained by refined plate-based analysis. However, it has remained to be difficult to obtain satisfactory results using a higher-order beam theory for a vehicle frame having a number of beam-joints because the exact field matching conditions for the higher-order modes at a joint are difficult to establish for beams of arbitrarily-shaped cross-sections. This difficulty comes from the fact that the higher-order modes generate no stress resultant over the beam cross-section, making the coordinate transformation matrix commonly used for the sectional rigid-body modes invalid for the case of the higher-order modes. Here, we newly propose an approach to define the joint condition for a one-dimensional higher-order beam model that is applicable to the higher-order modes as well as the sectional rigid-body modes. To confirm the validity of the proposed method, several numerical case studies are examined, including static and modal analyses of a simplified vehicle frame made of beams of various cross-sections.

© 2021 by the authors. Published by the Resource Efficient Vehicles Conference.  
This is an open access article under the CC BY license (<http://creativecommons.org/licenses/by/4.0/>).

## 1. Introduction

The use of a one-dimensional model is efficient to analyse frame structures because of simplicity of its modeling process and mathematical expression. However, conventional one-dimensional models based on the Euler-Bernoulli beam theory or the Timoshenko beam theory incorrectly evaluate the stiffness, since they cannot express detailed deformations like cross-section distortion. To overcome the inaccuracy of the conventional beam theories, many approaches have been developed since Vlasov proposed the inclusion of higher-order modes in addition to the six conventional cross-section modes,  $\{U_x, U_y, U_z, \theta_x, \theta_y, \theta_z\}$  [1]. Due to the consideration of higher-order modes, detailed behaviors of a beam can be captured by a higher-order beam theory leading to the accurate analyses of both displacement and stress fields [2, 3].

Although the use of higher-order modes improves the accuracy of one-dimensional analyses, they also make it difficult to define the coupling relations among their cross-section deformation shapes at a joint in which multiple beams are connected. For example, for the joint in Fig. 1, the coupling

relation for the six conventional rigid-body cross-section modes can be simply defined using a coordinate transformation matrix for the joint angle  $\phi$  because their directions are defined on the cross-section as illustrated in Fig. 2(a). However, this transformation matrix is not applicable if higher-order mode as in Fig. 2(b) are also considered in a beam theory.

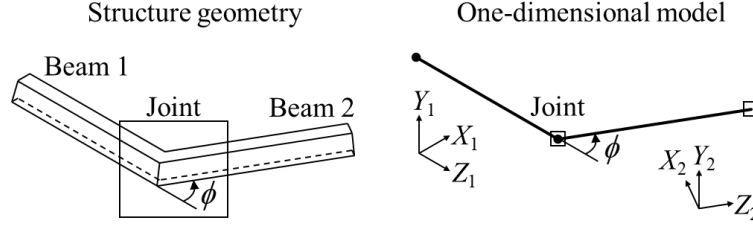


Figure 1: One-dimensional model of a beam structure.

To define coupling relations among higher-order modes, many attempts have been made. Jang and Kim [4] proposed a cross-sectional displacement continuity condition at a joint. They introduced a virtual section that is referred to as the joint section to define the displacements at a joint. Then they defined the mode coupling relations by minimizing the mismatches of displacements on the joint section. If the minimization is applied, the mode coupling relations can be described in terms of a square matrix relating the field variables in two adjacent beams meeting a joint. Although this approach was found to be effective for various cross-sections, their approach is appropriate mainly for two-beam joints; since the minimization process becomes complicated when three or more beams are connected. Towards this direction, efforts using the Generalized Beam Theory (GBT) were made to deal with beam structures made of multiple beams [5]. While the approach in [5] yielded accurate results, it appears to be most effective in open-sectioned thin-walled beams but requires some further efforts to be effective for more complicated structures, for example, vehicle frames, as it requires additional considerations for different cross-sections and connections. Our approach presented is, on the other hand, consistently applicable for general cases while it can employ as many higher-order modes as desired.

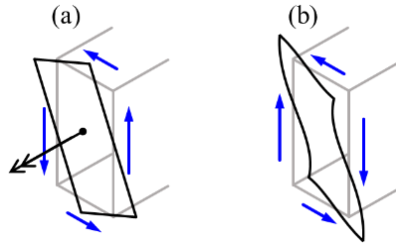


Figure 2: Cross-section modes of a box beam: (a) torsional rotation mode and (b) distortion mode.

## 2. Proposed joint condition

The proposed joint condition is inspired by some earlier studies; as in the GBT [5], displacement and rotation continuities at the connection points are taken into account, and the definition of the joint section as proposed by Jang and Kim [4] is used. Here, we newly propose some approaches to overcome some difficulties in using these techniques for complicated beam-joint structures. First, a consistent rationale to set the connection points for general cases is proposed – as shown in Fig. 3, the connection points are set to be located at the cross-section corners and at the joint axis. This rationale can be applied consistently to beams of any cross-sectional shape. At each connection point on the midline along the cross-section wall, the continuities in three dimensional displacements and rotations are imposed. Second, additional displacements on a joint section are taken into account. Because the cross-section of a beam is normal to the beam axis, the beam section and the joint section

do not match in general, as can be seen in Fig. 3. Therefore, displacements on the joint section should be carefully assessed to be able to accurately match the field quantities at a joint. The additional displacements on the joint section are calculated by using the rotations of the beam section, allowing the correct evaluation of displacements at the joint. The merit of the proposed method is that it can be applied “consistently” to beam structures of any cross-sectional shapes.

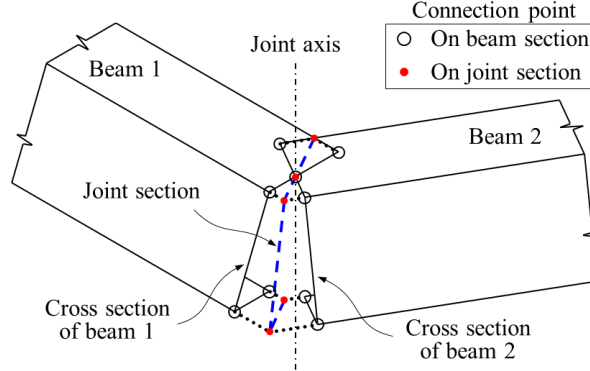


Figure 3: Proposed joint condition for a beam structure in Fig. 1.

### 3. Numerical examples

For the verification of the proposed joint matching condition, two numerical problems are considered. In Section 3.1, an L-type joint structure shown in Fig. 4, which was dealt with in Ref. [6], is analysed for varying joint angles. In Section 3.2, static and modal analyses are conducted for a simplified vehicle frame that is composed of various shapes of beams. All results obtained by the proposed beam-based matching method are compared with those by shell finite elements (ABAQUS S8R elements). The same material properties are used for all examples;  $E = 200$  GPa,  $\nu = 0.3$  and  $\rho = 7850$  kg/m<sup>3</sup>.

#### 3.1 L-type joint structure with rectangular section

An L-type joint structure shown in Fig. 4 is considered. One end of the structure is fixed while the other end is assumed to be rigidly constrained and subjected to a vertical force. The static analyses were carried out for several joint angles ( $\phi = 30^\circ, 60^\circ, 90^\circ$ ).

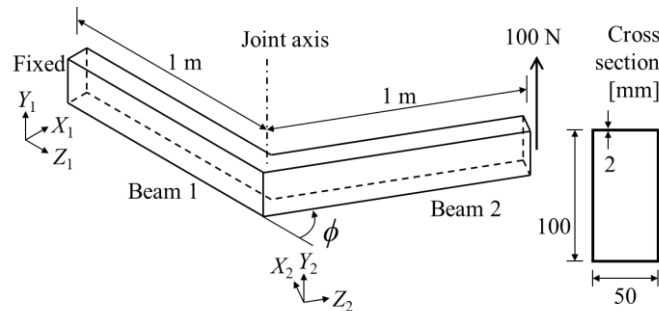


Figure 4: L-type joint structure with a rectangular section subjected to a vertical force.

The static analysis results by the shell elements, the Timoshenko beam theory, those in Ref. [6] and those by the proposed approach are compared in Fig. 5. Figure 5 shows that the results by [6] and the proposed approach agree with the shell results consistently for the joint angle, while the Timoshenko beam results do not.

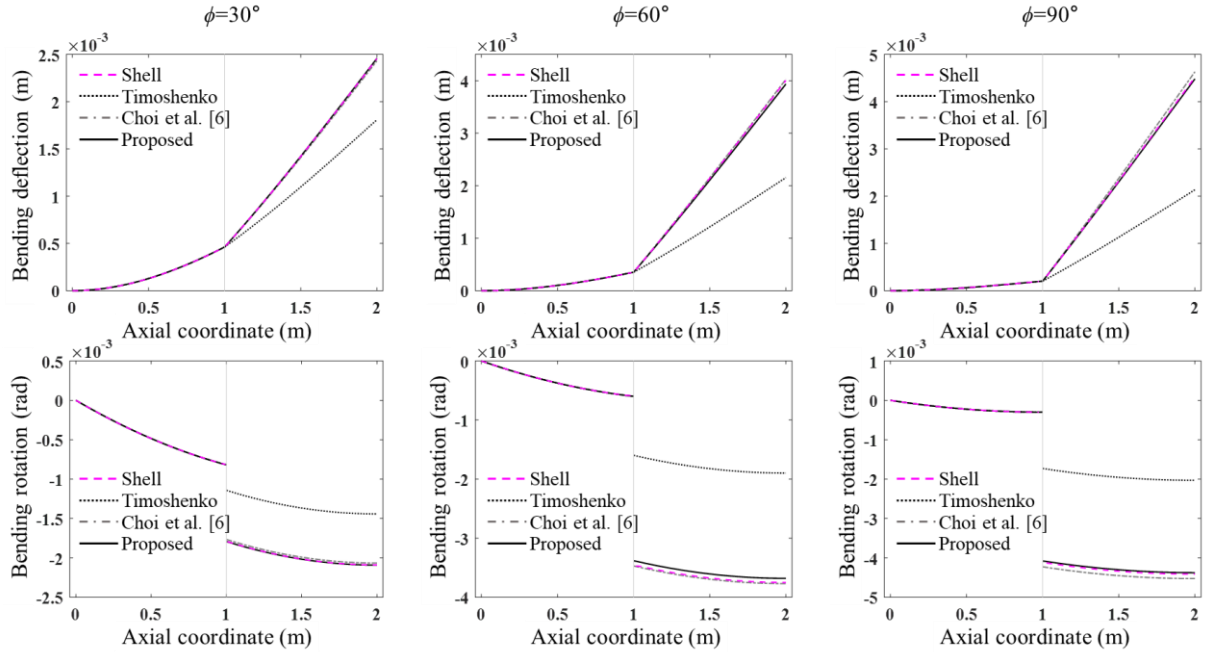


Figure 5: Analysis results of the problem in Fig. 4 for  $\phi=30^\circ$ ,  $60^\circ$ , and  $90^\circ$ .

### 3.2 Simplified vehicle frame

Figures 6(a) and 6(b) show a simplified vehicle frame and its one-dimensional model, respectively. The frame is fixed at two rear points and subjected to torsional forces at two points in the front. The beam sections in which forces are applied are assumed to be rigid.

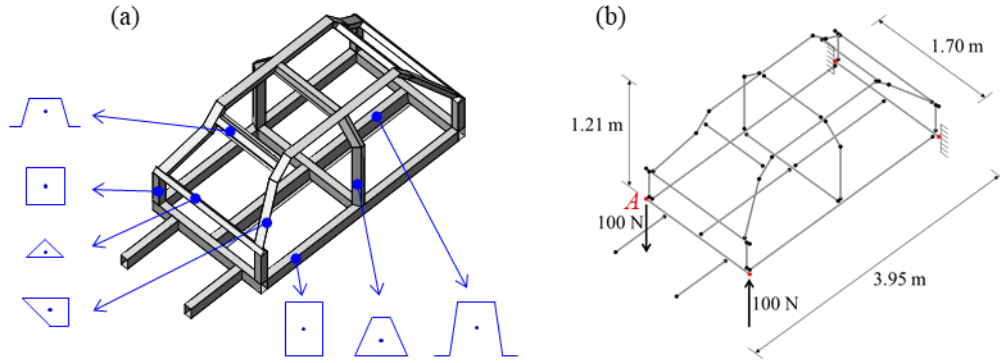


Figure 6: (a) A simplified vehicle frame and (b) its one-dimensional model.

While the detailed results here are skipped, it was found that the deformed shape by the proposed approach matches well with that by the shell elements, while the Timoshenko beam results are too stiff. Specifically, the difference in the vertical displacement at point A in Fig. 6(b), one of the loading points, is calculated as 0.4% for the proposed approach and 45.5% for the Timoshenko beam theory, compared to the shell finite element result. Also, the proposed approach gives accurate results in the free vibration analysis of the vehicle frame. The eigenfrequencies are compared in Table 1.

Table 1: Natural frequencies (Hz) of the vehicle frame in Fig. 6.

<b>Mode #</b>	<b>1</b>	<b>2</b>	<b>3</b>
<b>Motion</b>	<b>Torsion</b>	<b>Pulling</b>	<b>Bending</b>
<b>Shell</b>	31.15	38.97	51.77
<b>Timoshenko</b>	52.44	67.39	69.92
<b>Proposed</b>	32.19	39.76	52.24

## 4. Conclusion

While a one-dimensional higher-order beam analysis is preferred for fast and efficient analysis, it is known to be difficult to find field matching conditions at a joint of multiple thin-walled beams of possibly different cross-sections, especially closed cross-sectioned beams, when higher-order cross-section modes are included. Although many earlier attempts were made to define the coupling relations of the higher-order modes, they were limited only to specific joint types or cross-section types. To overcome these limitations, a new joint condition was proposed based on the continuities at the connection points. The validity of accuracy by the proposed methods was checked using numerical examples including the static and vibration analyses of a simplified vehicle frame.

## References

1. V.Z. Vlasov, Thin-walled elastic beams, Israel Program for Scientific Translations, Jerusalem, 1961.
2. A. Genoese, A. Genoese, A. Bilotta, G. Garcea, A generalized model for heterogeneous and anisotropic beams including section distortions, Thin-Walled Structures 74, 2014, pp. 85-103.
3. A.W. Ruggerinia, A. Madeob, R. Gonçalvesc, D. Camotimd, F. Ubertinia, S. de Miranda, GBT post-buckling analysis based on the Implicit Corotational Method, International Journal of Solids and Structures 163, 2019, pp. 40-60.
4. G. W. Jang, Y.Y. Kim, Fully coupled 10-degree-of-freedom beam theory for piecewise straight thin-walled beams with general quadrilateral cross sections, Journal of Structural Engineering 136, 2010, pp. 1596-1607.
5. C. Basaglia, D. Camotim, H.B. Coda, Generalised beam theory (GBT) formulation to analyse the vibration behaviour of thin-walled steel frames, Thin-Walled Structures 127, 2018, pp. 259-274.
6. S. Choi, G.-W. Jang, Y.Y. Kim, Exact matching condition at a joint of thin-walled box beams under out-of-plane bending and torsion, Journal of Applied Mechanics 79(5), 2012, 051018.

# Topological core design of multifunctional sandwich structures

Johan Larsson<sup>1,2,\*</sup>, Peter Göransson<sup>1,2</sup> and Per Wennhage<sup>1,2</sup>

<sup>1</sup>*KTH Royal Institute of Technology, Teknikringen 8, 100 44 Stockholm, Sweden*

<sup>2</sup>*The Centre for ECO<sup>2</sup> Vehicle Design, Teknikringen 8, 100 44 Stockholm, Sweden*

<sup>\*</sup>*Corresponding author. Email: jlar6@kth.se*

Topology optimization is used to design multifunctional sandwich panels that fulfill multiple functional constraints. The purpose is to expand the methodology for multifunctional design in early stages of the vehicle design process, to allow for design of multifunctional vehicle systems that can replace multiple subsystems and reduce the total mass of the vehicle. The focus of the research is the inclusion of dynamic behaviour into the topology optimization framework. The case study for this research is a train cabin sandwich structure, with the functional requirements being the structural and acoustic properties of the structure. The core of the sandwich panel is the design domain of the optimization. The problem is modelled and solved as a mass minimization topology optimization problem with the structural requirements being translated into constraints on the static response of the structure and the acoustic requirements being translated into constraints on the response when subjected to time-harmonic loads. The topology optimization problem is solved using the Topology Optimization of Binary Structures (TOBS) method.

©2021 by the authors. Published by the Resource Efficient Vehicles Conference.  
This is an open access article under the CC BY license (<http://creativecommons.org/licenses/by/4.0/>).

## 1. Introduction

Sandwich structures with distinct face and core materials play a major part in many engineering applications because of their high bending stiffness to weight ratio. They also offer excellent opportunities to customize the structure according to the specific application. The material and thickness of the faces and core are natural choices as design parameters when optimizing the sandwich structure according to the specific demands. A lot of research has been done in this area [1, 2]. However these studies often have some assumptions on the macroscopic core topology, it is either solid or has some predefined topological pattern, such as honeycomb. This restricts the freedom of the engineer to find solutions to the problems though some studies have been made regarding the topology of the core in sandwich structures.

The problems that have been treated can be divided into two categories. The first category is static problems that have been treated in [3] and [5]. In [3], the minimum compliance problem is studied for a sandwich beam with a periodic core topology using the Bidirectional evolutionary structural optimization (BESO) method. The same type of problem is solved in [5], but using a morphable moving components (MMC) method, which uses the size and placement of a number of discrete struts in the core as design variables.

The other category of problems are time-harmonic where the dynamic properties of sandwich beams are studied. The fundamental resonance frequency is maximized for a sandwich with a periodic core topology in [4] using the BESO method. In [6], the authors instead focus on minimizing

and maximizing the dynamic compliance of sandwich structures with graded core materials using a moving isosurface threshold (MIST) method.

Most of the research so far has been focused on minimizing or maximizing some type of physical response of the structure, such as compliance, eigenfrequencies etc with some constraint on the amount of volume or mass in the structure. From a lightweight structures perspective, it is more interesting to instead minimize the mass of a structure subjected to constraints on the physical response. In [7] the mass of a multifunctional sandwich panel is minimized subjected to constraints on the static compliance, fundamental resonance frequency and fundamental buckling load.

The work in this paper seeks to extend the optimization schemes used in [7]. The focus of the presented work is the mass minimization of a sandwich beam subjected to constraints on static and time-harmonic response using the topology optimization of binary structures (TOBS) method [8]. The proposed method is demonstrated on an example problem of a sandwich beam. The effects of a core material much weaker than the face sheets is also studied and discussed.

## 2. Problem description

The response of an elastic, hysterically damped structure to static or time-harmonic loading is governed by the finite element equation

$$(\mathbf{K} - \omega^2 \mathbf{M})\mathbf{u} = \mathbf{f} \quad (1)$$

where  $\mathbf{K}$  is the global damped stiffness matrix,  $\omega$  is the frequency of excitation,  $\mathbf{M}$  is the global mass matrix,  $\mathbf{u}$  is the vector of nodal displacements and  $\mathbf{f}$  is the vector of nodal loads. If the load is static then  $\omega = 0$ . The damping is assumed to be independent of excitation frequency and the damped stiffness matrix is given by the following equation.

$$\mathbf{K} = (1 + i\eta)\mathbf{K}_0 \quad \begin{cases} \eta = \eta_0 & \text{for } \omega > 0 \\ \eta = 0 & \text{for } \omega = 0 \end{cases} \quad (2)$$

where  $\mathbf{K}_0$  is the undamped global stiffness matrix,  $\eta$  is the structural loss factor and  $\eta_0$  is the prescribed constant value of  $\eta$ .

The topology optimization problem is formulated as follows

$$\begin{aligned} & \min m(\mathbf{x}) \\ & \text{s.t. } g_j(\mathbf{x}) \leq \bar{g}_j \\ & \quad x_i \in \{0, 1\} \end{aligned} \quad (3)$$

Here  $m$  is the mass of the structure,  $g_j$  is the  $j$ th constraint function,  $\bar{g}_j$  is the  $j$ th constraint value and  $\mathbf{x}$  is the vector of design variables, where 0 means that the element is not present in the design and 1 means that the element is present, and  $x_i$  being the  $i$ th element of  $\mathbf{x}$ . The problem is a non-linear integer program that is very hard to solve.

In the TOBS method, the problem in Eq. (3) is linearized using a first-order Taylor approximation, giving the new integer linear program (ILP)

$$\begin{aligned} & \min \Delta m(\Delta \mathbf{x}) = \frac{\partial m}{\partial \mathbf{x}} \Delta \mathbf{x} \\ & \text{s.t. } \Delta g_j(\mathbf{x}) = \frac{\partial g_j}{\partial \mathbf{x}} \Delta \mathbf{x} \leq \bar{g}_j - g_j(\mathbf{x}) \\ & \quad \Delta x_i \in \{0 - x_i, 1 - x_i\} \end{aligned} \quad (4)$$

which is then solved in every iteration of the optimization. The  $\Delta m$  and  $\Delta g_j$  are the change in mass and constraint functions caused by the change  $\Delta \mathbf{x}$  in the design variables according to the linear



approximation. The design is then updated according to

$$\mathbf{x}^{k+1} = \mathbf{x}^k + \Delta \mathbf{x}^k \quad (5)$$

where  $k$  is the number of the current iteration.

The constraints are relaxed according to

$$\Delta g_j(\mathbf{x}) \leq \Delta \bar{g}_j \quad (6)$$

where  $\Delta \bar{g}_j$  is given by

$$\Delta \bar{g}_j = \begin{cases} -\varepsilon_j g_j(\mathbf{x}) & \text{if } (1 - \varepsilon_j)g_j(\mathbf{x}) > \bar{g}_j \\ \bar{g}_j - g_j(\mathbf{x}) & \text{if } (1 - \varepsilon_j)g_j(\mathbf{x}) \leq \bar{g}_j \leq (1 + \varepsilon_j)g_j(\mathbf{x}) \\ \varepsilon_j g_j(\mathbf{x}) & \text{if } (1 + \varepsilon_j)g_j(\mathbf{x}) < \bar{g}_j \end{cases} \quad (7)$$

Here  $\varepsilon_j$  is some small number set by the user. This is to ensure that the ILP has feasible solutions, otherwise problems could arise where the ILP demands such a large change in the constraint functions that the problem becomes infeasible. The relaxation means that only small changes in the constraints are aimed for in every iteration.

A neighbourhood constraint is also used to limit how much the design can change in each iteration, this is formulated as

$$\sum_{x_i \in \text{solid}} \Delta x_i \geq -\epsilon_r N \quad \text{and} \quad \sum_{x_i \in \text{void}} \Delta x_i \leq \epsilon_a N \quad (8)$$

where  $\epsilon_r$  and  $\epsilon_a$  are the maximum ratio of elements allowed to be removed and added in each iteration and  $N$  is the total number of elements in the design domain.

The objective function is the mass of the sandwich structure, this can be formulated as

$$m = m_{\text{faces}} + \sum_{i=1}^n m_i^{(e)} x_i \quad (9)$$

where  $m_{\text{faces}}$  is the mass of the faces,  $n$  is the number of elements in the sandwich core and  $m_i^{(e)}$  is the mass of the  $i$ th element.

The static constraint function is the static compliance

$$C_{\text{stat}} = \mathbf{f}_{\text{stat}}^T \mathbf{u}_{\text{stat}} \quad (10)$$

while the dynamic constraint function is the dynamic compliance

$$C_{\text{dyn}} = |\mathbf{f}_{\text{dyn}}^T \mathbf{u}_{\text{dyn}}| \quad (11)$$

In order to formulate the linearized ILP, the sensitivities of the objective and constraints are needed.

The sensitivity analysis is identical to the one used for the soft-kill BESO method [9]. The material properties are interpolated according to the scheme suggested in [10] in order to avoid artificial modes in the low-density regions. The interpolation is

$$E(x_i) = E_s \left( \frac{x_{\min} - x_{\min}^p}{1 - x_{\min}^p} (1 - x_i^p) + x_i^p \right) \quad (12)$$

$$\rho(x_i) = \rho_s x_i$$

where  $E$  is the elastic modulus,  $\rho$  is the density,  $E_s$  is the elastic modulus of a solid element,  $\rho_s$  is the density of a solid element,  $x_i$  is the relative density of element  $i$ ,  $x_{\min}$  is the minimum value on  $x_i$  and  $p$  is the penalty exponent.

Based on Eqs. (1), (2) and (9)-(12), the sensitivities can be derived as

$$\frac{\partial m}{\partial x_i} = m_i^{(e)} \quad (13)$$

$$\frac{\partial C_{stat}}{\partial x_i} = -\mathbf{u}_{stat,i}^T \left( \frac{1 - x_{min}}{1 - x_{min}^p} p x_i^{p-1} \mathbf{K}^{(s,i)} \right) \mathbf{u}_{stat,i} \quad (14)$$

$$\frac{\partial C_{dyn}}{\partial x_i} = \frac{1}{|\mathbf{f}_{dyn}^T \mathbf{u}_{dyn}|} \text{Re} \left( -\mathbf{u}_{dyn,i}^T \left( \frac{1 - x_{min}}{1 - x_{min}^p} p x_i^{p-1} \mathbf{K}^{(s,i)} - \omega^2 \mathbf{M}^{(s,i)} \right) \mathbf{u}_{dyn,i} (\mathbf{f}_{dyn}^T \mathbf{u}_{dyn})^* \right) \quad (15)$$

where  $\mathbf{K}^{(s,i)}$  is the stiffness matrix of element  $i$  if the material is solid,  $\mathbf{M}^{(s,i)}$  is the mass matrix of element  $i$  if the element is solid,  $\mathbf{f}_{dyn}$  and  $\mathbf{f}_{stat}$  are the loads from the static and dynamic load cases and  $\mathbf{u}_{dyn}$  and  $\mathbf{u}_{stat}$  are the nodal displacement vectors from the static and dynamic load cases. The \* stands for the complex conjugate. The ILP is then solved using a branch-and-cut method [11].

### 3. Example problem

The optimization is demonstrated on the example problem illustrated in Fig. 1. It is a beam with the dimensions 1x0.2x0.05 m. Both face sheets are 5 mm thick and the core is 190 mm thick. The beam is clamped at both ends and is subjected to a uniform pressure acting on the middle 0.2 m of the top face sheet. The beam is discretized into 200x40 4-node plane stress elements. The top and bottom layers of elements constitute the face sheets and are exempt from the optimization, the material properties of these elements can also be different from the properties of the other elements in order to allow for different face sheet and core materials.

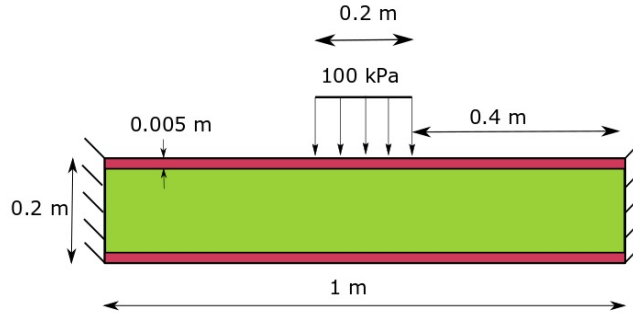


Figure 1: Example problem, the 0.05 m thickness is out of the plane in the image.

Three beams with different material combinations were considered in the optimization, all of them have a face sheet material with mechanical properties similar to glass fiber reinforced polymer (GFRP). The core materials considered have properties similar to GFRP, polylactide (PLA), often used in additive manufacturing, and a structural polymer foam, see Table 1. The face sheets are assumed to have damping coefficient 0.001 and the core materials are assumed to have damping coefficient 0.02. The different material combinations are chosen to illustrate how the difference in material properties between the face sheets and core affect the results of the optimization. The starting topology is the full design domain for each optimization.

#### 3.1 Changes in fundamental resonance frequency during optimization with a static constraint

First, the three beams were optimized with a single constraint on the static compliance. The fundamental resonance frequency was tracked during the optimization in order to investigate how the

Table 1: Mechanical properties of the different materials.

Material	Density [kg/m <sup>3</sup> ]	Young's Modulus [GPa]	Poisson's Ratio [-]
GFRP	1800	20	0.27
PLA	1200	4	0.3
Foam	100	0.13	0.3

fundamental eigenfrequency behaves during a static optimization for the different combinations of face sheet and core materials. The static compliance constraint for each of the beams can be seen in Table 2 and the result can be seen in Fig. 2, where the fundamental eigenfrequency is plotted as a function of optimization iteration for the different beams. The starting topology was the fully populated design domain. A solid GFRP beam is also included in order to investigate if the non-removable face sheets have a large impact on the first eigenfrequency.

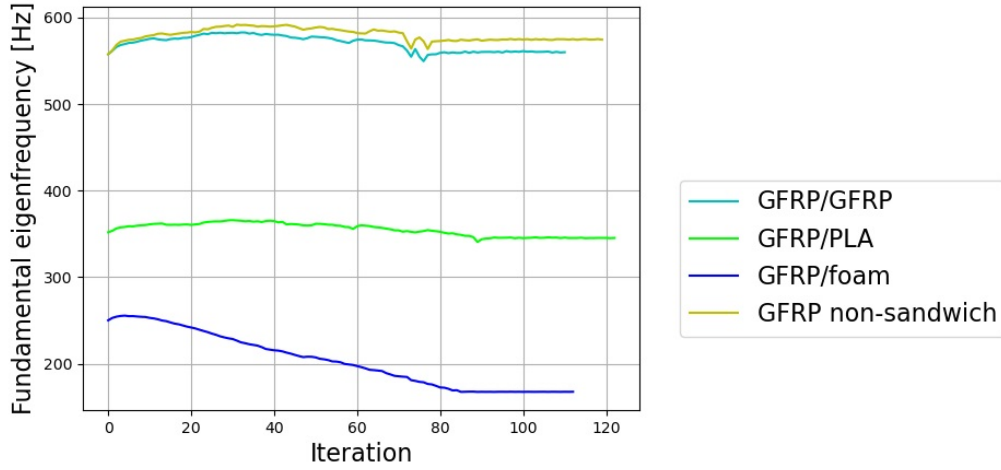


Figure 2: Fundamental eigenfrequency as a function of iterations for an optimization with only the static compliance constraint.

### 3.2 Optimization of multifunctional sandwich beams subjected to static and dynamic constraints

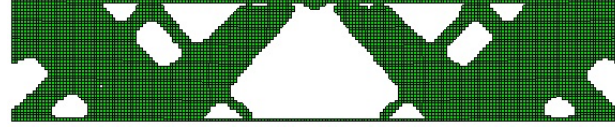
The different sandwich beams were then optimized with constraints on both the static and the dynamic compliance. The constraints and the excitation frequencies for each of the beams can be found in Table 2, the different resonance frequencies were selected so that they were below the fundamental resonance frequency for each of the beams, based on Fig. 2. The resulting topologies can be seen in Fig. 3. The mass, static compliance and dynamic compliance can be seen plotted against the optimization iterations for the GFRP/foam and GFRP/GFRP beams in Fig. 4. The optimization parameters for all beams are  $\varepsilon_j = 0.01$  for all constraints and  $\epsilon_a = \epsilon_r = 0.04$ .

## 4. Results and Discussion

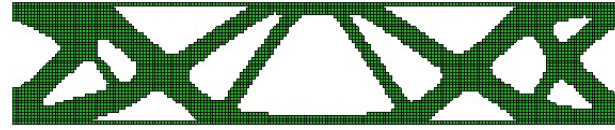
In Fig. 2 it is seen that the beam with a foam core behaves differently during optimization compared to the other beams. For the beams with GFRP and PLA cores and the non sandwich GFRP beam, the eigenfrequency is increased during the 30-40 first iterations and then slowly starts to decrease until it reaches roughly the same value as it had at the full design domain. Although the

Table 2: Constraints and excitation frequencies for the different beams

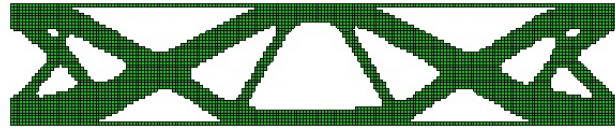
Core material	Static compliance constraint [Nm]	Dynamic compliance constraint [Nm]	Excitation frequency [Hz]
GFRP	0.02	0.06	520
PLA	0.08	0.2	320
Foam	1	1.5	160



(a) GFRP/Foam.



(b) GFRP/PLA.



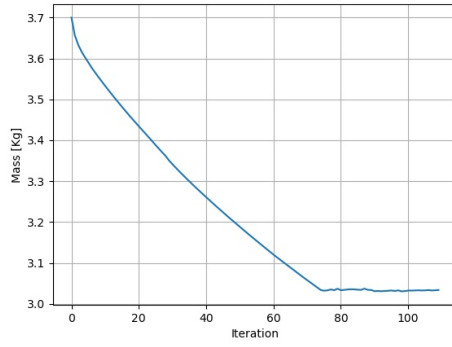
(c) GFRP/GFRP.

Figure 3: Final topologies for the different core materials.

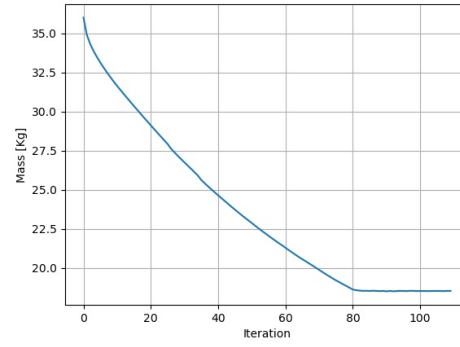
sandwich beam with GFRP core has a slightly lower eigenfrequency than the non-sandwich beam, the overall behaviour is still similar. This is in agreement with [12], where it was shown that maximizing the static compliance usually correlates to a high fundamental resonance frequency.

The foam core sandwich beam instead has a small increase in the first eigenfrequency during the first few iterations and then decreases rapidly until it reaches a much lower value than it had at the full design domain, in contrast to the behaviour of the other beams. The results seem to imply that if the core material is much weaker and lighter than the face sheet material, the fundamental resonance frequency will decrease no matter what elements are removed. The results in Fig. 4 also support this. For the GFRP sandwich beam, both the static and dynamic compliance constraints are active at the solution, as is seen in Figs. 4d and 4f. But for the foam core sandwich beam, only the dynamic compliance constraint is active, see Fig. 4c and 4e. This means that the optimizer cannot find a way to reduce the dynamic compliance even at the cost of a higher static compliance, which in turn means that the fundamental resonance can not be increased any more and pushed further from the exciting frequency through element removal.

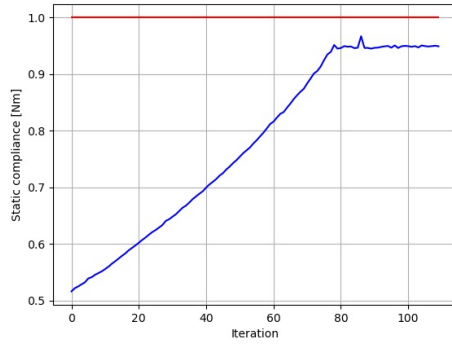
This highlights some of the difficulties in setting the constraints and choosing a start topology for the optimization. In this work the excitation frequency is chosen so as to be below the fundamental resonance even for the beam with only a static constraint. However, if the exciting frequency of the foam beam is a little higher, say 200 Hz, it would be below the fundamental resonance of the fully populated design domain, but above the fundamental frequency of the statically optimized foam beam. Starting the optimization from these two starting topologies could result in very different solutions, as one solution would strive to push the fundamental resonance as far up as possible and would be governed by the dynamic compliance constraint. The other solution would attempt to lower



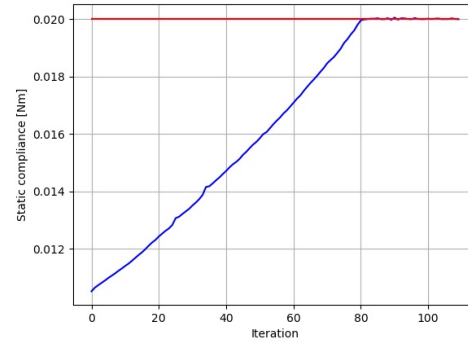
(a) Mass (objective) of the GFRP/foam beam.



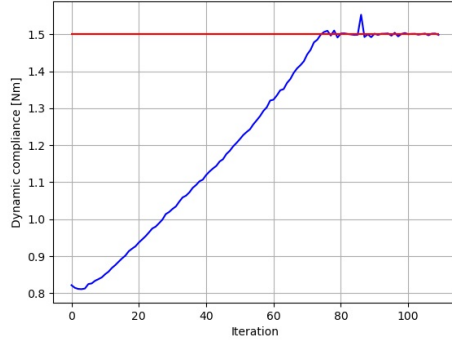
(b) Mass (objective) of the GFRP/GFRP beam.



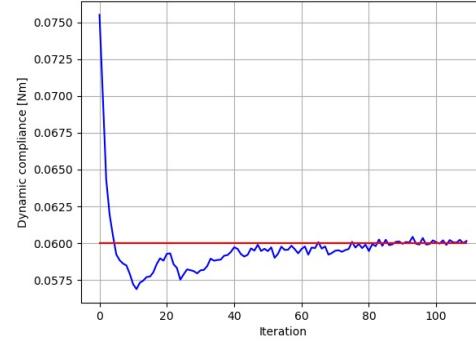
(c) Static compliance for the GFRP/foam beam, the red line is the constraint.



(d) Static compliance for the GFRP/GFRP beam, the red line is the constraint.



(e) Dynamic compliance for the GFRP/foam beam, the red line is the constraint.



(f) Dynamic compliance for the GFRP/GFRP beam, the red line is the constraint.

Figure 4: Objective function and constraints for the GFRP/foam and GFRP/GFRP beams during the optimization.

the fundamental resonance which, according to Fig. 2, correlates to the purely static optimization. This solution could be governed by the static compliance constraint or by both constraints.

Another thing no notice is that the resulting topologies of the PLA and GFRP core sandwich beams have roughly the same topological layout, they have structural members in roughly the same places, while the foam beam has a very different topology. This seems reasonable, as the difference in material properties between core and face sheet material is far smaller for the GFRP and PLA beams than for the foam beam. The topologies also seem reasonable, because according to beam theory, the core in the GFRP and PLA beams should carry a large part of the bending moment in the beam, since the difference between core and face sheet material is small. Looking at Fig. 3b and 3c, the core

reinforces the face sheets where the bending moment is large and is concentrated around the center line of the beam cross section at the inflexion points where there is no bending moment.

The foam beam core should instead, according to beam theory, mainly carry the shear force in the beam, because of the weak core. From 3a this seem to be the case, as the structural members in the beam are at an angle of about  $45^\circ$ , which is known to give high shear stiffness.

## 5. Conclusions

Multifunctional sandwich structures subjected to static and dynamic compliance constraints have been mass minimized using the TOBS method. The effects of differences in material properties between face sheets and core have been investigated and the potential difficulties caused by these differences have been discussed.

## Acknowledgments

The authors would like to thank the Centre for ECO2 Vehicle Design, which is funded by the Swedish Innovation Agency Vinnova (Grant Number 2016-05195).

## References

1. D. Wennberg, S. Stichel, P. Wennhage, Optimization of Sandwich Panels for the Load Carrying Structure of High-Speed Rail Vehicles, *International Journal of Aerospace and Lightweight Structures* 2 (2012) 19–40.
2. C.J. Cameron, P. Wennhage, P. Göransson., Structural-acoustic Design of a Multi-functional Sandwich Panel in an Automotive Context, *Journal of Sandwich Structures and Materials* 12 (2012) 684–708.
3. X. Huang, Y.M. Xie, Optimal design of periodic structures using evolutionary structural optimization, *Structural and multidisciplinary optimization* 36 (2008) 597–606.
4. Z.H. Zuo, X. Huang, Y.M. Xie, Optimal Topological Design of Periodic Structures for Natural Frequencies, *Journal of structural engineering* 137 (2011) 1229–1240.
5. S. Chu, L. Gao, M. Xiao, H. Li, Design of sandwich panels with truss cores using explicit topology optimization, *Composite Structures* 210 (2019) 892–905.
6. M. Alfounh, J. Ji, Q. Luo, Optimal design of multi-cellular cores for sandwich panels under harmonic loading, *Composite Structures* 248 (2020).
7. C. Cameron, E. Lind, P. Wennhage, P. Göransson, On the balancing of structural and acoustic performance of a sandwich panel based on topology, property and size optimization, *Journal of Sound and Vibration* 248 (2014) 2677–2698.
8. R. Sivapuram, R. Picelli, Topology optimization of binary structures using Integer Linear Programming, *Finite Elements in Analysis and Design* 139 (2018) 49–61.
9. Y.M. Xie, X. Huang, Bi-directional evolutionary topology optimization of of continuum structures with one or multiple materials, *Computational Mechanics* 43 (2009) 393–401.
10. X. Huang, Y.M. Xie, Evolutionary topology optimization of vibrating structures for natural frequencies, *Computers and Structures* 88 (2010) 357–364.
11. M. Conforti, G. Cornuéjols, G. Zambeli, *Integer Programming*, Springer Berlin Heidelberg, 2014, pp. 5–16.
12. C.S. Jog, Topology design of structures subjected to periodic loading, *Journal of Sound and Vibration* 253 (2002) 687–709.

# Redesign and structural optimization for lightweighting of a truck door

Jan Stroobants<sup>1,\*</sup>, Freek de Bruijn<sup>2</sup>, Saïcha Gerbinet<sup>3</sup>, Jean Pierre Heijster<sup>2</sup>, Carlos López<sup>1</sup>, Reginald Diltoer<sup>4</sup>, Jasper Mols<sup>5</sup>, Johan Potargent<sup>6</sup>, Angélique Léonard<sup>3</sup>, Elke Deckers<sup>7,8</sup>, Bert Pluymers<sup>7,8</sup> and Philip Eyckens<sup>1</sup>

<sup>1</sup>*Flanders Make, CoDesignS core lab, Oude Diestersebaan 133, 3920 Lommel, Belgium*

<sup>2</sup>*RAI Automotive Industry NL, Automotive Campus 30, 5708 JZ Helmond, The Netherlands*

<sup>3</sup>*University of Liège, Chemical Engineering, PEPs, Quartier Agora, B6a, Allée du Six Août 15, 4000 Liège, Belgium*

<sup>4</sup>*Flanders Make, MotionS core lab, Oude Diestersebaan 133, 3920 Lommel, Belgium*

<sup>5</sup>*GBO, Wethouder den Oudenstraat 6, 5706 ST Helmond, The Netherlands*

<sup>6</sup>*AMS Robotics, Kieleberg 5, 3740 Bilzen, Belgium*

<sup>7</sup>*Flanders Make, DMMS-D core lab, Celestijnenlaan 300, 3001 Heverlee, Belgium*

<sup>8</sup>*KU Leuven, Department of Mechanical Engineering, Celestijnenlaan 300, 3001 Heverlee, Belgium*

\*Corresponding author. Email: [jan.stroobants@flandersmake.be](mailto:jan.stroobants@flandersmake.be)

To advance on automotive lightweighting and sustainability, different design strategies can be followed, such as material substitution, functionality integration, structural design optimization and design for novel production processes. In the presented ab initio re-design use case of a truck door, all these strategies are combined to realize substantial weight reduction in combination with improved life cycle assessment. The traditional steel sheet body is hereby replaced with a short-fiber reinforced PE shell structure designed for a novel robomoulding process, and supported by a steel beam structure as an insert in the same production process. This contribution focuses on the various adopted strategies for structural design optimization throughout the design process, from the early conceptual design up to the detailed design and the validation stage. In early design stage, a simplified quasi-2D model is established to optimize the placement of a beam structure under static and vibrational load cases. In this process, a few hundred automatically generated and evaluated beam structures have been considered within an in-house design software tool. In the subsequent, detailed design stage, further FE-based optimization of the structural part is performed starting from a (3D) CAD design for additional lightweighting while retaining structural requirements. In this step, a commercial design optimization tool is adopted. The result is an optimized design with integrated functionalities, a mass reduction of at least 10 % and a corresponding reduction in CO<sub>2</sub>eq emissions. The optimized design will be realized as a physical prototype.

©2021 by the authors. Published by the Resource Efficient Vehicles Conference.  
This is an open access article under the CC BY license (<http://creativecommons.org/licenses/by/4.0/>).

## 1. Introduction

Climate change and transportation costs make legislation and OEMs strive for weight reduction and improved ecological impact of vehicles [1] [2] [3]. Two technological barriers typically hinder the step towards improvement in these areas: a more complicated design process when shifting to more

advanced materials and production processes, and an increased cost. Efforts like these demonstrate the capabilities of new design tools, whereas increased costs are mitigated by integrating and extending functionalities.

This work focuses on the re-design of a truck door. Not only a weight decrease is achieved, but it is combined with an improved ecological impact. The two-stage design process is explained, where a novel tool is used for early design decisions and a typical CAD/CAE process is used for detailed design. Finally, a life cycle assessment (LCA) compares the current door with the new door design.

## 2. Current design of a truck door

As a reference, a truck cabin door has been chosen from a truck manufacturer located in the Interreg Euregio Meuse-Rhine. The current design of this door was introduced in 2012. The door itself went into production in 2013. Since then, more than 370.000 trucks with this reference door have been sold worldwide. The cabin design at the time was considered aerodynamic and modern with a spacious interior [4] [5].

As a first step in the investigation of the current design, a thorough analysis was performed to obtain an indication of the physical properties of the reference door. The door has been dismantled, with all parts being weighed and measured in terms of dimensions. Furthermore from all parts, material, production method and service treatments have been investigated. The reference door is divided into four sub-assemblies: the sheet metal frame, the interior panel, the window elevator system and the door under-spoiler. The reference door is mainly composed of steel, ABS, polyester, tempered glass, rubber and bitumen as materials. Table 1 shows the weight breakdown. The door has an overall weight of 59,5 kg.

Table 1: Weight of the current truck door, split by material type

Material	Est. weight [kg]
Steel	24,1
Plastics (ABS, polyester)	11,8
Tempered glass	16,0
Miscellaneous (rubber, bitumen, etc.)	7,6
Total	59,5

A second step is the analysis of current functionalities and possible improvements towards improving the human machine interaction (HMI). The reference door is attached to the cabin via two hinge points, a lock and a door asset. In terms of functionalities, the reference door is equipped with a mechanical door handle and lock, an electrical operated mechanically window and electrically operated exterior mirrors.

## 3. Conceptual design

In a first step towards a new design, the first design change is to replace the steel panels by plastic panels. The idea is that this material change results in less weight. On the other hand, the imminent stiffness reduction needs to be compensated by a reinforcing structure. Therefore, the lower part of the door (below the waistline) is approximated by a plate structure, reinforced with beams. Based on a design methodology for computational design synthesis, the optimal position of these reinforcements is computed. Details of the design methodology are explained in [6]. An optimisation is set up to achieve a maximum stiffness for the loadcases of table 2. The design variables of the optimisation



problem are the possible start and end locations for the beams, as shown by the dots in Fig. 1 (left), and the number of beams. The cross section shape for the steel beams in this conceptual study is a solid square beam of 15x15 mm. Fig. 1 (right) shows the optimal conceptual design. This conceptual design is subsequently detailed in terms of material thicknesses in section 4.

Table 2: Loadcases (coordinate system according to Fig. 1 (left))

Loadcase	Constraints	Load dir & mag	Load location
Static-1	Door open	-Z 1000 N	handle
Static-2	Cabin tilted & door open	-Y $1000/\sqrt{2}$ N & -Z $1000/\sqrt{2}$ N	handle
Static-3	Door locked	-Y 300 N	handle
Static-4	Door locked & touching cabin on circumference	+Y 750 N	distributed
Modal	Touching cabin on circumference	n/a	n/a

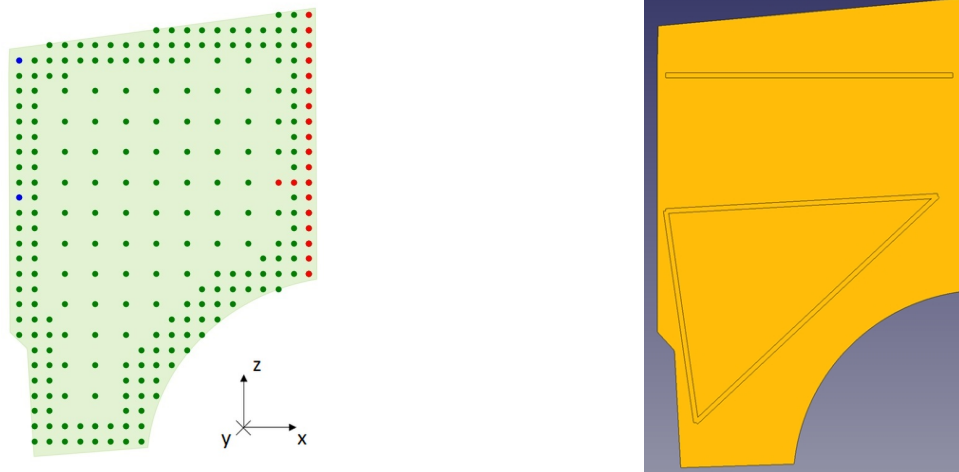


Figure 1: Conceptual design: possible reinforcement beam locations (left) and resulting design (right)

## 4. Detailed design and optimization

This section explains the steps and approximations to evolve from the conceptual design, through a detailed design (consisting of a CAD model and an FE model) to an FE-based optimization.

### 4.1 From conceptual design to detailed design

Based on the beam positions identified during the conceptual design, Fig. 2 shows the detailed 3D CAD drawing as conceived by an industrial designer and engineer. It consists of solid parts for the outer panel, the glass, the beams and the plastic inner panel. This drawing is converted into an FE model, where all parts are meshed using a 2D quad-based mesh. The steel beams are modelled with a hollow, square section which is compatible with a traditional extrusion process. Standard material properties were used for steel, glass and plastic (PE).

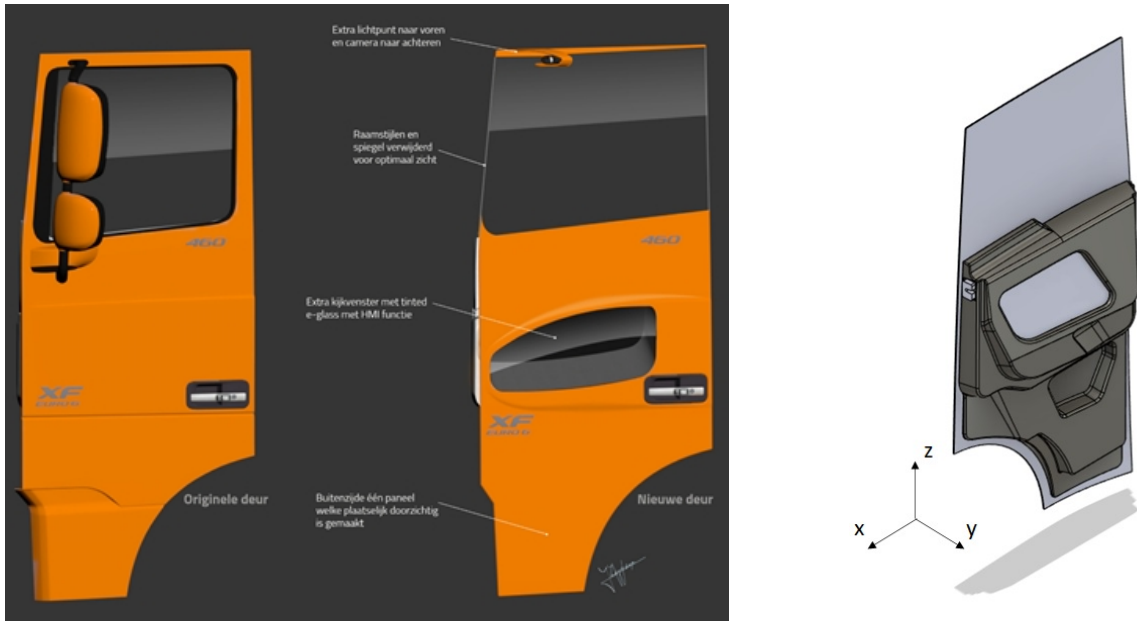


Figure 2: Design drawings of the reference and concept doors (left) and detailed CAD design (right)

## 4.2 Incorporation of new materials and production techniques

The inner part of the door consists of a plastic robomoulded structure. The material is a metallocene PE based material [7] with a skin-foam-skin construction, each skin having a thickness of 3 mm. Since no detailed material model exists, the material was approximated in the FE model by a standard PE material, which is sufficient for this design study. However, the density was adapted such that it depends on the thickness of the structure. The skin weight is  $1200 \text{ kg/m}^3$ , whereas the foam weight is  $120 \text{ kg/m}^3$ . Eq. 1 represents the material density  $\rho$  in  $\text{kg/m}^3$  related to the thicknesses  $t$  of the skins and foam, as to obtain the correct panel weight.

$$\rho = (1200 * t_{skins} + 120 * t_{foam}) / (t_{skins} + t_{foam}) \quad (1)$$

All shell meshes represent plate-like structures, except the mesh of the inner part, which encloses a volume. Consequently, the shell mesh is offset relative to the CAD surface by half the thickness. To accomodate for thicknesses that can be modified by the optimization of section 4.3, the shell offset of this part depends on the shell thickness.

## 4.3 Optimization

For the optimization of the design, the two most stringent loadcases were used: Static-2 & Modal from table 2. Table 3 shows the setup of the optimization problem. The Design Space Exploration module of the Simcenter 3D software [8] modifies the design variables in the corresponding FE model in order to find designs that fulfil the objective and constraints. The total mass of the truck door was used as an objective, whereas the CO2eq was calculated in post-processing based on the mass breakdown per material and on the LCA of section 5. Results show that these two attributes are heavily correlated, so the optimization result is not affected by choosing mass or CO2eq as objective.

Figure 3 shows the optimization results. The baseline design, based on the detailed design of section 4.1, is in red. The optimal design is in green. The dotted line represents the Pareto front. Relaxing the deformation constraint above 5 mm results in the purple design. The green and purple design exhibit a mass reduction of respectively 10 % and 12 % compared to the reference design. In terms of material breakdown (table 4, in comparison to table 1), the main material has shifted from steel to glass, and the relative presence of plastic has increased. The strength was verified by

comparing calculated stresses with their corresponding material yield stress, resulting in safety factors of at least 1,5. Other feasible designs easily reach the eigenfrequency constraint and are on or close to the Pareto front, which is a trade-off between stiffness on one hand and mass/CO<sub>2</sub>eq on the other hand. Mass and CO<sub>2</sub>eq are strongly correlated, so conclusions in that respect are interchangeable.

The green and purple design contain beams that are on the lower limit of the allowed thickness range. Designs where these beams are omitted, were checked but are not feasible in terms of stiffness, which highlights the value of the conceptual design phase of section 3.

Table 3: Setup of the optimization problem

	Design variable	Constraint	Objective
Top beam thickness	1 - 27 mm		
Tria beam thicknesses	1 - 6 mm		
Plastic thickness	6 - 23 mm		
Static-2 deformation		<5 mm	
First eigenfrequency		>50 Hz	
Mass			minimize

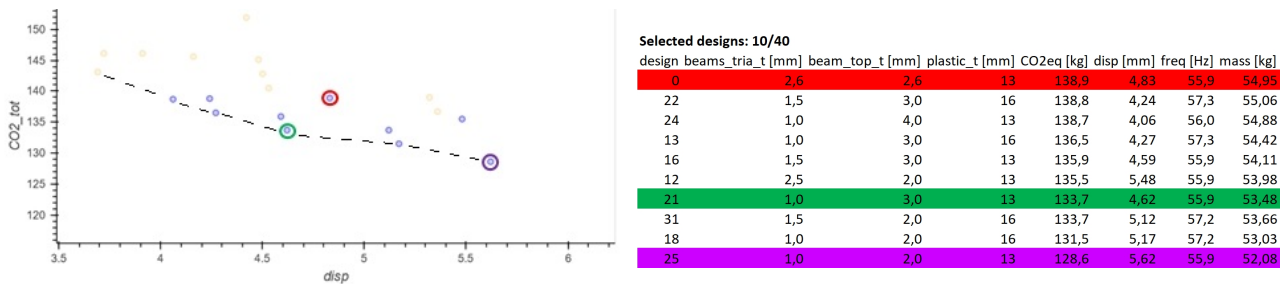


Figure 3: Feasible designs in the CO<sub>2</sub>eq-disp design space (left) and sorted by CO<sub>2</sub>eq (right)

Table 4: Weight of the redesigned truck door, split by material type

Material	Est. weight [kg]
Steel	4,1
Plastic (PE-based)	21,1
Tempered glass	26,9
Total	52,1

## 5. Life cycle assessment

To have a better understanding of the environmental impact of the door, a complete life cycle assessment (LCA) has been performed for the reference door. This LCA was done following the ISO 14040 [9] and ISO 14044 [10] standards and the ILCD recommendations [11]. The functional unit is a single door and the system boundaries only included raw materials, production and shaping.

Due to lack of data, the transport of the raw materials to the production site has not been included in this study. Nevertheless, some sensitivity analyses have been performed and show their small contribution on the overall impact. This study is done using the Environmental footprint method v1, focusing on the following impact categories: climate change, photochemical ozone formation, impact on human health (HH), respiratory inorganic effects, resource use, energy carriers, and mineral and metals. These indicators have been selected according to the goal of the study and after a detailed analysis of the results (including normalization and an EndPoint method). The data described in section 2 have been used for the inventory. The study is performed in Simapro using the ecoinvent v3.6 [12] database for background data. For the finishing process of painting, the data from Bianco et al [13] have been used and adapted to Simapro.

To support the optimization of section 4.3, table 5 shows the CO<sub>2</sub>eq contributions per kg of material. In the absence of data, the contribution for robomoulding is assumed similar to injection moulding.

Table 5: Climate change contribution by material type

Material	CO <sub>2</sub> -eq [kg] per kg of material
Steel (extruded)	3,60
Plastic (PE-based) (injection moulded)	2,99
Tempered glass	1,89

The detailed results for the complete door are presented in figure 4. Regarding climate change, the door construction leads to the emission of 159,5 kg CO<sub>2</sub>-eq, mostly related to the door frame, with a contribution of 74,8 kg CO<sub>2</sub>-eq. The contributions of the three other parts (main panel, window, and spoiler) are between 26 and 31 kg CO<sub>2</sub>-eq. Looking at the materials, most of the impact comes from the steel (56,7 kg CO<sub>2</sub>-eq), followed by the plastics (45,5 kg CO<sub>2</sub>-eq), the paint (34 kg CO<sub>2</sub>-eq) and finally the glass (19,8 kg CO<sub>2</sub>-eq). The parts contribution and its main material are accurate. The large contribution of the painting process can be seen, ranging from 10 % of the impact in the respiratory inorganics effects category to 20 % in climate change and energy use. The large contribution of the steel components is clear, with a total contribution from 20 % in energy use to 70 % in resources use. The differences in share between impact categories for the different steel materials is related to the different types of steel and to the different production processes, especially the large contribution of the spoiler part in resources is linked to its galvanization. The glass and ABS contributions are also non-negligible.

This analysis shows that a reduction of weight of the steel components would be the most pertinent path to reduce the environmental impact of the door production, which is in line with the optimization results of section 4.3. This reduction could also have a positive contribution on the use phase (out-of-scope of this study) by reducing the weight to transport. The large contribution of the finishing step (galvanization and painting) is also underlined.

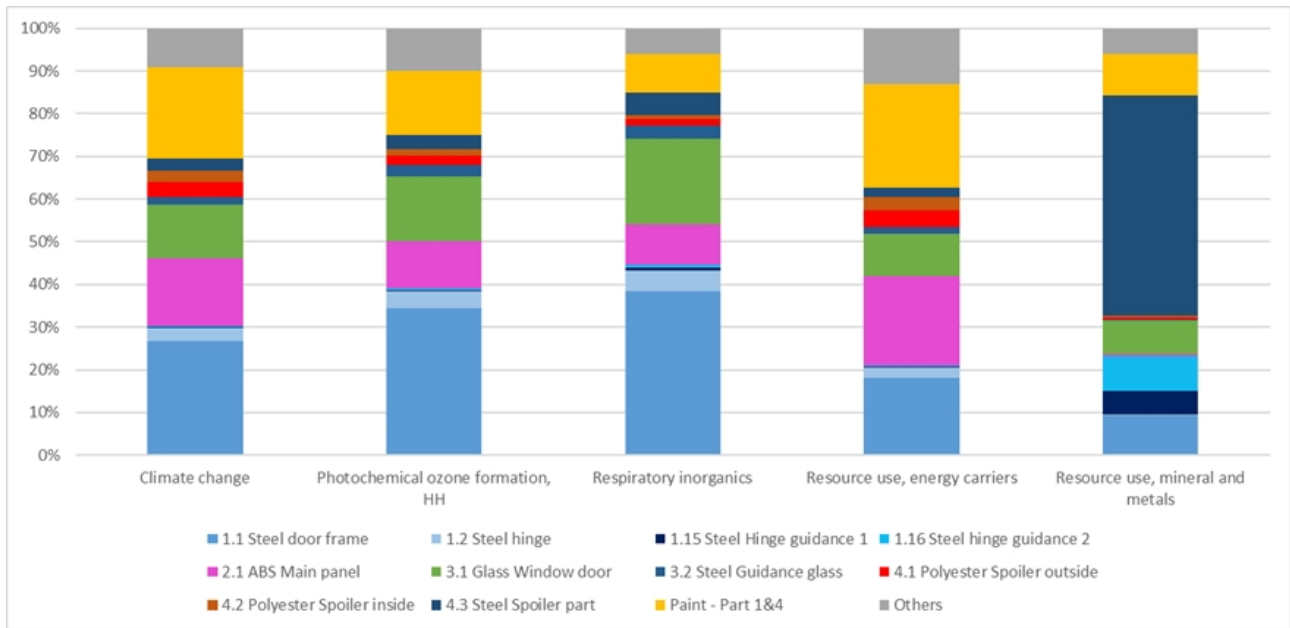


Figure 4: Results using Environmental footprint method v1 for a single truck door, conventional production: detailed analysis

## 6. Conclusion

This work showed the redesign of a truck door, based on material substitution (mainly steel by PE), functionality integration (HMI and optimised viewing angles), structural design optimization (in a conceptual design phase as well as a detailed design phase), design for novel production processes (robomoulding), while taken into account the environmental consequences (life cycle analysis). We have shown how design and optimisation methodologies can incorporate data for new materials and production processes. By keeping a close eye on the material breakdown, also a comparison in terms of environmental effects was made. Two proposed redesigns are able to achieve a weight reduction of at least 10 % and a reduction in CO<sub>2</sub>-eq of at least 4 %.

More extensive research on this topic might include an optimisation of the beam cross sections, the inclusion of crash loadcases, a complete LCA on the redesigned door, investigating the use of thinner glass and testing a physical prototype.

## 7. Acknowledgements

This research was partially supported by Flanders Make, the strategic research centre for the manufacturing industry. This paper is realized in the LightVehicle project (<https://www.lightvehicle2025.eu/>), which is funded by Interreg Euregio Meuse-Rhine and supported by the European Regional Development Fund. The Interreg V-A Euregio Meuse-Rhine (EMR) programme invests almost EUR 100 million in the development of the Interreg-region until 2020. This area stretches out from Leuven in the west to the borders of Cologne in the east, and runs from Eindhoven in the north all the way down to the border of Luxemburg. Over 5,5 million people live in this cross-border region, where the best of three countries merges into a truly European culture. With the investment of EU funds in Interreg projects, the European Union directly invests in the economic development, innovation, territorial development and social inclusion and education of this region.

## References

1. LIGHTer (Sweden, <https://lighter.nu/>) “Strategic research and innovation agenda for lightweight, 2019-2039”, 2021
2. G Koning, M. van Schijndel-de Nooij, F Willems, HTSM Automotive Roadmap 2020-2030, Holland High Tech, 2020, pp. 46, 48, 58.
3. J Heijster, Vision paper Automotive Manufacturing in the Netherlands, RAI Automotive Industry NL, June 2020, pp. 8, 10-14.
4. DAF, Mijlpalen in de geschiedenis van DAF. Retrieved at 14th of April 2021 from: <https://www.daf.nl/nl-nl/over-daf/history-of-daf/hoogtepunten-historie-daf?Page=2>
5. Truckstar, Praktijktest DAF XF 460 Euro 6 Space Cab. Retrieved at 14th of April 2021 from: <https://truckstar.nl/praktijktest-daf-xf-460-euro-6-space-cab/>
6. C. López, P. Eyckens, J. Stroobants, V. Iliopoulou, S. Jonckheere, B. Pluymers, W. Desmet, K. De Grave, J. Goos, A design methodology for engineering structures featuring automatic design concept generation by constraint programming and objective ranking by multi-attribute evaluation, High Performance and Optimum Design of Structures and Materials IV, WIT Transactions on The Built Environment 196 (2020) 193–204.
7. Total, Materials dedicated to robomoulding. Retrieved at 16th of April 2021 from: <https://www.polymers.total.com/markets/dedicated-rotomoulding>
8. Siemens Digital Industries Software, Simcenter 3D. Retrieved at 16th of April 2021 from: <https://www.plm.automation.siemens.com/global/en/products/simcenter/simcenter-3d.html>
9. ISO, ISO 14040 : Management environnemental - Analyse du cycle de vie - Principes et cadre, (2006).
10. ISO, ISO 14044 : Management environnemental - Analyse du cycle de vie - Exigences et lignes directrices, (2006).
11. European Commission - Joint Research Centre, Institute for Environment and Sustainability, International Reference Life Cycle Data System (ILCD) Handbook- Recommendations for Life Cycle Impact Assessment in the European context., 2011.
12. ecoinvent Center, The life cycle inventory data version 3, 2013.
13. I. Bianco, D. Panepinto, G.A. Blengini, M. Onofrio, M. Zanetti, Inventory and life cycle assessment of an Italian automotive painting process, Clean Technol. Environ. Policy. 22 (2020) 247-258. doi:10.1007/s10098-019-01780-3.

## Day 1: P04 – Driveline Aspects

Session P04 – Driveline Aspects, Monday 14 June

---

Session chairs: José Luis Olazagoitia and Eva Lundberg

- 14:20-14:30    **P04.A**  
*Methodology for the design of Stirling thermoacoustic engines based on the reactive power*  
Carmen Iniesta, Jaime Gros, José Luis Olazagoitia, Jordi Vinolas and Javier Aranceta
- 14:30-14:40    **P04.B**  
*Hydrogen powered trains challenges: normative constraints and operational assessment*  
Livia Maria Gandini, Stefano Ricci and Francesca Verrascina
- 14:40-14:50    **P04.C**  
*Product Cost Estimation in the early Development Phases – The Case of Powertrain Systems and Battery Packs*  
Simon Röhrenbacher, Oliver Moerth-Teo, Lukas Schwarz, Hans Schnöll and Christian Ramsauer
- 14:50-15:00    *Questions and Answers*
-

# Methodology for the design of Stirling thermoacoustic engines based on the reactive power.

Carmen Iniesta<sup>1</sup>, Jaime Gros<sup>1</sup>, José Luis Olazagoitia<sup>1,\*</sup>, Jordi Vinolas and Javier Aranceta<sup>1,2</sup>

<sup>1</sup>Nebrija University, Campus de la Dehesa de la Villa, Calle Pirineos, 55, 28040 Madrid, Spain

<sup>2</sup>CS Centro Stirling, S. Coop., Avda. Alava, 3 E-20550 Aretxabaleta-Guipúzcoa, Spain

\*Corresponding author. Email: jolazago@nebrija.es

The recovery of residual thermal energy is a critical issue in many industrial processes and engines. Stirling thermoacoustic engines are proving to have an interesting potential for recovering energy. The description of the internal physical phenomena to support the design process of these devices is far from simple. Conventional methods only consider so far, the flow of “active power” circulating, and do not pay attention to the “reactive power” that also flows through the system. This communication presents a simple methodology to analyse the energy flow (active and reactive power) for Stirling thermoacoustic engines. The results show that the amount of reactive acoustic power distributed towards the core branch is a good indicator of the grade of traveling-wave phasing. This new indicator can be used as an effective tool to design and study thermoacoustic devices.

© 2021 by the authors. Published by the Resource Efficient Vehicles Conference.  
This is an open access article under the CC BY license (<http://creativecommons.org/licenses/by/4.0/>).

## 1. Introduction

In view of the fact that road transport is one of the largest contributors to greenhouse gas (GHG) emissions in the EU, the regulation (EU) 2019/631 aims to reduce these emissions by setting limits for new passenger cars to make road transport cleaner and meet the EU’s greenhouse-gas-emission-reduction targets for 2021-2030 (by 30% compared to 2005) and to contribute to the goals of the Paris Agreement [1]. If manufacturers want to continue with the current model based on combustion vehicles, they must continue to support research and development of new technologies in every possible way to enable them to cope with the change.

The largest energy losses in a vehicle, almost 60%, are caused by heat dissipation from the exhaust system into the environment. Among the existing technologies for energy harvesting, it is worth highlighting: Organic Rankine Cycle (ORC) [2]; Turbo-Compound Technology (Mechanic [3] and electric [4] Turbo-Compound, TC and eTC); thermoelectric generators (TEG) [5] and Stirling type thermoacoustic engines (Thermoacoustic Stirling Like Cycle Engine, TA-SLiCE) [6].

Table 1 shows the virtual results for a complete car model corresponding to a study presented by Tenneco at the Vehicle Thermal Management Systems (VTMS) Congress [7]. The study evaluates and compares the amount of waste heat recovered by each technology and the type of energy generated, as well as its impact on fuel savings. Interestingly, it was found that there is no correlation between the amount of waste heat recovered and fuel savings.



Table 1: Comparative performance indicators for vehicle waste heat recovery technologies.

Technology	Energy collected in the exhaust [%]	Fuel savings [%]	Fuel savings vs. Energy harvested Ratio [%]
ORC	7	4	57
TC & eTC	19	1	5
TEG	2.5	0.7	28
TA-SLiCE	3.5	2.7	77

Fuel savings vs. Energy harvested Ratio data in Table 1, identifies TA-SLiCE to be the most promising technology in terms of efficiency and, at the same time, it is one of the technologies with the most options for innovation, given that it has not yet reached a high degree of maturity. This fact, leave room for improvement in TA-SLiCE's most significant limitation: it's low power density. Among the advantages of TA-SLiCE technology over the other technologies shown in Table 1, the most important are its simple configuration with almost no moving parts, making it particularly reliable, reducing low manufacturing and maintenance costs, and avoiding the use of damaging lubricants. Since they are external combustion engines, they can be powered by renewable thermal sources as well as thermal energy dissipated in other processes as is the case for the exhaust system of a vehicle combustion engine.

The convergence of the Stirling engine study with the development of thermoacoustic energy conversion is quite recent, with a history of only 40 years. Ceperley observed in 1979 that the flow paths of the working fluid molecules followed a sequence similar to that of the Stirling cycle. Since then, Backhaus and Swift presented the first thermoacoustic Stirling-like cycle engine (TA-SLiCE), based on travelling-wave phasing [8]. It became the latest evolution in conventional Stirling engines, dramatically simplifying their mechanics since the TA-SLiCE lacks pistons. Figure 1 shows the main components of a TA-SLiCE concept design.

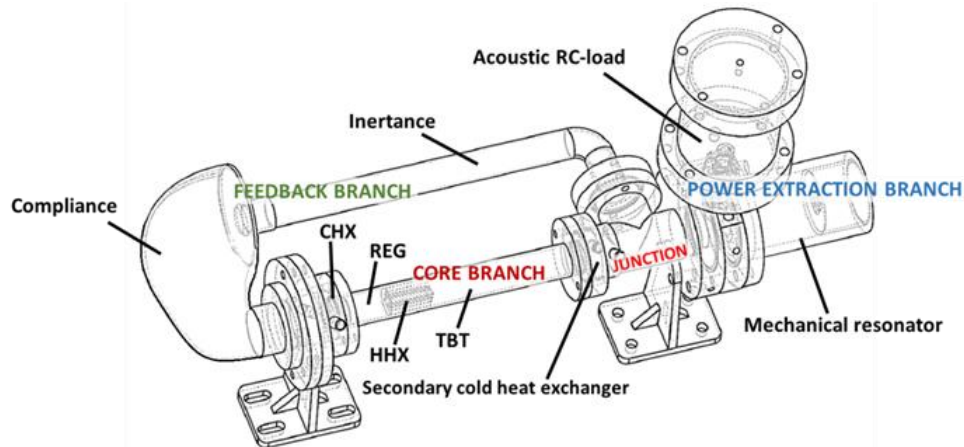


Figure 1: Diagram of the main components of a TA-SLiCE.

For the TA-SLiCE generator to work, a resonant passive acoustic circuit, consisting of a feedback branch (Compliance and inertance) and a resonating power extraction branch, is required to originate and maintain oscillations in a compressible fluid (gas) [9]. The acoustic circuit houses a set of key components for the thermoacoustic effect to take place, named the active core of the TA-SLiCE (a heater (HHX), a cold heat exchanger CHX and a regenerator (REG) interposed between them, in addition to the thermal buffer tube, TBT). On the other hand, the generated acoustic energy can be extracted using different types of electroacoustic transducers [10].

In contrast to the traditional Stirling engines the gas parcels into the regenerator experience the Stirling cycle at a microscopic scale inside the regenerator of a TA-SLiCE upon which a thermal gradient has been established. The work undergone by each of the gas parcels when completing a

whole Stirling cycle inside the regenerator results in amplification of the wave. In this way, the acoustic power at the output of the regenerator is amplified.

In a TA-SLiCE, the feedback branch design (compliance and inertance segments) is critical to the efficient integration of the travelling wave characteristic motion with the Stirling cycle performance.

The Design Environment for Low-Amplitude Thermoacoustic Energy Conversion software (DeltaEC) is the most widely used software for simulating TA-SLiCE technology. The conventional energy analysis of thermoacoustic devices made by DeltaEC models takes into account only the active power, based on the Rott linear theory published by Swift [11]. That approach considers that feedback inertances and compliances do not dissipate or produce acoustic energy, but simply transmit it by modifying the phase of the pressure  $p_1$  or the volumetric velocity rate  $U_1$  of the wave [11]. However, it is not always obvious, simply from the conventional analysis provided by the general theory, to intuitively define how the impedance of the components of the resonant network affects the pressure phasors  $p_1$  or volumetric velocity  $U_1$  by modifying their phase  $\phi_{pv}$  [12].

This paper captures the work done in theoretically modelling and simulating the operation of a TA-SLiCE concept from a methodology which considers the active and reactive acoustic power flows. This additional information is essential for the energy analysis to establish the TA-SLiCE design.

Section 2 describes the theoretical basis of the reactive acoustic power flow modelling of the conceptual TA-SLiCE design. Section 3 discusses the design of the TA-SLiCE demonstrator following the energetic methodology guideline. The most relevant conclusions and are made in section 4.

## 2. Design strategy

In this section is important to note that, when the amplified acoustic wave leaves the core branch, it has both a standing and a progressive contribution. This fact highlights the relevance of feedback for travelling wave adequacy at the input of the core branch. The methodology used in this paper proposes to take advantage of the information provided by the reactive acoustic power flow about the phase in which the wave arrives at the regenerator. The reactive acoustic power refers to the power that exists in a pure standing acoustic wave. The amount of reactive acoustic power delivered to the core branch varies depending on the dimensions of feedback branch compliance. When the feedback branch delivers less reactive acoustic power to the core branch, the wave arrives at the regenerator with a lower standing wave contribution, which means that the wave is closer to the desired progressive wave phase. Based on this analysis, the amount of reactive acoustic power distributed towards the core branch is a good indicator of the degree of travelling wave phase adequacy. Therefore, the reactive acoustic flow method leads to a straight and comprehensive design process for the resonant acoustic network of a TA-SLiCE.

### 2.1 Reactive acoustic power modelling

This section briefly introduces the description of the passive resonant acoustic network of the TA-SLiCE in terms of lumped elements on the basis of the linear theory [11]. Among the important electroacoustic analogies,  $p_1$  and  $U_1$  correspond to  $V_1$  and  $I_1$ , where  $V_1$  is the voltage, and  $I_1$  the current of the electric circuit.

The relationship between  $p_1$  and  $U_1$  is the acoustic impedance ( $Z_a$ ), and is analogous to the impedance ( $Z$ ) in an electric circuit [13]:

$$Z_a = p_1/U_1 = R_a + j(\omega L_a - 1/\omega C_a) \leftrightarrow Z = V_1/I_1 \quad (1)$$

$Z_a$  defines the resistive elements, inductive and capacitive waveguide to adapt the phase  $\phi_{pv}$ . At the acoustic networks, these elements are the acoustic resistance, the inertance and the compliance

(in electric circuits: resistance, coil, and capacitor, respectively). An acoustic resistor dissipates energy by viscosity and by thermal relaxation when it is crossed by the fluid. It acts as a resistance would in an analogous electric circuit. It always consumes (or absorbs) useful power. The resistive load is totally real (it has no imaginary part) as shown in Eq. (1). However, inductive and reactive loads are elements that delay or advance respectively the volumetric velocity phase with respect to the pressure one. Compliance introduces positive phase changes, i.e., it acts as a capacitive load and introduces a  $90^\circ$  phase change between  $|p_1|$  and  $|U_1|$  so that the volumetric velocity advances  $90^\circ$  with respect to the pressure. Inertance introduces negative phase changes, i.e., it acts as an inductive load that introduces a  $-90^\circ$  phase change between  $|p_1|$  and  $|U_1|$  so that the volumetric velocity is delayed by  $90^\circ$  with respect to the pressure. Both inertance and compliance are totally imaginary as seen in Eq. (1) and yield or absorb power according to the instant considered. The impedance, defined in Eq. (1), has a real resistive part and an imaginary capacitive and inductive part.

Considering Eq. (1), the total power of the inductance  $P_Z = V_1 \times I_1$  is a phasor that can be expressed graphically in the complex field as shown in Fig. 2.

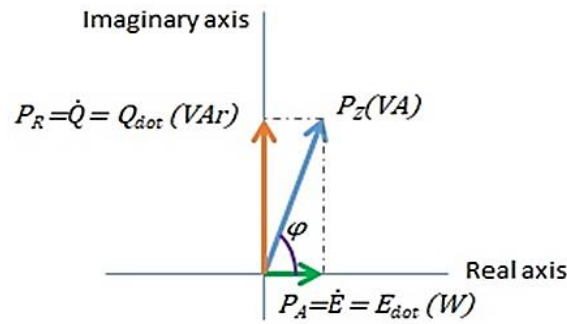


Figure 2: Representation of the total power  $P_Z$ , this can be broken down into active power on the real axis  $P_A$ , and into reactive power on the imaginary axis  $P_R$ .

Applying the electroacoustic analogy, the real part of the phasor  $P_Z$  is analogous to the active acoustic power flow. This variable averaged over an integral number of cycles, circulating in the  $x$  direction through a duct is given, according to the Rott approximation [11], by the second order expression:

$$\begin{aligned} \dot{E}(x) &= \frac{\omega}{2\pi} \oint p U dt = \text{Re} [p_1(x) e^{i\omega t}] \text{Re} [U_1(x) e^{i\omega t}] dt = \frac{1}{2} \text{Re}(\tilde{p}_1 U_1) = \frac{1}{2} \text{Re}(p_1 \tilde{U}_1) \\ &= \frac{1}{2} |p_1| |U_1| \cos \phi_{pU} \end{aligned} \quad (2)$$

The imaginary part of the  $P_Z$  phasor is analogous to the reactive acoustic power flow:

$$\dot{Q}(x) = \frac{1}{2} \text{Im}(\tilde{p}_1 U_1) = \frac{1}{2} |p_1| |U_1| \sin \phi_{pU} \quad (3)$$

where  $\phi_{pU}$  is the angle between the pressure  $p_1$  and the volumetric velocity  $U_1$  of the acoustic wave. Using the electroacoustic analogy again, it follows that  $\phi = \phi_{pU}$ .

The active acoustic power  $\dot{E}(x)$ , given by Eq. (2), represents the useful power since it is the only one that is transformed into work. The reactive power given by Eq. (3) is the one consumed by all the devices that have some type of coil or inductance. This type of energy only overloads any circuit, increasing the current (the volumetric velocity of the acoustic wave, by electro-acoustic analogy) that circulates through it, without producing work. When an AC receiver absorbs reactive power, this power is positive and when it gives up, it has a negative value. As the reactive power of any coil is positive, it can be said that all coils absorb reactive energy. Following the same reasoning, the reactive power of any capacitor is negative and, therefore, all capacitors supply reactive power.

## 2.2 TA-SLiCE DeltaEC reference model

The analysis of the active and reactive acoustic power flow distribution in a TA- SLiCE is necessarily carried out based on an initial DeltaEC model of that device. This section presents the numerical model corresponding to the reference feedback branch design. The parameters used for the model set up are those presented in Table 2.

Table 2: Main design parameters of the reference TA-SLiCE model.

Parameters		Values
<b>Operating conditions</b>		
Working gas		Air
Mean Pressure ( $p_m$ )		100 kPa
Operating frequency ( $f$ )		40 Hz
Mean gas temperature ( $T_m$ )		328 K
Estimated initial pressure amplitude ( $ p_1 $ )		5 kPa
<b>Core branch (CB)</b>		
Main cooler:	Length ( $L_{CHX}$ )	0.015 m
	Porosity ( $\phi_{CHX}$ )	60%
Regenerator:	Length ( $L_{REG}$ )	0.025 m
	Porosity ( $\phi_{REG}$ )	85%
	Hydraulic radius ( $r_{hREG}$ )	0.000184 m
Heater:	Length ( $L_{HHX}$ )	0.03 m
	Porosity ( $\phi_{HHX}$ )	60%
	Estimated thermal input power ( $\dot{Q}_H$ )	8 W
TBT:	Length ( $L_{TBT}$ )	0.085 m
	Cross-sectional area ( $A_{TBT}$ )	0.00025 m <sup>2</sup>
Secondary cooler:	Length ( $L_{SCHX}$ )	0.01 m
	Porosity ( $\phi_{SCHX}$ )	70%
<b>Reference Feedback Branch ("Fba")</b>		
Compliance:	Internal diameter ( $D_{Ca}$ )	0.02 m
	Length ( $L_{Ca}$ )*	0.41 m
	Volume ( $V_{Ca}$ )	129x10 <sup>-6</sup> m <sup>3</sup>
Inertance:	Internal diameter ( $D_{La}$ )	0.015 m
	Length ( $L_{La}$ )*	0.185 m

The DeltaEC software considers a thermoacoustic device as a one-dimensional set of connected segments, so that it always integrates all the governing equations for each of these segments. It solves the systems using a fourth order Runge-Kutta integration method and a guess-target approach, achieving convergence of the calculations. The accuracy of the virtual results obtained is given by the convergence tolerance parameter which, in all cases, satisfies a value less than 10<sup>-8</sup>.

### 2.3 Methodology guideline

The methodology for the TA-SLiCE design employed in this paper provides a comprehensive and easy-to-understand description of the phenomenon of progressive wave fitting due to the impedance of the acoustic network components. This is going to be illustrated by the following procedure: Based on the reference model, the dimensional parameters of the compliance are going to be modified twice to reduce the reactive power at the input of the active core. This modifications in the design, according to the established method, will lead to a more progressive acoustic wave.

The two compliance modifications give rise to three TA-SLiCE design models which share the set up summarized in Table 2, the difference between them is given by the dimensions of the feedback branch compliance:

*Reference model (feedback branch "Fba"):* A tube with 20 mm inside diameter used as compliance and another tube with 15 mm inside diameter is used for inertance.

*First design variation model (feedback branch "Fbb"):* By increasing the inside diameter of the compliance to 25 mm.

*Second design variation model (feedback branch "Fbc"):* By increasing again the inside diameter of the compliance to 66 mm.

The compliance depends on its volume in a similar way as the capacitance of a given capacitor depends on its geometry. Each model variation has supposed an increment of compliance volume, which in the equivalent AC circuit implies a proportional condenser capacity increase.

### 3. Results and discussion

The following paragraphs highlight the most important aspects of the analysis of the power flows and the modification of the feedback branch TA-SLiCE for the reference model, where the active and reactive acoustic power have been numerically calculated in the points labelled from 1 to 10.

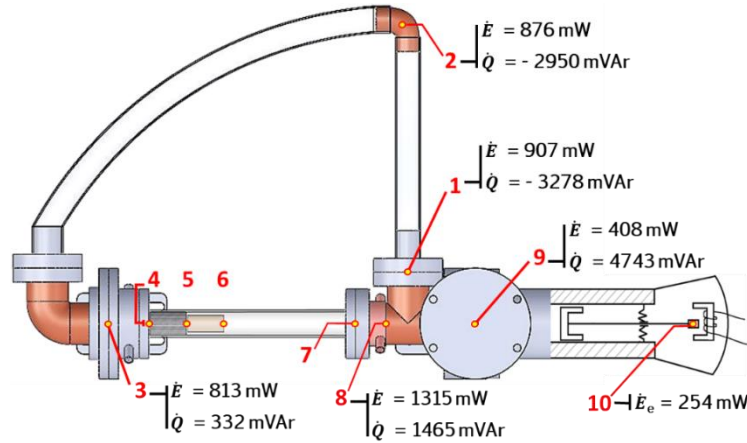


Figure 3: Diagram of the reference model TA-SLiCE with the "Fba" feedback branch. The distributions of active power flow  $\dot{E}$  and reactive power flow  $\dot{Q}$  are shown for the relevant points in the analysis. The numerically calculated electric power is also shown in point 10.

Once the acoustic power flows have been analysed in the reference model with "Fba" feedback (see Fig. 3), the system design can be modified. A trade-off strategy is employed between the loss of active acoustic power through the feedback branch and the delivery of reactive acoustic energy to the core branch. These requirements result in an increase in the inside diameter and a reduction in the length of the compliance for the "Fbb" feedback branch. These modifications result in an active acoustic power similar to that obtained with the feedback branch "Fba" and a lower reactive acoustic power flow to the core branch at point 3, as shown in Fig. 4.

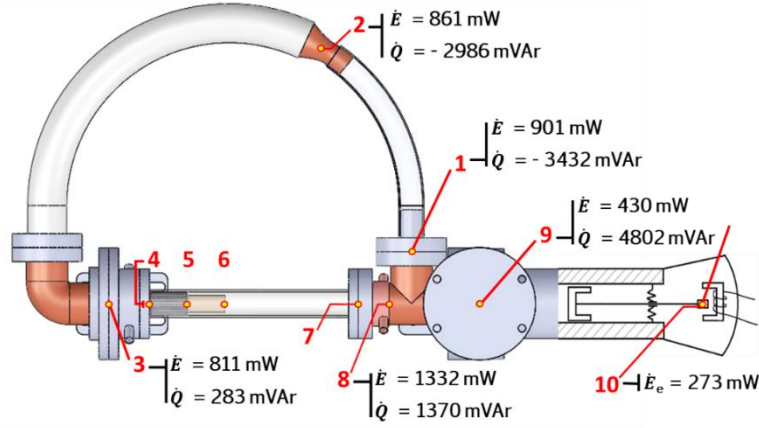


Figure 4: Diagram of the first design variation model with "Fbb" feedback branch.

When comparing the data in Figs. 3 and 4, the amplification of the active acoustic power through the core branch is slightly higher for feedback branch "Fbb" (813 to 1315 mW for "Fba" compared to "Fbb" from 811 to 1332 mW). For the "Fba" feedback branch shown in Fig. 3, the reactive acoustic power delivered to the core branch is high and the wave arrives with less travelling wave condition, compared to the results obtained for the "Fbb" configuration shown in Fig. 4 (332 mWAr for "Fba" versus 283 mWAr for "Fbb"). This means that, without the information of the reactive acoustic power flow, it is possible to select the "Fba" when it is not the best option. Thus, the knowledge of the reactive acoustic power flow provides a straight TA-SLiCE design criterion.

With the "Fbc" feedback branch, a second modification is made that brings further improvements to the performance of the system. This configuration shown in Fig. 5 has a much shorter compliance and a larger section, compared to the other two previous configurations ("Fba" and "Fbb").

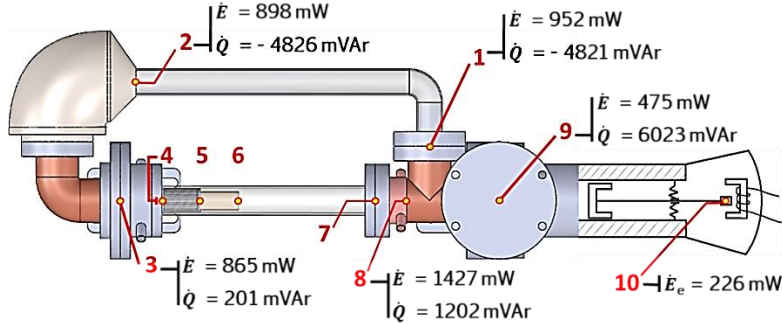


Figure 5: Diagram of the second design variation model improved with feedback branch "Fbc".

The comparative of the power flow distribution data from Figs. 4 and 5 shows that the active acoustic power is higher, and the reactive acoustic power is much lower (both calculated in point 3) for the feedback branch "Fbc" than for the feedback branch "Fbb" (865 mW/201 mWAr versus 811 mW/283 mWAr). This means that the "Fbc" feedback branch provides a more powerful wave while reaching the core branch with a better travelling wave condition.

When evaluating the results obtained for the reactive acoustic power calculated in point 3, it can be observed that the feedback branch "Fbc" distributes much less reactive acoustic power towards the core branch, indicating that the acoustic wave arrives at the regenerator with a more adjusted phase to the travelling wave condition compared to the other two feedback branch options. Furthermore, it follows that compliance should provide the minimum reactive acoustic power towards the core branch with the least active power loss. These requirements to improve the performance of the device using the reactive acoustic power flow method, suggest considering increasing the inside diameter and decreasing the length of the compliance, this leads to select a cavity type compliance with a section much larger than its length, instead of using duct type compliance, to achieve a similar volume.

## 4. Conclusions

The method of reactive acoustic power distribution significantly provides comprehension about the traveling-wave phasing, critical for efficient regenerator operation, and how various components of the feedback branch affect these properties. Numerical modelling of the demonstrator previously described is used to evaluate by comparing three feedback branch options. The effectiveness to distribute the reactive acoustic power, generated by the compliance, in order to favour adjusting of traveling-wave phasing is assessed for each of the three feedback branches under study. Besides, the presented method uses simply algebraic power sums, and it has not the need to handle complex phasor notation. This is analogous to the analysis carried out in an electric circuit, emphasizing the importance of the reactive power, in addition to the active power through each segment of the system.

## Acknowledgements

The authors thank the Global Nebrija-Santander Chair of Energy Recovery in Surface Transport for their financial support. This work was also supported by the Agencia Estatal de Investigación [grant RETOS 2018-RTI2018-095923-B-C22].

## References

1. EUR-Lex. Reduction in CO<sub>2</sub> emissions of new passenger cars and of new light commercial vehicles [Internet]. Summaries of EU Legislation. 2021. Available from: <https://eur-lex.europa.eu/legal-content/EN/TXT/?uri=LEGISSUM%3A4396542>
2. Kölsch B, Radulovic J. Utilisation of diesel engine waste heat by Organic Rankine Cycle. *Appl Therm Eng.* 2015 Mar;78:437–48.
3. Zhao R, Zhuge W, Zhang Y, Yin Y, Zhao Y, Chen Z. Parametric study of a turbocompound diesel engine based on an analytical model. *Energy.* 2016;115:435–45.
4. Pasini G, Lutzemberger G, Frigo S, Marelli S, Ceraolo M, Gentili R, Capobianco M. Evaluation of an electric turbo compound system for SI engines : A numerical approach. *Appl Energy.* 2016;162:527–40.
5. Kim TY, Kwak J, Kim B. Energy harvesting performance of hexagonal shaped thermoelectric generator for passenger vehicle applications: An experimental approach. *Energy Convers Manag.* 2018 Mar;160(January):14–21.
6. Sahoo D, Kotrba A, Steiner T, Swift G. Waste Heat Recovery for Light-Duty Truck Application Using ThermoAcoustic Converter Technology. *SAE Int J Engines.* 2017 Mar 28;10(2):196–202.
7. Uppuluri S, Khalane H, Naiknaware A, Sahoo D, Kotrba A. Exhaust Technologies in Support of LD and HD Reductions of GHGs and Criteria Pollutants. In: *Vehicle Thermal Management Systems Conference*. London, UK, 17-18 May; 2017. p. 127–40.
8. Backhaus S, Swift GW. A thermoacoustic-Stirling heat engine: Detailed study. *J Acoust Soc Am.* 2000 Jun;107(6):3148–66.
9. Yu Z, Jaworski AJ. Impact of acoustic impedance and flow resistance on the power output capacity of the regenerators in travelling-wave thermoacoustic engines. *Energy Convers Manag.* 2010;51(2):350–9.
10. Timmer MAG, de Blok K, van der Meer TH. Review on the conversion of thermoacoustic power into electricity. *J Acoust Soc Am.* 2018;143(2):841–857. DOI: 10.1121/1.5023395.
11. Swift GW. *Thermoacoustics: A Unifying Perspective for Some Engines and Refrigerators*. 2nd ed. Cham, Switzerland: ASA Press/Springer. ISBN:978-3-319-66932-8; 2017.
12. Hu ZJ, Li ZY, Li Q, Li Q. Evaluation of thermal efficiency and energy conversion of thermoacoustic Stirling engines. *Energy Convers Manag.* 2010;51(4):802–12.
13. Jin T. Preliminary Study on Circuit Simulation of Thermo Acoustic Engines. In: *AIP Conference Proceedings*. AIP; 2006. p. 1103–8.



---

# Hydrogen powered trains challenges: Normative constraints and operational assessment

Livia Maria Gandini<sup>1</sup>, Stefano Ricci<sup>1,\*</sup> and Francesca Verrascina<sup>1</sup>

<sup>1</sup>*Sapienza Università di Roma, DICEA, Via Eudossiana 18, 00184 Roma, Italy*

<sup>\*</sup>*Corresponding author. Email: stefano.ricci@uniroma1.it*

---

The use of hydrogen-powered propulsion in railways is very promising and already found relevant commercial applications. Some potential barriers emerged anyway as critical issues addressed by the scientific community, such as the hydrogen distribution and storage onboard: Hydrogen Refuelling Stations (HRS) and tankers has to fulfil safety criteria not yet consolidated in railway regulations and to manage effectively recharging time constraints. In this context, the present study, developed in cooperation with Trenitalia (Italian incumbent Railway Undertaking), focuses on two key aspects of the problem. The first is the identification of the existing normative constraints, at various levels, in the process to produce guidelines for the design of sustainable and harmonized safety rules based on systematic and robust risk analysis approach. The second is the comparative assessment of the present diesel powered operation on the case study of a not electrified line in Southern Italy with the radical solution of hydrogen-powered trains, without need of investments on overheads line and with a requirement of 800 km autonomy.

© 2021 by the authors. Published by the Resource Efficient Vehicles Conference.  
This is an open access article under the CC BY license (<http://creativecommons.org/licenses/by/4.0/>).

---

## 1. Introduction

Railways demonstrated to be the least polluting transport mode, thanks to electrification policies, which led to a major reduction in carbon fuel consumption. The extension of not electrified lines is anyway dramatically variable with top values of 90% and full electrification in Switzerland only. Electrification policies partly solved the problem of local polluting emissions and reduced the energy consumption thanks to the higher efficiency of the electric engines respect to the diesel. In this context, the use of hydrogen could be a valid alternative to the classical electrification, particularly in sensible areas and low traffic lines, where the related investment are not justified. Indeed, the use of Fuel Cell Electrical Vehicles (FCEV) is able to ensure a total limitation of gaseous and particulate emissions. The use of hydrogen-powered propulsion can anyway encounter a number of problems addressed by the scientific community, mainly in terms of hydrogen distribution and storage onboard. In particular, the design and the construction of Hydrogen Refuelling Stations (HRS) and tankers has to fulfil safety criteria not yet consolidated in railway regulations and to tackle recharging time constraints.



## 2. Perspectives for hydrogen-powered rail-based transport systems

In 2013, the European Commission announced a series of measures aimed at ensuring the development of the use of alternative energy sources, including electricity, hydrogen, biofuels, natural gas and liquefied petroleum gas (LPG) [1]. In this panorama the search for new solutions applicable to transport systems, capable of reducing greenhouse gas emissions, to comply with ambitious EU standards, the use of hydrogen-powered trains is an attractive alternative.

A specific recognized advantage of the train as a natural candidate for the use of these technologies, is the space available on board, larger than in road vehicles, and the operation of fleets on a territorial basis and with recurring use programs under the responsibility of individual operators. This feeds the disputes concerning the best solutions for replacing internal combustion traction, between the electrification of the lines and the use of solutions without fixed line systems. Hydrogen does not require the construction of an expensive electrical infrastructure, concentrating the investments mainly on rolling stock to achieve comparable performance in terms of gas and noise emissions.

The Coradia iLint, in operation in Germany, is the first train of its kind, equipped with fuel cells to convert hydrogen and oxygen into electricity, with a range of about 1000 km. This train is also equipped with batteries for the accumulation of energy recovered during braking and usable during acceleration. Beyond Germany, countries that are testing hydrogen trains or planning to do so in the near future are Austria, Canada, Denmark, France, Norway, Spain, UK and USA.

Hydrogen-powered Hydroflex trains are under tests in the UK since 2019, as part of the national plan to eliminate diesel traction by 2040 [2]. Furthermore, St. Andrew University in Scotland has started a project to convert a train consisting of three coaches into hydrogen as part of the Zero Emission Train project in collaboration with Scottish public and private enterprises. They look forward to presenting this technology at the United Nations Conference on Climate Change (COP 26) scheduled for December 2021. The decarbonisation goal of Scotland's railways is currently one of the most ambitious: the Scottish government hopes to eliminate related pollutant emissions to passenger transport by 2035. In Italy, the declared goal is to achieve Carbon Neutrality by 2050, as defined by the EU strategy and the hydrogen-based projects are an issue.

### 2.1 Present normative panorama

The focus is here the identification of the existing normative constraints, at various levels, in the process to produce guidelines for the design of sustainable and harmonized safety rules for hydrogen-powered rail-based transport systems. The purpose of the study is to provide the necessary support to identify a clear regulatory framework applicable to the introduction of hydrogen technology in the railway field and to present the risk assessment aimed at providing support to produce guidelines for the design of sustainable and harmonized safety rules based on systematic and robust risk analysis approach.

Already the Directive 2009/28/EC [3] establishes a common framework for the promotion of energy from renewable sources. It sets mandatory national general targets for the overall share of energy from renewable sources in gross final energy consumption and for the share of energy from renewable sources in transport (Article 3 and Part A of Annex I), as well as a legally binding target of 10% (energy content) for renewable energy in transport in 2020. Furthermore, it defines the role and scope of guarantees of origin of electricity, heat and cooling produced from renewable energy sources (Article 15).

More recently, the Directive for an Alternative Fuels Infrastructure (DAFI) of the European Parliament and of the Council (2014/94/EU) on the construction of an infrastructure for alternative fuels (including hydrogen), establishes a common framework of measures and minimum requirements in order to minimize dependence on oil and mitigate the environmental impact of transport. The transposition of this Directive was decisive for an opening towards hydrogen transport, such as a common technical specification for charging and refuelling points and

information requirements for users [4].

Moreover, a set of ISO international standards is in place to regulate the hydrogen production and use in transport systems applications [5] [6] [7] [8] [9] [10] [11] [12] (Figure 1).

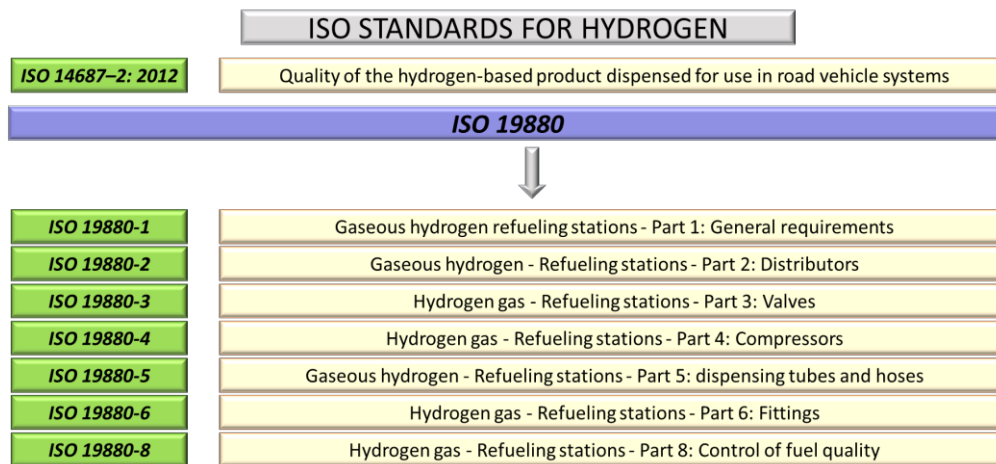


Figure 1: ISO standards dealing with production and use of hydrogen in transport systems

## 2.2 Approach to risk assessment in the use of hydrogen in transport systems

The world of transportation needs to find alternative solutions are able to meet the needs of the market for the production of reliable, high quality and affordable energy, while contemplating a reduction in harmful emissions to the environment. To achieve all this, as well as to ensure that transport systems closes the era of fossil fuels, it is necessary that they are and appear reliable and safe, as well as competitive on the market. In such a scenario, fuel cells are a very interesting technology offering great efficiency, negligible emissions and a wide range of applications. Though the costs are still high for the most part of them, it is certainly possible a significant reduction in prices. However, a fundamental element that could hinder the affirmation of these devices in the transport scenario is the perception of the risk in the use of hydrogen as a fuel.

Therefore, the present study is aiming to set up a methodology that makes it possible to assess the risk relating to hydrogen-powered vehicles. Central component of the study are hydrogen-powered fuel cells and, specifically, vehicles and infrastructures related to the use of hydrogen to generate electricity, basing on the main chemical and physical characteristics of hydrogen. Indeed, the main criticality found in the use of hydrogen as a fuel in transport systems consists of its low density, which provides for storage systems with significant safety-related implications.

Among the various methods for hydrogen storage, the most used technique is compression. Therefore, a typical refuelling station includes various safety-related aspects due to the risk of hydrogen leaks from various components of the structure, which could be easily under analysis by event-tree risk assessment methods.

Indeed the risk analysis is *the development of an estimate quantitative risk based on a technical assessment and mathematical techniques to combine estimates of the consequences of accidents and frequencies* [13]. In this context, it includes the description of the system and the identification of hazards that may arise from physical properties of substances and materials, temperature and pressure, as well as the processes themselves.

After the identification of hazards, the analysis of possible accidents includes the events that can aggravate the occurrence of the accident itself in terms of human injury, environmental damage and loss of production and equipment. For the identification of probabilities of events, references are reliable data published or estimated basing on recognized mathematical models. Meanwhile, the consequences estimation bases on statistics and simulated evolution of events

measured in terms of losses of human life and monetary cost. The combination of probability and consequences determines the risk.

Despite this robust approach, the public reactions to accidents are largely basing on the effects of media on the materialization of the population's opinions. Acceptable risk levels essentially depend on value judgments, not standardized by default. As an example, the amplified effects of the rare accidents involving trains or planes largely overpasses those of the many accidents involving cars and motorbikes, with which the population is generally more familiar and ready to accept their larger risks in change of the benefits brought by their daily use.

### 3 Comparative use of hydrogen-powered solutions on not electrified railways

In view of European restrictions requiring a 40% reduction in greenhouse gas emissions by 2030 (compared to 1990) and the target of a 90% reduction in emissions by 2050 [14] the need to eliminate the thermal propulsion in railway systems is self-evident. The hydrogen is one of the most promising solution to achieve effectively this target with reasonable times and investments. Therefore, the second part of the study is willing to assess this perspective on a real case study. The choice of the case study was for a line operated today exclusively by highly noisy and polluting diesel trains, where the assessed perspective is to employ hydrogen-powered trains. It is the Ionian line, located in Southern Italy, and particularly the section between Reggio Calabria Centrale and Catanzaro Lido for a total length of 177.5 km, with the only exception of the suburban section (29.8 km) between Reggio Calabria Centrale and Melito Porto Salvo.

Although electrification is an environmentally sound solution, it is a very expensive practice, which, according to [15] could cost in the range 1.0-1.4 Meuro/km, without taking into account local complications due to the interactions with urban or natural sensible environments.

For this reason, the proposed solution focuses on a possible radical alternative solution involving the use of hydrogen-powered vehicles.

### 4 Case study simulation

The energy study considers as a reference the four-coach train *Jazz* ETR 324, part of a wider family of electric trains built by Alstom Ferroviaria Spa. Table 1 shows the main characteristics used in the simulation.

Table 1: Main characteristics of ETR 324 [16]

Train parameters	Unit	Value
Max Speed	Km/h	160
Capacity	passengers	202 seats + 145 standing
Mass in service	t	168
Empty mass	t	136
Dimensions (L x W x H)	m	67.550 x 2.950 x 3.820
Power supply	kV	1.5-3.0 d.c.
Traction units	-	2

The aim of the study is to find the power required by the train under consideration and then the energy needed for the various phases of motion including 13 stops between Reggio di Calabria Centrale and Catanzaro Lido. This is the basis to estimate the approximate need of hydrogen required for the entire run and the possible economic advantage in addition to the environmental convenience of a fuel cell based operation.

Since the project does not envisage any changes to the infrastructure, the maximum design

speed of 130 km/h and the local limits currently imposed on the line are unchanged. The inputs for the calculation model are the traditional ones, namely traction/speed function of the train, Planimetry and profile of the line, affecting the operational performances in addition to the driving style adopted [17]. The coastal morphology of the line is quite flat with maximum slope of 10.4‰ and a corresponding moderate energy consumption of about 900 kWh for a single run between Reggio Calabria Centrale and Catanzaro Lido.

As far as the braking phase is concerned, the assumption of regenerative braking would allow great energy savings. The recovered energy, approximately calculated in 180 kWh (Figure 2), can recharge the accumulators used to energize the auxiliary services and to contribute to the high power requirements in the acceleration phases.

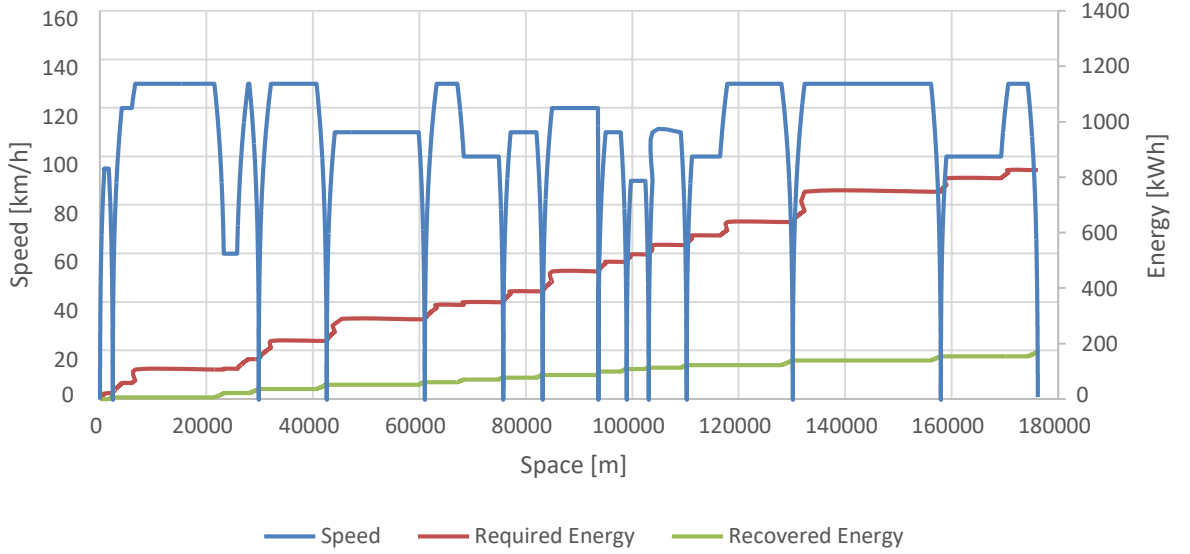


Figure 2: spatial variation of speed [km/h], required and recovered energy [kWh] along the Reggio Calabria – Catanzaro Lido section

The calculation of the required hydrogen starts from the power required, calculated as follows [18]:

$$P_{\text{required}} = P_{\text{el}} + P_{\text{aux}} \quad (1)$$

Where  $P_{\text{el}}$  is the electric traction power expressed by (2), equal to the ratio between the mechanical power ( $P_{\text{me}}$ ) and the efficiency (assumed 90%) during the acceleration phase and their product during the braking phase:

$$P_{\text{el}} = \begin{cases} \frac{P_{\text{me}}}{\eta} & \text{if } P_{\text{me}} \geq 0 \\ P_{\text{me}} * \eta & \text{if } P_{\text{me}} < 0 \end{cases} \quad (2)$$

However, for a more precise study, it is necessary to consider that  $P_{\text{aux}}$ , although constant for limited periods, varies according to the seasons and times of day, assuming a higher value during the winter or summer seasons and during the hottest or coldest time within the day, when the air conditioning system needs more.

As represented in Figure 2, the power is mainly below 400 kW and demands for higher values occur for short periods. Since sizing the fuel cells for such peak values would lead to an expensive and oversized system, a solution could be to size the fuel cells and calculate the amount of hydrogen required, taking into account the average value of the power demand, i.e. 475.4 kW, and cover the surplus power demand by the accumulators.

Considering the volumetric energy density of compressed hydrogen variable in the range 2.5-5.0 MJ/l and the efficiency of a fuel cell around 50% [19], the necessary quantity of hydrogen is estimable considering the capacity of the 700 bar hydrogen tank at 25°C equal to 0.039 kg/l. Therefore, the corresponding quantity of hydrogen required is approximately 48 kg.

Assuming a cost of hydrogen variable between in the range 2.50-6.80 \$/kg [20] and an intermediate value, optimistic in view of future expected costs reduction, of 3.50 \$/kg (2.90 Euro/kg), the approximate cost of hydrogen on the whole section (117.5 km) is about 138 Euro.

The economic viability in comparison with a diesel-powered train with the same performances, such as ETR 324, has to consider for this solution an energy density of approximately 35 MJ/l and an efficiency around 30% [21]. On this basis, the approximate resulting cost of the diesel fuel is about 226 Euro, about 64% more expensive than the hydrogen.

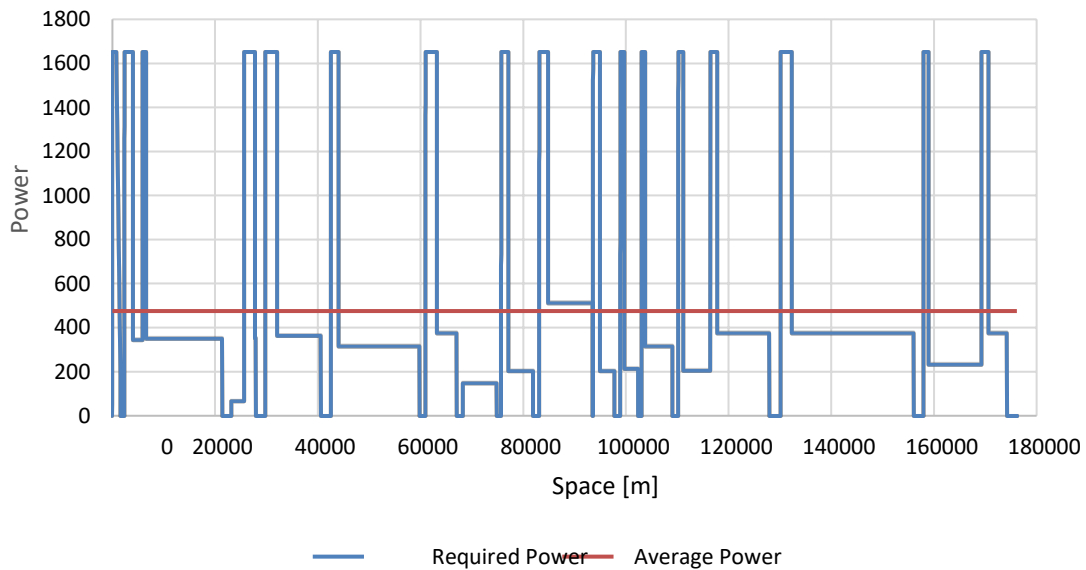


Figure 2: spatial variation of power demand and average power on the entire section towards Catanzaro Lido.

These estimated costs do not include fuel production, distribution and the modification of existing vehicles/purchase of new vehicles, etc. but the difference is relevant enough to ensure that an economic advantage, additional to the obvious environmental benefits, will be achievable.

Concerning the vehicle architecture, Figure 3 depicts a functional example of the hydrogen-powered train inspired by the Coradia iLint, where the hydrogen tanks and cells are on the roof of the vehicle in order to fulfil safety requirements. The energy exceeding the need from the fuel cells production and braking recovery is stored in battery packs that could be under the train bed, where also the inverter supplying the traction motor with the appropriate electrical power during accelerating and cruising phases and recovering kinetic energy under braking.

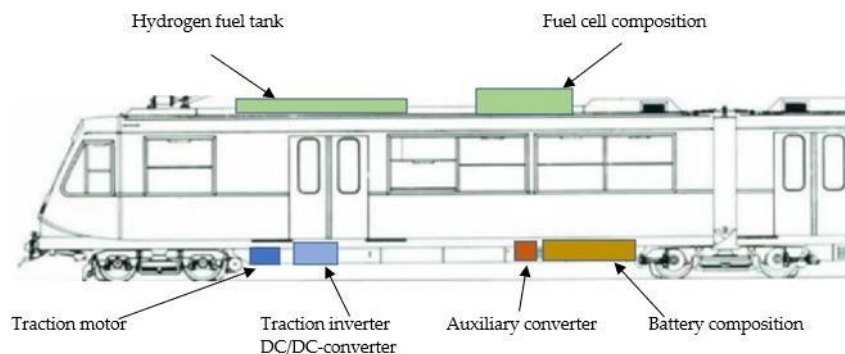


Figure 3: Schematic demonstration of a fuel cell train

## 5 Conclusions

This paper discusses the idea of upgrading old railway lines served by combustion engine trains, for which electrification work would be largely expensive, with new hydrogen-powered trains. The systematic application of the methodology demonstrated that, in specific conditions, considerable savings could be achievable. Far away from definitive conclusions, unjustified at the present implementation stage, the results encourage to orient in various directions the research concerning the potential application of hydrogen in rail transport systems. On one side, the next steps should be towards the development of simple and systematic regulatory framework basing on robust risk analysis approaches to prevent excessive restrictive constraints. On the other side, the most relevant need is to analyse the problem of the application fields of hydrogen-powered solution in a systemic vision, including, in addition to the vehicle itself, the production and distribution technical and operational open issue. At the present state of the knowledge, the competitive solutions for a cleaner operation on not electrified lines seems restricted to solution based on hydrogen and fast recharge of batteries during stops in stations. A key open issue, requiring a combination of technology and operation competences is to identify the most appropriate application fields for them, having in mind both long distance and urban-suburban systems, both related to the mobility of passengers but also, and maybe more, to the mobility of goods.

## References

1. European Commission - Clean energy for transport: a European strategy on alternative fuels – Brussels, 2013.
2. Hirschlag A. - Next stop, hydrogen-powered trains – BBC, 2020.
3. Directive 2009/28/EC of the European Parliament and of the Council of 23 April 2009 on the promotion of the use of energy from renewable sources and amending and subsequently repealing Directives 2001/77/EC and 2003/30/EC.
4. Directive 2014/94/EU of the European Parliament and of the Council on the Deployment of Alternative Fuels Infrastructure (DAFI).
5. ISO 14687-2:2012 Hydrogen fuel — Product specification — Part 2: Proton exchange membrane (PEM) fuel cell applications for road vehicles.
6. ISO 19880-1 Gaseous hydrogen fueling stations. Part 1: General requirements - ISO, 2020.
7. ISO 19880-2 Gaseous hydrogen fueling stations. Part 2: Dispensers - ISO, 2020.
8. ISO 19880-3: Gaseous hydrogen fuelling stations. Part 3: Valves - ISO, 2018.
9. ISO 19880-4: Gaseous hydrogen fueling stations. Part 4: Compressors - ISO, 1970.
10. ISO 19880-5: Gaseous hydrogen fuelling stations. Part 5: Dispenser hoses and hose assemblies - ISO, 2019.
11. ISO 19880-6: Gaseous hydrogen fueling stations. Part 6: Fittings – ISO, 2013.

12. ISO 19880-8: Gaseous hydrogen fuelling stations. Part 8: Fuel quality control – ISO, 2019.
13. Crowl D.A., Do Jo Y. - The hazards and risks of hydrogen, - 40th Annual Loss Prevention Symposium, AIChE Spring Natural Meeting, vol. 20, 337–349, 2006.
14. [https://ec.europa.eu/clima/policies/strategies/2050\\_en](https://ec.europa.eu/clima/policies/strategies/2050_en)
15. Fisher S. - Hydrogen rides the rails – ENI, 2020.
16. Ferrovie.it - Focus sugli ETR.324 ed ETR.425 – Approfondimenti, 2014.
17. Bruno F., Coviello N., Dalla Chiara B., Di Paola A., Pagliero P., Viktorov V. - The energy consumption of trains in operation: simulation, a methodology for the analysis and influence of the driving style - Ingegneria Ferroviaria, vol.4, 327-357, 2015.
18. Tian Z., Zhao N., Hillmansén S., Su S., Wen C. - Traction Power Substation Load Analysis with Various Train Operating Styles and Substation Fault Modes - Energies, 13, 2788, 2020
19. Wolf J. - Liquid-hydrogen technology for vehicles - MRS Bulletin, September 2002, 684-687.
20. Collins L. - Global news and intelligence for the Energy Transition, A wake-up call on green hydrogen: the amount of wind and solar needed is immense - Recharge, 2020.

---

# Product Cost Estimation in the early Development Phases – The Case of Powertrain Systems and Battery Packs

Simon Röhrenbacher<sup>1</sup>, Oliver Moerth-Teo<sup>1,\*</sup>, Lukas Schwarz<sup>1</sup>, Hans Schnöll<sup>1</sup>,  
Christian Ramsauer<sup>1</sup>

<sup>1</sup>*Institute of Innovation and Industrial Management, Graz University of Technology, Austria*

<sup>\*</sup>*Corresponding author. Email: [oliver.moerth@tugraz.at](mailto:oliver.moerth@tugraz.at)*

---

In the automotive industry, high competition, volatile markets and short development cycles are commonplace. In addition, the transition to new drive technologies brings further challenges and complexity for car manufacturers. Improved product cost estimation especially during the early development phases enhances design decisions to better address this situation. Due to the lack of data availability in this stage, exact calculations are very difficult and require a lot of experience. Even though various methods to estimate the product cost already exist, they usually vary greatly in accuracy and applicability. Therefore, the focus of this paper is to investigate different qualitative and quantitative product cost estimation methods in the early development phases.

First, a literature review provides the fundamental understanding about existing cost estimation methods. Aiming for a data triangulation, documents were collected, experts interviewed and a survey conducted, all at one engineering company dealing with powertrain development. Based on these three sources, two empirical studies were performed (study A: documents and interviews; study B: survey). A subsequent comparison allowed statements about the applicability of qualitative and quantitative cost estimation methods in the early development phases. Finally, two of these methods (case based and fuzzy logic) were applied at two different points in the early stage of battery pack development. In order to represent the increasing data availability when progressing in the development process, different parameters were included. While the reference data for the product cost estimation came from literature, the case company provided the input data for six battery packs of existing electric vehicles. This allowed a comparison of the estimated cost to the actual cost, whereas the calculation of derivations built the basis to evaluate the accuracy of the methods at both points.

© 2021 by the authors. Published by the Resource Efficient Vehicles Conference.  
This is an open access article under the CC BY license (<http://creativecommons.org/licenses/by/4.0/>).

---

## 1. Introduction

Estimating the product cost accurately represents a difficult challenge in general, but even more in case only little data is available as in the early development stage. Improving decision making, an appropriate product cost estimation is essential to deal with increasing market competition, shortening development cycles and general market volatility. This is especially true in the automotive industry, typically characterised by large and complex projects. However, with the shift to new eco-friendly technologies and a great attention of customers on topics such as sustainability, estimating the future vehicle cost has become more challenging for car manufacturers. While cars with internal combustion engines have been produced for many decades, new automotive trends such as electrification appeared rather suddenly and caused a quick shift to new technologies, resulting in a lack of experience and a lot of uncertainties [1, 2].



Product cost comprises all financial resources used for development, production and distribution. Important decisions need to be made during the development phase, whereas future production and distribution cost should be considered. The high relevance of these early decisions is illustrated in Figure 1. While decisions during product development already cause high cost commitments, most of the actual costs are incurred much later. Therefore, Ehrlenspiel and Meerkamm (2013) express the significance of systematic development approaches to effectively realize benefits such as product cost minimization [3]. An appropriate pre-calculation of the product cost in the early development phase is consequently highly relevant.

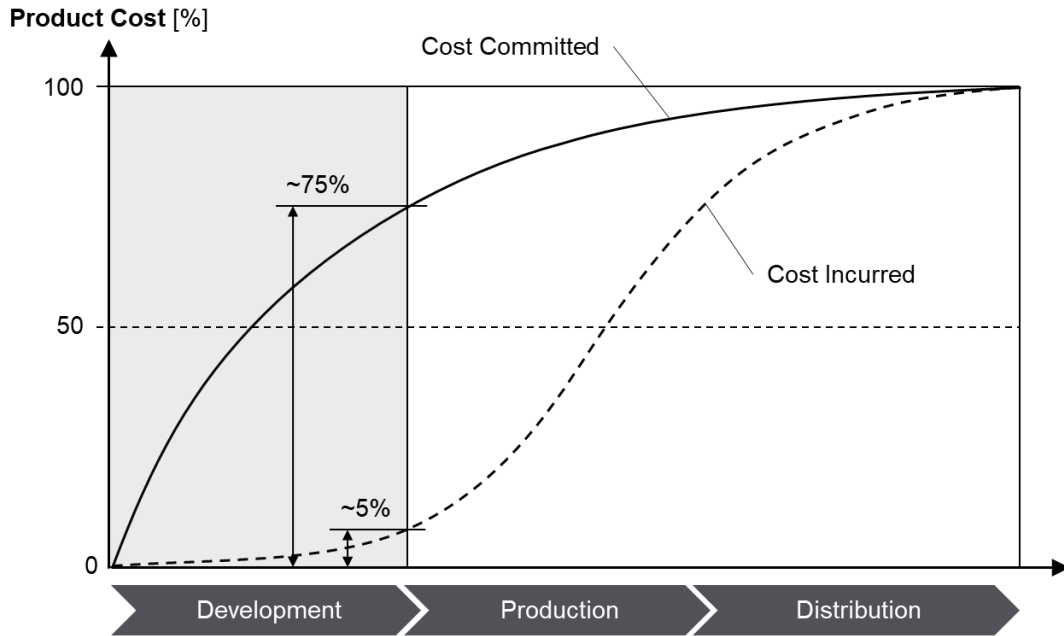


Figure 1: Impact on Product Cost [adapted from 3]

Schlink (2015) stated different principles for preliminary cost calculations during the development process. The basic approach of each method is identifying the main cost influencing factors. For example, the predicted used materials or the predicted weight of the product. Another approach is to identify certain performance parameters of the future product. The appropriate selection of a method depends on three aspects: the properties of the project, the experience of the developing company and the time of the project [4]. Lindemann et al. (2014) summarized the problem of early cost recognition such as that a company already wants to know the future cost when hardly having information about the product. They suggest a cost tracking on basis of the whole product or on single systems and elements. While some of the elements are purchased from suppliers, other parts might be produced in-house. Sometimes, the costs can also be derived from reference projects. The decisive factor for the accuracy of a calculation mainly depends on its purpose. In case of a quotation costing, the result must be very accurate. If the price is set too high, the customer will not order the product and if it is too low, the company will lose money. On the other hand, for a comparison of variants, the results simply need to be accurate enough to enable clear decisions and selections between them. Any higher accuracy only means an unnecessary use of resources [5, 6].

The previous statements underline that an appropriate product cost estimation in the early development phases might be crucial for a company to remain competitive. The literature provides several different qualitative and quantitative methods for such product cost estimations, whereas a specific group is investigated in the next section of this paper. On the basis of a powertrain development process, the applicability of different product cost estimation methods in the early development phases is subsequently evaluated. Finally, two of these methods are applied at two different points in the early stage of battery pack development.

## 2. Theoretical Basis

Based on the purpose of building a common base to different actors, a product development process also enables continuous tracking of the progress, detecting deviations from chosen targets and avoiding mistakes by integrating the lessons learned of previous projects. Developing a powertrain system, it is crucial to consider all interfaces between the involved systems, upwards to the whole vehicle and downwards to the elements. An entire vehicle can be divided into several systems, such as a powertrain or chassis, whereas these systems consist again of many elements, such as a battery pack or transmission [7]. Typically, a powertrain development process is structured in phases, Q-gates and milestones, starting with innovation or concept activities and ending with the start of production (SOP) [8].

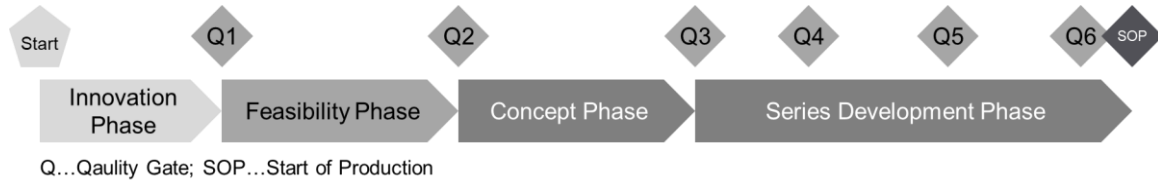


Figure 2: General Powertrain Development Process with Example Quality Gates [adapted from 7]

Figure 2 shows a general powertrain development process, whereas the innovation, feasibility and concept phase are part of the early stage [7]. The product cost is mainly set during the development by aspects like the product design, the production processes and the production location [4].

There are different characteristics of cost models. The applicability characteristic describes the state of the system. While predicting future cost is usually the aim in the early project phase, the estimation of already incurred cost might be the focus of a later stage. In contrast, the granularity level characterizes the “direction” of the cost model. The third characteristic relates to two approach types: qualitative and quantitative [9]. These qualitative and the quantitative methods can be further divided as illustrated in Figure 3. The included methods for estimating the cost of a new product can also be structured in four levels. Differing between qualitative and quantitative approaches represents the first level. In the second level, they can be further split into intuitive, analogical, parametric and analytical techniques. The third level already provides specific methods, whereas only decision support techniques also include a fourth level [10].

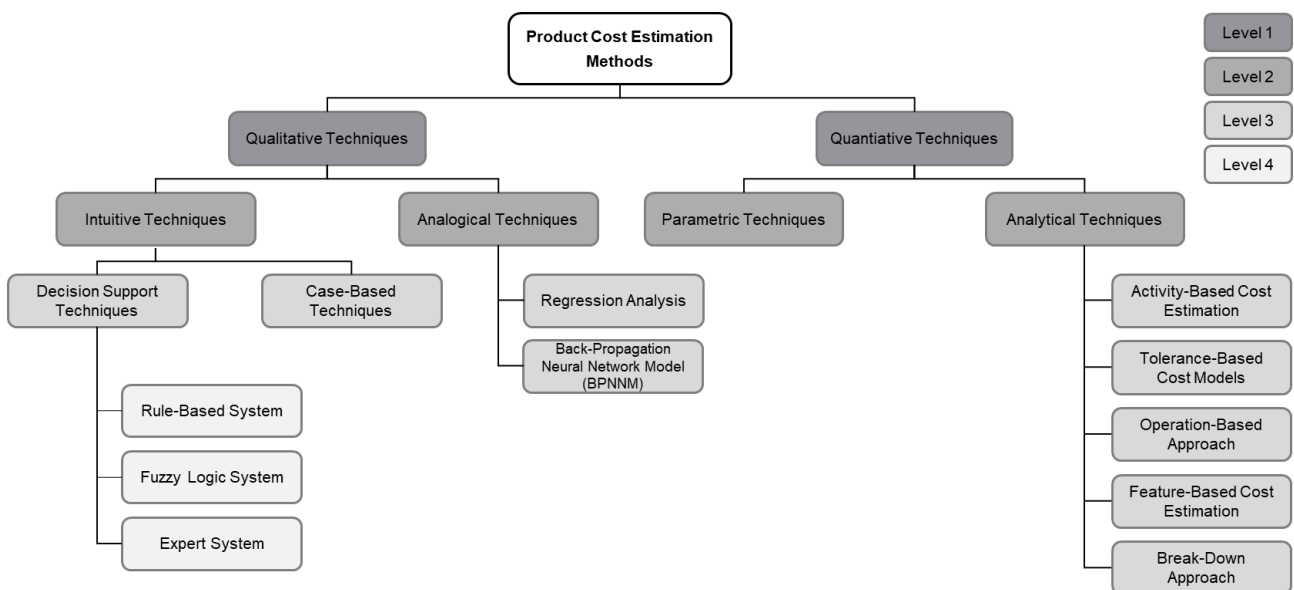


Figure 3: Classification of Product Cost Estimation methods [adapted from 10]

Table 1 provides brief descriptions of each product cost estimation method from Figure 3.

Table 1: Descriptions of available Product Cost Estimation methods [10]

#	Title	Description
1	Rule Based System	Based on design/manufacturing constraints which are reflected as IF-THEN rules
2	Fuzzy Logic System	Based on a decision table with IF-THEN rules. Handles uncertainties of variables through linguistic expressions (low/med/high)
3	Expert System	Based on experts' knowledge to a specific topic that is transferred through a rule-based programming into a knowledge database
4	Case Based Technique	Based on the idea that similar product characteristics cause similar cost
5	Regression Analysis Model	Based on historical cost data, aiming to establish a linear relationship between cost of past and current values of design variables
6	Neural Networks	A neural network is a type of artificial intelligence which is able to processes big data amounts to extract valuable information
7	Parametric Techniques	Based on applying statistical methodologies, aiming to express product cost as a function of its main cost drivers
8	Activity Based Approach	Based on performed activities to manufacture a product
9	Operation Based Approach	Based on the sum of the cost associated with production times, non-productive times and setup times
10	Tolerance Based Approach	Based on design tolerances. Different design variables are linked to manufacturing processes and further to costs
11	Feature Based Approach	Based on identifying the product's cost driving features for determining their associated costs. (design, process planning, manufacturing processes)
12	Break Down Approach	All cost that arise during a product lifecycle are summed up. Comparable with Lifecycle Costing

### 3. Empirical Studies

The data acquisition is based on an engineering company dealing with the development, simulation and testing of powertrain systems for different kinds of vehicles. A single case design was chosen due to the uniqueness of the case [11] as well as the opportunity for a greater depth of investigation [12]. Aiming for a data triangulation [13], the first step was collecting documents. The typically used powertrain and battery development processes provided information about data availability in the different early phases. Subsequently, four semi-structured interviews with individual experts of the case company were conducted to gain practical knowledge. Merging the extracted data from the documents with the expert knowledge from the interviews represents study A. Based on the information from these two sources, the authors qualitatively assessed the applicability of the twelve qualitative and quantitative product cost estimation methods in the early development phases. Additionally, a survey was conducted in the department "Production & Cost Engineering" of the partner company, representing study B. The aim was to assess the costing approaches regarding their complexity and accuracy in the same early phases of powertrain and battery development. The seven participants therefore rated the complexity and accuracy of each cost estimation method separately from one to four, whereas "one" stood for high complexity or low accuracy, and "four" for low complexity or high accuracy. The applicability value was calculated through Formula 1, and in case it was greater than the threshold value of 2, the product cost estimation method was assumed to be applicable.

$$Applicability = \frac{Accuracy}{Complexity}$$

Formula 1: Calculation of the Applicability Value in Study B

## Comparison of Study A & B

In the following section, the results of the two studies A & B are compared. Table 2 shows the applicability of each method in the three defined early development phases. While a letter “A” indicates an applicability according to study A, a letter “B” means the same for study B. “A & B” represents an assumed applicability in both studies, whereas “NA” means that it was neither in study A nor in study B seen applicable.

Table 2: Applicability of the Product Cost Estimation methods based on Study A & B

			Early Development Phases		
			Innovation Phase	Feasibility Phase	Concept Phase
Product Cost Estimation Methods	Qualitative Methods	Rule Based	A	A	A & B
		Fuzzy Logic	A	A	A
		Expert	A & B	A & B	A & B
		Case Based	A & B	A & B	A & B
		Regression Analysis	A & B	A & B	A & B
		Neural Networks	A & B	A & B	A & B
	Quantitative Methods	Parametric	B	B	B
		Activity Based	NA	B	B
		Operation Based	NA	B	NA
		Tolerance Based	A	A	A
		Feature Based	A	A	A
		Break Down	B	B	B

Starting with the innovation phase, qualitative methods are mainly rated applicable in both studies. On the other hand, quantitative methods are only partially applicable with limitations, for example on specific components. The results for qualitative methods are identic in the feasibility phase, while the results of the quantitative methods also show only a partial applicability. The manufacturing related methods such as the operation based and break down method are not favourable due to the lack of information caused by a low project maturity. Moving to the concept phase, qualitative approaches still show the highest applicability and manufacturing related methods the lowest. The results indicate that the maturity of quantitative methods provides little applicability during the early development phases, whereas the lack of required input data can be stated as reasonable explanation. Furthermore, the results of study A and study B demonstrate big differences within the group of quantitative methods. On the other hand, qualitative methods that strongly rely on experience and need less quantitative data mainly show a rather high applicability throughout the entire early stage.

## 4. Practical Application

Two of the investigated qualitative methods, case based and fuzzy logic, were also applied to estimate the product cost of the powertrain element “battery back”. They were selected due to their high relevance mentioned in literature. On the other hand, the battery pack was chosen as this technology is rather new and shows high relevance in the future of the automotive industry [2]. Furthermore, sufficient reference and input data is available. As seen in Figure 4, the methods were applied at two points in the early stage of the development process to enable a comparison.



Figure 4: Application of two Product Cost Estimation methods at Point A and B

In order to represent the lack of available input data at point A (innovation phase), only information about the two parameters “annual pack production” (strongly determining production resources), and the “vehicle range” (correlating with total battery pack energy capacity), was included. As the available data increases with progressing in the development process, at point B (feasibility phase) was also information about two the additional parameters “total pack mass” (correlating with amount of used materials) and the “number of cells” (affecting the battery power and used electrode materials) included. The output variable was stated as “Total Battery Pack Cost to OEM in €”. The reference data used in the methods came from the report “BatPaC – modelling the performance and costs of lithium-ion batteries for electric-drive vehicles”, which was created by the Argonne National Laboratory [14]. In contrast, the case company provided the input data for six battery packs of existing electric vehicles to perform six cost estimations. Additionally, also the cost of these six battery packs calculated by the engineering company were provided. As these calculations are based on highly detailed data from benchmark studies, their results were assumed as actual costs. The comparison of the six estimated battery pack costs in the early development stage with the related actual costs enabled the calculation of derivations, building the basis to evaluate the accuracy of the two methods at point A and B.

### Application of the Case Based Method

The purpose of this method is to compare a new “case” with existing reference “cases” to find similarities, based on the idea that similar product characteristics cause similar cost [10]. Therefore, it is important to systematically arrange the relevant information of the reference cases in a database. Even though this sounds quite obvious, in practice it is often not executed appropriately and consistently enough. Such databases need continuous maintenance and must be regularly updated. However, this effort ideally results in a quite strong support for cost engineering departments [9]. For this paper, the gathered data from the “BatPaC” was arranged into seven cases using a “Microsoft Office Excel” document as database. An input mask for the four chosen parameter was also created. In order to ensure a quick and simple application of the tool, the best fitting cases were highlighted. Therefore, cost engineers can directly see the cases with the closest values and decide which one to choose as final reference for the new project.

### Application of the Fuzzy Logic Method

Its purpose is to handle uncertain knowledge with linguistic expressions by connecting input variables to output variables through IF-THEN rules. For this application, the two input variables of point A and the four input variables of point B were connected to the single output variable. An actual tool was created using the “Fuzzy Logic Designer” provided by Mathworks Matlab. Having identified all input and output variables as first step, the next includes the creation of membership functions (MFs) to all variables. A MF defines the fuzziness of the variables and outlines the degree of membership, and therefore describes the belonging of a value to a function. In general, every variable is described through linguistic expressions. An example would be, “if the tomato is red, it is ripe”. But what if the tomato is not totally red and still has some green spots? In cases a decision with 0 or 1 is not fully clear or possible, the application of a fuzzy logic system is preferred as it is able to describe such situations [15]. There are many different ways to create membership functions. After intensive investigations of the topic “fuzzy logic systems”, the authors decided to take an “Intuition” approach using triangular MF. This decision was mainly based on the little data available, as most of

the other approaches need bigger datasets. Furthermore, it is also easier to use by non-experts compared to the others. It was assumed that the variables have a linear relation, hence the triangular shape [16, 17]. For the actually created fuzzy logic system, a base of 81 IF-THEN rules was created to connect the input variables with the output variable.

## Comparison of Results

In general, the bigger the reference database for case-based cost estimations, the higher the probability to obtain more accurate results. Using only two input parameters resulted in an average deviation of around 30% at point A. Increasing the number of included parameters to four at point B also caused a reduction of the deviation to around 12%. As expected, the small database comprising only seven reference cases and the low amount of input parameters provided a rather low accuracy of the product cost estimation. Nevertheless, the values at point B could already be used by cost engineers for a quick and simple project evaluation. Taking a look at the fuzzy logic system, achieving very accurate results also needs much more reference and input data as well as deeper expert knowledge and experience regarding the single variables. In point A, the average deviation of the cost was around 16%. This could already be used for a first assessment of the project. In point B, the deviation shows results similar to the case based cost estimation with around 12%.

Comparing both methods at both points, it is obvious that more input data also led to more accurate results. While both methods show a similar deviation at point B, the results of the fuzzy logic cost estimation provided a much higher accuracy at point A. However, realizing a fuzzy logic system also requires more effort. It can be concluded that for an accurate product cost estimation of complex systems such as a powertrain or battery pack, broader reference data and more than just four input parameters are greatly required. Nevertheless, the applications showed their potential and provided also with less data acceptable results. Therefore, both methods are assumed to be a supportive tool for cost engineers in the early phases of developing a powertrain or related elements.

Table 2: Comparison of Case Based & Fuzzy Logic System

	Point A			Point B		
	Average	Max	Min	Average	Max	Min
<b>Case Based System</b>	+/-30 %	-54 %	+28 %	+/-12 %	-38 %	-8 %
<b>Fuzzy Logic Sstem</b>	+/-16 %	+40 %	-18 %	+/-12 %	-27 %	-6 %

## 5. Discussion and Conclusion

An appropriate product cost estimation in the early development phases is essential for automotive companies to remain competitive. While the literature already provides several qualitative and quantitative methods, the applicability of twelve was evaluated in the innovation, feasibility and concept phase. Based on data from one engineering company, two empirical studies were therefore performed (study A: documents and interviews; study B: survey). The results indicate that the maturity of quantitative methods provides little applicability, whereas the lack of required input data can be stated as reasonable explanation. On the other hand, qualitative methods that strongly rely on experience mainly show a rather high applicability throughout all early development phases. The application of a hybrid approach could allow combining the advantages of both types. However, only assumptions can be mentioned at this point and further research for a clear statement is still necessary.

Finally, two of these methods (case based and fuzzy logic) were applied at two different points in the early stage of battery pack development. While the reference data came from literature, the case company provided the input data for six battery packs of existing electric vehicles. This allowed a comparison of the estimated cost to the actual cost. Basically it can be stated that more input data also led to more accurate results. Even though the outcomes provided a broad range of deviations, some might be already acceptable for quick and simple project evaluations. Therefore, both methods are

assumed to be a supportive tool for cost engineers in the early phases of developing a powertrain system or related elements such as battery packs.

This work represents a basis for future investigations into the topic of product cost estimation in the early development phases. Further research regarding main cost drivers is essential to simplify the process while increase the accuracy of its results. This should always happen in accordance to data availability to ensure the applicability of methods in the early development stage.

## Acknowledgements

This work has been conducted as part of the research project P2-Opti (Product- and production optimization covering the entire automotive powertrain lifecycle). Sincere thanks to the Austrian Research Promotion Agency (FFG) for the project funding.

## References

1. S. Volker, G. Prosteian, Research of Automotive Change Management and Combined Management Models, 13<sup>th</sup> International Symposium in Management, 2015, pp. 395-396.
2. Roland Berger & Lazard, Global Automotive Supplier Study 2018, 2017, available at <https://www.rolandberger.com/en/Insights/Publications/Global-Automotive-Supplier-Study-2018.html>.
3. K. Ehrlenspiel, H. Meerkamm, Integrierte Produktentwicklung - Denkabläufe, Methodeneinsatz, Zusammenarbeit, Carl Hanser Verlag, Germany, 2013.
4. H. Schlink, Wirtschaftlichkeitsrechnung für Ingenieure, Springer, Germany, 2015.
5. U. Lindemann, K. Ehrlenspiel, A. Kiewert, M. Mörtl, Kostengünstig Entwickeln und Konstruieren – Kostenmanagement bei der integrierten Produktentwicklung, Springer, Germany, 2014.
6. U. Lindemann, Handbuch Produktentwicklung, Carl Hanser Verlag, Germany, 2016.
7. P. Kranabittl, M. Bajzek, M. Atzwanger, D. Schenk, H. Hick, Automotive Development Process - Systems Engineering for Automotive Powertrain Development, Springer, Switzerland, 2020.
8. P. Fietkau, B. Kistner, J. Munier, Virtual Powertrain development, Journal of Automobile Engineering, 2020, pp. 3288-3301.
9. A. Salmi, A review of cost estimation models for determining assembly automation level, Computer & Industrial Engineering 98, 2016, pp. 246-259.
10. A. Niazi, Product Cost Estimation - Technique Classification and Methodology Review, Journal of Manufacturing Science and Engineering 128(2), 2006, pp. 563-575.
11. R.K. Yin, Case study research - Design and methods, Sage Publications, United States of America, 2009.
12. C. Karlsson, Research methods for operations management, Routledge, United States of America, 2016.
13. J. Freeman, T. Chen, Green supplier selection using an AHP – Entropy-TOPSIS framework, Supply Chain Management: An International Journal (20), 2015, pp. 327-340.
14. Argonne National Laboratory, BatPaC Model Software, 2020, available at <https://www.anl.gov/cse/batpac-model-software>.
15. A. J. O'Brien, FLIHI: Fuzzy Logic Implemented Hill-based Model, Washington, 2018.
16. T. J. Ross, Fuzzy Logic – With Engineering Applications, John Wiley & Sons, United States of America, 2010.
17. H. Unbehauen, Regelungstechnik 1 – Klassische Verfahren zur Analyse und Synthese linearer kontinuierlicher Regelsysteme, Fuzzy Regelsysteme (Bd. 15), Vieweg + Teubner, Germany, 2008.

## Day 1: P05 – Energy Consumption I

Session P05 – Energy Consumption I, Monday 14 June

---

**Session chairs:** Mario Hirz and Malte Rothhämel

- 15:20-15:30    **P05.A**  
*A more efficient braking system for heavy vehicles*  
Pontus Fyhr and Leon Henderson
- 15:30-15:40    **P05.B**  
*Development of rolling resistance measurement set-up  
in order to enable energy optimisation of vehicle-road  
interaction taking into account safety and performance*  
Lisa Ydrefors, Mattias Hjort, Sogol Kharrazi, Jenny Jerrelind and  
Annika Stensson Trigell
- 15:40-15:50    **P05.C**  
*Regenerative braking for an electric vehicle with a high-  
speed drive at the front axle*  
Ektor Karyotakis, Rémi Mongellaz and Mathias Lidberg
- 15:50-16:00    *Questions and Answers*
-



# A more efficient braking system for heavy vehicles

Pontus Fyhr<sup>1,2\*</sup> and Leon Henderson<sup>3,4</sup>

<sup>1</sup>*Haldex brake products AB, Box 501, 261 24 Landskrona, Sweden*

<sup>2</sup>*Industrial electrical engineering and automation, Lund university, Box 118, SE-221 00 Lund, Sweden*

<sup>3</sup>*Chalmers university of technology, SE-412 96 Gothenburg, Sweden*

<sup>4</sup>*Volvo technology, SE-405 08, Gothenburg, Sweden*

\*Corresponding author. Email: [pontus.fyhr@haldex.com](mailto:pontus.fyhr@haldex.com)

Electric powertrains increase efficiency in road vehicles and enable zero tailpipe emissions, but introduce practical limitations in on board energy storage capacity, due to the low energy density in battery systems when compared with chemical fuels in tanks. The increased powertrain efficiency and lower on-board energy storage levels place focus on other energy consumers in the vehicle system, such as the braking system. Our measurements indicate that a conventional pneumatic electronic braking system for heavy vehicles consumes 2-3% of the mission energy in a typical city bus cycle for a battery electric vehicle. The newly developed electromechanical braking system offers a more efficient energy conversion for the braking function, consuming 0.4-0.7% of the mission energy under similar driving conditions. This work focuses on an energy analysis of the conventional and the novel system in the context of a city bus application. The data is sourced from measurements of a battery electric bus, driven on a proving ground in tests repeated three times, in unladen condition. The measurements include comparative tests for the vehicle equipped with a traditional electro-pneumatic braking system and the same vehicle equipped with the new electro-mechanical braking system.

© 2021 by the authors. Published by the Resource Efficient Vehicles Conference.  
This is an open access article under the CC BY license (<http://creativecommons.org/licenses/by/4.0/>).

## 1. Introduction

The energy used by the longitudinal actuators in a battery electric bus were studied experimentally, by driving an emulated city bus schedule featuring frequent stops on a proving ground. An illustration of the test vehicle is shown in figure 1. Energy consumption in battery electric city buses has been

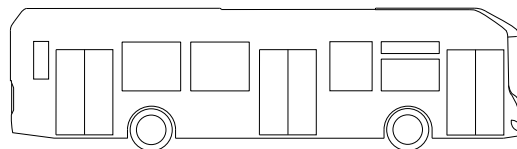


Figure 1: The object under study, a low floor 4x2 battery electric bus.

studied in [1], which does not go into detail on the energy use of the braking system. One work that does investigate the pneumatic system in heavy vehicles is [2], but the authors unfortunately hide the axes on significant results.

Table 1: Vehicle properties.

Property	value	unit
Unladen mass	12800	kg
Pneumatic tank energy	256	kJ
Capacitor bank energy	44	kJ

## 2. Methodology

A test vehicle, powered by a battery electric powertrain, was run over a 5 km loop on a proving ground, starting and stopping in the same location. This cycle was repeated three times in succession for each of the tested braking systems, the reported cases are in an unladen vehicle state. The tests were performed on separate occasions, as the same vehicle was used with both systems.

### 2.1 Test cycle

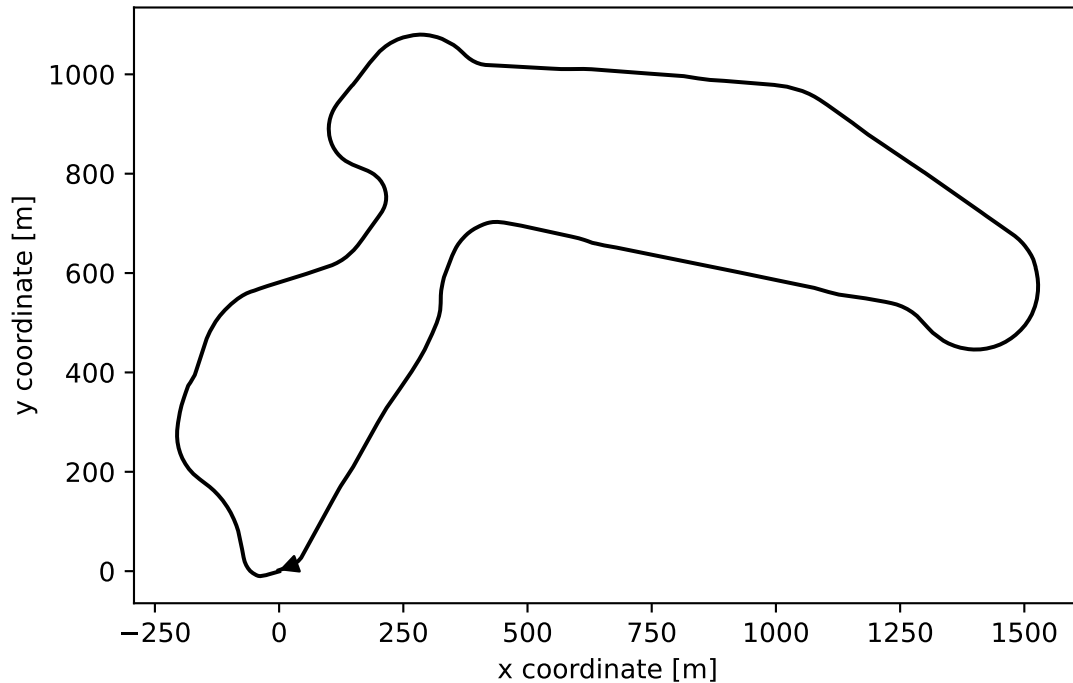


Figure 2: The test track coordinates, the arrow indicates the driving direction and location of the start and finish for each test.

The loop is driven on an asphalt road, forming a closed circuit, as depicted in figure 2. Tests are driven at targeted speeds of 8.5 m/s, the lateral acceleration content is minimal, and the longitudinal accelerations are in the 1 m/s<sup>2</sup> range. The velocity and altitude profile of the track are depicted in figure 3. At each stop a halt brake function is activated in the EBS case, which applies a service brake pressure of 200 kPa, roughly 17 % of the system capability. On steeper inclines this system retains a slightly higher pressure. In the EMB case this functionality is emulated by the use of its parking brake function, which uses a clamping force equal to 25 % of the system capability.

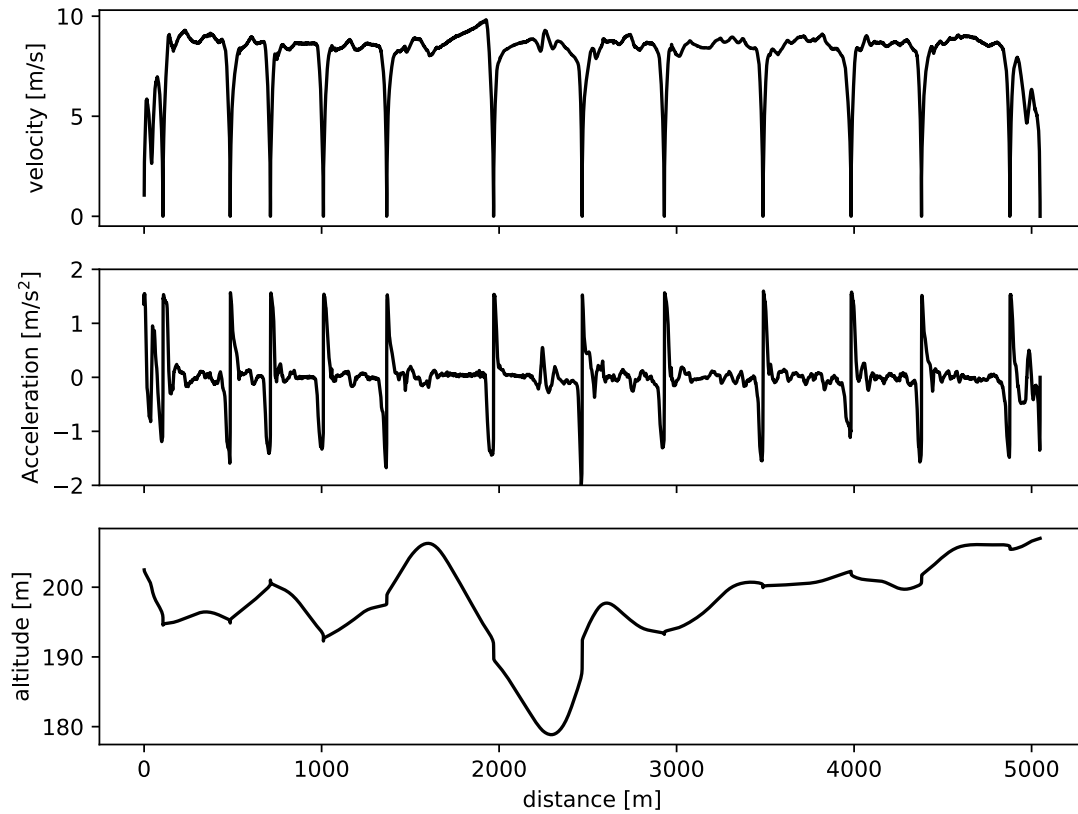


Figure 3: The test cycle velocity, acceleration and altitude, the discontinuities on each stop location are caused by the GPS receiver altitude drift, indicating low accuracy in altitude.

## 2.2 Experimental setup and data

The energy converted by the longitudinal actuators were gathered at a sample rate of 10 ms on the vehicle CAN-bus, together with two GPS devices at 10 ms and 100 ms respectively.

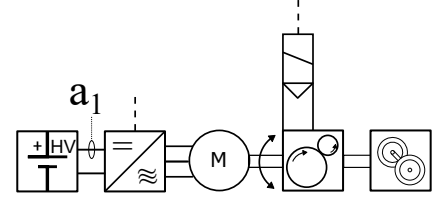
The longitudinal actuators in the vehicle, including the two braking system variants, are depicted in figure 4. These are a) the powertrain, b) the compressed air system, and c) the EMB system. The data gathered by the CAN-logger is saved in a vendor-proprietary message based binary format. After completion of the experiments, the data is converted to ASCII values, utilizing the CAN message data specification in order to generate sampled physical value data at a 10 Hz rate. This data is subsequently processed and displayed in section 4.

## 2.3 Experimental uncertainty

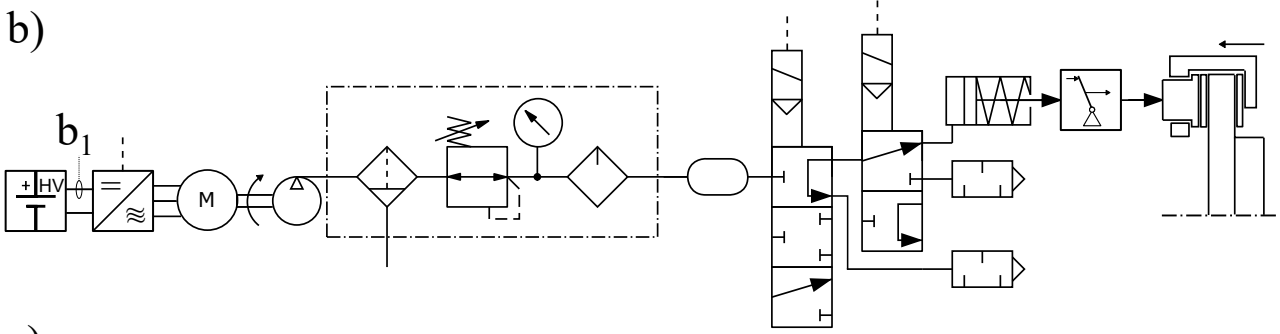
As the experiments are performed with a human driver over several different days, the repeatability of the experiments is not perfect. For example, some average driving speed disparities can be seen in the comparison tests, where the EBS runs are on average performed with a slightly lower driving speed than with EMB. The number of stops performed in the EBS case is 13, and in the EMB case 10, when counting the final stop at the take off location, as indicated by the arrow in figure 2.

The EMB system consumption is measured from the low voltage (24 V), which means that the losses stemming from the conversion from high voltage to low voltage systems is not captured in this measurement. The reasoning behind this choice is that many other consumers that are out of scope for this work would be included in the measurement if it was performed on the high voltage side of the DC/DC converter. The efficiency of such converters is typically >95 %.

a)



b)



c)

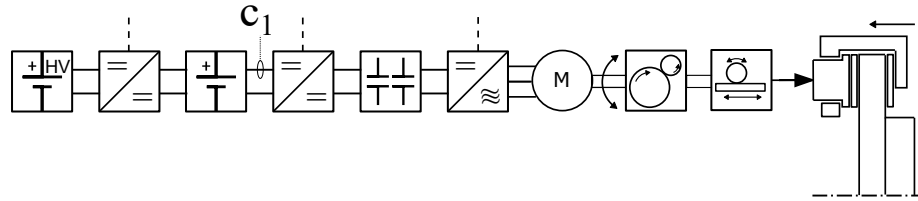


Figure 4: Diagram of the actuators under study. a) is the traction system, b) is the EBS system, and c) is the EMB system. The points  $\{a,b,c\}_1$  indicate where the energy used is measured by the actuator in question as voltage at the terminals of the device times current flowing into the device.

Other consumers of compressed air exist in the vehicle, such as air-suspension and other body-functions, the use of these functions have been minimized, by not utilizing for example the kneeling function. Still some consumption of compressed air exists in excess of that used by the EBS system. The consumption of these systems is captured implicitly, by subtracting the air use that remains in the EMB case from the EBS cases in Section 5.

It should be noted that most of the braking effort, slowing the vehicle down, is performed by the regenerative braking from the powertrain. The controller requesting this action is not identical between the two systems. This may affect the acceleration levels and velocities triggering powertrain and braking system actions, but efforts have been made to align their actions.

### 3. Analysis

The energy used by each actuator over a cycle is

$$W_{*1} = \int_{t_0}^{t_1} P_{*1} dt \quad (1)$$

where  $*$  is the actuator, the value is calculated numerically using Simpson's rule. The total energy consumed by the longitudinal actuators in the vehicle is defined as

$$W_{tot} = W_{a1} + W_{b1} + W_{c1} \quad (2)$$

The maximum available energy inside the pneumatic reservoirs, from the common gas law and assuming isothermal expansion would be

$$W_p = p_t V_t \ln \frac{p_a}{p_t} + (p_t + p_a) V_t \quad (3)$$

where  $*_t$  denotes the reservoir, and  $*_a$  denotes atmosphere. The energy stored in the capacitor bank is

$$W_c = \frac{1}{2} U^2 C \quad (4)$$

## 4. Results

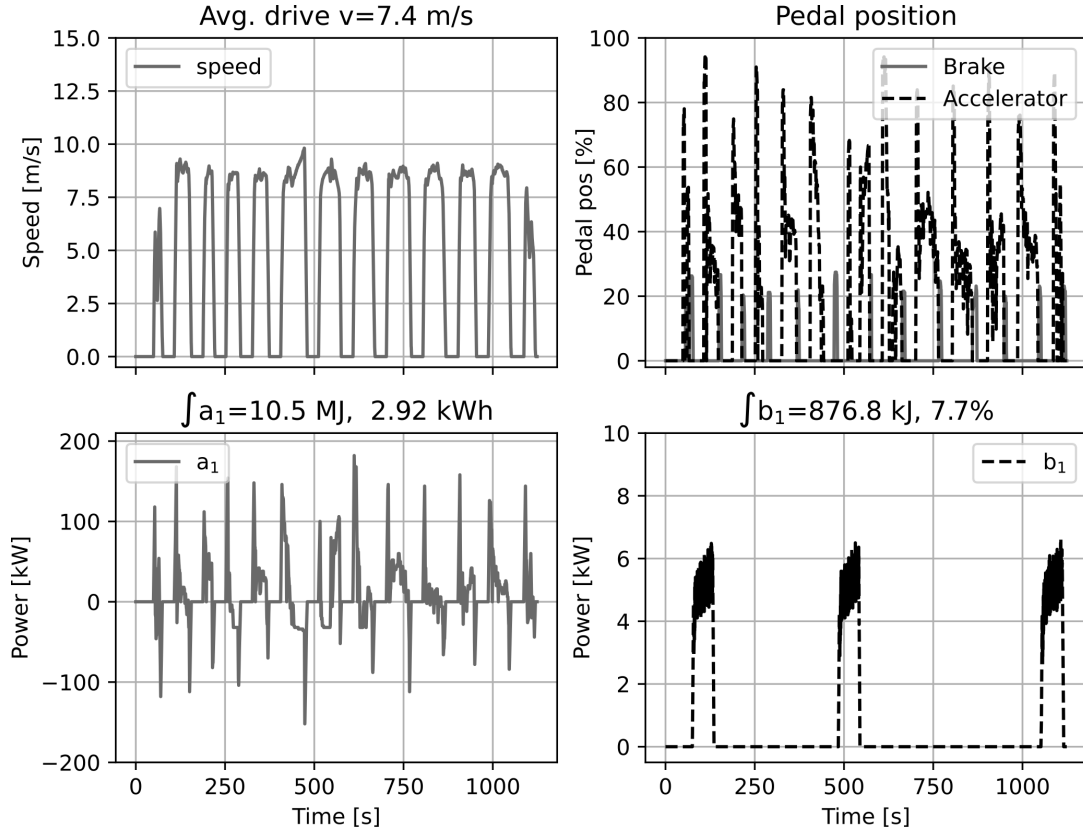


Figure 5: EBS run 3

Figures 5-6 show the third run with each vehicle configuration, as this allows the systems in the vehicle approach operating temperature, the earlier repeat runs are included in the appendix, Figs. 7-10. Each result plot includes the calculated energies converted by the longitudinal actuators during the the run. On the top left is the velocity as measured at the wheels, the top right shows pedal positions used by the driver. The lower left shows the powertrain power, which is both positive for tractive effort and negative for regenerative braking, the lower right shows the pneumatic compressor, and where applicable also the power consumed for charging the capacitor bank energy storage in the EMB case.

The measured energies consumed by the powertrain and braking systems over all runs for the three cases are presented in Tab. 2. This table also contains some information regarding irregularities in the driven cycles, stemming from the use of a human driver.

## 5. Discussion

In the EBS case, the  $b_1$  actuator consumed on average 587 kJ, with the pneumatic electronic braking system removed and the electromechanical braking system installed, the energy consumption of  $b_1$  was reduced to 276 kJ on average. This indicates that the energy used to actuate the pneumatic brakes was 311 kJ, as measured at the terminals of the compressor system. In comparison to the powertrain energy, in the EBS case was 10.6 MJ, the pneumatic braking system used 2.8% of the total energy

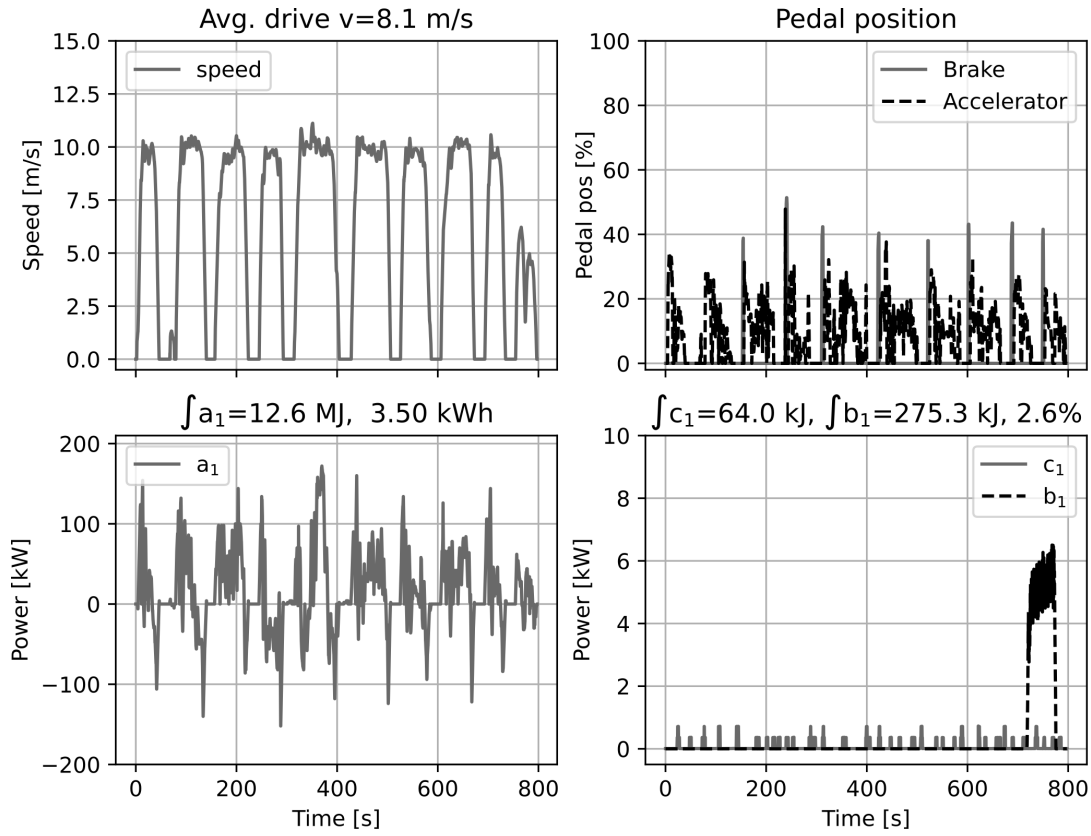


Figure 6: EMB run 3

for the measured actuators,  $a_1$  and  $b_1$ . The remaining compressed air energy may be used in body functions, one example being pneumatic suspension.

In comparison, the EMB system used 62 kJ for a similar mission, albeit with fewer stops and higher average driving speeds, leading to higher powertrain energy consumption. Here the energy consumption in the  $b_1$  system is 276 kJ, leading to a total  $b_1+c_1$  energy use of 338 kJ, significantly lower than the average of the EBS runs. If calculated as a fraction of the total mission energy, the  $c_1$  system used 0.45% of the energy for the measured actuators  $a_1$ ,  $b_1$  and  $c_1$ .

This indicates that the electromechanical braking system is clearly more efficient than the pneumatic electronic braking system, but the comparison is slightly unfair as fewer stops were performed and the powertrain energy was higher. So if a careful extrapolation effort is undertaken and the EMB system consumption,  $c_1$ , is scaled up by a factor relating to the number of stops, 1.3, its consumption could have been 81 kJ, and  $b_1$  from EMB is scaled up by the same factor, giving 359 kJ. These numbers, if combined with a powertrain consumption from the EBS case of 10.6 MJ, would have resulted in 0.73% of the total energy used by the EMB system, and 3.25% used by  $b_1$ . Alternatively, the average amount of energy used by the EBS can be estimated per bus stop and compared to the same metric measured for the EMB system. Such a calculation gives values of 24 kJ/stop and 6 kJ/stop for the EBS and EMB systems respectively.

According to these results the electromechanical energy conversion in the EMB system is more efficient than the combined air compressor and EBS system, by a factor between 3 and 4, while performing the duties of stopping and holding a battery electric city bus stationary, during the stops on a typical city bus driving schedule.

The amount of compressed air used by other systems on the bus was not studied in detail in this work. It is, however, interesting to observe that, according to the energy use measured, the EBS only accounted for around 60% of the total compressed air use. Further experiments are needed to identify which systems are responsible for this additional compressed air energy use.

Table 2: Averages over 3 runs.

	EBS	EMB	unit
a1, powertrain	10.6	13.5	MJ
b1, compressed air	587	276	kJ
c1, EMB	-	62	kJ
b1+c1 % of total	5.2	2.5	%
Velocity	7.4	8.5	m/s
Stops	13	10	-
Ambient temperature	12	6	°C

## References

1. A. Łebkowski, “Studies of energy consumption by a city bus powered by a hybrid energy storage system in variable road conditions,” *Energies*, vol. 12, no. 5, 2019.
2. B. Karanja and P. Broukhiyan, “Commercial vehicle air consumption: Simulation, validation and recommendation,” Master’s thesis, KTH, Machine Design (Dept.), 2017.

## Appendix

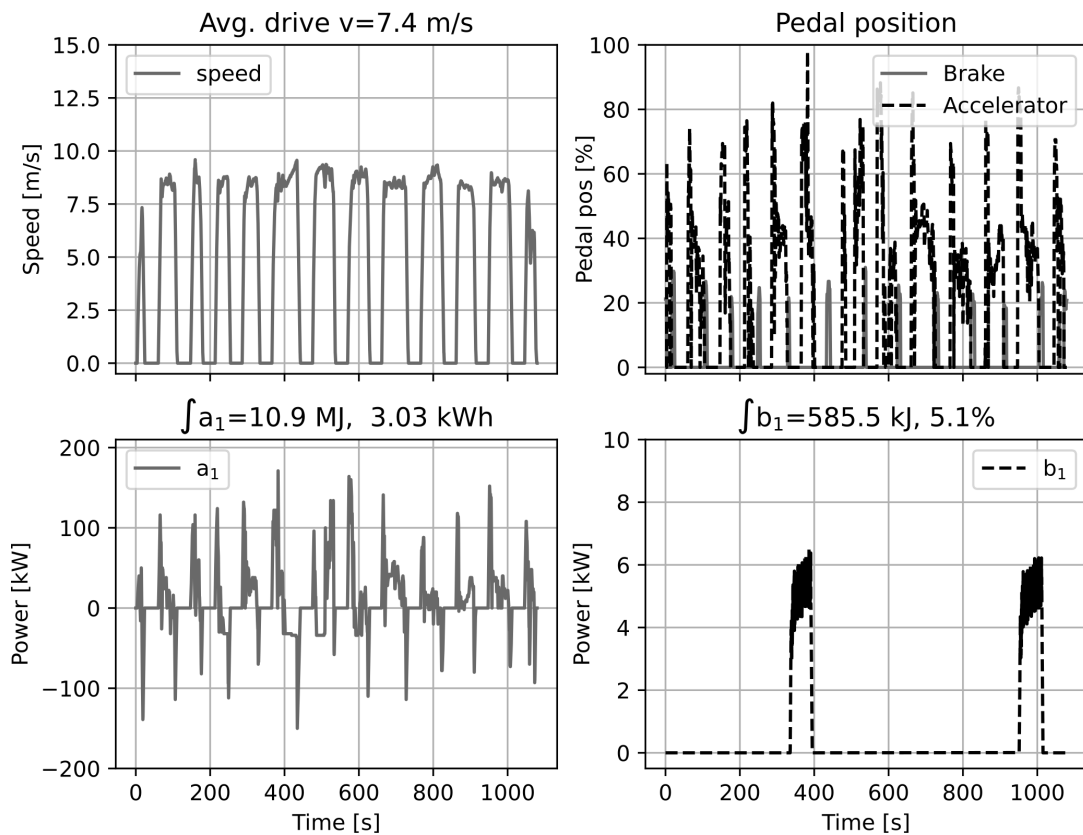


Figure 7: EBS run 1

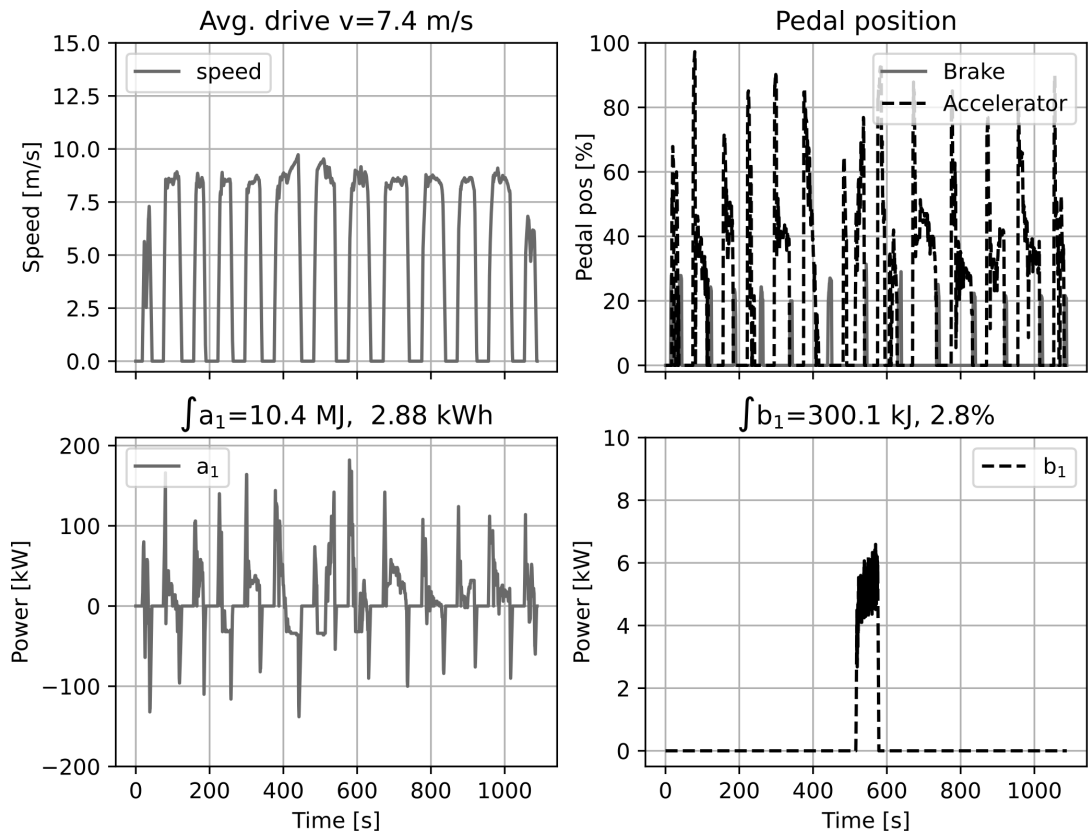


Figure 8: EBS run 2

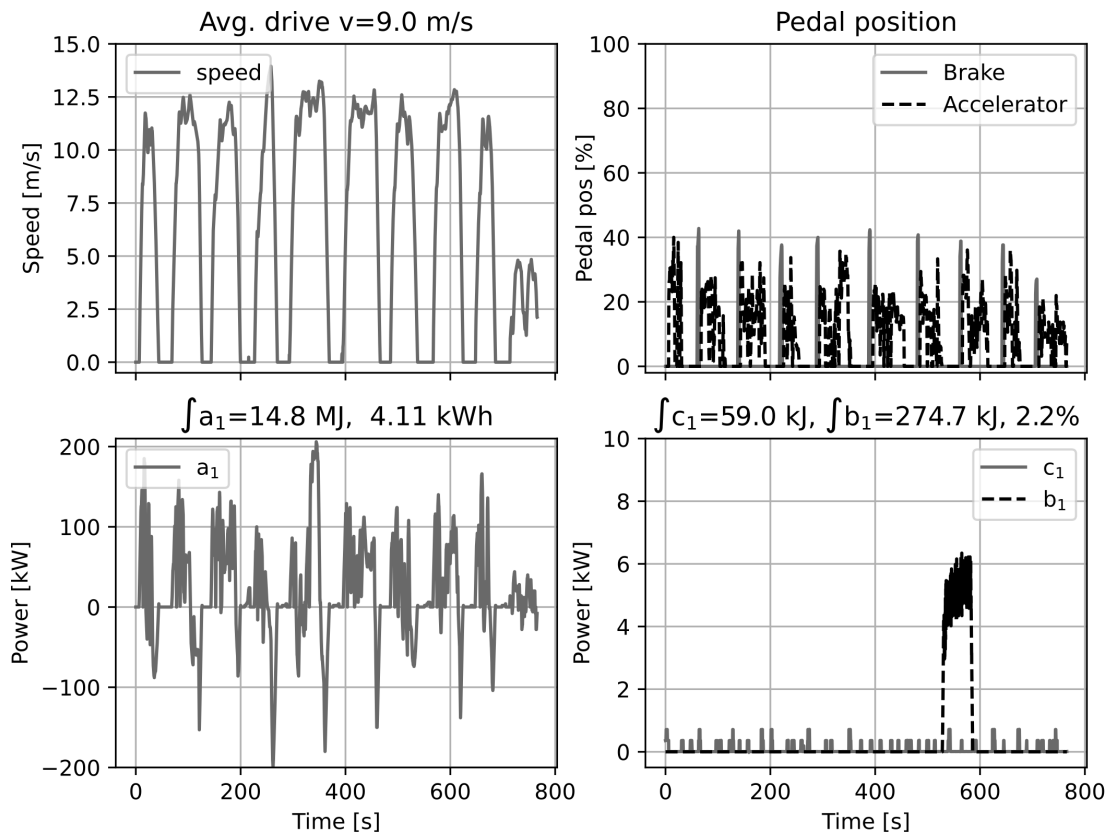


Figure 9: EMB run 1



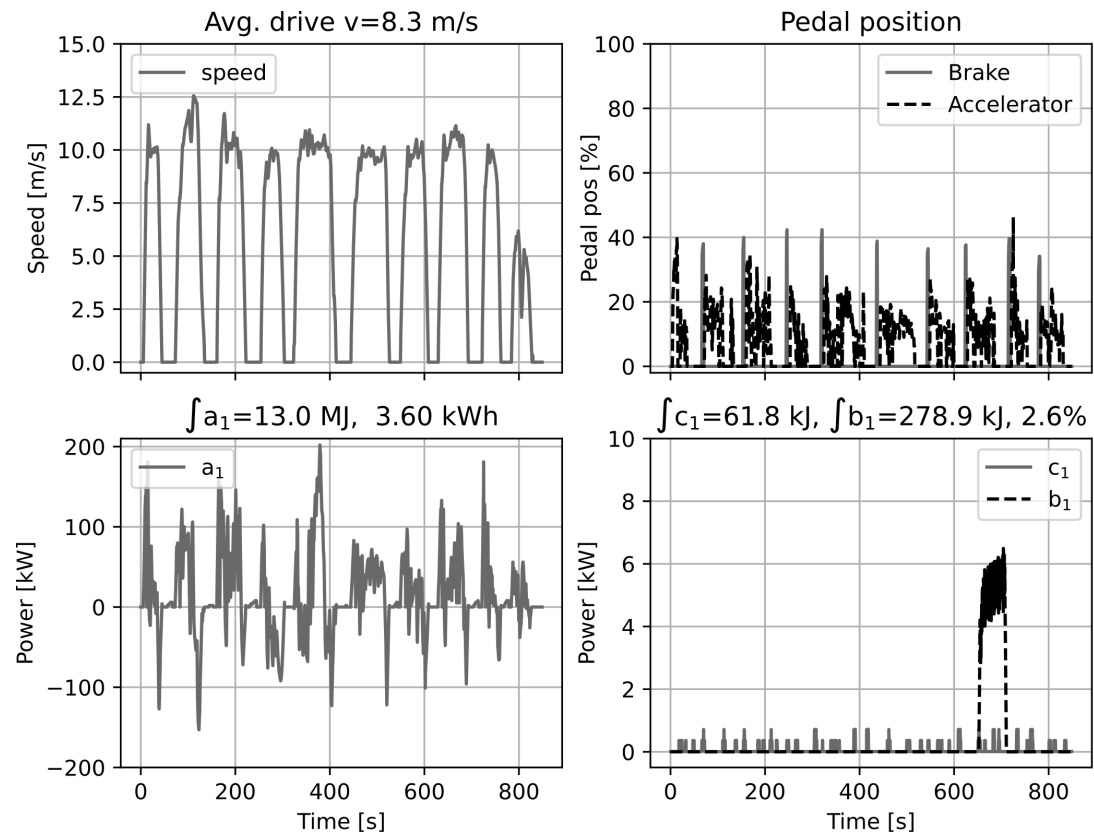


Figure 10: EMB run 2

---

# Development of rolling resistance measurement set-up in order to enable energy optimisation of vehicle-road interaction taking into account safety and performance

Lisa Ydrefors<sup>1,2,3\*</sup>, Mattias Hjort<sup>1,2</sup>, Sogol Kharrazi<sup>1,2</sup>, Jenny Jerrelind<sup>2,3</sup> and Annika Stensson Trigell<sup>2,3</sup>

<sup>1</sup>*The Swedish National Road and Transport Research Institute (VTI), Linköping, Sweden*

<sup>2</sup>*The Centre for ECO<sup>2</sup> Vehicle Design, KTH Royal Institute of Technology, Stockholm, Sweden*

<sup>3</sup>*Department of Engineering Mechanics, KTH Royal Institute of Technology, Stockholm, Sweden*

*\*Corresponding author. Email: lisa.ydrefors@vti.se*

---

Reducing the rolling resistance for future vehicle designs creates a possibility to reduce the fuel consumption and make the future vehicles more economical and ecological. For electric vehicles it is also an enabler to increase their driving range per charge. When optimising for reduced rolling resistance, contradictory requirements such as force generation for maintaining safety and performance need to be considered. Furthermore, it is important to include both the effects of road surface and vehicle, to avoid sub-optimisation regarding only the tyres. A cross-functional conflict on the component level is well known, in form of energy consumption versus wet grip (traffic safety). On the system level, different wheel settings to optimise energy consumption conflicts with vehicle dynamical properties related to traffic safety, such as stability or steer response. The long term vision of the work presented is to create tools for more energy efficient vehicles by reducing the rolling resistance during driving. The first part is to establish a credible measurement method for rolling resistance on road under controlled conditions (lab environment). Today's existing measurement methods on rolling resistance under laboratory conditions commonly utilise a rotating drum, whose curved surface affects the results. Therefore, rolling resistance influence of vehicle settings such as camber or toe angles is difficult to assess using standard methods, and there is a need for measurements using a more realistic contact patch, which would need a flat surface. The existing unique tyre testing facility at the Swedish National Road and Transport Research Institute, VTI, is used as a base for developing the new rolling resistance set-up. The tyre test facility is today used to determine tyre characteristics such as brake and steering forces. The method to measure rolling resistance with this equipment under highly controlled conditions is under development, and some preliminary results are presented.

---

© 2021 by the authors. Published by the Resource Efficient Vehicles Conference.  
This is an open access article under the CC BY license (<http://creativecommons.org/licenses/by/4.0/>).

## 1. Introduction

As the number of vehicles on the roads increases, the need to make the vehicles more resource efficient in order to reduce their environmental impact increases. One way to influence the energy consumption of the vehicles is to reduce the resistive forces during travelling. The main resistive forces for road vehicles to overcome are aerodynamics, inertia, internal friction and rolling resistance.

Reducing vehicles rolling resistance has been in focus during many years for both economic and environmental reasons. It started with economic considerations of fuel to conventional combustion vehicles and has intensified with the introduction of electric vehicles. Electric vehicles have been promoted as one part of the solution in reducing greenhouse gases and energy use. To accelerate the increase of electric vehicles, several countries have today a set date to begin phasing out combustion driven vehicles. Vehicle manufacturers are also adapting to this, offering hybrid and electric vehicles in their product portfolio. Some vehicle manufacturers even goes further, one example being Volvo Cars that announced during 2021 that from 2030 the company will only sell electric cars [1]. However, for the complete success of all-electric vehicles there is a need of increasing their driving range per charge without adding more battery weight, thereby lower rolling resistance is highly beneficial.

When optimising for reduced rolling resistance contradictory requirement such as force generation for maintaining safety and performance, as well as the road surface need to be taken into account. For example, a cross-functional conflict on the component level (the tyre) is well known, in form of rolling resistance (energy consumption) versus wet grip (traffic safety). Tyre manufacturers commonly talk about the Magic tyre triangle which illustrates the conflicting requirements between fuel efficiency (i.e., low rolling resistance), wear and grip, see Figure 1. On the higher system level, different wheel settings in order to optimise energy consumption conflicts with vehicle dynamic properties related to traffic safety, such as stability or steer response.

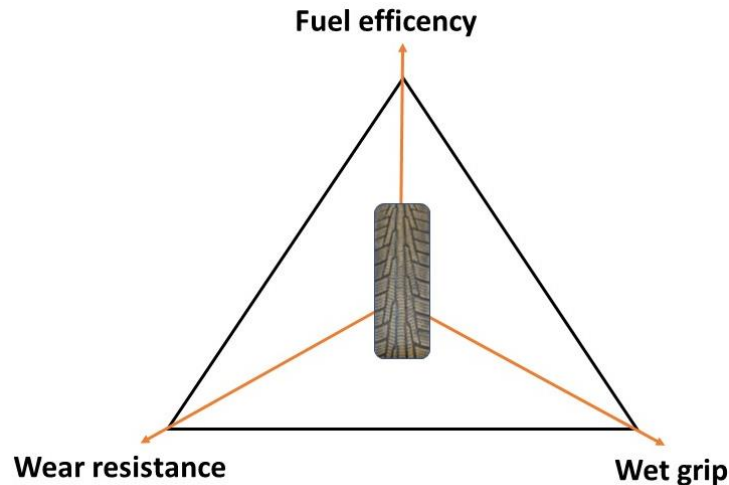


Figure 1. The Magic tyre triangle.

The overall vision of this work is creating tools for more energy efficient vehicles by reducing the rolling resistance during driving. More specifically, this work focuses on development of good measurement methods and verified simulation models for rolling resistance, in order to enable optimisation of vehicles to reduce rolling resistance while maintaining safety and performance. The work is divided in four parts, as can be seen in Figure 2. The first part is to establish a credible measurement method for rolling resistance on road under controlled conditions (lab environment). Secondly, to investigate the influential parameters on rolling resistance. Thirdly, to create a simulation model of tyre rolling resistance and friction forces for vehicle dynamics simulations which will be validated by measurements. Finally, the combined knowledge and tools from the previous steps will be used to perform rolling resistance optimisation studies with maintained safety and

performance. New possibilities for control strategies open up by assuming that the vehicle to be optimised has wheel corner modules, i.e., electric motors at each wheel with integrated suspensions which implies that for each wheel, traction, braking and wheel angles can be controlled.

Currently, the focus is on part one of Figure 2 and the progress so far will be presented in this article. The emphasis of the work is on car tyres and the effect of different driving conditions. The influence of changes in the tyre construction is not included. The outline of the article is as follows. In Section 2 an introduction to rolling resistance is given followed by a short general overview of rolling resistance measurement equipment in Section 3. The equipment and measurement method used in this work, together with some measurements are presented in Section 4. Finally, Section 5 presents the conclusions.



Figure 2. An overview of the work to be performed to full fill the overall vision.

## 2. Rolling resistance

Rolling resistance (RR) can be defined as “the mechanical energy converted into heat by a tire moving for a unit distance on the roadway” [2], or the part of the energy transferred to the tyres, which will not contribute to the forward motion of the vehicle. The main source of this energy loss is the hysteresis in the tyre rubber which means that the energy lost in the deformation of the tyres is greater than the energy regained at its relaxation. The magnitude of the rolling resistance varies between different tyres and different driving conditions. For passenger cars, the rolling resistance stands for about 5-20% of the fuel consumption, which can be compared to 15-40% for trucks [3], [4]. A 10% reduction of the rolling resistance has shown to generate 0.5-3% lower fuel consumption for cars [5].

The rolling resistance of a tyre is determined by its construction and operating conditions. Operating conditions are for example the inflation pressure, the tyre temperature, the vehicle speed, the tyre load, the road surface, the driving torque and wheel angles, such as the slip and camber angles. In general, the rolling resistance increase with increased vehicle speed, tyre load, driving torque, road surface roughness or tyre angles, and decrease with increased inflation pressure or tyre temperature [6], [7]. The tyre temperature is an important driving condition which have a large effect on the tyre rolling resistance.

## 3. Equipment for rolling resistance measurements

There are several different sorts of measurement equipment that can be used to measure rolling resistance in laboratories and in the field. The laboratory measurements have the advantage of a higher precision and repeatability compared to field measurements, since the measurement conditions are easier to control.

The most common laboratory measurement method is external drum measurements. This is the only rolling resistance method which is standardised. There are four different standards to measure rolling resistance on an external drum; ISO 28580 [8], ISO 18164 [9], SAE J1269 [10] and SAE J2452 [11]. The main idea is to run the tyre on the drum until it has reached a steady-state level and then measure the rolling resistance. Reaching steady-state implies that the tyre and the equipment have reached a heat balance, which causes the rolling resistance to remain at the same level independent of further running of the tyre at the same conditions. The main advantages of this method are the relatively low cost, and the good repeatability. The main drawbacks are the curvature of the drum and the limitation in possible road materials for the tyre to run on. Both the road material and the curvature have a large effect on the rolling resistance. The curvature of the drum increases the tyre deformations which will result in a higher rolling resistance and tyre temperature compared to running the tyre on a flat surface. An external drum is very useful for comparing the rolling resistance of different tyres at the same conditions, but the tyre is tested at very limited conditions. Besides external drums, internal drums also exist. Figure 3 illustrates how the tyre runs against the different drums. In contrast to the external drum which deforms the tyre more than a corresponding flat surface, the internal drum deforms it less. Moreover, real asphalt can be used in an internal drum, due to its much larger curvature. However, both types of equipment have a curvature which will affect the relationship between rolling resistance and wheel angles.

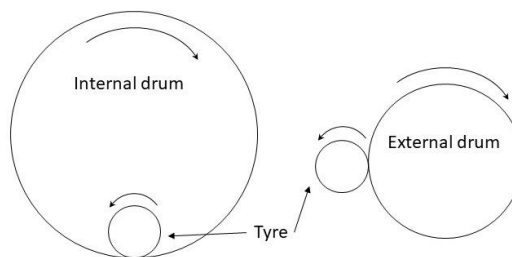


Figure 3. Difference between internal and external drum.

Another group of testing equipment for rolling resistance measurements are flat tracks. The most common flat track equipment is a rolling belt run around two big drums, where the belt becomes a flat surface for the tyre to run on. While this method is more expensive than the drum method, it maintains the drum's advantage of steady-state measurements but without the drawback of the curvature effects. The flat surface thereby enables studies of the effect of slip and camber angles on rolling resistance without any curvature effects. However, the equipment is limited regarding road surface types that can be used on it, since the belt must be flexible enough to bend around the drums.

For further details about rolling resistance measurement equipment's see for example [12].

#### 4. Development of VTI tyre test facility for rolling resistance measurements

The existing tyre testing facility at the Swedish National Road and Transport Research Institute, VTI, is used as a base for developing the new rolling resistance set-up, see Figure 4. The tyre test facility is today used to determine tyre characteristics such as brake and steering forces. This type of flat track tyre test facility is rather rare. The tyre is placed in a measurement rig and pressed against the ground with a specified load, while the ground, in the shape of a large metal beam, moves beneath the tyre at a speed up to 30 km/h. The advantage with this kind of equipment is that real asphalt can be used, and that the road surface can be covered by water to simulate wet conditions or covered by ice to simulate winter conditions. Another advantage is that the flat surface removes the curvature effects inherent in the drum measurements, which makes it easier to measure the effect of camber and slip angles. A drawback is however that it cannot be used for steady-state measurements due to the limited

length of the metal beam simulating the road. The beam is 55 m long and if running the equipment with the maximum speed 30 km/h the measurements are over in less than 13 seconds.

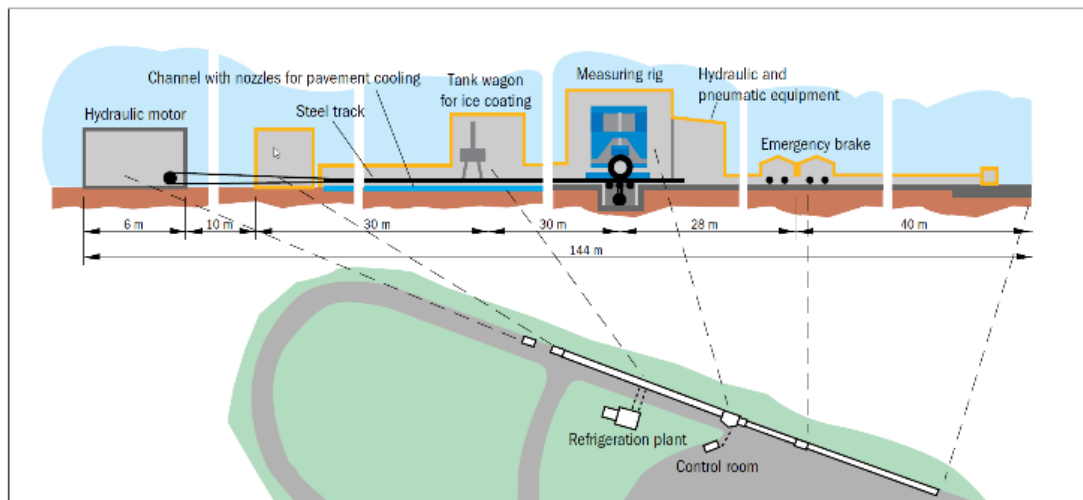


Figure 4. An overview of the VTI Tyre test facility.

This equipment has been used for almost 40 years, mainly to measure brake forces. To be able to use it for measuring rolling resistance, the sensor accuracy needs to be examined since rolling resistance forces are much smaller than brake forces. The equipment measures the force in the direction of travel, which gives the rolling resistance. The measured value includes internal equipment losses which needs to be measured and subtracted. In addition, any misalignment between the applied vertical force and the beam will produce a force in the direction of travel which needs to be compensated for.

As mentioned earlier the measurement only takes seconds, thereby the tyre will not be significantly heated. This can be compared to drum tests which are made at steady-state temperature, or running the tyre in traffic which generally will result in a heat up of the tyre. Therefore, to be able to compare the measurement results from the VTI tyre test facility, with test results from field tests or drum tests, the tyre must be heated. The heating will affect both the tyre temperature and inflation pressure, which both affect the rolling resistance. To better control the measurements and to be able to study the relationship between these properties and the rolling resistance, the inflation pressure as well as the inside and outside tyre surface temperatures are also measured. The internal tyre rubber temperature distribution of the tread will vary between the measured inside and outside tyre surface temperatures. Figure 5 gives an example of measurement results where the rolling resistance coefficient (RRC) is plotted versus the temperature. The RRC, which is a commonly used measure for rolling resistance, is the rolling resistance divided by the load on the tyre. As can be seen, the rolling resistance decreases with temperature, which is expected [6]. The strong temperature dependence of the RRC, emphasise the importance of maintaining a stable and repeatable tyre temperature. The tests accounted for in Figure 5, are measured on unheated tyres, which results in much lower tyre temperatures than measurements on the road or a drum. This emphasises the need to heat the tyres to get comparable rolling resistance levels. The tested tyre is a Standard Reference Test Tyre (SRTT). Tests on an internal drum performed at the Federal Highway Research Institute (BAST) in Germany, at steady state temperature and 50 km/h, but otherwise similar conditions, gave an RRC

that varied between 0.008-0.015 [13]. This difference in RRC could be attributed to the difference in tyre temperatures between the two measurements.

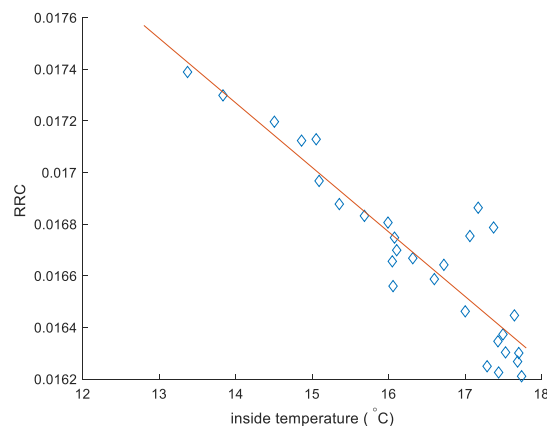


Figure 5. The relationship between the rolling resistance coefficient (RRC) and the tyre inside surface temperature, as measured in the VTI tyre test facility. Each square corresponds to a single RRC-measurement and the line is a linearisation of the results to emphasise the trend.

## 5. Conclusions

In the paper, the needs behind a new rolling resistance measurement method are described along with the methodology for using the VTI tyre test facility to measure rolling resistance. The results presented are shown to be promising. When the rolling resistance measurement method is completed the work to develop and validate a tyre model for simulation of rolling resistance and force generation will be initiated. The development of a rolling resistance model will facilitate complete vehicle dynamic simulations to find control strategies for different driving conditions, considering energy consumption, performance and safety, to handle the mentioned conflict of interest.

## 6. Acknowledgements

The authors would like to thank the Centre for ECO2 Vehicle Design, funded by the Swedish Innovation Agency Vinnova (Grant Number 2016-05195), and VTI for financial support.

## References

- [1] T. Augustsson and J. Carlström, ‘Volvo satsar på el och säljer bara digitalt’, *SvD Näringsliv*, 2021.
- [2] D. Schuring, ‘A new look at the definition of tire rolling loss’, 1977.
- [3] D. E. Hall and J. C. Moreland, ‘Fundamentals of rolling resistance’, *Rubber Chem. Technol.*, vol. 74, no. 3, pp. 525–539, 2001, doi: 10.5254/1.3547650.
- [4] J. Barrand and J. Bokar, ‘Reducing tire rolling resistance to save fuel and lower emissions’, *SAE Tech. Pap.*, 2008, doi: 10.4271/2008-01-0154.
- [5] H. S. Aldhufairi and O. A. Olatunbosun, ‘Developments in tyre design for lower rolling resistance: A state of the art review’, *Proc. Inst. Mech. Eng. Part D J. Automob. Eng.*, vol. 232, no. 14, pp. 1865–1882, 2018, doi: 10.1177/0954407017727195.
- [6] A. N. Gent and J. D. Walter, *The Pneumatic Tire*. 2005.
- [7] D. Schuring, ‘The Rolling Loss of Pneumatic Tires Schuring.pdf’, *Rubber Chem. Technol.*, vol. 53, no. 3, pp. 600–727, 1980.

- [8] 'ISO 28580. Passenger car, truck and bus tyre rolling resistance measurement method: single point test and correlation of measurement results'. 2018.
- [9] 'ISO 18164. Passenger car, truck, bus and motorcycle tyres: methods of measuring rolling resistance'. 2005.
- [10] 'SAE J1269. Rolling resistance measurement procedure for passenger car, light truck, and highway truck and bus tires'. 2006.
- [11] 'SAE J2452. Stepwise coastdown methodology for measuring tire rolling resistance'. 2017.
- [12] L. Ydrefors, M. Hjort, S. Kharrazi, J. Jerrelind, and A. Stensson Trigell, 'Rolling resistance and its relation to operating conditions – a literature review', *Proc. Inst. Mech. Eng. Part D J. Automob. Eng.*, April 2021, doi: 10.1177/09544070211011089
- [13] A. Bergiers *et al.*, 'Comparison of Rolling Resistance Measuring Equipment - Pilot Study', 2011.



---

# Regenerative braking for an electric vehicle with a high-speed drive at the front axle

Ektor Karyotakis<sup>1,\*</sup>, Rémi Mongellaz<sup>2</sup> and Mathias Lidberg<sup>1</sup>

<sup>1</sup>*Chalmers University of Technology, Mechanics and Maritime Sciences, 412 96 Gothenburg, Sweden*

<sup>2</sup>*Siemens Digital Industries Software, 19 bd Jules Carteret, 69007, Lyon, France*

\*Corresponding author. Email: [ektorkar@gmail.com](mailto:ektorkar@gmail.com)

---

The main contribution of this paper lies in the development of a novel front-to-rear axle brake force distribution strategy for the regenerative braking control of a vehicle with a high-speed electric drive unit at the front axle. The strategy adapts the brake proportioning to provide extended room for energy recuperation of the electric motor when the vehicle drivability and safety requirements permit. In detail, the strategy is adaptive to cornering intensity enabling the range to be further extended in real-world applications. The regenerative braking control features a brake blending control algorithm and a powertrain controller, which are decisive for enhancing the braking performance. Lastly, the regenerative braking control is implemented in the high-fidelity simulation environment *Simcenter Amesim*, where system efficiency and regenerative brake performance are analysed. Results confirm that the designed regenerative braking greatly improves the effectiveness of energy recuperation for a front-wheel driven electric vehicle with a high-speed drive at the front axle. In conclusion, it is shown that it is feasible to use the high-speed drive with the proposed control design for regenerative braking.

© 2021 by the authors. Published by the Resource Efficient Vehicles Conference.  
This is an open access article under the CC BY license (<http://creativecommons.org/licenses/by/4.0/>).

---

## 1. Introduction

In the past decades, electrically propelled vehicles have been under the spotlight for their sustainable energy potential. One of their key features is their ability to recuperate energy back into the battery through regenerative braking [1]. Research on regenerative brake systems has focused mainly on two areas: optimising energy recuperation efficiency through analysing the brake energy management and improving the blended brake dynamics through cooperative control of the regenerative braking and the hydraulic brakes [2,3].

In brake energy management, there have been many ideas on changing the brake force distribution (BFD) to increase the regeneration potential. However, incorporating the vehicle handling requirements early in the design is usually only limited to the ideal brake curve. That is because the BFD curve is fixed in conventional brake systems. A brake-by-wire system though enables the dynamic manipulation of the BFD. This is useful for increasing the recuperation potential when stability and safety requirements are satisfied. For instance, regenerative braking can be expanded for use during cornering [4,5].

To increase the dynamic brake response and at the same time improve regeneration efficiency, cooperative control of the hydraulic brakes and the electric motor is favourable. The main difficulty of the coordination comes because of flexibilities in the driveshafts, which make smooth torque transfer from the electric motor to the wheels challenging [2]. Finally, regenerative braking and anti-lock braking can be combined to incorporate wheel-slip control in the design, as in [6].

In this article, a complete regenerative braking control (RBC) is presented for an electric vehicle with a high-speed drive at the front axle. The innovative electric powertrain was designed for the ModuED EU project, and a prototype was built featuring high motor efficiency and augmented power density [7]. The work presented here investigates the challenges and performance of regenerative braking for the high-speed drive with a two-gear transmission mainly in terms of energy recuperation efficiency, limited by vehicle drivability and handling requirements. The backbone of the RBC is a BFD strategy. The BFD strategy considers the vehicle handling–energy maximization trade-off and is made adaptive to the cornering intensity. Furthermore, to support a smooth brake response two control functions are developed: a powertrain controller to suppress oscillations at the driveshafts and a brake blending control algorithm to enhance the braking performance.

Specifically, this article starts with the analysis behind the brake energy management motivated by the driver's habits, which shows how the brake proportioning can both support the driver and increase the driving range. Furthermore, the developed RBC architecture and its key features are presented. Lastly, the results of full-vehicle simulations carried out in the high-fidelity environment *Simcenter Amesim* for various driving cycles with and without regenerative braking are analysed.

## 2. Brake energy management

### 2.1 Efficiency and driver's habits

The amount of energy that can be recovered using regenerative braking depends mainly on two factors: driver's habits and the recuperation efficiency of the regenerative braking system. According to the collected data from real-world driving provided by Renault [8], there is a significant potential for energy recovery not only during straight-line braking but also during cornering. In detail, as shown in Figure 1, the energy recuperation potential statistics are presented for various combinations of braking and cornering. On the horizontal axes the longitudinal and lateral acceleration levels are plotted, while on the vertical axis the energy recuperation potential statistics are plotted accordingly.

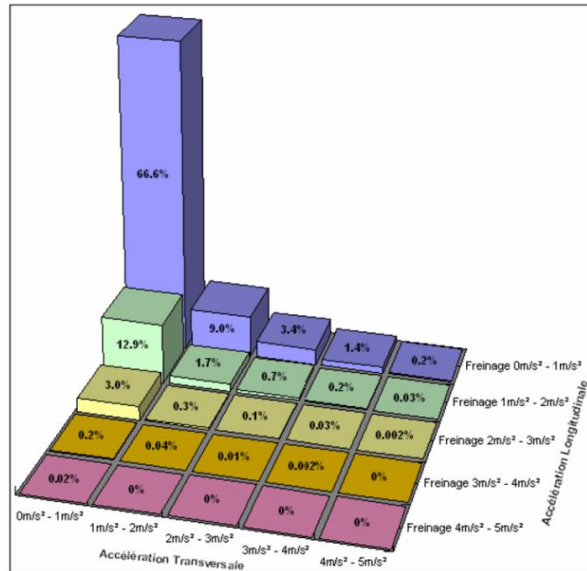


Figure 1: Energy recuperation potential statistics on various braking and cornering levels [8]

From the figure, up to 15.3% of energy can be recuperated for lateral acceleration values in the range 1–3 m/s<sup>2</sup>. Above that, the stability control algorithms (ABS, ESC) usually take control as the tire limits are approached. Under these circumstances, safety takes priority over energy recuperation. The main objective of the brake energy management development here is to cover the regenerative braking operating range for combined braking and cornering most efficiently, while driver comfort and safety are maintained.

## 2.2 Brake force distribution

Increasing the utilization of the front axle increases the available capacity that can be used for regeneration. Increasing the brake torque at the front axle though, reduces vehicle stability and manoeuvrability during cornering [4,5]. Based on this trade-off, a brake force distribution strategy, first proposed in [9], is improved to adapt to the current driving situation.

In a conventional brake system, the BFD is determined by the design of the brake system itself. In a brake-by-wire system though the BFD can be adapted to the current driving conditions. A typical BFD diagram is presented in Figure 2. The ideal- and ECE regulation curves are depicted, which limit the design for best handling and maximum regeneration, respectively. The Conventional, constant brake proportioning curve is also depicted in the diagram. Finally, the proposed “ModulED” BFD strategy is presented. Here, the ModulED curve is made adaptive to the predicted cornering intensity ( $a_{yg} = a_y/g$ ) to consider the combined effects of braking and cornering. Based on the current predicted cornering intensity level, the adaptation moves the [A, B, C] points between a selected fixed position for straight-driving and the Conventional strategy. In detail, a cornering intensity limit is chosen, above which the Conventional strategy is used entirely, while in between, a convex combination of the two strategies (Conventional and straight-driving) is used instead.

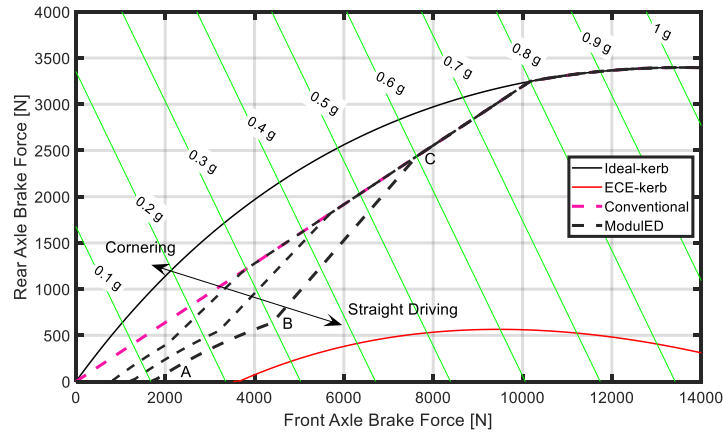


Figure 2: Brake force distribution diagram.

To assess the ideal energy recuperation potential for the various BFD strategies, the energy information from Figure 1 is first extracted. Then, for each strategy the front-to-rear axle brake proportioning is calculated for the same longitudinal and lateral acceleration data points. This ratio is assumed to be equal to the maximum amount of energy that can be recuperated by the electric motor of a front wheel drive vehicle. Therefore, multiplying the brake proportioning with the energy data of each point and summing it up gives the total energy recuperation potential of the strategy. The results are gathered in Table 1.

Table 1. Energy recuperation potential for the various braking strategies

	Conventional	ModulED
Energy recuperation potential	76%	94%

The Conventional strategy has a constant brake proportioning of roughly 76% of the brake torque on the front axle for the showcased vehicle and it is assumed that it maintains drivability in most driving conditions. Therefore, from the energy recuperation potential data [8], an energy value exactly equal to its distribution can be attained. The adaptive ModulED strategy on the other hand achieves higher energy recuperation levels. Specifically, a total of 18 pp (percentage points) more energy can be attained when using the ModulED strategy instead of the Conventional. This number shows the

potential energy benefit when the drivability requirements are included in the design. Focusing only on energy recuperation maximization, as when following strictly the ECE curve, cannot give optimal results due to drivability implications with combined braking and cornering.

### 3. Regenerative brake control

#### 3.1 Adaptive regenerative brake strategy

In Figure 3, a flow chart is presented, which explains the logic behind the complete regenerative brake strategy with adaptive brake force distribution. The brake demand coming from the driver is first split between the front- and the rear axle based on the adaptive ModuED BFD strategy. Here the strategy is only adaptive to cornering intensity, however, it can be made adaptive to different driving conditions in a similar manner. Then, at the front axle, the total front axle demand,  $T_{afd}$ , is split between the motor and the hydraulic brakes based on the current speed-dependent motor torque limitations, which translate to the maximum available driveshafts torque that can be provided by the motor,  $T_{ds,max}$ . The strategy is serial [3], i.e. it is set to always use as much regeneration as possible, while any missing brake torque to fulfil the demand is delivered by the hydraulic brakes.

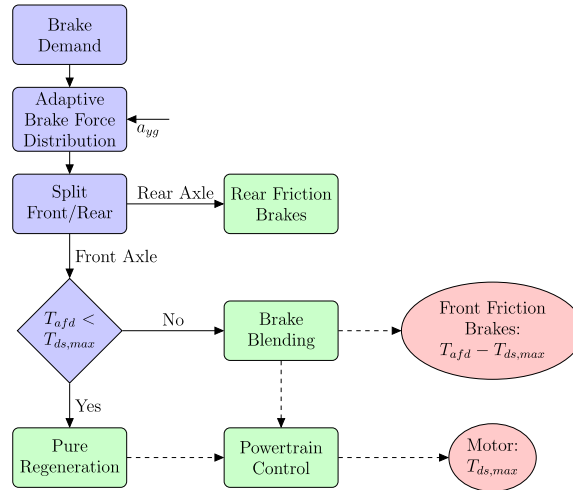


Figure 3: Flow chart of the adaptive regenerative brake strategy

#### 3.2 Powertrain and brake blending control

The longitudinal dynamics of an electric vehicle is examined using a four-DOF nonlinear one-axle vehicle model. The mechanical system of the vehicle comprises three rigid bodies for the body, the front axle, and the electric motor. The tire and motor dynamics are also modelled.

In literature, the stiffness of the driveshafts is commonly reduced to match the first natural frequency of the powertrain, the shuffle [10]. The shuffle's effect is the occurrence of oscillations in the driveshafts when the powertrain applies torque, which in the case of electric drivetrains is important both for acceleration and deceleration. Including this effect into other relevant dynamics, the nonlinear model is first linearized and then reduced for control design, creating a model similar to [11]. The model reduction is done rigorously and gives a model with its gain being adaptive to road conditions, in a similar manner to [12].

To ensure an enhanced braking performance two control algorithms are designed a powertrain controller and a brake blending control algorithm. The powertrain controller is designed to follow a desired driveshafts torque reference model, in a similar manner as in [13]. This controller actively suppresses the occurring oscillations at the driveshafts while ensures a fast and smooth torque transfer from the motor to the wheels. The powertrain controller is based on the simplified model of the powertrain described above. The primary function of the brake blending control is to speed up

blended brake response at the front axle and secondary to reduce any significant steady-state error between the demand and the actual delivered front axle brake torque. This is necessary because there are nonlinear variations in the brake response and torque delivered, which mainly occur due to the flexibility of the driveshafts [2]. The coordination of these two systems is essential, mainly for a fast and smooth brake response contributing to increased regeneration efficiency and safety.

#### 4. Vehicle energy efficiency

To assess energy efficiency in detail, a vehicle simulation model is built in *Simcenter Amesim*. The simulation model is comprised of separate models for the vehicle body, nonlinear tires, electric motor, battery and features the control subsystems presented in Sec. 3.2, as well as an automatic gear-shift algorithm for the project's two-speed gearbox. The model's architecture is shown in Figure 4.

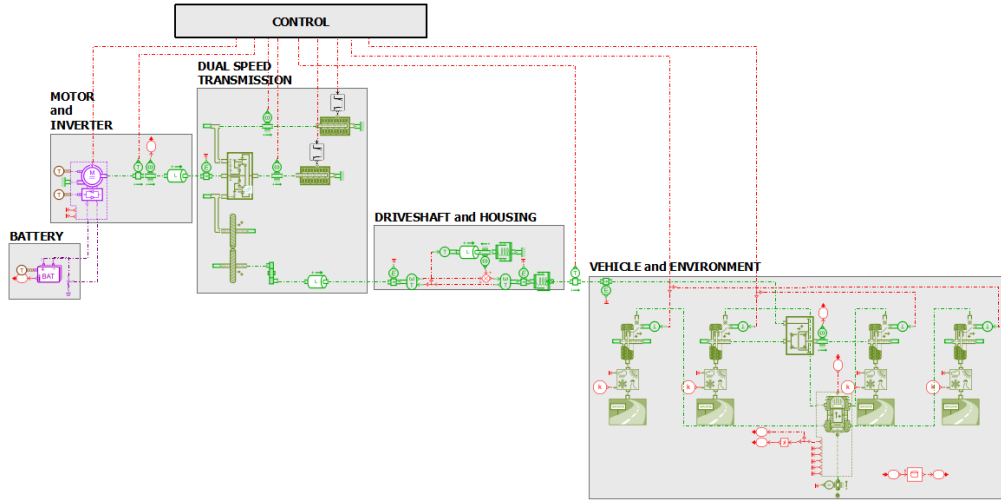


Figure 4: Vehicle model in *Simcenter Amesim*

To evaluate the contribution of regenerative braking on the vehicle's energy efficiency there are two main measures used, namely the energy consumption reduction rate and the driving range extension rate [3]. The energy consumption reduction rate  $\Delta_E$  is defined as:

$$\Delta_E = \frac{E - E_{reg}}{E} \quad (1)$$

where  $E_{reg}$  and  $E$  are the net energy consumption with and without regenerative braking, respectively.

In a similar manner the driving range extension rate  $\Delta_S$  is defined as:

$$\Delta_S = \frac{S_{reg} - S}{S} \quad (2)$$

where  $S_{reg}$  and  $S$  are the energy consumption with and without regenerative braking, respectively.

##### 4.1 Simulation scenarios

To get a better understanding of how the RBC affects energy recuperation efficiency, several driving cycles are analysed. Specifically, the NEDC, WLTC Class 3, and SFTP-US06 have been chosen as the most suitable for a common electric passenger car.

To evaluate the braking intensity content of a driving cycle, the Relative Negative Acceleration (RNA) measure is used. The RNA is calculated by focusing only on the points of the driving cycle where there is deceleration. In mathematical form this is expressed as (adapted from [14]):

$$a_{RNA} = \frac{\sum v_i a_i^-}{x} \quad (3)$$

where  $v_i$  and  $a_i^-$  are the velocity and deceleration at each timepoint of deceleration, and  $x$  is the total driving cycle distance.

The regeneration efficiency of a driving cycle varies with the BFD strategy [15]. To assess this, the regeneration efficiency is expressed as:

$$\eta_{reg} = \frac{E_e^-}{W_b} \quad (4)$$

where  $E_e^-$  is the recuperated energy and  $W_b$  is the total braking work. This measure shows in fact how much of the total braking work is recuperated for given driving cycle and BFD strategy.

## 4.2 Simulation results

A set of results is presented for each driving cycle in Table 2. On the left-hand side, the deceleration intensity content of each driving cycle is given, represented by the RNA and the portion of deceleration that is under  $1 \text{ m/s}^2$ . On the right-hand side, the efficiency of the two brake strategies is evaluated, through the regeneration efficiency  $\eta_{reg}$ , the energy consumption reduction rate  $\Delta_E$ , and the driving range extension rate  $\Delta_S$  measures.

Table 2: Driving cycle results

Cycle dec. content			Efficiency evaluation					
Driving cycle	RNA [m/s <sup>2</sup> ]	Dec. < 1 m/s <sup>2</sup> [%]	$\eta_{reg}$ [%]		$\Delta_E$ [%]		$\Delta_S$ [%]	
			Conv.	ModulED	Conv.	ModulED	Conv.	ModulED
NEDC	0.22	90	73.4	99.5	+21.1	+27.4	+26.8	+37.7
WLTC-C3	0.30	87	73.2	99.1	+20.5	+26.5	+25.8	+36.1
SFTP-US06	0.41	73	74.0	95.4	+20.6	+25.8	+26.0	+34.7

For the ModulED BFD strategy, it is observed that the efficiency measures increase inversely proportional to the deceleration intensity content of the cycle. This can be traced back to the BFD curve since for deceleration levels higher than  $1 \text{ m/s}^2$  (point A in Figure 2) the load is gradually switched to the rear to enhance handling. For all driving cycles, the ModulED strategy achieves significant energy efficiency levels, close to the maximum possible. For the Conventional BFD strategy though, there is no such clear trend. Since its brake proportioning is constant, the regeneration efficiency is also relatively constant, changing slightly depending on the energy consumption profile, as it will be shown in the energy consumption analysis later. The ModulED strategy exhibits an overall better efficiency, by recuperating more energy and extending the driving range further than the Conventional. This is in fact evaluated through the regeneration efficiency of the strategy, where the ModulED achieves an average 24.5 pp more than the Conventional. This is translated in an average 5.8 pp less energy consumed or 10 pp driving range extension gain. In Figure 5, the efficiency results from Table 2 are visualized.

Comparing the simulated configuration with the high-speed drive at the front axle and the developed regenerative brake control to the literature [3,15] the results are in favor of the former. This confirms that the high-speed drive can be used successfully for regenerative braking, resulting in very efficient solutions.

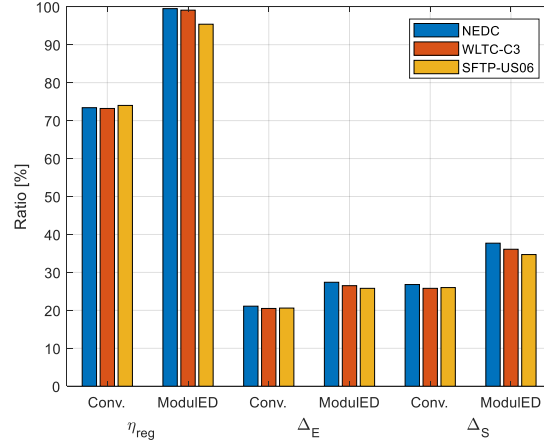


Figure 5: Regeneration efficiency  $\eta_{reg}$ , energy consumption reduction rate  $\Delta_E$ , and driving range extension rate  $\Delta_S$  results for the two brake force distribution strategies in each driving cycle

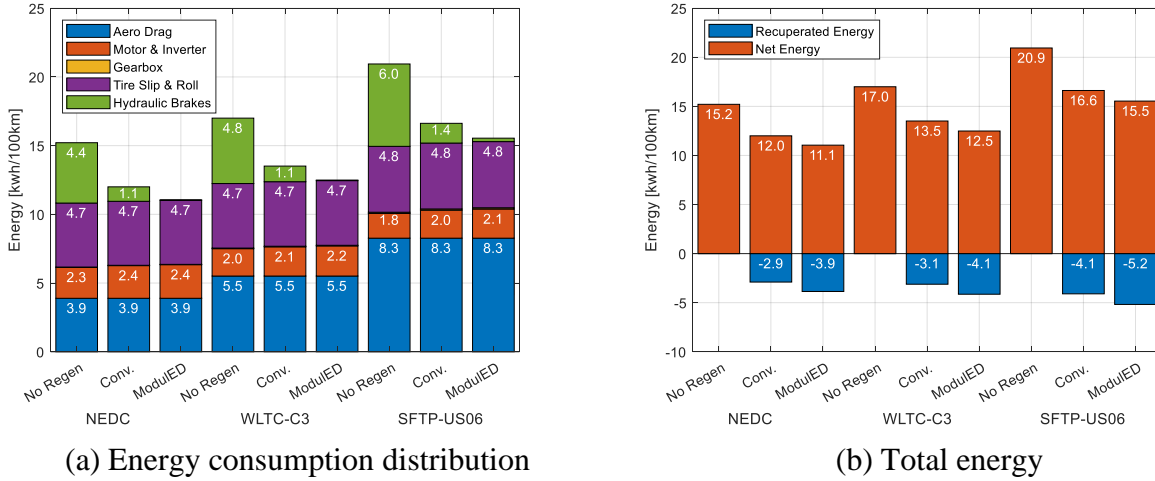


Figure 6: Energy consumption distribution for the various driving cycles and brake force distribution strategies

The analysis of energy consumption for the various driving cycles and BFD strategies is presented in Figure 6. The aerodynamic drag and rolling resistance depend only on the driving cycle and are therefore constant between the various strategies, see Figure 6a. The thermal losses in the motor and inverter though, increase slightly the more the regenerative braking is used. However, the gain reducing the use of the hydraulic brakes is more significant. The energy consumption due to the rolling resistance and slip of the tyres is almost constant between the different driving cycles. A small increase in tire slip is seen in the SFTP-US06 cycle. Reviewing the SFTP-US06 cycle in detail it is observed that the motor and inverter thermal losses are decreasing, but the hydraulic brakes are utilized more for this driving cycle compared to the other two cycles. The combination of these two losses explains mainly why there is a small increase in the efficiency of the Conventional strategy for this cycle. In Figure 6b, an increase in the total energy consumption is observed when regeneration is off. This is traced back to the increased use of the hydraulic brakes. Specifically, there is an inertial resistance at the driveshafts coming from the powertrain when the hydraulic brakes are applied, which is significantly reduced with the use of blended braking.

## 5. Conclusion

This article focuses on the regenerative brake system of an electric vehicle with a high-speed drive at the front axle. After analysing the trade-off between energy recuperation efficiency and drivability



during braking, an adaptive to cornering intensity brake force distribution strategy is proposed to handle it. It is calculated that making the brake force distribution adaptive to cornering can give a recuperation potential up to 18 percentage points relative to conventional, constant brake proportioning. Furthermore, a regenerative brake control algorithm is presented, for increased braking performance and regeneration efficiency, featuring a powertrain controller and a brake blending control algorithm. Conducted full vehicle simulations focus on the energy analysis of various driving cycles. The results show significant energy recuperation gains with the proposed regenerative brake system. In detail, the energy consumption analysis shows that using blended braking benefits the total energy consumption due to inertia effects at the driveshafts. Finally, through this work, it is shown that it is feasible to use the high-speed drive with the proposed control design for regenerative braking.

## Acknowledgments

This paper is part of the ModuLED project that has received funding from the European Union's Horizon 2020 research and innovation programme under grant agreement No 769953.

## References

1. S. A. Oleksowicz, K. J. Burnham, A. Southgate, et al., Regenerative braking strategies, vehicle safety and stability control systems: critical use-case proposals, *Vehicle System Dynamics* 51:5 (2013) 684-699
2. C. Lv, J. Zhang, Y. Li, Extended-Kalman-filter-based regenerative and friction blended braking control for electric vehicle equipped with axle motor considering damping and elastic properties of electric powertrain, *Vehicle System Dynamics* 52:11 (2014) 1372-1388, DOI: 10.1080/00423114.2014.938663
3. C. Lv, J. Zhang, Y. Li, Y. Yuan, Mechanism analysis and evaluation methodology of regenerative braking contribution to energy efficiency improvement of electrified vehicles, *Energy Convers. Manag.* 92 (2015): 469-482.
4. C. N. Kumar, S. C. Subramanian, Brake force sharing to improve lateral stability while regenerative braking in a turn, *P I MECH ENG D-J AUT* 233.3 (2019): 531-547.
5. J. Olafsdottir, M. Lidberg, P. Falcone, Energy Recuperation in Fully Electric Vehicles Subject to Stability and Drivability Requirements, *The 11th International Symposium on Advanced Vehicle Control*, 2012.
6. M. Rosenberger, R. A. Uhlig, T. Koch Uhlig, M. Lienkamp, Combining Regenerative Braking and Anti-Lock Braking for Enhanced Braking Performance and Efficiency, No. 2012-01-0234, *SAE Technical Paper*, 2012.
7. J. Hemsén, D. Kieninger, L. Eckstein, et al., Innovative and Highly Integrated Modular Electric Drivetrain, *World Electric Vehicle Journal* 10:89 (2019), DOI: 10.3390/wevj10040089
8. G. Pita-Gil, S. Amara, T. Raste, B. Bayer, Electric vehicles, a new opportunity for brake-by-wire systems, *Proc. of 16th International SIA Conference in Vehicle Dynamics*, 2011.
9. C. Lv, J. Zhang, Y. Li, Y. Yuan, Regenerative braking control algorithm for an electrified vehicle equipped with a by-wire brake system, No. 2014-01-1791, *SAE Technical Paper*, 2014.
10. V. Hermansson, K. Moparthy, Control of an electric vehicle powertrain to mitigate shunt and shuffle, *Master's Thesis*, Chalmers University of Technology, Gothenburg, 2016.
11. F. Bottiglione, A. Sorniotti, L. Shead, The effect of half-shaft torsion dynamics on the performance of a traction control system for electric vehicles, *P I MECH ENG D-J AUT* 226.9 (2012): 1145-1159.
12. Y. Hori, Y. Toyoda, Y. Tsuruoka, Traction control of electric vehicle: basic experimental results using the test EV "UOT Electric March", *IEEE transactions on Industry Applications* 34.5 (1998): 1131-1138.
13. A. Masato, Vehicle Active Motion Controls, in *Vehicle handling dynamics: theory and application*, Butterworth-Heinemann, 2015, pp. 201-229.
14. M. Weiss, P. Bonnel, R. Hummel, et. al, Analyzing on-road emissions of light-duty vehicles with Portable Emission Measurement Systems (PEMS), *JRC Scientific and Technical Reports*, EUR 24697 (2011).
15. J. Ruan, P. D. Walker, P. A. Watterson, N. Zhang, The dynamic performance and economic benefit of a blended braking system in a multi-speed battery electric vehicle, *Applied Energy* 183 (2016): 1240-1258.



## Day 2: P06 – Energy Consumption II

Session P06 – Energy Consumption II, Tuesday 15 June

---

**Session chairs:** Mathias Lidberg and Rickard Persson

- |             |  |
|-------------|--|
| 10:00-10:10 | <b>P06.A</b><br><i>Development of a vehicle-road interaction analysis framework for truck tyres</i><br>Jukka Hyttinen, Rickard Österlöf, Jenny Jerrelind and Lars Drugge     |
| 10:10-10:20 | <b>P06.B</b><br><i>Possible reduction of energy consumption with single axle running gears in a metro train</i><br>Rickard Persson, Zhendong Liu and Rocco Libero Giossi     |
| 10:20-10:30 | <b>P06.C</b><br><i>Cargo bikes – sustainable means of transportation</i><br>Saskia Biehl, Heinz Kaufmann, Artur Schönemann, Tobias Melz, William Kaal and Wilfried Kolodziej |
| 10:30-10:40 | <i>Questions and Answers</i>   |
-

## Development of a vehicle-road interaction analysis framework for truck tyres

Jukka Hyttinen<sup>1,2,3\*</sup>, Rickard Österlöf<sup>1,3</sup>, Jenny Jerrelind<sup>2,3</sup> and Lars Drugge<sup>2,3</sup>

<sup>1</sup>Scania CV AB, Södertälje, Sweden

<sup>2</sup>Engineering Mechanics, KTH Royal Institute of Technology, Stockholm, Sweden

<sup>3</sup>The Centre for ECO<sup>2</sup> Vehicle Design, KTH Royal Institute of Technology, Stockholm, Sweden

\*Corresponding author. Email: [jahyt@kth.se](mailto:jahyt@kth.se)

The current state of global warming requires immediate measures to reduce greenhouse gases and resource efficient vehicles act as a part of the solution. Rolling resistance of truck tyres is one of the main contributors to the environmental impact of road freight transport. To achieve adequate range for future battery electric trucks, parameters influencing rolling resistance and other tyre properties need to be researched carefully. Tyre manufacturers are able to affect rolling resistance by optimising tyre design, rubber compounds, and by balancing between conflicting properties such as rolling resistance, wear, particulate emissions and grip. Vehicle manufacturers on the other hand can focus on enhancing the optimal usage of the tyre with simulations and testing. The aim of the present work is to develop an FE truck tyre and road modelling framework to be able to quantify and optimise the energy consumption due to rolling resistance and its potential trade-offs with e.g. damaging vehicle forces and road damage. To build an accurate FE truck tyre model, different measurements has been performed to characterise material properties and the tyre structure. Furthermore, a suitable constitutive model is chosen which takes into account amplitude and frequency dependent stiffness and dissipation characteristics. To model the tyre rubber, a parallel rheological framework is used to simulate amplitude and frequency dependency of storage and loss modulus. Currently, there are no simple parametrisation methods and the usage of more advanced constitutive models have a trade-off between tuneable parameters and accuracy. Therefore a simple and robust parametrisation technique for filled rubber with clear and understandable tuneable parameters that can be used in FE tyre simulations is under development. The objective of the tyre model is to enable trade-off evaluations between different properties such as energy consumption and wear of truck components. The ultimate goal is to assess the society-benefit of innovative vehicle chassis and tyre technologies with the developed vehicle-road interaction framework.

© 2021 by the authors. Published by the Resource Efficient Vehicles Conference.  
This is an open access article under the CC BY license (<http://creativecommons.org/licenses/by/4.0/>).

## 1. Introduction

Rolling resistance (RR) of truck tyres consumes a very large part of the driving torque. This directly affects greenhouse gases and the profitability of truck operation. In 2019, the European Union (EU) set new targets for heavy duty vehicles to reduce average certified truck CO<sub>2</sub> emissions by 15% by 2025 and with 30% by 2030 in the EU [1]. All of the manufacturers must comply with these targets or otherwise they are given financial penalties per manufactured vehicle for excess emissions, 4250 €/gCO<sub>2</sub>/tkm by 2025 and 6800 €/gCO<sub>2</sub>/tkm by 2030. These targets require at least partial electrification of the heavy duty segment. Although the electrical motor losses are low, the batteries are much larger and heavier than the fuel tanks. This makes reduction of the aerodynamic drag and rolling resistance even more important to be able to build electrified trucks with sufficient range.

Even though rolling resistance is a well-known and researched phenomenon, it is still one of the most cumbersome tyre properties to measure and simulate. For measurements this is partly due to vertical loading forces being multiple orders of magnitude higher than measured longitudinal resisting forces and all the parameters affecting the RR. Great difficulty to characterise filled rubber behaviour arises from its highly nonlinear mechanical behaviour. Filled rubber properties are frequency, amplitude and temperature dependent [2]. Rubber even changes its mechanical properties depending on the previously applied maximum load (Mullins effect) [3], and the properties change over time when tyre experiences ageing. The mechanical behaviour of filled rubber is hysteretic, and 80-95% of rolling resistance is generated by the hysteretic behaviour of the rubber. Due to this hysteretic behaviour, a rolling tyre has a centre of contact pressure in front of the rotation axis [4] which results in a braking moment (Figure 1). Therefore accurate modelling of the tyre rubber properties is crucial for rolling resistance simulations.

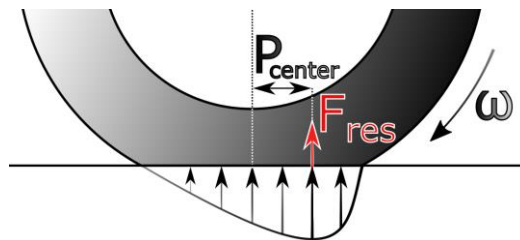


Figure 1: Contact pressure due to hysteretic behaviour of rubber in rolling motion.

The remaining part of the rolling resistance is due to frictional effects (adhesion, stick and slip) at the contact patch. These are highly dependent on the surface roughness and the rigidity of the road. All these properties together with a composite steel-rubber-fabric structure make RR highly nonlinear and difficult to model and measure. FE simulations of tyres often include nonlinear elasticity and viscoelasticity, near incompressibility, damage, large strains and rotations, follower forces, frictional effects, and possibly temperature effects.

EUs tyre labelling system ranks truck tyre rolling resistance from grade A to F and provides an easy way to compare different tyres. A is the lowest value (< 4 kg/ton) for rolling resistance and F is the most energy-inefficient tyre ( $\geq 8.1$  kg/ton). The tyre is warmed up by rolling it against a drum with 85% of the maximum tyre load, constant speed and temperature (+25 °C) until the tyre reaches a stable temperature distribution and rolling resistance, according to ISO 28580:2009 [5]. The warmup takes three hours and then a single RR value is measured. This way to evaluate RR is a major simplification and lots of information is lost by having only one measurement point. Examples of lost information are tyre pressure, different loading conditions, velocity and temperature dependency, tyre cooling and the effect of different surfaces. Rolling resistance is usually at its highest value when the tyre is cold [6]. This is interesting to note since for example distribution vehicles often drive only 10-20 minutes and then stop to unload or load the vehicle. In this case the vehicle would almost always have cold tyres and from this perspective EU labelling of rolling resistance is an insufficient indicator for these type of vehicles. Furthermore in Europe, truck drivers are not allowed to drive continuously more than four and half hours, which means that the labelled value is correct at its best only 50% of

the time during highway driving. Therefore, there is a need to develop more detailed testing and simulation methods to assess rolling resistance more accurately.

Reducing rolling resistance usually has undesirable effects on braking and handling properties and usually influences negatively the wear properties and product cost. Tyre wear generates PM1.0-PM10 size particles which can end up in alveoli and cause harmful diseases. Currently, there are no standard procedures to assess tyre particle emissions and it is difficult to know where all the particle emissions end up [7]. In certain operating conditions the benefits in lower rolling resistance might be less important than actually having a better wear resistant tyre that dissipates more energy. Better tyre recommendations based on the specific usage conditions could yield more resource efficient vehicles. It is important to be able to simulate tyres in a more accurate way to understand and balance different tyre aspects. To achieve this, the objective is to develop a vehicle-road analysis framework (Figure 2).

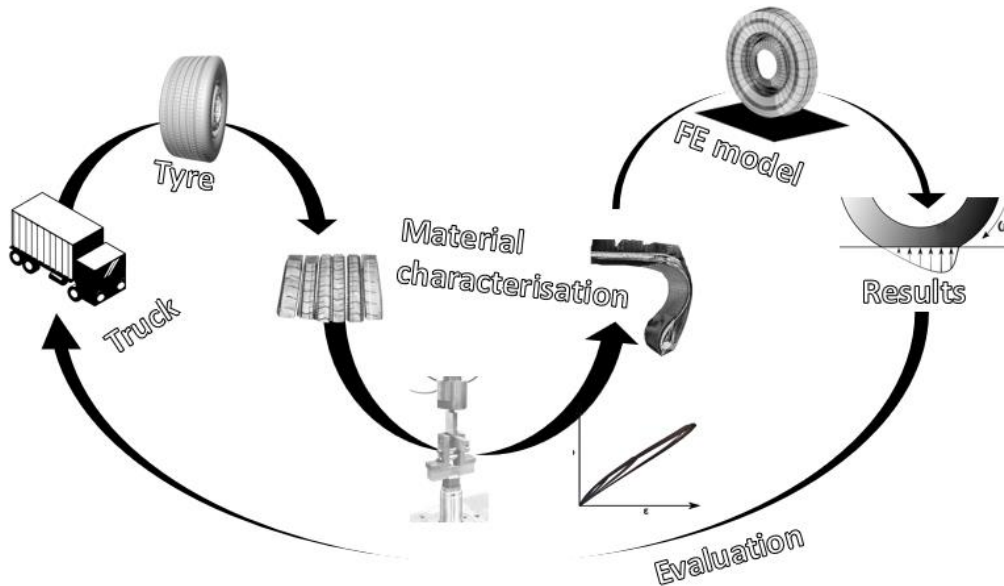


Figure 2: Framework for vehicle-road analysis.

## 2. Vehicle-road interaction

Rolling resistance can be defined as a longitudinal force resisting the motion of the vehicle. The coefficient of rolling resistance ( $C_{rr}$ ) is unitless and described as the ratio between longitudinal resisting force ( $F_x$ ) and vertical force ( $F_z$ ),  $C_{rr} = \frac{F_x}{F_z}$ . The measurements done according to the ISO 28580:2009 testing standard are correlated to a drum that has an outer diameter of 2 m with a correction equation because the contact area is smaller than driving on a flat road [5]. The usual drum values result in slightly erroneous measurement values, since a smaller diameter alters the contact pressure of the tyre and results in a too high tyre temperature. The measurements can be improved with a load cell that can be used in real road traffic.

Tyre manufacturers can reduce the rolling resistance by rubber compounding but this causes a compromise with other critical properties, e.g. comfort, grip and abrasion resistance. Rubber compounding is always balancing between conflicting goals. Vehicle manufacturers on the other hand can focus on enhancing the optimal usage of the tyre with FE simulations in an early stage of vehicle design rather than reducing rolling resistance by compounding. Parameters that contribute to rolling resistance, wear and load carrying capacity are for example number of axles, axle loads, wheel alignment, steering and suspension solutions, tyre pressure, tyre and ambient temperature. Directing cooling airflow away from the tyres could be an effective way to increase tyre temperature and reduce rolling resistance [8]. An example of the complexity of the RR and the need to understand tyre-road interaction is the effect of tyre pressure on rolling resistance. On hard surfaces, increasing tyre

pressure has a decreasing effect on rolling resistance, whereas on soft surfaces a higher tyre pressure can have an inverted effect. This is due to the larger penetration of the surface [9].

For constitutive modelling purposes it is important to take into account the amplitude dependency of the storage and loss modulus, which is called the Fletcher-Gent effect or the Payne effect [10]. Storage and loss modulus are measures of stiffness and dissipation, respectively. The Fletcher-Gent effect can be explained as a rapid decrease of storage modulus after a certain strain amplitude.

By far the most popular way to simulate hysteretic effects of tyre rubber is using Prony series in combination with a hyperelastic model [11]. The problem with linear viscoelastic models such as Prony series is that the viscoelastic properties are not dependent on the strain amplitude as they are for the rubber used in tyres. Therefore different parts of the tyre require a new set of parameters to accurately simulate the tyre rubber even if the used material would be identical. Nonlinear viscoelastic material models on the other hand are able to simulate the Fletcher-Gent effect but the parameters are not intuitive and require stress-strain data as an input for the parameter optimisation. Especially when multiple nonlinear viscoelastic models are organised in parallel the parameters lose their meaning and tuning of the parameters after optimisation becomes cumbersome. More accurate models usually have a trade-off between number of parameters and accuracy.

In this research, a viscoplastic parallel rheological modelling technique is chosen to simulate tyre rubber and it is able to capture the Fletcher-Gent effect. A parametrisation method that reduces the tuneable parameters of the constitutive model is being developed where the amount of tuneable parameters is not dependent on the number of different viscoelastic or plastic networks. Figure 3 shows the combined effects of viscoelastic, plastic and total response of all parallel models in different amplitudes and frequencies. The Prony series gives the model the rate dependency (frequency stiffening) whereas the plastic elements give the amplitude dependency for the model (Fletcher-Gent effect) and additional width of the hysteresis loops.

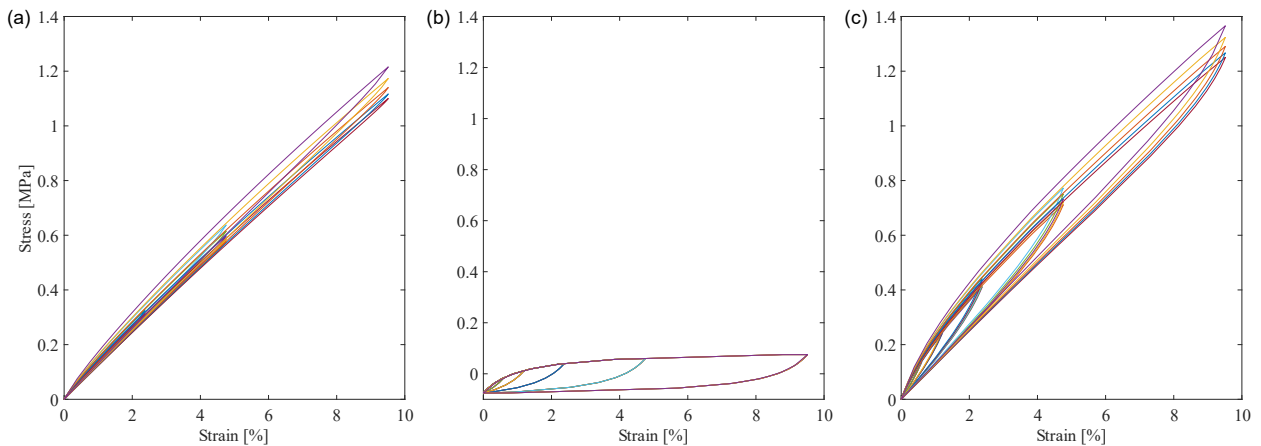


Figure 3: Example results of parametrised material model. Hysteresis loops from Prony series (a), hysteresis loops from plastic networks (b) and the total response (c).

Figure 4 illustrates the calculated storage and loss modulus values over a large range of frequencies and amplitudes. Increased rubber temperature above glass transition temperature increases the molecular movement of the rubber which reduces hysteretic effects. Thus, the rolling resistance reduces with increasing tyre temperature. The simulations can be done by parametrising the rubber in its working temperature or by making the parameters temperature dependent.

An FE truck tyre model is currently being developed with the help of reverse engineering techniques. To be able to model the tyre 3D-scanning is used for the outer geometry of the tyre. X-ray (Figure 5) and CT-scanning are used for reconstructing the belt structure. Dynamic mechanical analysis (DMA) is used to test the tyre rubber properties and is used for parametrisation. To measure different parameters a measurement fixture has been built to test the stress-strain response in shear and tension. To be able to choose sufficient amount of rubber specimens to DMA tests,



thermogravimetric analysis, laser spectrometry and IRHD hardness tests have been conducted to samples from different positions from the tyre section.

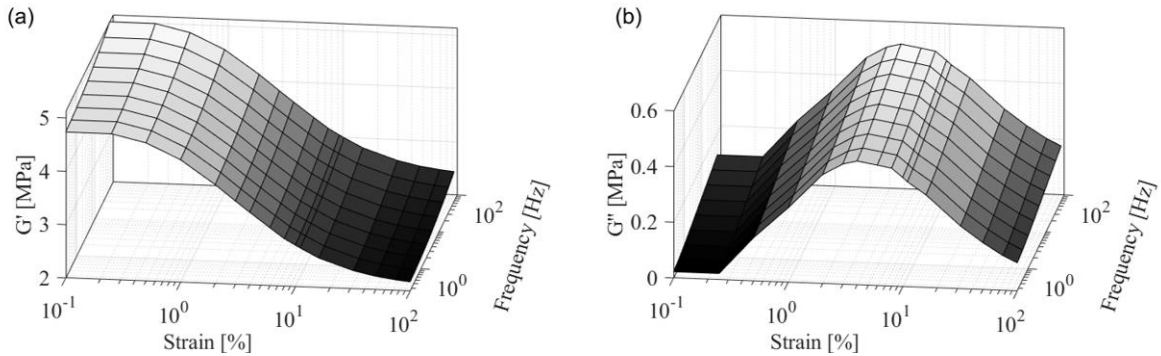


Figure 4: Amplitude and frequency dependency for the parametrised material model. (a) Storage modulus  $G'$  and (b) loss modulus  $G''$ .

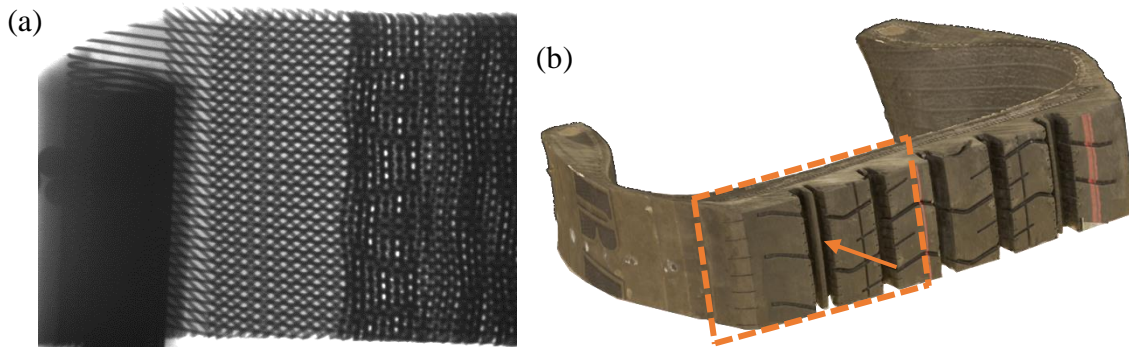


Figure 5: (a) X-ray image from the belt structure and (b) photoscanned 3D-model of a tyre section and the position of the X-ray image.

### 3. Discussion and conclusions

Understanding tyre behaviour and being able to simulate tyres accurately is essential to reach the strict green-house gas emission goals. For the tyre rubber, a suitable modelling technique has been chosen and a parametrisation technique to effectively capture the Fletcher-Gent effect is being developed. Parametrisation methods are as important as the constitutive models employed. A simple and robust parametrisation technique enables quick parameter studies and removes the need to have a set of rubber test data to conduct sensitivity studies. Moreover, the same parametrisation technique could be used with other rubber simulations such as bushing and vibration isolator simulations.

Further on, the developed FE truck tyre model is intended to be used in balancing between conflicting requirements, such as rolling resistance, wear, handling and damaging forces to the vehicle and road. With the help of an accurate physical model of a tyre within the vehicle-road simulation framework, an assessment of society-benefit of future vehicle technologies is more feasible.

In the near future, whole tyre measurements will be conducted in a climate wind tunnel using different ambient temperatures to quantify the temperature effects on transient and stabilised rolling resistance. Not only is the goal to create a vehicle-road interaction simulation framework but also to develop a convenient method to test tyre rolling resistance in real road operation. Therefore a load cell that can be used in real road rolling resistance measurements instead of usual drum and flat belt measurements is planned to be developed.

## Acknowledgements

The authors would like to thank the Centre for ECO2 Vehicle Design, funded by the Swedish Innovation Agency Vinnova (Grant Number 2016-05195), and Scania for financial support.

## References

- [1] “Road transport: Reducing CO2 emissions from vehicles,” European Union, [Online]. Available: [https://ec.europa.eu/clima/policies/transport/vehicles/heavy\\_en](https://ec.europa.eu/clima/policies/transport/vehicles/heavy_en). [Accessed 7.4 2021].
- [2] J. Bergström, *Mechanics of Solid Polymers*, Elsevier, 2015.
- [3] J. Diani, B. Fayolle and P. Gilormini, “A review on the Mullins effect,” *European Polymer Journal*, vol. 45, pp. 601-612, 3 2009.
- [4] Y. Li and R. L. West, “Rolling Resistance Revisited,” *Tire Science and Technology*, vol. 47, pp. 77-100, 3 2019.
- [5] “ISO28580 Passenger car, truck and bus tyres — Methods of measuring rolling resistance — Single point test and correlation of measurement results,” Geneva, 2009.
- [6] M. Greiner, H.-J. Unrau and F. Gauterin, “A model for prediction of the transient rolling resistance of tyres based on inner-liner temperatures,” *Vehicle System Dynamics*, vol. 56, p. 78–94, 6 2017.
- [7] M. E. Dalmau, K. Augsburg, F. Wenzel and V. Ivanov, “Tire Particle Emissions: Demand on Reliable Characterization,” *Tire Science and Technology*, vol. 48, pp. 107-122, 3 2020.
- [8] M. L. Janssen and G. L. Hall, “Effect of Ambient Temperature on Radial Tire Rolling Resistance,” in *SAE Technical Paper Series*, 1980.
- [9] J. Y. (. Y. Wong, *Theory of ground vehicles*, 3. ed.. ed., New York: Wiley, 2001.
- [10] T. Dalrymple, J. Hurtado, I. Lapczyk and H. Ahmadi, “Parallel rheological framework to model the amplitude dependence of the dynamic stiffness in carbon-black filled rubber,” in *Constitutive Models for Rubbers IX*, CRC Press, 2015, pp. 189-195.
- [11] P. N. Zitelli, G. N. Curtosi and J. Kuster, “Rolling Resistance Calculation Procedure Using the Finite Element Method,” *Tire Science and Technology*, vol. 48, pp. 224-248, 10 2019.

---

## Possible reduction of energy consumption with single axle running gears in a metro train

Rickard Persson<sup>1\*</sup>, Zhendong Liu<sup>1</sup>, Rocco Libero Giossi<sup>1</sup>

<sup>1</sup>*KTH Royal Institute of Technology, Teknikringen 8, 100 44 Stockholm, Sweden*

<sup>\*</sup>*Corresponding author. Email: patper@kth.se*

---

Running gears form a significant part of the weight of a railway vehicle, and if the weight of these could be reduced, this would affect the vehicle's energy consumption, especially for services with many stops. In the project RUN2Rail, a part of the EU-funded initiative Shift2Rail, a single axle running gear was proposed for metro vehicles. Active suspensions were suggested to overcome deficiencies in terms of ride comfort and wheelset steering, which are well known for such vehicles. The concept has been further developed in the project NextGear, also part of Shift2Rail, where the material of the running gear frame has been changed from steel to composite to further reduce the weight and the wheelset guidance updated to decrease the running resistance in curves. Prototypes of frame and wheelset steering actuator will be built and tested in the laboratory to validate the performance.

The present study is comparing a reference vehicle from Metro Madrid with the proposed vehicle in terms of energy consumption for simulated service on Metro Madrid Line 10 with curvature, gradients, stops and speed profiles considered. Only parameters with relation to the weight, curving performance and auxiliary energy consumption for the active system are assumed different for the vehicles. The vehicles are further assumed to use regenerative braking, hence the energy needed to accelerate the vehicle will be regenerated when braking, but there will be transformation losses with relation to the weight. The simulation results show that the very innovative NextGear vehicles will reduce energy consumption by 8% compared to the reference vehicles. The lower weight and the decreased running resistance in curves contribute about as much to the savings.

© 2021 by the authors. Published by the Resource Efficient Vehicles Conference.  
This is an open access article under the CC BY license (<http://creativecommons.org/licenses/by/4.0/>).

---



## 1. Introduction

Single axle running gears have been used for rail vehicles from the beginning. Most of the applications have been for freight service where performance has been less important than the acquisition cost. By adding active suspensions, the performance can be improved and brought up to level with conventional bogie vehicles. Active suspension with solutions as active tilting, hold-off-devices and active secondary suspensions have been employed on top of the line rail products [1], [2]. In the project RUN2Rail [3], a part of the EU-funded initiative Shift2Rail, active wheelset steering was proposed for a single axle running gear [4], [5]. The concept has been further developed in the project NextGear, also part of Shift2Rail, where the material of the running gear frame has been changed from steel to composite to further reduce the weight and the wheelset guidance updated to decrease the running resistance in curves.

The present study is comparing a reference vehicle from Metro Madrid with two proposed vehicles in terms of energy consumption for simulated service on Metro Madrid Line 10 with curvature, gradients, stops and speed profiles considered. The hypothesis is that the reduced weight and the active wheelset guidance will reduce the energy consumption in a metro application.

## 2. The vehicles

Metro Madrid is member of both the RUN2Rail and the NextGear projects, and it is therefore natural to take their vehicle as reference for the present study. Key data for the reference vehicle, MM S8000 [6], and the two proposed innovative 2-axle vehicles with single axle running gears (SARG) are shown in Table 1. The reference vehicle is 55 m long and challenging vehicles are given data as they would have for the same length. Parameters without relation to vehicle weight and curving resistance is assumed to be the same for all three vehicles, this group includes system efficiency, b and c-term for running resistance, acceleration and retardation. Parameters with relation to weight are assumed to vary linearly to weight, this group includes rotating masses, the a-term for running resistance, the maximum power and the tractive/braking effort. The passenger load is assumed as 500 kg/train meter. All dynamic braking is assumed for all vehicles and the auxiliary power is taken as 1 kW/train meter + the power for any active suspensions.

Table 1: Key data for the vehicles

Property	Unit	MM S8000	RUN2Rail	NextGear
Length	m	55	55	55
Tare weight	kg	104200	82500	80500
Addition due to rotating masses	kg	5210	4125	4025
Passenger load	kg	27500	27500	27500
Running resistance, term a	N	521	413	403
Running resistance, term b	N/(km/h)	10	10	10
Running resistance, term c <sup>a)</sup>	N/(km/h) <sup>2</sup>	0.3	0.3	0.3
Maximum tractive power	kW	2280	1901	1866
Auxiliary power	kW	55	62	62
Starting tractive /braking effort	kN	137	114	112
Maximum acceleration	m/s <sup>2</sup>	1	1	1
Maximum retardation	m/s <sup>2</sup>	1	1	1
Maximum speed	m/s	33.3	33.3	33.3
Breaking speed <sup>b)</sup>	m/s	16.7	16.7	16.7

a) At open air, b) The speed where the tractive /braking effort begin to reduce due to available tractive power

The reduction in tare weight is directly derived from the design of the running gear. The innovative running gear has the axle boxes on the inside of the wheels, which makes the wheel axle shorter and the frame more compact. One suspension step is eliminated, and the remaining suspension step can be a simple coil spring design. The anti-roll function is integrated into the frame instead of being a separate part, Figure 1. The shape of the running gear composite frame designed within NextGear is shown in Figure 2. A prototype of the frame will be built and tested in the laboratory to validate the performance. The additional weight for any active system is included in the estimated weights.

The reduced weight of the running gear itself leads to that less axles can carry the payload per meter train and yet complying with the maximum allowed axle load of 15 tons. The weight of propulsion equipment and other components will be reduced as spinoffs of the reduced running gear weight and is estimated to 5500 kg per vehicle.



Figure 1: Conventional bogie design (left), the innovative running gear (right)

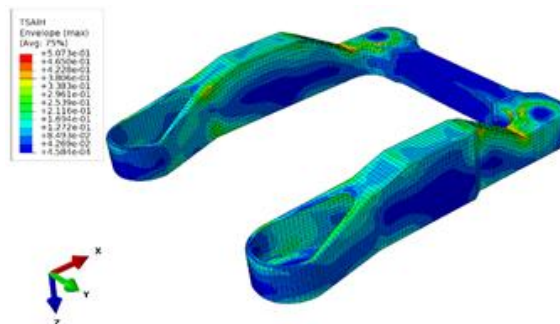


Figure 2: Strength calculation of the composite frame designed in NextGear

### 3. The active wheelset guidance

A vehicle with a passive suspension and as long wheelbase suggested for the vehicle with single axle running gears will have worse curving performance than the reference vehicle. On a metro line as the Madrid line 10 this would not only lead to unacceptable wear on wheels and rail, but also to unnecessary running resistance in curves. Active wheelset steering will improve the curving performance for the suggested vehicle to become better than the reference vehicle. For a curve with 300 m radius, which is typical on the line, the curve resistance will drop from 2676 N for the reference vehicle to 330 N for the RUN2Rail vehicle and even lower for the NextGear vehicle.

The actuators for the wheelset guidance are located directly between the axlebox and the carbody, Figure 3. The actuator has the passive wheelset guidance integrated into the same unit and is setup to work in parallel with the active system. The passive wheelset guidance ensures safety and the active system improves the curving performance. The drawback with this setup is that the active system must balance the forces from the passive guidance to create the needed yaw angle between axle and carbody [7]. In NextGear, the passive characteristic has been modified from linear to nonlinear to reduce the active force needed to achieve a radial wheelset position relative the track. A prototype of the wheelset steering actuator will be built and tested in the laboratory to validate the performance.

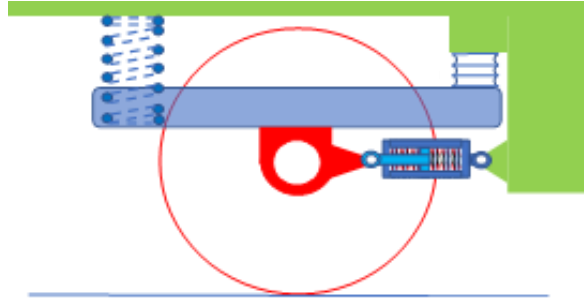


Figure 3: Side view of the single axle running gear with its wheelset steering actuator located between axlebox and carbody

## 4. The track network

The class 8000 vehicle is used on several lines of the Metro Madrid network. Line 10 is selected as reference as this line has sections with tight curves and other sections with relatively high speed making it suitable as a reference track, see Figure 4. The line goes from Hospital Infanta Sofía via Tres Olivos to Puerta del Sur. The low speed section located at 21.000 m contains as small curve radius as 100 m. Beside the speed profile and curvature, gradients and stops are considered.

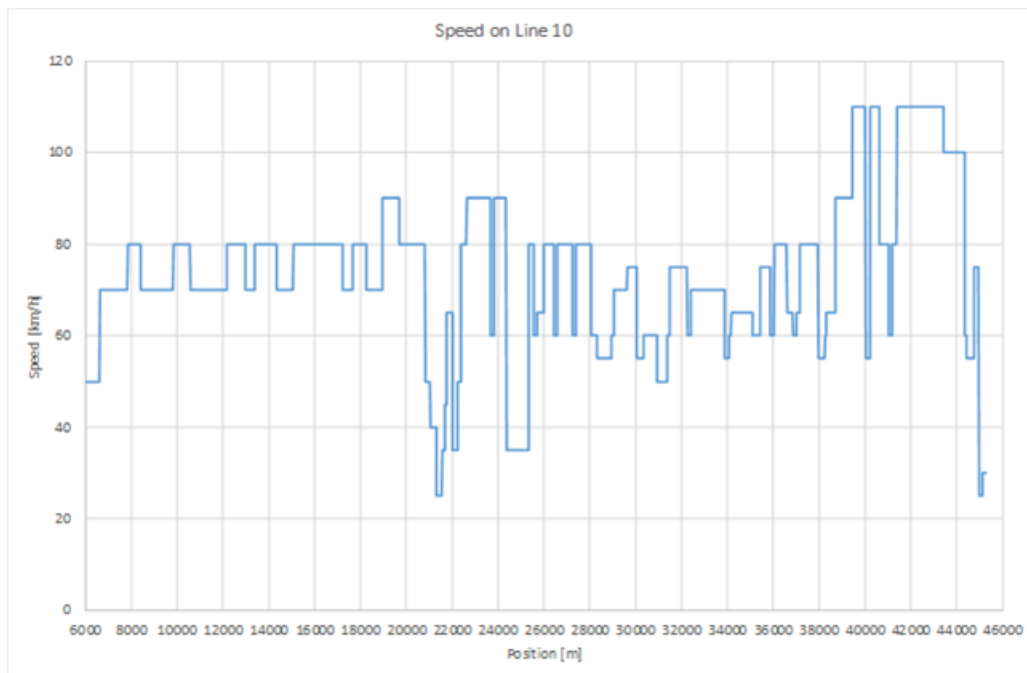


Figure 4: Line speed profile on Metro Madrid Line 10

## 5. Energy consumption

### 5.1 Calculation setup

The energy consumption is simulated for three vehicle types. The Metro Madrid class 8000 is the existing vehicle type on Line 10 and is therefore taken as reference for the study. The vehicle proposed in RUN2Rail and the further improved vehicle in NextGear are the challenging vehicles. The energy consumption for simulated service on Metro Madrid Line 10 with curvature, gradients, stops and speed profiles considered. Only parameters with relation to the weight, curving performance and auxiliary energy consumption for the active system are assumed different for the vehicles. The

vehicles are further assumed to use regenerative braking only, hence the energy needed to accelerate the vehicle will be regenerated when braking, but there will be transformation losses with relation to the weight. The calculations are made in two steps, first the vehicles are simulated on straight track with gradients and stops considered, which are performed with an in-house software STEC (Simulation of Train Energy Consumption) [8]. Most of Line 10 run in tunnels, where the aerodynamic drag is larger than in open air, this influence is considered by a standard add on derived by the Shift2Rail project FINE1 [9]. In the second step the curve resistance is added to the energy consumption.

## 5.2 Straight track

The simulation starts from Hospital Infanta Sofía via Tres Olivos to Puerta del Sur including all intermediate stops. The running resistance take account the increased drag in tunnels by an 80% addition on the running resistance c-term [10]. The auxiliary power consumption is considered as 1kw/train meter. On top of this 750 W constant power for the active suspensions per running gear is considered. It is here assumed that the running gear is equipped with active wheelset steering and active dynamic suspension in both vertical and lateral direction. The simulated gross power and reclaimed power is shown in Figure 5 and is summarized in Table 2. The reduction of about 5% in energy consumption is purely due to the weight difference as all other parameters are kept unchanged.

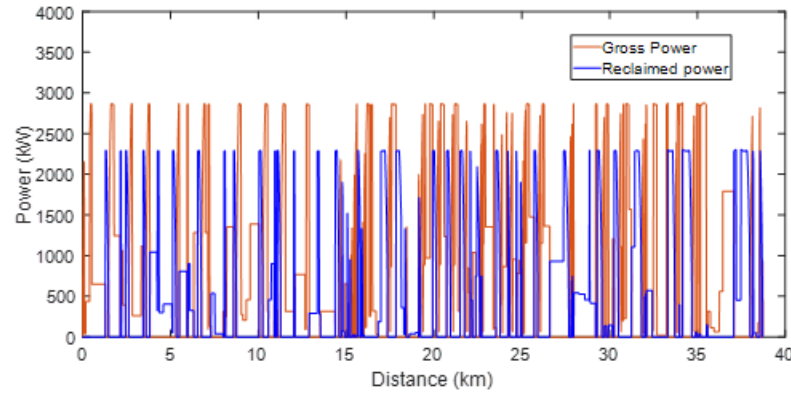


Figure 5: Gross power and reclaimed power as function of distance

Table 2: Energy consumption for one run at straight track

	Unit	Vehicle		
		MM S8000	Run2Rail	NextGear
Gross energy	kWh	520.9	454.8	448.4
Reclaimed energy	kWh	-334.5	-277.0	-271.8
Net energy	kWh	186.4	177.8	176.6
Reduction	%	-	4.6	5.3

## 5.3 Curve contribution

The additional resistance in curves and curve transitions is very dependent of wheelset guidance. Simulations are made with a multi body simulation tool (SIMPACK) where the vehicle with its masses, springs, dampers etc. are modelled. These simulations are made for a set of curves with constant radii aiming to find a regression between curve radius and curve resistance. The result is summarized in Figure 6. Different track segments are connected by clothoid transitions, where the curvature change linearly. Hence, also the curving resistance in transitions can be considered by the simulated results.

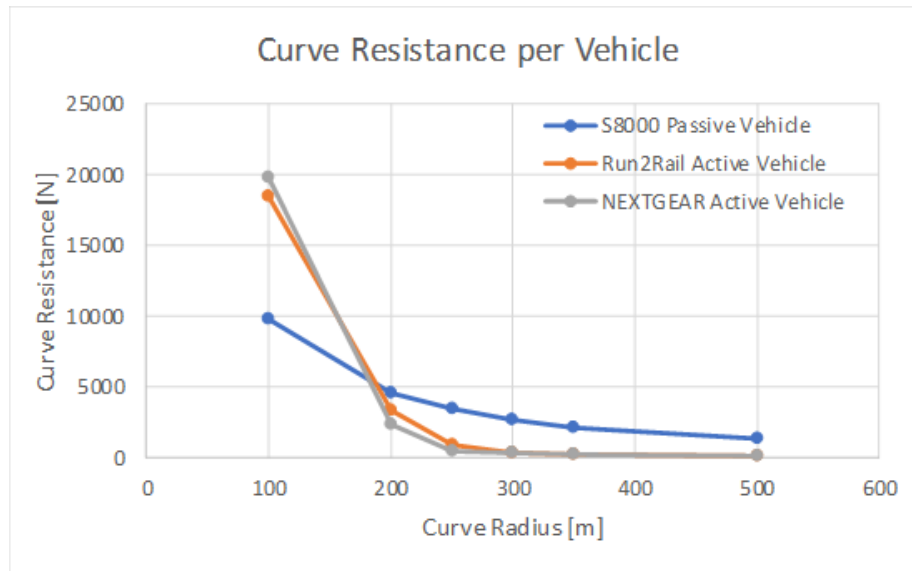


Figure 6: Curving resistance as function of curve radius for the three vehicles

The results for the two vehicles with active wheelset guidance are very good as long as the radii is not very small. At the smallest radius, the active wheelset guidance cannot compensate for the longer wheelbase compared to the reference vehicle due to the assumed actuation force limitation at 30 kN. However, as the number of small radii curves is low and the length of them limited the benefit with the challenging vehicles becomes a reduction with more than 80%, see **Error! Reference source not found..**

Table 3: Additional energy consumption in curves for one run

	Unit	Vehicle		
		MM S8000	Run2Rail	NextGear
Circular curves	kWh	6.5	1.3	1.1
Curve transitions	kWh	1.3	0.2	0.2
Total addition	kWh	7.8	1.5	1.3
Reduction	%	-	80.8	83.3

## 5.4 Total energy consumption

The total energy consumption is calculated as the sum of the energy consumption on straight track and the additional energy consumed in curves and curve transitions, see Table 4. The total energy consumed for one run on Metro Madrid Line 10 drops from 194.2 kWh for the reference vehicle to 179.3 kWh for the Run2Rail vehicle and even slightly lower for the NextGear vehicle.

Table 4: Total energy consumption for one run

	Unit	Vehicle		
		MM S8000	Run2Rail	NextGear
Straight track	kWh	186.4	177.8	176.6
Curves	kWh	7.8	1.5	1.3
Total	kWh	194.2	179.3	177.9
Reduction	%	-	7.7	8.4

## 6. Conclusion

The hypothesis is that the reduced weight and the active wheelset guidance will reduce the energy consumption in a metro application has been validated. Compared with a reference vehicle from Metro Madrid the simulated energy consumption on Metro Madrid Line 10 with curvature, gradients, stops and speed profiles considered the challenging vehicles reduce energy consumption by 8%. The lower weight and the decreased running resistance in curves contribute about as much to the savings.

## 7. Acknowledgement

This project has received funding from the Shift2Rail Joint Undertaking under the European Union's Horizon 2020 research and innovation program under grant agreement (No. 777564). The content of this paper reflects only the author's view and the JU is not responsible for any use that may be made of the information it contains.

## References

1. Goodall R., Active railway suspensions: implementation status and technological trends. *Veh Syst Dyn* 28:87-117, 1997.
2. Fu B., Giossi R., Persson R., Stichel S., Bruni S., and Goodall R., Active suspension in railway vehicles: a literature survey, *Railw. Eng. Sci.*, Mar. 2020.
3. Shift2Rail – RUN2Rail, Innovative RUNning gear soluTiOns for new dependable, sustainable, intelligent and comfortable RAIL vehicles, <http://www.run2rail.eu/>
4. Shift2Rail - Run2Rail, Innovative running gear solutions for new dependable, sustainable, intelligent and comfortable rail vehicles - Deliverable 3.2 - New actuation systems for conventional vehicles and an innovative concept for a two-axle vehicle, 2019
5. Giossi R., Persson R., Stichel S., Improved curving performance of an innovative two-axle vehicle: a reasonable feedforward active steering approach. *Veh Syst Dyn*, 2020.
6. Via Libre, Los nuevos trenes de Metro de Madrid, mayo 2010
7. Mei T. and Goodall R., "Wheelset Control Strategies for a Two-Axle Railway Vehicle," *Veh. Syst. Dyn.*, vol. 33, no. sup1, pp. 653-664, Jan. 1999.
8. MS Excel based software for Simulation of Train Energy Consumption (version 2.7), Div. of Rail Vehicles, KTH, Stockholm.
9. Shift2Rail - FINE1, Future Improvement for Energy and Noise, <https://shift2rail.org/fine1/>
10. Shift2Rail - FINE1, Future Improvement for Energy and Noise - Deliverable 3.1 - Energy baseline, 2017

---

## Cargo bikes – sustainable means of transportation

Saskia Biehl\*, Heinz Kaufmann, Artur Schönemann, Tobias Melz, William Kaal and Wilfried Kolodziej

*Fraunhofer Institute for Structural Durability and System Reliability LBF, Bartningstr. 47, 64289 Darmstadt, Germany*

\*Corresponding author. Email: [saskia.biehl@lbf.fraunhofer.de](mailto:saskia.biehl@lbf.fraunhofer.de)

---

Nowadays, mobility in cities is undergoing a visible change. Cargo bikes are becoming a key alternative to cars. They are not only flexible and fast but moreover environmentally- and climate-friendly. Young families, craftspeople and delivery services are using cargo bikes and the demand thereof is skyrocketing. This development is particularly favorable, given the climate targets that have been set not only for Germany but worldwide. Therefore, Fraunhofer LBF develops sustainable, comfortable, lightweight solutions for the next generation of cargo bikes. The key aspects of development lie in investigation of a multifunctional frame with integrated sensor and battery systems and mission-depending cargo boxes. As the starting point for these advancements, a commercial cargo bike is used.

© 2021 by the authors. Published by the Resource Efficient Vehicles Conference.  
This is an open access article under the CC BY license (<http://creativecommons.org/licenses/by/4.0/>).

---

### 1. Introduction

In 2020 for the first time more than 100.000 cargo bikes were sold in Germany of which 78.000 had electric drive [1]. There are many good reasons to expect a significant global rise in sale for these bikes within the next few years. One important reason is the global climate. The negotiated Paris Agreement of 2015 set the limit of global warming to 2 °C. This necessitates an extreme reduction of the global greenhouse gas emission. Germany has set its goal to reach an emission reduction of 65 % until 2030 in comparison to the emission values of 1990. A shift in the transportation device from car to cargo bike, is hence a good contribution in that direction. Especially for last-mile-logistics cargo bikes are very important [2-4]. Another benefit in using cargo bikes, is that it improves the quality of life. It has positive effects on health, for noise reduction in urban environment, for fast travel beside the road, for prevention of parking problems and it becomes a life-style-piece [5]. Particularly during the corona pandemic, the need for health-protecting transportation-alternative is rising and the cargo bike is one important option. To shift the cargo bike out of its technological niche into a standard means of transportation, especially in Europe, improvements are necessary, i.e. in safety, in comfort, in battery system, in the reduction of weight and in the integration of new features such as sustainable cargo boxes, sensor systems for monitoring the payload and the environment. In other markets, such as India, the requirements can be different with focus on efficient, inexpensive and agile cargo bikes. This paper presents the latest investigations in these research fields of the Fraunhofer LBF.



## 2. Experimental

### 2.1 Multifunctional lightweight frame

A commercial tricycle shown in Figure 1 presents the base case for the investigations. The front end of the tricycle was selected to demonstrate the targeted lightweight design. As a basis for this redesign, the initial data for the weight and geometry of all individual components of the front end were recorded. Driving measurements were then carried out. In the next step, the frame was redesigned by creating computer added design (CAD) models and finite elements models (FEM) derived from the initial data. Figure 2 shows a comparison of the old design and the new one in CAD.



Figure 1: Commercial tricycle with checker plate on the left hand side and with a direct view onto the front end frame on the right hand side.

The core of the new design is a tube out of an aluminum alloy (AlMgSi1) with an inner diameter of 70 mm and a thickness of just 5 mm. This tube is not only an element of the frame. It is also the housing of the new tubular designed energy system explained under 2.2. U-shaped profiles are welded to the left- and the right hand side of the tube. Also, in the new construction the checker plate is welded to the frame elements, so it gets a load-bearing function. Four load sensor systems developed for this application are mounted directly onto the checker plate as joining element for the cargo box. They are described further in 2.3 and the cargo box systems in 2.4.

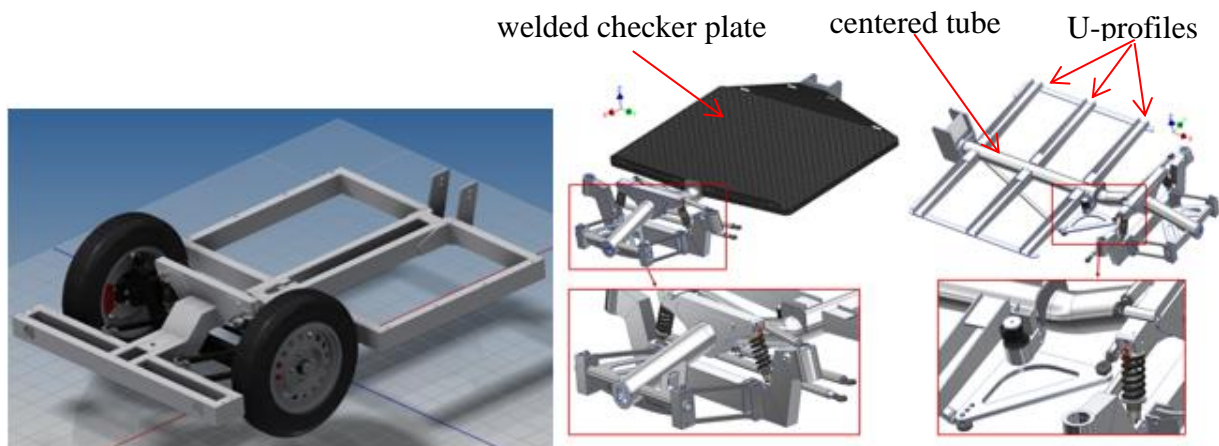


Figure 2: CAD design of the old front end on the left hand side and the new design on the right.

The new frame encloses the design and fabrication of lightweight corrugated rims (wobbly-web wheel rims), also shown in Figure 4 together with the whole modified cargo bike.



## 2.2 Tubular energy system (TES)

As shown in Figure 1, the commercial tricycle has a battery system mounted outside to the frame. It exists of 40 Li-Ion-cells and has a capacity of 500 Wh. The newly developed tubular energy system TES consists of 10 modules, each with eight Li-Ion cells (18650 round cells) connected by resistance spot welding with power connectors on the top and bottom as shown in Figure 3. These connectors are made of diffusion-annealed steel with a specially-shaped electrolytic nickel coating. On the material side, this ensures low contact resistance and high corrosion protection.

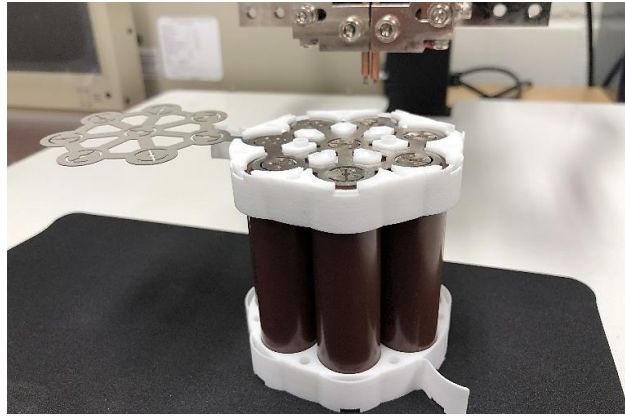


Figure 3: One module of the TES after the resistance spot welding process.

TES provides a capacity of 1.000 Wh. It is designed in a way that it can be easily integrated into the frame tube. The placement of the TES, shown in Figure 4, guarantees a weather-resistant and thief-proof place without the need of an additional case.



Figure 4: The modified cargo bike is shown on top and the TES, integrated in the frame tube under the checker plate, is arranged below.

The TES has its own battery management system and an app developed for the driver. This is very important as depending on the season, cargo bikes are not used for a longer period of time. In order to guarantee the desired reliability of the energy storage, the TES is equipped with an energy efficient storage monitoring system that continuously detects the charge and aging status of the modules and, if necessary, sends a request directly to the drivers smartphone to recharge the battery.

### 2.3 Load sensor system as joining element

The load sensor system is based on a capacitive measuring principle [6]. The schematic set-up and the real one are shown in Figure 5. An arrangement of thin elastomer foils in combination with micro-patterned metal electrodes is housed in an aluminum case with threaded connection. The whole system has a height of just 8 mm and is placed inbetween the cargo bike frame and the transport box floor. With four of these sensor systems in each corner, the box is joint with the frame very stably. These sensor systems measure the distribution and the mass of the payload in the box during the ride.

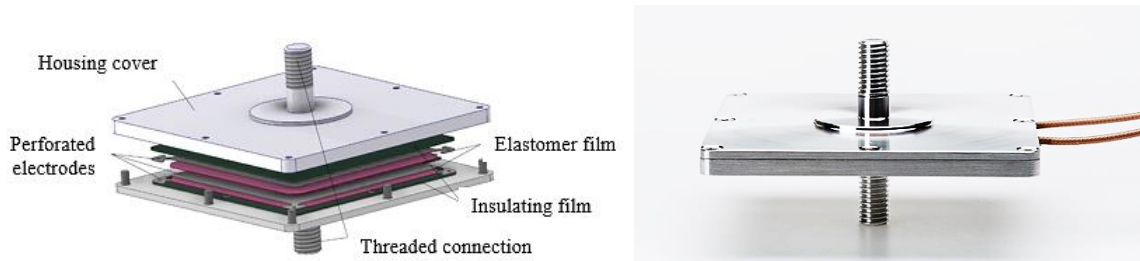


Figure 5: Schematic set-up of the sensor system on the left hand side and the ready-for-use sensor on the right hand side.

### 2.4 Mission depending cargo box development

Commercial cargo boxes are fabricated mainly out of aluminum, wood or plastic. According to customers needs, three different cargo box systems were designed with regard to sustainability and ultralightweight in combination with safety and bio-compatibility. Therefore a frame construction out of aluminum alloy was designed for different inlets to easily be integrated into this frame.

The inlets for the ultralightweight box are fabricated by additive manufacturing made of polyamide (PA6) and have different lightweight designs, like a honeycomb structure. For safety, box crash protecting structures were embedded (Figure 6 left). They absorb the impact energy and convert it into deformation energy, as demonstrated in the center of Figure 6. Also carbon fiber reinforced plastic is used for the inlets.

One hundred percent biological box inlets were fabricated out of cork granules, meadow grass, flax fiber, bark mulch in different combinations as shown in Figure 6 (to the right). Each natural inlet was bound with the biopolymer polylactide (PLA).

One hundred percent sustainable boxes with inlets out of recycling materials were fabricated as sandwich systems consisting of top layers (organic sheet made out of flax fiber reinforced recycled polypropylene (PP)) and cores (cork grist, polyurethane (PU) out of old mattresses or tearing fiber fleece out of old textiles).

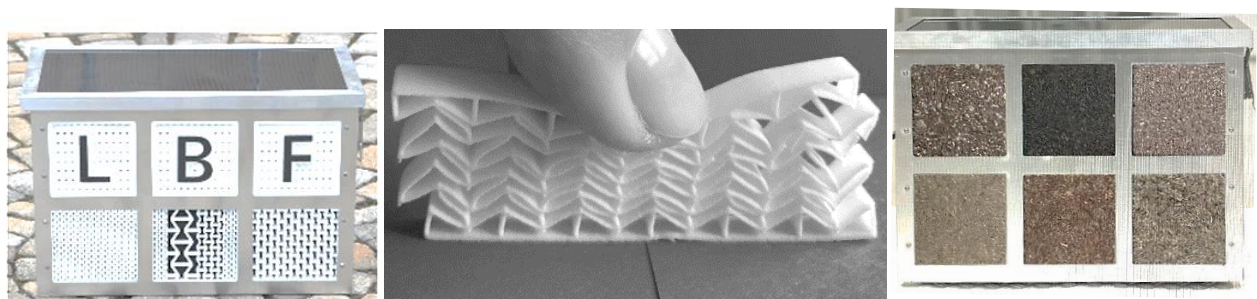


Figure 6: Transport box with ultralightweight inlets out of PA6 in different crash designs and the demonstration of the possible deformation of these structures in the center. On the right-hand side the box with 100 % natural inlets is shown.

### 3. Results and Discussion

A weight comparison of all changed parts of the front end is summarized in Table 1. It was possible to manufacture a frame that is 39 percent lighter than the commercial front end, while still having the capacity to carry the same loads of about 200 kg.

Table 1: Weight comparison between the original parts of the front end and the new ones.

Destination		Weight	Savings
Tricycle front part		105,9 kg	<b>-39 %</b>
Lightweight front part		64,7 kg	
Destination	Material	Weight	Savings
Original frame	Al	47,8 kg	-48 %
Lightweight frame	Al	24,7 kg	
Original axis	Steel	8,4 kg	-58 %
Lightweight axis	Al	3,5 kg	
Coupling elements	Steel	9,7 kg	-73 %
Lightweight coupling elements	Al	2,6 kg	
Original wheel rim	Steel	5,92 kg	-61 %
Corrugated rim	Al	2,3 kg	

With the new TES, it is possible to integrate the battery safely into the frame structure. This offers the advantages to increase the capacity up to 1.000 Wh, to extend the time of bicycling and to reduce the weight, as in this method of battery integration there is no need of a normal housing.

The joining elements with integrated sensor layer system show a linear capacitance dependency on the applied load (Figure 7 left). In this application, they not only measure the mass distribution in the box but also give the driver a monitoring system during the tour on the stability of the payload. The values are shown directly on a display mounted in front of the driver (Figure 7 right).

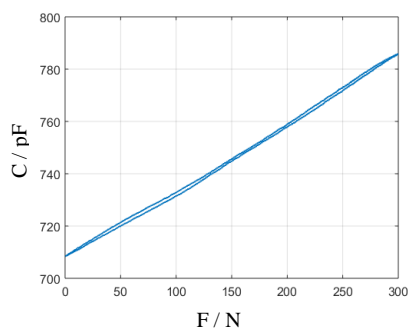


Figure 7: The characteristic linear dependency of the sensor capacitance on the load for two load-unload cycles on the left hand side and the display arrangement for the monitoring of the sensor signals on the right.

In view of a sustainable life, alternative cargo box systems will be in fashion. They ensure an effective means of transportation, due to the fact that box systems, fabricated out of natural and recycled materials show a very good thermal isolation so they enable the driver the transportation of cooked or cool food. Special lightweight crash structures offer the transportation of fragile goods.

## 4. Summary and Outlook

A change in mobility is taking place. Even for last-mile-transportation cargo bikes are playing an increasing, important role. Therefore it is important to introduce new investigations into this technology to improve the safety, the comfort, the quality and the sustainability of these vehicles. This paper shows some effective changes with regard to the battery system, the cargo box and the multifunctional lightweight frame. In the future, an active stabilization system for long john bikes, rain protecting systems for display and driver with special bio-based coatings and different sensor systems based on dielectric elastomers will be presented.

## 5. Acknowledgments

The authors would like to thank Andre Jöckel and Markus Laubenheimer for their extraordinary support in the field of ultralightweight front end development, Jan Hansmann and Marco Jackel for the driving measurements, Ye Ji Park and Sebastian Rieß for their assistance in building up the joining sensor systems and Roland Klein, Felix Weidmann, Martin Lehmann, Lena Mavie Herkenrath and Reinhold Riesner for their support in the development of the three different transport box systems.

## References

1. Zweirad-Industrie-Verband, Marktdatenpräsentation 2021, [https://www.ziv-zweirad.de/fileadmin/redakteure/Downloads/Marktdaten/PM\\_2021\\_10.03\\_ZIV-Praesentation\\_10.03.2021\\_mit\\_Text.pdf](https://www.ziv-zweirad.de/fileadmin/redakteure/Downloads/Marktdaten/PM_2021_10.03_ZIV-Praesentation_10.03.2021_mit_Text.pdf).
2. L. Rosenberg, N. Balouka, Y. T. Herer, E. Dani, P. Gasparin, K. Dobers, D. Rüdigers, P. Pättiniemi, P. Portheine, S. van Uden, Introducing the Shared Micro-Depot Network for Last-Mile Logistics, Sustainability 2021, 13, 2067, <https://doi.org/10.3390/su13042067>.
3. B. Rajesh, J. Rajan, Sustainable Performance of Cargo Bikes to Improve the Delivery Time Using Traffic Simulation Model, FME Transactions (2020) Vol. 48, No 2, 2020, pp. 411-418
4. D. L. Sárdi, K. Bóna, A Geometrical Structure-Based New Approach for City Logistics System Planning with Cargo Bikes and Its Application for the Shopping Malls of Budapest, Applied Sciences 2021, 11,3300, <https://doi.org/10.3390/app11083300>
5. L. Heinrich, W. H. Schulz, I. Geis, The impact of product failure on innovation diffusion: The example of the cargo bike as alternative vehicle for urban transport, ScienceDirect, Transportation Research Procedia 19 (2016), pp. 269-271.
6. F. Carpi, I. Anderson, S. Bauer, G. Frediani, G. Gallone, M. Gei, C. Graaf, C. Jean-Mistral, W. Kaal, G. Kofod, M. Kollosche, R. Kornbluh, B. Lassen, M. Matysek, S. Michel, S. Nowak, B. O'Brain, Q. Rei, R. Pelrine, B. Rechenbach, S. Rosset, H. Shea, Standards for dielectric elastomer transducer, IOP Publishing, Smart Materials and Structures 24 (2015), <https://doi.org/10.1088/0964-1726/24/10/105025>.

## Day 2: P07 – Life Cycle Aspects I

Session P07 – Life Cycle Aspects I, Tuesday 15 June

---

**Session chairs:** Mathias Janssen and Ciarán O'Reilly

- 11:00-11:10    **P07.A**  
*Potential for CO<sub>2</sub> equivalent emission reduction in future passenger car fleet scenarios in Europe*  
Thu Trang Nguyen, Helmut Brunner, Mario Hirz, Alexander Rust and Johann Bachler
- 11:10-11:20    **P07.B**  
*A preliminary investigation of robust design and uncertainty quantification within the life cycle energy optimisation methodology*  
Hamza Bouchouireb, Ciarán J. O'Reilly and Peter Göransson
- 11:20-11:30    **P07.C**  
*Life cycle assessment of distribution vehicles: Battery electric vs diesel driven*  
Dora Burul and David Algesten
- 11:30-11:40    **Questions and Answers**
-



# Potential for CO<sub>2</sub> equivalent emission reduction in future passenger car fleet scenarios in Europe

Thu Trang Nguyen<sup>1\*</sup>, Helmut Brunner<sup>1</sup>, Mario Hirz<sup>1</sup>, Alexander Rust<sup>1,2</sup> and Johann Bachler<sup>2</sup>

<sup>1</sup>*Institute of Automotive Engineering, Graz University of Technology, Inffeldgasse 11/II, 8010 Graz, Austria*

<sup>2</sup>*Department Research and Technology Development, Powertrain Systems, AVL List GmbH, Hans-List-Platz 1, 8020 Graz, Austria*

*\*Corresponding author. Email: t.nguyen@tugraz.at*

The CO<sub>2</sub> emission performance standards (CO<sub>2</sub> standards) set limits for fleets of new cars sold in Europe at 95 gCO<sub>2</sub>/km in 2021 and targeted 59 gCO<sub>2</sub>/km in 2030. Furthermore, the European Green Deal aims to reduce at least 55% total greenhouse gas (GHG) emissions in the continent by 2030. These legislations will undoubtedly shape future passenger car fleets in Europe. However, the current standards are solely based on Tank-to-Wheel (TTW) analysis, even though other stages of the product life cycle (LC) can contribute significantly to the overall emissions. Therefore, this paper aims at answering the question: what are possible GHG emission reduction potentials, measured by CO<sub>2</sub> equivalent (CO<sub>2</sub>eq), over the whole LC of future EU-wide passenger car fleets that meet the CO<sub>2</sub> standards? Firstly, LC CO<sub>2</sub>eq emissions of several state-of-the-art propulsion systems are examined. The technologies considered are internal combustion engine, battery electric, hybrid, plug-in hybrid and fuel-cell. Data on CO<sub>2</sub>eq emissions in different LC stages are identified via literature review and own calculations. Reduction potentials of the technologies are addressed for three scenarios, namely 2020 as a basis, 2030, and 2050. Secondly, fleet configurations are defined for the years 2020 and 2030 in order to meet the CO<sub>2</sub> standards, by considering specific TTW CO<sub>2</sub> emissions of the technologies and their shares in the EU passenger car fleet. Finally, LC CO<sub>2</sub>eq emissions of possible future fleets are calculated. The results indicate that only increasing the number of low emission vehicles entering the fleet until 2050 will not be sufficient to achieve the transport GHG emission targets. Other measures such as technology improvements, renewable-based electricity grid and e-fuels, need to be taken into account as well. Moreover, TTW-based analysis does not reflect the whole sectoral emissions, thus Well-to-Wheel or even LC emissions should be considered in legislations.

© 2021 by the authors. Published by the Resource Efficient Vehicles Conference.  
This is an open access article under the CC BY license (<http://creativecommons.org/licenses/by/4.0/>).

## 1. Introduction

The European Union aims to reduce emissions significantly by 2030 with at least 55% reduction of greenhouse gas (GHG) emissions in comparison to the 1990 level, as stated in the European Green Deal [1]. As the transport sector contributes to about one fifth of the total greenhouse gas emissions in Europe, being the second largest GHG producer after the energy sector [2], decarbonization in the transport sector has become a crucial measure to achieve stated targets. Within the transport sector, road transport is the main emitter, responsible for more than 70% of the transport GHG emissions [3]. Particularly, passenger cars cause the highest amount of emissions in comparison to other vehicle categories. Therefore, CO<sub>2</sub> standards for passenger cars were introduced in order to bring averaged

emissions from the passenger car fleet down to a limit 95 gCO<sub>2</sub>/km in 2021 (by measuring the 2020 fleet), and to further reduce to a targeted amount of about 59 gCO<sub>2</sub>/km by 2030 [4]. Thanks to this legislation, manufacturers around Europe have been improving their technologies, as well as attempt to increase the sales of zero and low carbon emission vehicles (ZLEVs) in their fleets. However, existing legislations regarding emissions of passenger cars only consider emissions occurring during the use phase (TTW). Despite the fact that LC phases of vehicle production, fuel production, electricity production (in the case of electric vehicles), and end-of-life treatment can contribute remarkably to the overall emissions of the vehicles, they are not considered in the current regulations and policies. However, as the European Union sets the vision to become the first carbon-neutral continent in the world, it may become necessary to take the whole LC, expressed via CO<sub>2</sub>eq emissions, and the entire mobility system [5], into consideration.

There are several studies on LC assessment of different propulsion systems at the European level, such as [6] [7] [8] [9] [10], as well as reports on how EU-wide passenger car fleets could meet the CO<sub>2</sub> standards [11] [12] [13]. However, studies linking TTW-based legislations and LC emissions of current and future fleets are still missing. This paper intends to fill this gap by 1) identifying CO<sub>2</sub>eq emission reduction potentials over the whole LC of EU-wide passenger car fleets that meet the CO<sub>2</sub> standards, and 2) comparing these fleet emissions with the current GHG emission targets for the transport sector.

## 2. Methodology

Based on real-life data, this paper considers the passenger car fleet in Europe consisting of ICEVs powered by gasoline, diesel, liquefied petroleum gas (LPG), and natural gas (NG), as well as BEVs, PHEVs, HEVs, and FCEVs [14]. Ethanol- and E85-powered vehicles are not considered due to their insignificant share in the fleet [15]. The same applies to HEVs with diesel engines. Currently, FCEVs also just have a small share in new car registration. However, they are included due to the fact that they can play an important role in the future [16].

At first a fleet model is created in order to examine shares of the considered vehicle technologies at present and in the future. In the second step, LC CO<sub>2</sub>eq emissions from several drive systems are identified via literature review and own calculations. Next, LC CO<sub>2</sub>eq emissions of the whole passenger car fleet are calculated according to two fleet scenarios and then compared to the transport GHG emission targets.

Three scenarios are conducted for different time points according to the CO<sub>2</sub> standards and the Green Deal goals, namely 2020, 2030, and 2050. Even though the 95 gCO<sub>2</sub>/km target is set for 2021, the data is in fact accounted for the 2020 fleet and hence scenario 2020. As the CO<sub>2</sub> standards are defined according to the New European Driving Cycle (NEDC), which is replaced by the more realistic Worldwide Harmonised Light Vehicles Test Procedure (WLTP) from 2021 on, it is important to convert the NEDC-based standards. Under the WLTP, the CO<sub>2</sub> fleet limits are approximately 109 g/km and 69 g/km for 2021 and 2030, respectively [17]. WLTP is also the basis for all scenarios.

### 2.1 Possibilities for future EU-wide passenger car fleet configurations

Data regarding the fleet of new passenger cars and the total number of vehicles-in-use are collected for the period 2010-2020 from difference statistic sources, such as the European Automobile Manufacturers Association (ACEA) [18] [19] and the International Council on Clean Transportation (ICCT) [20]. By using a simple stock-flow analysis and the historical data, numbers of different vehicle technologies are calculated.

Possible new passenger car fleet configurations to meet the CO<sub>2</sub> standard are addressed for 2020 and 2030 by combining EU-averaged specific CO<sub>2</sub> (TTW-based) emissions of the considered technologies and their respective shares in the new car sales in the market. Data from the fleet of 2019 is set as a reference to validate the calculations based on available datasets from the European Environment Agency [15]. Shares of car sales are collected for 2020 and are assumed for 2030 and

2050 [21] [22] [23]. Note that as 2020 is counted as the “transition” time, only 95% of the fleet is used for calculating the fleet-average emissions. A “super credit factor” is also considered, based on the EC regulation [4]. In order to examine how different shares of the technologies will affect the whole passenger car fleet emissions in 2050, two fleet scenarios are created for 2030, namely FS1 and FS2. In FS1, the shares of technologies in the new car fleet are assumed to meet the CO<sub>2</sub> standard. On the other hand, in FS2, an extreme case is considered, in which ZLEVs will be accounted for 90% of the new car fleet.

## 2.2 Life cycle CO<sub>2eq</sub> emissions of different propulsion systems

This paper focuses on the LC emissions of mid-size passenger cars in the European context. To extract vehicle-specific LC CO<sub>2eq</sub> emissions, various studies are compared with each other regarding their boundary conditions (e.g. vehicle mass, electricity mix, battery capacity and materials) in order to derive the most reliable data required for calculations, as shown in Table 1.

Table 1: Main parameters for calculation of LC CO<sub>2</sub> emissions

Parameter	Unit	2020		2030		2050	
		Value	Source	Value	Source	Value	Source
Vehicle lifetime	Km	161000	[18], [13]	168000	Assumed	168000	Assumed
Battery energy density	kg/kWh	4	[24]	3,6	Assumed 10% improvement since 2020	3,2	Assumed 20% improvement since 2020
BEV battery size	kWh	58	[6]	64	[6]	74	[6]
HEV battery size	kWh	2	Assumed	3	Assumed	4	Assumed
PHEV battery size	kWh	10	Assumed	15	Assumed	20	Assumed
Battery production	kgCO <sub>2eq</sub> /kWh bat	75	[7]	64	[7]	46	Assumed, based on [7]
Electricity production	gCO <sub>2eq</sub> /kWh	439	[6]	254	[6]	20	Assumed 100% renewable
Hydrogen production (NG-based)	gCO <sub>2eq</sub> /MJ	96	[9]	88,3	Assumed 8% improvement since 2020	-	
Hydrogen production (electrolysis)	gCO <sub>2eq</sub> /MJ	-		137,5	[6]	10	[9] (100% renewable)
Synthetic gasoline production	gCO <sub>2eq</sub> /MJ	-		-		57,2 (without CC) -13,8 (with CC)	[6] (20% improvement since 2020)
Synthetic diesel production	gCO <sub>2eq</sub> /MJ	-		-		34,4 (without CC) -34,8 (with CC)	[6] (20% improvement since 2020)
Battery recycling potential	kgCO <sub>2eq</sub> /kg bat	-3	[25] [26]	-10	Assumed	-12	Assumed



The total mileage is considered to be 161000km for 2020, and 168000km for both 2030 and 2050, as it is argued that ownership models could have an impact on life time expectations, as well as a potential future legislation and/or labelling of LC emissions. Data for glider and powertrain production and their recycling potential are taken from [6], with exception for the production of ICEVs. Due to noteworthy differences in the results, the average of [6] and [8] is used to represent the ICEVs production emissions. ICEVs operated with LPG and NG (alternative fuels) are presented as a joint average (ICEV-AF). The baseline scenario, representing the starting point in 2020, is mainly based on literature. Particularly, TTW emissions of vehicles operated by fossil fuels are taken from the European dataset for 2019 [15], with a 2% improvement for the assumed 2020 scenario. Based on these values, the Well-to-Tank (WTT) emissions are calculated with an online tool of the Austrian Environment Agency [27]. Beside the fossil fuels, the electricity/hydrogen consumption of BEV, PHEV and FCEV is based on the data sheets of individual cars [28] [29] [30].

For the outlook to 2030, a further 3% efficiency improvement is assumed for ICEVs and 8% for the other technologies. These gains are assumed to be acquired through fuel production (e.g. gasoline, diesel, LPG, NG, hydrogen), fuel/electricity consumption and energy density of batteries. All other influencing parameters are still based on previous studies. Regarding FCEVs, an average of NG-based hydrogen and hydrogen produced by electrolysis is calculated for representing the WTT emissions. Additionally, electrolysis process is assumed for hydrogen production, but not for e-fuels, due to the fact that e-fuel production is much less efficient than hydrogen production.

The 2050 scenario is assumed to be the best-case scenario, as assumptions are made to realize the highest emission reduction potential. The efficiency increase is assumed to be 5% for fossil fuel-based technologies and 10% for the others, compared to 2030 level. Vehicle production and recycling, as well as maintenance, are directly based on literature. The fuels used for operating are based on 100% renewable energy (e.g. synthetic gasoline, synthetic diesel, electricity, hydrogen). Furthermore, benefits from carbon capture (CC) are considered for the synthetic fuels, as it is assumed that the amount of carbon contained in those fuels can be bound from the atmosphere or from waste streaming processes. In case of LPG and NG, no e-fuels are considered due to unavailable data. For the depiction of the WTT phase, CO<sub>2</sub> capture is also included.

## **2.3 Life cycle CO<sub>2</sub>eq emissions of potential future fleets**

Vehicle-specific LC emissions are combined with their numbers in the fleet scenarios modelled in the first step to extract the LC emissions values for the whole fleets. It is important to note that for a simplified reflection, this paper assumes that the whole passenger car fleet consists of mid-size vehicles. The results are then compared with the European GHG targets for the transport sector published in 2018, namely 929 Mt CO<sub>2</sub>eq for 2030 and 337 Mt CO<sub>2</sub>eq for 2050 [3]. Even though sectoral emissions are defined as the total amount of GHG emitted in that sector according to IPCC procedures, current transport regulations are based on TTW CO<sub>2</sub> emissions, therefore there are mismatches when different boundaries are considered [31]. Thus, this paper will compare the transport GHG targets to fleet emissions against three system scales: TTW, WTW, and the whole LC. To translate these targets to the passenger car fleet only, this paper assumes that road transport still contributes to about 72% of total transport emissions, and passenger cars are responsible for roughly 44% of road transport emissions, as they are today [3].

## **3. Results and discussion**

### **3.1 Vehicle-specific CO<sub>2</sub>eq emission**

Figure 1 shows the LC CO<sub>2</sub>eq emissions of average mid-size cars, equipped with the different propulsion systems for all three scenarios. In the 2020 scenario, the BEV clearly outweighs all other drive technologies in terms of CO<sub>2</sub>eq LC emissions. Among the fossil fuel-based vehicles there are

only narrow differences due to the rather small deviations in efficiency of the ICEs. The PHEV and the FCEV line up in the middle of the field. The outlook to 2030 shows only slight CO<sub>2</sub>eq emission reduction potentials for ICE-based drive technologies, while the BEVs carbon footprint can be reduced by more than 37%. This mainly lies in the improvement of the European electricity mix, but also in an increase of battery energy density. For this scenario, conventional fossil fuels are still used for powering the ICEs, because the production of e-fuels by means of electrolysis using the European electricity mix would result in higher CO<sub>2</sub> emissions than the production of conventional fossil fuels. Also, biofuels are not considered due to the high level of sensitivity for conducting an LCA for biofuels. In scenario 2050, since the production process for synthetic diesel is much more efficient than for synthetic gasoline [6], this technology shows the greatest GHG reduction potential for ICE-based technologies. Nevertheless, the BEV provides the lowest LC emissions in the best-case scenario too, with almost half of the emissions compared to 2030. However, the FCEV's carbon footprint can get reduced by more than 67% and thus this type becomes competitive to the BEV.

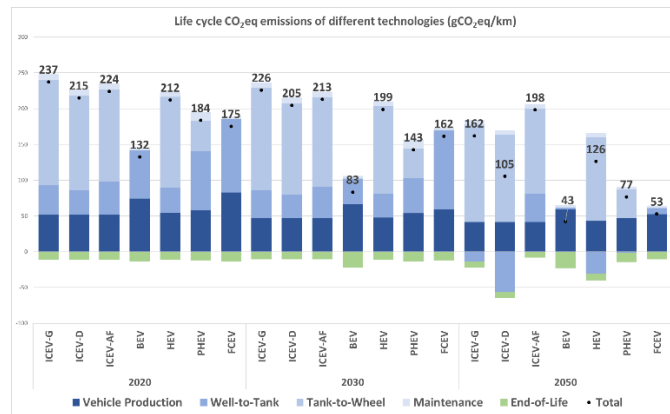


Figure 1: vehicle-specific LC CO<sub>2</sub>eq emissions for mid-size cars.

## 3.2 Fleet CO<sub>2</sub>eq emission

### 3.2.1 New passenger car fleet configurations to meet the emission targets

Table 2 indicates that the new passenger car fleet in 2020 comes closely to the demanded CO<sub>2</sub> standards, with the fleet-calculated emissions stand at 124 gCO<sub>2</sub>/km. Shares of BEVs and PHEVs increase more than double and triple in comparison to 2019, respectively. HEVs also witness a remarkable growth, almost two times more than in 2019. Alternative fuel powered vehicles also grow by 23%. In 2030 fleet scenario 1 (2030\_FS1), a new passenger car fleet with about 55% ZLEVs and a significant reduction of ICEVs powered by gasoline and diesel will be able to meet the CO<sub>2</sub> standards. Particularly, the shares of ICEV-G and ICEV-D drop by 67%. In this scenario, AF-powered vehicles, rise to account for 10% of the market share. The market for FCEVs will also grow tremendously with a share of 5%. While both BEVs and PHEVs are expected to increase exceptionally to a joint 50% share, share of HEVs will reduce moderately in comparison to 2020. Due to the large shares of ZLEVs, 2030\_FS2 demonstrates a tremendous reduction of fleet emission, with more than 50%.

Table 2: Shares in the new passenger car fleet in 2020 (actual) and 2030 (assumed)

Parameter	Technology	2019	2020	2030_FS1	2030_FS2
EU-average CO <sub>2</sub> emission based on WLTP [gCO <sub>2</sub> /km]	ICEV-G	151.0	148.0	143.5	143.5
	ICEV-D	157.0	153.8	149.2	149.2
	BEV	0.0	0.0	0.0	0.0
	PHEV	57.7	56.5	51.9	51.9
	HEV	129.2	126.6	116.3	116.3
	FCEV	0.0	0.0	0.0	0.0
	ICEV-AF	121.6	119.2	115.5	115.5

Share of sale volume in the fleet [%]	ICEV-G	58.9	47.5	15.0	0.0
	ICEV-D	30.5	28.0	10.0	0.0
	BEV	2.4	5.2	30.0	40.0
	PHEV	1.6	5.4	20.0	40.0
	HEV	5.9	11.9	10.0	5.0
	FCEV	0.0	0.0	5.0	10.0
	ICEV-AF	1.7	2.1	10.0	5.0
Super credit factor		1	2	1	1
Percentage of the fleet to be considered [%]		100	95	100	100
Fleet-calculated emissions [gCO <sub>2</sub> /km] (WLTP)		147.4	124	68.7	32.4
Fleet-average standards [gCO <sub>2</sub> /km] (WLTP)		-	109	69	69

### 3.2.2 Numbers of new vehicles, replacement and vehicles-in-use

Figure 2 indicates the number of new vehicles entering the new passenger car fleet for each scenario. In the present scenarios, the volume of new cars sales increases steadily from 12 million units in 2020 to almost 16 million in 2030 and ends up at roughly 21 million in 2050. While the 2030 fleets in FS1 and FS2 are different in terms of their configuration, the 2050 fleets have the same shares of different technologies. Regarding replacement of cars over the year, the total replaced cars are the same for both fleet scenarios in 2030 and 2050. Yet, FS1 shows higher mounts of replacement for ICEVs and HEVs, while FS2 witnesses more replacement of BEVs, PHEVs, and FCEVs, as illustrated in Figure 3. Due to the differences in in-flow and out-flow, the number of vehicles-in-use is slightly higher in FS1 than FS2 for both 2030 and 2050, as can be seen in Figure 4. The passenger car fleet in the EU rises from 248 million units in 2020 to about 277 million in 2030, and roughly 367 million in 2050. In 2030, ICEVs still contribute to the largest share of the fleet, namely 81% and 75% for FS1 and FS2, respectively. Yet by 2050, only 35% (FS1) or 25% (FS2) of the total passenger car fleet are ICEVs. It is important to note that FS2 points out that even in the case no ICEVs powered by diesel or gasoline will be sold from 2030 on, this technology will still be responsible for at least one fourth of the passenger car fleet by 2050.

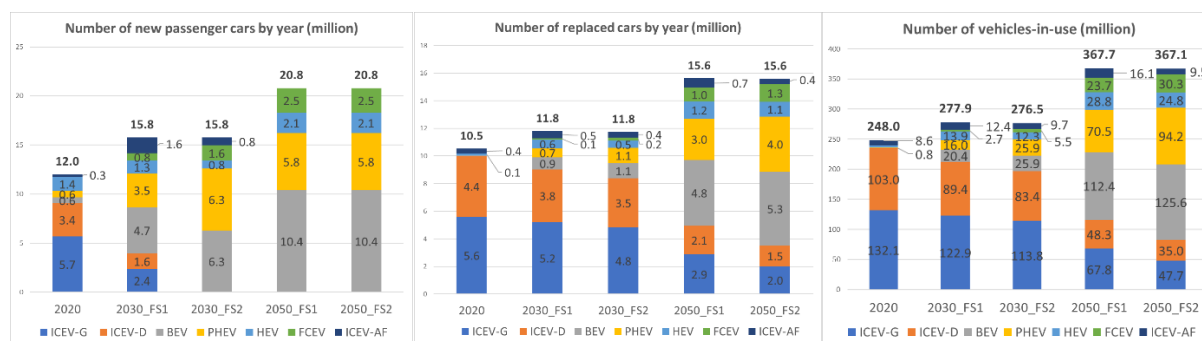


Figure 2: number of new passenger cars. Figure 3: number of replaced cars. Figure 4: number of vehicles-in-use.

### 3.2.3 Fleet emissions versus transport GHG emission targets

In Figure 5, total fleet emissions per year are illustrated according to three scales. Between 2020 and 2050, LC fleet emissions reduce by 39% in FS1 and 46% in FS2. Meanwhile, TTW emissions decrease by 33% and 46% in FS1 and FS2, respectively. If WTW emissions are considered, then a reduction of 56% in FS1 and up to 64% in FS2 is achieved. Furthermore, if passenger cars will still be responsible for the same share of road transport GHG emissions as today, 2030 and 2050 transport GHG emission targets will not be met. In 2030, passenger car TTW emissions take up to 69% (FS1) and 64% (FS2) of road transport emissions. These shares raise to 91% (FS1) and 87% (FS2) if WTW

emissions are considered. When the whole LC emissions are counted, emissions from passenger cars will surpass the transport GHG emission targets.

It is even more problematic for the fleet of 2050, as TTW emissions from passenger cars are higher than the road transport emission targets for both fleet scenarios. So even in the case of FS2, where no new ICEVs enter the fleet from 2030 on, emissions from conventional technologies still impact significantly the passenger car fleet by 2050. Due to advancements of the technologies, e-fuel production, and a higher share of renewable energy in the electricity mix in 2050, passenger cars have in fact lower WTW emissions than their TTW values. It shows that e-fuels in an electricity mix with a high renewable energy share can contribute to the efforts of making transport carbon-neutral.

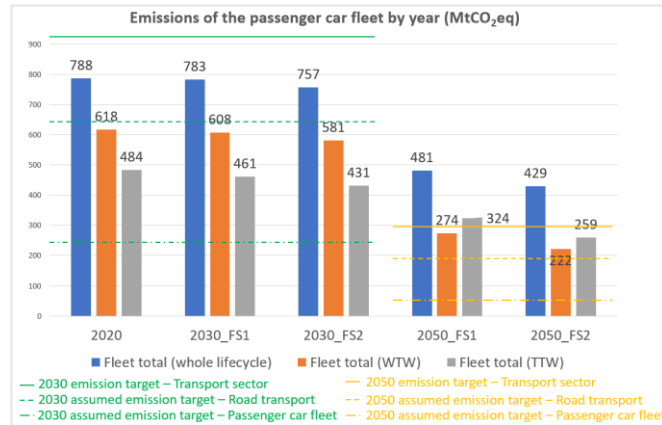


Figure 5: Emissions of the passenger car fleet by year

## 4. Conclusion

The results show that it is unlikely to achieve the European GHG emission targets for the transport sector if increasing the number of ZLEVs is the only measure. Further improvements of the technologies and efforts to lower GHG emissions from all LC stages are also necessary, as well as a transition to a renewable-based electricity mix coupling with e-fuels production. Additionally, a careful and targeted planning of incentives is in demand. It is important to focus on research to realize the upscale of technologies, such as charging, hydrogen, e-fuels, battery production. Moreover, even though passenger cars emit the highest amount of GHGs in the sector, it is critical that all other vehicle categories and transport modes also reduce their emissions significantly. TTW emissions do not reflect the real sectoral emissions, and therefore broader system boundaries should be considered, such as WTW, or at large, the whole product LC. By 2050, GHG emissions can be reduced by more than 50% if WTW emissions become the basis for calculation. As renewable energy sources contribute more and more to the European grid, e-fuels could play an important role in the future, due to the moderate amount of ICEVs still exist in the fleet by 2050.

The limitations of this paper include the simplification of the fleet configurations, as well as the various assumptions in the LC emission analysis. Future work will address these issues to gain a deeper insight of the topic. Nevertheless, the general statements regarding the impact of different car fleet scenarios on the CO<sub>2</sub> reduction shown in this paper give a holistic overview on the potentials of different technologies.

## References

1. European Commission, Communication from the Commission The European Green Deal, 11/12/2019. [Online]. Available: <https://eur-lex.europa.eu/legal-content/>. [Accessed 08/03/2021].
2. European Environment Agency, Greenhouse gas emissions by aggregated sector, 19/12/2019. [Online]. Available: <https://www.eea.europa.eu/data-and-maps/>. [Accessed 08/03/2021].
3. European Environment Agency, Greenhouse gas emissions from transport in Europe, 17/12/2019. [Online]. Available: <https://www.eea.europa.eu/data-and-maps/indicators/>. [Accessed 08/03/2021].

4. European Parliament, Regulation (EU) 2019/631 setting CO<sub>2</sub> emission performance standards for new passenger cars and for new light commercial vehicles, 17/04/2019. [Online]. Available: <https://eur-lex.europa.eu/legal-content/>. [Accessed 08/03/2021].
5. H. Brunner, M. Hirz, W. Hirschberg, K. Fallast, Evaluation of various means of transport for urban areas, *Energy, Sustainability and Society* 8 (9), 2018.
6. N. Hill, S. Amaral, S. Morgan-Price, T. Nokes, J. Bates, H. Helms, F. Horst, K. Biemann, N. Abdalla, J. Jöhrens, E. Cotton, L. German, A. Harris, S. Ziem-Milojevic, S. Haye, Determining the environmental impacts of conventional and alternatively fuelled vehicles through LCA, European Commission Brussels, 2020.
7. Transport & Environment, How clean are electric cars? T&E's analysis of electric car lifecycle CO<sub>2</sub> emissions, T&E, 2020.
8. M. Wietschel, Klimabilanz, Kosten und Potentiale verschiedener Kraftstoffarten und Antriebssysteme für PKW und LKW, Fraunhofer-Institut für System- und Innovationsforschung ISI, Karlsruhe, 2019.
9. A. Valente, D. Iribarren, D. Candelaresi, G. Spazzafumo, J. Dufour, Using harmonised life-cycle indicators to explore the role of hydrogen in the environmental performance of fuel cell electric vehicles, *International Journal of Hydrogen Energy* 45 (47), 2020, pp. 25758-25765.
10. S. Merschak, P. Hehenberger, J. Bachler, A. Kogler, Data relevance and sources for carbon footprint calculation in powertrain production, International Conference on Product Lifecycle Management - Product Lifecycle Management Enabling Smart X Rapperswil, 2020.
11. International Council on Clean Transportation, CO<sub>2</sub> emissions from new passenger cars in Europe: Car manufacturers' performance in 2019, ICCT, 2020.
12. Deloitte, Cutting CO<sub>2</sub> emissions from passenger cars - Towards a greener future for the European automotive industry, Deloitte, 2020.
13. B. Witkamp, R.-v. Gijlswijk, M. Bolech, T. Coosemans, N. Hooftman, The transition to a Zero Emission Vehicles fleet for cars in the EU by 2050, EAFO project, 2017.
14. European Automobile Manufacturers Association, Fuel types of new passenger cars, 01/08/2020. [Online]. Available: <https://www.acea.be/statistics/>. [Accessed 05/03/2021].
15. European Environment Agency, CO<sub>2</sub> emissions from new passenger cars, 23/06/2020. [Online]. Available: <http://co2cars.apps.eea.europa.eu/>. [Accessed 12/02/2021].
16. Fuel Cells and Hydrogen , Hydrogen Roadmap Europe, Publication Office of the European Union Luxembourg, 2019.
17. The International Council on Clean Transportation, 2020–2030 CO<sub>2</sub> standards for new cars and light-commercial vehicles in the European Union, ICCT, 2016.
18. European Automobile Manufacturers Association, Size and distribution of the EU vehicle fleet, 01/02/2021. [Online]. Available: <https://www.acea.be/statistics/>. [Accessed 14/02/2021].
19. European Automobile Manufacturers Association, Vehicles in use in Europe, ACEA, 2021.
20. The International Council on Clean Transportation, European Vehicle Market Statistics Pocketbook 2020/21, ICCT Europe, 2020.
21. A. Tsakalidis, C. Thiel, Electric vehicles in Europe from 2010 to 2017: is full-scale commercialisation beginning? - An overview of the evolution of electric vehicles in Europe, Publications Office of the European Union Luxembourg, 2018.
22. A. Mayyas, M. Mann, Manufacturing competitiveness analysis for hydrogen refueling stations, *International Journal of Hydrogen Energy* 44 (18), 2019, pp. 9121-9142.
23. Transport & Environment, Roadmap to decarbonising European cars, European Federation for Transport and Environment AISBL, 2018.
24. R. Haslinger, Mehr Effizienz und Reichweite, Netzintegration, 2017, pp. 113-115.
25. M. Buchert, J. Sutter, Aktualisierte Ökobilanzen zum Recyclingverfahren EcoBatRec für Lithium-Ionen-Batterien, Öko-Institute E.V. Darmstadt, 2016.
26. M. Buchert, J. Sutter, Aktualisierte Ökobilanzen zum Recyclingverfahren LithoRec II für Lithium-Ionen-Batterien, Öko-Institute E.V. Darmstadt, 2016.
27. Umwelt bundesamt, Berechnung von Treibhausgasen (THG)-Emissionen verschiedener Energieträger, 10/2019. [Online]. Available: <https://secure.umweltbundesamt.at/co2mon/co2mon.html>. [Accessed 10/03/2021].
28. ADAC, VW ID.3: Das Volks-Elektroauto im ADAC Test, 03/02/2021. [Online]. Available: <https://www.adac.de/rund-ums-fahrzeug/autokatalog/marken-modelle/vw/vw-id-3/>. [Accessed 10/03/2021].
29. ADAC, Volvo XC40 T5 Twin Engine: Das kann der Plug-in-Hybrid, 27/10/2020. [Online]. Available: <https://www.adac.de/rund-ums-fahrzeug/autokatalog/marken-modelle/volvo/volvo-xc-40/>. [Accessed 10/03/2021].
30. Toyota, Mirai Basis, [Online]. Available: <https://www.toyota.de/automobile/mirai/>. [Accessed 18/03/2021].
31. Innovation for Life, Consideration of alternative approaches to regulating CO<sub>2</sub> emissions from light duty road vehicles for the period after 2020, TNO Delft, 2013.

# A preliminary investigation of robust design and uncertainty quantification within the life cycle energy optimisation methodology

Hamza Bouchouireb<sup>1,2,\*</sup>, Ciarán J. O'Reilly<sup>1,2</sup> and Peter Göransson<sup>1,2</sup>

<sup>1</sup>*KTH Royal Institute of Technology, Teknikringen 8, 100 44 Stockholm, Sweden*

<sup>2</sup>*The Centre for ECO<sup>2</sup> Vehicle Design, Teknikringen 8, 100 44 Stockholm, Sweden*

\*Corresponding author. Email: hamzab@kth.se

The Life Cycle Energy Optimisation (LCEO) methodology aims at finding a design solution that uses a minimum amount of cumulative energy demand over the different phases of the vehicle's life cycle, while complying with a set of functional constraints. This effectively balances trade-offs, and therewith avoids sub-optimal shifting between the energy demand for the cradle-to-production of materials, operation of the vehicle, and end-of-life phases. The present work describes the inclusion of robust design aspects and uncertainty quantification into the LCEO framework. In particular, uncertainty is introduced through the assumption that the material and energy properties of a subset of the optimisation's candidate materials are described by statistical distributions as opposed to a priori fixed values. Subsequently, the nature of the LCEO-associated optimisation problem is changed from deterministic to stochastic. This change is handled by defining a multilevel representation hierarchy, and using the Multilevel Monte Carlo (MLMC) approach in the optimisation process to evaluate the expected compliance of a given design with the transport-related functional requirements. The extended framework is applied to the robust design optimisation of a subsystem of a vehicle model which is both mechanically and geometrically constrained. The ability of the LCEO methodology to include robust design aspects early during the vehicle design process, while simultaneously handling functional conflicts, to result in a robust life cycle energy optimal design is demonstrated. Furthermore, the performance increase obtained by the use of the MLMC approach instead of the classical Monte Carlo approach within an optimisation under uncertainty framework is illustrated.

© 2021 by the authors. Published by the Resource Efficient Vehicles Conference.  
This is an open access article under the CC BY license (<http://creativecommons.org/licenses/by/4.0/>).

## 1. Introduction

Between 2009 and 2017, the fleet average CO<sub>2</sub> emissions from new cars have decreased by 18.6% [1], with these improvements being mostly the result of changes targeting the vehicle's propulsion system [2] and lightweight design [3]. However, several studies have underlined the necessity to take into consideration the entire life cycle of vehicles when addressing their environmental impact through incremental design alteration or radical architecture change [3, 4, 5]. Furthermore, most of the existing methodologies that support such engineering design activities have a re-active character [6]. They are often applied to assess the environmental performance of a limited subset of design alternatives, and only use the environmental performance indicators as criteria in a down-selection process [5] rather than main design drivers. These obstacles limit their ability to lead to the emergence of radically new vehicle concepts.

The life cycle energy optimisation (LCEO) methodology [6] has been proposed as a systematic approach that yields concrete design choices while addressing the critical conflict between functionality and environmental impact [7] existing in vehicle engineering design. The methodology is intended to enable early-stage life cycle energy (LCE) efficient vehicle design through solving an optimisation problem with the LCE as its objective function, while the functional requirements that the design is subject to are implemented as optimisation constraints.

Previous work on the LCEO methodology has concerned: the introduction and the formalisation of the methodology, and the investigation of the impact of the inclusion of the production and use-phase energies [6]; the impact of end-of-life (EOL) modelling [8]; the functional extension of the framework through the preliminary examination of the effect of vehicle shape and aerodynamic drag estimations [9]; as well as the expansion of the framework to enable vehicle production system design optimisation [10].

Beyond widening the area of applicability of the framework and uncovering fundamental links between the very mechanisms enabling the embodiment of the LCE optimal designs and the vehicle's life cycle parameters, the aforementioned works also underscore the high dependency of the optimal solutions on a number of parameters. Some of these parameters are characterised with a high level of uncertainty, whether intrinsically or due to the circumstances of conceptual vehicle design. For instance, EOL parameters are characterised with a high level of uncertainty as they are related to the lifespan of vehicles and their future use; while the uncertainty of the use phase-related energy estimates is due, in part, to the use of relatively lower fidelity models. The *epistemic uncertainty* introduced by such models is related to the so-called design paradox [11]: the amount of vehicle-specific knowledge is at its lowest when it is most needed, that is during the conceptual stage. Furthermore, due to the intrinsic variability of manufacturing – and EOL – processes, *aleatoric uncertainty* is expected in such quantities as the material properties.

Thus, in order to identify solutions – or classes of solutions – to the LCE optimisation problem that remain stable within a reasonable range of variation of these aforementioned parameters, it is necessary to include aspects of robust design and uncertainty quantification within the LCEO methodology. This is particularly relevant for cases including vehicle, or vehicle subsystem, models that are characterised by large design landscapes, and that are therefore more likely to feature large variations in optimal design outcomes based on changes in the optimisation parameters; and remains relevant for smaller models as it allows for the quantification of the impact of parameter uncertainty on the mechanisms enabling the optimal solutions.

This paper constitutes a first proof of concept of the introduction of uncertainty quantification within the LCEO framework. Therefore, it only targets one of the dimensions of the larger robustness problematic and does not aim at providing a comprehensive treatment of the latter within the LCEO methodology. In particular, this work targets the introduction of uncertainty in some of the parameters influencing the mechanical performance of a subset of the constitutive materials of a vehicle subsystem. This uncertainty may stem from the intrinsic variation in production processes, or even more so from mixing recycled materials with the virgin material stock. Indeed, the properties of the vehicle's constitutive materials can be significantly degraded depending on the EOL processing options considered.

The consideration of uncertainty in the mechanical parameters of the constitutive materials alters the nature of the optimisation problem at hand. The latter becomes constrained by a stochastic system of partial differential equations rather than a deterministic one. This is handled by using the non-intrusive, and relatively more computationally efficient, Multilevel Monte Carlo (MLMC) [12] approach in order to evaluate the verification of the functional transport-related constraints at any given design point during the optimisation loop.

The results show the gap in LCE between the deterministic solution and the robust formulation, as well as the performance increase obtained from the use of the MLMC approach instead of the classical Monte Carlo (MC) one within an Optimisation Under Uncertainty (OUU) framework. Furthermore,



a discussion of how additional aspects of robustness can be included in the LCEO framework is also provided.

Section 2 provides an overview of the LCEO methodology, as initially introduced in [6] and further elaborated in [8], as well as a brief description of the MLMC approach as introduced in [12]. Subsequently it presents the benchmark illustrative case study that has been established in previous works [6, 8, 9, 10, 13] and extends it to a stochastic formulation in order to accommodate the introduction of forward uncertainty quantification into the methodology. Following this, Section 3 presents some preliminary results that establish the optimality gap between the robust solutions and the deterministic ones and illustrates the performance increase associated with the use of the variance reduction scheme of the MLMC approach in lieu of the MC alternative. Finally, a summary outlook on the steps necessary to provide a more comprehensive treatment of uncertainty within the LCEO methodology is provided in Section 4.

## 2. Methodology

### 2.1 LCEO methodology

The LCEO method formally integrates environmental considerations into a design methodology through the formulation of a mathematical multidisciplinary design optimisation framework. The life cycle energy is used as the objective function to be minimised, as detailed in [6]. Functional requirements stemming from structural mechanics, and eventually other disciplinary fields, act as constraints on the design. Thus, this methodology does not compromise design requirements, but rather changes design variables so as to find the design solution which features the minimum life cycle energy use while fulfilling all the transport related functional requirements.

The life cycle energy is formulated as

$$E_L(X) = E_P(X) + E_U(X) + E_E(X), \quad (1)$$

where  $E_L$  is the life cycle energy,  $E_P$  is the production energy,  $E_U$  is the use-phase energy,  $E_E$  is the end-of-life energy, and  $X$  is the set of design variables.

The production energy is obtained from the embodied energy of the constitutive materials of a given design; while the EOL energy is obtained from the sum of two distinct contributions, and is expressed as

$$E_E(X) = E_{Pro}(X) + E_{Rec}(X). \quad (2)$$

$E_{Pro}(X)$  corresponds to the energy burdens and credits associated with the EOL processing of the material entering into the composition of the vehicle subsystem considered, while  $E_{Rec}(X)$  corresponds to the corrected energy credits resulting from the EOL processing phase of the aforementioned vehicle subsystem [8]. A scenario-based approach is adopted for the treatment of the different material candidates entering into the composition of the vehicle subsystem, with more specific details about these scenarios being provided along with the description of the case study considered in this work in Section 2.3.1.

Finally, the use phase energy is obtained through multiplying the energy required to move the vehicle according to a prescribed drive cycle (New European Drive Cycle) by the number of such cycles during the entire use phase of a vehicle. The associated optimisation problem is expressed as

$$\min(E_L(X)), \quad (3)$$

subject to constraints of the form:

$$T_{(I)}(X) \leq 0, \quad (4)$$

$$T_{(E)}(X) = 0, \quad (5)$$

$$X_{min} \leq X \leq X_{max}. \quad (6)$$



Equation 4 corresponds to functional requirements expressed as inequalities, while Equation 5 refers to the functional requirements which are expressed as equalities. The last equation, Equation 6, is the set of design variable boundaries.

## 2.2 Multilevel Monte Carlo

The central idea of the MLMC approach is that Monte Carlo samples can be simultaneously and independently drawn on several approximations of the studied problem on a hierarchy of computational grids – or levels – with an associated decreasing sequence of mesh sizes  $h_0 > h_1 > h_2 > \dots > h_L$  and an accordingly increasing number of degrees of freedom.

The linearity of the expectation operator  $\mathbb{E}[\cdot]$  enables the expression of the expectation of a given Quantity of Interest (QoI)  $Q$  at the finest level,  $\mathbb{E}[Q_L]$ , to be rewritten as a telescopic sum of the expectation of the QoI at the coarsest level,  $\mathbb{E}[Q_0]$ , and a sum of correction terms adding the difference in expectation of the QoI between evaluations at the consecutive levels denoted by the subscript  $l$ :

$$\mathbb{E}[Q_L] = \mathbb{E}[Q_0] + \sum_{l=1}^L \mathbb{E}[Q_l - Q_{l-1}]. \quad (7)$$

Using sample average approximations, the MLMC estimator of  $\mathbb{E}[Q]$  can be defined as the following:

$$\mathbb{E}^{MLMC}[Q_L] := \frac{1}{M_0} \sum_{m_0=1}^{M_0} Q_0^{(m_0)} + \sum_{l=1}^L \frac{1}{M_L} \sum_{m_l=1}^{M_L} (Q_l^{(m_l)} - Q_{l-1}^{(m_l)}). \quad (8)$$

where  $Q_i^{(m_j)}$  refers to the  $j^{th}$  realisation of the QoI at the  $i^{th}$  mesh refinement level. Thus, the term  $(Q_l^{(m_l)} - Q_{l-1}^{(m_l)})$  comes from two discrete approximations at two different refinement levels ( $l$  and  $l-1$ ) evaluated for the same samples. A presumption of this approach is that the mesh hierarchy provides errors and computational costs that respectively decrease and increase algebraically with  $h_l$ .

A computational complexity analysis of the error of the MLMC estimator shows that it is composed of a discretisation error and a statistical error. For a given error tolerance level, a splitting parameter can be introduced to split the tolerance requirements over both error sources. Subsequently, the optimal number of samples at different levels can be obtained by minimising the computational cost of the MLMC estimator subject to the accuracy constraint based on the statistical error; while a stopping criterion for the amount of levels to be added can be derived using the discretisation error constraint. More details about the MLMC algorithm can be found in [12].

## 2.3 Illustrative case study

This section reformulates the previously established LCEO benchmark problem [9] as a multilevel stochastic PDE-constrained optimisation problem with the QoIs intervening at the level of the design constraints. It also describes the simplifying assumptions made in order to compute the relevant QoIs more easily.

### 2.3.1 Description of the target vehicle subsystem

The MLMC augmented LCEO methodology is applied to the case study of the design of a vehicle component to illustrate the impact of uncertainty quantification into the framework. In particular, the vehicle component considered is the roof of a car, which has already served as a benchmark for previous LCEO studies [6, 8, 9, 10, 13]. The model considered here is two dimensional and relies on symmetry to reduce the size of the problem.

The car roof panel is assumed to be a sandwich panel consisting of three layers: two thin face sheets and a thicker core. This design choice introduces the face sheet layer thicknesses  $t_i$ , the core

layer thickness  $t_c$  and the material volume fractions  $V_{i,j}$  as the design variables. The face sheets of the panel may be composed of a blend of carbon fibres (CF) and glass fibres (GF) as reinforcements to a thermosetting epoxy matrix. The core of the panel can be composed of a blend of polyvinylchloride (PVC), polyethylene (PET), and polyurethane (PUR). The material properties and embodied energies of these materials are provided in [6]. The hybridisation concept is used to allow for the continuous representation of the intra-layer material properties [14].

Two EOL scenarios are considered for the processing of the materials entering into the composition of the panel: a high and a low recycling scenario. In the first idealised reference scenario, it is assumed that little to no material property degradation takes place for CF and GF and that their resulting recyclates can entirely replace virgin fibres. On the other hand, in the second scenario, only a modest amount of recovered fibres is presumed to be able to be mixed with the virgin fibres. In order to limit the complexity of the study, the materials of the core layer are assumed to be incinerated with energy recovery in both scenarios. The processes as well as energy burden and credit values used in the optimisation are shown in Table 1.

Table 1: Overview of the two EOL scenarios modelled and the EOL credit and burden energy values used in the optimisation. Adapted from [8].

Nr.	Description	$E_{Pro}$ [MJ/kg]					$C_f$		$E_{Rec}$ [MJ/kg]	
		CF	GF	PET	PVC	PUR	CF	GF	CF	GF
1	CF Pyrolysis GF Shredding	30	0.17	-23.8	-22.9	-24	1	1	-286	-30
2	CF Milling GF Shredding	0.27	0.17	-23.8	-22.9	-24	0.3	0.3	-85.8	-9

Typical automotive design requirements that can be formulated on a vehicle's roof are related to loading cases in the event of the car rolling over [15], flutter behaviour under driving conditions [16] as well as fundamental sound transmissions properties. Therefore, two maximum displacement under load and two minimum frequency constraints are formulated on the panel. The maximum displacements allowed under local and global unit static pressures are set to  $d_{1,max} = d_{2,max} = 2.5 \times 10^{-6}$ ; while the minimum frequencies for the first and second natural frequencies of the panel are set to  $f_{1,min} = 330$  Hz and  $f_{2,min} = 520$  Hz.

### 2.3.2 A multilevel stochastic formulation of the associated design problem

As a result of the application of the EOL processing alternatives presented in Table 1, as well as the inherent variability in production processes, the material properties of CF and GF can vary. In order to more accurately capture the impact of this effect on the optimal solutions, the material properties associated with these candidate materials are described through presumed probability distributions, instead of deterministically. Therefore, the LCEO problem presented in Section 2.1 becomes an optimisation problem constrained by a system of partial differential equations with random coefficients.

Consequently, the deterministic inequality constraints  $d_i(X) \leq d_{i,max}$  and  $f_i(X) \geq f_{i,min}$ , for  $i = 1, 2$ , have to be reformulated as the chance constraints  $P(d_i(X) \leq d_{i,max}) = 1$  and  $P(f_i(X) \geq f_{i,min}) = 1$ . However, the computation of such constraints can be challenging, and it is suggested here to relax them using statistics of the displacement and normal mode QoIs. Such a relaxation has been previously used in the context of reliability-based design optimisation of aircraft components [17].

The relaxed constraints for  $i = 1, 2$  are formulated as

$$\mathbb{E}[d_i(X)] + n\sigma[d_i(X)] \leq d_{i,max}, \quad (9)$$

$$\mathbb{E}[f_i(X)] - n\sigma[f_i(X)] \geq f_{i,min}, \quad (10)$$

with  $n$  an integer and  $\sigma[\cdot]$  the standard deviation operator.

The MLMC solver is used, in conjunction with a deterministic solver of the system of elastostatic equations implemented in FreeFem++ [18], in order to estimate the relevant statistics of the QoIs introduced in the relaxed constraints within the Differential Evolution population-based optimiser [19]. To this end, a mesh hierarchy is defined for the FEM model of the sandwich panel. In this work, a geometric mesh hierarchy is defined by taking  $h_l = h_0\beta^{-l}$ , where  $h_l$  is the mesh size at level  $l$ ,  $h_0$  the mesh size at the coarsest level and  $\beta \geq 2$  is a constant integer.

### 3. Results

The preliminary results presented here are obtained for the inclusion of uncertainty at the level of the Young's modulus of the CF material candidate. It is assumed that the modulus follows the uniform distribution  $\mathcal{U}(0.95E_N, 1.05E_N)$  centred around its nominal value  $E_N$ . The stochastic optimisation results are obtained for a relatively generous tolerance level of  $\epsilon_{TOL} = 0.1$ ,  $\beta = 2$  and  $n = 3$ . Both deterministic and stochastic results shown in Tables 2 and 3 are obtained for a total driving distance of 60,000 km, and are optimised for both EOL scenarios presented in Table 1.

Table 2: Deterministic optimisation results.

EOL Scenario	$E_L$ [MJ]	$m$ [kg]	$V_{CF}$ [%]	$V_{GF}$ [%]	$t_1$ [mm]	$V_{PVC}$ [%]	$V_{PUR}$ [%]	$t_c$ [mm]
1	220	0.71	100	0	0.43	62	38	24.6
2	248	0.51	100	0	0.2	41	59	29.7

Table 3: Stochastic optimisation results.

EOL Scenario	$E_L$ [MJ]	$m$ [kg]	$V_{CF}$ [%]	$V_{GF}$ [%]	$t_1$ [mm]	$V_{PVC}$ [%]	$V_{PUR}$ [%]	$t_c$ [mm]
1	222	0.81	100	0	0.44	92	8	22.9
2	250	0.58	81	19	0.22	46.3	53.7	30.8

Table 4: Typical number of deterministic model evaluations observed per mesh hierarchy level in the MLMC approach.

Mesh level	0	1	2	3
Number of model evaluations	868	50	50	1

A comparison between the stochastic and deterministic optimisation results presented in the aforementioned tables shows that the uncertainty characterising CF's Young modulus can be handled with a sub 1% LCE premium and with significant design changes. Indeed, the inclusion of robustness in the optimal designs leads to a mass increase of roughly 14% in both scenarios. However, this mass increase is arrived at differently depending on the EOL scenario considered.

In the first scenario, CF-associated uncertainty is neutralised by increasing the amount of CF used as well as increasing the amount of the stiffer PVC in the core of the panel. On the other hand, in the

second scenario, the same is achieved by replacing a fifth of the amount of CF with the previously unused GF.

These large variations in the optimal design with a relatively small impact on the LCE are likely the result of the multimodality of the design optimisation problem considered. However, it remains to be seen if this demonstrated flexibility would endure were the material properties of the other constitutive materials to also be described stochastically.

Finally, the performance of the MLMC approach can be illustrated by the break-down of model evaluations per mesh hierarchy level shown in Table 4. The latter shows that, for the design point considered, most of the FEM model calls are performed at the lowest level (0), and only one call is performed at the highest level (3). Conversely, fulfilling a similar tolerance level using the MC approach would typically require a number of model calls of the order of  $10^3$  at a mesh level comparable to mesh level 2 in Table 4.

## 4. Summary and outlook

In this paper, it was demonstrated on an illustrative case study how uncertainty can be systematically and efficiently included in the LCEO methodology to enable robust design aspects to be considered early during the vehicle engineering design process. This was achieved by capitalising on the relatively increased computational efficiency offered by the MLMC approach within an OUU context. The results of this study have shown that – under the assumption of the stochastic variation of the material properties of one of the constitutive materials of a vehicle subsystem – robust alternative LCE optimal designs can be obtained at a marginal LCE increase relative to the deterministic optimal solution. Additionally, these robust designs constitute a significant departure from the deterministic ones, with the design changes varying depending on the life cycle scenario considered.

Further work includes more rigorously handling the estimation of the higher order statistical moments of the constraints-related QoIs using estimators such as the ones introduced by Bierig & Chernov [20] or Pisaroni [21], as well as considering uncertainty at the level of the material's energy properties. The latter step would lead to a reformulation of the optimisation problem introduced in Equations 3, 4, 5 and 6 to involve statistics of  $E_L(X)$  in the objective function to minimise. It is worth noting here that this reformulation significantly increases the computational complexity of the problem as it would involve solving a nested optimisation problem (that may itself involve a sampling-based approach similar to that presented in this paper) at every sample needed for the computation of the LCE's statistics.

## 5. Acknowledgement

The authors would like to thank the Centre for ECO<sup>2</sup> Vehicle Design at KTH, funded by the Swedish Innovation Agency Vinnova, aimed at supporting the development of resource efficient vehicles in a sustainable society; and the strategic research area TRENoP and the Swedish Research Council Formas for their financial contributions to this work.

## References

1. European Environment Agency. Monitoring CO<sub>2</sub> emissions from new passenger cars and vans in 2016. EEA Report No. 19/2017, 2017.
2. Constantine Samaras and Kyle Meisterling. Life cycle assessment of greenhouse gas emissions from plug-in hybrid vehicles: Implications for policy. *Environmental Science & Technology*, 42(9):3170–3176, 2008.
3. Hyung-Ju Kim, Colin McMillan, Gregory A. Keoleian, and Steven J. Skerlos. Greenhouse gas emissions payback for lightweighted vehicles using aluminum and high-strength steel. *Journal of Industrial Ecology*, 14(6):929–946, 2010.

4. Troy R. Hawkins, Bhawna Singh, Guillaume Majeau-Bettez, and Anders Hammer Strømman. Comparative environmental life cycle assessment of conventional and electric vehicles. *Journal of Industrial Ecology*, 17(1):53–64, 2013.
5. S. Poulikidou, C. Schneider, A. Björklund, S. Kazemahvazi, P. Wennhage, and D. Zenkert. A material selection approach to evaluate material substitution for minimizing the life cycle environmental impact of vehicles. *Materials & Design*, 83:704–712, 2015.
6. Ciarán J. O’Reilly, Peter Göransson, Atsushi Funazaki, Tetsuya Suzuki, Stefan Edlund, Cecilia Gunnarsson, Jan-Olov Lundow, Pontus Cerin, Christopher J. Cameron, Per Wennhage, et al. Life cycle energy optimisation: A proposed methodology for integrating environmental considerations early in the vehicle engineering design process. *Journal of Cleaner Production*, 135:750–759, 2016.
7. Daniel P. Fitzgerald, Jeffrey W. Herrmann, and Linda C. Schmidt. A conceptual design tool for resolving conflicts between product functionality and environmental impact. *ASME J. Mech. Des.*, 132(9), 2010.
8. Hamza Bouchouireb, Merle-Hendrikje Jank, Ciarán J. O’Reilly, Peter Göransson, Josef-Peter Schögggl, Rupert J. Baumgartner, and José Potting. The Inclusion of End-of-Life Modeling in the Life Cycle Energy Optimization Methodology. *Journal of Mechanical Design*, 143(5), 11 2020. 052002.
9. Hamza Bouchouireb, Ciarán J. O’Reilly, Peter Göransson, Josef-Peter Schögggl, Rupert J. Baumgartner, and José Potting. The inclusion of vehicle shape and aerodynamic drag estimations within the life cycle energy optimisation methodology. *Procedia CIRP*, 84:902–907, 2019.
10. Hamza Bouchouireb, Ciarán J. O’Reilly, Peter Göransson, Josef-Peter Schögggl, Rupert J. Baumgartner, and José Potting. Towards holistic energy-efficient vehicle product system design: the case for a penalized continuous end-of-life model in the life cycle energy optimisation methodology. In *Proceedings of the Design Society: International Conference on Engineering Design*, volume 1, pages 2901–2910. Cambridge University Press, 2019.
11. Mattias Lindahl and Erik Sundin. Product design considerations for improved integrated product/service offerings. In *Handbook of Sustainable Engineering*, pages 669–689. Springer, 2013.
12. Michael B. Giles. Multilevel monte carlo path simulation. *Operations research*, 56(3):607–617, 2008.
13. Hamza Bouchouireb. Advancing the life cycle energy optimisation methodology. Licentiate thesis, KTH Royal Institute of Technology, 2019.
14. M.F. Ashby and Y.J.M. Bréchet. Designing hybrid materials. *Acta materialia*, 51(19):5801–5821, 2003.
15. Tengfei Bi, Haibin Li, and Kun Wang. Research on the test and assessment method for roof crush resistance. In *2017 9th International Conference on Measuring Technology and Mechatronics Automation (ICMTMA)*, pages 232–235. IEEE, 2017.
16. David Stotera, Terence Connelly, Bryce Gardner, Eric Seifferlein, and Ricardo de Alba Alvarez. Testing and simulation of anti-flutter foam and high damping foam in a vehicle roof structure. Technical report, SAE Technical Paper, 2013.
17. Shantaram S. Pai, Rula Coroneos, and Surya N. Patnaik. Reliability-based design optimization of a composite airframe component. NASA Tech Briefs, NASA Glenn Research Center, 2011.
18. F. Hecht. New development in FreeFem++. *Journal of Numerical Mathematics*, 20(3-4):251–265, 2012.
19. Kenneth Price, Rainer M. Storn, and Jouni A. Lampinen. *Differential evolution: a practical approach to global optimization*. Springer Science & Business Media, 2006.
20. Claudio Bierig and Alexey Chernov. Convergence analysis of multilevel monte carlo variance estimators and application for random obstacle problems. *Numerische Mathematik*, 130(4):579–613, 2015.
21. Michele Pisaroni. *Multi level monte carlo methods for uncertainty quantification and robust design optimization in aerodynamics*. PhD thesis, EPFL, École Polytechnique Fédérale de Lausanne, 2017.



Life cycle assessment of distribution vehicles

# Battery electric vs diesel driven





# Executive summary

Scania's purpose is to drive the shift towards a sustainable transport system. A holistic view is key both to support our customers' business as well as addressing environmental impacts. Life Cycle Assessment (LCA) is an ISO 14040/44 method to calculate the environmental impacts of products or services over their entire life cycle: in this case the vehicle and battery production, use, maintenance and recovery.

LCA in Scania is used to evaluate the product's environmental impacts and setting internal project targets in product development. Scania has built up in-house capacity and competence to conduct LCA and guides the organisation via LCA as a fact base. With this external LCA publication Scania takes a step further to inform stakeholders of key LCA findings.

Scania is in the middle of a transformation with already connected, more electrified and arising autonomous products and services. For Scania's product development this means more than producing a few electrified vehicles – a complete modular toolbox is needed to offer the great variety of commercial vehicles also as electrified. Scania's first fully serial produced BEV was launched during the autumn of 2020. This made the choice easy to conduct this first publicly available LCA as a comparison between a representative distribution BEV, available in the first launch, with a corresponding ICEV.

The study covers the entire vehicle life cycle from cradle to grave, starting at the extracting and refining of raw materials and ending at the recovery of the vehicles. The chosen functional unit has the aim to reflect and represent a full life of operation for the vehicles. The functional unit is: 500 000 km driven in a representative distribution cycle with an average payload of 6,1 ton.

The vehicle technical properties, besides the drive trains, are kept as similar as possible to make the comparison as fair as possible. The installed battery capacity in the BEV is 300kWh. European grid mix with reference year 2016 is used as the baseline for the carbon intensity in the electricity used in the BEV. Additional grid mixes have been investigated to analyse the impact from future prognosed mixes as well as green electricity. The fuel used for the ICEV is B7 diesel with 7% RME drop-in, representative for European conditions.

The production of the BEV entails a higher environmental impact, mainly due to energy intensive battery cell manufacturing. GHG emission raises from 27,5 tonnes CO<sub>2</sub>eq (ICEV production) to 53,6 tonnes CO<sub>2</sub>eq (BEV production). GHG emissions coming from production of battery cells are 74kg CO<sub>2</sub>eq/kWh of installed battery capacity. Despite the increased production burden, the total life cycle impact on climate change shows a dramatic reduction potential for the BEV, thanks to the much lower impact from the use phase. Depending on the carbon intensity in the EU electrical grid, the life cycle GHG reduction spans from 38% (EU mix 2016) to 63% (prognosed EU mix 2030). Powering the vehicle with green electricity is the way to fully utilise the potential with the BEV. The results show a life cycle GHG reduction of 86%.

*"a BEV entering the EU market after 2020 will have more than 50% life cycle GHG reduction compared to the diesel alternative"*





Due to the higher GHG emissions from the production, BEV vehicles can be seen as having a carbon debt in comparison to ICEV. The GHG debt will somewhere in time be repaid due to the lower use phase emissions per km. This is usually called the break-even point, the point in time when the BEV starts having a smaller total GHG impact than the ICEV. Depending on the carbon intensity, the break-even occurs between 33 000 km (green electricity) to 68 000 km (baseline 2016). This indicates that the BEV has the potential to have less climate impact than the ICEV already within one or two years of operation, for all investigated electricity mixes in the report.

At the End-of-Life Scania traction batteries are collected, dismantled, shredded and recycled by collection and recycling partners. The exact recycling process depends on geographical location and partner setup. Due to the varying market setups (pilot vs large scale recovery) and limited relevant data, the choice has been to exclude the battery recycling from the recovery model. Further, no second life of the battery is assumed in the LCA model, meaning that the full production burden is attributed to the Scania vehicle's life cycle.

There is also a dramatic reduction potential for other impact categories like fine particle formation, ozone creation and terrestrial acidification. The reduction in these categories lies between 83-97%, mainly due to eliminating tailpipe emissions.

Fossil resource use and eutrophication of marine- and freshwater also decrease significantly (18-48%) for the BEV, even though there are a considerable impact related primarily to coal in the electricity generation. The main reason is that well-to-tank impact from diesel production is higher than the impact coming from electricity generation.

*“With sustainable battery production and green electricity, GHG reduction potential for the BEV will be well more than 90%”*

This LCA gives a view of the magnitude and relationship between environmental impacts for the BEV and the ICEV distribution trucks. However, the LCA results, especially in absolute terms are not intended to be compared to other OEMs. The choice of functional unit, methodology, scope and access to primary data will have a great influence on the final result.

All facts and figures in this report are third party verified in a background report (Scania internal). The verification was done by IVL Svenska Miljöinstitutet following the ISO 14040/44 standard.

## Authors

Dora Burul  
Energy Economy and Sustainability  
Scania R&D

David Algesten  
Energy Economy and Sustainability  
Scania R&D

## Contact

Andreas Follér  
Head of Sustainability  
[andreas.foller@scania.com](mailto:andreas.foller@scania.com)



## Day 2: P08 – Life Cycle Aspects II

Session P08 – Life Cycle Aspects II, Tuesday 15 June

---

**Session chairs:** Marco Pierini and Mathilda Karlsson Hagnell

- 11:50-12:00    **P08.A**  
*System-wide impact of vehicle innovations – Evaluating Track-friendliness during vehicle design*  
Carlos Casanueva, Visakh V Krishna and Sebastian Stichel
- 12:00-12:10    **P08.B**  
*A life cycle energy and weight comparison of a carbon fiber composite versus metallic component in a commercial vehicle*  
Sara Eliasson, Mathilda K. Hagnell, Robert Jonsson, Per Wennhage and Zuheir Barsoum
- 12:10-12:20    **P08.C**  
*The environmental benefits and challenges of the composite car with structural battery materials*  
Frida Hermansson, Ivan Berg, Kevin Sandberg, Leif E. Asp, Matty Janssen and Magdalena Svanström
- 12:20-12:30    *Questions and Answers*
-

---

# System-wide impact of vehicle innovations – Evaluating track-friendliness during vehicle design

Carlos Casanueva<sup>1</sup>, Visakh V Krishna<sup>1\*</sup> and Sebastian Stichel<sup>1</sup>

<sup>1</sup>*Department of Engineering Mechanics, KTH Royal Institute of Technology, Teknikringen 8, 100 44 Stockholm, Sweden*

<sup>\*</sup>*Corresponding author. Email: [visakh@kth.se](mailto:visakh@kth.se)*

---

The cost of maintenance of railway tracks due to vehicle passage is a major limiting factor to the competitiveness of railway sector in EU. For instance, in Sweden in 2017 only, 2800 million SEK was spent on track maintenance and reinvestment due to wear and tear caused by traffic. Considering this, there is a major incentive to operate track-friendly vehicles that also facilitate economically feasible maintenance strategies. In this context, the NEXTGEAR project aims to incorporate a track-friendliness module in the ‘Universal Cost Model 2.0’ that can estimate operating costs for a given set of operational parameters such as vehicle suspension design, energy usage, track geometry, etc. Such a tool could be useful in estimating the costs for a train operator for a given route and application. However, estimation of costs due to track damage is a complex cross-disciplinary task encompassing varying domains such as vehicle dynamics, tribology, economics, maintenance policy etc so that actual damage in the infrastructure can be linked to maintenance actions and thus costs. Currently there are two major diametrical approaches such as the ‘Bottom-up’ Engineering approach that seeks to create accurate engineering models of vehicle, track, etc. Then there is the ‘Top-down’ Econometric approach that seeks to create statistical models linking the operating variables with historically recorded cost data. Also, track damage itself manifests in various forms such as wear RCF and settlement and it is extremely useful to understand the distribution of costs amongst them. Nowadays a Hybrid approach is being developed that can bridge the limitations of the other two methods. Eventually all these models seek to calculate differential operating costs due to the introduction of vehicle innovations during the design stage, hence contributing to the overall economic feasibility of the railway system.

© 2021 by the authors. Published by the Resource Efficient Vehicles Conference.  
This is an open access article under the CC BY license (<http://creativecommons.org/licenses/by/4.0/>)

---

## 1. Introduction

In the European Railway Sector, track owners and vehicle operators have been separated for the last decades, which decouples the different railway subsystems (infrastructure ownership, vehicle operation, maintenance for either of them, and rail vehicle manufacturing) so that there can be new players that compete for the commercial exploitation of these subsystems. The theoretical promise is that this allows for a better optimisation of the different subsystems. While technically true, there are still interactions between these actors, so the actions taken by one of them do affect the rest of the stakeholders.

In this context there are usually no issues regarding the daily operation of railway systems, where the individual optimisation of the subsystems can still be the optimal system case. However, vehicle innovations have almost completely disappeared due to the fact that the stakeholder that pays for the

vehicles, the Vehicle Operator (VO), does not receive a significant economic benefit out of these innovations. There are certain benefits for the VO, such as reduced need for wheel maintenance, or lower energy consumption, but the economic savings that impact the vehicle directly are not enough for justifying a higher initial cost. However, if a system perspective is adopted, there are also benefits for the Infrastructure Manager (IM) as track damage is reduced, which might have a significant impact on the long-term savings for the whole railway system. A solution to try to overcome this limitation is to charge vehicle operators a variable Track Access fee that depends on how the specific vehicle influences track deterioration, but in the existing schemes the cost is calibrated against the marginal cost of track maintenance, so the operator would need existing experimental measurements and actual costs for the vehicles being studied. So an innovative running gear at a prototype stage (or lower TRL) cannot be used for the calibration of these models.

EU project Roll2Rail developed the so-called Universal Cost Model (UCM) that accounts for all aspects of running gear innovations that influence the whole railway system's Life Cycle Costs (LCC) [1]. The main objective is to create simulation-based framework and tools that will allow to compare a reference vehicle against an innovative one, showcasing the differential costs and benefits due to a certain innovation. It will increase the awareness of the impact of different bogie design concepts on different costs of the railway system, allowing Infrastructure Managers to assess different vehicle offers for a certain system, or the influence on an existing track of a novel vehicle concept, and even contribute to optimize maintenance and replacement cycles for Infrastructure Maintainers. Eventually, the usage of the UCM by a critical mass of stakeholders will steer the railway market to a minimisation of system-wide LCC.

## 2. Track-Friendliness

A key step towards calculation of life-cycle costs incurred at the wheel-rail interface is the assessment of track-friendliness of a wagon during its design stage. 'Track-friendliness' of a wagon/bogie design is its propensity to cause minimal damage to track during its passing, which indirectly gives a measure of the expected costs incurred by the infrastructure manager in maintaining and replacing track components. Track damage itself manifests in different forms, each governed by a complex physical phenomena and requiring separate mitigating measures.

A lot of prior work exist to assess track-friendliness of freight wagons to help decide track access pricing strategies in the EU. These can be broadly classified into two approaches as explained by Smith et al. [2]:

- *Bottom-up approach*: They involve engineering simulation methods that estimate the track damage caused by the rail vehicles. Since the physical phenomena that cause damage is modelled step-wise and scaled up for a required running distance/ tonnage passage of wagons, it is regarded as 'Bottom-up'
- *Top-down approach*: These involve econometric methods that estimate a relationship between the actual maintenance costs obtained historically and the different attributes of traffic passing on the track using econometric methods. They do not explicitly consider the physical phenomena responsible for the creation and propagation of damage. They directly start from the final costs incurred to the infrastructure manager and therefore regarded as 'Top-down'.

Both approaches carry some distinct advantages and address a part of the multi-disciplinary nature of track access pricing. There exist multiple methods in literature that come under each of the above approaches. Some of these methods are described in this section.

### 2.1 Engineering approach

Figure 1 illustrates a 'pure' engineering approach where detailed characteristics of vehicle, track operation (suspension design, track radii, wheel-rail contact friction levels, speeds, etc) are taken as inputs. Based on various running scenarios, the damage caused to track via various damage modes are calculated through Multi-Body-simulations (MBS) simulations. The outputs from simulations

help quantify the damage. Öberg et al. [3] for instance identifies four modes of track damage and lists the damage quantification expression.

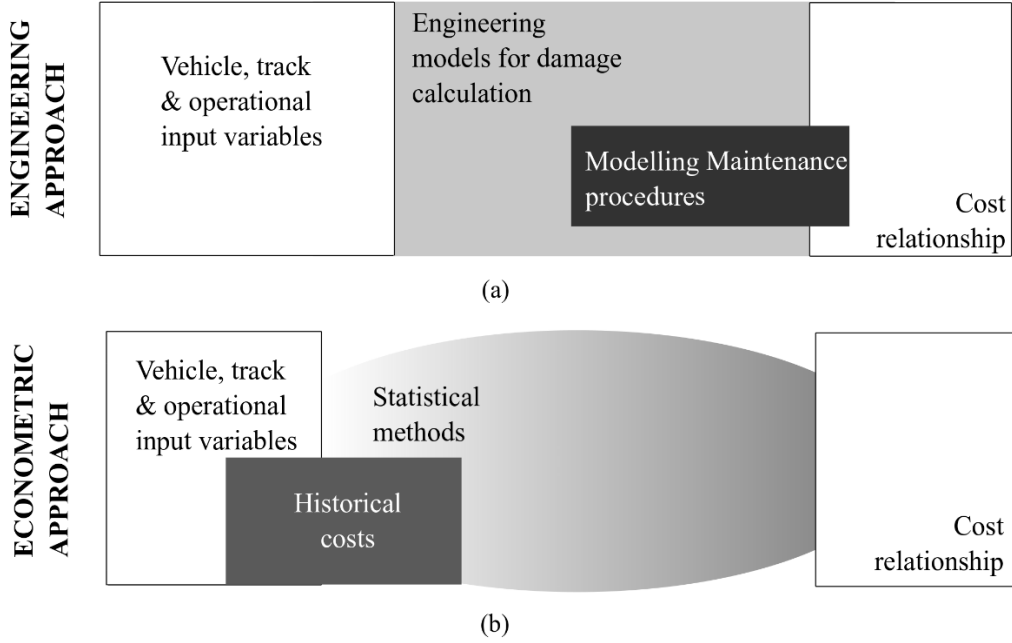


Figure 1. Different approaches to evaluate Track-friendliness to obtain a cost relationship between vehicle operational inputs and costs incurred by an infrastructure manager

They calculate the marginal cost for the passage of wagons as:

$$e_{ton-km,z}(R_j) = \begin{cases} k_1 \cdot Q_{tot}^3 \\ + k_2 \left[ \sqrt{Q_{tot}^2 + Y_{qst}^2} \right]^3 \\ + k_{34} \cdot \frac{\sum_{i=1}^{n_z} [f(T\gamma)_i]}{m_z} \end{cases} \quad (1)$$

Where  $Q_{tot}$  and  $Y_{qst}$  stand for vertical and lateral quasistatic wheel-rail forces respectively and  $T\gamma$  stands for energy dissipated on the contact patch. The first term reflects the engineering output quantifying damage due to track settlement ( $Q_{tot}^3$ ), the second reflects the same due to track component fatigue ( $[Q_{tot}^2 + Y_{qst}^2]^{3/2}$ ) and the third reflecting the damage due to rail surface damage ( $T\gamma$ ). Rail surface damage itself is further comprised of two damage modes namely wear and rolling contact fatigue, the effects combined in the form of a function  $f$ . Each term has a calibrated coefficient ( $k_1, k_2, k_{34}$ ) forming a linear function between marginal costs and the engineering outputs. A similar approach was also adopted by [4] to compare track-friendliness of bogie designs. This approach of individually identifying the contribution of each track damage mode and calculation of the total costs was also adopted in the EU project Roll2Rail [5] that put forward one of the first UCMs in the area [1]. Similar track access pricing methods rooted in the engineering approach are also in use to a certain extent by infrastructure managers in the UK [6], Austria and Switzerland [7].

More advanced methods capable of predicting the evolution of rail geometry with increasing tonnage passage are also recently being developed. They take the engineering approach a step further from calculating dynamic forces such as the terms in equation (1) to predicting the shape of the rail profile after a large tonnage passing such as the work done by [8]. More recently, the impact of intermediate maintenance measures and the interaction between different modes of rail surface damage were also implemented in [9]. The main benefit of these methods is an increased accuracy as they integrate the physical damage modelling and simulation with the actual maintenance actions required during the operational cycles off the designed vehicles, but a salient feature in these more

advanced methods is that they require a lot of computational time and therefore is more challenging to cover all operating scenarios. Especially in the stage of vehicle design, this is important since the

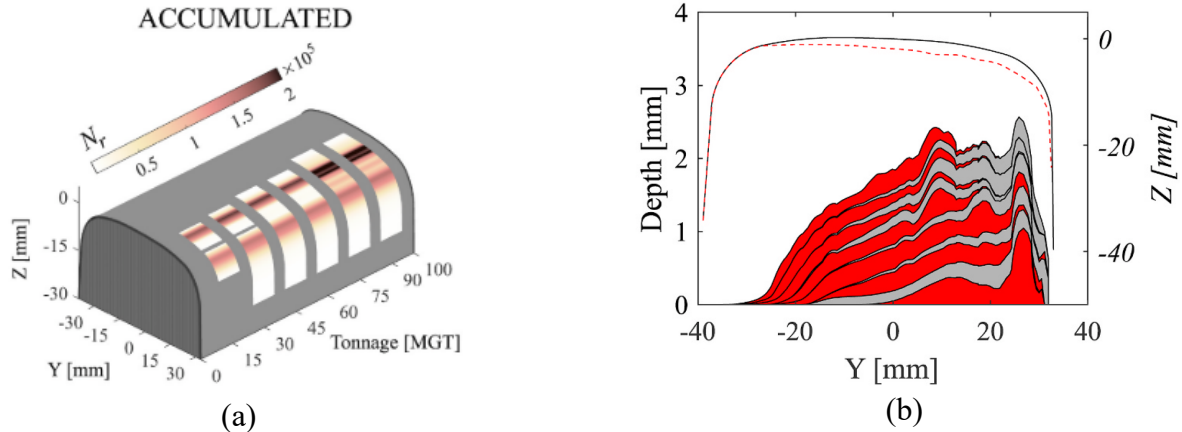


Figure 2. Example of result from a more 'purely' engineering approach. (a) RCF concentrations depicted by  $N_r$  (b) Rail profile evolution due to wear by vehicle and maintenance actions

'track-friendliness' of a wagon should not be limited to simulating a particular set of scenarios. An example of results from a pure engineering approach is depicted in Figure 2. It shows the evolution of rail surface damage modelled because of vehicle-induced and maintenance-induced wear and Rolling Contact Fatigue over an accumulated tonnage of 100 MGT (typically a period of 3-4 years in the Swedish iron-ore line).

Overall, engineering approaches tend to be relatively rigid in their methodology, i.e., they require meticulous modelling of all phenomena from vehicle-track interaction and maintenance strategies to costs. They also require extensive inputs in the calculation stage, being a 'Bottom-up' approach. While they are suitable to obtain physical indicators governing track deterioration, it can be quite difficult to link them to costs using simple linear relationships since cost modelling involve several non-linear components such as availability of personnel, workshops, etc which are difficult to model using purely engineering-based approaches. Therefore, some works also define relative 'track-friendliness' at the vehicle design stage by using only physical outputs such as  $\langle T \rangle$  as seen in [10]. However for cost relationships, a 'purely' engineering based approach may not be suitable.

## 2.2 Econometric approach

Figure 1b illustrates a 'pure' econometric approach where basic characteristics of vehicle, track and operational variables are taken as inputs (axle load, sections). However, they are also complemented with a detailed set of section-wise cost data available from historical actions of maintaining and replacing track components. This essentially accounts for a wide set of non-linear cost components derived from prior experience, which was otherwise absent in the engineering approaches. Work done by Andersson et al. [11] in UK, Bugarinovic et al. [12] in Serbia and Gaudry et al. [13] in France are some examples of econometric approaches to guide track access pricing strategies. They provide results in the form of elasticity of track renewal costs with respect to usage by traffic classes using different regression models. 'Track usage' in these approaches are generally expressed in terms of gross-tonnes passage, regardless of the wagon designs that pass through. A simple example for this approach is the Translog regression model used to model costs in [13]:

$$\ln(C) = \beta_0 + \sum_k^r \beta_k \ln(X_k) + \sum_i^r \sum_j^r \beta_{ij} \ln(X_i) \ln(X_j) \quad (2)$$

Here  $C$  refers to cost data and  $X$  refers to operational variables such as traffic class, axle loads, etc.  $\beta$  refer to coefficients used to fit the available cost data  $C$  with the variables. The first term in equation (2) corresponds to fixed costs, the second term refers to the effect of variables and the third refers to

the effect of interdependency between the variables on cost  $C$ . Several other regression models are also in use. Typically, many sample sections are taken with  $C$  and  $X$  known. The calculation of coefficients  $\beta$  that ensures the best fit between  $C$  and  $X$  using methods such as least squares approximation give a cost relationship. This makes it a ‘Top-down’ approach since the calculation already starts with system-wide costs. This is contrast to the simpler linear coefficients approximated in the engineering approach seen earlier.

While this approach tends to give a realistic cost estimate ( $C$ ) for the infrastructure manager with change in payload, age of track components, etc (represented by  $X$ ), they do not necessarily estimate potential savings that can be achieved with more ‘track-friendly’ wagon designs. This is so since the impact of vehicle design is largely absent in the econometric methodologies. They are more reliable in guiding pricing strategies with incremental changes in tonnage, running distance, etc for the existing traffic and are generally unable to guide vehicle designers to manufacture more ‘track-friendly’ wagons. However, within the context of the present work, one of the main objectives of the UCM2.0 is to incentivise wagon designs that cause less damage to track by providing a cost calculation tool that can guide manufacturers during the vehicle design stage. Therefore, a purely econometrics-based approach is not suitable.

### 3. Hybrid approach

In the previous section, two different approaches to propose effective track access pricing strategies were studied. Both approaches came with their own set of advantages and challenges. Within the context of developing ‘Universal Cost Model 2.0’, the proposed cost relationship should:

- include the effect of innovative vehicle designs on costs to be borne by the infrastructure manager in lieu of its passing.
- give a reasonable estimate of expected costs and a good estimate of the relative difference between different solutions that arise due to track damage by wagon designs.
- be presentable in the form of a simple tool for the infrastructure managers to differentiate various traffic class to assign track access charges.

While the first requirement presents a case for using an engineering approach, the second favours an econometric approach. Therefore, for UCM 2.0, a hybrid approach that combines the advantages of both approaches has been proposed.

Figure 3 illustrates a simple hybrid approach built from elements of both engineering and econometric approaches in Figure 1. Hybrid approaches have previously been studied such as in the recent work by Smith et al [14]. The more advanced engineering approaches are typically not considered in a hybrid approach to ensure more operating scenarios are considered at the vehicle design stage. The cost modelling as depicted by the diagram consists of two steps. To simplify the hybrid approach as much as possible, a clear interface is presented between the cost modeling and the engineering calculations in the figure. Econometric models on that are then simplified as much as possible, linking them to specific maintenance actions, in order to create a streamlined simulation process where the economic results can be directly linked to the simulation results.

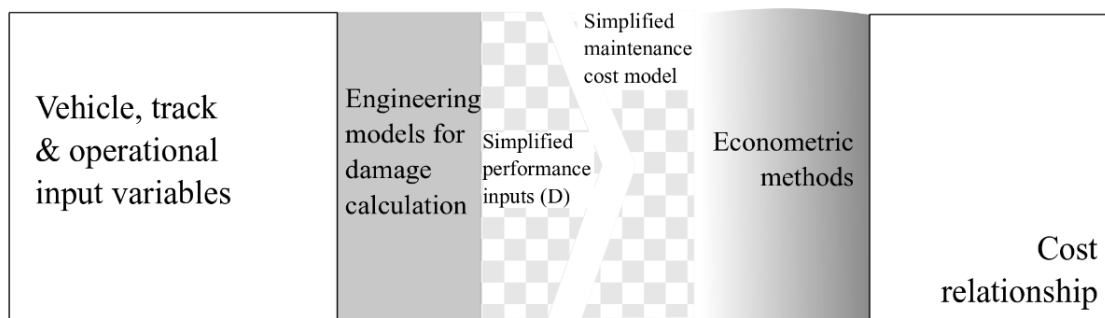


Figure 3. General example of a simple hybrid approach

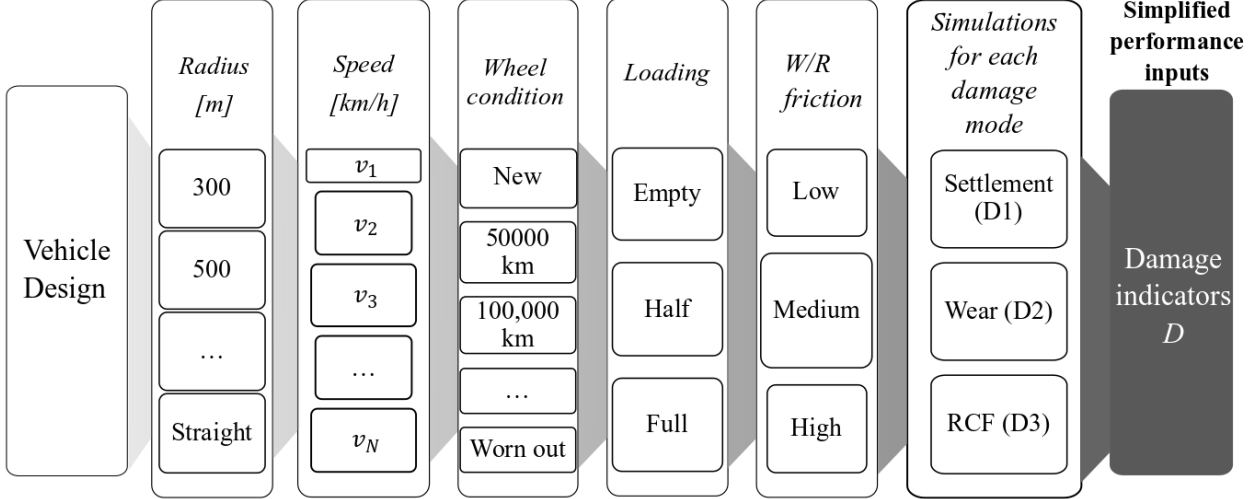


Figure 4. Engineering outputs constituting the first step of the hybrid approach

Initially, simulations are performed for a matrix of intersecting operating scenarios depicted in Figure 4 to obtain engineering outputs. At the end of this step, damage contributions  $D$  corresponding to each damage mode ‘ $a$ ’ is obtained. For the damage mode of rail surface damage for instance,  $D_{wear} = T\gamma$ . The cost relationship in step 2 of the hybrid approach then takes the form:

$$\begin{aligned} \ln(C) = & \beta_0 + \sum_{a=1}^A \beta_a \ln(D_{ai}) + \sum_{a=1}^A \sum_{b=a}^A \beta_{ab} \ln(D_{ai}) \ln(D_{bi}) + \sum_{k=1}^K \beta_k \ln(X_{ki}) \\ & + \sum_{k=1}^K \sum_{l=a}^K \beta_{kl} \ln(X_{ki}) \ln(X_{li}) + \sum_{a=1}^A \sum_{k=1}^K \beta_{ak} \ln(X_{ai}) \ln(X_{ki}) + e \end{aligned} \quad (3)$$

In equation (3), the damage contributions  $D$  account for the effect of vehicle design. This is input into an econometric model in step 2 along with other track variables  $X$  to obtain the form like the one seen in equation (2). However, cost modelling now includes the effect of vehicle design on track-friendliness due to the presence of damage variables ( $D$ ).

This approach consisting of two steps brings the balance between the modelling of vehicle design in reflecting its ‘track-friendliness’ and at the same time capturing of the non-linear cost components that constitute typical cost functions used to estimate maintenance. It must be noted however that the Hybrid approach itself can vary depending on how ‘pure’ engineering or econometric approaches are used in the respective steps. It is possible to use simpler models on both engineering and econometric steps and at the same time more advanced models in either steps. This must be decided on an application-basis depending on whether the whole network/traffic is studied or only specific sections/ traffic classes.

From UCM2.0 standpoint that aims to provide general guidance to vehicle manufacturers regarding the track-friendliness of their prospective vehicle designs (which often are purchased by diverse networks across the world), maximum operating scenarios need to be considered in the design stage. This calls for prioritizing general trends in the track-friendly behaviour of vehicle designs on any given track section rather than an operation-specific analysis. Therefore, the authors recommend the use of simpler econometric models in the hybrid approach at the same time covering a large matrix of operating scenarios as depicted in Figure 4.

## 4. Conclusions

In this paper different cost modelling approaches are analysed to find the right one for the UCM2.0 user base. A hybrid approach is found to be the most promising, as it can reasonably model Life Cycle Costs incurred by infrastructure managers during the vehicle design stage. This is achieved by calculating the expected costs of track deterioration during the vehicle design stage by considering the vehicle and infrastructure as a single system.

## References

- [1] J. Meléndez *et al.*, “Roll2Rail: Deliverable D4.3 Cost model methodology: EU Project Deliverable R2R-T4.3-D-CEI-049–06,” 2017.
- [2] A. Smith, S. Iwnicki, A. Kaushal, K. Odolinski, and P. Wheat, “Estimating the relative cost of track damage mechanisms: combining economic and engineering approaches,” *Proc. Inst. Mech. Eng. Part F J. Rail Rapid Transit*, vol. 231, no. 5, pp. 620–636, 2017.
- [3] J. Öberg and E. Andersson, “Determining the deterioration cost for railway tracks,” *Proc. Inst. Mech. Eng. Part F J. Rail Rapid Transit*, vol. 223, no. 2, pp. 121–129, 2009.
- [4] M. Hiensch, N. Burgelman, W. Hoeding, M. Linders, M. Steenberg, and A. Zoeteman, “Enhancing rail infra durability through freight bogie design,” *Veh. Syst. Dyn.*, vol. 56, no. 10, pp. 1532–1551, 2018.
- [5] C. Casanueva, B. Dirks, M. Berg, and T. Bustad, “Track damage prediction for Universal Cost Model applications,” in *25th International Symposium on Dynamics of Vehicles on Roads and Tracks*, 2017.
- [6] Network Rail, “Control Period 5 ( CP5 ) Variable Usage Charge ( VUC ) guidance document (November 2017),” 2017.
- [7] S. Marschnig, “Innovative Track Access Charges,” *Transp. Res. Procedia*, vol. 14, pp. 1884–1893, 2016.
- [8] W. Zhai, J. Gao, P. Liu, and K. Wang, “Reducing rail side wear on heavy-haul railway curves based on wheel-rail dynamic interaction,” *Veh. Syst. Dyn.*, vol. 52, no. SUPPL. 1, pp. 440–454, 2014.
- [9] V. V. Krishna, S. Hossein-nia, C. Casanueva, and S. Stichel, “Long term rail surface damage considering maintenance interventions,” *Wear*, vol. 460–461, no. July, p. 203462, 2020.
- [10] V. V. Krishna, C. Casanueva, S. Hossien-Nia, and S. Stichel, “FR8RAIL Y25 running gear for high tonnage and speed,” in *Proceedings of the 12th International Heavy Haul Association IHHA*, 2019.
- [11] M. Andersson, A. Smith, Åsa Wikberg, and P. Wheat, “Estimating the marginal cost of railway track renewals using corner solution models,” *Transp. Res. Part A Policy Pract.*, vol. 46, no. 6, pp. 954–964, 2012.
- [12] M. Bugarinovic and B. Boskovic, “A systems approach to access charges in unbundling railways,” *Eur. J. Oper. Res.*, vol. 240, no. 3, pp. 848–860, 2015.
- [13] M. Gaudry, B. Lapeyre, and É. Quinet, “Infrastructure maintenance, regeneration and service quality economics: A rail example,” *Transp. Res. Part B Methodol.*, vol. 86, pp. 181–210, 2016.
- [14] A. S. J. Smith *et al.*, “Estimating the marginal maintenance cost of different vehicle types on rail infrastructure,” *Proc. Inst. Mech. Eng. Part F J. Rail Rapid Transit*, 2021.



# A life cycle energy and weight comparison of a carbon fiber composite versus metallic component in a commercial vehicle

Sara Eliasson<sup>1,2,3,\*</sup>, Mathilda K. Hagnell<sup>2,3</sup>, Robert Jonsson<sup>2,3</sup>, Per Wennhage<sup>2,3</sup> and Zuheir Barsoum<sup>3</sup>

<sup>1</sup>Scania CV AB, Södertälje, Sweden

<sup>2</sup>The Centre for ECO<sup>2</sup> Vehicle Design, SE-100 44 Stockholm, Sweden

<sup>3</sup>KTH Royal Institute of Technology, The Department of Engineering Mechanics, SE-100 44 Stockholm, Sweden

\*Corresponding author. Email: saraeli@kth.se

Lightweight design is important for Battery Electric Vehicles (BEVs), to minimize the effects from the added weight of the batteries. The study looks at the benefits and disadvantages of choosing a Carbon Fiber Reinforced Polymer (CFRP) material in comparison to metallic material for a specific battery electric commercial vehicle component. A Life Cycle Energy (LCE) and weight analysis are the basis for the comparison. Other aspects that could be considered important for the industrial implementation, such as cost, are also discussed. The LCE is assessed using a combination of engineering process modelling, available data from industrial partners, and data available in the literature. The analysis is aimed to support a holistic comparison, which means the modelling is performed on an overarching level of detail.

©2021 by the authors. Published by the Resource Efficient Vehicles Conference.  
This is an open access article under the CC BY license (<http://creativecommons.org/licenses/by/4.0/>).

## 1. Introduction

More than 6 million Heavy Duty Vehicles (HDVs) circulate European roads today [1] and account for a quarter of the EU's CO<sub>2</sub> road emissions [2]. From 2030 and onwards a 30 % reduction of the CO<sub>2</sub> emissions for HDVs manufacturers is dictated [3], hence the need has risen for commercial vehicle manufacturers to improve their HDV design towards climate neutral goals.

To reduce the CO<sub>2</sub> emissions of HDVs, their energy consumption need to be reduced. On a system level an effective approach could be to increase the efficiency of each transport by reducing the distance driven and increase the payload utilization. From the suppliers end, important design topics can include lightweight design and Battery Electric (BE) drivetrains. Battery Electric Vehicles (BEVs) can, apart from CO<sub>2</sub> emissions, potentially reduce toxic emissions, e.g. NO<sub>x</sub>, in comparison to traditional combustion-engine systems, however, their load capacity and range can be limited [4]. In addition, the weight of batteries is an added concern, making lightweight design of essence. The introduction of higher performance materials such as composites, sandwich materials, aluminum or high strength steels shows great potential for reduced energy consumption and increased payload, but does not necessarily imply lower environmental impacts. The entire life cycle should be considered in this direction; from resource extraction to End-of-Life (EoL).

In a review on the topic of life cycle engineering, Herrmann et al. [5] emphasizes the importance of utilizing Life Cycle Analysis (LCA) to get input on the environmental impact of designs and

evaluate if the lightweight design actually contributes to a lowered environmental impact. O'Reilly et al. [6] introduced Life Cycle Energy (LCE) as an overarching design criteria in an optimization methodology. In this way, a homogeneous measure over the complete life cycle is utilized.

Burd et al. [7] deliberates on the cost for a lightweight design, comparing high strength steel and aluminum for a BEV design. In his approach, only the increased cost effectiveness of steel is considered rather than effects on the complete life cycle, which is crucial especially for HDVs where up to 98 % of the energy consumption occur during the use phase [8]. There are only a few studies focusing on HDVs. Earl et al. [9] conducted a study comparing the energy consumption for an HDV with a BE drivetrain and an HDV with a diesel ICE drivetrain for a long haulage application concluding a three times lower energy consumption for the HDV with a BE drivetrain. The high mileage for HDVs yield great potential, e.g. Rupp et al. [10] concluded that the emission and energy reduction potential per vehicle of a semi-trailer is much larger than the potential of a passenger car.

This work aims to give input on what lightweight design could be worth for an HDV with BE or ICE drivetrain. The component analyzed is an HDV chassis, designed for metallic materials or for CFRP material. An LCE analysis [11] was applied for three different designs of the HDV chassis.

## 2. A Life Cycle Energy Analysis

The LCE analysis conducted, included five phases of the life cycle: (1) Resource extraction, (2) Material processing, (3) Product manufacturing, (4) Product use and (5) End-of-Life (EoL) treatment. The LCE analysis was implemented in Python.

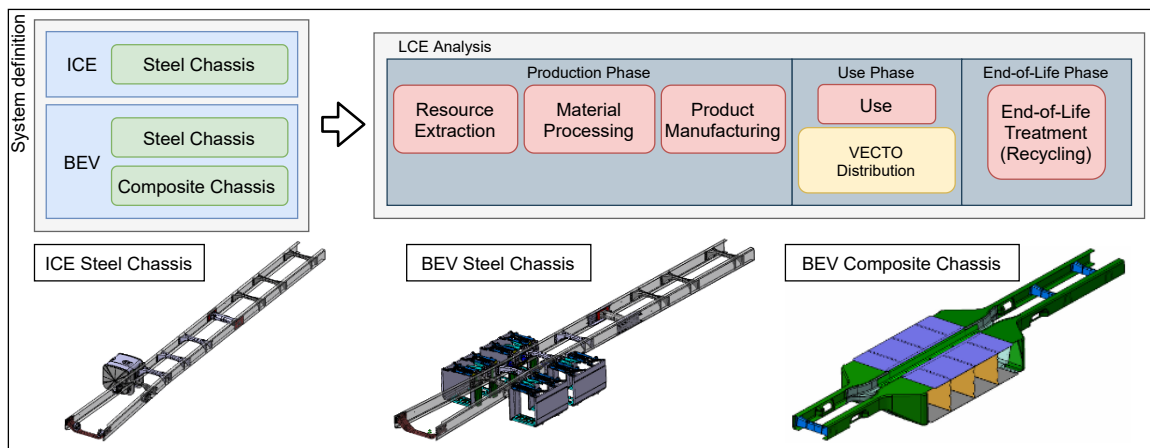


Figure 1: The LCE analysis.

### 2.1 HDV Chassis

Three different designs of an HDV chassis were analysed. The first chassis is a regular steel chassis developed for an ICE drivetrain (ICE Steel). The second chassis is a steel chassis designed for a BE drivetrain (BEV Steel). The third chassis is a composite chassis, also designed for a BE drivetrain (BEV Composite). All chassis are designed with regards to a distribution use profile. The steel chassis are existing manufactured designs, meaning they are designed for stiffness, strength, fatigue and crash load cases. The composite chassis is a design proposal in a step towards a design using advanced lightweight materials. The composite chassis is designed for stiffness and strength. Fatigue strength characterization has been conducted on the unidirectional CFRP material used in the composite chassis design, where preliminary results shows that the fatigue endurance limit is approximately 70 % of the Ultimate Tensile Strength (UTS) [12].

A HDV with a BE drivetrain, today, is powered with lithium batteries, 165 kWh or 300 kWh [13]. However, these were not included in the analysis. For a distribution HDV a reasonable amount of

batteries is four, to optimize the range and cost. This meant that for the steel chassis, four battery carriers were added to the design. The analysed designs contained the structural parts of the chassis and the energy carriers. The energy carriers were defined as the diesel tank for the ICE Steel chassis and the battery carriers for the BEV chassis, not the diesel or batteries themselves. The engine suspension was also part of the designs compared. No fasteners were included in the analysis. Although more components could be added, the system definitions are chosen to keep the results conservative. The main input to the LCE analysis was mass and material and there was no in depth details for the different manufacturing methods. An overview is illustrated in Figure 1.

### 2.1.1 Materials and weights

The data presented for the chassis designs has the ICE Steel chassis as a reference, representing 100 %. The components for the ICE and BEV Steel chassis are not only manufactured in steel. Information and complete composition of the chassis can be found in Table 1.

Table 1: Data for the LCE analysis, with the ICE Steel chassis as the reference measurement.

Chassis Design	No. Components	No. Different Components	Materials *	Total Weight [-]
ICE Steel (ref)	100%	100%	1, 2, 3 and 4	100%
BEV Steel	560%	248%	1, 2, 3 and 5	150%
BEV Composite	73%	57%	6	47%

\* (1) Steel - Standard steel; (2) Cast Iron - Iron used for casting; (3) Aluminum - Standard wrought aluminum; (4) Cast Aluminum - Aluminum used for casting; (5) Foam - Crushable foam used for impact zones; (6) CFRP - NCF fabric with epoxy matrix

## 2.2 LCE Phases

The different phases of the life cycle were chosen according to Jonsson [11]. A short description of the energy in the different phases are found in Table 2. The input for each phase is described in the coming sections.

Table 2: Life cycle phases' energy consumption modelled in the LCE analysis.

Cycle Phase Energy	Description
Resource extraction	Energy to produce 1kg of raw material (embodied energy).
Material processing	Energy to transform 1kg of raw material to 1kg of material used for the manufacturing.
Product manufacturing	Energy needed to produce the component.
Product use	Energy consumed during the component's usage life-time.
End-of-Life treatment	Energy that is consumed during recycling and energy that can be returned back to the life cycle for a circular energy flow.

### 2.2.1 Resource Extraction

The energy consumption for the resource extraction was computed using the embodied energy of the material and multiplying it by the component mass. For steel the data was more elaborated, utilizing the work of Shetye [14]. The component mass was compensated with regards to a material utilization factor of 0.8 for all materials. This factor shall compensate for any scrap during the production phase. The data for resource extraction is presented in Table 3.

Table 3: Energy data for the resource extraction in the LCE analysis.

Material	Resource Extraction	Material Utilization Factor	Data Source
Steel	0.576 MJ/kg	0.8	[14]
Cast Iron	33.9 MJ/kg	0.8	[15]
Aluminium Wrought	213 MJ/kg	0.8	[15]
Aluminium Casted	198 MJ/kg	0.8	[15]
CFRP	Fibers: 286 MJ/kg Resin: 80 MJ/kg	0.8	[16, 17]
Foam	89.2 MJ/kg	0.8	[15]

### 2.2.2 Material Processing

The material processing, is the step where the raw material is transformed in to a material which can be used in the product manufacturing phase. In Table 4 the different material processes assumed for the materials of the components are presented, alongside, the energy to process the material.

Table 4: Energy data for the material processing in the LCE analysis.

Material	Material Processing	Process	Data Source
Steel	15.9 MJ/kg	Typical steel process	[14]
Cast Iron	11.3 MJ/kg	Casting process	[15]
Aluminium Wrought	4.484 MJ/kg	Smelting and roll forming process	[18, 15]
Aluminium Casted	1.404 MJ/kg	Smelting process	[18]
CFRP	Fabric: 0.772 MJ/kg Resin: 24.2 MJ/kg	Resin and Fabric production	[17]
Foam	18.7 MJ/kg	Molding process	[15]

### 2.2.3 Product Manufacturing

The product manufacturing energy is the energy needed to produce the final component. There can be several steps involved in this phase, but the choice was taken to keep it simple and add only the obvious steps of the product manufacturing. The components from the chassis are manufactured with a few dominating processes which were applied (Table 5). The calculations were based on an annual production of 80,000 vehicles, two shift work and 261 work days per year.

### 2.2.4 Use Phase

The energy consumed during the use phase of an HDV is very dependent on the load, road and the driving style adopted and it is very hard to standardize a typical driving behavior for an HDV. The driving cycle used for this study was extracted from VECTO (Vehicle Energy Consumption Calculation Tool), that is a simulation tool developed by the European Commission and used to determine CO<sub>2</sub> emissions and fuel consumption for HDVs [19]. The mission profile extracted from VECTO was the Urban Delivery (UD) profile, which is the tougher of the delivery mission profiles, consuming more energy. In VECTO the mission profiles are described by velocity (km/h) and distance (m), and

Table 5: Energy data for the product manufacturing processing in the LCE analysis.

Material	Process	Manufacturing Energy	Data Source
Steel	Pressed	8.3 MJ/Part	[11]
Steel	Fine Machining	7.66 MJ/rmvd kg	[15]
Steel	Casted	11.3 MJ/kg	[15]
Aluminum	Pressed	8.3 MJ	[11]
Aluminum	Extruded	5.85 MJ	[15]
Aluminium	Casted	12.1 MJ/kg	[15]
CFRP	HP RTM	13.4 MJ/kg	[15]
Foam	Fine Machining	0.557MJ/rmvd kg	[15]

complemented with an acceleration scheme for a typical driver. This data was altered in MATLAB to get the acceleration and velocity over time.

With the mission profile from VECTO the energy needed for the component to move according to the profiles was calculated according to Bouchouireb [20]. The energy needed,  $W_T$ , can be calculated as the sum of the energy needed to overcome two types of driving resistances, the rolling resistance,  $W_R$ , and the inertial resistance to acceleration,  $W_A$ . The aerodynamic energy was neglected since the component is not in a position where it is effected by the aerodynamic drag of the vehicle. The resulting energy is expressed as:

$$W_T = W_R + W_A = m_{comp} * c_r(1 - r)g \int v dt + m_{comp} \int a(t)v(t)dt \quad (1)$$

Where  $c_r$  ( $= 0.01$ ) is the rolling resistance coefficient and  $r$  ( $= 0.15$ ) the fraction of kinetic energy regained during deceleration. With these equations the energy needed to move the given component mass placed on the vehicle was calculated. However, this energy needed to be converted to the energy consumed (fuel or electricity) with regards to the drivetrain. This conversion was done by considering the two drivetrains' energy efficiency. The energy efficiencies were taken from Earl et al. [9], where an ICE has a 40 % energy efficiency and a BE drive train has an 85 % efficiency.

The total use energy over the life cycle was calculated based on an annual driving distance of 55,500 km for a typical regional delivery HDV [21]. The total service life was set to 20 years. It is not unusual for the life length of HDVs to be short since the amount of annual kilometers and use frequency can be very high.

### 2.2.5 End-of-Life

For a circular economy the EoL phase is intended to recycle as much material as possible. In the EoL phase the assumption was that the product system must be processed in order to be recyclable. This means that the total energy available from the EoL-phase was the extractable energy from reusing recycled material, minus the energy of processing the material.

The recycling of steel was implemented as done by Shetye [14]. The energy to process recycled steel is lower compared to processing of the primary metal. Aluminum utilized the same approach. However, creating new metal from recycled aluminum requires only 5 % of the energy needed to produce the primary aluminum [22]. For all metals a 95 % recycling rate was assumed. The foam in the study was assumed to have a recycling rate of 20 %.

Recycling of composites is still a challenge because of the necessity to separate the matrix from the fibers. The currently available methods are e.g. thermolysis recycling methods. However, adding heat damages the fibers and can affect and lower the mechanical properties. Pyrolysis also has a quite

high energy demand of 30 MJ/kg. A promising method that doesn't have as high energy demand, 19.2 MJ/kg, is a chemical method called solvolysis. This method chemically extracts the fibers with a minimal decrease of the mechanical properties [11].

In this study pyrolysis and solvolysis were compared. Pyrolysis has a 65 % reuse efficiency,  $RC_{eff}$ , meaning the UTS is 65 % of that of the virgin carbon fibers. The solvolysis method has a reuse efficiency of 91 %. Reusing fibers, the demand was to maintain a UTS of at least 95 %. The fraction of recycled fibers was calculated as:  $V_{recCF} = (0.95 - 1)/(RC_{eff} - 1)$ . The amount of reused fibers were 15 % for the pyrolysis method and 56 % for the solvolysis method.

## 2.3 Cost Analysis

To conduct a cost analysis data was collected on electricity prices [23] and average diesel prices [24] for five different European countries (Table 6). The electricity price is for non-household consumers, assuming the HDVs are charged at a company with an annual consumption of at least 500 MWh. The energy content in diesel was set to 37 MJ. Converting the diesel to energy the combustion irreversibilities were set to 25 % [25].

Table 6: Cost for electricity and diesel for five different European countries.

Country	Electricity Price [EUR/kWh]	Diesel Price [EUR/Liter]
Germany (DE)	0.179	1.29
Sweden (SE)	0.065	1.545
The Netherlands (NL)	0.128	1.385
United Kingdom (UK)	0.163	1.492
Poland (PL)	0.109	1.145

## 3. Results

The LCE analysis was performed for all three chassis designs (Figure 2). A relatively small fraction of the total energy is actually consumed during the production phase for both the ICE Steel and BEV Steel chassis. Instead the majority of the energy is consumed during the use phase and is strongly dependent on the structural mass. Looking at the results for the BEV Composite chassis, a majority of the energy consumed can be attributed to the production phase. Even so, the results from the LCE analysis show that the total sum of LCE is the lowest for the BEV Composite chassis, assuming a service life of 20 years and an annual mileage of 55,500 km.

The energy demand to recycle the CFRP material with pyrolysis is higher than with solvolysis (Figure 2). If solvolysis was to be used as a recycling method for CFRP, the sum of the LCE would be decreased by the EoL treatment, as it is for the ICE Steel and the BEV Steel chassis.

The evolution of LCE over time for the different components is shown in Figure 3. The ICE Steel chassis has an advantage in the beginning of its life span, since the energy for production is much lower than for both the BEV Steel and the BEV Composite chassis. Adding the yearly contribution of the energy from the use phase to the fixed energy (Production phase and End-of-Life phase) it is possible to find the intersection point of when the ICE Steel chassis have consumed more energy than the BEV Steel chassis and the BEV Composite chassis. The BEV Steel chassis only need approximately 5 years to break even with the ICE Steel chassis, while the composite chassis need 9.6 years.

The cost to keep each chassis moving was calculated and compared based on the use phase. In Figures 4a, 4b and 4c, the running cost up to the different intersection points from Figure 3 for the different chassis are presented. A comparison between different countries is also conducted since

the diesel price and electricity price varies (Table 6). The largest difference in cost is between the ICE Steel chassis and the BEV Composite chassis (Figure 4b). The BEV Composite chassis is the cheapest one to move annually because of the low weight (Figure 5).

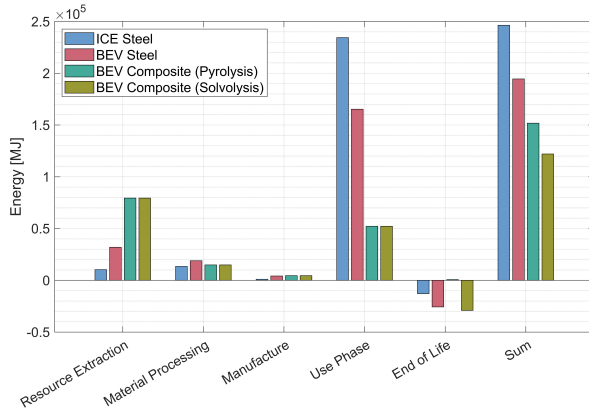


Figure 2: Energy for complete life cycle of the three different chassis designs.

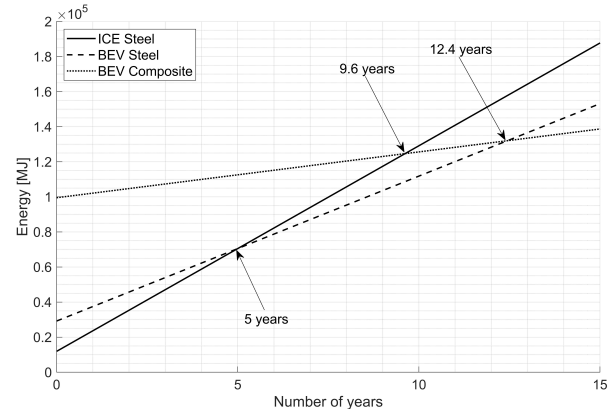
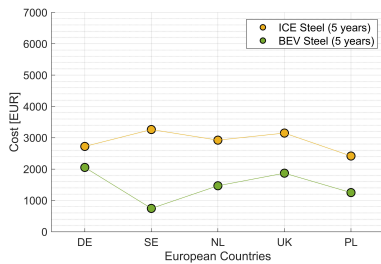
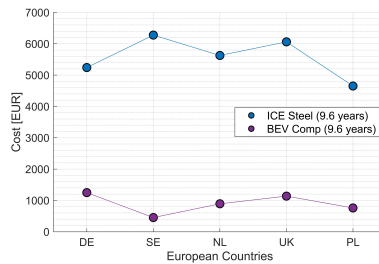


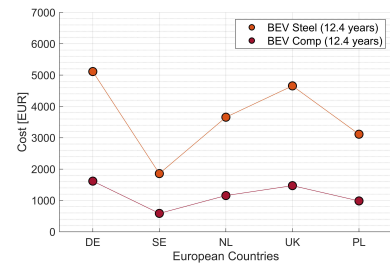
Figure 3: The increase of energy consumption over time.



(a) Intersection 5 years.

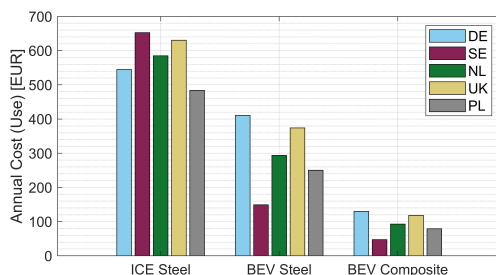


(b) Intersection 9.6 years.

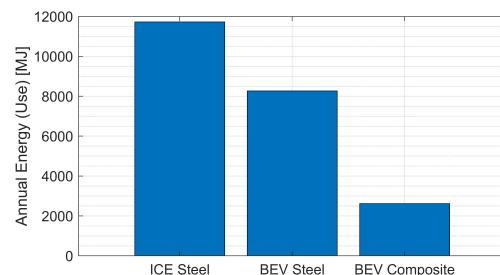


(c) Intersection 12.4 years.

Figure 4: Total cost until break even for the comparison of two chassis (refer back to Figure 3).



(a)



(b)

Figure 5: The (a) annual cost and the (b) annual energy for the different chassis designs.

An existing next generation design for the BEV Steel chassis has a weight reduction of 21 % compared to the original design. If the same percentual improvement is extrapolated for the BEV, the potential of future solutions can be highlighted. The LCE analysis shows that both the slope of the curve and the intersection point with the y-axis is decreased (Figure 6). The new intersection points for when the ICE Steel chassis has consumed more energy than the BEV Steel chassis and the BEV Composite chassis, is 2.7 years and 7.4 years respectively.

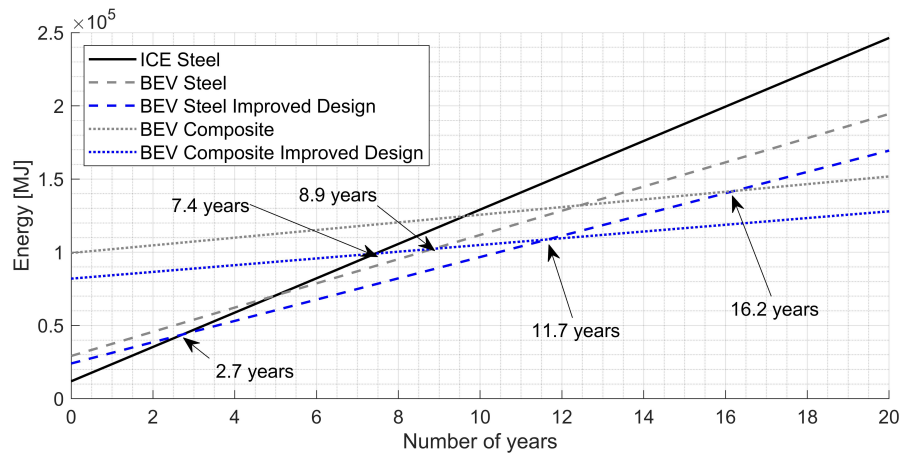


Figure 6: The increase of energy consumption over time for the new designs

## 4. Conclusions and Discussion

An LCE analysis has been presented for three chassis designs. Some conclusions are

- For service life longer than 5 years, BE drivetrain components are preferable and for service life longer than 12.4 years composite design becomes more energy efficient than steel.
- Increasing efforts in the design we lower the LCE and lower necessary service life of the chassis with a BE drivetrain to 2.7 years for the steel chassis and 7.4 years for the composite chassis.
- Mass for the steel chassis with an ICE drivetrain cost more to move. Saved weight for the chassis with a BE drivetrain will lower the slope of the curves and decrease the LCE.

For CFRP, the production phase is still very high-priced, both with regards to energy and cost. However, over time the higher energy demand of the production phase can be compensated by the reduced energy consumption in the use phase. This is important to consider if calculating cost for investment. Considering a complete life cycle, a lower weight is the goal for HDVs and an increased cost in the production process could to some extent be covered by a saved use cost for the owner. Lightweight design also have positive effects on payload. If the addition in payload would be enough to reduce the number of transports needed it could potentially reduce the number of years to the break even point between the composite and the steel chassis for the BE drivetrain.

This work has highlighted the importance to consider and compare the R&D effort for evaluated structures, given the maturity of the steel chassis contra the novelty of the composite chassis. When designing with a CFRP material the effort and possible improvements need to be considered in correlation to the costs.

## Acknowledgments

The authors would like to thank the Centre for ECO2 Vehicle Design, funded by the Swedish Innovation Agency Vinnova (Grant Number 2016-05195), and Scania CV AB for financial support.

## References

1. ACEA European Automobile Manufacturers Association. About the Automobile Industry – Trucks, Vans and Buses – Trucks, <https://www.acea.be/automobile-industry/trucks>, Accessed 2021-03-17.
2. European Commission. EU Transport in Figures, Publications office of the European Union, 2018.
3. European Commission. Reducing CO2 emissions from heavy-duty vehicles, [https://ec.europa.eu/clima/policies/transport/vehicles/heavy\\_en](https://ec.europa.eu/clima/policies/transport/vehicles/heavy_en), Accessed 2021-03-17.



4. S. Sripad and V. Viswanathan. Performance metrics required of next-generation batteries to make practical electric semi truck, *ACS Energy Letters* 2, 2017, pp.1669–1673.
5. C. Herrmann, W. Dewulf, M. Hauschild, A. Kaluza, S. Kara and S. Skerlos. Life cycle engineering of lightweight structures, *CIRP Annals - Manufacturing Technology*, vol. 67, 2018, pp. 651–672.
6. C. O'Reilly, P. Göransson, A. Funakazi, T. Suzuki, S. Edlund, C. Gunnarsson, J.-O. Lundow, P. Cerin, C. J. Cameron, P. Wennhage and J. Potting. Life cycle energy optimisation: A proposed methodology for integrating environmental considerations early in the vehicle engineering design process, *Journal of Cleaner Production*, vol. 135, 2016, pp. 750–759.
7. J. T. Jameson Burd, E. A. Moore, H. Ezzat, R. Kirchan and R. Roth. Improvements in electric vehicle battery technology influence vehicle lightweighting and material substitution decisions, *Applied Energy* 283, 2021, pp. 116269.
8. Volvo Trucks Global. Environmental Footprint Calculator,  
<https://www.volvotrucks.com/en-en/trucks/alternative-fuels/environmental-footprint/environment-footprint-calculator.html>, Accessed 2021-04-20.
9. T. Earl, L. Mathieu, S. Cornelis, S. Kenny, C. Calvo Ambel and J. Nix. Analysis of long haul battery electric trucks in EU, 8th Commercial Vehicle Workshop, Graz, Austria, 2018.
10. M. Rupp and S. Schulze and I. Kuperjans. Comparative life cycle analysis of conventional and hybrid heavy-duty trucks, *World Electric Vehicle Journal*, vol. 9, 2018, pp. 797–804.
11. R. Jonsson. Life cycle energy optimization as a tool to compare and evaluate the optimal design in the automotive industry, Degree Project, 2020, TRITA-SCI-GRU ; 2020:228, KTH, School of Engineering Sciences and Engineering Mechanics, SE-100 44 Stockholm, Sweden.
12. S. Eliasson, S. Wanner, Z. Barsoum and P. Wennhage. Development of fatigue testing Procedure for unidirectional carbon fiber composites, *Procedia Structural Integrity* 19, 2019, pp. 81–89.
13. Scania CV AB. Battery Electric Truck - Technical Specifications,  
<https://www.scania.com/group/en/home/products-and-services/trucks/battery-electric-truck.html>, Accessed 2021-04-26.
14. N. Shetye. Life-Cycle Energy Analysis of a High Strength Steel Application, Degree Project, 2020, TRITA-SCI-GRU 2020:314, KTH, School of Engineering Sciences and Engineering Mechanics, SE-100 44 Stockholm, Sweden.
15. CES EduPack software, Granta Design Limited, Cambridge, UK, 2009.
16. T. Suzuki and J. Takahashi. Prediction of energy intensity of carbon fiber reinforced plastics for mass-produced passenger cars, The 9th Japan International SAMPE Symposium, 2005, pp. 14–19.
17. Y. S. Song, J. R. Youn and T. G. Gutowski. Life cycle energy of fiber-reinforced composites, *Composites: Part A* 40, 2009, pp. 1257–1265.
18. U.S. Department of Energy. U.S. Energy Requirements for Aluminum Production - historical perspective, theoretical limits and current practices, 2007.
19. European Commission. Vehicle Energy Consumption calculation Tool - VECTO,  
[https://ec.europa.eu/clima/policies/transport/vehicles/vecto\\_en](https://ec.europa.eu/clima/policies/transport/vehicles/vecto_en), Accessed 2021-04-21.
20. H. Bouchouireb. Advancing the life cycle energy optimization methodology, Licentiate Thesis, 2019, TRITA-SCI-FOU ; 2019:60, KTH, School of Engineering Mechanics, SE-100 44 Stockholm, Sweden.
21. K. Natanaelsson, M. Lindgren, E. Rydén, B. Hasselgren, K. Palo and S. Grudemo. Analysera föutsättningar och planera för en utbyggnad av elvägar, 2021, TRV 2020/113 361, Trafikverket, Borlänge, Sweden
22. Constellium. Going Full Circle - The life-cycle of aluminium,  
[https://www.constellium.com/sites/default/files/constellium\\_-\\_life\\_cycle\\_of\\_aluminium.pdf](https://www.constellium.com/sites/default/files/constellium_-_life_cycle_of_aluminium.pdf), Accessed 2021-04-22.
23. European Commission. Electricity price statistics,  
[https://ec.europa.eu/eurostat/statistics-explained/index.php/Electricity\\_price\\_statistics#Electricity\\_prices\\_for\\_non-household\\_consumers](https://ec.europa.eu/eurostat/statistics-explained/index.php/Electricity_price_statistics#Electricity_prices_for_non-household_consumers), Accessed 2021-04-20, Data extracted in November 2020.
24. Global Petrol Prices. Diesel prices, liter, 19-Apr-2021,  
[https://www.globalpetrolprices.com/diesel\\_prices/](https://www.globalpetrolprices.com/diesel_prices/), Accessed 2021-04-19.
25. G. Bourhis and P. Leduc. Energy and exergy balances for modern diesel and gasoline engines, *Oil & Gas Science and Technology*, vol. 65, 2010, pp. 39–46.

---

# The environmental benefits and challenges of a composite car with structural battery materials

Frida Hermansson<sup>1,\*</sup>, Ivan Berg<sup>1</sup>, Kevin Sandberg<sup>1</sup>, Leif E. Asp<sup>2</sup>, Matty Janssen<sup>1</sup>, and Magdalena Svanström<sup>1</sup>

<sup>1</sup>*Environmental Systems Analysis, Chalmers University of Technology, 412 96 Gothenburg, Sweden*

<sup>2</sup>*Material and Computational Mechanics, Chalmers University of Technology, 412 96 Gothenburg, Sweden*

\*Corresponding author. Email: [frida.hermansson@chalmers.se](mailto:frida.hermansson@chalmers.se)

---

One way to reduce the environmental impact of an electric vehicle is to reduce the vehicle's mass. This can be done by substitution of conventional materials such as steel, aluminium, and plastics with carbon fibre composites, or possibly even with structural battery composite materials. In the latter case, another consequence is that the size of the vehicle battery is reduced as the structural battery composite not only provides structural integrity, but also stores energy. This study assesses the change in life cycle environmental impacts related to transitioning from a conventional battery electric vehicle to a vehicle with components made from either carbon fibre composites or structural battery composites, with the aim of identifying environmental challenges and opportunities for cars with a high share of composite materials. Results show that a transition to carbon fibre composites and structural battery composite materials today would (in most cases) increase the total environmental impact due to the energy intensive materials production processes. The two major contributors to the environmental impacts for the structural battery composite materials are energy intensive structural battery material manufacturing process and carbon fibre production process, both of which can be expected to decrease their energy consumption as the technology maturity level increases and other production and manufacturing processes are developed. For future assessments, more effort needs to be put on collecting primary data for large-scale structural battery composites production and on assessing different technology development routes.

© 2021 by the authors. Published by the Resource Efficient Vehicles Conference.  
This is an open access article under the CC BY license (<http://creativecommons.org/licenses/by/4.0/>).

---

## 1. Introduction

Around 30% of the total European greenhouse gas emissions in 2017 came from the transport sector, to which road transports contributed more than 70% [1]. To reduce these emissions, there needs to be a transition from fossil to renewable fuels, but also a reduction in fuel consumption. A reduction in fuel consumption can be accomplished by making vehicles lighter, for example by substituting conventional structural materials with lighter ones, such as composites. It has also been suggested for battery electrical vehicles (BEVs) that the heavy batteries are replaced by structural batteries (SBs) that would integrate energy storage into the structural components, and thereby would reduce weight even further by decreasing the size of the battery. A drawback with composite materials

is however that they, in some cases, are very energy intensive to produce compared to conventional materials. Therefore, lightweighting does not always lead to a reduced environmental impact throughout a vehicle's life cycle [2].

This study assesses the possible environmental benefits from using composite materials in vehicles, both conventional carbon fibre composites and SBs. The aim is to investigate what possibilities a transition to multifunctional lightweight materials introduces in terms of reducing vehicle weight and, to identify future areas of research for reducing the environmental impact of structural battery composites.

## 2. Methodology

The methodology of this study is divided into two main parts: 1) the conceptual design of a composite vehicle with carbon fibre composites (also known as carbon fibre reinforced polymers, CFRPs) or SBs (Section 2.1), and 2) the cradle-to-grave environmental life cycle assessments (LCA) of these conceptual composite vehicles (Section 2.2). The purpose of the conceptual design was to demonstrate the potential mass-savings of the vehicle by using CFRPs and SBs while keeping or increasing the system performance. The result from the conceptual design functioned as input data for the inventory analysis of the LCA. The purpose of the LCA was to assess the influence the use of CFRPs and SBs could have on the environmental impact of electric vehicles as well as to identify areas that need further research for decreasing the environmental impact.

### 2.1 Design of a conceptual composite vehicle

Three different types of vehicles were considered: One conventional BEV, one vehicle where selected components are replaced with CFRPs, and one vehicle where the components are replaced with SBs.

The components of the conventional BEV that were being replaced with CFRPs and SBs are listed in Table 1. The components' material type and properties were obtained from Pradeep et al. [3], while the dimensions of the components were assumed after discussions with technical experts. The input data for the components in the conventional BEV are presented in Table 1 and are used to estimate the dimensions of the replacing composite components as well as the lightweighting of the vehicles.

Table 1: The components considered in this study and the input data for the assessment. Based on data from Pradeep et al. [3] and discussions with technical experts.

Component	Material	$\rho$ (kg/m)	E (GPa)	l (m)	w (m)	t (mm)	m (kg)
Outer door panels	Aluminium	2700	69	1.2	0.8	3	31.1
Roof	Steel	7800	206	2.2	1.1	0.8	15.1
Bumpers	Polypropylene	950	1.4	2	0.5	5	9.50
	CFRP	1310	50	2	0.5	2	5.24
A and B roof arches	Steel	7800	206	1.1	0.05	1	0.858
C roof arch	Steel	7800	206	1.1	0.05	5	2.15
Hood	Steel	7800	206	1.6	1.1	0.8	11.0
Dashboard	Polypropylene	950	1.4	1.8	0.5	2	1.71

(continued)

(continued)

Component	Material	$\rho$ (kg/m)	E (GPa)	l (m)	w (m)	t (mm)	m (kg)
Inner door panels	Polypropylene	950	1.4	1	0.6	2	4.56
Luggage floor	Polypropylene	950	1.4	1	0.88	2	1.67
Luggage wall	Polypropylene	950	1.4	0.5	0.88	2	1.67

For the composite vehicles, the analysis included calculations of the CFRPs' and SBs' effective modulus of elasticity and energy density, to assess how much composite materials that would be needed to maintain the components' structural integrity. Input data for the calculation of the SBs' effective modulus of elasticity are presented in Table 2. The CFRP scenario followed the same methodology as for the SB scenario, but the energy density was not considered due to the CFRPs' monofunctional characteristics.

Table 2: Input data for calculations of the effective modulus of elasticity for the SBs, estimated based on current state-of-the-art [4].

Parameter	Metric	Unit
$v_{xy}$	0.3	-
$v_{yx}$	0.05	-
$E_x$	75	GPa
$E_y$	10	GPa
$G_{xy}$	5	GPa
d	60	$\mu\text{m}/\text{cell}$

The calculations of the effective modulus of elasticity were based on classical laminate theory and resulted in a value of 32.5 GPa. The calculations were based on a cell design with 6 laminates where the orientation code is  $[0/60/60]_s$ . Constitutive relationships for the fibre reinforced lamina was determined to express the reduced stiffness matrix where the fibre lamina was assumed to be in the plane stress state. The constitutive relationships were transformed from a fibre-oriented coordinate system to a global coordinate system by multiplying the reduced stiffness matrix with the stress transformation matrix as well as the strain transformation matrix. Midplane strains, plate curvatures and material properties were assumed to be the same within each lamina. The effective modulus of elasticity was obtained by summing the product of the transformed reduced stiffness matrix and the thickness for each lamina. The energy density of the SBs was set to 75 Wh/kg, and was based on the findings by Carlstedt and Asp [5]. For the CFRP case, the effective modulus of elasticity was assumed to be 50 GPa. The same type of analysis was applied for the CFRP case as for the SB case, but with the exception that, as earlier mentioned, the energy density was excluded.

To calculate the amount of composite material needed to replace the components in the conventional BEV, the input data in Table 1 were combined with the effective modulus of elasticity as well as the energy densities of SBs and CFRP to create a case with a vehicle with the components replaced by CFRP, and one case with a vehicle with the components replaced with SBs while still maintaining the components' structural integrity. The changes in mass of the components and the changes in size of the battery are found in Table 3 in Section 2.2.

## 2.2 Life cycle assessment

The goal of this LCA was to assess the influence a transition towards using CFRPs and SBs could have on the environmental impact of electric vehicles, as well as to identify main contributors to the

environmental impact of CFRP and SBs to aid further material development. The LCA of the three different vehicles is based on the modelling done for the conceptual composite vehicle in Section 2.1, where the conventional BEV (i.e., the base case) is based on the data found in Table 1. The lightweighting potential of the CFRPs and SBs in the vehicles are found in Table 3. Note that this LCA builds on the modelling of the conceptual vehicle as described in Section 2.1, but processes in the vehicles' LCA build on literature and database data and, consequently, the results should be seen as an early screening LCA for hotspot identification. Figure 1 shows a simplified outline of the vehicles' life cycle (either conventional electric vehicle, vehicle with CFRP components, or a vehicle with SBs). The technical system is further described below.

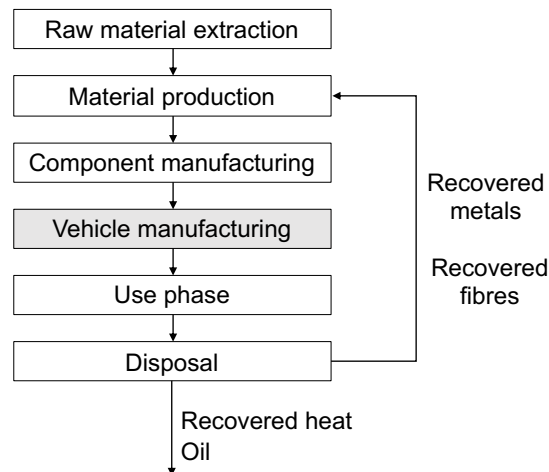


Figure 1: The basic outline of the product life cycle. The grey box is outside the scope of this study and is not included in the assessment.

The functional unit of the study was defined to include the function of the vehicle components listed in Table 1, as well as the battery of the electric vehicle. This was needed to consider the multiple functions of the SBs. The study assesses three different cases as defined in the previous section: a base case considering a conventional BEV with parts made from materials specified in Table 1, one vehicle where these parts are replaced with mono-functional composites (CFRP), and one vehicle where the parts are replaced with multifunctional composites (SBs). The study is cradle-to-grave which means it includes the raw material extraction, composite and structural batteries production, the use phase as well as the end-of-life treatment. It was assumed that the vehicle was driven for 200 000 km before being discarded, which is in line with other studies for composite vehicles, but with internal combustion engines (see for example Duflou et al. [6] and Das [7]). The production, use, and disposal of the composites is assumed to take place in Germany, using German or European specific data as far as possible.

All LCA modelling was done using OpenLCA. If not stated otherwise, the Ecoinvent APOS database version 3.3 [8] was used. The materials of the components in the conventional BEV are listed in Table 1. All CFRPs were assumed to consist of 60% carbon fibres and 40% epoxy. The modelling of the carbon fibre production was based on a life cycle inventory by Romaniw [9]<sup>1</sup> and the polyacrylonitrile (a fossil based polymer usually used for carbon fibre production) precursor fibre production data were provided by Fazio and Pennington [10] and was found in the ELCD database [11]. The composites are assumed to be produced by means of resin transfer moulding (RTM), which requires 12.8 MJ/kg [12] and it is assumed that all energy used in the RTM process is electricity. Models for the SBs were based on data provided by Zackrisson et al. [13], where the polyvinylidene fluoride was excluded due to data availability. Data for  $\text{LiFePO}_4$  (used to coat the fibres in the SB positive electrode) production was taken from Zackrisson et al. [14] and Dunn et al. [15], and data for diammonium production (used to produce  $\text{LiFePO}_4$ ) from Manjare and Mohite [16]. The

<sup>1</sup> See Table C4 in Romaniw [9]

electrolyte used in the structural batteries was approximated to be equivalent to an electrolyte used in the production of NiMH batteries. The battery of the electric vehicle was assumed to be a Li-ion battery that could be used for the mechanical drive of an electric vehicle.

The vehicle components are assumed to be fully recycled after use, and the recycling is modelled using system expansion by substitution, where a credit for avoided production is given to the system. The metals used in the base case vehicle are assumed to be collected and reused again in secondary applications (however any collection and treatment has been excluded due to uncertainties as these are very case specific), and the polymer parts are assumed to be incinerated, and the heat recovered and given as a credit to the system. It was assumed that polypropylene had an energy content of 45 MJ/kg (the calculated net combustion heat for polypropylene according to Ioelovich [17]) which was assumed to be turned fully into heat. The CFRPs are assumed to be recycled by means of pyrolysis, which requires 30 MJ electricity per kg CFRP [18]. Note that the pyrolysis process in this study does not include any emissions, other than emissions related to the energy input. It is also assumed that the structural batteries can be recycled via pyrolysis to recover the carbon and glass fibres; this is however something that is not done today and needs more research. The recovered carbon fibres are assumed to have lost 18% of their tensile strength [19] and the glass fibres are assumed to have a tensile strength degradation of 50% [20] (both tensile strength reduction values are originally used for fluidized bed recycling, but are used as a proxy for pyrolysis in this study), and the credit given is for avoided production is adjusted in line with these values using a quality correction factor. It is assumed that the polymer is degraded to an oil during pyrolysis (see for example Cunliffe et al. [21]) with the corresponding impact/function as petroleum, and is thus given a credit for avoided petroleum production. In this study we assume that the polymer is degraded to 100% oil, in reality this value is probably lower. Any recycling or end-of-life treatment of the Li-ion battery has been left out of this study due to lack of data.

In the cases where the material substitution leads to a lighter weight of the vehicles, the fuel consumption of the vehicle will be reduced [22]. The change in fuel consumption can be calculated using Eq. 1 [23].

$$\Delta FC = \Delta m * FRV \quad (1)$$

Where  $\Delta FC$ =fuel consumption,  $\Delta m$ =difference in mass between the original vehicle and the conceptual vehicle and  $FRV$ =fuel reduction value. In this study, the fuel reduction value is assumed to be 0.069 Wh/kg/km (Forell et al. (2016) as cited in Johannisson et al. [24]).

The fuel reduction over the vehicle's lifetime of 200 000 km is then calculated using the  $\Delta FC$  as calculated using Eq. 1 for each conceptual vehicle, by multiplying the resulting value by the milage. The fuel saved is then given as a credit for the avoided energy use. The mass savings and fuel savings are found in Table 3.

Table 3: The mass reductions, changes in fuel consumptions and the total amount of fuel saved throughout the vehicle's life cycle.

	$\Delta m$ (kg) Material substitution	$\Delta m$ (kg) Battery size	$\Delta m$ (kg) Total	Fuel saved (kWh)
Conventional BEV	n/a	n/a	n/a	n/a
CFRP vehicle	-37.6	0	-37.6	-519
SB vehicle	+3.68	-42.0	-38.4	-529

In the case of SBs, the mass of the vehicle changes due to a transition from conventional materials to SBs, as well as due to a reduction in the size of the battery, as the SBs store some of the energy. This means that the SB vehicle could be given both a credit or a burden for the total change of mass, which leads to a changed fuel consumption in the use phase, as well as credits related to the avoided production of parts of the battery.

This study considers climate impact using the CML2001 assessment method as provided by Ecoinvent 3.3 [8] and the crustal scarcity indicator developed by Arvidsson et al. [25]. Climate impact is included as it is a widely recognized environmental issue, that is strongly connected to energy use in production processes and vehicle use phases. The crustal scarcity indicator is chosen to account for minerals used in the electric vehicle batteries and other parts of the vehicle.

### 3. Results and discussion

Figures 2a and Figure 2b show the climate impact and crustal scarcity impact of the three different vehicles.

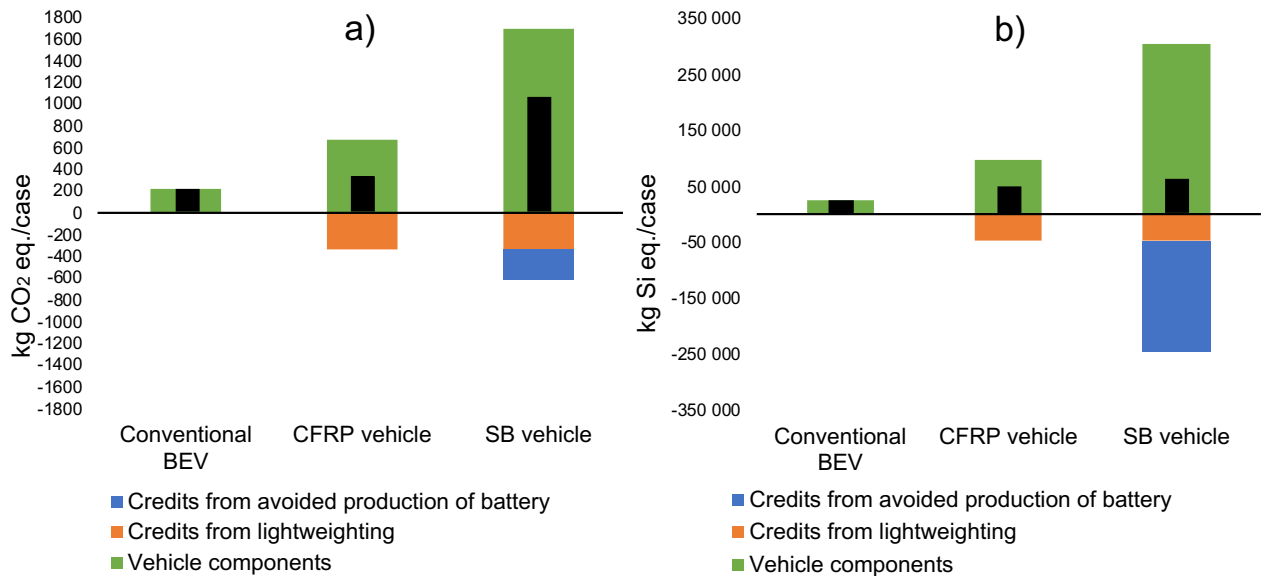


Figure 2: The a) climate impact and b) crustal scarcity impact of the three vehicles in the study. The black bar shows the net impact.

Figure 2a) shows that the net climate impact is almost the same for the conventional BEV and the CFRP vehicle (slightly higher for the CFRP vehicle), even as the lightweighting of the composite vehicles provides a benefit in the use phase. This is due to the very energy intensive carbon fibre production process, which is not weighed up for by the fuel saved in the use phase. It is also related to that a high recycling rate and recovery quality is expected for the metals (in fact, it is assumed that the parts are reused) while the fibres in the composite materials are degraded, and the polymer matrix is recovered as an oil corresponding to petroleum (which production process has a relatively low climate impact). The vehicle with the SBs has the highest climate impact of the three cases, even considering the lightweighting and the avoided Li-ion battery production. This is related to the energy intensive carbon fibre production process (used as electrodes in SBs), but also to the fact that the structural batteries themselves are very energy intensive to manufacture. It should be mentioned that the technology maturity level is very different between the three cases, where the conventional vehicle is having the highest technology maturity level and the SB vehicle the lowest, which means that the impact of the SB vehicle can be expected to decrease as manufacturing technology matures and the energy needed in manufacturing decreases. As an example, the SB manufacturing process has a cumulative energy demand that is almost 9 times higher than for the RTM process used in the CFRP manufacturing process. It is not unlikely that the energy consumption in the SB manufacturing process will approach the RTM energy consumption as technology is further developed. In addition to this, carbon fibre production can be made more energy efficient, which would decrease the impact of both CFRPs and SBs, for example by the use of bio-based raw materials (see for example: Das [7], Janssen et al. [26] and Hermansson [27]), and the use of microwave technology in carbon fibre production (see for example Lam et al. [28]).

Figure 2b) shows the crustal scarcity impact for the different cases. Here, the conventional vehicle also has the lowest impact, which is partly related to the high recycling and recovery rate of the metals. For this impact category, the SB vehicle is more competitive than for the climate impact. This is partly because of the avoided use of energy consumption in the use phase, but mostly because of the avoided production of part of the Li-ion battery, where the avoided production of the battery cell and the integrated circuit offsets most of the impacts. However, also for this impact category, the high energy use in the SB manufacturing phase and the carbon fibre production contributes significantly. In addition to this, the production of the  $\text{LiFePO}_4$  (used to coat the carbon fibres in positive electrode production) also contributes significantly, where the main contributor is the lithium carbonate production. A development in SB manufacturing and carbon fibre production would therefore also benefit this impact category.

## 4. Conclusions

CFRPs and SBs show great potential to decrease the weight of electrical vehicles. However, the very energy intensive carbon fibre production process and structural batteries manufacturing process counteract the environmental benefits from lightweighting and, for the SBs, reduced battery size. While the results in this paper show that the CFRPs and SBs do not automatically provide an environmental benefit over conventional materials today, results indicate that the use of composites in vehicles could very well decrease the impacts compared to conventional vehicles if the energy use in the manufacturing phase, as well as in the carbon fibre production, is decreased.

More efforts need to be put into modelling the vehicle components, especially for structural batteries, using primary data. Modelling of different technology development routes are seen as particularly important to identify which route would have the largest influence on reducing the CFRPs and SBs environmental impact.

## 5. Acknowledgements

This study is partly based on the work done within the scope of a master thesis done during the spring of 2021 by Ivan Berg and Kevin Sandberg at the division of Environmental Systems Analysis, Chalmers University of Technology, Gothenburg Sweden.

The authors of the paper would like to acknowledge that this study was conducted as a part of the LIBRE (Lignin Based Carbon Fibres for Composites) project, which has received funding from the Bio-Based Industries Joint Undertaking under the European Union's Horizon 2020 research and innovation program under grant agreement No 720707. The study has also been carried out in association with Batteries Sweden (BASE) and the Strategic Innovation Programme LIGHTer.

## References

1. European Environment Agency. Greenhouse gas emissions from transport in Europe. 2019 [cited 2021 2:nd of March]; Available from: <https://www.eea.europa.eu/data-and-maps/indicators/transport-emissions-of-greenhouse-gases/transport-emissions-of-greenhouse-gases-12>.
2. Hermansson, F., M. Janssen, and M. Svanström, Prospective study of lignin-based and recycled carbon fibers in composites through meta-analysis of life cycle assessments. *Journal of Cleaner Production*, 2019. 223: p. 946-956.
3. Pradeep, S.A., et al., 30 - Automotive Applications of Plastics: Past, Present, and Future, in *Applied Plastics Engineering Handbook (Second Edition)*, M. Kutz, Editor. 2017, William Andrew Publishing. p. 651-673.
4. Asp, L.E., et al., A Structural Battery and its Multifunctional Performance. *Advanced Energy and Sustainability Research*, 2021. 2(3): p. 2000093.
5. Carlstedt, D. and L.E. Asp, Performance analysis framework for structural battery composites in electric vehicles. *Composites Part B: Engineering*, 2020. 186: p. 107822.



6. Duflou, J., et al., Environmental impact analysis of composite use in car manufacturing. *CIRP Annals-Manufacturing Technology*, 2009. 58(1): p. 9-12.
7. Das, S., Life cycle assessment of carbon fiber-reinforced polymer composites. *The International Journal of Life Cycle Assessment*, 2011. 16(3): p. 268-282.
8. Wernet, G., et al., The ecoinvent database version 3 (part I): overview and methodology. *The International Journal of Life Cycle Assessment*, 2016. 21(9): p. 1218-1230.
9. Romaniw, Y.A., The relationship between light-weighting with carbon fiber reinforced polymers and the life cycle environmental impacts of orbital launch rockets. 2013, Georgia Institute of Technology.
10. Fazio, S. and D. Pennington, Polyacrylonitrile fibres (PAN); from acrylonitrile and methacrylate; production mix, at plant; PAN without additives (Location: EU-27), J.R.C.J. European Commission, Editor. 2005, European Commission, Joint Research Centre (JRC).
11. European Platform on Life Cycle Assessment, ELCD, European Platform on Life Cycle Assessment, Editor. 2018.
12. Suzuki, T. and J. Takahashi. Prediction of energy intensity of carbon fiber reinforced plastics for mass-produced passenger cars. in Ninth Japan International SAMPE Symposium JISSE-9, Tokyo, Japan. 2005.
13. Zackrisson, M., et al., Prospective Life Cycle Assessment of a Structural Battery. *Sustainability*, 2019. 11(20): p. 5679.
14. Zackrisson, M., L. Avellán, and J. Orlenius, Life cycle assessment of lithium-ion batteries for plug-in hybrid electric vehicles – Critical issues. *Journal of Cleaner Production*, 2010. 18(15): p. 1519-1529.
15. Dunn, J.B., et al., Material and Energy Flows in the Production of Cathode and Anode Materials for Lithium Ion Batteries. 2015: United States.
16. Manjare, S. and R. Mohite, Application Life Cycle Assessment to Diammonium Phosphate Production. *Advanced Materials Research*, 2012. 354-355: p. 256-265.
17. Ioelovich, M., Energy Potential of Natural, Synthetic Polymers and Waste materials-A Review. *Acad. J. Polym. Sci*, 2018. 1(1): p. 1-15.
18. Witik, R.A., et al., Carbon fibre reinforced composite waste: an environmental assessment of recycling, energy recovery and landfilling. *Composites Part A: Applied Science and Manufacturing*, 2013. 49: p. 89-99.
19. Pickering, S., et al. Developments in the fluidised bed process for fibre recovery from thermoset composites. in 2nd Annual Composites and Advanced Materials Expo, CAMX 2015; Dallas Convention Center Dallas; United States. 2015.
20. Pickering, S.J., Recycling technologies for thermoset composite materials—current status. *Composites Part A: applied science and manufacturing*, 2006. 37(8): p. 1206-1215.
21. Cunliffe, A.M., N. Jones, and P.T. Williams, Recycling of fibre-reinforced polymeric waste by pyrolysis: thermo-gravimetric and bench-scale investigations. *Journal of Analytical and Applied Pyrolysis*, 2003. 70(2): p. 315-338.
22. Koffler, C. and K. Rohde-Brandenburger, On the calculation of fuel savings through lightweight design in automotive life cycle assessments. *The International Journal of Life Cycle Assessment*, 2010. 15(1): p. 128-135.
23. Del Pero, F., M. Delogu, and M. Pierini, The effect of lightweighting in automotive LCA perspective: Estimation of mass-induced fuel consumption reduction for gasoline turbocharged vehicles. *Journal of cleaner production*, 2017. 154: p. 566-577.
24. Johannisson, W., et al. Modelling and design of structural batteries with life cycle assessment. in 22nd International Conference on Composite Materials (ICCM22). 2019.
25. Arvidsson, R., et al., A crustal scarcity indicator for long-term global elemental resource assessment in LCA. *The International Journal of Life Cycle Assessment*, 2020. 25(9): p. 1805-1817.
26. Janssen, M., et al. Life cycle assessment of lignin-based carbon fibres. in 14th Conference on sustainable development of energy, water and environment systems (SDEWES), 1-6 October 2019, Dubrovnik. 2019.
27. Hermansson, F., Assessing the future environmental impact of lignin-based and recycled carbon fibres in composites using life cycle assessment, in Technology Management and Economics. 2020, Chalmers University of Technology: Chalmers Reproservice, Gothenburg.
28. Lam, S.S., et al., Cleaner conversion of bamboo into carbon fibre with favourable physicochemical and capacitive properties via microwave pyrolysis combining with solvent extraction and chemical impregnation. *Journal of Cleaner Production*, 2019. 236: p. 117692.

## Day 3: P09 – Materials and Modelling I

Session P09 – Materials and Modelling I, Wednesday 16 June

---

Session chairs: Elke Deckers and Romain Rumpler

- 10:00-10:10    **P09.A**  
*Green chips urethane based poroelastic materials: An opportunity for up to 80% recycled and 100% recyclable content coming from recycled PU mattresses*  
Arnaud Duval, Guillaume Crignon, Maxime Roux and Dominique Lemaire
- 10:10-10:20    **P09.B**  
*Periodic resonator-based optimization of an acoustic package made of glass wool*  
Giuseppe Catapane, Dario Magliacano, Giuseppe Petrone, Francesco Franco and Sergio De Rosa
- 10:20-10:30    **P09.C**  
*3D tunable anisotropic metamaterial for low-frequency vibration absorption*  
Huina Mao, Romain Rumpler and Peter Göransson
- 10:30-10:40    *Questions and Answers*
-

# Green chips urethane based poroelastic materials: an opportunity for up to 80% recycled and 100% recyclable content coming from recycled PU mattresses

Arnaud Duval<sup>1,\*</sup>, Guillaume Crignon<sup>1</sup>, Maxime Roux<sup>1</sup> and Dominique Lemaire<sup>1</sup>

<sup>1</sup>Treves Product, Services & Innovation, 2-4, rue Emile Arquès, CS 70017, 51686 Reims Cedex 2, France

\*Corresponding author. Email: [arnaud.duval@treves-group.com](mailto:arnaud.duval@treves-group.com)

Chips urethane porous materials usage is known in the automotive industry as spacer function mainly or stiff porous barriers in hybrid stiff insulators, using both resin based or thermoplastic based binders, with injected foam as poroelastic spring traditionally. The switch from thermoset resin binders to thermoplastic PET bi-component fibers makes the material 100 % recyclable and improves drastically the poroelastic spring vibro-acoustic properties. Indeed, hybrid stiff insulators or under carpet insulators are thus feasible with 100 % usage of this thermoplastic chips urethane based recycled material called Polyfoam T used for both stiff absorbing barriers and poroelastic spring functions.

Transformed in one shot processes, these innovative hybrid stiff insulators presents excellent mechanical decoupling properties even at high densities above  $150 \text{ kg/m}^3$  and up to  $300 \text{ kg/m}^3$  typically. This is particularly interesting in these one shot thermoforming processes where low thickness areas may exist due to complex package management (available space) in the automotive industry. As these low thickness areas are the poorest performing areas of the insulators, a Transmission Loss improvement of more than 7 dB in average compared to traditional porous injected or thermoformed materials improves drastically the insulator performance allowing further weight reduction while keeping the recyclability advantage even for the End of Life Vehicles phase.

© 2021 by the authors. Published by the Resource Efficient Vehicles Conference.  
This is an open access article under the CC BY license (<http://creativecommons.org/licenses/by/4.0/>).

## 1. Introduction

The automotive industry is entering now a new era with a very fast growing electrification as well as ambitious sustainability goals. Beyond new environmental regulations discussed at the European Union level, most OEMs have set up internal recyclability goals which goes up to 40% recycled polymers (plastics) entering the manufacturing processes. Regarding the recyclability, the End of Life Vehicles (ELV) EU directive under revision for 2022 stipulates up to now that a minimum of 85% weight per vehicle should be reusable and/or recyclable and that a minimum of 95% weight per vehicle should be reusable and/or recoverable. This is this latter value and particularly the exact meaning of *recoverability* that is particularly targeted by the new upcoming ELV EU directive. This means that innovative Noise Vibration & Harshness (NVH) products should not only come from recycled or renewable resources but also that the final NVH parts should be 100% recyclable after a potential separation phase.

This former statement implies that thermoset binding should be avoided and thus that thermoplastic binding should be generalized whenever the working temperatures enable it [1]. This issue is easily

solved here for recycled polyurethane (PU) chips by using CoPET bi-component fibers, which makes the Polyfoam T material up to 80% recycled and 100% recyclable. Within the hybrid stiff family hard porous layer / impervious layer / soft porous layer, the first challenge of this acoustic study has been to define one shot processes for more efficient lay-ups with heavier recycled impervious barriers and mass localization. The second challenge has consisted in quantifying precisely the -20% average weight reduction brought by the chips urethane material bound with bico fibers for both hardness (static compressibility) and acoustic Insertion Loss whenever used as poroelastic spring in shape [2]. Indeed, the NVH performance proved to be density dependant with a huge improvement of more than 7 dB in average for high densities typically occurring at low thicknesses for thermoforming processes above  $150 \text{ kg/m}^3$  and up to  $300 \text{ kg/m}^3$ .

## 2. Chips urethane recycled raw material

The recycling process and raw material Polyfoam T blank manufacturing can be described as follows. A first anti-bacterial and anti-fungal decontamination step is carried out on the recycled used PU mattresses. Then, a shredding process in order to get the recycled PU flocks followed by a mixing step with bi-component fibers takes place (cf. Fig. 1).



Figure 1: Mattresses shredding (left) and PU flocks with PET bico mixing (right)

The resulting chips urethane mixture is then airlay carded as well as calandered and thermofixed in a hot air oven. Final chips urethane blanks are thus obtained after a last cutting step (cf. Fig. 2).



Figure 2: Airlay carding & thermofixing (left) and chips urethane blanks cutting (right)

## 3. Poroelastic spring vibro-acoustic properties

The recycled chips urethane material used as poroelastic spring presents the advantage of drastically increasing the insulation performance for the low thicknesses (high densities). Indeed, the cotton felt material becomes very hard above  $200 \text{ kg/m}^3$  up to  $300 \text{ kg/m}^3$  with Young's modulus

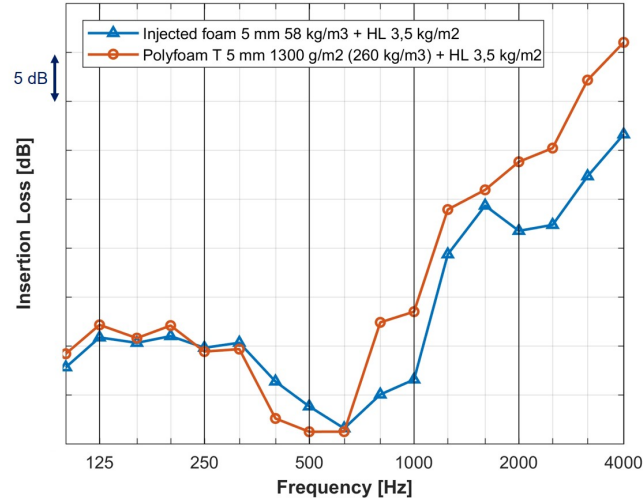


Figure 3: Polyfoam T Insertion Loss small cabin measurements at low thicknesses

between  $1E6$  Pa up to  $1E8$  Pa progressively depending on the binder percentage and nature, whereas the Polyfoam T made of chips urethane coming from shredded used mattresses remains below  $5E5$  Pa with an optimal percentage of Co-PET bi-component fibers (density  $260\text{ kg/m}^3$ )... Fig. 3 shows a measured Insertion Loss improvement of 7 dB in average compared to an injected foam  $58\text{ kg/m}^3$ , which remains relatively soft at 5 mm thickness with Young's modulus below  $1E5$  Pa, proving that the increased density is thus favorably contributing here, as well as the strongly increased airflow resistance. The comparison with the super hard cotton felt as poroelastic spring does not make sense (thus not reported here) and would be highly in favor of the still soft highly compressed Polyfoam T material anyway [3]... This 7 dB Insertion Loss improvement result is much better than the mass law, knowing that the mass per unit area of the heavy layer is  $3.5\text{ kg/m}^2$  here.

#### 4. Chips urethane based dash insulator

For manufacturing a Hybrid Stiff dash insulator, the chips urethane blanks are then superposed depending on the targeted acoustic lay-up, heated with contact heating and thermoformed in a cold mold with air pressure in order to compress the top hard absorbing layer thanks to the PET film presence in sandwich (cf. Fig. 4). The originality of this one shot process lies in the thickness relaxation at temperature of the Polyfoam T material, enabling strong compression during the heating time which allows to speed up the overall cycle time.

Fig. 5 presents recomposition Insertion Loss results of the lower area of a dash insulator coming from measured database every 5 mm and a thickness 3D map. For this lower area, the acoustic principle remains a mass-spring system with a contributing or not contributing insulating or absorbing carpet. Indeed, the insulating carpet with its hard felt backing and its glued lower film brings the mass of the total carpet as if it were an heavy layer in the middle and high frequency range [5]. The latter enables a further weight reduction beyond poroelastic spring Polyfoam T vs. injected foam intrinsic decoupling properties resulting in a 7 dB improved global recomposed Insertion Loss in the high frequency range.

Fig. 6 shows the recomposition results in the Noise Reduction sense, meaning Sound Pressure Level difference in (dB) between two cavities of  $1\text{ m}^3$  coupled by a  $1\text{ m}^2$  panel covered by an insulating and absorbing trim. The Noise Reduction  $NR$  is computed following this equation  $NR = TL + 10 * \log(A)$ , with  $TL$  being the Transmission Loss (dB) and  $A$  the absorption area ( $\text{m}^2$ ) close to the diffuse field absorption coefficient of the noise treatment technology here. Compared to the



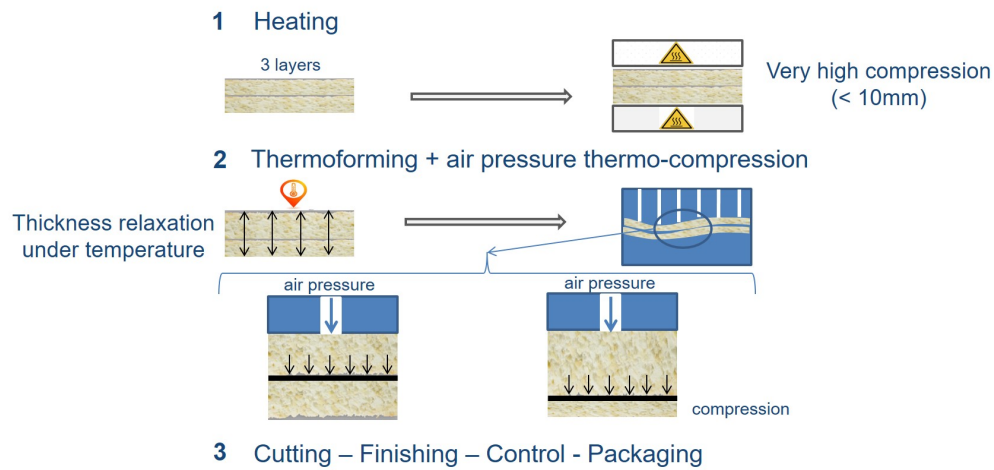


Figure 4: Hybrid Polyfoam T one shot process

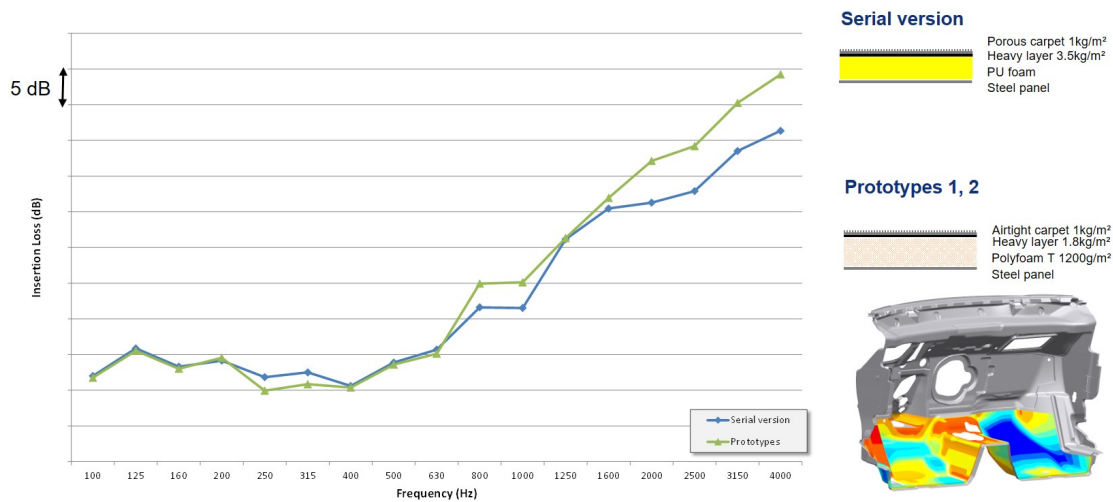


Figure 5: Hybrid Polyfoam T Hi-perf lower area: Insertion Loss (dB)

ABA Absorber/Barrier/Absorber reference (already) lightweight technology, the Hybrid Polyfoam T Hi-perf one shot presents the advantage of delivering absorption everywhere on the part leading to a higher absorption area in the high frequency particularly due to the limited coverage of the polyester (PET) felt of less than 50 %.

In order to increase the absorption in the middle frequency range, a solution consists in using also an ultra-soft highly compressible PET felt out of the available thickness CAD of the insulators (with a tuned AirFlow Resistance nonwoven on top). Therefore, this ultra-soft PET felt will be locally in interference with components behind the Instrument Panel (up to 70 % or 80 % of the total PET felt thickness) like the HVAC air-conditioning unit or glove box for example etc... The latter added middle and high frequency absorption allows an additional weight reduction from - 8 % globally on the dash insulator part down to - 15 % for this Hybrid Polyfoam T Hi-perf Ultimate technology beyond the good decoupling properties of the chips urethane material.

## 5. Chips urethane based floor insulator

As mentioned earlier, the chips urethane material used as poroelastic spring enables not only a weight reduction regarding acoustic Insertion Loss performances behind barriers but also regarding

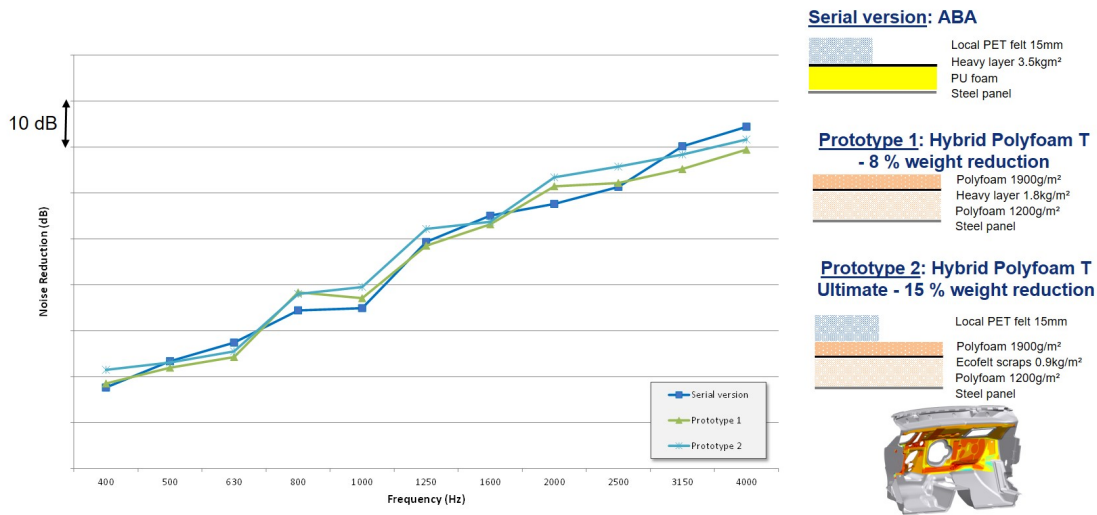


Figure 6: Hybrid Polyfoam T Hi-perf upper area: Noise Reduction (dB)

hardness (static compressibility) particularly requested for under carpet insulator applications. Even against thermoplastic felt at relatively low densities between  $50 \text{ kg/m}^3$  and  $150 \text{ kg/m}^3$ , the - 15 % to - 20 % weight reduction is happening for both aforementioned characteristics. For high densities above  $150 \text{ kg/m}^3$  up to  $300 \text{ kg/m}^3$ , the acoustic performance differences are even larger allowing even further weight reduction.

For the 2.5 D chips urethane under carpet prototyped in the vehicle using a large blank and small local patches, the weight reduction has been above - 20 % with 1,2 kg saved globally for the under carpet insulator. As shown Fig. 7 the reciprocal airborne transfer functions at vehicle level are even better in the high frequency range with 1 dB to 2 dB improvement despite this strong weight reduction thanks to both the mentioned good decoupling properties as well as switch from an absorbing carpet to an insulating one keeping anyway nice absorption properties with the carpet with a hard under felt backfoiled.

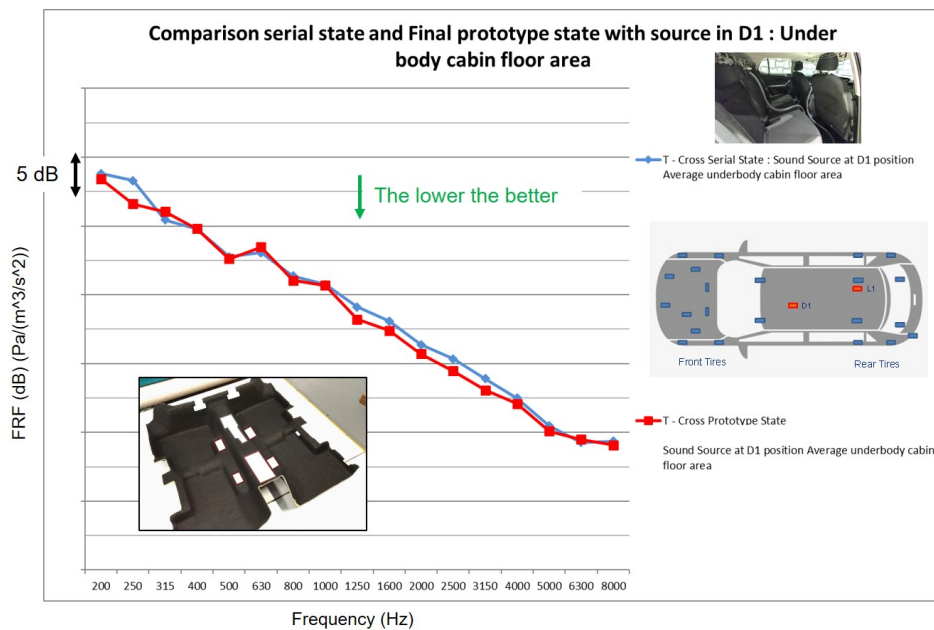


Figure 7: Polyfoam T under carpet: reciprocal airborne transfer functions

## 6. Vehicle acoustic measurements on a four wheels chassis dyno

The chassis dyno acoustic results for the final prototype state show equivalent or better results in the middle and high frequencies up to 1 dB in average for all microphones. This performance tends to increase to 2 dB for the rolling noise contribution due to the very good performance of the insulating carpet combined with the Polyfoam T light poroelastic spring.

This good performance of the carpet is confirmed by the microphones close to the footwell with up to 3 dB improvement there for all configurations with an Articulation Index improvement of up to 8 %.

## 7. Conclusion

Beyond its one shot competitive process, the Hybrid Polyfoam T concept (without PET felt optionally) presents the additional advantage for the hard absorbing barrier layer to be easily charged with solid inclusions in the volume up to 30 % while maintaining a good absorption [1] or powdered below backfoiled here for even higher equivalent masses [6], in order to increase the overall Transmission Loss and thus address upper segment vehicles (so-called Hi-perf versions).

With superior middle and especially high frequency acoustic global performance within actual available spaces, the Hybrid Polyfoam T Ultimate insulator with its ultra-soft PET felt is thus particularly adapted to electric or hybrid electrified vehicles with easily tunable acoustic performances and good mechanical stability.

The sustainable 80 % recycled and 100 % recyclable chips urethane material used as poroelastic spring allows thanks to its maintained softness an excellent low thickness high density performance even above  $150 \text{ kg/m}^3$  and up to  $300 \text{ kg/m}^3$  versus injected foam or cotton felt (which is even worse at these densities). This chips urethane based green insulator has proven here to be very efficient for 2.5 D under carpet applications with a - 20 % weight reduction which could go even further with a 3 D process allowing an even more precise localized density control.

## 8. Acknowledgment

We would like to thank warmly Thomas Semerak and Thomas Platz from the NVH department of Volkswagen in Wolfsburg for the fruitful discussions and support during this acoustic study.

## References

1. A. Duval, G. Crignon, M. Goret and M. Roux, Comprehensive hybrid stiff insulators family: the chips urethane contribution, SAE Conference - 2017-01-1883, Grand Rapids (MI), USA, 2017.
2. A. Duval, M. Goret, D. Lemaire and G. Crignon, Hybrid Polyfoam T Ultimate: an efficient chips urethane based green & light insulator, SAPEM Conference, West Lafayette (IN), USA, 2021.
3. J.-F. Allard and N. Atalla, Propagation of sound in porous media: modelling sound absorbing materials, Wiley & Sons, 2009.
4. A. Duval, J.-F. Rondeau, L. Dejaeger, F. Lhuillier and al., Generalized Light-Weight Concepts: A New Insulator 3D Optimization Procedure, SAE Conference - 2013-01-1947, Grand Rapids (MI), USA, 2013.
5. A. Duval and L. Bischoff, Stiff textiles or felts glued on light impervious layers: a new green light septum fiber technology, SAPEM Conference, Ferrara, Italy, 2011.
6. A. Duval, G. Crignon, M. Goret, D. Lemaire and al., Ecofelt Hybrid Stiff NVH Tunable Insulator, ISNVH Conference - 2018-01-1494, Graz, Austria, 2018.



---

# Periodic resonator-based optimization of an acoustic package made of glass wool

G. Catapane<sup>1,\*</sup>, D. Magliacano<sup>1</sup>, G. Petrone<sup>1</sup>, F. Franco<sup>1</sup> and S. De Rosa<sup>1</sup>

<sup>1</sup>PASTA-Lab (Laboratory for Promoting experiences in Aeronautical Structures and Acoustics), Department of Industrial Engineering - Aerospace Section, Università degli Studi di Napoli "Federico II", Via Claudio 21, 80125 Naples, Italy

\*Corresponding author. Email: [g.catapane@studenti.unina.it](mailto:g.catapane@studenti.unina.it)

---

Nowadays, modern urbanization and traffic increase could cause severe noise-induced health damages, such as annoyance, sleep disturbance, or even ischemic heart disease, and thus the interest on environment noise control is quickly growing.

Unfortunately, a sound absorbing material that well performs in overall the frequency range is not present in nature. For instance, acoustic solutions such as Helmholtz resonators have good performances at low frequencies, while porous media, whose foam cavities dissipate the energy by viscous and thermal losses, perform better at high frequencies.

The scope of this work is to investigate the sound transmission loss of an acoustic package made of glass wool, as well as to propose innovative solutions based on the inclusion of a periodic pattern of Helmholtz resonators inside its core, aiming at passively improving the acoustic performance in a chosen range of frequencies. In order to reach this goal, a numerical model is studied, and the effect of Helmholtz resonators tuned at several frequencies are simulated. For each of these layouts, also the mass increase of the so-called meta-core, compared to that of its classical homogeneous counterpart, is estimated. Results obtained herein may constitute a good basis in order to perform preliminary design considerations that could be interesting for further generalizations.

©2021 by the authors. Published by the Resource Efficient Vehicles Conference.  
This is an open access article under the CC BY license (<http://creativecommons.org/licenses/by/4.0/>).

---

## 1. Introduction

Acoustic meta-materials offer great flexibility for manipulating sound waves and promise unprecedented functionality, ranging from transformation acoustics, super-resolution imaging to acoustic cloaking. However, the design of acoustic meta-materials with exciting functionality remains challenging with traditional approaches using classic acoustic elements such as Helmholtz resonators (HR). Helmholtz resonators are used in a variety of applications to reduce the transmission of unwanted sound.

Alster [2] derived the classical formula for calculation of resonant frequencies of Helmholtz resonators, under the assumptions that all mass significant for oscillation of a resonator is concentrated in the neck of the resonator and that the spring constant is given by the volume of the resonator. Tang *et al.* [13] developed the theory of a generalized Helmholtz resonator, based on the jet-flow model which is manifested in the non-linearity of the orifice flow upon the passage of a high intensity wave. Fahy *et al.* [6] coupled a single Helmholtz resonator to an enclosure and tuned it to the natural frequency of one of its low order acoustic modes, also analyzing the effect on the free, and forced, vibrations of the fluid in the enclosure. Chanaud [3] developed an equation for the resonance frequency

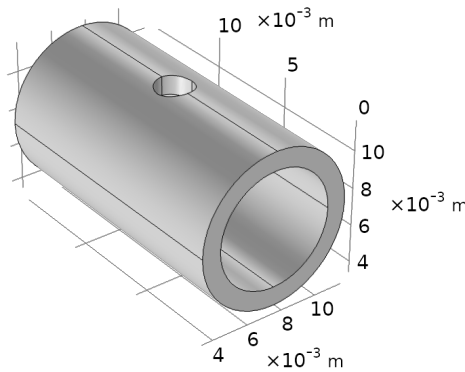


Figure 1: Geometry of Helmholtz resonator tuned at 3000 [Hz].

of a Helmholtz resonator from the wave equation for the case of a cavity volume that has the shape of a rectangular parallelepiped and orifices of different geometries. de Bedout *et al.* [5] presented a tunable Helmholtz resonator and a feedback-based control law that achieves optimal resonator tuning for time-varying tonal noise control applications. Lei *et al.* [8] described a strategy to characterize power and ground-plane structures using a full cavity-mode frequency-domain resonator model. Griffin *et al.* [7] demonstrated that mechanically coupled resonators can be used to design a particular transmission loss response, provide a wider bandwidth of attenuation, and adapt the transmission loss characteristics of a structure to attenuate disturbances of varying frequency. Tang [14] experimentally and theoretically investigated the acoustical properties of Helmholtz resonators with necks having cross-section dimensions decreasing away from the entry of the resonator cavities. Park [12] introduced micro-perforated panel absorbers backed by Helmholtz resonators in order to improve sound absorption in the low-frequency region, where conventional micro-perforated panel absorbers cannot provide sufficient absorption. Cheng *et al.* [4] demonstrated an ultraslow-fluid-like particle with intense artificial resonances for low-frequency airborne sound.

In the present work, a new concept of acoustic package is numerically studied and investigated, with the target of taking advantage from the exploitation of the combined effects of periodicity-induced and Helmholtz resonances; this may result in a meaningful increase of acoustic performance in two desired frequency ranges at the same time without any increase in terms of package thickness, thus allowing to pursue the target of resource efficiency.

In Section 2, the properties of the studied acoustic package are introduced, together with the 3-dimensional finite element (FE) geometries that are investigated in the following sections. Then, in Section 3, some possible meta-core solutions based on a glass wool layer are proposed and discussed. Furthermore, a numerical test campaign is performed for five setups, each with Helmholtz resonators tuned at different frequencies; for each of these configurations, also the mass increase of the meta-core, compared to that of its classical homogeneous counterpart, is estimated. In this context, the obtained results may constitute a good basis in order to perform preliminary design considerations that could be interesting for further generalizations. In conclusions, in Section 4, the results of this investigation are commented, and some possible future expansions of the present research are evaluated.

## 2. Definition of the problem

In this section, an innovative configuration based on an acoustic package made of commonly-used glass wool with embedded periodic Helmholtz resonators made of steel is numerically modeled and studied. Helmholtz resonators are considered in the shape of a hollow cylinder, with a hole acting as the neck, as shown in Figure 1.

<b>Color</b>	Yellow
<b>Material</b>	Glass wool
<b>Porosity</b>	0.99
<b>Tortuosity</b>	1
<b>Airflow resistivity [Pa*s/m<sup>2</sup>]</b>	9000
<b>Viscous characteristic length [mm]</b>	0.192
<b>Thermal characteristic length [mm]</b>	0.384

Table 1: Properties of JCA-modeled glass wool.

<b>Color</b>	Green
<b>Material</b>	Steel
<b><math>\rho</math> [kg/m<sup>3</sup>]</b>	7800
<b><math>E</math> [Pa]</b>	210E+09
<b><math>\nu</math></b>	0.30

Table 2: Properties of solid layers.

## 2.1 Geometrical and material properties

The physical properties of the studied acoustic package are reported in Tables 1 and 2, together with a legend of colors. Properties of air (indicated with pink-colored layers) are: density  $\rho_0 = 1.213 \left[ \frac{\text{kg}}{\text{m}^3} \right]$ , speed of sound  $c_0 = 342 \left[ \frac{\text{m}}{\text{s}} \right]$ . The total thickness of the different studied packages  $T = 75[\text{mm}]$  is kept constant.

The glass wool is modeled as an equivalent fluid through the Johnson-Champoux-Allard (JCA) approach; the FE implementation and analysis of this kind of materials has already been validated by the authors in their previous works [11], as well as for more complicated di-phasic behaviors through the use of Biot theory of poro-elasticity [9]. Unit cells with Helmholtz resonators tuned at different frequencies are shown in Figure 2.

## 2.2 Finite Element implementation

For what concerns the FE implementation, the module “Pressure Acoustics and Frequency Domain” of COMSOL MultiPhysics is used both as modeling environment and numerical solver. For all configurations presented in this work, the acoustic package consists of a repetition of five unit cells, meshed with tetrahedral elements generated through physics-controlled algorithms that are pre-implemented in the software. Since the analyses are carried out considering an excitation consisting of a normal incidence plane wave acting along  $z$ -axis, the only fundamental boundary condition to apply is the so-called Perfectly Matched Layer (PML) on the very bottom face of the models: indeed, this represents an artificial absorbing layer for wave equations, commonly used to truncate computational regions in numerical methods in order to simulate problems with open boundaries; this allows

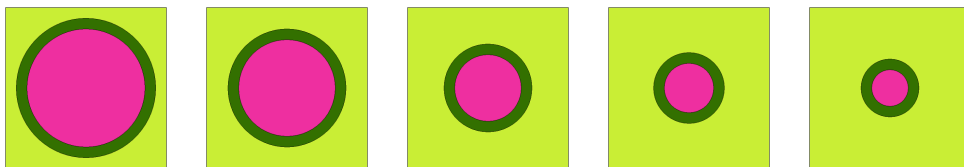


Figure 2: From left to right, meta-core unit cells with Helmholtz resonators tuned at 1000, 2000, 3000, 4000 and 5000 [Hz].

Configuration	HR tuning freq. [Hz]	HR resonance freq. [Hz]	Domain elem.	Boundary elem.	Edge elem.
1	1000	980	15950	7870	1272
2	2000	2010	16059	7084	1186
3	3000	2890	26816	8232	1296
4	4000	3850	29266	8400	1331
5	5000	5100	22587	7622	1261

Table 3: Number of FE mesh elements for each of the studied configurations.

the PML to strongly absorb outgoing waves from the interior of a computational region, without reflecting them back into the interior. Such property essentially simulates the interior of the aircraft cabin. On the contrary, boundary conditions applied on faces normal to  $x$ - and  $y$ - axes are not relevant for analyses with the above-mentioned kind of excitation, since under this condition the waves do not have propagating components along those directions; thus, for the sake of computational simplicity, a Sound Hard Boundary Wall (SHBW) boundary condition is applied herein. Eventually, for different angles of excitation, proper periodic conditions should be used instead.

In Table 3 the number of FE mesh elements for each of the studied configurations are reported; it should be pointed out that the difference between the values reported in “HR tuning frequency” and “HR resonance frequency” columns is that the first ones represent the ideal resonance frequency targets, while the second ones are the actual resonance frequencies that the authors were able to achieve. The sound transmission loss may be estimated through different approaches, such as the Transfer Matrix Method (TMM) [1], the Finite Element Method (FEM) [10], the Wave Finite Element Method (WFEM) [16] and the Statistical Energy Analysis (SEA) [15, 18], all having their own advantages and limitations [17]. In the context of this research, TMM and FEM are used. In particular, for a plane wave configuration at normal incidence  $\theta = \phi = 0$ , and thus oriented towards the negative direction of  $z$ -axis, the transmission loss is computed as reported in Eq. 1.

$$TL = 10\log_{10} \frac{\Pi_{incident}}{\Pi_{transmitted}}. \quad (1)$$

In the context of this work, the TLs related to the homogeneous (which has no inclusions) and the meta-core models are estimated through a FE implementation of Eq. 1. It should be highlighted that homogeneous results are compared with those obtained through TMM, as defined in Eq. 2 and Eq. 3.

$$TL = 10\log_{10} \left( \frac{1}{4} |T_{11} + \frac{T_{12}}{\rho_0 c_0} + \rho_0 c_0 T_{21} + T_{22}|^2 \right), \quad (2)$$

$$\text{with } \begin{bmatrix} T_{11} & T_{12} \\ T_{21} & T_{22} \end{bmatrix} = \begin{bmatrix} \cos(kd) & j \sin(kd) Z_c \\ \frac{j \sin(kd)}{Z_c} & \cos(kd) \end{bmatrix}. \quad (3)$$

### 3. Analyses and results

The well-known analytical formula for predicting the resonance frequency  $f_{HR}$  of a Helmholtz resonator is:

$$f_{HR} = \frac{c_0}{2\pi} \sqrt{\frac{S_n}{V_c (l_n + d_n \cdot CF)}}, \quad (4)$$

where  $S_n$  is the wetted surface of the neck,  $V_c$  is the cavity volume,  $l_n$  is length of the neck,  $d_n$  is the equivalent diameter of the neck and  $CF$  is a correction factor, which may need to be tuned according to the case of interest. In the context of the configurations analyzed herein, the aforementioned quantities are reported in Table 4.

Configuration	$l_n[\text{m}]$	$d_n[\text{m}]$	$S_n[\text{m}^2]$	$V_c[\text{m}^3]$	$CF$
1	0.001	0.001	7.85E-07	1.43E-06	0.71
2	0.001	0.002	3.14E-06	9.54E-07	0.71
3	0.001	0.002	3.14E-06	4.53E-07	0.74
4	0.001	0.002	3.14E-06	2.49E-07	0.77
5	0.001	0.002	3.14E-06	1.36E-07	0.82

Table 4: Geometrical characteristics of Helmholtz resonators, with reference to Configurations 1-5 described in Table 3.

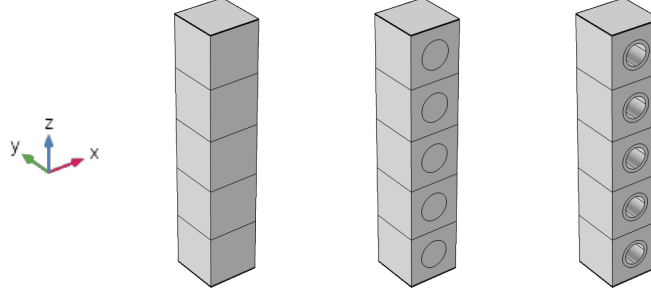


Figure 3: From left to right, acoustic packages made of glass wool: homogeneous, with periodic inclusions and with HRs (the latter being studied either filled by foam or air).

### 3.1 Investigation about several meta-core configurations

In this subsection, some possible meta-core solutions based on a glass wool layer are proposed and discussed. With reference to Figure 3, TL performance are estimated for:

- A homogeneous layer of glass wool (both through TMM and FEM);
- A layer of glass wool with a periodic pattern of five steel plain inclusions;
- A layer of glass wool with a periodic pattern of five Helmholtz resonators (Configuration 3 of Table 3), with steel walls and filled by glass wool;
- A layer of glass wool with a periodic pattern of five Helmholtz resonators (Configuration 3 of Table 3), with steel walls and filled of air.

All the aforementioned models have the same total thickness  $T = 75[\text{mm}]$ . Looking at Figure 4, it is evident how TL results related to the model having homogeneous layers show an almost perfect agreement with those analytically computed through the TMM; therefore, this comparison plays the role of an analytical validation of numerical results related to the multi-layered configuration without inclusions. Unfortunately, it is not conceptually possible to directly perform the same kind of validation also for the meta-configurations. As expected, through the adoption of a periodic pattern of five steel plain inclusions, the meta-core shows a performance peak related to periodicity effects, when half of the wavelength  $\lambda$  is equal to periodicity dimension (i.e. to the unit cell thickness along  $z$ -axis); it should be noted that, since this kind of acoustic resonance still relates on the thickness of the unit cell, it may be challenging to obtain performance peaks at low frequencies, when only a limited volume is available. Going further, the plain inclusions are replaced with specifically tuned Helmholtz resonators, thus awakening the correspondent resonance behavior: clearly, the related TL peak is significantly lower and slightly wider when the HR is filled by glass wool rather than air, due to the higher dissipation in the first system; anyway, solutions based on air-filled HRs may be more interesting with reference to the mass variation of the whole acoustic package (this aspect is thoroughly faced in Subsection 3.2).

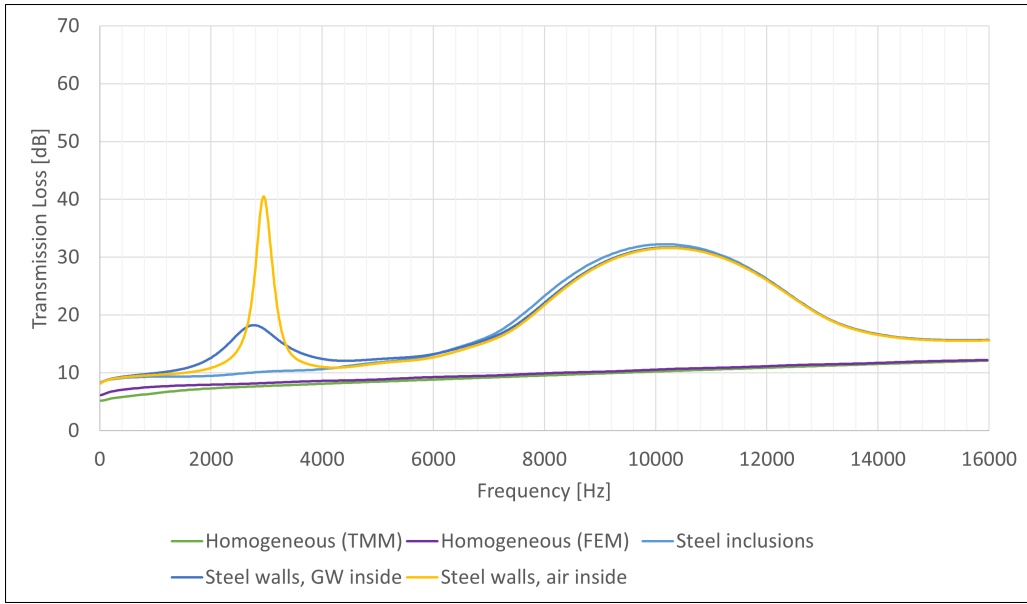


Figure 4: Transmission loss study performed on several meta-core solutions.

Configuration	Mass [kg]	Surface density $\left[\frac{\text{kg}}{\text{m}^2}\right]$	Mass increase [%]
1	2.21E-02	2.95E-01	8036
2	1.84E-02	2.46E-01	6721
3	1.33E-02	1.78E-01	4833
4	1.04E-02	1.39E-01	3730
5	8.21E-03	1.09E-01	2940

Table 5: Mass data of Configurations 1-5 described in Table 3, with air-filled HRs.

### 3.2 Numerical study on Helmholtz resonators tuned at different frequencies

In this subsection, a numerical test campaign is performed for five geometrical setups, each with Helmholtz resonators tuned at different frequencies; results are presented in Figure 5. In addition, considering that the homogeneous configuration has mass  $=2.70\text{E-}04$  [kg] and surface density  $=3.60\text{E-}03$   $\left[\frac{\text{kg}}{\text{m}^2}\right]$ , also the mass increases of the meta-cores are estimated and reported in Table 5. Concentrating on Figure 5, first of all one may notice that, at increasing HR resonance frequencies, the periodicity peak does not shift in frequency, but decreases its amplitude: this is explained by the fact that, in order to work at higher frequencies, the HR needs to have a smaller cavity; clearly, this has a non-negligible effect also on the amplitude of the periodicity-induced resonance peak. Furthermore, it should be noted how the resonance peaks computed in the (purely academic) cases of Helmholtz resonator walls modeled as SHBW almost perfectly agree with those analytically predicted through Eq. 4; instead, in general, when using a real material (e.g.: steel) to model such walls, HR resonance frequencies present a slight shift in their precise value, compared to those analytically calculated. The authors empirically verified that such a shift meaningfully increases for decreasing HR mass, thus representing a non-trivial obstacle to overcome in order to find an acceptable compromise between accuracy in resonance designability and mass increase. The latter consideration is useful to justify the very high values in terms of mass increase reported in Table 5, which therefore classify this solution concept, in its present form, as mainly viable for civil applications.

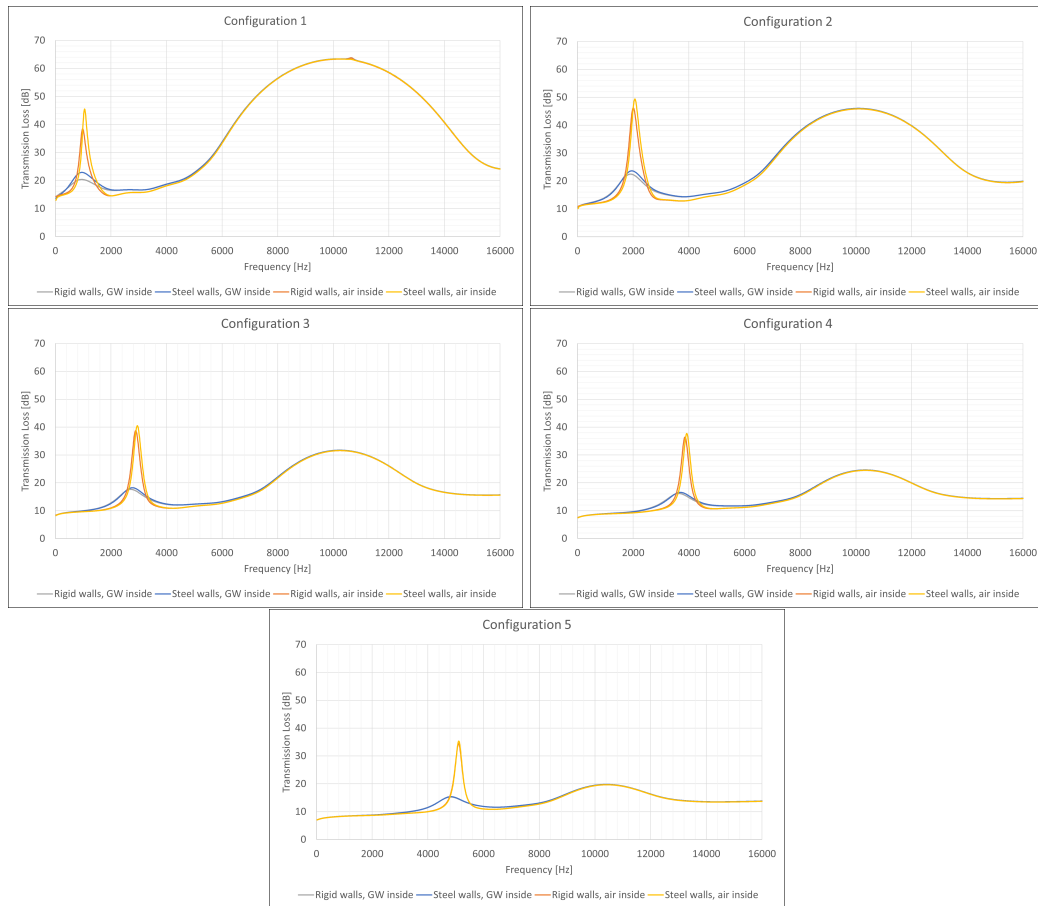


Figure 5: Transmission loss comparisons for Configurations 1-5 of Table 3.

## 4. Conclusions

In the present work, a new concept of acoustic package is numerically studied and investigated, with the target of taking advantage from the exploitation of the combined effects of periodicity-induced and Helmholtz resonances; this results in a meaningful increase of acoustic performance in two desired frequency ranges at the same time without any increase in terms of package thickness, thus allowing to pursue the target of resource efficiency. After having introduced the properties of the studied acoustic package, some possible meta-core solutions based on a glass wool layer are proposed and discussed. Then, a numerical test campaign is performed for five setups, each with Helmholtz resonators tuned at different frequencies; for each of these configurations, also the mass increase of the meta-core, compared to that of its classical homogeneous counterpart, is estimated. Future works could focus on the estimation of the correction factor of the analytical formulation of Helmholtz resonance frequency for different cavity geometries, and possibly for different cavity/neck ratios. Also a parametric analyses on different resonator patterns could represent an interesting extension of the concept presented herein. Most of all, it would be fundamental to investigate a way to further reduce the mass increase related to the use of meta-cores, thus making this solution viable also for applications in transportation engineering and increasing its overall resource efficiency.

## Acknowledgments

The authors acknowledge the support of the Italian Ministry of Education, University and Research (MIUR) through the project DEVISU, funded under the scheme PRIN-2107 - grant agreement No. 22017ZX9X4K006.

## References

1. J.F. Allard and N. Atalla. *Propagation of sound in porous media: Modelling sound absorbing materials*. Wiley, 2<sup>nd</sup> edition, 2009.
2. M. Alster. Improved calculation of resonant frequencies of helmholtz resonators. *Journal of Sound and Vibration*, 24(1):63–85, 1972.
3. R.C. Chanaud. Effects of geometry on the resonance frequency of helmholtz resonators. *Journal of Sound and Vibration*, 178(3):337–348, 1994.
4. Y. Cheng, C. Zhou, B.G. Yuan, D.J. Wu, Q. Wei, and X.J. Liu. Ultra-sparse metasurface for high reflection of low-frequency sound based on artificial mie resonances. *Nature Materials*, 14(10):1013–1019, 2015.
5. J.M. De Bedout, M.A. Franchek, R.J. Bernhard, and L. Mongeau. Adaptive-passive noise control with self-tuning helmholtz resonators. *Journal of Sound and Vibration*, 202(1):109–123, 1997.
6. F.J. Fahy and C. Schofield. A note on the interaction between a helmholtz resonator and an acoustic mode of an enclosure. *Journal of Sound and Vibration*, 72(3):365–378, 1980.
7. S. Griffin, S.A. Lane, and S. Huybrechts. Coupled helmholtz resonators for acoustic attenuation. *Journal of Vibration and Acoustics, Transactions of the ASME*, 123(1):11–17, 2001.
8. G.-T. Lei, R.W. Techentin, and B.K. Gilbert. High-frequency characterization of power/ground-plane structures. *IEEE Transactions on Microwave Theory and Techniques*, 47(5):562–569, 1999.
9. D. Magliacano, S. Ahsani, M. Ouisse, E. Deckers, G. Petrone, W. Desmet, and S. De Rosa. Formulation and validation of the shift cell technique for acoustic applications of poro-elastic materials described by the biot theory. *Mechanical Systems and Signal Processing*, 147, 2021.
10. D. Magliacano, M. Ouisse, S. De Rosa, F. Franco, and A. Khelif. Computation of acoustic properties and design guidelines of periodic biot-modeled foams. *Applied Acoustics*, 168, 2020.
11. D. Magliacano, M. Ouisse, A. Khelif, S. De Rosa, F. Franco, N. Atalla, and M. Collet. Computation of dispersion diagrams for periodic porous materials modeled as equivalent fluids. *Mechanical Systems and Signal Processing*, 142, 2020.
12. S.-H. Park. Acoustic properties of micro-perforated panel absorbers backed by helmholtz resonators for the improvement of low-frequency sound absorption. *Journal of Sound and Vibration*, 332(20):4895–4911, 2013.
13. P.K. Tang and W.A. Sirignano. Theory of a generalized helmholtz resonator. *Journal of Sound and Vibration*, 26(2):247–262, 1973.
14. S.K. Tang. On helmholtz resonators with tapered necks. *Journal of Sound and Vibration*, 279(3-5):1085–1096, 2005.
15. T. Wang, S. Li, S. Rajaram, and S.R. Nutt. Predicting the sound transmission loss of sandwich panels by statistical energy analysis approach. *Journal of Vibration and Acoustics, Transactions of the ASME*, 132(1):41–47, 2010.
16. Y. Yang, B.R. Mace, and M.J. Kingan. Wave and finite element method for predicting sound transmission through finite multi-layered structures with fluid layers. *Computers and Structures*, 204:20–30, 2018.
17. C. Yuan, O. Bergsma, and A. Beukers. Sound transmission loss prediction of the composite fuselage with different methods. *Applied Composite Materials*, 19(6):865–883, 2012.
18. R. Zhou and M.J. Crocker. Sound transmission loss of foam-filled honeycomb sandwich panels using statistical energy analysis and theoretical and measured dynamic properties. *Journal of Sound and Vibration*, 329(6):673–686, 2010.



# 3D tunable anisotropic metamaterial for low-frequency vibration absorption

Huina Mao<sup>1,2,\*</sup>, Romain Rumpler<sup>1,2</sup> and Peter Göransson<sup>1,2</sup>

<sup>1</sup>*KTH Royal Institute of Technology, Teknikringen 8, 100 44 Stockholm, Sweden*

<sup>2</sup>*The Centre for ECO<sup>2</sup> Vehicle Design, Teknikringen 8, 100 44 Stockholm, Sweden*

*\*Corresponding author. Email: huina@kth.se*

In the well-known conflict between design space and performance requirements e.g. in terms of noise and vibration insulation, the emergence of new materials exhibiting exceptional insulation properties for a reduced weight or volume increase has received much attention in the last decade. Metamaterials with artificially designed architectures are increasingly considered as new functional materials with unusual properties. This paper presents a group of novel 3D lattice metamaterials for low-frequency vibration absorption. The novel lightweight cellular microstructures for vibro-acoustic metamaterials are designed by modification of the Kelvin cell. Interesting anisotropic material properties are generated by controlling the geometries, e.g., high-stiffness, auxetic, and strong compression-torsional coupling properties. The interesting meta-properties enable to tune the cellular resonators of the structures at a low-frequency range. Previous research is mostly focused on metamaterials for vibration absorption along only one or two directions. In this paper, wide-band high sound absorption properties of energy transfer coupling in all three directions are achieved by tuning the frequency-dependent meta-structures in controlling the geometry and material properties. Additive manufacturing technologies are used for making the 3D complex tunable metamaterials.

© 2021 by the authors. Published by the Resource Efficient Vehicles Conference.  
This is an open access article under the CC BY license (<http://creativecommons.org/licenses/by/4.0/>).

## 1. Introduction

Metamaterials with artificially designed architectures are increasingly considered as new functional materials with unusual properties. Vibro-acoustic metamaterial gained a lot of attention due to their superior noise and vibration insulation properties in a frequency range where wave propagation is prevented [1, 2]. One way to achieve the wave attenuation is to add resonant structures of sub-wavelength sizes to a host material or structures [1, 3]. The interaction between resonant inclusions and host structures can lead to an increased vibro-acoustic performance in the lower frequency ranges with light weight solutions. This work is based on previous developed cellular materials by the authors with rigid body twist, tilt or stretch of Kelvin cells (KC) [4, 5]. The new modified KC demonstrates light-weight, high stiffness and tunable anisotropic material properties [4, 6].

This paper focuses on design of vibro-acoustic resonant structures based on the anisotropic cells in [4]. An innovative metamaterial model is designed for sound absorption: novel cellular resonant structures are added to cavities of a periodic core sandwich structure to create and increase the sound transmission behaviour. Parametric studies of the cellular geometry are discussed to investigate the application and demonstrate a method allowing to design vibro-acoustic metamaterials by controlling cellular meta-resonators.

## 2. Cellular meta-resonators

The novel properties of metamaterials are dictated by the structure of the metamaterial, which will be different from its constituent material properties. An isometric KC arrangement exhibiting cubic material symmetry is chosen as the reference micro-structure in the design of cellular meta-resonators, see Fig. 1a. The geometrical modifications of KC include twist, tilt and stretch [4]. Here only rigid body rotations are applied to the square faces of the reference KC geometry while keeping these squares undeformed during the rotation [4, 7]. Fig. 1 shows examples of auxetic cells leading to negative Poisson's ratios generated by twisting (in-plane rotation) of one to three pairs of square faces of the reference KC. Topologically, the cell is not modified and all vertices remain connected through the same struts (with altered lengths) as in the KC geometry. The rotational angles applied on each pair of square faces are anti-symmetric, *i.e.* rotated with opposite angles, equal in absolute value. The twisted cell exhibits chirality with respect to each middle plane parallel to the pairs of twisted faces. Negative Poisson's ratios from one to three directions are found by controlling the twisting faces and angles, *i.e.*, the cell becomes thinner when compressed, as shown in Fig. 2d.

Additive manufacturing technologies are applied to manufacture the complex geometry. Fig. 2a shows a 3D printed single cell that has negative Poisson's ratios in all three directions. Fig. 2 shows three interesting mode shapes of the auxetic single cell which might be interesting for vibro-acoustics purposes in energy transfer: spring-mass-like functional mode shape which may be introduced to exhibit an internal-resonator-like behaviour [3], see Fig. 2b; or extension-torsion coupled mode shapes due to chiral symmetry in Fig. 2c-Fig. 2d. In order to verify the application in vibro-acoustics, a simple sandwich composite structure embedded with cellular arrays is proposed in following Section 3.

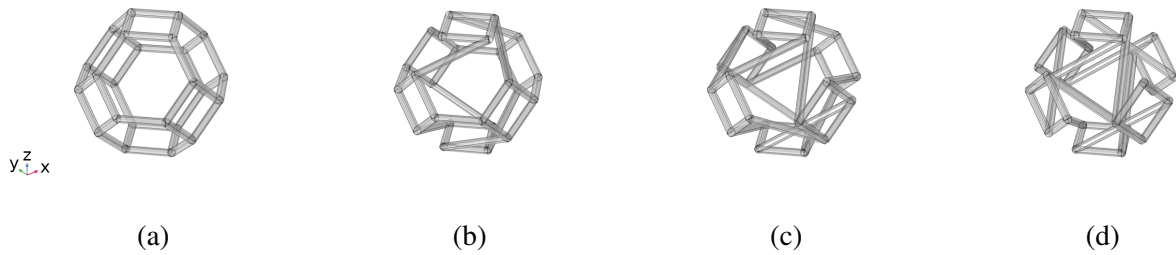


Figure 1: a) Reference Kelvin cell; auxetic cells with negative Poisson's ratios generated by rigid body rotations of the square faces of the reference Kelvin cell of  $90^\circ$  along: b)  $z$  direction ( $\nu_{yx} < 0$ ); c)  $z$  and  $y$  directions ( $\nu_{yx} \approx \nu_{zx} < 0$ ); d)  $z$ ,  $y$  and  $x$  directions ( $\nu_{yx} \approx \nu_{zx} \approx \nu_{zy} < 0$ ).

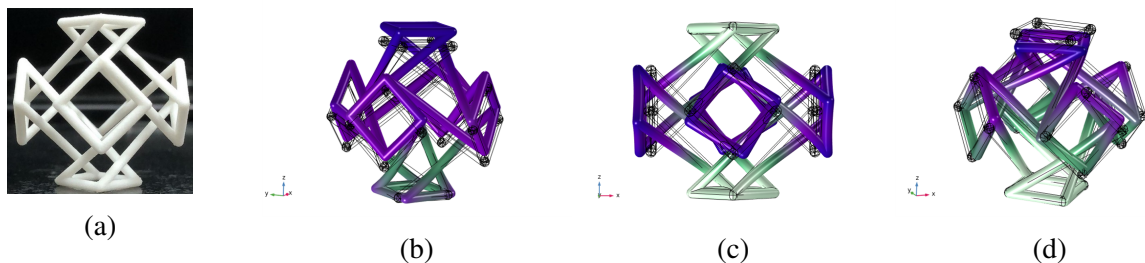


Figure 2: 3D printed auxetic cell twisted along  $z$ ,  $y$  and  $x$  direction; Selected interesting mode shapes of a single twisted cell: b) a spring-mass-like system, c) extension-torsion coupling between transverse directions, d) extension-torsion coupling between longitudinal and transverse directions where the cell becomes thinner under compression (auxetic/negative Poisson's effect).

### 3. Vibro-acoustics model

In connection with the specific applications and special properties, multiple cellular structures are currently under study. Here we focus on an application in vibro-acoustics of auxetic cells for sound insulation purposes in sound transmission loss (STL): a sandwich panel with a cell-based structural foam as core material to generate internal-resonator-like behaviour.

Fig. 3a shows the finite element model of the metamaterial sandwich plate (periodic sandwich plate with infinite lateral dimensions). A cellular array consisting of two cells in the thickness are assembled as a meta-structure core material of the sandwich plate [7]. Table 1 shows the dimension and material properties of the model, where the diameter of the cross-section of the cell is 1.5 mm.

Table 1: Geometry and material properties of the finite element model in Fig. 3a

Material	Density [kg/m <sup>3</sup> ]	Young's Modulus [GPa]	Poisson's Ratio [-]	Thickness [mm]
Cell	10340	16	0.3	25
Foam	920	0.8	0.3	5
Aluminium	2700	69	0.33	2

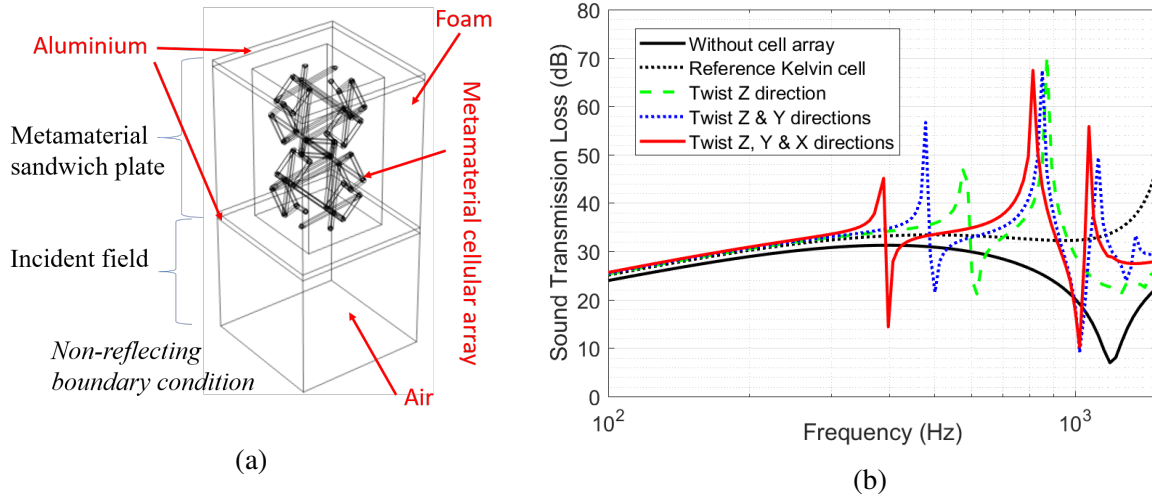


Figure 3: The finite element model of the metamaterial sandwich plate, b) Sound transmission loss (STL) of the metamaterial single-layer plate with different embedded cellular arrays.

### 4. Results

Fig. 3b illustrates the resulting trend of the STL in the frequency range up to 1500 Hz of different cell structures in Fig. 1. The case without internal resonator is plotted in black solid line, and the potential associated with the addition of the reference KC array corresponds to the black dashed line. The added KC array acts as an internal-resonator, similar to a spring-mass-like system as in Ref. [3]. The coincidence region is clearly visible on the reference calculation without the cellular array. In addition to the effect of spring-mass-like system, three cases with different auxetic cell arrays, plotted in coloured lines, clearly show an increased STL in a relatively low frequency range compared with the reference KC case. The auxetic cell with twists in all three directions, see 1d, provides a wider band-gap at a lower frequency range than the other two auxetic cells (cell twisted

around the  $x$  direction, and cell twisted around the  $x$  &  $y$  directions). The results show that tuning the cell geometry offers the possibility to improve the STL in a low frequency region.

Fig. 4 shows the resonant deformation of the reference KC and the auxetic cell of twist in all three directions (Fig. 3b). The reference KC model only has one resonance as spring-mass-like deformation under 1500 Hz, see 4a. However, the auxetic one (red curve in Fig. 3b) has three resonances with complex coupling deformations in all three directions, see Fig. 4b-Fig. 4d. Such configurations will be further studied to better understand, control, and advantageously use these resonances for STL improvements.

In addition to tuning the STL by controlling the geometry of the cellular array, Fig. 5a shows that the STL can also be improved by controlling the material properties of the cellular struts. The results naturally show, for instance, that by increasing the density of the struts, thus slightly increasing the mass of the resonator, a shift to lower frequencies with a wider gap were found. Conversely, increasing the stiffness of the struts, a shift to higher frequencies with a wider gap were found. Interestingly, Fig. 5b shows that by adding mass on the square faces in  $x$  and  $y$  directions (side faces), the second and third resonances merge and generate a wider STL. Since the focus is here only on demonstration of the idea for novel vibro-acoustic metamaterials with cellular structures, the cases with auxetic cells are presented.

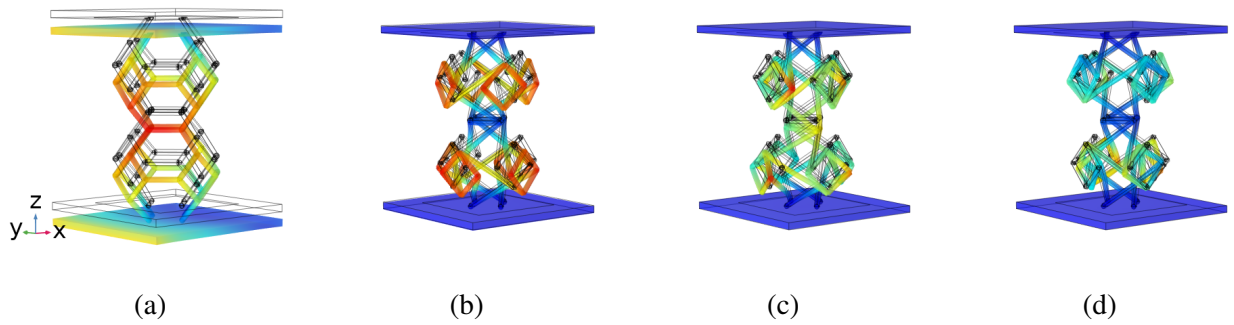


Figure 4: a) a spring-mass-like deformation of the reference Kelvin cell at frequency of 1500 Hz; resonant deformation of the auxetic cell in Fig. 1d at frequency of: b) 380 Hz, c) 812 Hz, and d) 1072 Hz.

## 5. Discussion and Conclusion

Novel light-weight open cells are proposed in this paper as meta-resonators for sound transmission applications. Example results of sandwich meta-structures show that the sound transmission properties are tunable by controlling the cellular geometry and material properties. High STL are found in a relatively low frequency range with embedded auxetic cellular array meta-structures. Coupling dynamics between longitudinal and transverse directions contributes to potentially increase further the transmission performance of such panels. The gap and amplitude of the STL are also tunable by adjusting the size, geometry, mass and material properties of the added cellular meta-structures. Ongoing studies seek to fully tune multiple resonances of the proposed resonators in order to exhibit exceptional sound transmission performance over wide frequency bands.

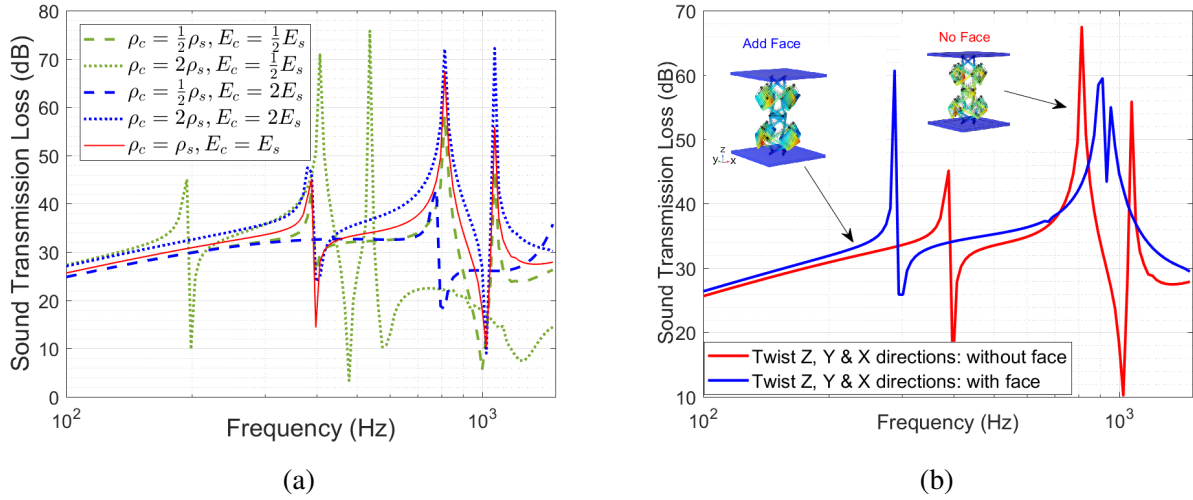


Figure 5: Sound transmission loss (STL) of the metamaterial single-layer plate of the auxetic cell (twist  $x$ ,  $y$  and  $z$  directions as shown in Fig. 1d): a) with different stiffness and densities where  $\rho_s$  and  $E_s$  are the default density and stiffness of the cell as shown in Table 1; b) add mass on square faces in  $x$  and  $y$  directions.

## References

1. NGR de Melo Filho, Lucas Van Belle, Claus Claeys, Elke Deckers, and Wim Desmet. Dynamic mass based sound transmission loss prediction of vibro-acoustic metamaterial double panels applied to the mass-air-mass resonance. *Journal of Sound and Vibration*, 442:28–44, 2019.
2. Giorgio Palma, Huina Mao, Lorenzo Burghignoli, Peter Göransson, and Umberto Iemma. Acoustic metamaterials in aeronautics. *Applied Sciences*, 8(6):971, 2018.
3. Zibo Liu, Romain Rumpler, and Leping Feng. Broadband locally resonant metamaterial sandwich plate for improved noise insulation in the coincidence region. *Composite structures*, 200:165–172, 2018.
4. Huina Mao, Romain Rumpler, Mathieu Gaborit, Peter Göransson, John Kennedy, Daragh O'Connor, Daniel Trimble, and Henry Rice. Twist, tilt and stretch: From isometric kelvin cells to anisotropic cellular materials. *Materials & Design*, 193:108855, 2020.
5. Huina Mao, Romain Rumpler, and Peter Göransson. An inverse method for characterisation of the static elastic Hooke's tensors of solid frame of anisotropic open-cell materials. *International Journal of Engineering Science*, 147:103198, 2020.
6. Huina Mao, Mathieu Gaborit, Romain Rumpler, and Peter Göransson. Vibro-acoustic behaviour of low-to high-density anisotropic cellular foams. In *ISMA2020 International Conference on Noise and Vibration Engineering, September 07-09, 2020, Leuven, Belgium*, 2020.
7. Huina Mao, Romain Rumpler, Mathieu Gaborit, and Peter Göransson. A tunable architected core material exhibiting auxetic behaviour for sound transmission control.

## Day 3: P10 – Materials and Modelling II / Early Design I

Session P10 – Materials and Modelling II / Early Design I, Wednesday 16 June

---

---

**Session chairs:** Thilo Bein and Peter Göransson

- 11:00-11:10    **P10.A**  
*Analytical method for predicting micro-geometry-based flow resistivity in anisotropic foams to improve sound absorption of vehicle panels*  
Eva Lundberg, Brad P. Semeniuk, Huina Mao, Romain Rumpler and Peter Göransson
- 11:10-11:20    **P10.B**  
*Optimization of deep drawing process parameters for multiple functional requirements*  
V. K. Balla, E. Deckers, B. Pluymers, J. Stroobants, H. G. Sakinala and W. Desmet
- 11:20-11:30    **P10.C**  
*Systematic design of a generic Life Cycle Inventory model construct*  
Patrick Haun, Philipp Müller and Marzia Traverso
- 11:30-11:40    *Questions and Answers*
- 
-



---

# Analytical method for predicting micro-geometry-based flow resistivity in anisotropic foams to improve sound absorption of vehicle panels

Eva Lundberg<sup>1,2,\*</sup>, B. P. Semeniuk<sup>1</sup>, Huina Mao<sup>1,2</sup>, Romain Rumpler<sup>1,2</sup> and Peter Göransson<sup>1,2</sup>

<sup>1</sup>*KTH Royal Institute of Technology, Teknikringen 8, 100 44 Stockholm, Sweden*

<sup>2</sup>*The Centre for ECO<sup>2</sup> Vehicle Design, Teknikringen 8, 100 44 Stockholm, Sweden*

\**Corresponding author. Email: eval@kth.se*

---

Vehicle structures such as train floors or car roofs are usually built as multi-layer panels, where a foam is placed between a load-carrying structure and an interior panel. The foam adds acoustical and thermal performance, but very little weight. In most contributions introducing foams for acoustic treatment, these have been considered isotropic, with acoustic losses mainly depending on properties in the thickness direction. Another mechanism investigated here is the possibility for the acoustic flow in the foam to change from acting only in the thickness direction but rather to be re-directed to also travel in-plane, where dimensions are substantially larger than in the thickness direction, permitting more losses as the wave travels through the material. That kind of effect would result in higher acoustic losses without increasing the thickness of the vehicle panel and better use of the allowable space to achieve acoustic and functional requirements, i.e. a better functional density. A first step is to investigate how the absorption properties of an anisotropic foam differs from an isotropic foam. The chosen approach is to use an analytical micro-model to calculate the dynamic drag impedance (flow resistivity on micro-scale) for an anisotropic open cell foam material. Based on a simple micro-scale geometry of Kelvin cells, it has been shown that simple cell alterations to the micro-geometry, such as stretching, twisting and tilting results in an anisotropic foam structure. The anisotropic flow resistivity tensor is not diagonal and uniform, but different directions can have different magnitudes and it can display off-diagonal coupling terms. The influence of such micro-scale distortions on the flow resistivity, and on the resulting sound absorption is investigated with the purpose of improving the acoustic performance without adding volume. Future steps include to modify the functional density and tailor the sound transmission loss to a specific application.

© 2021 by the authors. Published by the Resource Efficient Vehicles Conference.  
This is an open access article under the CC BY license (<http://creativecommons.org/licenses/by/4.0/>).

## 1. Introduction

The vehicle panels such as roof and floor are used for the structural integrity of vehicles. In addition to the load carrying function, it has additional functions e.g. reducing noise and give thermal insulation. To achieve the latter requirements, lightweight materials such as foams are often used. Since typical foam materials can consist of more than 90% air, they contribute to thermal and acoustic performance while adding very little extra weight. Still, the fundamental principles of sound absorption in isotropic materials require that the thickness is about a quarter of a wavelength in thickness for efficient absorption. This is a serious limitation making it hard to reduce noise in particular at lower frequencies. A thick vehicle panel also reduces the inner space which should be optimised for passenger comfort and/or payload capacity. The idea explored here is if there are possibilities to exploit the large inplane dimensions of the panel more efficiently for noise reduction by applying anisotropic foams. This analysis requires a tool where such foams can be modelled and investigated. Currently there are few such tools, but one that does exist is a transfer matrix method code based on a state-space formulation [1]. This method allows anisotropic input data for the foam material, e.g. dynamic drag impedance (or flow resistivity) and dynamic stiffness. Since measured anisotropic data is extremely rare, those properties are instead calculated from a simplified micro-geometry model. Material models based on micro-geometry for transversely isotropic materials have been validated in [2] and validation of analytical isotropic foam models are found in [3]. Here the foam models are extended to anisotropic acoustic properties, using the same micro-geometry as presented in [4]. Using the same basic micro-geometry for both stiffness and acoustics permits the two to be combined and further investigated as a next step, e.g. analyzing sound transmission loss of multi-layer panels.

Biot's theory [5] [6] [7] allow for accounting for anisotropic effects, but most current tools do not allow for it in practice. To estimate the Biot parameters, measurements on an actual sample exhibiting a degree of anisotropy is needed,, and even with samples available it is not an easy and straightforward process to go from microstructure to macro-level parameters [8] [9]. The results from these research tools give deep insights and interesting results, but demands a lot of resources and knowledge. Numerical models based on micro-geometry are currently very costly, in particular for thin struts, and even more so if symmetry due to isotropy cannot be used. Here these challenges are addressed by instead using a simplified analytical micro-geometry model for the foam. Using an analytical model based on micro-geometry is computationally efficient and can be used as a complementary technique in particular in early project phases for design decisions. Since it is fast, many different types of designs can be explored in order to make design decisions. It can also be used as a part of design optimization with the objective of balancing different requirements.

## 2. Analytical model for open cell foams

With the goal of having a simple and fast method, a number of assumptions are introduced. The primary focus is on obtaining the two most important parameters describing the acoustics of the foam material: the porosity and the dynamic drag impedance, which is equivalent to the flow resistivity on micro scale. The method has been described in detail in references [2] and [3]. For completeness the most important assumptions and formulas are given in Section 2.2. In order to obtain a simple model a number of assumptions are made: the struts are assumed to be so long that the effects of drag at the end of the struts and at the joints can be neglected and all interactions between the struts are neglected. The struts are straight with circular cross section making an analytical formulation possible. The cell and strut dimensions are assumed to be much smaller than the sample size and the wavelength of the acoustic waves, allowing the fluid to be modelled as viscous and in-compressible. The frame of the struts is assumed to be motions-less, and the viscous losses are assumed to be generated at the interface between the moving fluid and solid frame. The thermal influence is included in a non equilibrium model: the thermal transfer from the solid to the fluid is included, while the solid



strut temperature is assumed to remain constant. The thermal influence is taken into account via a factor  $\chi$  which modifies the governing equations. Even though this is a very simple model, the results for a fully isotropic material have been validated with excellent results against numerical models in Semeniuk et al [3]. Here the results are extended to include acoustic effects of anisotropic materials.

## 2.1 Microgeometry and porosity

The basic geometry is a Kelvin cell, whose repeated unit cell will have 24 struts in order to avoid double counting and allow packaging to fill space, see Fig. 1. Applying rotations of the square faces creates an anisotropic structure, as described in Mao et al [4]. Due to the way the transformation is applied, a supercell consisting of 8 cells in a 2x2x2 pattern will be symmetric. The porosity for a regular cell is defined as  $\phi = 1 - V_s/V_K$ , where  $V_s$  is the total strut volume in one cell and  $V_K$  is the cell volume. However, for a twisted cell, the cell volume cannot be easily estimated and another way of calculating the porosity has to be found.

A supercell of 8 Kelvincells in a 2x2x2 pattern is enclosed in a rectangular box of dimension  $2L_x 2L_y 2L_z$ . In addition to the 8 Kelvincells, a total additional volume corresponding to 8 Kelvincells must be added to completely fill space: 1 cell in the center of the supercell, 1/2 cell at each of the 6 centers of side faces, 1/4 cell associated with each of the 12 edges and 1/8 in each of the 8 corners see Fig. 1. The porosity for the geometry is calculated as  $\phi = 1 - (16V_{s,cell})/(8L_x L_y L_z)$ . For the cases considered here the geometry has been described in detail in [4]. Three cases for which the stiffness was calculated in [4] will here be investigated in terms of the effect on the dynamic drag impedance and the absorption. The three cases are: the isotropic case (NISO), the case with 60 degree twist around z-axis (NTw1), and the case with 60 degree twist applied in sequence z, y, x around the three global Cartesian directions (NTw2), see Fig 1. The geometrical parameters are given in Table 1.

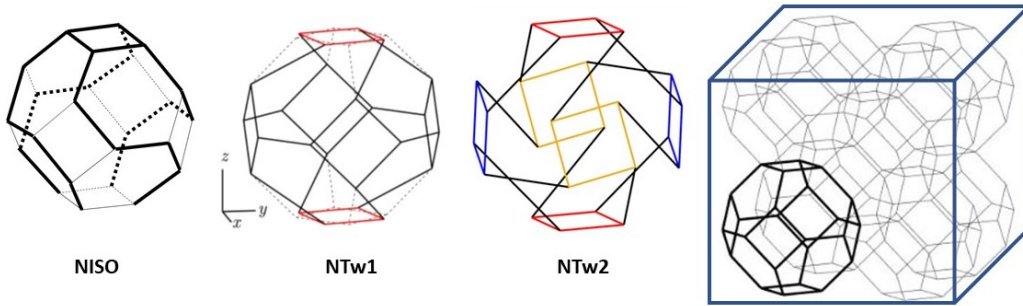


Figure 1: From left to right the micro-geometries for the isotropic cell (ISO), the cell twisted around z-axis (NTw1), the cell twisted around z,y and x axis (NTw2) and the symmetric supercell of 2x2x2 regular Kelvin cells (partial Kelvin cells filling cubic space are not shown) [4]

## 2.2 Analytical model for dynamic drag impedance

The governing equations are based on the  $\{\mathbf{u}^s, \mathbf{u}^t\}$  formulation of Biot's equations by Dazel in [10] and implemented in a transfer matrix method using state-space formulation by Parra Martinez[1].  $\mathbf{u}^s$  is the solid displacement and  $\mathbf{u}^t$  the total displacement. The formulation including the thermal factor  $\chi$  follows from [3]. The notations and material properties in Table 2 are used in the derivation and calculation of the dynamic drag impedance from the micro-geometry. For the case of motionless frame, the fluid pressure  $p$  can be related to the divergence of  $\mathbf{u}^t$  using the equivalent fluid bulk modulus  $\tilde{K}_{eq} = K_f/(\phi\chi)$  with the fluid bulk modulus  $K_f$ , as

Tabell 1: Geometric properties with models according to Fig 1 and Mao [4]

Property	Symbol	Model NISO	Model NTw1	Model NTw2
strut length/radius	$l_n/r_n$	100/2.5 $\mu\text{m}$	100/2.5 $\mu\text{m}$	100/2.5 $\mu\text{m}$
porosity	$\phi$	0.9959	0.9953	0.9939
twist around Z-axis		0 deg	60 deg	60 deg
twist around Y-axis		0 deg	0 deg	60 deg
twist around X-axis		0 deg	0 deg	60 deg

Tabell 2: Material properties

Property	symbol	value	unit
fluid density	$\rho_f$	1.2044	kg/m <sup>3</sup>
solid density	$\rho_s$	1574	kg/m <sup>3</sup>
fluid dynamic viscosity	$\mu_f$	$1.8140 \times 10^{-5}$	kg/ms
fluid bulk modulus	$K_f$	101325	Pa
fluid thermal conductivity	$\kappa_f$	0.02577	W/m K
solid thermal conductivity	$\kappa_s$	0.5	W/m K
fluid specific heat	$C_{pf}$	1005	J/kg K
solid specific heat	$C_{ps}$	1200	J/kg K
fluid expansion coefficient	$\eta$	$3.43 \times 10^{-3}$	-

$$\chi p = -\tilde{K}_{eq} \nabla \cdot \mathbf{u}^t. \quad (1)$$

The thermal influence has been derived in [3] and is given by  $\chi = \left(1 - \alpha \eta \phi (K_f / \phi) / j \omega \rho_f C_{pf}\right)$  where  $\alpha$  is a factor relating acoustic pressure to rate of heat input from solid to fluid. With  $\tilde{\alpha}$  defined by  $\tilde{\alpha} = \mathbf{I} - i \mathbf{Z} / (\omega \rho_f \phi)$ , the momentum equation for the fluid phase is given by

$$-\phi \nabla p \mathbf{I} = -\rho_f \omega^2 \tilde{\alpha} \mathbf{u}^s - \rho_f \omega^2 \tilde{\alpha} \mathbf{u}^f \quad (2)$$

The dynamic drag impedance is calculated from drag forces created by viscous losses at the solid-fluid interface from transverse (T) and longitudinal (L) flow with respect to three directions in a local coordinate system aligned the strut, see Eqs. (4) and (5). Since all struts can have different orientations, the contributions from each strut are rotated back to the global coordinate system with rotation matrix  $\mathbf{R}$  and then added. The porosity and total strut volume is then used to get the total dynamic drag force per unit volume, divided by the flow velocity, i.e. the dynamic drag impedance  $\mathbf{Z}$ .

$$\mathbf{Z}_{cell} = \begin{bmatrix} Z_{11} & Z_{12} & Z_{13} \\ Z_{21} & Z_{22} & Z_{23} \\ Z_{31} & Z_{32} & Z_{33} \end{bmatrix} = \frac{1 - \phi}{V_s} \sum_{n=1}^N \mathbf{R}_n \begin{bmatrix} Z_{Ln} & 0 & 0 \\ 0 & Z_{Tn} & 0 \\ 0 & 0 & Z_{Tn} \end{bmatrix} \mathbf{R}_n^T. \quad (3)$$

$$Z_{Ln} = 2\pi \int_0^{l_n} r_n k_\beta \mu_f \frac{H_1^{(2)}(k_\beta r_n)}{H_0^{(2)}(k_\beta r_n)} dz = 2\pi r_n l_n k_\beta \mu_f \frac{H_1^{(2)}(k_\beta r_n)}{H_0^{(2)}(k_\beta r_n)} \quad (4)$$

$$Z_{Tn} = i\pi r_n^2 l_n \rho_f \omega \left( 1 - \frac{4H_1^{(2)}(k_\beta r_n)}{k_\beta r_n H_0^{(2)}(k_\beta r_n)} \right) \quad (5)$$

$Z_{cell}$  is the dynamic drag impedance for the material and  $k_\beta = \sqrt{-(i\omega\rho_f/\mu_f)}$  is the shear wave number for the viscous fluid. To use the properties calculated on micro-scale in a TMM code developed for macro scale models, the method developed for a fibrous material in [2] is applied on the foam. The derived dynamic drag impedance is expressed in terms of modified Biot complex densities.

### 3. Results

#### 3.1 Dynamic drag impedance of anisotropic foam

To see the effect of anisotropy on the dynamic drag impedance, the method described in Section 2 is applied on the geometries in Table 1. In Table 3 the components of the dynamic drag impedance tensor at 0.01 Hz, related to the static flow resistivity, are compared for the three cases shown in Fig. 1. The anisotropy introduces effects that cannot be observed in isotropic materials. The diagonal elements in the anisotropic models NTw1 and NTw2 are larger than for the isotropic case NISO and are no longer identical. At the same time a negative term  $Z_{13}$  is introduced for NTw1 and NTw2. The effect is stronger when the unit cell is twisted around all three axes, but the trend is the same for both cases NTw1 and NTw2. The terms  $Z_{12}$  and  $Z_{23}$  remain approximately zero for these geometries. The isotropic dynamic drag impedance at 0.01 Hz is  $4531 \text{ N s/m}^4$ , which is a realistic value.

Tabell 3: Components of dynamic drag impedance normalized to the isotropic value

Component	model NISO	model NTw1	Model NTw2
$Z_{11}/Z_{iso}$	1	1,38	2,02
$Z_{22}/Z_{iso}$	1	1.32	1,49
$Z_{33}/Z_{iso}$	1	1.51	2,03
$Z_{12}/Z_{iso}$	0	0	0
$Z_{13}/Z_{iso}$	0	-0,06	-0,14
$Z_{23}/Z_{iso}$	0	0	0

Even though the porosity and strut dimensions are about the same for all three models, the drag impedance approximately doubles for the NTw2 geometry compared to the isotropic NISO case. The only change introduced is different degrees of anisotropy in the material. The introduction of the negative off-diagonal coupling term is also a very interesting feature.

#### 3.2 Transfer Matrix Calculation of absorption

When the dynamic drag impedance has been evaluated for the different micro-geometries, the absorption can be calculated on macro scale for a typical sample size using the method in [1]. To go from the micro-model-based properties associated with Eqs. (1) – (2) to the parameters used in a TMM calculation based on Biot formulation, the modified Biot complex densities  $\rho_{11}, \rho_{12}, \rho_{22}$  are calculated according to [11]. Together with the equation for  $\tilde{K}_{eq}$  in Eqn. (1), input data for an absorption calculation can be generated. With the notations from Section 2

$$\rho_{11} = \chi \left[ (1 - \phi) \rho_s \mathbf{I} - i \frac{\mathbf{Z}}{\omega} \right] \quad (6)$$

$$\rho_{12} = i\chi \frac{Z}{\omega} \quad (7)$$

$$\rho_{22} = \chi \left[ \phi \rho_f \mathbf{I} - i \frac{Z}{\omega} \right]. \quad (8)$$

### 3.3 Absorption of isotropic foam

In order to validate the method for the isotropic case, a calculation of an example where both measurement results and another implementation of the analytical method are available has been carried out. In Figure 19 in reference [3], a comparison is made for a measurement of a 51 mm thick sample of melamine. The material is modelled as isotropic Kelvin cell foam with a cell height of 0.3 mm (strut length 0.1 mm) and strut diameter of  $5\mu\text{m}$ . Motionless frame is assumed. The absorption is measured and calculated at normal incidence up to 6000 Hz. The result is compared to the measurement from [12] as well as another analytical implementation based on the same assumptions by Semeniuk and the result agrees very well.

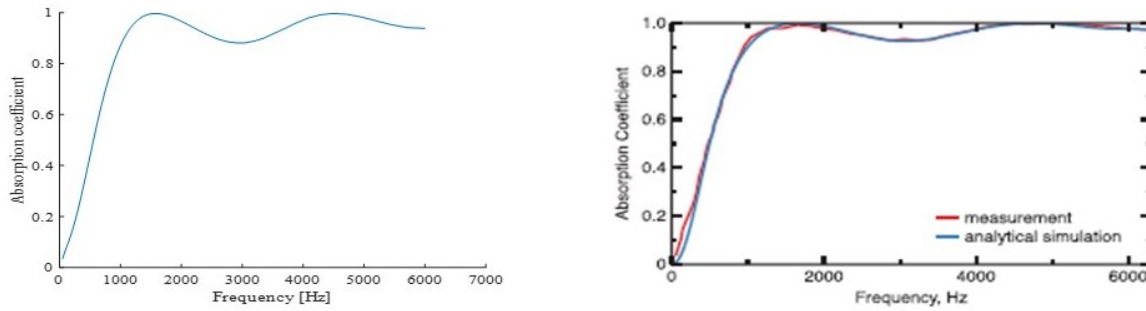


Figure 2: Measured and calculated absorption coefficient of isotropic melamine using two different analytical foam model, compared to measurements. The presented model to the left and measurements compared to a similar analytical model on the right. [12], [3].

### 3.4 Absorption of anisotropic foam

The three different cases are compared in terms of absorption coefficient for both normal and oblique incidence. The absorption coefficient is calculated using a transfer matrix method according to Parra Martinez et al [1], using the formulation described in Section 3.2. The oblique incidence gives higher absorption than normal incidence. The absorption coefficient at low frequencies below 1 kHz increases within a range of 0,1-0.15 with increasing anisotropy. Although the increase is rather modest, this gain is achieved without any change in strut dimension, porosity or thickness.

## 4. Discussion

Tools for analyzing the acoustics of anisotropic foams has until now been rarely presented. Numerical modelling including visco-thermal fluid is an alternative, but if the strut diameter is small and results for the entire frequency range should be calculated directly it can take hours, if not days or weeks. Since the dynamic drag impedance increases with decreasing strut diameter, this is one of the most interesting applications for noise reduction. In addition, most tools assume that it is possible to measure a sample in an impedance tube to obtain asymptotic values, something which is not possible in an early phase of designing a foam material since it does not exist physically.

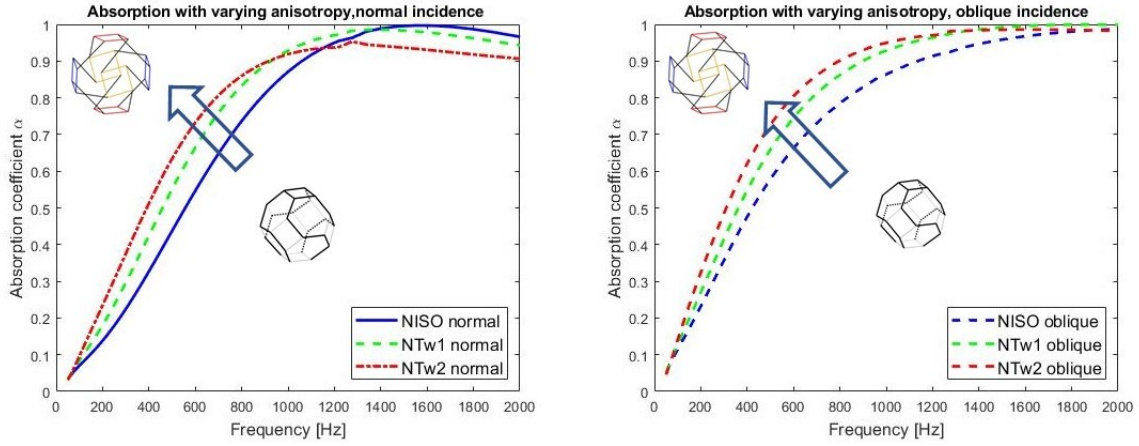


Figure 3: Calculated absorption coefficient with increasing anisotropy, models NISO, NTw1 and NTw2 for normal incidence (left) and oblique incidence of 45 deg (right).

Here an analytical model for estimating the dynamic drag impedance based on a simplified micro-structure model is presented. It is based on a number of simplifications: the cell size is assumed to be small both in relation to the wavelength and the sample size. This allows the drag force from the incompressible viscous fluid flow across the rigid circular strut to be estimated using an analytical expression. All interactions between the struts are neglected and so are the contributions from the joints between the struts. The thermal influence is included through a non equilibrium formulation: the temperature of the strut is assumed constant, while the temperature dissipation into the fluid is included. Given the difference in thermal capacity between the strut material and the air this is a justified assumption. At lower frequencies the assumption of no interaction between struts is strictly not correct, but at higher frequencies it is more reasonable. The validation in [2] and [3] show that the numerical and analytical models agree well, and also compare well to measurements for the isotropic case.

For anisotropic foams it is very difficult to find published measurements that can be used for validation. A numerical validation should be carried out to see how well the anisotropic dynamic drag impedance models the visco-thermal losses. The preliminary calculation do however show very interesting features. The magnitude of the dynamic drag impedance increases without changing strut diameter, cell size or porosity. In addition a negative coupling term is introduced. Future detailed evaluations are needed to show the exact significance of the introduced off-diagonal coupling term. One possibility to be investigated is whether the generated term indicates the possibility of energy dissipation along an in-plane direction. The positive diagonal terms of the dynamic drag impedance represent viscous losses, so a negative term may represent a generated energy, in a direction perpendicular to the flow direction, i.e. in an in-plane direction of the panel. If that feature can be exploited, the in-plane dimension, which is substantially larger than the thickness of the layer, can be used to increase the acoustic losses. If so, the thickness required for efficient noise reduction through vehicle multi-layer panels such as walls or floors may be reduced, or provide better acoustic performance in the same available space.

## 5. Conclusions

An analytical method for calculating the dynamic drag impedance of anisotropic foams based on micro-geometries based on Kelvin cells has been developed. The preliminary results show that when a foam with exactly the same strut thickness is made anisotropic by deforming it, it results in higher drag impedance than the isotropic design, up to double the isotropic value. In addition a negative

off-diagonal coupling term is introduced. The exact significance of the negative term remains to be explored in detail. The next steps are to fully validate the method for anisotropic microstructures and then investigate the effects on the sound transmission loss when using anisotropic instead of isotropic foam materials in multilayer panels for noise reduction in vehicles.

## 6. Acknowledgements

The authors would like to thank the Centre for ECO2 Vehicle Design, which is funded by the Swedish Innovation Agency Vinnova (Grant Number 2016-05195). Eva Lundberg would also like to thank for support from GKN ePowertrain.

## References

1. J. P. Parra Martinez, O. Dazel, P. Göransson and J. Cuenca , Acoustic analysis of anisotropic poroelastic multilayered systems, *J. of Applied Physics* 119, 084907 (2016)
2. B. P. Semeniuk, P. Göransson and O. Dazel, Dynamic equations of a transversely isotropic, highly porous, fibrous material including oscillatory heat transfer effects, *J. of the Acoustical Society of America* 146(4), 2019, pp. 2540-2551.
3. B. P. Semeniuk, E. Lundberg and P. Göransson, Acoustics modelling of open-cell foam materials from microstructure and constitutive properties, *J. of the Acoustical Society of America* 149, 2021, pp. 2016-2026.
4. H. Mao, R. Rumpler and P. Göransson, Twist tilt and stretch: From isometric Kelvin cells to anisotropic cellular materials, *Materials & Design* 193(2020) 108855
5. M.A. Biot, Theory of Propagation of Elastic Waves in a Fluid-Saturated Porous Solid. II. Higher Frequency Range, *The Journal of the Acoustical Society of America* 28, 179 (1956), pp. 168-178
6. M.A. Biot, Theory of Propagation of Elastic Waves in a Fluid-Saturated Porous Solid. II. Higher Frequency Range, *The Journal of the Acoustical Society of America* 28, 179 (1956), pp. 179-191
7. J.F. Allard and N. Atalla, *Propagation of Sound in Porous Media: Modelling Sound Absorbing Materials*, 2nd edition, John Wiley&Sons Ltd, 2009
8. V. H. Trinh, V. Langlois, J. Guilleminot, C. Perrot, Y. Khidas and O. Pitois, Tuning membrane content of sound absorbing cellular foams: Fabrication, experimental evidence and multiscale numerical simulations, *Materials & Design* 2019 Vol. 162, pp.245-361
9. T. G. Zielinski, R. Venegas, C. Perrot, M. Cervenka, F. Chevillotte, K. Attenborough, Benchmarks for microstructure-based modelling of sound absorbing rigid-frame porous media, *J. of Sound and Vibration* 2020 Vol 483 pp. 115441
10. O. Dazel, B. Brouard, C. Depollier and S. Griffiths, An alternative Boit's displacement formulation for porous materials. *J. of the Acoustical Society of America* 121(6), 2007, pp. 3509-3516.
11. B. P. Semeniuk, P. Göransson and O. Dazel, Microstructure based modelling of the thermal and viscous dissipation of a transversely isotropic porous fibrous insulation material, *Proc. of ISMA 2018 and USD 2018, International Conference on Noise and Vibration Engineering* , Leuven, Belgium, (September 17-19, 2018)
12. H.-Y. Lai, C. Gentry-Grace, M. Bonilha and C.A. Yoerkie, Experimental characterization of materials for acoustic performance with applications, in *Proceedings of Inter-Noise 2000* , Nice, France (August 27-30, 2000)

# Optimization of deep drawing process parameters for multiple functional requirements

V. K. Balla<sup>1,3,\*</sup>, E. Deckers<sup>1,2</sup>, B. Pluymers<sup>1,2</sup>, J. Stroobants<sup>4</sup>, H. G. Sakinala<sup>3</sup> and W. Dismet<sup>1,2</sup>

<sup>1</sup>*KU Leuven, Department of Mechanical Engineering, Celestijnenlaan 300, B-3001, Heverlee, Belgium*

<sup>2</sup>*DMMS Core Lab, Flanders Make, Belgium*

<sup>3</sup>*Member R&D, TVS Motor Company Ltd., Hosur-635110, Tamilnadu, India*

<sup>4</sup>*CodesignS Core Lab, Flanders Make, Belgium*

\*Corresponding author. Email: vamsikrishna.balla@kuleuven.be

In this work, a cylindrical cup design is investigated for meeting the dimensional accuracy, vibro-acoustic and crash performance simultaneously. Cylindrical cup forming simulations are performed using different deep drawing process parameters—Blank Holder Force (BHF), Friction Coefficient, Blank thickness and misalignment—to predict geometric profile and thickness variations. The formed geometry is used to simulate the vibro-acoustics performance of the design. The cylindrical cup has nominal dimensions of 80 mm diameter, 24 mm deep and 0.97 mm thickness. Forming simulations are performed to quantify the vibro-acoustic variability caused by changes in process parameters. The vibro-acoustic variability is attributed to the geometry profile and thickness distribution changes of the deep drawing manufacturing process. To investigate the same, the Design Of Experiments (DOE) studies, based on Taguchi orthogonal arrays, are carried out to characterize the effect of individual process parameters on the response. The deep drawing analysis and the subsequent vibro-acoustic simulations are instrumental in optimizing both functional requirements. The crash performance of the component is predicted using the empirical formula mentioned in the literature. It is shown that a careful selection of process parameters help to optimize the response for multiple functional requirements.

© 2021 by the authors. Published by the Resource Efficient Vehicles Conference.  
This is an open access article under the CC BY license (<http://creativecommons.org/licenses/by/4.0/>).

## 1. Introduction

The ever-increasing demands of customers must be satisfied in order to improve the brand image of products. The number of components required to meet functional needs is increasing due to reason as mentioned earlier. Furthermore, stringent mass emission and other regulatory standards prevent weight addition, thus limiting the number of components in the product. Consequently, there are multiple functional requirements for a component. Optimization of design parameters that aim to meet the most often not the contradictory functional requirements shall be carried out during the initial phase to take advantage of the maximum possible design space. Although the design space at the initial stage of the product is less restricted, the domain knowledge—generated through virtual simulations, surrogate product experiments, or empirical models—is crucial to select the optimum design parameters.

The deep drawing manufacturing process is used for manufacturing sheet metal components [1]. The weight advantages of sheet metal components over castings or forged components help to design



resource-efficient products. The advancements in the sheet metal industry are likely to benefit the automobile industry as a typical Body-In-White (BIW) weight of an automobile consists of about 75% sheet metal parts [2] produced through stamping or deep drawing processes. The sheet metal part contribution to dimensional stability, vibro-acoustic and crash performance is quite significant, and this work emphasizes achieving the attributes mentioned above simultaneously by studying an archetype sheet metal cylindrical cup component.

## 2. Component description

The cylindrical cup has a nominal diameter, depth and thickness of 80 mm, 24 mm and 0.97 mm, respectively, as shown in Figure 1. Additionally, cylindrical cups with the same diameter and depth but with a thickness of 1.21 mm are also produced. The BHF used for cylindrical cup manufacturing is 35 kN or 45 kN. The cylindrical cup is made of DP600. Table 1 presents the details of the combinations of cylindrical cups considered in the present work. The blank diameter used for the manufacturing is 100 mm, along with a punch diameter of 50 mm. The die opening is 52.88 mm, and the die entry radius is 3 mm. The punch speed is 50 mm/min.

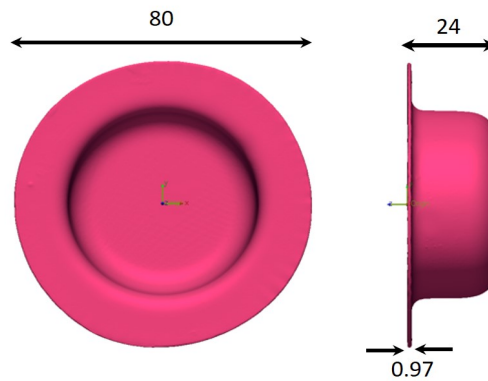


Figure 1: Top and side views of the cylindrical cup (All dimensions are in mm).

Table 1: Cylindrical cup geometry, BHF, part number description, and weight details.

Depth (mm)	BHF (kN)	Thickness (mm)			
		0.97		1.21	
		Cup no.	Weight (g)	Cup no.	Weight (g)
24	45	1	59.17	9	74.47
	35	2	58.52	10	76.07

The cylindrical cup geometries are manufactured using two different BHF values. The acceptable range of BHF variation, as mentioned in literature [3], is about 25%. The vibrational behaviour can be assessed by studying the dynamic behaviour of these cups subjected to two different BHF values. Cups 1, 2 are produced using 45 kN BHF and 35 kN BHF respectively .

## 3. Results and Discussion

### 3.1 Simulation model validation

The deep drawing analysis is carried out using the explicit finite element method. The main goal of this analysis is to arrive at a more representative geometry to imitate the actual manufactured part and predict the influence of the geometry profile and thickness variations on the natural frequencies and the mode shapes. Additionally, having a numerical model in place also allows verifying the influence of process parameter variations. The analysis is performed using Radioss software [4]. The deep drawing of the cylindrical cup is complete, and the thickness distribution is shown in Figure 2a.



The thinning occurs at the bottom of the cup, and thickening occurs at the top of the cup. A thickness distribution comparison between the experimental and simulation results is shown in Figure 2b. The thickness distribution is compared with the experimental results of the reference [5]. The frequency response analysis has been carried out by exciting the physical cup at response location no.22 (driving point response). The simulation results are compared with the experimental results, as shown in Figure 3. It can be seen from the results that there is a reasonable match between the results. Hence, the simulation framework is validated, and further parametric analyses can be performed to understand the process parameter sensitivity.

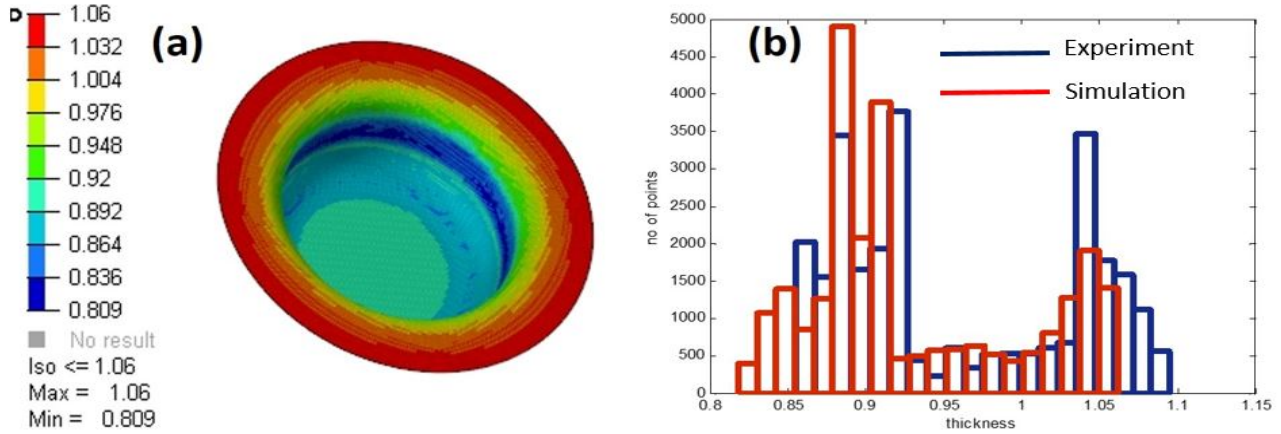


Figure 2: Comparison of thickness distribution of cylindrical cup-1 a) Contour map b) Histogram with experimental results.

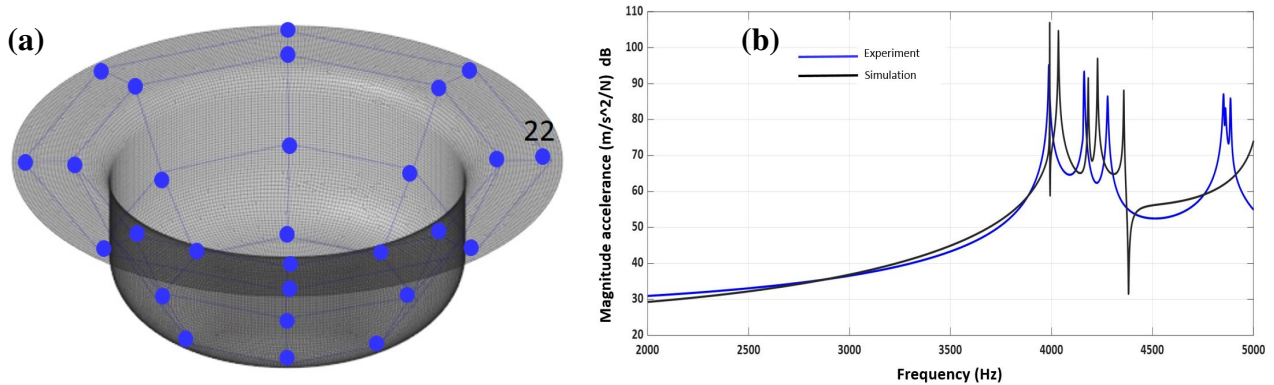


Figure 3: Cylindrical cup-3 a) FEM model b) FRF comparison of experimental and simulation results.

### 3.2 Functional performance metrics

The vibrational, acoustic, and crash performance of the component is optimized in this work. The component's double hat cross-section is considered as a representative section for analyzing the aforementioned attributes.

#### 3.2.1 Vibro-Acoustic analysis

The vibrational analysis is carried out as explained in the previous section by exciting at point-22, and responses are computed at all 32 locations (represented as blue dots in Figure 3). The global behaviour of the component is represented using a sum of FRFs [6] computed at all the locations.

The radiated noise of the cylindrical cup is predicted using the equivalent radiated power (ERP) approach [7]. It is possible to identify the structural regions that contribute most in the frequency range of interest. This computation mainly depends on the evaluation of velocity responses on the radiating surface, and it is defined as:

$$ERP = \frac{1}{2} \rho c \sum_{e=1}^{N_e} A_e V_e^2. \quad (1)$$

where  $A_e$  is elemental area, and  $V_e$  velocity magnitude at the element centre,  $\rho$  is fluid density,  $c$  speed of sound.

### 3.2.2 Crash analysis

Crash-worthiness is described as the ability of a part to withstand crash loads without undue deformation while also absorbing and dissipating the kinetic energy of the impact. The midrail component and a quarter vehicle subsystem from a General Motors' production vehicle are investigated [8]. According to the author, the general formula for the energy absorbed can be written as:

$$E_{TR,SR} = E_{BT,BS} (1.467 * TR - 0.447) (0.791 * SR + 0.208) \quad (2)$$

where  $TR$  is thickness ratio relative to baseline thickness and  $SR$  stress ratio relative to baseline stress.

## 3.3 Parametric studies

The following parameters are considered for quantifying the performance of deep drawn parts: i) blank holder force, ii) friction coefficient, iii) nominal blank thickness variation iv) misalignment, based on the literature. The manufacturing/misalignment error is defined as the angle between the punch and the die cavity.

The individual effects of each of these process parameters are assessed by keeping all other variables at the nominal level. For example, the effect of BHF is evaluated by varying it at different levels 35 kN, 45 kN, 55 kN while keeping friction coefficient as 0.1 and nominal blank thickness as 0.97 mm with no misalignment. The thickness distribution histogram and the sum of the FRFs of all the nodes corresponding to the measurement locations are given in Figure 4a & b, respectively. The lower and upper bounds of BHF values are obtained from the reference [9]. The high BHF value increased the resistance of material flow into the die cavity and thus increased the thinning phenomenon. This phenomenon reduced the stiffness of the geometry, and hence eigenfrequencies have shifted to the lower side with the highest BHF value. Figure 4c & d show the impact of friction changes on both thickness distribution and frequency response function. The thinning phenomenon reduced with the reduction in friction value, and eigenfrequencies shifted to the higher side. The lower and upper bounds of friction values are obtained from the reference [3]. The effect of blank nominal thickness is shown in Figure 4e & f.

The lower and upper bounds of thickness variation are obtained from the reference [10]. The higher nominal thickness increased the highest thickness of the formed cup, while the lower nominal blank thickness increased the propensity of thinning. The shift in eigenfrequencies and amplitude changes are more evident due to variations in the nominal blank thickness. Hence, it can be stated that the effect of these process parameters is different and the nominal thickness has the highest impact on the vibro-acoustic properties. In addition, a small misalignment that could possibly happen during the deep drawing process is also considered. Slavic et al. [11] showed that misalignments cause unbalanced thickness and increase the load required for the drawing process. The upper and lower bounds of variation in the present study are obtained from [11, 12].

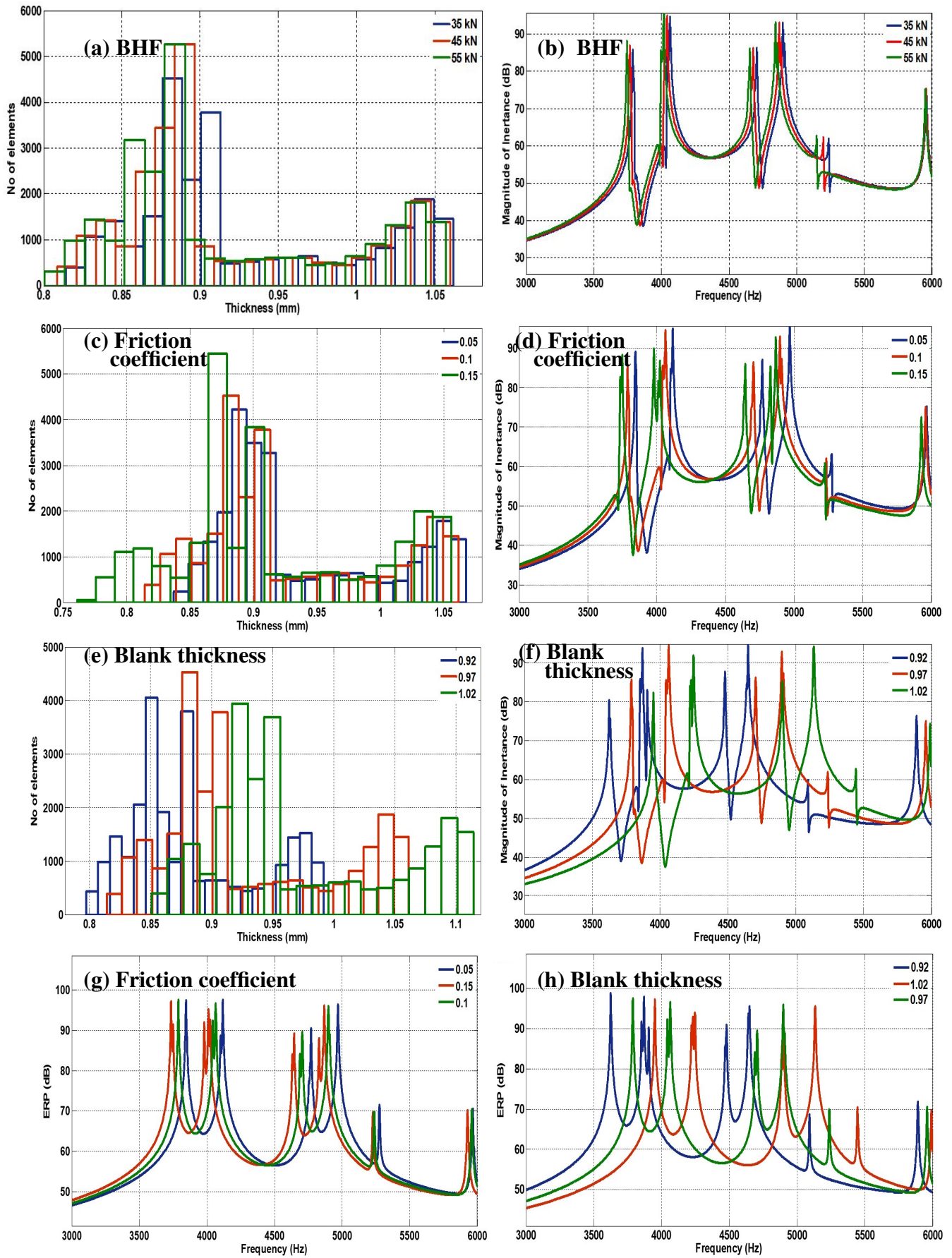


Figure 4: Influence results of a) BHF on thickness distribution b) BHF on FRF c) Friction on thickness distribution d) Friction on FRF e) Blank thickness on thickness distribution f) Blank thickness on FRF g) Friction on ERP h) Blank thickness on ERP.

The ERP values of all the configurations mentioned above are computed. However, the results of the friction and the nominal blank thickness effects are only shown in Figure 4g & h, respectively. The amplitude and frequency changes are quite evident from the results.

### 3.4 Design of Experiments

In order to further quantify the effect of the process parameters, a Design of Experiments (DOE) of the simulation model is carried out in the Minitab software [13]. The four factors considered are BHF, friction coefficient, blank nominal thickness and misalignment. The process parameters are varied at three levels, except for BHF, which is varied at two levels. The full factorial experiments 54 ( $2^1 \times 3^3$ ) are required to analyze the complete design. However, to reduce the computational time without compromising the accuracy of findings, the orthogonal array ( $L_{18}$ ) proposed by Taguchi [14] is used in the present study. The control factors and corresponding levels of all the experiments are as shown in Table 2.

Table 2: Control factors and levels.

Sl. No.	BHF (kN)	Friction	Thk (mm)	Misalign (deg)
1	35	0.05	0.92	0.00
2	35	0.05	0.97	0.05
3	35	0.05	1.02	0.10
4	35	0.10	0.92	0.00
5	35	0.10	0.97	0.05
6	35	0.10	1.02	0.10
7	35	0.15	0.92	0.05
8	35	0.15	0.97	0.10
9	35	0.15	1.02	0.00
10	45	0.05	0.92	0.10
11	45	0.05	0.97	0.00
12	45	0.05	1.02	0.05
13	45	0.10	0.92	0.05
14	45	0.10	0.97	0.10
15	45	0.10	1.02	0.00
16	45	0.15	0.92	0.10
17	45	0.15	0.97	0.00
18	45	0.15	1.02	0.05

The mean square response is considered as a metric to characterize the vibro-acoustic response. The mean square response,  $\overline{R^2}$  in any preferred frequency band, is the integral of the spectral density response within the frequency limits of the specified band, i.e., the area under the response spectral density curve [15] as follows:

$$\overline{R^2} = \int_{f_1}^{f_2} f(\omega) |H(\omega)|^2 d\omega \quad (3)$$

where  $f(\omega)$  and  $H(\omega)$  are force and transfer functions, respectively.

The vibration response at all of the corresponding measurement locations is computed, and ERP is evaluated for the complete cup geometry. The vibration and ERP levels i.e.,  $\overline{R^2}$  of each configuration in the design of experiment (DOE) runs, is considered as the corresponding response. Figure 5a & b show  $\overline{R^2}$  results of vibration and ERP response, respectively. It can be seen from the results that the vibration  $\overline{R^2}$  response of Run-15 has registered the lowest response. Similarly, the same DOE run's ERP can be considered the lowest in the case of radiated noise of the cups.

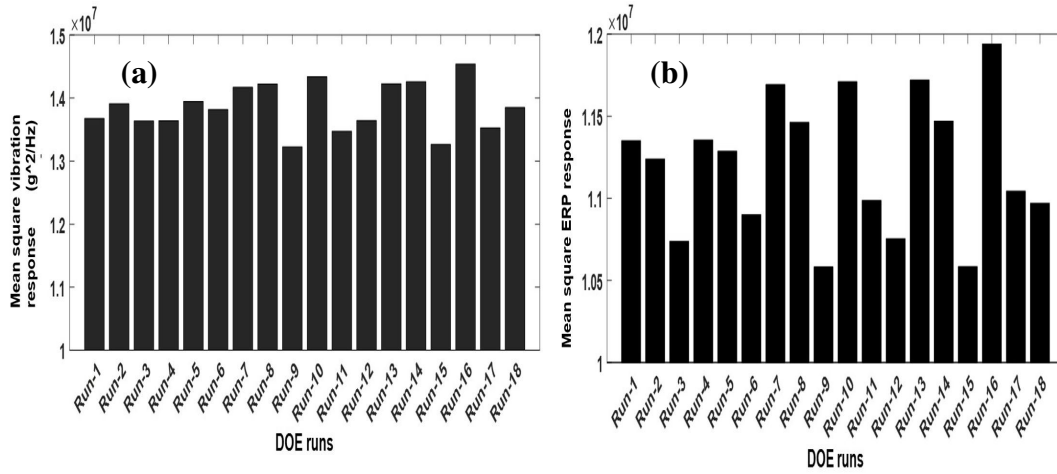


Figure 5: Comparison of a) vibration response b) ERP response of DOE runs.

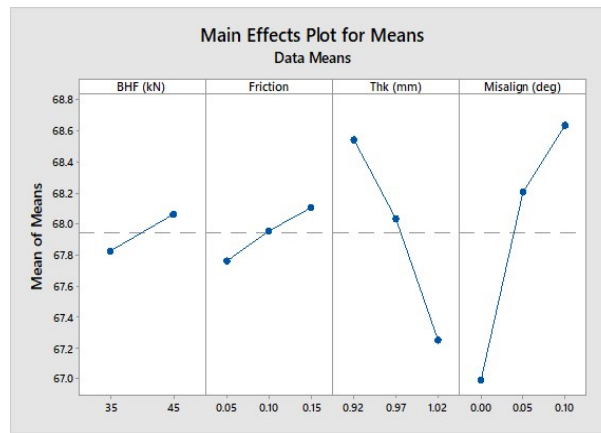


Figure 6: Vibration response main effect results of design parameters.

Figure 6 shows the main effect results of individual control parameters of vibration response. The highest and lowest design responses are obtained by selecting the process parameters corresponding to the higher and lower values of the main effect results. The difference between the foremost and the latter is the highest design variability in the manufacturing process. Figure 7 shows the highest possible performance variability that can be obtained due to process parameter changes. It is found that the total average vibration and ERP response levels in terms of  $\overline{R^2}$  values vary by 38% & 34%, respectively, within the total frequency range. The results show that 3.1 dB and 3.7 dB in vibration and radiated noise levels can be expected.

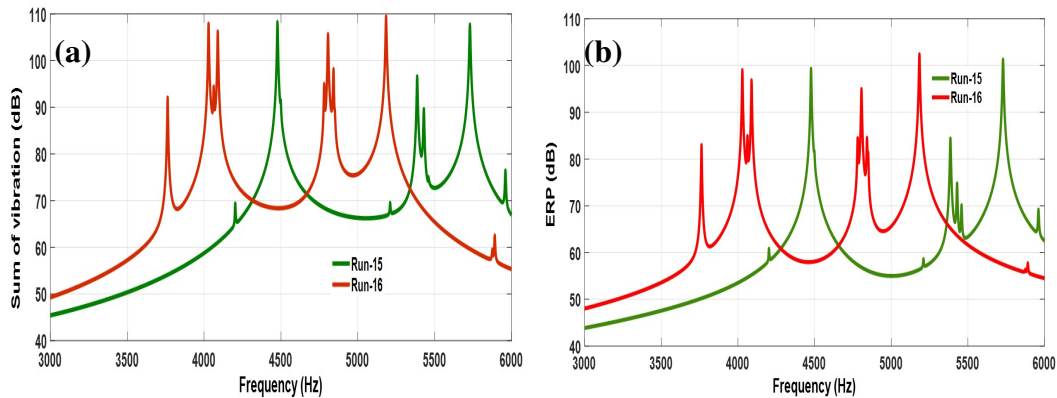


Figure 7: Comparison results of highest variability configuration a) vibration response b) ERP response of DOE runs.

The optimization of vibro-acoustic response can be carried out by a careful selection of process parameters. The lowest vibration response value achieved is 66.2 dB for the Run-15. However, further reduction of mean response can be achieved by keeping all the process parameters at the lowest levels, as indicated by the main effects plot. The variability can be controlled most effectively by minimising the nominal blank thickness variation and misalignment changes during the process.

The crash response is determined by the minimum thickness and stresses induced in the component. Figure 8 shows DOE results of minimum thickness and stresses induced in the component. The thickness and stress changes among the runs are about 19% and 43%, respectively. According to the literature, for a specific thickness, a 10% change in stress (relative to the baseline stress) results in a 7.03% and for a specific stress, a 10% change in thickness (relative to the baseline thickness) results in a 14.71% change in energy absorption respectively. Since the changes in stresses and thickness are greater than mentioned in the literature, the crash performance of these components is likely to vary significantly.

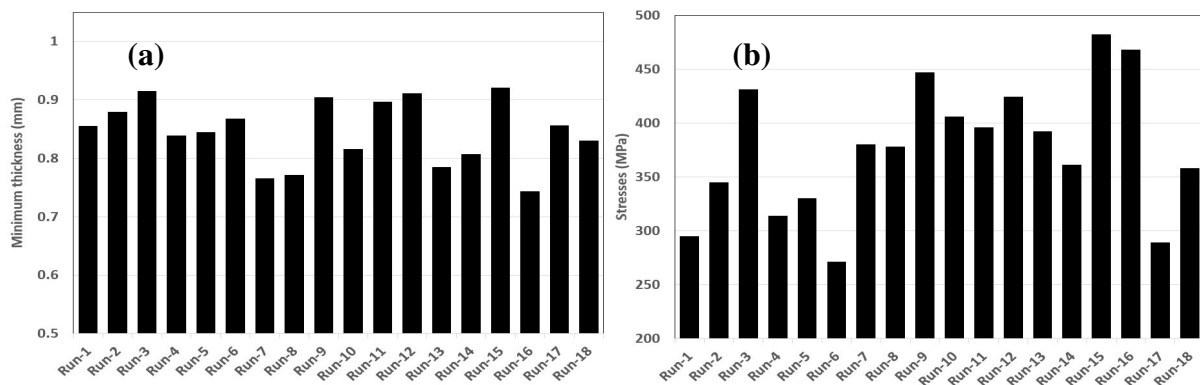


Figure 8: Comparison results of a) Minimum thickness b) Stresses of DOE runs.

## 4. Conclusions

The forming simulations of cylindrical cups are carried out, and the simulation results of thickness distribution and frequency response functions are validated with the experimental results. The individual process parameter changes, i.e. BHF, friction coefficient, blank thickness and misalignment of the press showed considerable changes in the thickness distribution, vibration responses. Besides, the sensitivity of these parameters to the radiated noise variability—rather difficult to quantify through physical experiments, due to difficulties in repeatability concerns of lightweight components—is demonstrated through equivalent radiated power (ERP) simulation results. Starting from these results, the authors carried out further analysis using a Design of Experiments (DOE) Taguchi approach to identify process parameters to optimize vibro-acoustic and crash performance. The authors propose future work to carry out the crash analysis to quantify the influence of the process parameters. Besides, the interaction of control factors is not considered in the present study, due to the nature DOE table. The authors consider the study of interactions as another interesting field of this research work.

## References

1. H. Tschaetsch, Deep drawing. In: Metal Forming Practise, Springer, Berlin, Heidelberg, 2006.
2. Hirsch, J. Aluminium in innovative light-weight car design. *Materials Transactions*, 52(5) (2011), 818–824.

3. S. Yossifon, K. Sweeney, M. Ahmetoglu, T. Altan, On the acceptable blank-holder force range in the deep-drawing process, *Journal of Materials Processing Technology* 33 (1992) 175–194.
4. Radioss, 10.0 version, *RADIOSS Theory Manual*, Altair Hyperworks software (2009).
5. F. Greco, E. Deckers, J. Stroobants, S. V. Poppel, K. Linck, W. Desmet, Finite element simulation of the dynamic behaviour of deep drawn components with accurate thickness description, *Finite Elements in Analysis and Design* 138 (2018) 12–20.
6. V. K. Balla, L. Coox, E. Deckers, F. Greco, B. Pluymers, W. Desmet, A study of vibro-acoustic behaviour variation of thin sheet metal components manufactured through deep drawing process, *Applied Acoustics* 153 (2019) 110–126.
7. M. Luegmair, H. Munch, Verbesserte equivalent radiated power (erp) -berechnung, in: *DAGA2015 – 41. Jahrestagung für Akustik*, 2015, pp. 834–836.
8. J. D. Reid, Towards the understanding of material property influence on automotive crash structures, *Thin-Walled Structures* 24 (1996) 285–313.
9. J. F. Siekirk, Process variable effects on sheet metal quality, *Journal of Applied Metalworking* 4 (1986) 262–269.
10. R. Sniekers, Friction in deep drawing, Ph.D. thesis, Department of Mechanical Engineering (1996).
11. J. Slavic, S. Bolka, V. Bratus, M. Boltezar, A novel laboratory blanking apparatus for the experimental identification of blanking parameters, *Journal of Materials Processing Technology* 214 (2014) 507–513.
12. H. Vairavan, A. Abdullah, Die-punch alignment and its effect on the thinning pattern in the square-shaped deep drawing of aluminium alloy, *Int. J. Materials and Product Technology*, 54 (2017) 147–164.
13. Minitab, 17.0 version, *Minitab Theory Manual*, Minitab 17 Statistical Software (2010).
14. G. Taguchi, *System of Experimental Design: Engineering Methods to Optimize Quality and Minimize Costs*, UNIPUB/Kraus International Publications - Two Volumes, 1987.
15. A. J. Curtis, N. G. Tinling, H. T. Abstein, *Selection and performance of vibration tests*, United States dept. of Defence, 1971.



---

# Systematic design of a generic Life Cycle Inventory model construct

Patrick Haun<sup>1,2,\*</sup>, Philipp Müller<sup>2</sup> and Marzia Traverso<sup>1</sup>

<sup>1</sup>*RWTH Institute of Sustainability in Civil Engineering, Mies-van-der-Rohe-Str. 1, 52074 Aachen, Germany*

<sup>2</sup>*Dr.-Ing. h.c. F. Porsche AG Body Advanced Engineering, Porschestraße 911, 71287 Weissach, Germany*

\*Corresponding author. Email: [patrick.haun@porsche.de](mailto:patrick.haun@porsche.de)

---

With increasing awareness on environmental issues, there is a necessity to make the environmental performance of a product assessable. The most valid and scientifically recognized methodology to achieve this target is the Life Cycle Assessment (LCA). In the automotive industry, the carbon footprint is the main focus when it comes to the environmental performance. A vehicle consists of many components. This makes an overall LCA of a vehicle a complex project, which cannot be done without the support of databases and software tools. One possibility to handle the complexity is the assignment of components to pre-defined Life Cycle Inventory (LCI) models based on secondary data, which can lead to inaccuracies if the assignment is not done by the most influencing component attributes. This paper tackles the conflict of inaccuracy and modelling effort of the automated LCAs with assigned LCI models. A methodology to build a construct of generic LCI models under constraints regarding accuracy and modelling effort is here presented and discussed throughout an example. For this approach, the relevant factors influencing the Global Warming Potential (GWP) of the component have to be identified. A distinction has to be made as to whether the influencing factors are described by discrete or continuously variable parameters. Considering the constraints on accuracy and modelling effort, the parameters have to be discretized and grouped to meaningful grid points. The number of grid points can be reduced when technical constraints are considered. The method is applied on the cradle-to-gate modelling of aluminium automotive components for the main technologies casting, deep-drawn sheets and extrusion. Due to a systematic construct of pre-defined LCI models, the assignment of LCI models is more flexible and the effect of the most relevant component attributes on the GWP are observable.

© 2021 by the authors. Published by the Resource Efficient Vehicles Conference.  
This is an open access article under the CC BY license (<http://creativecommons.org/licenses/by/4.0/>).

---

## 1. Introduction

The Life Cycle Assessment (LCA) is the most recognized methodology to quantify environmental impacts of a product along its life cycle [1] [2]. While the necessity of reducing environmental impacts of vehicles is widely realized by car manufacturers, vehicles are complex products that consists of thousands of components. Performing LCAs can in general be very time consuming due to collection of the required information [3] [4] and becomes more time consuming the more complex a product is [1] [5]. Therefore, performing LCAs on vehicles manually is not recommended for the sake of efficiency and consistency of the LCA [6]. To tackle the challenges of complexity, streamlining approaches are recommended and discussed in literature [3] [4] [7] [8] [9] [10] [11].



## 2. State of the art of streamlining LCAs

While streamlining LCAs in order to reduce the complexity of an LCA is a widely discussed and applied approach [7], the simplification by automation is a suitable approach to reduce manual workload by over 80 % [6]. By assigning the same material and process information to the same pre-defined LCI model, the consistency of the LCA is strengthened due to the automation approach [6]. However, the pre-defined models have to be flexible regarding parameters that have high relevance on the LCA results since oversimplifications lead to high uncertainties [1]. To avoid major uncertainties and keeping the modelling effort low BECCALI et. al., ZAH et. al. and FERRARI et. al. suggest to only consider few parameters as customizable in the LCI model since only few parameters have a significant influence on the LCA results [3] [10] [11].

To combine these approaches, the pre-defined LCI models must consider these most-influencing parameters (MIPs). In this, paper a systematic design of a LCI model construct is discussed, that considers MIPs and enables automated assessment during the LCI phase of an LCA. The LCI model construct is applied to automotive aluminium components with the production processes deep-drawn sheets, casting and extruded profiles.

## 3. Methodology

To combine the approaches from Section 2, the pre-defined LCI models must consider these most-influencing parameters (MIPs). In this, paper a systematic design of a cradle-to-gate LCI model construct is discussed, that considers MIPs and enables an automated assignment during the LCI phase of a LCA. Furthermore, only the Global Warming Potential (GWP) with the characterization model CML 2001- Jan 2016 is considered since the reduction of CO<sub>2</sub>e-emissions is a highly considered objective when it comes to environmental pledges of car manufacturers. [12] The considered database is the GaBi Professional database with the service pack 39 [13] [14]. For the production process of aluminium components the scrap rate (SR), the recycled content (RC) and the mix of alloy elements represented by the content of magnesium are identified as three MIPs.

Therefore, a generic LCI model was designed which is displayed as a flow chart in Fig. 1 and consists in the provision of semi-finished products and the production process of the component. The RC and the SR are defined by the auxiliary processes *recycled content* and *scrap rate*. For each of the production processes (deep-drawn sheets, casting and extruded profiles) a fitting process for *component production process* has to be selected. Since the production process was not identified as a MIP, no further variations of the process are included in this paper. The processes *virgin semi-finished product* and *semi-finished product process* are represented by datasets that are dependent from the respective production process. Since datasets for all virgin semi-finished products are available but not for recycled semi-finished products, the *virgin semi-finished product* is represented by a single dataset and the recycled semi-finished product by the *recycled aluminium ingot* and the respective *semi-finished product process*. For the process *recycled aluminium ingot* no variation of datasets is considered in this paper since the datasets for secondary aluminium contain virgin alloy elements and it is assumed, that the recycled scrap already contains alloy elements. Therefore, the dataset for *secondary aluminium ingot* is the dataset with the lowest alloy element content available. For the produced scrap, no credits for the GWP are given since the selected allocation methodology on recycling is the recycled content approach described in the GREENHOUSE GAS PROTOCOL PRODUCT STANDARD [15].

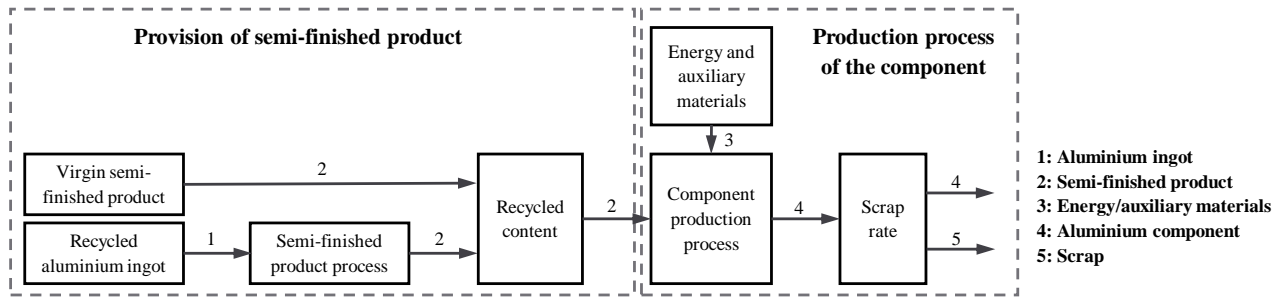


Figure 1: flowchart of the generic LCI model of aluminium components

### 3.1 Classification of the MIPs

It can be seen that the characteristics of the MIPs differ. While the magnesium content of the virgin semi-finished products is based on available datasets in the given database, the RC and the SR can be varied arbitrarily within the technical realizable boundaries. Therefore, the denotations discrete variable parameters (DVP) and continuously variable parameters (CVP) are introduced to distinguish between the parameter specific characteristics. CVPs are parameters that define the ratio of input and output flows of processes within a LCI model. An example is the parameter of the RC of a material because it defines the ratio between virgin and recycled material [16]. The parameter can be implemented in the LCI model with an auxiliary process that has no environmental impact by itself (see Fig. 1 *Recycled content*). DVPs can be varied by selecting different datasets from a given database. The variation of the parameter is therefore restricted by the available datasets.

Since the pre-defined LCI models offer discrete solutions, CVPs have to be discretized while DVPs have to be grouped to create meaningful grid points for the LCI model construct. The number of LCI models within the LCI model construct equals the product of the number of all the grid points of the MIPs. While the reduction of grid points leads to lower modelling effort, it can also lead to higher uncertainties. A grouping strategy for the virgin semi-finished products and a discretization of the RC and the SR or the considered aluminium components are discussed subsequently.

### 3.2 Grouping of the DVP

The virgin semi-finished products are dependent from the component production process. For deep-drawn sheets aluminium sheet processes, for casting components aluminium ingots processes and for extruded profile components extruded profile processes were considered. For the sake of simplicity, no variation of the location of the raw material and only European (EU-28) semi-finished products were considered. It has to be emphasized, that the location and especially the electricity mix during the aluminium production can have significant influence on the GWP and is not considered in this paper due to a lack of available datasets. For aluminium sheets 9 datasets, for aluminium ingots 4 datasets and for extruded profiles 10 datasets with information of the alloy element content were identified. By analysing the correlation between alloy elements and the GWP of 1 kg of the semi-finished product, high correlations between the magnesium content and the GWP for sheets (correlation coefficient: 0.98) and extruded profiles (correlation coefficient: 0.95) were calculated. Only for aluminium ingots the correlation coefficient was low with only 0.22. As mentioned in Section 3.1 it is reasonable to reduce the number of grid points for the MIPs. SUN et. al. published an approach to group material datasets based on their environmental impact with the constraint, that the relative standard deviation of the groups is less than 30 % [17]. A similar approach for the grouping of the datasets is applied in this paper. The datasets for semi-finished products are grouped based on the content of magnesium content and with the requirement of a relative standard deviation less than 5 % and with a maximum difference between the GWP of the datasets of 1 kg CO<sub>2</sub> eq. / kg semi-finished product. In contrast to the approach of SUN et. al., the LCI models do not use the average value of the group, but rather a representative dataset whose GWP is closest to the average GWP.

With the defined requirements the number of datasets were reduced significantly from 23 to 5. The 9 aluminium sheet datasets and the 10 extruded profile datasets were reduced each to 2 datasets for low magnesium content ( $< 2.8\%$  for sheets and  $< 3.0\%$  for extruded profiles) and high magnesium content ( $\geq 2.8\%$  for sheets and  $\geq 3.0\%$  for extruded profiles). The aluminium ingot datasets were grouped into one group with one representative dataset since the difference in GWP was low enough to group them with the defined requirements.

### 3.3 Discretizing of the CVPs

As stated in Section 3.1, CVPs describe a ratio of inputs and outputs of processes. Therefore, the influence of CVPs on the environmental impact of an output dependent from an environmental impact of an input can be described by  $I_{\text{output}} = f(\text{CVP}) * I_{\text{input}}$  with  $I$  describes the environmental impact (GWP in this case). After the function  $f(\text{CVP})$  is identified, the grid points for the CVP can be discretized. This is necessary to enable the automated assignment of components attributes to discretized parameters in pre-defined LCI models. Therefore, it has to be defined what kind of inaccuracy is acceptable for the assignment of the component's attributes represented by CVP to the discretized grid points represented by  $\text{CVP}_d$ . In this paper only a relative deviation of the assignment is discussed as in Eq. 1 although also the absolute difference of environmental impacts can be applied.

$$\delta \leq \left| \frac{f(\text{CVP})}{f(\text{CVP}_d)} - 1 \right|, \quad (1)$$

With

$\delta$ : relative deviation between  $f(\text{CVP})$  and  $f(\text{CVP}_d)$  [%]

With this context, a range limited by  $\text{CVP}_{d,\min}$  and  $\text{CVP}_{d,\max}$  can be calculated for a CVP that fulfils the requirement of Eq. 1 for the assignment to the respective  $\text{CVP}_d$ . Since a CVP shall have  $\text{CVP}_d$ s for the whole range of realizable values, a variety of  $\text{CVP}_d$ s have to exist to enable a gapless assignment. The requirement of the gapless assignment leads to the connections of  $\text{CVP}_d$ s as described in the equation  $\text{CVP}_{d,\max,i} = \text{CVP}_{d,\min,i+1}$ . For a given start value of  $\text{CVP}_{d,\min,1}$ ,  $\text{CVP}_{d,1}$  or  $\text{CVP}_{d,\max,1}$  all grid points for a CVP can be calculated in an iterative calculation as shown in Fig. 2. The necessary inputs for this calculations are the requirement of deviation  $\delta$ , a start value for  $\text{CVP}_{d,\min,1}$ ,  $\text{CVP}_{d,1}$  or  $\text{CVP}_{d,\max,1}$  and an end value for  $\text{CVP}_{\max}$  that defines the limit of the CVP. The discretization of the SR and the RC are discussed subsequently in Section 3.3.1 and 3.3.2.

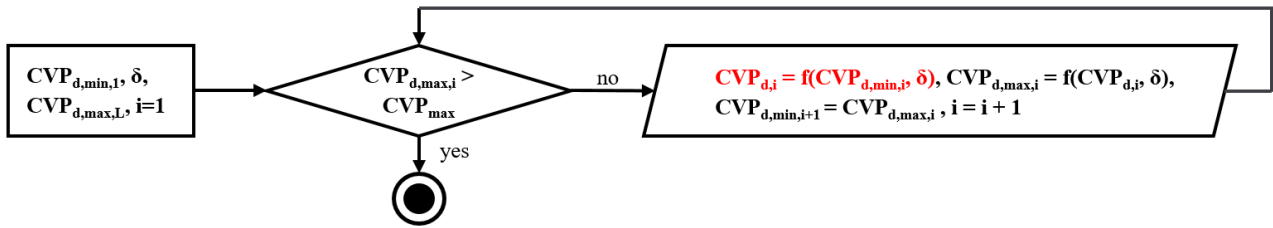


Figure 2: iterative calculation of the grid points  $\text{CVP}_{d,i}$  for a given start value of  $\text{CVP}_{d,\min,1}$

#### 3.3.1 Scrap rate

The SR is defined by the equation  $\text{SR} = (m_{\text{input}} - m_{\text{output}}) / m_{\text{input}}$  with  $m_{\text{input}}$  is the mass of input materials and  $m_{\text{output}}$  is the output mass. Thereby,  $m_{\text{input}} - m_{\text{output}}$  equals the mass of the produced scrap. In Fig. 1 it can be seen that the SR influences the quantity of all flows since it has an influence on the required amount of raw materials and the production process of the aluminium component. The context of Eq. (2) was deduced that defines  $f(\text{SR})$ .

$$I_{component} = f(SR) * (I_{mat.pro.} + I_{comp.prod.}) = \left( \frac{1}{1 - SR} \right) * (I_{mat.pro.} + I_{comp.prod.}) \quad (2)$$

With

$I_{component}$ : GWP of the component [kg CO<sub>2</sub> eq.]

$I_{mat.pro.}$ : GWP of the material provision [kg CO<sub>2</sub> eq.]

$I_{comp.prod.}$ : GWP of the component production [kg CO<sub>2</sub> eq.]

In Fig.3 the course of  $f(SR)$  is shown and it can be seen that the course of the function is not linear but increasing progressively with increasing SR. Since all relevant equations for the iterative calculation of Fig. 2 can be deduced, the input values have to be defined. For the relative deviation  $\delta$ , 10 % deviation were defined as acceptable. Since all aluminium components produce some scrap during their production, the first grid point  $SR_d$  shall not be 0 %. Therefore,  $SR_{d,min,1} = 0$  % is defined as the start value. The maximum SR considered in this paper is  $SR_{max} = 80$  %. Since high SRs make a significant difference in the GWP of the component, high SRs have to be considered. However, higher SRs are assumed to be uneconomical and unlikely for most components because more than five times of input material compared to output material is needed to produce the component. With the iterative calculation, 9 grid points  $SR_{d,1} - SR_{d,9}$  were calculated. They are shown in Table 1. It has to be emphasized, that the calculated grid points can be applied to every process, independent from the considered technology or impact category.

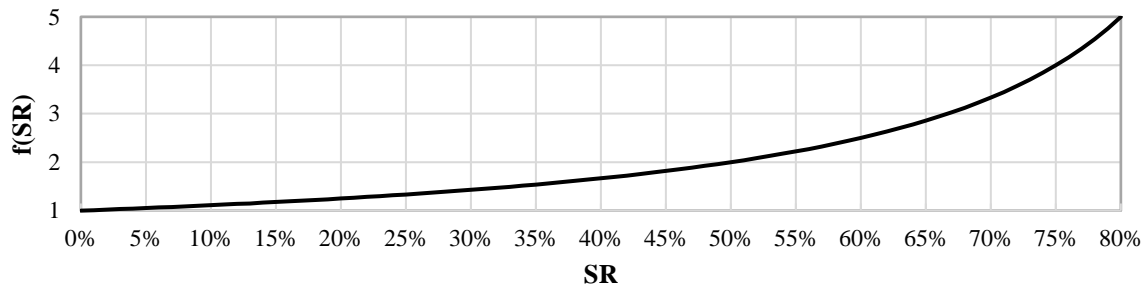


Fig. 3:  $f(SR)$  dependent from SR in the range of  $SR = 0 - 80$  %

Table 1: grid points  $SR_d$  with the respective range from  $SR_{d,min}$  to  $SR_{d,max}$

Number of grid points	$SR_d$ [%]	$SR_{d,min}$ [%]	$SR_{d,max}$ [%]
1	10.0	<b>0.0</b> <sup>1</sup>	18.2
2	26.4	18.2	33.1
3	39.8	33.1	45.2
4	50.7	45.2	55.2
5	59.7	55.2	63.3
6	67.0	63.3	70.0
7	73.0	70.0	75.5
8	77.9	75.5	79.9
9	81.9	79.9	83.6

<sup>1</sup> start value

### 3.3.2 Recycled content

The RC is a CVP but does not influence the GWP of the whole LCI model but only the material provision (see in Fig. 1). The GWP of the material provision can be calculated as shown in Eq. 3 and can be simplified with Eq. (4) to Eq. (5)

$$I_{mat.pro.} = RC * (I_{rec.ingot} + I_{s.-f.prod.process}) + (1 - RC) * I_{virgin s.-f.prod.} \quad (3)$$

$$\varepsilon = \frac{I_{rec.ingot} + I_{s.-f.prod.process}}{I_{virgin s.-f.prod.}} \quad (4)$$

$$I_{mat.pro.} = (RC * (\varepsilon - 1) + 1) * I_{virgin s.-f.prod.} = f(RC, \varepsilon) * I_{virgin s.-f.prod.} \quad (5)$$

With

- $I_{rec.ingot}$ : GWP of the recycled aluminium ingot [kg CO<sub>2</sub> eq.]  
 $I_{s.-f.prod.process}$ : GWP of the semi-finished product process [kg CO<sub>2</sub> eq.]  
 $I_{virgin s.-f.prod.}$ : GWP of the virgin semi-finished product [kg CO<sub>2</sub> eq.]

The course of  $f(RC, \varepsilon)$  is shown in Fig. 4. It can be seen that the RC has a linear influence on the GWP of the material provision but is also dependent on  $\varepsilon$ , which describes the proportion of the GWP of virgin and recycled semi-finished product. For the discretization however,  $\varepsilon$  is considered to be constant and the lowest realizable value within the datasets is selected ( $\varepsilon = 14.9\%$ ). This is because the absolute slope of  $f(RC, \varepsilon)$  is higher for low values of  $\varepsilon$  and more grid points are required to fulfil the requirement of Eq. 1 making it a worst case regarding the number of grid points. With the constant value for  $\varepsilon$ , the function  $f(RC)$  is only dependent from the parameter RC and the grid points  $RC_d$  can be calculated with the iterative calculation. For the relative deviation  $\delta$ , the value  $\delta = 10\%$  was set as for the SR. For the case that the RC is unknown,  $RC = 0\%$  is a worst-case assumption and potential default value. Therefore, the start value of  $RC_{d,1} = 0\%$  is set to guarantee the most accurate assignment of this worst case. Since aluminium is a highly recyclable metal, RCs of up to 100% are considered to be possible ( $RC_{max} = 100\%$ ). With the selected start values, 10 grid points were calculated with the iterative calculation from Fig. 2 that are listed in Table 2.

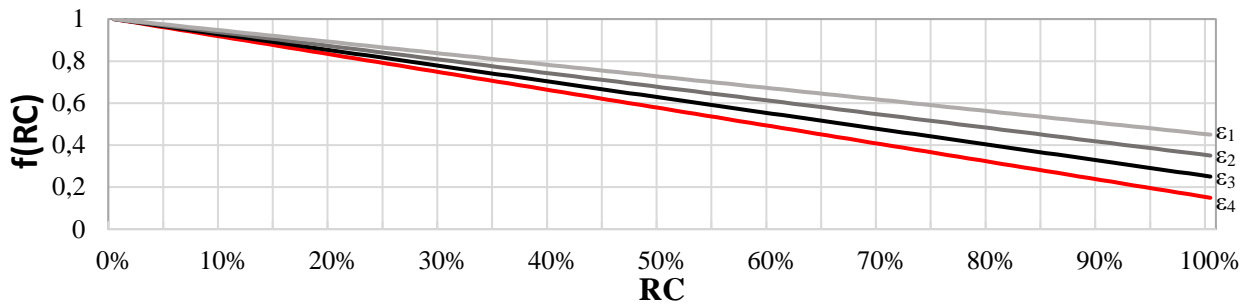


Figure 4:  $f(RC, \varepsilon)$  dependent from RC for different values for  $\varepsilon$

Table 2: grid points  $RC_d$  with the respective range from  $RC_{d,min}$  to  $RC_{d,max}$

Number of grid points	$RC_d$ [%]	$RC_{d,min}$ [%]	$RC_{d,max}$ [%]
1	<b>0.0</b> <sup>1</sup>	-11.8	11.8
2	21.4	11.8	31.0
3	38.9	31.0	46.7
4	53.2	46.7	59.6
5	64.9	59.6	70.1
6	74.5	70.1	78.8
7	82.3	78.8	85.8
8	88.7	85.8	91.6
9	94.0	91.6	96.3
10	98.2	96.3	100.2

<sup>1</sup> start value

### 3.4 Building the LCI model construct

After the DVPs are grouped and the DVPs are discretized to meaningful grid points, the grid points can be applied to parametrize the generic LCI model from Fig. 1. The solution area of this LCI model construct consists N models, while N is the product of the number of the grid points of the considered MIPs. Therefore, 180 models each for deep-drawn sheet components and extruded profile components (number of grid points: 2 x magnesium content, 9 x SR, 10 x RC) and 90 models for casting components (number of grid points: 1 x magnesium content, 9 x SR, 10 x RC) making it 450 models. To lower the modelling effort, further assumptions can be applied to reduce the number of grid points. For an example it is assumed that the SR of casting and extruded profile components is not higher than 33 %, and the RC of wrought alloys is less than 45 %. This reduces the number of grid points for the SR of casting and extruded profile components to 2 and the number of grid points for the RC for deep-drawn sheet and extruded profile components to 3. As a consequence, the number of LCI models were reduced from 450 to 86 which is a manageable modelling effort if the generic LCI model from Fig. 1 is used as a base line.

## 4. Discussion and Conclusion

As shown in Section 2, approaches for automated LCIs exist to keep the effort on performing LCAs on complex products manageable. While efficiency and consistency are benefits of automated LCIs, there is no guarantee that the influence of relevant parameters are observable within an LCA. This is because relevant attributes of a product are not necessarily considered in the assignment to the pre-defined models in a LCI due to inflexible assignments. As by the authors observed, there are no existing approaches in literature to systematically design an LCI model construct to make the assignment of pre-defined LCI models more flexible in an automated LCI.

In this paper, a possible LCI model construct for deep-drawn sheet, casting, and extruded profile aluminium components is presented. By grouping DVPs and discretizing CVPs with an iterative calculation, grid points for the selected parameters were identified that result in 450 LCI models. With further assumptions, the number of LCI models were reduced to 86. The aluminium component attributes magnesium share, SR, and RC can now be assigned to grid points in the LCI model construct as shown in Fig. 5. The influence of these parameters is now observable in an automated LCI with a defined inaccuracy. Since overall vehicle LCAs with automated LCIs are done with information provided by suppliers [6], the LCA can only be done at the later stage of the development stage. Many authors however, recommend to make an assessment in the early stage of development to elaborate measures to reduce the environmental impact of a product [3] [9] [18] [19]. Because the LCAs in the early stage of development are not necessarily limited by automation, the influence of all relevant parameters can be observed, while an overall vehicle LCA with automated LCA may fail to make these parameters customizable. With the systematic design of the LCI model construct, the influence of relevant parameters is also observable in an automated LCI which leads to a comparability between early and later stage LCA.

It has to be emphasized that the equations and results may vary with different assumptions regarding the considered product, the selection of the MIPs, the design of the generic LCI model, the deviation of the assignment and the allocation methodology on recycling. However, the methodology is customizable to other assumptions and therefore gives an idea of a procedure to systematically design LCI models in an automated LCI.

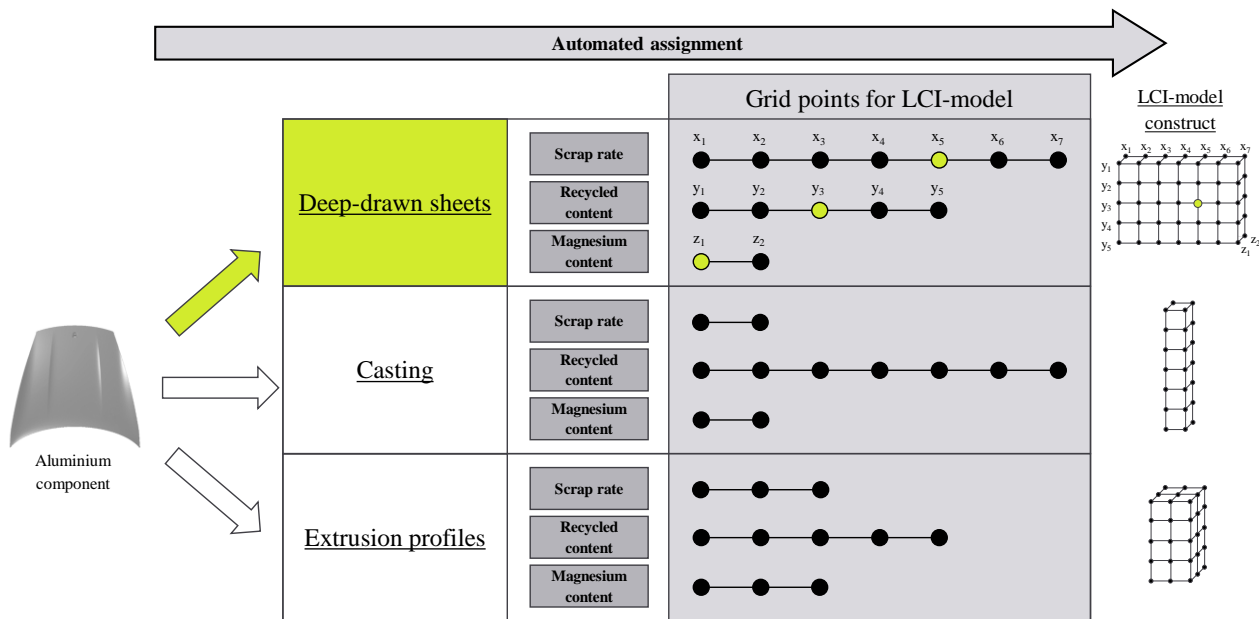


Figure 5: Automated assignment of an aluminium component to a pre-defined LCI model in a LCI model construct. The number of grid points displayed is arbitrary and does not represent the elaborated grid points of Section 3.

## References

1. D. Millet, L. Bistagnino, C. Lanzavecchia, R. Camous, T. Poldma, Does the potential of the use of LCA match the design team needs?, *Journal of Cleaner Production* 15 (4), 2007, pp. 335-346.
2. M. Delogu, S. Meltese, F. Del Pero, L. Zanchi, M. Pierini, A. Bonoli, Challenges for modelling and integrating environmental performance in concept design, *International Journal of Sustainable Engineering* 11 (2), 2018, pp. 135-148.
3. A. Ferrari, L. Volpi, D. Settembre-Blundo, F. García-Muiña, Dynamic life cycle assessment (LCA) integrating life cycle inventory (LCI) and Enterprise resource planning (ERP) in industry 4.0 environment, *Journal of Cleaner Production* 286, 2021.
4. J. Pascual-González, C. Pozo, G. Guillén-Gosálbez, L. Jiménez-Esteller, Combined use of MILP and multi-linear regression to simplify LCA studies, *Computers & Chemical Engineering* 82, 2015, pp. 34-43.
5. M. Arena, G. Azzone, A. Conte, A streamlined LCA framework to support early decision making in vehicle development, *Journal of Cleaner Production* 41, 2013, pp. 105-113.
6. C. Koffler, S. Krinke, L. Schebek, J. Buchgeister, Volkswagen slimLCI: a procedure for streamlined inventory modelling within life cycle assessment of vehicles, *Int. J. Vehicle Design* 46 (2), 2008, pp. 172-188.
7. S. Beemsterboer, H. Baumann, H. Wallbaum, Ways to get work done: a review and systematisation of simplification practices in the LCA literature, *The International Journal of Life Cycle Assessment* 25, 2020, pp. 2154-2168.
8. Society of Environmental Toxicology and Chemistry (SETAC), Streamlined Life-Cycle Assessment: A Final Report from the SETAC North America Streamlined LCA Workgroup, 1999, pp. 15-30
9. H. Kaebernick, M. Sun, S. Kara, Simplified Life Cycle Assessment for the Early Design Stages of Industrial Products, *CIRP Annals* 52, 2003, pp. 25-28.
10. R. Zah, M. Faist, J. Reinhard, D. Birchmeier, Standardized and simplified life-cycle assessment (LCA) as a driver for more sustainable biofuels, *Journal of Cleaner Production* 17, 2009, pp. 102-105.
11. M. Beccali, M. Cellura, S. Longo, D. Mugnier, A simplified LCA tool for solar heating and cooling systems, SHC 2015, *International Conference on Solar Heating and Cooling for Buildings and Industry*, 2016.
12. Science Based Targets initiative (SBTi), Companies taking action, Retrieved from <https://sciencebasedtargets.org/companies-taking-action?sector=Automobiles%20and%20Components#table>, 2021

13. Sphera, GaBi ts Version History, Retrieved from <http://www.gabi-software.com/deutsch/my-gabi/gabi-version-history/gabi-ts-version-history/>, 2021
14. Sphera, GaBi Data – Important notes, Correction of EU-28: Aluminium sheet (AlMg4.5), wrong Mg content, <http://www.gabi-software.com/international/support/gabi-data-important-notes/>, 2021
15. P. Bhatia, C. Cummis, A. Brown, L. Draucker, D. Rich, H. Lahd, Greenhouse Gas Protocol – Product Life Cycle Accounting and Reporting Standard, World Resource Institute, World Business Council for Sustainable Development, 2011, pp. 70-74.
16. International Organization for Standardization (ISO), ISO 14021 – Environmental labels and declarations – Self-declared environmental claims (Type II environmental labelling), 2016, pp. 15-17.
17. M. Sun, C. J. Rydh, H. Kaebernick, Material Grouping for Simplified Product Life Cycle Assessment, The Journal of Sustainable Product Design 3 (1), 2003, pp. 45-58.
18. G. I. Broman, K. H. Robèrt, A framework for strategic sustainable development, Journal of Cleaner Production 140, 2017, pp. 17-31.
19. D. Jasiński, J. Meredith, K. Kirwan, A comprehensive framework for automotive sustainability assessment, Journal of Cleaner Production 135, 2016, pp. 1034-1044.



## Day 3: P11 – Early Design II

Session P11 – Early Design II, Wednesday 16 June

---

**Session chairs:** Josef-Peter Schögggl and Tracy Bhamra

- 11:50-12:00    **P11.A**  
*Concept of a digital product passport for an electric vehicle battery*  
Katharina Berger, Josef-Peter Schögggl and Rupert J. Baumgartner
- 12:00-12:10    **P11.B**  
*A generic approach to capitalize manufacturing experience in design and optimization*  
Philip Eyckens, Frank Naets, Elke Deckers, Eveline Rosseel, Hendrik Schuette, Ioanna Koutla, Reginald Diltoer, Carlos Lopez and Pierre Duysinx
- 12:10-12:20    **P11.C**  
*Validation of a novel XiL setup for frontloaded testing of an electric vehicle powertrain*  
Bart Forrier, Thomas D'hondt, Leonardo Cecconi and Mathieu Sarrazin
- 12:20-12:30    *Questions and Answers*
-

---

# Concept of a digital product passport for an electric vehicle battery

Katharina Berger<sup>1,\*</sup>, Josef-Peter Schögggl<sup>1</sup> and Rupert J. Baumgartner<sup>1</sup>

<sup>1</sup>*Christian Doppler Laboratory for Sustainable Product Management enabling a Circular Economy, Institute of Systems Sciences, Innovation and Sustainability Research, University of Graz, Merangasse 18/I, 8010 Graz, Austria*

\*Corresponding author. Email: [katharina.berger@uni-graz.at](mailto:katharina.berger@uni-graz.at)

---

The concept of circular economy (CE) has recently gained momentum due to being perceived as a potential facilitator of sustainable development. In the context of electric vehicles, it is argued that the value chain (VC) of an electric vehicle battery (EVB) would benefit from transitioning from a linear to a circular one due to the potential of the latter one to reduce environmental pressures and enhance the security of supply of raw materials. However, VC loop-closing pathways may not necessarily contribute to enhanced VC sustainability performance. Information technologies such as the digital twin (DT) could be used to support VC stakeholders in identifying sustainable loop-closing pathways. The DT technology has recently received attention because it is perceived as a potential technology for driving so-called “digital product passport”. The idea of such applications is currently being discussed due to their potential to function as unique identifiers of their corresponding physical counterparts by containing specific product/material-related data and gathering real-time data over the entire life cycle of a product. Such an application could support value chain stakeholders in their efforts to manage the sustainable circularity on the product level. In this context, this study provides a preliminary concept of the information model of an EVB’s digital product passport. This information model details data types, sources, and requirements for different use cases of sustainable and circular battery management. Conducting a dynamic life cycle assessment of an EVB or deciding on an EVB’s potential second life serve as examples of such use cases. The findings stem from conducting a systematic literature review, as well as a preliminary model validation by three industry experts. In summary, the preliminary conceptual information model presented shall provide a first building block for a comprehensive EVB digital product passport concept.

© 2021 by the authors. Published by the Resource Efficient Vehicles Conference.  
This is an open access article under the CC BY license (<http://creativecommons.org/licenses/by/4.0/>).

## 1. Introduction

The European Commission's recently presented proposal for a new regulation on batteries and waste batteries is demanding the transition from traditional linear to circular battery value chains [1] due to the latter one offering potential benefits (e.g., reduction of environmental stresses, security of critical raw material supply) [2]. However, a more circular value chain does not automatically equate to a more sustainable one [cf. 3]. As a result, possible positive and negative effects of more circular value chains with respect to their sustainability performance require investigation [cf. 3]. An assessment of the sustainability and circularity performance on product level, however, requires high-quality data and adequate assessment tools [4]. In particular, the former one is currently lacking due to, for example, information losses along product value chains, or lacking access to needed data, such as energy, emissions and waste-related data [cf. 4]. Those challenges could be taken on by digitalization and its respective information technologies, such as the Digital Twin [cf. 5].

A Digital Twin (DT) is initially described as a virtual real-time representation of a physical product that is able to gather, contain and monitor real-time value chain and life cycle data of its physical counterpart [5]. In general, a DT is in need of three components that have to work seamlessly together; one of them being a (pre-defined) information model that abstracts specifications of the respective physical object [6]. Due to its prior described properties, DT technology shows promising potential to be employed in various fields, such as supply chain management and product life cycle management [7]. In addition, DT has received attention recently due to it being perceived as potential underlying technology of *digital product passports* [8], which in turn are perceived as tools to support the transition from a linear to a sustainable circular economy [1]. In general, digital product passports are described as a product's unique identifier due to containing respective value chain and life cycle data [8], thus being further able to function as *digital product declarations*.

The idea of digital product passports (DPP) has also caught the attention of policymakers, such as the European Commission, who is explicitly demanding the implementation of digital battery passports (DBP) in their proposal for a new regulation on batteries and waste batteries [1]. As a result, DBPs, in particular for electric vehicle traction batteries (EVB), are currently discussed and pursued by initiatives and practitioners [e.g. 9]. However, there is currently little scientific coverage with respect to DBPs in the context of sustainable and circular product management. Consequently, there is a lack of understanding with respect to data that a DBP has to provide, to support value chain stakeholders, or rather its users, in their sustainable battery management efforts. To address this currently existing research gap, this work pursues the following question: *What kind of data should a digital battery passport's underlying information model contain to support its users in their sustainable battery management efforts?*

The paper at hand provides a preliminary conceptual information model of a DT-driven digital battery passport, or digital product declaration of an EVB in the context of sustainable product management. The term *sustainable product management* is defined as product management, which aims to minimize respective negative social and environmental impacts, whilst pursuing value chain loop-closing pathways to increase a product's circularity performance. The presented concept in this work further provides the foundation of a comprehensive information model that may support value chain stakeholders in respective decision-making situations.

## 2. Methods

The preliminary conceptual information model was developed by conducting a systematic literature review following the PRISMA guidelines [10], as well as seeking preliminary validation by consulting three industry experts from an automotive engineering centre.

The literature review was conducted to (1) identify potential users of a DBP, (2) derive potential use cases and respective decision-making situations, as well as (3) identify respective data needs and requirements. Pursuing these aspects allowed to gather information, which served as building blocks of the information model presented in this work. To identify suitable references, the database Scopus

and search engines (Google Scholar, Ecosia) were employed. With respect to selection criteria, publications in the English and German language, published between 2010-2021, were considered. The time horizon was chosen due to electric vehicles entering the mass market in 2009 [11]. Publications were not excluded based on their geographical context due to the global character of battery value chains [12]. Furthermore, publications in form of peer-reviewed journal articles (e.g., research articles, review papers, conceptual papers), as well as grey literature (e.g., pre-prints, reports, conference contributions, product specification sheets) were considered. Employed keywords are depicted in Table 1.

Table 1: (exemplary) keywords used for the systematic literature review

(exemplary) keywords	“traction battery” AND “value chain” “traction battery” AND “supply chain” “lithium battery” AND “value chain”	“lithium battery” AND “supply chain” “lithium battery” AND “second life” “battery” AND “value chain” “battery” AND “supply chain”	“digital battery passport” “battery” AND “state of health assessment” “battery” AND “state of health indicator”
-------------------------	---	--	--

The initial search, which was conducted between October 2020 and January 2021, led to an initial sample of 1140 peer-reviewed articles and 50 references in the form of grey literature. The initial sample was subjected to a screening process of titles and abstracts. Publications were excluded when they did not have any relation to the electric vehicle battery value or supply chain, the electric vehicle battery life cycle, battery second life, battery health, digital product or battery passports, or potential use cases and respective data needs. The remaining publications were subjected to a full-text screening. During the full-text screening stage, additional references were identified by following the snowballing principle. The overall process resulted in identifying 129 references that were used for developing the conceptual information model presented in this work. The prior described literature review process is depicted in Figure 1. After conducting the literature review, respectively derived information was used to develop the preliminary conceptual information model by pursuing a bottom-up approach. Thus, aspects considered relevant by analysed literature for supporting decision-making situations in the context of sustainable product management were compiled. Data relevant for conducting life cycle assessments, purchasing decisions, maintenance operations, or end-of-first-life treatments serve as examples of such decision-making situations. Gathered aspects were furthermore grouped into main and sub-categories to structure the information model meaningfully.

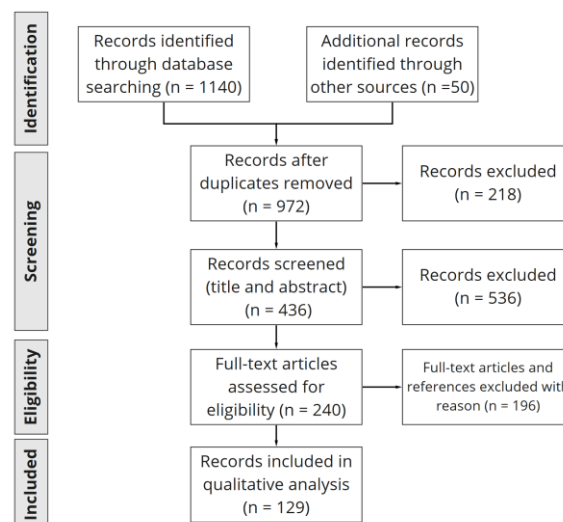


Figure 1: Literature review process following the PRISMA guidelines [10]

In addition, a preliminary model validation was provided by three industry experts (one project manager, one head of global R&D, one specialist of technical legislation). With respect to expert selection criteria, industry experts were considered who had affiliations to EVB-related industries and a minimum of five years of experience in the aforementioned industries. The three industry experts, who provided the preliminary model validation, fulfilled these criteria because of their affiliation to an automotive engineering centre that concerns itself with the development of (electric) powertrain systems, as well as experience of five and more years in the industry. The experts were recruited from the network of company partners in the authors' research project.

### 3. Preliminary conceptual information model

The developed preliminary conceptual information model comprises four main information categories: (1) *Battery*, (2) *Sustainability and circularity*, (3) *Diagnostics, maintenance, and performance*, and (4) *Value chain actor*. These four categories, illustrated in Figure 2, further constitute underlying information layers containing more granulated qualitative and quantitative data that allows potential users to obtain more in-depth information. The information model includes a total of five information layers, of which Lv. 1 and Lv. 2 are illustrated in Figure 2. The information layers, however, do not indicate the degree of data confidentiality. A description of the information categories' content and function, as well as development, is provided in the proceeding sub-sections. With respect to the model development, three industry experts reviewed each information category (details see below).

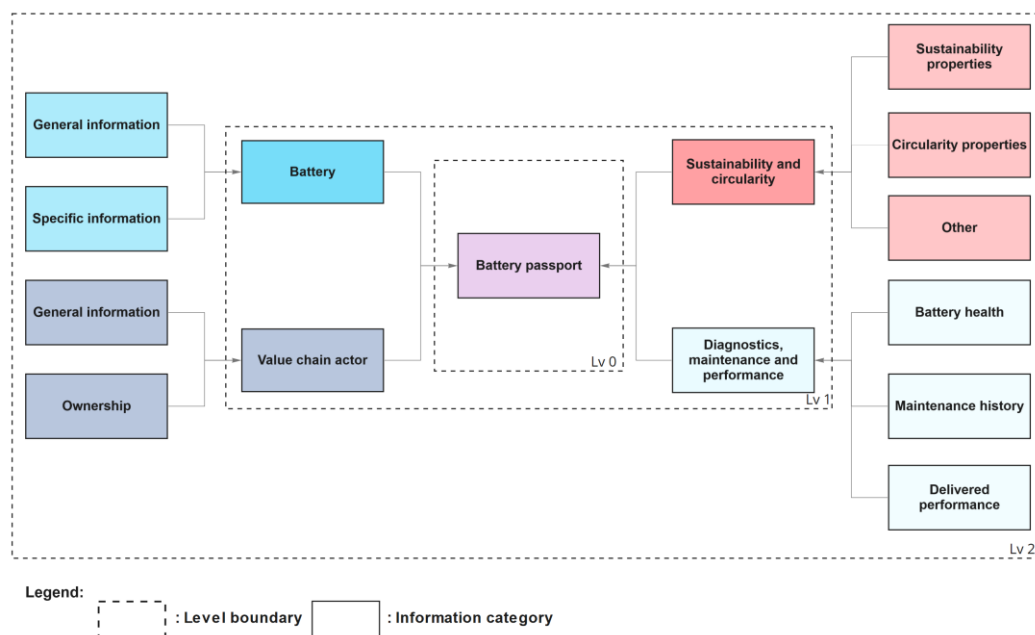


Figure 2: Preliminary conceptual information model of a digital battery passport

#### 3.1 Battery

When pursuing sustainable product management efforts contextualization is needed, meaning that the product of interest needs to be clearly identified in order to be managed. Therefore, the main information category *Battery* provides information that can be used to identify the EVB at hand. Information presented in this category is further divided into two sub-categories: *general product information* and *specific product information* (cf. Fig. 2). The sub-category *general product information* contains information on the battery type (e.g., EVB), battery chemistry, battery identifier (e.g., serial number, batch number), and manufacturing-related information (e.g., name of battery pack manufacturer, location of production site). The sub-category *specific product information* provides information on battery performance (e.g., driving range, lifespan, charging times, energy

consumption); battery structure specifications (e.g., dimensions, number modules, number of cells, employed assembly processes) with respect to pack, module and cell level; electro and electrochemical engineering-related specifications (e.g., energy density, power density, energy content) with respect to cell, module and pack level; material-related properties (e.g., type, function, production-related properties).

The content of the main information category *Battery* was developed by consulting publications by policymakers, such as the European Commission, who is demanding the disclosure of a certain degree of product-related information [1]. Also, publications by CE-related initiatives [9], and material passport-related research [8,13] provided input for the concept development. In addition, literature with a focus on EVBs and their performance [14–16], structure [17–19], as well as DT technology in the context of waste electronic and electrical equipment (WEEE) [20] was consulted.

### 3.2 Sustainability and circularity

In case of pursuing the improvement of the sustainability and/or circularity performance of a product, value chain stakeholders require knowledge of the status quo of respective performances. This information may support, for example, an OEM in defining new product sustainability and circularity targets, as well as identifying potential levers that may be pulled to improve respective performances of an EVB. Thus, the main category *Sustainability and circularity* contains information related to a battery's sustainability and circularity performance. Information presented in this category can be further distinguished into three sub-categories: *sustainability properties*, *circularity properties*, and *other* (cf. Fig. 2). The sub-category *sustainability properties* contains data that allows to obtain information on the environmental and social impact of the EVB of interest. Thus, this sub-category contains respective indicators, as well as information on corresponding impact categories, indicator calculation methods, used inventory data in social and environmental life cycle assessments, as well as applied standards and impact assessment methods. In addition, this sub-category further contains information with respect to employed material types (e.g., hazardous, critical). The sub-category *circularity properties* contains information on the EVBs circularity performance. This sub-category follows the same logic in terms of structure and content as the prior described one. The sub-category *other* contains underlying data that allows to derive information with respect to battery module and pack assembly processes (e.g., welding, gluing, wiring), product designs (e.g., design for recycling), as well as disassembly instructions.

The content of the main information category *Sustainability and circularity* was developed by consulting publications by policymakers, such as the European Commission, who is setting sustainability and circularity performance-related targets of EVBs [1]; that describe already existing material passports (e.g., in the building sector) [8,13], or that illustrate the use of DT technology in the context of WEEE [20] and sustainable supply chain management [21,22]. In addition, literature on the technical specifications and structure of EVBs [19] served as inspiration.

### 3.3 Diagnostics, maintenance, and performance

To identify potential value chain loop-closing pathways other than recycling, respective value chain stakeholders (e.g., waste battery collectors) require information on an EVB's health to identify EVB packs or modules that qualify for loop-closing pathways, such as second life pathways [1,9,19]. Therefore, the main-information category *Diagnostics, maintenance, and performance* contains data that allows deriving information which can be further distinguished into three sub-categories: *battery health*, *maintenance history*, and *delivered performance* (cf. Fig. 2). The sub-category *battery health* contains data that provides information on battery health-related indicators (e.g., state-of-health, state-of-charge, depth-of-discharge, rest of useful life). The sub-category *maintenance history* contains data that allows accessing information on maintenance and repair work that has been done, triggers of carried out maintenance and repair work, as well as the involved party that carried out respective work. The sub-category *delivered performance* allows to obtain quick information on the

so far delivered performance of the EVB at hand (e.g., charging/discharging cycles, provided range, provided operation time).

This information category was developed by consulting publications by policymakers, such as the European Commission [1], and CE-related initiatives, such as the Circular Economy Initiative Deutschland [9]. Both preceding references emphasise the importance of battery health-related data for remanufacturing and repurposing-related stakeholders due to respective parameters being not allowed to fall below a certain threshold when remanufacturing or repurposing efforts are pursued [1,9]. In addition, literature related to battery diagnostics and battery second life [23–25], as well as recycling [19] was consulted for model development purposes.

### 3.4 Value chain actor

To enhance and ensure transparency along a product's entire value chain, information on involved actors and their respective roles and responsibilities need to be provided. This, in turn, may also enhance trust between value chain stakeholders, as well as support respective decision-making situation. A potential EV user, for example, might be able to identify EVBs that have shorter supply chains, which in turn might support an EV user's buying decision. Therefore, the main-information category *Value chain actor* provides information that can be further distinguished into two sub-categories: *general actor-related information* and *ownership-related information* (cf. Fig. 2). The sub-category *general actor information* contains data that allows to derive information on actors that concern themselves with the EVB during its entire life cycle, regardless to which extent (e.g., supplier of active materials, manufacturer of cells, recycler). Such information is, for example, the name of involved actors (e.g., company name), actor type and function (e.g., supplier of active materials), geographical location of the value-activity (e.g., production site of cells), and actor identifier (e.g., trade registration number). The sub-category *ownership-related information* provides data that allows to derive chain-of-custody-related information. Thus, this sub-category provides information that allows to identify value chain actors' responsibility related to the EVB. This does not only include responsibility of the physical product, respective components, or related services (e.g., maintenance), but also responsibility of sustainability- and circularity-related performances.

The content of this information category was developed by consulting publications provided by policymakers, such as the European Commission who emphasises the importance of extended producer responsibility to enhance transparency along battery supply and value chains [1]. In addition, literature with focus on DT [5], as well as digitalization and sustainable supply chain management [21,22] was consulted.

## 4. Limitations

As one limitation, the process of conducting the systematic literature review can be named because potential references might have been excluded during the title and abstract screening process. Furthermore, the presented conceptual information model has been developed by assuming a “perfect world” in terms of data availability and accessibility. Even though the concept has been subjected to a preliminary validation by three industry experts, a full validation by a representative sample consisting of value chain stakeholders, who are likely to take on the role of potential data providers and DBP users, is still lacking. Thus, the concept outlined in this paper lacks a view through the lens of practical applicability.

## 5. Discussion

The conceptual information model contains information based on qualitative, as well as quantitative data. Next to sustainability and circularity performance-related information, the systematic literature review and the preliminary model validation by industry experts revealed that

additional information, such as product- [8,13], battery health- [1,9,11] and value chain actor-related information [1,21,22] is required to support value chain stakeholders in their sustainable product management efforts. These additional categories reflect the need for a having a detailed digital representation of the EVB to be managed, as only such a representation can contextualize sustainability and circularity performance-related information. In addition, further information is needed to identify and pursue potential value chain loop-closing pathways (e.g., battery second life, adequate recycling treatment) [9,19], as well as to further enhance the value chain's transparency [21,22]. Thus, an information model with sustainability and circularity performance-related information only, might be a less useful tool to potential users. The conducted systematic literature review further allowed to identify different potential use cases for a DBP, such as decision-making support in early product design stages [cf. 8,13], for buying decisions [cf. 21,22], and end-of-first-life treatment options [cf. 8,19]. These use cases will guide further empirical and prescriptive research. With respect to potential data sources for the presented information model, value chain stakeholders are likely to take on this role. However, the question with respect to stakeholders' willingness to contribute needed data remains open. In addition, some information outlined in the developed model might not be available at all (e.g., due to data losses along the value chain) or might be available but not accessible (e.g., due to confidentiality concerns) [cf. 21,22]. In addition, further barriers for DBP implementation perceived by value chain stakeholders need to be identified to develop solutions to overcome them.

## 6. Conclusion and further outlook

In this paper, a preliminary conceptual information model for a DBP of an EVB in the context of sustainable product management was presented. The current version of the model comprises four main information categories, which further comprise underlying sub-categories to provide a first meaningful structure of information. Due to the current lack of validation, next research steps will comprise the conduct of focus group workshops, as well as interviews and surveys with industry experts (e.g., from R&D, battery supply chain, production, and end-of life) to develop a fully validated conceptual information model. The validation process will aim to identify and validate (1) data needs and requirements, (2) availability of critical data, (3) use cases, and (4) implementation barriers for a DBP. The fully validated conceptual information model will be used as the foundation for developing a comprehensive information model.

## References

- [1] European Commission, Proposal for a Regulation of the European Parliament and of the Council concerning batteries and waste batteries, repealing Directive 2006/66/EC and amending Regulation (EU) No 2019/1020, (2020), <https://eur-lex.europa.eu/legal-content/EN/TXT/?uri=CELEX%3A52020PC0798> (accessed March 26, 2021).
- [2] A. Buruzs, A. Torma, A Review on the Outlook of the Circular Economy in the Automotive Industry, *International Journal of Environmental and Ecological Engineering* 11, (2017), pp. 576–580.
- [3] J.-P. Schöggel, L. Stumpf, R.-J. Baumgartner, The narrative of sustainability and circular economy - A longitudinal review of two decades of research, *Resources, Conservation and Recycling* 163, (2020), pp. 1–22.
- [4] M. Saidani, B. Yannou, Y. Leroy, F. Cluzel, A. Kendall, A taxonomy of circular economy indicators, *Journal of Cleaner Production* 207, (2019), pp. 542–559.
- [5] F. Tao, J. Cheng, Q. Qi, M. Zhang, H. Zhang, F. Sui, Digital twin-driven product design, manufacturing and service with big data, *International Journal of Advanced Manufacturing Technology* 94, (2018), pp. 3563–3576.
- [6] Y. Lu, C. Liu, K. Wang, H. Huang, X. Xu, Digital Twin-driven smart manufacturing: Connotation, reference model, applications and research issues, *Robotics and Computer-Integrated Manufacturing* 61, (2020), pp. 1–14.
- [7] D. Jones, C. Snider, A. Nassehi, J. Yon, B. Hicks, Characterising the Digital Twin: A systematic literature review, *CIRP Journal of Manufacturing Science and Technology* 29, (2020), pp. 36–52.



- [8] M. Heinrich, W. Lang, Materials Passports - Best Practice, (2019), [https://www.bamb2020.eu/wp-content/uploads/2019/02/BAMB\\_MaterialsPassports\\_BestPractice.pdf](https://www.bamb2020.eu/wp-content/uploads/2019/02/BAMB_MaterialsPassports_BestPractice.pdf) (accessed March 26, 2021).
- [9] Circular Economy Initiative Deutschland, Ressourcen- schonende Batteriekreisläufe (2020), <https://www.acatech.de/publikation/ressourcenschonende-batteriekreislaeufe> (accessed March 26, 2021).
- [10] D. Moher, A. Liberati, J. Tetzlaff, D. G. Altman, Preferred reporting items for systematic reviews and meta-analyses: The PRISMA statement, *BMJ* 339, (2009), pp. 332–336.
- [11] R. Reinhardt, B. A. Garcia, L. C. Casals, S. G. Domingo, Critical evaluation of European Union legislation on the second use of degraded traction batteries, *International Conference on the European Energy Market*, 2016.
- [12] A. Mayyas, D. Steward, M. Mann, The case for recycling: Overview and challenges in the material supply chain for automotive li-ion batteries, *Sustainable Materials and Technologies* 19, (2019), pp. 1–13.
- [13] M. Honic, I. Kovacic, G. Sibenik, H. Rechberger, Data- and stakeholder management framework for the implementation of BIM-based Material Passports, *Journal of Building Engineering* 23, (2019), pp. 341–350.
- [14] D. Stampatori, P. P. Raimondi, M. Noussan, Li-ion batteries: A review of a key technology for transport decarbonization, *Energies* 13, (2020), pp. 1–23.
- [15] M. Philippot, G. Alvarez, E. Ayerbe, J. Mierlo Van, Eco-Efficiency of a Lithium-Ion Battery for Electric Vehicles : Influence of Manufacturing Country and Commodity Prices on GHG Emissions and Costs, *Batteries* 5 (1), (2019), pp. 1-23.
- [16] W. Chen, J. Liang, Z. Yang, G. Li, A review of lithium-ion battery for electric vehicle applications and beyond. *Energy Procedia* 158, (2019), pp. 4363–4368.
- [17] D. Coffin, J. Horowitz, The Supply Chain for Electric Vehicle Batteries The Supply Chain for Electric Vehicle Batteries *Journal of International Commerce and Economics* | 2, *Journal of International Commerce and Economics* (2018), pp. 1–21.
- [18] A. C. Jussani, J. T. Coulter Wright, R. K. Motomatsu, Battery global value chain and its technological opportunities for electric vehicle in Brazil, *EVS 2017 - 30th International Electric Vehicle Symposium and Exhibition* 14, (2017), pp. 333–338.
- [19] Y. Bai, N. Muralidharan, Y. K. Sun, S. Passerini, M. Stanley Whittingham, I. Belharouak, Energy and environmental aspects in recycling lithium-ion batteries: Concept of Battery Identity Global Passport, *Materials Today* 41, (2020), pp. 1–12.
- [20] X. V. Wang, L. Wang, Digital twin-based WEEE recycling, recovery and remanufacturing in the background of Industry 40, *International Journal of Production Research* 57, (2019), pp. 3892–902.
- [21] M. Kouhizadeh, S. Saberi, J. Sarkis, Blockchain technology and the sustainable supply chain: Theoretically exploring adoption barriers, *International Journal of Production Economics* 231, (2021), pp. 1-21.
- [22] S. Saberi, M. Kouhizadeh, J. Sarkis, L. Shen, Blockchain technology and its relationships to sustainable supply chain management, *International Journal of Production Research* 57, (2019), pp. 2117–2135.
- [23] R. Xiong, L. Li, J. Tian, Towards a smarter battery management system: A critical review on battery state of health monitoring methods, *Journal of Power Sources* 405, (2018), pp. 18–29.
- [24] M. Lipu, M. A. Hannan, A. Hussain, M. M. Hoque, P. J. Ker, M. Saad, A review of state of health and remaining useful life estimation methods for lithium-ion battery in electric vehicles: Challenges and recommendations, *Journal of Cleaner Production* 205, (2018), pp. 115–133.
- [25] L. Canals Casals, M. Barbero, C. Corchero, Reused second life batteries for a aggregated demand response services, *Journal of Cleaner Production* 212, (2019), pp. 99–108.

---

## A generic approach to capitalize manufacturing experience in design and optimization

Philip Eyckens<sup>1,\*</sup>, Frank Naets<sup>2,3</sup>, Elke Deckers<sup>2,3</sup>, Eveline Rosseel<sup>1</sup>, Hendrik Schuette<sup>4</sup>, Ioanna Koutla<sup>5</sup>, Reginald Diltor<sup>6</sup>, Carlos Lopez<sup>1</sup>, Pierre Duysinx<sup>5</sup>

<sup>1</sup> Flanders Make, CodesignS corelab, Gaston Geenslaan 8, 3000 Leuven, Belgium

<sup>2</sup> Flanders Make, DMMS corelab, Celestijnenlaan 300, 3000 Leuven, Belgium

<sup>3</sup> KU Leuven, Department of Mechanical Engineering, Celestijnenlaan 300, 3000 Leuven, Belgium

<sup>4</sup> Code Product Solutions, Breinder 26, 6365CX Schinnen, The Netherlands

<sup>5</sup> University of Liege, A&M - Automotive Engineering, Allée de la Découverte 13A, 4000 Liege, Belgium

<sup>6</sup> Flanders Make, MotionS corelab, Gaston Geenslaan 8, 3000 Leuven, Belgium

\*Corresponding author. Email: philip.eyckens@flandersmake.be

---

As design changes in the production phase can be hundreds of times more costly than in the design phase, it is crucial to make sure that the designed product is actually manufacturable before start of production. To this aim nowadays often many manual iterations are needed between the designers and manufacturing experts, which leads to an inefficient design process and delayed time-to-market that in turn are detrimental for company competitiveness. Here we present the outline of a research effort to realize a substantially more integrated design process tailored towards both performance aspects and manufacturability. Key to this is the formalisation of Design for Manufacturing (DfM) rules within the functional CAD design stage. The traditional design approach is exemplified further in this work for the design of a gearbox housing for electric vehicle transmission systems. To realize substantial weight reduction without compromising performance, a novel multi-material design is proposed, constituting of both aluminium, to ensure structural integrity, and high performance polymer for additional structural integrity and leak-tightness under operating condition. Results shown include Topology Optimization (TO) under realistic loading conditions, scrutinizing material volume fraction boundary conditions and mesh sensitivity. Finally, some DfM rules and considerations in order to come to a manufacturable CAD design, are highlighted.

© 2021 by the authors. Published by the Resource Efficient Vehicles Conference.  
This is an open access article under the CC BY license (<http://creativecommons.org/licenses/by/4.0/>).

---

### 1. Manufacturing-informed Design and Optimization framework

Firstly, we present the main scope and first results of the Flanders Make ICON project ‘CAMEDO – Capitalizing Manufacturing Experience in Design and Optimization’. Its purpose is to develop and implement a generic and novel design approach that substantially reduces the time required to achieve a final manufacturable geometrical CAD design of a new mechanical component, by including and exploiting manufacturing information within the design process, both in late and early design phases. To ensure a continuous evaluation of the manufacturability of the component, Design for Manufacturing (DfM) rules are effectively integrated within the design process. Hereby three specific goals have been set, which are targeted within the project:

G1: establish a methodology to capture and formalize existing, heuristic manufacturing knowledge, in a structured database that can be exploited during the design phase of a new product.

G2: establish a prototype software tool able to assess the manufacturability of a mechanical component design based on a CAD file and accounting for the rules of G1.

G3: establish a methodology that embeds the manufacturing knowledge of G1 within a prototype topology optimisation tool, exploiting such rules in order to improve the manufacturability of the newly conceived designs.

A graphical abstract of CAMEDO is provided in Figure 1.

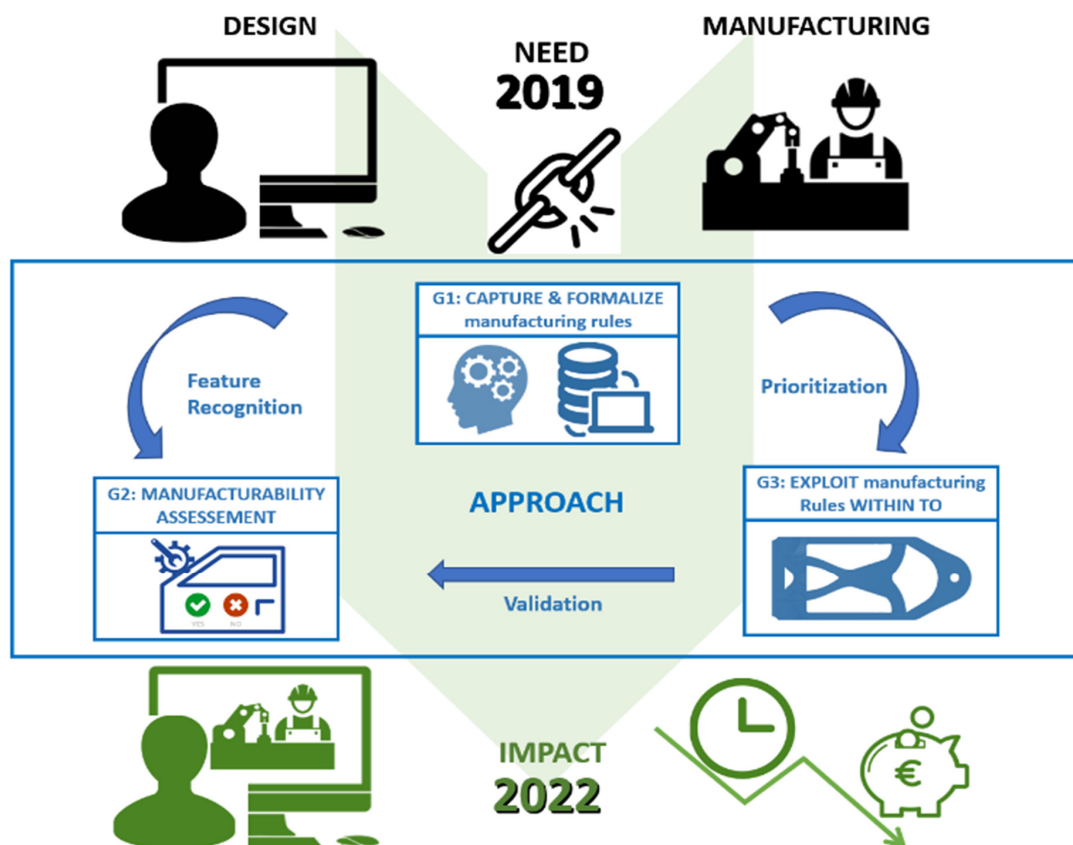


Figure 1: Flanders Make ICON project ‘CAMEDO – Capitalizing Manufacturing Experience in Design and Optimization’.

## 2. Multi-material gearbox housing for lightweight e-vehicle transmission systems

### 2.1 Use Case description

The use case studied is one of the four demonstrators developed in the Interreg project LightVehicle [1] and consists of a gearbox housing for Electric Vehicle (EV) applications. Traditionally, these components are manufactured fully in aluminium, but we aim to develop a novel multi-material design with two materials: aluminium and plastic (PA6 compounded with styrene

maleic anhydride). Figure 2 shows the geometry of the component, as well as the loads applied on it. Two load cases are defined as below:

- Load Case 1: load applied in the smaller shaft hole (point 1), boundary constraints applied along the contour.
- Load Case 2: load applied in the larger shaft hole (point 2), boundary constraints applied along the contour.

The load values are provided by one of the participating companies and are kept confidential.

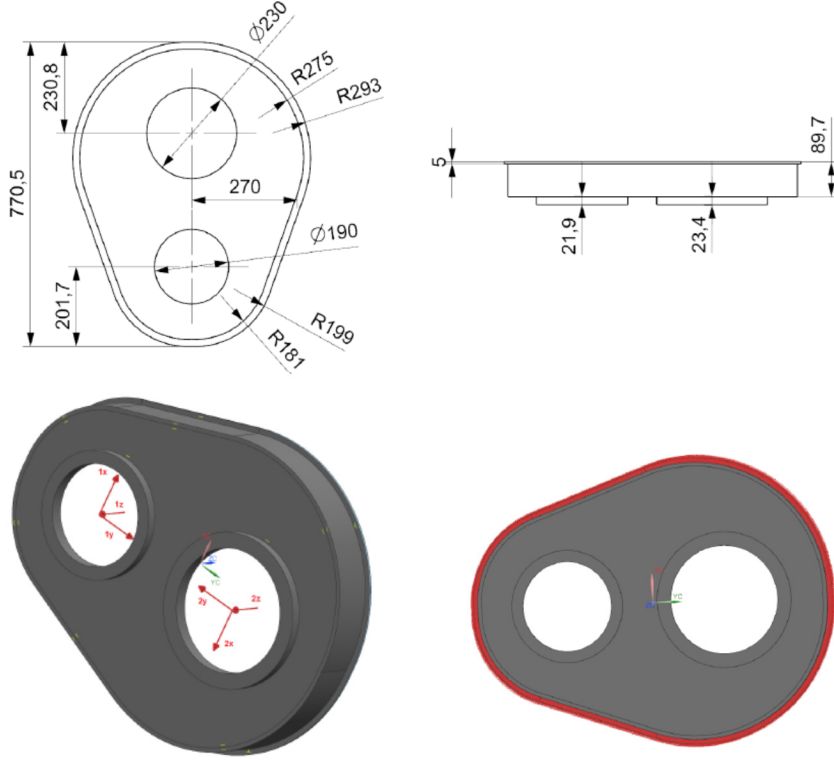


Figure 2: Multi-material gearbox design space and loadcases.

The goal is to maximize the performance of the gearbox housing while making sure that a certain weight reduction target is achieved. Therefore, the optimization problem proposed is defined as:

$$\begin{aligned} & \min \text{Compliance} \\ & \text{subject to:} \\ & \quad \text{mass} < 9 \text{ kg} \\ & \quad \text{material fraction} < P \% \end{aligned}$$

where *Compliance* refers to the strain energy and gives a measure of the structural stiffness (the lower the compliance, the higher the stiffness). We aim to study the influence of different plastic fraction constraints, as well as the influence of the mesh size.

## 2.2 Multi-material Topology Optimization

We start by solving the topological optimization problem described in Section 2.1 without imposing multi-material material fraction constraints. We employ the topology optimization tool [2], which is based on the method of moving asymptotes (MMA) [3]. The optimized result is shown in Figure 3. The yellow parts represent plastic material and the blue parts aluminium. We observe that nearly no plastic material appears in the final configuration, there is only some plastic at the

boundaries between the aluminium and the void parts. In order to obtain a more realistic and manufacturable balance between the plastic and aluminium materials in the final gearbox layout, we introduce next a material fraction constraint.

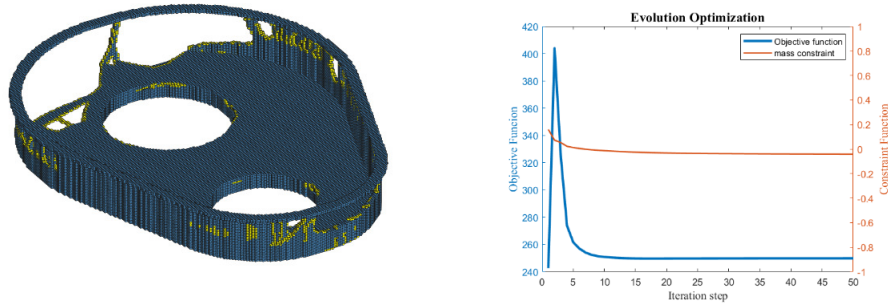


Figure 3: Topological optimization result of multi-material gearbox with mass constraint.

The material fraction constraint imposes a minimum percentage of plastic with respect to aluminium in the final layout. Figure 4 shows the layout of the gearbox after 100 optimization steps of the MMA algorithm for a material fraction constraint of respectively 40%, 50% and 60% of plastic. A consistent growth of the plastic islands can be observed for an increasing minimum fraction of plastic material. In order to maintain a sufficient stiffness – resulting from the minimization of the compliance – the central part of the gearbox housing in-between the shaft holes, is dominated by aluminium and also the vertical gearbox edges contain aluminium ribs as reinforcements.

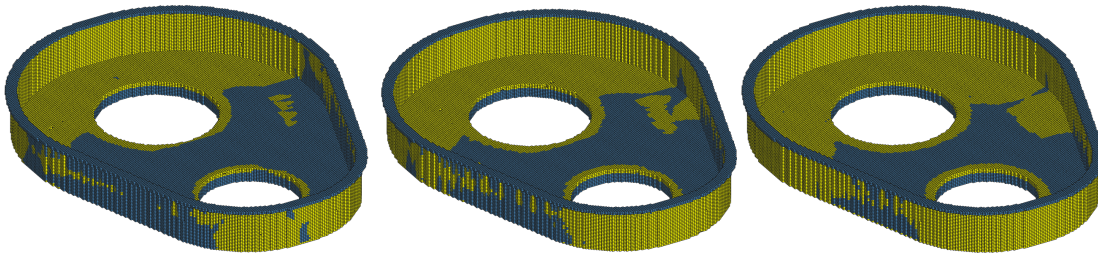


Figure 4: Final layout of the gearbox model for material fraction constraint of respectively 40%, 50% and 60% of plastic.

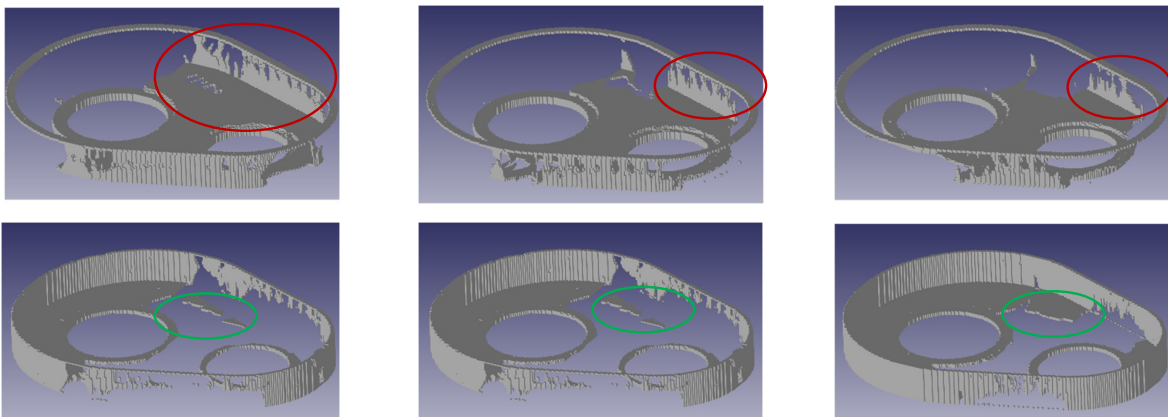


Figure 5: Aluminium (top) and plastic (bottom) fractions in the final gearbox layout for a minimum plastic fraction of respectively 40%, 50% and 60%.

By imposing a larger fraction of plastic material, these vertical aluminium ribs become more and more perforated which results in larger maximum compliance values, as can be seen in Table 1. The evolution of the aluminium/plastic ribs and the growth of the plastic islands is illustrated by the respectively the red and green circles in **Error! Reference source not found.5**, which shows the contributions of the 2 materials in the final layout separately.

The convergence of the optimization iterations is illustrated in Figure 6 and the final mass and compliance results are compared to the initial configuration in Table 1. As initial set-up, the entire gearbox layout is filled with aluminium material. In all optimization cases, the mass constraint of at most 9kg is satisfied and by imposing a larger plastic material fraction, a lower total mass is obtained, as expected from the lower mass density of the plastic material compared to the aluminium material. The convergence of the material fraction constraint becomes slower when imposing a larger fraction of plastic.

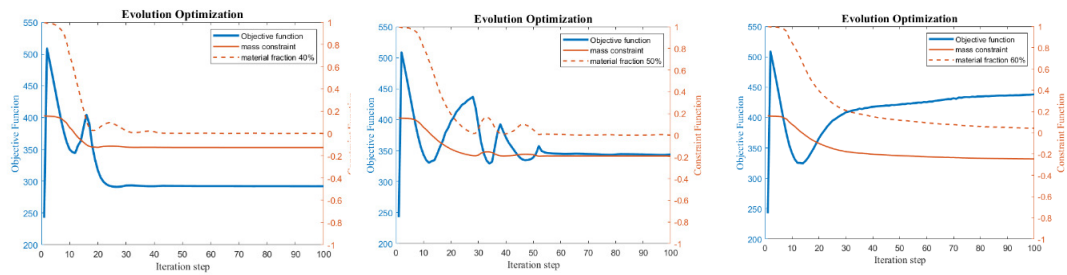


Figure 6: Optimization steps for a material fraction of respectively 40%, 50% and 60% of plastic.

	Initial set-up (full alum.)	Min. 40% plastic	Min. 50% plastic	Min. 60% plastic
Compliance	243	292	344	439
Mass	10.4	7.87	7.26	6.78
Max. displacement	0.41	0.47	0.54	0.69

Table 1: Optimized gearbox results compared to the initial configuration.

The above results consider a voxel based mesh with (160,240,36) voxels in the x-, y- and z-directions. From the gearbox dimensions of (608,771,110) mm, this corresponds to an element size of (3.8,3.1,3.1) mm. In order to illustrate the effect of mesh refinement on the topological optimization, Figure 7 shows the results for a (240,360,48) voxel mesh and a material fraction constraint of at least 50% plastic. This result is qualitatively and quantitatively very similar to the results from Figure 4 (central result with 50% plastic constraint), which illustrates the robustness of the optimization approach with respect to a larger set of design variables due to mesh refinement. We note however that for the refined mesh more iterations are required than for the coarser discretization in order to reach convergence. This complies with a general observation that for very fine meshes or



very strict constraints – for example imposing a very low mass or an extreme material fraction constraint – the convergence of the optimization algorithm can become slower or can even be lost.

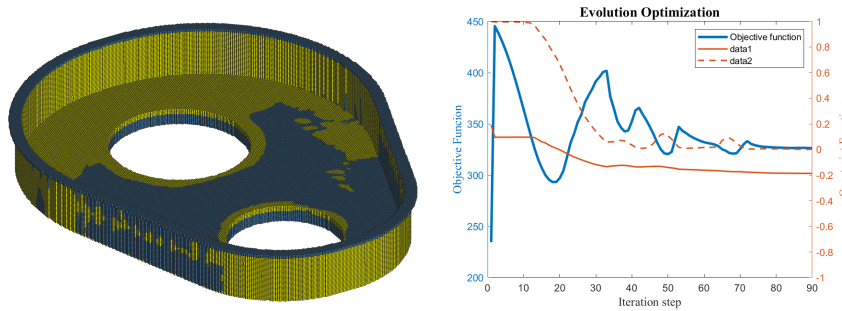


Figure 7: Final layout of the gearbox and optimization iterations for a 50% material fraction constraint and a finite element discretization using a (240,360,48) voxel mesh.

### 2.3 Translation to manufacturable CAD design

The obtained design that has been optimized for performance, is generally not or poorly manufacturable directly. In addition to this, different manufacturing methods, machines and materials impose very different requirements on the CAD design, and result in different properties, as illustrated in Table 2. Therefore, an iterative trial-and-error procedure traditionally needs to be adopted, involving manual iterations of CAD designs with accompanying manufacturing process simulation.

Production technology	Limitations	Batch Sizes	Tolerances*	Surface quality*	Costs
<b>Milling</b>	Almost no limitations design-wise, long processing times	Small volumes	Very precise	Very good	High costs
<b>Casting</b>	Difficult for thin wall thicknesses	Small to large volumes	Precise	Very good, if milled afterwards, otherwise moderate	Low costs in large series, secondary operations required
<b>Metal injection moulding</b>	Usually done for smaller parts in range of mm (tool cost, machine dimensions)	Small to large volumes	Very precise	Very good	<b>High tooling costs</b> (Assumption: most probably no price advantage towards current design)
<b>Stamping</b>	Not suitable for high and highly non-homogeneous wall thicknesses	Small to large volumes	Precise	Very good	Low costs in large series

Table 2: Manufacturing knowledge for different processes in scope for the multi-material gearbox.

Let's make this concrete for our use case. In a first design iteration the CAD engineer interprets the optimization results of section 2.1, resulting in the design shown in Figure 8. In this design, the “plastic islands” shown in Fig. 5 bottom row, are incorporated as 2 “bridges” of plastic between the 2 main plastic zones in the design, hereby realizing an additional design requirement, namely sufficient mechanical interlocking between the aluminium and plastic constituents. However, incorporating relatively thin bridges, as suggested by the Topology Optimization results, is in practice not manufacturable for the envisaged process, being injection (insert) moulding. This is due to excessive fill time (cf. right injection moulding simulation result in Fig. 8 with Moldflow [4]). Obviously, the bridges may be enlarged in the design for better manufacturability, but this has the risk of significantly deteriorating the performance, as the manufacturable CAD design “drifts away” from the performance-optimized TO design.

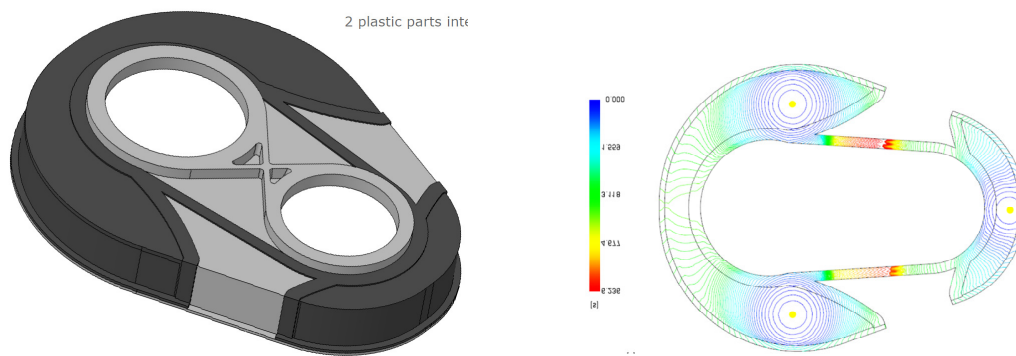


Figure 8: (left) CAD design with 2 plastic bridges providing mechanical interlock. It is however not manufacturable by injection insert moulding (simulation result on the right) due to excessive fill time causing weld lines and air traps.

In a next design iteration with modification to CAD and corresponding process simulation (Fig. 9), a compromise is found in removing the plastic bridges and incorporating smaller interlocks with geometries that are suitable for both the aluminium casting process and subsequent injection insert moulding process. Still, some compromises for manufacturability are required at the expense of performance. For instance, a single aluminium rib on either side of the gearbox wall is chosen, while for optimal performance in terms of weight and stiffness, Topology Optimization suggests multiple smaller aluminium ribs that are alternated by plastic, cf. Figure 5 top row.

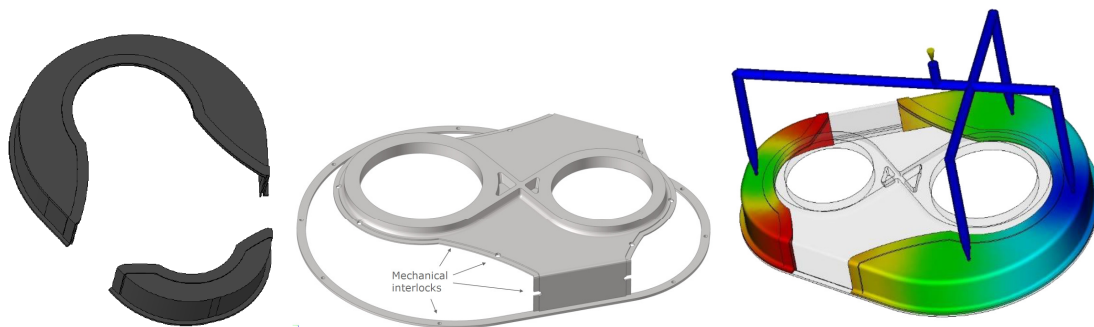


Figure 9: Next-iteration CAD design with 2 plastic parts (left) manufacturable by injection insert moulding (simulation result on the right). Additional details in the aluminium CAD (middle) provide mechanical interlocking between both materials.

### 3. Conclusions

This paper exemplifies a 2-stage design approach of firstly adopting topology optimization for performance optimization, followed by iteratively deducting manufacturable CAD designs that are simulated for one or more candidate manufacturing processes, possibly in conjunction with performance validation simulations.

The presented results demonstrate how by combining topological optimization with multi-material constraints the design of a gearbox can be substantially improved, realizing more than 30% weight reduction. To come to a manufacturable design however, post-processing of the optimal design, common state-of-the-art practise, means making concessions to the optimally performing solution, at the expense of additional effort in the design process.

As outlook, the CAMEDO project (Capitalizing Manufacturing Experience in Design and Optimization), shortly outlined in this work, will investigate how manufacturing design guidelines may be translated to Design for Manufacturing (DfM) rules that can be exploited as constraints in



Topology Optimization. Additionally, the envisaged Formalization Toolbox of DfM rules may be equally exploited to evaluate existing CAD designs for specific processes, machines and material choices. This will improve the overall design process significantly in terms of required resources and robustness.

#### **4. Acknowledgements**

This research was partially supported by Flanders Make, the strategic research centre for the manufacturing industry. This paper is realized in the framework of the LightVehicle project (<https://www.lightvehicle2025.eu/>), which is funded by Interreg Euregio Meuse-Rhine and supported by the European Regional Development Fund. The Interreg V-A Euregio Meuse-Rhine (EMR) programme invests almost EUR 100 million in the development of the Interreg-region until 2020. This area stretches out from Leuven in the west to the borders of Cologne in the east, and runs from Eindhoven in the north all the way down to the border of Luxemburg. Over 5,5 million people live in this cross-border region, where the best of three countries merges into a truly European culture. With the investment of EU funds in Interreg projects, the European Union directly invests in the economic development, innovation, territorial development and social inclusion and education of this region.

#### **References**

1. Interreg LightVehicle project: <https://www.lightvehicle2025.eu/>
2. C. López, S. Burggraef, P. Lietaert et al. Model-based, multi-material topology optimization taking into account cost and manufacturability. *Structural and Multidisciplinary Optimization* 62 (2020) 2951–2973.
3. K. Svanberg, The method of moving asymptotes-a new method for structural optimization. *International Journal for Numerical Methods in Engineering* 24(2) (1987) 359–373
4. Autodesk Moldflow (2020): <https://www.autodesk.com/products/moldflow/features>

---

# Validation of a novel XiL setup for frontloaded testing of an electric vehicle powertrain

Bart Forrier<sup>1,\*</sup>, Thomas D'hondt<sup>1</sup>, Leonardo Cecconi<sup>1</sup> and Mathieu Sarrazin<sup>1</sup>

<sup>1</sup>Siemens Industry Software NV, Interleuvenlaan 68, 3001 Leuven, Belgium

\*Corresponding author. Email: bart.forrier@siemens.com

---

The importance of electric vehicles to the automotive market continues to increase. Meanwhile, the demand for high levels of energy efficiency, performance and comfort leads to ever more integrated E-powertrains and sophisticated controllers. This complicates the vehicle development process and raises the need for frontloaded testing. Model based approaches, such as Hardware-in-the-Loop (HiL) tests, address this need. However, they approximate operational full-vehicle tests, rather than to replace them, and their performance assessments may be biased. This work focuses on an E-powertrain subsystem, consisting of its traction motor with inverter and controllers. The frontloaded assessment of this subsystem's in-vehicle performance is done on a new X-in-the-loop setup. In HiL mode, the real subsystem under test is coupled to an executable digital twin of the vehicle. The main contribution of this paper is that it provides a quantitative validation of the obtained HiL test results. The evaluation is made primarily in terms of energy consumption. The reference dataset is obtained in a full-vehicle on-road operational test campaign. The in-lab HiL test results correlate well with on-road full-vehicle operation. Their validated accuracy is also related to the use of HiL based explorative test results. This is done by studying the effect of design changes, e.g. a modified gearbox ratio or battery pack, on the energy consumption.

©2021 by the authors. Published by the Resource Efficient Vehicles Conference.  
This is an open access article under the CC BY license (<http://creativecommons.org/licenses/by/4.0/>).

---

## 1. Introduction

The fast-growing share of electric vehicles (EV) presents both opportunities and challenges to automotive OEMs and their suppliers [1]. Expectations are high with respect to powertrain efficiency, safety, and reliability, while customer acceptance also depends largely on cost. Those demands combined, lead to increased levels of integration for E-powertrains [2]. As such, they complicate both the EV design and its test-based verification [3]. Meanwhile, increasingly software-defined vehicles open the road towards regular performance- and comfort-enhancing updates [4]. In order to maintain appropriate safety and reliability, this evolution demands ever faster design and validation iterations.

Today's automotive development processes are largely model based. To further reduce design and validation efforts, the methodology of model based system testing is being adopted more widely. The combined use of simulation models with physical testing allows one to frontload performance assessments, and to avoid late and costly integration issues [5, 6]. In this context, the application scope of Hardware-in-the-Loop (HiL) testing has been extended significantly. More complete subsystems under test are considered [7], rather than only the electronic control unit [8]. Instead of one functionality, multi-attribute objectives are evaluated as well, e.g. drivability and consumption [9]. Both trends culminate in distributed HiL and X-in-the-Loop (XiL) testing of multiple subsystems [10].

In contrast to their widespread application in support of frontloaded verification testing, literature on the accuracy of such mixed virtual-real tests is sparse. Documented validations against real-world data seem to be oriented primarily towards the homologation of specific functional implementations, such as longitudinal velocity control [11] or lane-keeping assistance [12]. The validation of HiL based energy consumption assessments is documented also [9]. This validation employs standardized drive cycles on a chassis dynamometer, though, instead of actual on-road data.

The work presented here focuses on electric powertrain subsystem testing in view of frontloaded EV design verification and optimization. Its main contribution is the quantitative back-to-back validation of HiL test results against operational on-road data. The HiL results are acquired on a novel XiL setup<sup>1</sup>, which allows to couple a real E-motor with inverter and control unit to a virtual rest vehicle including a virtual driver. In view of HiL-based design optimization, the obtained accuracy is related to the observed variations in a series of explorative tests.

The remainder of the paper is structured as follows. The operational on-road test campaign is presented first. It includes the real vehicle, its instrumentation and the followed trajectory. Secondly, the test setup is discussed. The focus is on the safe execution of realistic HiL tests using a digital twin of the test vehicle, its driver and the environment. Thirdly, the back-to-back validation is performed, focusing mainly on the energy consumption of the EV powertrain. Next, the obtained accuracy is related to the results of an explorative test campaign. This illustrates its significance with respect to HiL based design optimization. The final section lists the main conclusions of this work.

## 2. On-road test campaign

In-vehicle operational data has been acquired for identifying a representative driving scenario and for validating model based results. During the on-road test campaign, an instrumented EV is driven on various public roads in and near Leuven, Belgium. Figure 1 shows the SimRod EV and the trajectory, called the *Leuven Drive Cycle*, for which the reference dataset is acquired. The SimRod EV is a commercially available battery electric vehicle, on which other research work has demonstrated the process of digital twin creation [13, 14]. Its E-powertrain contains a three-phase voltage inverter with field-oriented torque control and an induction machine with external air cooling. The latter has nominal and peak power values of 15 kW and 45 kW, respectively.

During the operational test campaign, the SimRod EV is instrumented as indicated in the non-exhaustive Table 1. The listed signals are used in the following discussions. The current transducers and voltage probes, on both sides of the inverter, are of type LEM IN 1000-S and Tektronix P5200A, respectively [14]. One motor winding temperature is read from the vehicle CAN and a K-type thermocouple is mounted on the inverter heatsink. The throttle signal is branched off between pedal and inverter. All data are acquired synchronously with a Simcenter SCADAS mobile system.

<sup>1</sup>The test setup is called a *XiL* setup because the real SuT can readily be replaced by an existing virtual counterpart.

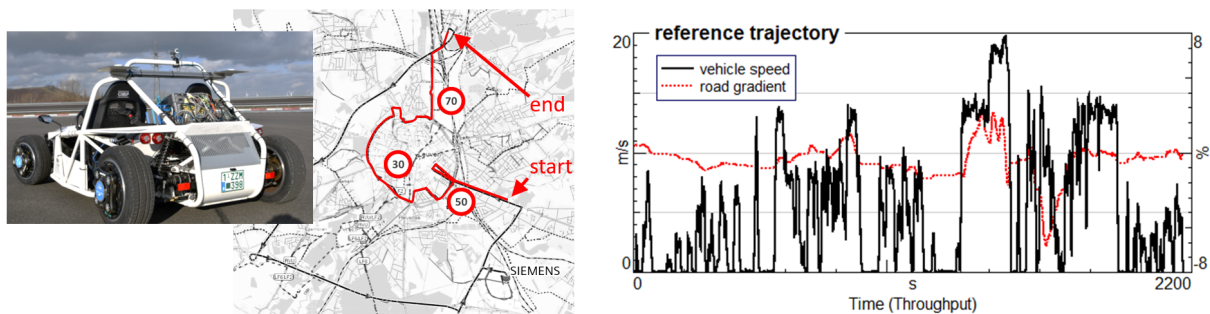


Figure 1: The instrumented SimRod EV (left) and the *Leuven Drive Cycle* (middle, right).

Table 1: Instrumentation of the SimRod EV during operational testing.

Domain	Description	Symbol	Unit	Sample rate [Hz]
Electrical	Inverter currents	$i_{dc}, i_u, i_v$	A	20480
	Inverter voltages	$v_{dc}, v_{uv}, v_{vw}$	V	
Thermal	Motor winding	$\theta_{mot}$	$^{\circ}\text{C}$	16
	Inverter heatsink	$\theta_{inv}$		
GPS	Lat., Lon., Alt.	$\phi, \lambda, h$	$^{\circ}, ^{\circ}, \text{m}$	4
	Speed	$v$	$\text{km h}^{-1}$	
Driver	Throttle voltage	$v_{\theta}$	V	1024

### 3. HiL setup for EV powertrain subsystem testing

The HiL operation of the new test setup primarily aims for near-operational loading of the system under test (SuT), i.e. the SimRod’s E-motor with inverter and control logic. This section will present the test setup and explain how it can replicate an operational test scenario. The remaining sections will show the back-to-back validation against the operational data, and indicate the significance of the obtained accuracy in an explorative test campaign.

#### 3.1 Overview of the HiL setup

Figure 2 provides a view on the HiL test setup. The SuT inverter is fed by an industrial DC/DC converter that acts as battery emulator. The latter supports two-quadrant operation and can deliver up to 250 A of current (bidirectionally). Its output voltage setpoint is adjustable in a range of 80 V to 120 V, to reflect the actual battery voltage. The load motor has torque and speed ratings similar to those of the SuT E-motor, but much higher overload capabilities. The torsionally stiff coupling between the SuT E-motor and the load motor is completed with a torque-measuring flange.

As indicated by the schematic, the measured torque is fed to the real-time platform, on which the executable digital twin of the rest vehicle is running. The latter provides the speed reference for the load motor, corresponding to the virtual vehicle speed. In order to control that speed, the virtual driver provides a throttle command to the SuT inverter. During execution of this real-time control loop and as in the operational measurement, physical sensor data is acquired on the SuT. Thus, Table 1 still applies, except for the GPS data. In addition, the HiL setup provides a torque measurement. Together with it, also a 2048-pulse encoder reading of the shaft speed and other model inputs and outputs (e.g. virtual vehicle speed, distance travelled) are logged onto the real-time execution platform.

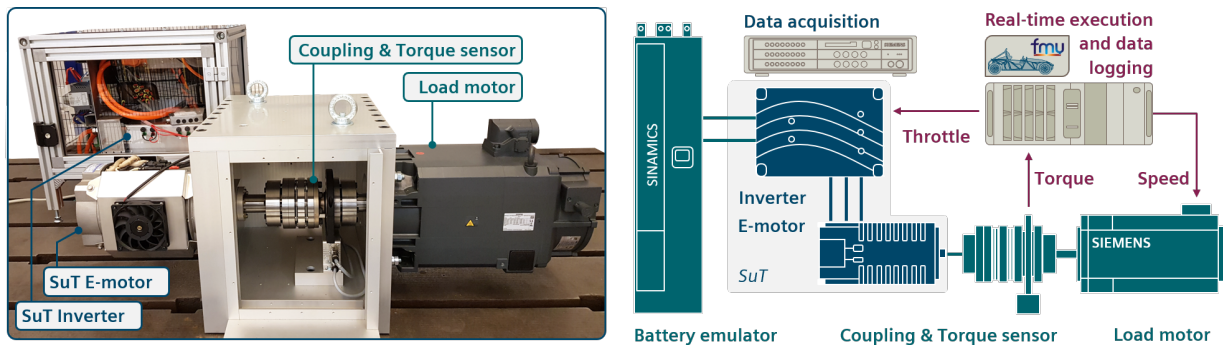


Figure 2: Actual and schematic view on the HiL setup with SimRod E-motor and inverter.

The overview of Fig. 2 does not show the industrial inverter that powers the load motor. This inverter is connected to the electrical grid ( $3 \times 400$  V) via an isolation transformer. Its 700 V DC bus is shared with the high-voltage side of the battery emulator, so that the electrical power can be re-circulated. A brake resistor, connected to the same DC bus, can dissipate excess power.

The selection of the above-described hardware allows the SuT to cover the current/voltage and torque/speed envelopes of the SimRod vehicle. For realistic loading of the SuT, though, the executable digital twin of the rest vehicle is equally essential to the complete HiL (and in fact XiL<sup>2</sup>) setup.

### 3.2 Executable digital twin of the rest vehicle

The executable digital twin of the rest vehicle has three main functionalities. Firstly, it represents the dynamics of the SimRod vehicle and its driver. Secondly, it contains the specification of the test scenario. Finally, it has control logic and interfaces for interacting safely with the real hardware.

The longitudinal vehicle dynamics follow the force balance of Eq. (1). In this expression,  $m$  is the vehicle mass and  $J_w$  the inertia of one wheel with a radius  $R_w$ . The propulsive force scales with the SuT E-motor torque  $\tau_m$ , the transmission efficiency  $\eta$ , the gear ratio  $r$ , and the inverse of the wheel radius  $R_w$ . This torque  $\tau_m$  is negative during regenerative braking. The hydraulic braking torque  $\tau_b$  is computed following [13]. Finally,  $F_r$  represents the longitudinal component of the resistive forces.

$$\left(m + 4 \frac{J_w}{R_w^2}\right) \ddot{x} = \frac{\tau_m r \eta - \tau_b}{R_w} - F_r \quad (1)$$

The resistive forces consist of a gravity component due to the road gradient, the aerodynamic drag, and rolling resistance. In Eq. (2),  $g$  is the constant of gravity and  $s$  is the road slope percentage.  $C_x$  is the aerodynamic drag coefficient of the vehicle with active frontal area  $S$ , moving at the speed  $\dot{x}$  in air with density  $\rho_{\text{air}}$ . Finally, the rolling resistance is proportional to the friction coefficient  $f$ .

$$F_r = \underbrace{mg \frac{s}{100}}_{F_{\text{grad}}} + \underbrace{C_x \rho_{\text{air}} S \frac{\dot{x}^2}{2}}_{F_{\text{drag}}} + \underbrace{mgf}_{F_{\text{roll}}} \quad (2)$$

From the measured motor torque  $\tau_m$ , Eqs. (1)–(2) thus predict the evolution of the vehicle speed  $\dot{x}$ . The speed reference for the load motor is set accordingly. Meanwhile, the virtual driver aims to match the simulated vehicle speed  $\dot{x}$  to its target value, by adjusting both the actual motor torque  $\tau_m$  and the simulated braking torque  $\tau_b$ . This is achieved by a combination of two PI-controllers [15], from which the resulting throttle command value is fed to the torque controller of the SuT inverter.

The test scenario is specified in terms of the target speed as a function of time, the road gradient as a function of traveled distance, and the parameter settings of model and SuT. Because the road gradient is specified as a function of distance, its faithful representation requires the speed tracking to be accurate and free of drift. This aspect will therefore be included in the validation.

The real-time model also includes various safety provisions. A throttle request to the SuT would lead to an uncontrolled speed increase if the load motor's speed control is inactive. The model therefore inhibits the test execution or switches off the SuT upon detection of such an unsafe situation. A safety state-machine manages this, and allows nonzero setpoints in safe conditions only. During normal operation, the analog setpoints and their rates of change are still limited. Lastly, to avoid thermal overloading, the SuT temperatures are monitored and used for controlling several cooling fans.

The real-time architecture is described in detail in [15]. The complete model is uploaded to the real-time platform in a format adherent to the FMI standard (version 2.0) for co-simulation [16]. This format allows model parameters to be changed after the model is uploaded, to study the effect of design changes. The communication with the power components goes via a real-time field bus and automotive CAN for the SuT. The rate of real-time execution and data logging is 1 kHz.

<sup>2</sup>Every new HiL test scenario is verified a-priori in MiL mode, coupling the rest vehicle model to a virtual SuT.

## 4. Back-to-back validation results

This section validates the HiL test results against their corresponding reference dataset. Firstly, it assesses the ability to follow the intended scenario in terms of speed and road gradient, cfr. Fig. 1. Next, it investigates the effect of different boundary conditions on the thermal behavior of the SuT. Finally it quantifies the accuracy of the HiL based evaluation of energy consumption by the E-powertrain. Because HiL tests can only aid decision-making if the results are accurate *and* consistent, three nominally identical tests are performed on different days and with varying preceding operations.

Figure 3 shows the speed tracking error for only one of the three HiL tests; the three error signals are virtually identical. The difference between the operational speed, i.e. the target, and the actual speed in the HiL test, has a  $3\text{-}\sigma$  value of 2 km/h. The tracking performance is thus in line with the state of the art in Vehicle-HiL based testing of longitudinal speed controllers [11]. By the end of the HiL test, the corresponding distance error is of 80 m on a total of 11.5 km. The right side of Fig. 3, shows that even these small errors lead to significant mismatches (up to 1.5 kW) in the instantaneous power required for ascending. The latter quantity is obtained, using Eq. (2), as  $\dot{x}F_{grad}$ .

Figure 4 shows the back-to-back validation against the operational reference of the SuT performance assessment. At the start of the HiL tests, the thermal state of the E-motor differs somewhat from the operational case. After about 15 min, all three HiL test results have converged to within  $\pm 2.5\text{ }^{\circ}\text{C}$  around the reference signal. This is not surprising, since the ambient temperature was almost equal in all (operational and HiL) cases. Moreover, both in the operational case and on the HiL setup the fan of the E-motor switches on/off upon reaching a winding temperature of  $60\text{ }^{\circ}\text{C}$ .

Larger discrepancies exist in the inverter heatsink temperatures. Also this is not surprising, since the inverter heatsink is cooled by a speed-dependent natural airflow in the operational test campaign. The HiL setup compensates for the lack of such cooling by means of two fans below the inverter. They are commanded by hysteresis control with low and high thresholds at  $45\text{ }^{\circ}\text{C}$  and  $50\text{ }^{\circ}\text{C}$ , respectively. In Fig. 4, the inverter temperature downslopes in the HiL data are markedly steeper than the rising portions of the same signals. In other words, the available cooling capacity exceeds the largest inverter loss power. This implies the possibility of tracking the operational temperature signal, by changing either the entire control algorithm or just its threshold values.

The net energy consumed by the SuT is displayed on the right side of Fig. 4, together with the energy regenerated in the operational and in all three HiL tests. These signals of consumed and regenerated energy are computed from the DC current and voltage measurements, as in Eqs. (3). Over the three HiL tests, the average and largest deviations from the operational consumption  $E_{cns}(t_f)$  amount to  $-1.1\%$  and  $-2.5\%$ , respectively. The corresponding respective deviations from the operational regeneration are of  $2.75\%$  and  $3.6\%$ .

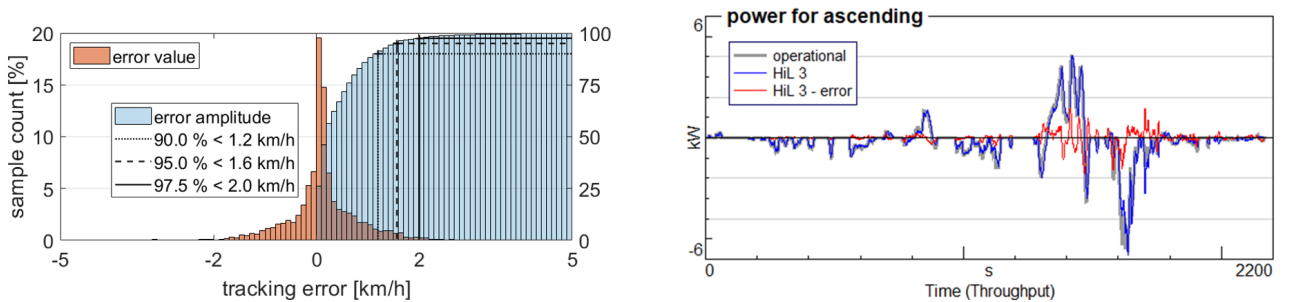


Figure 3: Speed tracking error (left) and its effect on the power required for ascending (right).



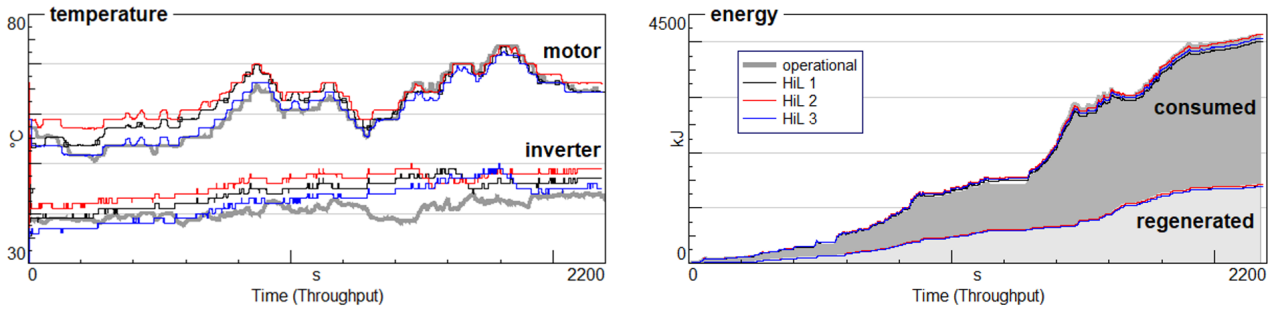


Figure 4: Back-to-back validation of HiL test results versus operational on-road data. Temperatures inside SuT motor/inverter (left) and energy consumed/regenerated by the SuT (right).

$$E_{\text{cnsm}}(t) = \int_0^t v_{\text{dc}} i_{\text{dc}} dt, \quad E_{\text{regen}}(t) = - \int_0^t v_{\text{dc}} i_{\text{dc}} (i_{\text{dc}} < 0) dt, \quad t \in [t_0 : 0 \text{ s}, t_f : 2190 \text{ s}] \quad (3)$$

In conclusion, the HiL test results approximate the operational test data with high accuracy in terms of the imposed speed profile, the corresponding traveled distance, the E-motor temperature, and the DC electrical energy exchange with the SuT. Larger differences exist in the power required for ascending and in the inverter temperature.

The usefulness of HiL-based E-powertrain testing in view of decision-making is further highlighted in Fig. 5. The left side of this figure shows the distance-averaged energy consumed by the SuT. It is obtained as the ratio between the final value of the consumed energy and the total distance traveled by the virtual vehicle. Besides the comparison between HiL and operational test results, it also includes those obtained from executing partial<sup>3</sup> NEDC and WLTC test cycles on the HiL setup. Such standardized test cycles are useful for verification testing, because of their inherent consistency.

The variations among the HiL test results are visualized using the grey rectangle. It shows that the test result is repeatable within a relatively small margin of 1.6 Wh/km. Its center, marked by the vertical orange line, matches closely the actual on-road consumption. The HiL tests thus reproduce the operational energy consumption consistently and with high accuracy. Different results originate from the standardized cycles. Hence the test scenario, or the variety in test scenarios to consider, is clearly important for the evaluation of energy consumption metrics.

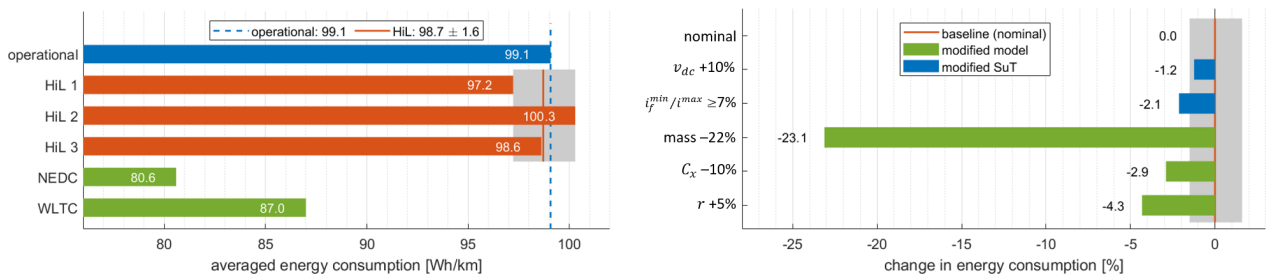


Figure 5: Nominal energy consumption (left) and the effects due to applied modifications (right). The grey rectangle (left & right) corresponds to the observed error margin of the HiL test results.

<sup>3</sup>For a better comparison with the operational scenario, only the part with the vehicle speed below 20 m/s is considered.

Table 2: Modifications applied on the HiL setup.

Indication	Nominal setting	Applied modification	Studied effect
$v_{dc} + 10\%$	$v_{dc} = 96\text{ V}$	Setpoint of battery emulator at 106 V	Modified battery
$i_f^{\min}/i^{\max} \geq 7\%$	$i_f^{\min} = 0\text{ A}$	Impose lower bound on SuT field current <sup>i</sup>	More responsive motor controller
mass $-22\%$	$m = 848\text{ kg}$	Change model parameter to $m = 665\text{ kg}$	Remove instrumentation and co-driver
$C_x - 10\%$	$C_x = 0.277$	Change model parameter to $C_x = 0.2493$	Improve vehicle's aerodynamic shape
$r + 5\%$	$r = 7.13$	Change model parameter to $r = 7.486$	Larger gear ratio

<sup>i</sup> This setting of the SuT inverter's torque controller is specified relative to the maximum motor current  $i^{\max}$ .

## 5. Explorative test results

The previous section has validated the HiL based assessment of the EV energy consumption. This section focuses on design optimization, in view of further reducing development efforts.

Five potential EV design modifications have been studied, each impacting on the E-powertrain. Table 2 explains how the first two affect directly the SuT, and the last three act on the rest vehicle. Each modification is straightforward to apply on the HiL setup<sup>4</sup>, whereas most equivalent prototype tests would be expensive and time consuming. The right side of Fig. 5 shows their effects on the energy consumption, as evaluated on the HiL setup. The relative differences are expressed with respect to the baseline value of  $98.7\text{ W h km}^{-1}$  and compared to the uncertainty margin of  $\pm 1.6\text{ W h km}^{-1}$ . Only one test ( $v_{dc} + 10\%$ ) yields an indecisive result. All other tests do provide a clear answer on whether a change decreases the energy consumption, as well as indicate the sensitivity.

The outcome of executing the equivalent on-road operational tests would likely be unclear, due to the latter's inherently lower repeatability. For example, the decision to maintain the E-motor magnetized at all times ( $i_f^{\min}/i^{\max} \geq 7\%$ ) could not be supported by an operational test. On the contrary, it might be expected, and falsely confirmed, to increase the consumption. The HiL test has made clear that in a realistic driving scenario, the maintained magnetization increases the amount of energy regeneration. Hence it combines a higher responsiveness with a lower net consumption.

## 6. Conclusion

This work has proposed and validated a novel test setup for the performance assessment of an EV powertrain subsystem. In HiL mode, it couples the real EV traction motor with inverter to an executable digital twin of the rest vehicle. The latter represents the longitudinal dynamics of the vehicle with its driver and follows a realistic driving scenario. The appropriate loading is imposed onto the SuT in real-time. The HiL test results are validated quantitatively against on-road operational measurement data, focusing mainly on the aspect of energy consumption. This back-to-back validation has proven the consistent accuracy with which the operational test scenario is replicated in-lab. The obtained accuracy is also brought in relation to an application case of design optimization. This shows the value of explorative HiL testing in view of optimizing the energy consumption of EV.

<sup>4</sup>All five modified 37-minute HiL test scenarios were prepared and executed within one day by the first two authors.



## Acknowledgement



This project has received funding from the European Union's Horizon 2020 research and innovation program under grant agreement No 769506. The content of this publication does not reflect the official opinion of the European Union. Responsibility for the information and views expressed therein lies entirely with the authors.

## References

1. IEA, Global EV Outlook 2020, Tech. rep., 2020, [iea.org/reports/global-ev-outlook-2020](https://www.iea.org/reports/global-ev-outlook-2020)
2. H. Shimizu, T. Okubo, I. Hirano, S. Ishikawa, M. Abe, Development of an integrated electrified powertrain for a newly developed electric vehicle, SAE Technical Paper 2013-01-1759, 2013.
3. F. Akkaya, W. Klos, T. Schammle, G. Haffke, H. Reuss, Holistic Testing Strategies for Electrified Vehicle Powertrains in Product Development Process, World Electric Vehicle Journal 9 (5), 2018.
4. V. H. Le, J. den Hartog, N. Zannone, Security and privacy for innovative automotive applications: a survey, Computer Communications 132, 2018, pp. 17–41.
5. H. Van der Auweraer, J. Anthonis, S. De Bruyne, J. Leuridan, Virtual engineering at work: the challenges for designing mechatronic products, Engineering with Computers 29, 2013, pp. 389–408.
6. Siemens DI Software, Model-based system testing: Efficiently combining test and simulation for model-based development, White paper, 2019, [plm.automation.siemens.com](https://plm.automation.siemens.com).
7. S. Jiang, M. Smith, J. Kitchen, A. Ogawa, Development of an engine-in-the-loop vehicle simulation system in engine dynamometer test cell, SAE Technical Paper 2009-01-1039, 2009.
8. V. Cioffi, F. Di Genova, M. de Manes, G. Di Mare, G. Flauti, F. Ferrara, Hardware in the loop simulation for PIAGGIO MP3 control systems validation, IEEE ISIE, 2008, pp. 2213–2218.
9. J.S. Bang, T. S. Kim, S. H. Choi, R. Rhot-Vaney, H. R. Pillai, Development of a hardware in the loop setup with high fidelity vehicle model for multi attribute analysis, 9th EUROSIM & 57th SIMS, 2016.
10. V. Schreiber, V. Ivanov, K. Augsburg, M. Noack, B. Shyrokau, C. Sandu, P. S. Els, Shared and distributed X-in-the-loop tests for automotive systems: feasibility study, IEEE Access 6, 2018, pp. 4017–4026.
11. S. Riedmaier, J. Nesensohn, C. Gutenkunst, T. Dueser, B. Schick, H. Abdellatif, Validation of X-in-the-loop approaches for virtual homologation of automated driving functions, 11th GSVF, 2018.
12. S. Riedmaier, D. Schneider, D. Watzenig, F. Diermeyer, B. Schick, Model validation and scenario selection for virtual-based homologation of automated vehicles, Appl. Sci. 11 (35), 2021.
13. T. D'hondt, B. Forrier, M. Sarrazin, T. Favilli, L. Pugi, L. Berzi, R. Viviani, M. Pierini, Modeling and identification of an electric vehicle braking system, SAE Technical Paper 2020-01-1094, 2020.
14. B. Forrier, A. Loth, Y. Mollet, In-vehicle identification of an induction machine model for operational torque prediction, 24th International Conference on Electrical Machines, 2020, pp. 1157–1163.
15. T. D'hondt, Y. Mollet, A. Joos, L. Cecconi, M. Sarrazin, J. Gyselinck, Scalable electric-motor-in-the-Loop testing for vehicle powertrains, 17th ICINCO, 2020, nr. 103.
16. Modelica Association, Functional mockup interface for model exchange and co-simulation (version 2.0), Tech. Std., 2014, [fmi-standard.org](https://fmi-standard.org).

## Day 3: P12 – Systems Aspects I

Session P12 – Systems Aspects I, Wednesday 16 June

---

**Session chairs:** Arnaud Can and Per-Olof Sturesson

- 13:30-13:40    **P12.A**  
*A methodology to assess the impact of driving noise from individual vehicles in an urban environment*  
Sacha Baclet, Siddharth Venkataraman and Romain Rimpler
- 13:40-13:50    **P12.B**  
*Analyzing interaction effects in a vehicle model using network theory*  
Sai Kausik Abburu, Carlos Casanueva Perez and Ciarán O'Reilly
- 13:50-14:00    **P12.C**  
*Open-source modeling chain for the dynamic assessment of road traffic noise exposure*  
Valentin Lebescond, Arnaud Can, Pierre Aumond and Pascal Gastineau
- 14:00-14:10    *Questions and Answers*
-

---

# A methodology to assess the impact of driving noise from individual vehicles in an urban environment

Sacha Baclet<sup>1,\*</sup>, Siddharth Venkataraman<sup>2</sup> and Romain Rumpler<sup>2</sup>

<sup>1</sup>*The Centre for ECO<sup>2</sup> Vehicle Design, Teknikringen 8, 100 44 Stockholm, Sweden*

<sup>2</sup>*The Marcus Wallenberg Laboratory for Sound and Vibration Research, KTH Royal Institute of Technology, Teknikringen 8, 100 44 Stockholm, Sweden*

\*Corresponding author. Email: [baclet@kth.se](mailto:baclet@kth.se)

---

Road traffic is a major source of environmental noise pollution in urban areas, while the intra-day distribution of road traffic is often leading to sub-optimal use of infrastructure and resources. In order to evaluate and enable improved distribution of traffic, taking into consideration its impact in terms of noise emissions and other externalities, the present contribution focuses on a methodology designed to assess the impact of the noise generated by individual vehicles on a city's population using NoiseModelling, an open-source library implementing the CNOSSOS-EU model, capable of producing environmental noise maps. The method was applied to delivery trucks in the city of Stockholm, comparing the population's exposure in a variety of scenarios.

The initial step consists in processing microscopic traffic data (simulated in the present contribution), where the traffic intensity is dependent on the time of day that is targeted. The micro-traffic data is subsequently used to generate background noise maps by simulating the propagation of traffic noise using NoiseModelling. Then, the impact of the noise from the vehicle of interest is simulated, based on several parameters (route followed, type of motorization: diesel or hybrid, etc.). Finally, the data is post-processed to calculate the "exceedance" (increase in ambient noise) caused by the vehicle, taking the previously calculated background noise maps as reference. The complete methodology, its underlying assumptions, and the associated criteria proposed in order to assess the impact of noise emissions from individual vehicles will be presented and demonstrated on realistic scenarios.

© 2021 by the authors. Published by the Resource Efficient Vehicles Conference.  
This is an open access article under the CC BY license (<http://creativecommons.org/licenses/by/4.0/>).

---

## 1. Introduction

The increasing prevalence as well as better understanding of noise exposure as a cause of health problems has motivated major developments in the estimation and assessment of noise pollution, of which road traffic noise is found to be a leading contributor. Traditional noise mapping allows for taking reactive measures to abate existing levels of noise pollution such as testing action plans using strategic noise maps [1]. In order to address further challenges associated with noise pollution at a more detailed level than that offered by the generation of strategic noise maps, more refined approaches are necessary. The present paper proposes such a methodology which is intended to allow for preemptive decision making when planning urban mobility strategies.

The methodology described in this contribution processes the output of a noise emission and propagation module which takes traffic flow as input, in order to extract the driving noise impact of individual vehicles within the flow. Time-dependent noise mapping, which is a variant of the

static noise mapping approach, currently in its developing stage [2, 3], is considered in the proposed approach due to the need to assess noise emissions under varying configurations of traffic flow. In that sense, the methodology also allows to overcome the limitations associated with time-averaged noise indicators during sparse nighttime traffic [4] by offering the possibility to introduce appropriate noise indicators [5].

After introducing an overview of the proposed methodology, its modelling steps and necessary input data in Section 2, case studies and the associated discussion are presented in Section 3 before drawing general conclusions.

## 2. Methodological Proposal

The proposed methodology aims at comparing how driving noise emissions from single vehicles impact a city's population in multiple scenarios. Establishing those scenarios consists in varying the values of one or more of the parameters introduced in our approach, whose general workflow is described in Fig. 1. These influential parameters include for example:

- time of day, *e.g.* peak hour, night time, specific time;
- vehicle route, including speed;
- vehicle noise emission model, depending on the type of vehicle, the type of propulsion system, etc.

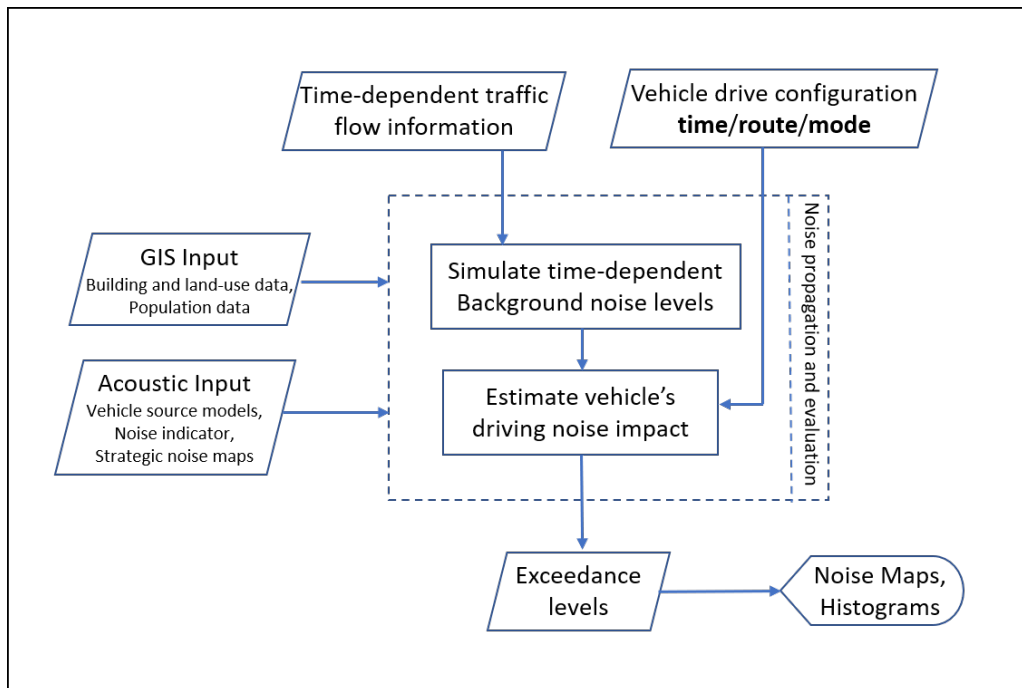


Figure 1: Flowchart of the methodology

### 2.1 General methodology steps

The methodology itself may be described following three main steps:

1. the first step consists in establishing an average background noise map for the area of study, which will serve as a noise level baseline;
2. the second step consists in simulating the propagation of the sound emitted by the individual vehicle of interest;
3. the final step consists in evaluating the impact of the individual vehicle with an indicator which reflects the increase in noise levels that citizens are exposed to, compared to the otherwise established baseline level.

### 2.1.1 Baseline: background noise maps

As previously mentioned, the first step consists in generating a reference noise map for each of the targeted time segments of the day.

To generate such a map, the initial choice made in this contribution is to aggregate micro-traffic data into average traffic per each road segment. NoiseModelling, an open source tool designed to produce environmental noise maps [6], is then used to generate sound sources from those road segments according to the harmonized noise modelling standards CNOSSOS-EU [7] and to subsequently calculate the sound level at each receiver. This sound level is converted to and stored as A-weighted, equivalent level,  $LA_{eq}$ .

### 2.1.2 Vehicle noise simulation

On the basis of a specific noise emission model associated with the studied vehicle and its speed, each position of the vehicle is assigned an emitted sound power level in each octave. NoiseModelling is subsequently used to simulate the propagation of the sound from the positions of the vehicle to the receivers. The outcome is stored as  $LA_{eq}$  levels for each receiver, and for each time step.

### 2.1.3 Noise impact evaluation via an exceedance indicator

The noise impact of an individual vehicle varies depending on the time of day or the neighbourhood in consideration, given that ambient noise can play an important role in the discomfort caused by a vehicle.

In order to evaluate that impact in connection with a baseline level associated with ambient noise, an *exceedance* indicator  $exc_i$  (in dB) is calculated at receiver  $i$  and defined as

$$exc_i = 10 * \log_{10} (10^{LA_{eq,i}/10} + 10^{bg_i/10}) - bg_i \quad (1)$$

where  $LA_{eq,i}$  is the sound level generated by the vehicle (without background noise) at receiver  $i$ , and  $bg_i$  is the average background noise level at receiver  $i$  at the given time of day.

This indicator therefore reflects an increase in sound power received due to the passing of the vehicle. It is calculated for each receiver, for each time step, from the previously generated background maps and vehicle noise emission and propagation simulation.

Subsequently, a local indicator associated with the *impact* of the vehicle on the population may be derived from the exceedance measure. For instance, when defining the impact in the case study of this contribution, a choice is made to evaluate the impact in terms of the quantity  $exc * pop$  for each receiver and for each time step, where  $pop$  refers to the aggregated number of citizens to each receiver.

Finally, a global impact indicator may be evaluated from this local indicator, in order to compare multiple scenarios easily, using a single metric. In the present contribution, the impact values of all time steps are summed, for each receiver, to calculate the vehicle's impact over the duration of the trip for each receiver. The impact values of all receivers may later be summed into a single metric to compare the global impact of multiple scenarios. Apart from the global indicator considered here, more specific indicators may be derived from the data, which is in itself a topic of interest beyond the scope of the present contribution [8].

## 2.2 Modelling and input data

Traffic noise modelling consists in the simulation of traffic sound emission and propagation in an area of study. The two main steps of such modelling are the prediction of the sound emission levels of sound sources (cars, trucks...), and the propagation of that sound in the area of study depending on the layout of the area (buildings, forests...).

In the present contribution, the CNOSSOS-EU framework is used for both noise emission and propagation models, though the methodology is not limited to these. As previously mentioned, Noise-Modelling, being almost compliant with the CNOSSOS-EU standard method [6], is used here for the simulation of road traffic sound emission and propagation. The following inputs are necessary for this purpose: sound sources (*e.g.* vehicles), the layout of the area of interest (buildings, parks...) and receivers, *i.e.* locations where the sound level is calculated. Those receivers may be defined in several ways, commonly as a regular grid of points, or as points around buildings, at a given distance from the facades. For the proposed methodology, the latter method is chosen, as it simplifies the aggregation of citizens to each receiver.

In the following, the key input data to the proposed methodology are detailed.

### 2.2.1 Geographical data

Multiple categories of geographical data describing the area of interest are necessary to model the impact of noise. This data is stored as shapefiles, which can be opened and processed using a GIS (Geographic Information System) application, unless specified otherwise.

The first category of geographical data of interest is the physical layout of the area, which includes:

- the road network;
- buildings, as two-dimensional shapes with the height of each building as an attribute;
- green areas, including parks and forests, *i.e.* highly sound absorbent spaces.

The second category of necessary geographical data is population data. It should be as spatially detailed as possible, ideally distributed at the level of each building. In this contribution, population is added as an attribute of each building. The population of a building is then spread equally among all of the receivers which are placed around it. This population distribution serves as a basis for the estimation of noise exposure.

### 2.2.2 Traffic data for reference background noise evaluation

*Microscopic traffic data* or *micro-traffic data* designates the position and speed of individual vehicles at short time intervals ( $\sim 1$  second) for different times of the day. It may either be measured data or simulated data. For instance, open-source software *Eclipse SUMO* can generate micro-traffic data based on measured traffic data for given streets. This data is then aggregated to the chosen time interval (*e.g.* 15 minutes, 1 hour...) as average traffic per road segment.

If micro-traffic data is not available for the area, then existing strategic noise maps or traffic flow data may be used instead as a starting point. These may either be used as is if the time granularity is fine enough, or post-processed with interpolation (*e.g.* based on complementary measurements) for coarser granularity.

### 2.2.3 Vehicle route

The routes followed by the vehicle whose impact is studied must be available for each scenario, including a specific timestamp, position, and associated speed of the vehicle. This data may be either retrieved from measurements (*e.g.* GPS receiver) or simulated (*e.g.* with *Eclipse SUMO*). If this data is measured data from a GPS receiver, it needs to be pre-processed to correct positioning errors so that every position is placed on the road. To refine the granularity of the data retrieved from the simulations, it is here interpolated (with an equal time interval between each position) such that the distance between 2 successive positions of the vehicle is short enough, *e.g.* less than the typical distance between buildings on the two sides of a road.

### 2.2.4 Vehicle-specific noise emission model

In the present contribution, noise emission models part of the CNOSSOS-EU framework are used. These imply a dependency of the sound power level on the vehicle category (car, truck, etc.), its driving speed, and a distinction between rolling noise and engine noise, see [7].

## 3. Case Study and Discussion

The previously described methodology was applied to evaluate the impact of a delivery truck on the island of Södermalm, in the city of Stockholm, Sweden. The following provides further details on the associated steps.

### 3.1 Baseline: background noise maps

Ideally, the reference noise maps may be established from measured data, or, as introduced in the introduction of the methodology, following an aggregation associated with micro-traffic simulations. The second approach is the one intended by the authors in their methodology, where an averaged traffic per road segment is to be introduced as a sound source in a tool such as NoiseModelling in order to generate baseline noise maps.

Unfortunately, measured micro-traffic data is usually not available for entire cities. When it is available for some roads, it may be extrapolated to other roads, but the resulting data could be inaccurate.

However, some strategic background noise maps exist for the city of Stockholm ( $L_{day}$ ,  $L_{night}$ ). These may be used, in an initial approximation, as a baseline, particularly if a time-dependent interpolation can be introduced on the basis of measured data, such that a more realistic set of noise maps may be derived as a reference. This is the approach chosen to be followed in the case study considered.

In order to obtain these maps for specific times of the day, those background noise maps were interpolated to the hour, using time series of sound levels measured by a microphone placed on the island. Figure 2 shows two examples of background noise maps resulting from this interpolation. It



Figure 2: Interpolated background noise maps for two times of the day on Södermalm. The colour scale is continuous, from purple (low noise levels) to yellow (high noise levels); white is for "no data".

should be noted that the results of those interpolations, while valid in the vicinity of that microphone, might be inaccurate in other parts of the city, if traffic dynamics depending on the time of day are different there.



### 3.2 Vehicle noise simulation

The truck's positions for this case study are based on GPS measurements carried out aboard a delivery truck. The data points were corrected, *i.e.* they were properly re-positioned on the road when meeting GPS inaccuracies, and subsequently interpolated such as to ensure one position per second. All positions of the truck are plotted in Fig. 3. It should be noted that the interpolation method chosen

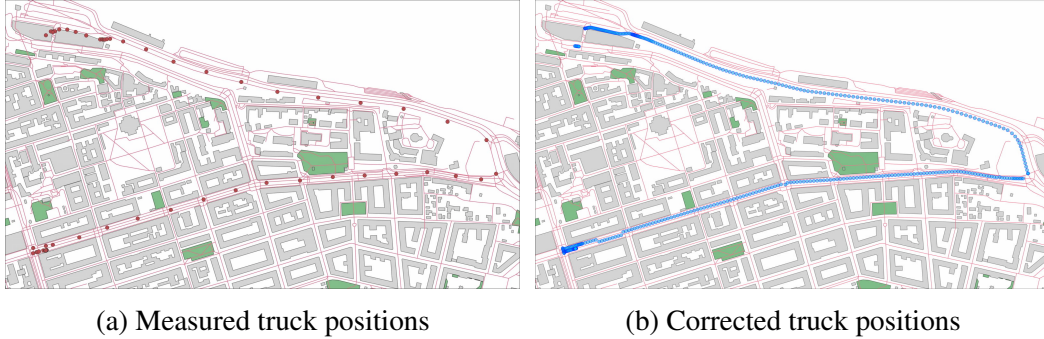


Figure 3: Positions of the truck (a) before and (b) after correction and interpolation.

here for the GPS positions doesn't take acceleration into account. The positions and attributes (speed, timestamp) of the data points are interpolated linearly.

Those truck positions are each associated with emission sound levels using the CNOSSOS-EU emission model for diesel trucks, and defined into NoiseModelling as sound sources. The acceleration of the vehicle is not taken into account in the emission model that we used, but another emission model could allow for this possibility, provided that the necessary input data is available. The result is a table containing, for each time step,  $LA_{eq}$  for each receiver at that time step.

### 3.3 Impact evaluation and discussion

The exceedance for each receiver and each time step is subsequently evaluated according to Eq. (1). Exceedance values are then summed for all time steps, for each receiver, and the resulting map is spatially interpolated into a continuous exceedance map. The resulting map is presented in Fig. 4. As shown on this map, exceedance levels – and thus the impact of the truck on population exposure – are higher when average traffic is lower, and spotting the areas of the neighbourhood which are most impacted by the noise emissions of the truck is straightforward.

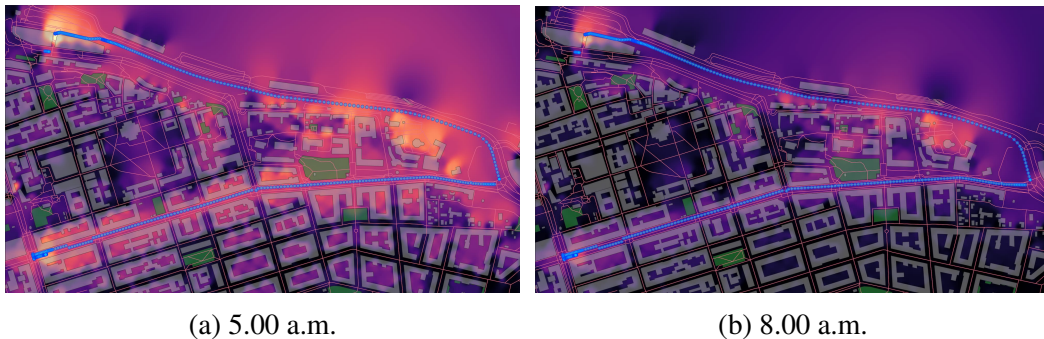


Figure 4: Map visualisation of the exceedance caused by the truck at two times of the day: (a) 5.00 a.m., (b) 8.00 a.m.; the colour scale is continuous, from black (low exceedance) to yellow (high exceedance).

This visualisation method doesn't show population data, even though this may provide valuable insight in areas where population is not spread homogeneously. Both population and exceedance may



be visualised on a map where the size of the receivers is modulated by the number of citizens while the colour of the receivers depends on the exceedance level (see Fig. 5). This approach makes it possible to determine the areas where high exceedance levels have the highest impact on the population. Used in conjunction with Fig. 4, Fig. 5 illustrates how some areas are exposed to high exceedance levels but are very sparsely populated (*e.g.* towards the North of the island).

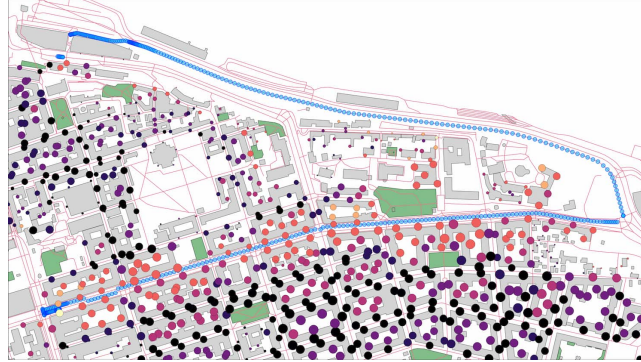


Figure 5: Population weighted exceedance map. Each circle is a noise receiver. Their colour represents noise levels, from black (low) to yellow (high); their size increases with the number of citizens affected.

However, this visualisation method also highlights some limitations associated with this case study: *i)* the dynamics of population density are not taken into account, implying that the citizens are always expected to be home, and *ii)* only permanent residents are taken into account, which overlooks the impact on sensitive zones such as schools, hospitals, etc. These considerations are however a problem of input data, which does not affect the potential of the approach proposed in itself.

It is also worth noting that the approach in the version detailed herein should only be applied at times and in places where traffic is not too sparse, *i.e.* places where *average* noise levels are meaningful. If traffic is very sparse, then analysing the noise level fluctuations caused by each vehicle makes more sense than having average noise levels as a baseline (as is the case in this methodology) to better characterize the exposure to sound. Moreover, sleep sensitivity models might be used to better assess the impact of the vehicle.

## 4. Conclusion

The present contribution describes a method which enables the assessment of the impact of an individual vehicle in an urban environment without the need for field measurements of the vehicle's sound emissions in the area of interest. It may be used as a way to qualitatively compare different scenarios, seeking to minimize the impact of a vehicle on the citizens in urban environments. In particular, it places a high focus on the choice of timing for routing, as well as taking into consideration an estimated number of citizens impacted. This later is highlighted to be a static input data in the case study introduced, which should ideally also be considered as time-dependent in a way similar to the fluctuating background reference noise levels. Finally, the sharp difference in properties of day-time vs. nighttime traffic implies that adjustments to the proposed methodology should be included, particularly in the context of sparse traffic.

Future developments and variants of the method will further allow for the assessment of the sensitivity of each road segment for sound emission and other applications.

## Acknowledgements

The authors would like to thank the Centre for ECO2 Vehicle Design, which is funded by the Swedish Innovation Agency Vinnova (Grant Number 2016-05195). The funding from the EIT Urban Mobility project "Zero Emission off-peak Urban DeliverieS (ZEUS)" (GA 20035) is also gratefully acknowledged.

## References

1. E. Directive, "Directive 2002/49/ec of the european parliament and the council of 25 june 2002 relating to the assessment and management of environmental noise," *Official Journal of the European Communities, L*, vol. 189, no. 18.07, p. 2002, 2002.
2. G. Zambon, R. Benocci, A. Bisceglie, H. E. Roman, and P. Bellucci, "The life dynamap project: Towards a procedure for dynamic noise mapping in urban areas," *Applied Acoustics*, vol. 124, pp. 52–60, 2017.
3. W. Wei, T. Van Renterghem, B. De Coensel, and D. Botteldooren, "Dynamic noise mapping: A map-based interpolation between noise measurements with high temporal resolution," *Applied Acoustics*, vol. 101, pp. 127–140, 2016.
4. A. Can, L. Leclercq, J. Lelong, and J. Defrance, "Capturing urban traffic noise dynamics through relevant descriptors," *Applied Acoustics*, vol. 69, no. 12, pp. 1270–1280, 2008.
5. J. Nygren, S. Boij, R. Rumpler, and C. J. O'Reilly, "An investigation of allocation strategies for internalizing the impact from traffic noise," in *ISMA2020 International Conference on Noise and Vibration Engineering, September 07-09, 2020, Leuven, Belgium*, 2020.
6. E. Bocher, G. Guillaume, J. Picaut, G. Petit, and N. Fortin, "Noisemodelling: An open source gis based tool to produce environmental noise maps," *Isprs international journal of geo-information*, vol. 8, no. 3, p. 130, 2019.
7. S. Kephelopoulou, M. Paviotti, and F. Anfosso-Lédée, "Common noise assessment methods in europe (cnossos-eu)," 2012.
8. A. Can, S. Michel, B. De Coensel, C. Ribeiro, D. Botteldooren, and C. Lavandier, "Comparison of noise indicators in an urban context," in *INTER-NOISE and NOISE-CON Congress and Conference Proceedings*, vol. 253, pp. 775–783, Institute of Noise Control Engineering, 2016.

---

# Analyzing interaction effects in a vehicle model using network theory

Sai Kausik Abburu<sup>1,\*</sup>, Carlos Casanueva Perez<sup>1</sup> and Ciarán J. O'Reilly<sup>1</sup>

<sup>1</sup>*KTH Royal Institute of Technology, The Centre for ECO<sup>2</sup> Vehicle Design, SE-100 44 Stockholm, Sweden*

<sup>\*</sup>*Corresponding author. Email: [abburu@kth.se](mailto:abburu@kth.se)*

---

The vehicle industry is moving towards developing more sustainable and efficient solutions. This movement towards sustainable and efficient solutions brings up the need to develop and integrate new subsystem technologies that are beneficial for the overall vehicle system. However, introducing new technology into an existing vehicle architecture may have knock-on effects on the dependent subsystems. Furthermore, there can be a bias towards the existing technological solutions as a large part of the architecture is developed pertaining to the established solutions. Therefore, sufficient knowledge is required to understand the level of impact the interdependencies, both direct and indirect, can have at a subsystem level and at the overall vehicle system level. To address and assess these interdependencies that arise during the conceptual design phase, a bottom-up design model is proposed. The model, utilizing network theory could represent each subsystem as nodes and their interaction effects on each other as edges. Thus, the interaction effects between different subsystems and their complex influence on the overall vehicle system are considered. This model could serve to evaluate an optimal solution in terms of functional density and economic benefits thus providing the opportunity to avoid any unintended negative indirect effects. Furthermore, it could help in identifying the technological limits in the current vehicle system and thus, identifying the areas that can be developed to further enhance the vehicle system performance. The method of implementation, its advantages, disadvantages, applications, and challenges in implementation are discussed.

©2021 by the authors. Published by the Resource Efficient Vehicles Conference.  
This is an open access article under the CC BY license (<http://creativecommons.org/licenses/by/4.0/>).

---

## 1. Introduction

The concept of sustainable design and sustainability oriented technology and innovation has been prevalent and gaining more traction over the past decade [1]. But, since the establishment of Sustainable Development Goals (SDGs) as a part of Agenda 2030 by the United Nations General Assembly in 2015, and the Paris Agreement in 2016, the concept of sustainability has gained more traction than ever in most industrial sectors. Especially the transportation industry, which is one of the highest contributor of the greenhouse gases, accounting for 24% of all greenhouse gas emissions in EU [2] has been an active participant in the ‘Sustainability Transition’. This transition entails changes across different dimensions such as technological, material, organizational, institutional and sometimes even political, economic, and socio-cultural [2]. As a part of this transition, most if not all of the vehicle manufacturers have introduced the aspect of ‘Sustainability’ in all of its processes, right from concept development, vehicle design, until the end of life of the product.

Moreover, in accordance with SDGs and the Paris agreement, stricter regulations have been established to reduce the carbon footprint. However, the current technology might be inadequate in order

to effectively contribute towards achieving these sustainability goals and to adhere the stricter regulations and standards that accompany. This brings about the need for developing better technological solutions that can fulfill the performance requirements while adhering to the need for developing sustainable and resource efficient products. However, while introducing this new technological solutions into existing vehicle architectures or even new vehicle designs, there are several uncertainties and challenges that needs to be accounted for at a subsystem level. This paper focuses on suggesting possible solutions to tackle these uncertainties and challenges.

## **2. Problem Background**

The central challenge in developing new technological subsystem solutions for the next generation of vehicles is the uncertainty of the direct and indirect impact of the new solutions. The new solutions can have direct and indirect effects on the other subsystems at a subsystem level and in turn they can have an effect on a system level. However, most of the traditional models consider the beneficial and adverse effects of improving a technology or integrating a new technology at a component level. Thus ignoring the direct and indirect effects the new solution can have on a subsystem and in turn on a system level.

This negligence of direct and indirect impact could lead to unintended negative effects on other subsystems, e.g. reducing the efficiency of the subsystems that is dependent on the subsystem where the new solution is implemented. The negligence could also cause inefficient utilisation of resources i.e. the solution could help in reducing the size of the dependent subsystem, but without enough knowledge of impact of subsystems at a system level, this benefit could be lost and thus could lead to over-sizing and redundancy of some components, leading to a inefficient vehicle design. The iterations required to identify the regions to improve the efficiency of the vehicle in different subsystems are rather expensive both in terms of time and money. Moreover, much of the existing solutions for the surrounding subsystem vehicle architecture are established and matured. Thus, while evaluating the benefits and limitations of implementing the new technology at a subsystem level there can be a bias towards the existing solutions.

Therefore, a model that captures the direct and indirect interaction effects on a subsystem level and the complex influence of this interaction on the overall attributes of the vehicle system is required.

## **3. Proposed Solution**

Vehicles are complex systems with several intricately connected subsystem which communicate with each other through complex interactions. Such complex interactions cannot be captured by the traditional design models that describe the vehicle in a top-down approach. Therefore, a bottom-up design model that sufficiently captures the complex interactions between the subsystems and its influence on the overall vehicle system is proposed.

### **3.1 Network Theory Approach**

To represent the complex vehicle system architecture and the relationship between the different subsystems within this vehicle system, a network model is proposed.

Network models are graphical representation of complex networks in which discrete objects or variables are represented as nodes or vertices and the relationship between these discrete objects or variables are represented as edges. Network models have been a popular way to abstract complex models across many disciplines including statistical mechanics, biology, neuroscience, psychology, and psychiatry [3]. With the rise of interest in autonomous vehicle and vehicle fleets, the network models are increasingly being used in the transportation and traffic models as well. Fig.1 depicts a network model with nodes and edges. It can be observed from Fig.1 that two nodes can have multiple edges connecting them indicating multiple relationships between two nodes.

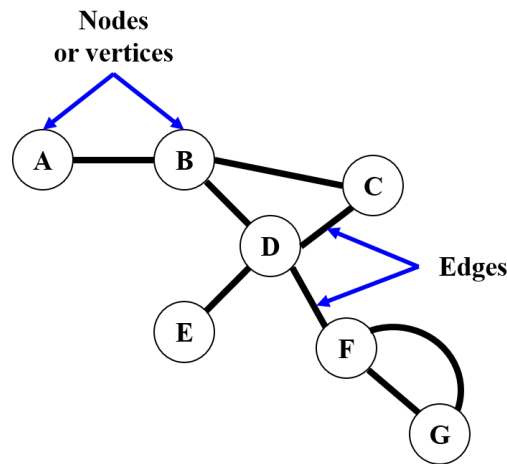


Figure 1: Example network model with nodes and edges

While representing the vehicle system architecture as a network model, we could consider each subsystem as a node and the relationship between two subsystems as edges. This representation could help us understand the ways in which the different subsystems are connected. Moreover, it could allow us to observe, identify and analyse the direct and indirect interaction effects between the different subsystems.

The first step in developing a network model representation of a vehicle system architecture is to identify the different subsystems that are involved in the functioning of the vehicle. Next, with the established knowledge of the physical and mathematical relationship between the different subsystems, the nodes in the network model are connected. As suggested earlier, it is possible for two subsystems to have multiple relationships, i.e., one subsystem may be connected to another subsystem physically, it could also be thermally dependent, and they could be connected through the same vibration transmission path. In such cases of multiple dependencies, there can be multiple edges connecting two subsystems.

To illustrate the method, a typical architecture of a rail vehicle is chosen. The different subsystems that are involved in the functioning of the train are identified and with the help of the known relationship between the identified subsystems, a network model is developed. Fig.2 depicts this network model for a typical rail vehicle.

Representing the vehicle system architecture using network models has multiple advantages. These models allow the possibility to analyse the network structure at a subsystem and system level. Thus, inferences on the behaviour of the whole system could be made which would have not been possible using the traditional design models [3]. Understanding the dependency of one subsystem over another could help in identifying the design bottlenecks i.e. it could be helpful in identifying which subsystems need to be developed further to achieve the design goals. It is to be noted that the proposed method could be used to represent any type of vehicle or even any system with interdependencies. Moreover, this type of design models are vital in the context of multidisciplinary approach where no overall model exists.

However, there are some limitations to the network model approach that need to be considered as well. Network models require considerable knowledge on the direct relationship between different subsystems to develop a model with appropriate level of detail. If not properly modelled, adding or eliminating nodes and edges in a complex network model could be quite cumbersome.

Despite these limitations, there has been considerable research performed in the domain of representing complex systems as abstract network models, and the applications of the network models are increasing as well. These models, when appropriately modelled with enough detail could predict the interaction effects of dependent subsystems that are far from each other in the network model (i.e.,

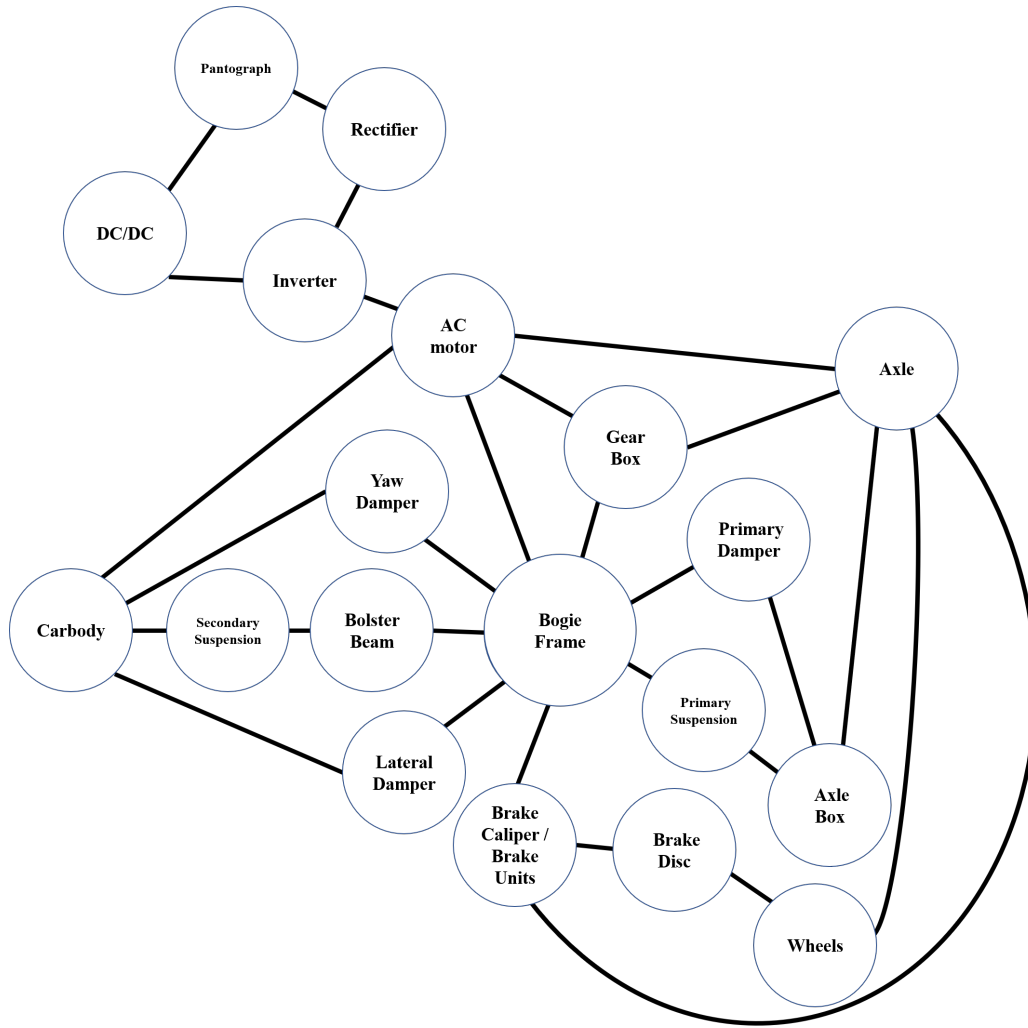


Figure 2: Example network model with nodes and edges

when they are not very evidently connected in real life). The interdependence of the subsystem parameters could be quantified if the models satisfy certain monotonicity or convexity requirements [4]. Furthermore, the interdependence of the subsystems could be quantified using Dijkstra's algorithm. Dijkstra's algorithm is generally used to find the shortest distance between two nodes and evidently finds its applications in traffic planning to find the shortest travel routes. However, by determining the distance between two nodes in a network diagram, we could quantify the level of dependency of one subsystem over another. Therefore, the applications of the network models could also be extended to the rail vehicle network model that is described.

### 3.2 Traction system modelling using network theory

The traction system of a rail vehicle provides the necessary tractive power required to accelerate the train and overcome the running resistance (i.e. air drag, rolling resistance, gradients, etc.) [5]. Due to the complex dependencies and the different indirect benefits that can be realized, traction systems are an interesting application to model using network theory. To illustrate, consider the Silicon Carbide (SiC) based semiconductors. Compared to the conventional Silicon based semiconductors, the SiC-based semiconductors have lower switching losses, can operate at higher switching frequencies, and can endure at higher voltages and temperatures [6]. These advantages of the SiC-based semiconductors could help in redesigning some components and their requirements, and in turn, could help in improving the efficiency of the vehicle. For example, due to the higher switching frequency and low

switching losses, the cooling system of the vehicle can be changed from a forced convection system to a natural convection system. Furthermore, the higher switching frequency opens the possibility to reduce the size of filters, motors, and transformers. This helps in developing a compact unit, freeing up volume. This further allows to reduce the weight of the vehicle which can be utilised for other purposes such as increasing payload, increasing vehicle performance, or even adding extra amenities for a more comfortable journey for the passengers. Furthermore, representing the traction system using network models could allow us to identify the bottlenecks i.e. to identify the critical components that needs to be improved to realise the design requirements. It is important to understand that these type of indirect vehicle-level benefits would go unexploited if there is not enough knowledge on the interaction effects of the subsystems in the vehicle system. And one good way to gain such knowledge about a vehicle system is by representing them using network models.

## 4. Challenges

Utilizing network theory to represent vehicle systems and the complex interactions of the subsystems could offer various advantages and consequently different applications. But, it also entails certain challenges when representing such complex vehicle systems.

While representing the different subsystems as nodes and their complex interactions as edges, it could be challenging to understand in what manner the subsystems are represented. They could be represented as physical components while optimising for volume and mass; they could be represented as objects in a vibration transmission path while optimising for noise and vibration reduction; they could be considered as heat exchange elements while optimising for thermal capabilities of the system. Therefore, understanding the manner in which the subsystems are represented could help in identifying the complex interactions between the subsystems in what ways the subsystems are connected.

Deciding the complexity of the models while representing vehicle systems using network models could also be a huge challenge. Here, complexity refers to the precision of the model. Highly complex models require high computational time and cost, and could produce plethora of data which could be not entirely useful. On the other hand, low complexity models may not be able to produce required level of detail on the data or even worse, it could produce inaccurate data. Therefore, understanding what type of data is relevant in the context of the chosen optimisation aspect (i.e. mass optimisation, noise and vibration reduction, power and efficiency optimisation) could help us understand the level of complexity that is required while modelling.

While optimising two subsystems with multiple interactions between them (e.g. they could be dependent on each other in terms of both mass dependency and heat exchange), conflicting situations may arise. For example, redesigning one subsystem could benefit the other subsystem in terms of mass, however, it could be detrimental in terms of thermal management. Therefore, it is important to quantify the interdependencies between different subsystems and find a method to handle the importance level of the interactions and the desired design requirements.

## 5. Future Work

To fully realize the described and desired model that captures the intricate interactions of different subsystem and its complex influence on the overall system, certain tasks must be performed:

- Initially, the manner in which the input and output of each of the subsystems and the manner in which each subsystem is represented will be identified. This allows to gain an understanding of how different subsystems are connected.
- The required optimisation goals (i.e. mass optimisation, heat exchange optimisation, noise and vibration reduction etc.) will be identified.
- The priority of the desired optimisation goals will be identified.
- To test the validity of the assumptions, a scaled problem including only few subsystems in traction system will be identified and tested with different optimisation algorithms.

## 6. Conclusion

This paper focuses on proposing a network model that is able to capture the intricate interaction effects of different subsystems and its complex influence on the overall attributes of the system. The need for such a network model was explained by comparing it with the traditional models and their limitations. The repercussions of ignoring the interaction effects of subsystems were addressed with examples, including a solution proposal to overcome these shortcomings. The steps involved in developing a network model for a vehicle system, the advantages, and the limitations of representing the vehicle model using network theory were explained. The application of network theory was exemplified with the traction system modelling. The implementation of such a network model does not lack challenges, and the focus for the upcoming work will be centered around finding the right variables to analyze and optimize, balancing model complexity such that the network methods would be able to handle the designed complexity levels while having accurate representation of the subsystems, and the methods to prioritize design variables and even the design process.

## Acknowledgement

The authors would like to thank the Centre for ECO<sup>2</sup> Vehicle Design, which is funded by the Swedish Innovation Agency Vinnova (Grant Number 2016-05195).

## References

1. J. Markard, R. Raven, and B. Truffer, “Sustainability transitions: An emerging field of research and its prospects,” *Research Policy*, vol. 41, no. 6, pp. 955–967, 2012.
2. V. Omahne, M. Knez, and M. Obrecht, “Social aspects of electric vehicles researchâtrends and relations to sustainable development goals,” *World Electric Vehicle Journal*, vol. 12, no. 1, pp. 1–13, 2021.
3. J. M. Haslbeck and L. J. Waldorp, “How well do network models predict observations? On the importance of predictability in network models,” *Behavior Research Methods*, vol. 50, no. 2, pp. 853–861, 2018.
4. S. W. Smith, P. Nilsson, and N. Ozay, “Interdependence quantification for compositional control synthesis with an application in vehicle safety systems,” *2016 IEEE 55th Conference on Decision and Control, CDC 2016*, no. Cdc, pp. 5700–5707, 2016.



5. E. Andersson, M. Berg, S. Stichel, and C. Casanueva, “Traction of rail vehicles,” in *Rail Systems and Rail Vehicles : Part 2: Rail Vehicles*, pp. 15–1–15–72, KTH Royal Institute of Technology, Stockholm, Sweden: KTH, The KTH Railway Group, 1 ed. QC 20160615.
6. J. Biela, M. Schweizer, S. Waffler, and J. W. Kolar, “SiC versus Si - Evaluation of potentials for performance improvement of inverter and DCDC converter systems by SiC power semiconductors,” *IEEE Transactions on Industrial Electronics*, vol. 58, no. 7, pp. 2872–2882, 2011.

---

# Open-source modeling chain for the dynamic assessment of road traffic noise exposure

Valentin Le Bescond<sup>1,3,\*</sup>, Arnaud Can<sup>1,3</sup>, Pierre Aumond<sup>1,3</sup> and Pascal Gastineau<sup>2,3</sup>

<sup>1</sup>UMRAE, Univ Gustave Eiffel, IFSTTAR, CEREMA, F-44344 Bouguenais, France

<sup>2</sup>AME-SPLOTT, Univ Gustave Eiffel, IFSTTAR, F-44344 Bouguenais, France

<sup>3</sup>Institut de Recherche des Sciences et Techniques de la Ville (IRSTV), CNRS, 44321 Nantes Cedex 3, France

\*Corresponding author. Email: [valentin.lebescond@univ-eiffel.fr](mailto:valentin.lebescond@univ-eiffel.fr)

---

In light of the growing concern about the adverse effects of noise pollution on health, a better understanding is needed of the relationships between urban transport and individual exposure. To improve the scientific community's modelling capabilities specific to this issue, we are proposing a noise exposure modelling framework that uses agent-based activity, multi-agent travel simulation and a European standardized noise emission and propagation model. Based on two open source software packages, MATSim and NoiseModelling, this framework aims to simulate the spatiotemporal distributions of daily individual activity and road traffic noise. As such, it enables both characterizing the individual exposure to road traffic-related noise and investigating noise exposure inequality problems based on the attributes of individuals and their activities.

© 2021 by the authors. Published by the Resource Efficient Vehicles Conference.  
This is an open access article under the CC BY license (<http://creativecommons.org/licenses/by/4.0/>).

---

## 1. Introduction

Awareness of the climate agenda and the need to limit transport-related energy consumption are driving the development of new urban transport policies. Noise is then an environmental externality of transport to be considered in the same way as environmental pollution or greenhouse gas emissions. Indeed, the significant health impacts from noise are universally acknowledged, with road traffic being rated as the primary contribution. Quantifying and reducing noise pollution exposure is a crucial issue for cities in terms of health, quality of life and attractiveness. In order to move towards cities in which all socioeconomic groups benefit from a quieter environment, it is necessary to improve understanding of the complex interactions taking place between transport policies and impacts in terms of distribution of noise exposure among the population.

From a decision-making perspective, traffic models are needed to assess the impact of mobility management policies on noise exposure. Microscopic traffic models have been used to compare the

noise impact of roundabouts and traffic signal intersections [1-2], to test speed reduction measures or green wave implementations [3]. In order to refine noise exposure calculations and assess the impact of transport policies on exposure, the development of efficient city-scale modelling chains, including a traffic module and an acoustic module, has thus become a key issue for the scientific community. As for now, Houot *et al.* coupled the MobiSim model with the MITHRA-GIS noise mapping software on a case study in Besançon (France) [4]. Kaddoura *et al.* proposed a coupling between MATSim and the RLS90 acoustic model [5]. Cucurachi *et al.* also relied on MATSim to evaluate the contribution of road transportation to the total noise footprint of land-based mobility [6]. All these studies have shown the value of using multi-agent modelling to analyse acoustic impacts. The aim is for this community to grasp the potential of multi-agent traffic modelling in order to rise new research questions on acoustic modelling, on associations with annoyance, or on the estimation of specific acoustic indicators.

In this paper, we propose an open source modelling framework that enables both characterizing the individual exposure to road traffic-related noise and investigating noise exposure inequality problems. The proposed modeling framework could: (i) be integrated within multi-dimensional environmental assessments, (ii) be mimicked for assessing the impacts of other road traffic externalities. A module for reading and integrating MATSim outputs has recently been integrated into the NoiseModelling noise prediction tool [7]. This paper extends this first publication and presents the open possibilities of the approach. Section 2 presents the resulting modelling chain. The potential of a modelling chain for use in exposure calculations and associated analyses is illustrated in Section 3 through examples from a case study in Nantes (France). Section 4 discusses the further developments and its interest for multi-dimensional traffic externalities assessment.

## 2. Methods

### 2.1 Modelling framework

The modelling framework is presented in details in [7]. The reader can refer to this paper for further details. In short, it consists of a coupling between the Multi-Agent Transport Simulation MATSim, and the noise modelling software NoiseModelling.

MATSim is described in [8]. In this model, agents are described by their daily schedules. For instance, an agent may wish to stay at home, then go to work at 9.00, go to leisure activity at 18.00 and go back home at 20.00. All agents seek to maximize their travel score while sharing the traffic network and its capacities with other agents. The model outputs the resulting daily schedules of all agents, and a list of traffic events. The mobility simulator is responsible for modelling the traffic interaction on the network, and is based on a FIFO (First In, First Out) queue model. The modelling is less accurate, but with a faster resolution, than the microscopic traffic models. In order to prepare the MATSim simulation inputs, and more importantly a simplified microscopic representation of the actual population, the Eqasim project, as developed by Hörl and Balac is used [9].

The noise modelling component of the modelling chain consists of NoiseModelling, which is a free and open source software developed primarily by the DECIDE team of the Lab-STICC (CNRS) and the Joint Research Unit in Environmental Acoustics UMRAE (Gustave Eiffel University) [10-11]. The noise calculation method implemented within NoiseModelling is based on the standard European method CNOSSOS, which serves as a reference method to use for the Directive 2015/996 relative to environmental noise assessment and management (Commission Directive, 2015). The calculation is split into three modules, namely: (i) a noise emission calculation module that estimates

the sound power level based on input data, such as the mean flow rates and mean speeds per road segment, (ii) a path-finding algorithm that searches the paths between sources and receivers, (iii) a calculation of attenuation value along each of the propagation paths for a selected range of octave bands, using the CNOSSOS-EU model. The sound level at a receiver is the sum of the contributions of all sources; its output consists of a grid of receivers with an attributed sound level value computed in dB.

## **2.2 Coupling**

### **2.2.1 Generalities**

The Eqasim project uses these inputs in order to generate a synthetic population, directly usable in the MATSim multi-agent traffic simulation. More in details, Eqasim generates a traffic network for the various transport modes such as car, train, bus, bike, etc., generates a list of agents, with characteristics such as age, gender, driver's license or household income, generates a list of a geographically placed activities (or facilities), and generates a schedule, i.e. the sequence of activities that they will try to follow during the day, for every agent.

These inputs are then used to run a MATSim traffic simulation. The MATSim simulation result is a list of events representing, among other things, vehicle movements. The elements in this list of benefit for noise calculations (time, position, vehicle, speed, etc.) are then extracted and used as noise sources in the noise modelling software. Buildings are directly imported from the OSM database. Noise receivers are determined from the agent's activity positions. The noise levels at the receiver positions can then be calculated. In knowing the time and position of every agent, their noise exposure at any given time and throughout the simulated day can also be calculated. In the work presented herein, the three following time discretization periods were implemented and can be chosen at runtime by the user: (i) day, evening, night; (ii) every hour; and (iii) every 15 minutes.

### **2.2.2 Noise calculation**

For each road segment, each vehicle type and each time period, the number of vehicles passing and their speed are stored. The average speed is then calculated and the NoiseModelling libraries are used to calculate a sound power level per meter for every road segment and every time period. Agents' activities are imported into NoiseModelling in order to directly place receivers at the activities position, which in turn makes it possible to calculate noise levels at the different positions that agents can occupy during the simulated day.

Noisemodelling libraries are used to calculate a noise map from a MATSim simulation output at the desired time slots.

### **2.2.3 Integration of the coupling**

Such a coupling was performed between MATSim version 11.0 and NoiseModelling version 3.3. Since both MATSim and NoiseModelling are written in Java programming language, this coupling was accomplished using this same language. The coupling code was released in version 3.3.2 of NoiseModelling, along with a specific tutorial ([https://noisemodelling.readthedocs.io/en/latest/Matsim\\_Tutorial.html](https://noisemodelling.readthedocs.io/en/latest/Matsim_Tutorial.html)) and can be found on the project Github repository: <https://github.com/Ifsttar/NoiseModelling>.

### 3. Case study

#### 3.1 Description of the study area

The study area is the agglomeration of Nantes, which contains more than 520 000 inhabitants, and a surface area of 317.5 km<sup>2</sup> (see Figure 1).

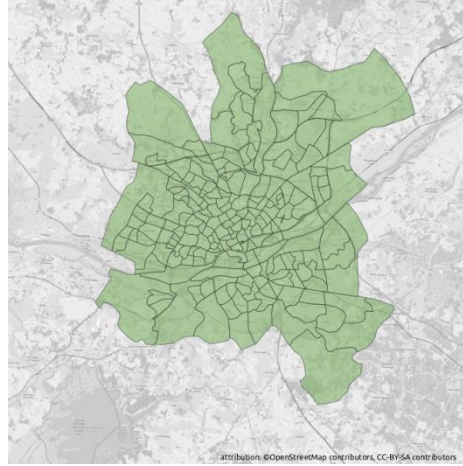


Fig. 1: The municipalities chosen for the Nantes case study, and their IRIS blocs<sup>1</sup>

Figure 2 illustrates the simulated vehicles resulting from the MATSim simulation, around the city center, at 9:00 am of the simulated day. The figure highlights areas of traffic slowdown within the area, particularly around certain intersections, due to high travel demand during this time slot. From this point forward, the previously presented framework is used to obtain noise levels every 15 minutes at each agent activities position. Hence each of the 96 computed noise maps corresponds to a 15-minute period during the simulated day.

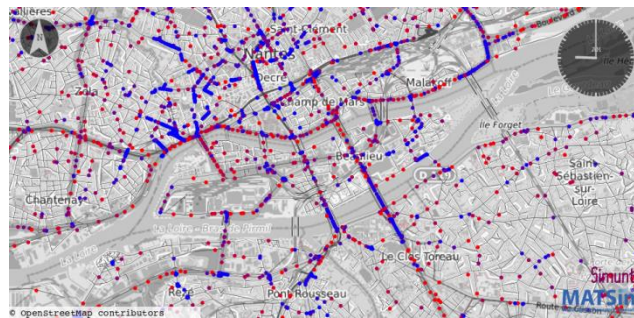


Fig. 2: Nantes area vehicles colored according to their speed (red: fast, blue: slow)

Figure 3 illustrates a noise map obtained at 9 a.m. This figure classically indicates the high noise levels along the main roads, especially the ring road. The originality of this approach lies in

<sup>1</sup> IRIS is the fundamental unit for dissemination of infra-municipal data.

considering the agents' position over the pertinent time slot, for purposes of both calculating noise levels and determining agents' exposure. This approach makes it possible to: (i) calculate the temporal evolution of noise levels throughout the day; and (ii) refine the calculation of agent exposure, by means of overlapping the dynamic noise map and the agents' position.

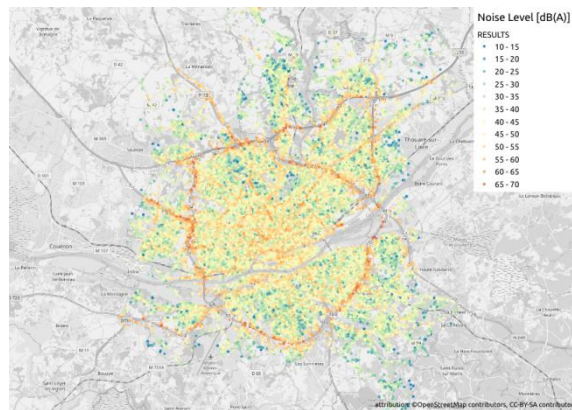


Figure 3: Noise levels, at agent activities positions, between 9 am and 9:15 am

From an agent's perspective, in moving from activity to activity throughout the daily plan, a noise level can be assigned every 15 minutes. The dose level plotted represents the cumulative noise exposure level of the agent-based or home-based activity. This value can only increase and its final value, at the end of the day, equals the equivalent noise level over the course of this same day. The agent depicted in Figure 4 has a worker-type activity plan: at home until 5:30 am, at work until 9 pm, and then back home again after 9 pm. The two curves Agent\_LAeq and Home\_LAeq are superimposed until 5:30 am since the agent is at home. Afterwards, the two curves diverge, with the agent being exposed to higher noise levels at the workplace than what would have been received had the agent stayed home. This curve shape is typical of an agent who lives outside the city center where noise levels are low, while working at a location with high noise pollution. The agent-based noise exposure calculation indicates that this agent is exposed to approx. 73dB(A) daily, whereas a standard noise map would only consider the home exposure of 40dB(A).

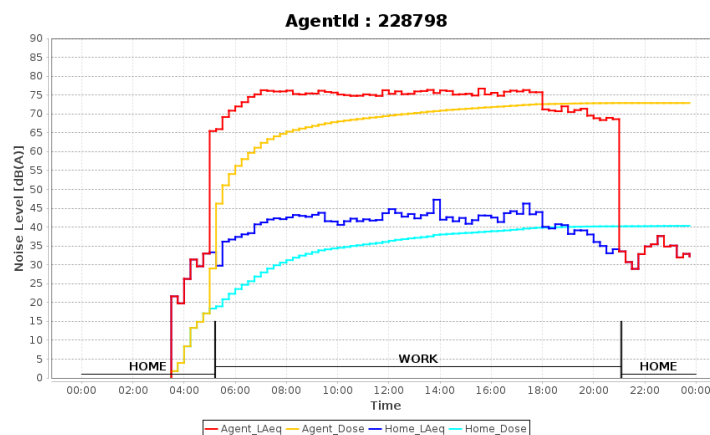


Figure 4: Evolution in exposure of a “student” agent during the day

## 4. Discussion

We are proposing a multi-agent noise modelling framework that relies on open source tools and data. The modelling framework presented comprises two distinct modelling systems: a multi-agent traffic simulation component, MATSim, and a noise modelling component, NoiseModelling. The application of this framework to a case study has illustrated its relevance when considering an assessment of the dynamic exposure of individuals to road traffic noise, as compared to classical noise exposure assessments, which assign inhabitants at their location of residence.

Further research is required to:

- Include the proposed modelling framework within multi-dimensional environmental assessments, including vehicle energy consumption and airborne pollutant emissions, so as to test transport policies such as the introduction of an urban toll, the spreading of demand, or the implementation of low emission zones, on all these dimensions;
- Propose indicators for the assessment of the noise environmental cost of transport policies indicators in view of the assessment of transport policies, as initiated in [12]. The indicators should address the different environmental dimensions (noise and air pollution) through separate or mixed indicators. Indicators should reflect both the long-term health impacts such as indicators based on Disability Adjusted Life Years estimates, and the short-term effects linked to the dynamics of exposure. Finally, particular attention should be paid to the issue of social and territorial equality in the proposal of indicators.

## 5. List of references

1. Can, A., Chevallier, E., Nadji, M., Leclercq, L., 2010. Dynamic traffic modeling for noise impact assessment of traffic strategies. *Acta Acustica united with Acustica* 96(3), 482-493.
2. Chevallier, E., Can, A., Nadji, M., Leclercq, L. 2009. Improving noise assessment at intersections by modeling traffic dynamics. *Transport. Res. Part D: Transp. Environ.* 14(2), 100–110D.
3. De Coensel, B., Can, A., Madireddy, M., De Vlieger, I., Botteldooren, D., 2010. Combined assessment of noise and air pollution caused by road traffic. *Proceedings of the Institute of Acoustics & Belgium Acoustical Society, Noise in the Built Environment, Ghent (Belgium), 29-30 April 2010*, 6p.
4. Houot, H., Antoni, J.P., Pujol, S., Lamiral, M., Mauny, F., 2015. Les mobilités urbaines et leur impact sur l'exposition au bruit : simulation de scénarios prospectifs appliqués à la ville de Besançon [Urban mobilities and their impact on noise exposure: simulation of prospective scenarios applied to the city of Besançon]. *Transports urbains, G.E.T.U.M. (Groupement pour l'étude des transports urbains modernes)*, 2015, 16-20.
5. Kaddoura, I., Kröger L., Nagel K., 2017. An activity-based and dynamic approach to calculate road traffic noise damages. *Transportation Research Part D: Transport and Environment* 54, 335-347.
6. Cucurachi, S., Schiess, S., Froemelt, A. Hellweg, S., 2019. Noise footprint from personal land-based mobility. *Journal of Industrial Ecology* 23(5), 1028-1038.
7. Le Bescond V., Can A., Aumond P., Gastineau P., 2021. Open-source modelling chain based on multi-agent systems for dynamic assessment of road traffic noise exposure, *Transport. Res. Part D: Transp. Environ.* 94.
8. Horni, A., Nagel, K., Axhausen, K.W., 2016. Introducing matsim. In: Horni, A., Nagel, K., Axhausen, K.W., editors. *The Multi-Agent Transport Simulation MATSim*. London: Ubiquity Press, p. 3–8.

9. Hörl, S., and Balac, M., 2020. Open data travel demand synthesis for agent-based transport simulation: A case study for Paris and Île-de-France. Preprint submitted to ETH Research Collection Nov 2020.
10. Bocher, E., Guillaume, G., Picaut, J., Petit, G., Fortin, N., 2019. NoiseModelling: An Open Source GIS Based Tool to Produce Environmental Noise Maps. ISPRS International Journal of Geo-Information, MDPI, 8(3), pp.130. {10.3390/ijgi8030130}. {hal-02057736}
11. Aumond, P., Fortin, N., Can, A., 2020. Overview of the NoiseModelling open-source software version 3 and its applications, Proceedings of the 49th International Congress and Exhibition on Noise Control Engineering e-congress, 20-23 Aout 2020, Seoul, South Korea.
12. Nygren, J, boij, S., Rumpler, R., O'Reilly, CJ. An investigation of allocation strategies for internalizing the impact from traffic noise , Proceedings of ISMA2020 and USD2020.



## Day 3: P13 – Systems Aspects II

Session P13 – Systems Aspects II, Wednesday 16 June

---

Session chairs: Gyözö Gidofalvi and Susann Boij

- 14:20-14:30    **P13.A**  
*Using Analytical Hierarchy Process (AHP) to introduce weights to Social Life Cycle Assessment of Mobility Services*  
Katharina Gompf, Marzia Traverso and Jörg Hetterich
- 14:30-14:40    **P13.B**  
*An initial exploration of measures of transport efficiency through optimising a simple truck model*  
Khashayar Shahrezaei, Ciarán O'Reilly, Timo Lähivaara and Peter Göransson
- 14:40-14:50    **P13.C**  
*Towards a multi-scale and multi-domain modelling of road cargo systems*  
Per-Olof Sturesson and Stefan Edlund
- 14:50-15:00    **P13.D**  
*On the trade-off between noise exposure cost and resource efficiency in traffic*  
Johan Nygren, Susann Boij, Romain Rumpler and Ciarán J. O'Reilly
- 15:00-15:10    *Questions and Answers*
-

# Using analytical hierarchy process (AHP) to introduce weights to social life cycle assessment of mobility services

Katharina Gompf<sup>1,2,\*</sup>, Marzia Traverso<sup>1</sup> and Jörg Hetterich<sup>2</sup>

<sup>1</sup> Institute of Sustainability in Civil Engineering, RWTH Aachen University, Aachen, Germany

<sup>2</sup> BMW Group, Knorrstraße 147, 80788 Munich, Germany

\*Corresponding author. Email: Katharina.Gompf@bmw.de

Decisions in sustainability assessment of mobility services and in particular in social sustainability, often pose a multi-criteria decision making issue, as trade-offs can occur between multiple alternatives and a participatory process should be used. Thus, the goal of this research is to support decision-making through determining weightings for different criteria and indicators within the five stakeholder groups presented by the UNEP/SETAC Guidelines and by implementing a participatory process. The selected indicators to be weighted were adopted from Gompf et al. (2020), who conducted an intensive literature review and suggested for the first time a holistic set of indicators for the evaluation of mobility services. The analytical hierarchy process (AHP) method was used to determine weightings for the chosen indicators. A participatory analysis has been used to identify those weightings. In total, 48 experts in the field of sustainable urban mobility were questioned for the weighting process. These experts were chosen from three different groups: academic institutions, city authorities and mobility service providers in order to be able to analyse differences as well as similarities between these groups. While some indicators resulted in clear prioritization, other indicators revealed large differences between the expert groups. For the majority of indicators, the weighting results are similar for all three groups of experts. Consequently, the results provide clear guidance for decision makers in the field of sustainable urban mobility. Further research should consider expanding the sample size, the geographical scope as well as investigating whether additional expert groups in the area of sustainable urban mobility should be included in the weighting process.

© 2021 by the authors. Published by the Resource Efficient Vehicles Conference.  
This is an open access article under the CC BY license (<http://creativecommons.org/licenses/by/4.0/>).

## 1. Introduction

Mobility is a basic need of humans. This need for mobility in combination with urbanization causes far-reaching implications and problems. The transportation sector is among the top three polluter with 14,3% of worldwide CO<sub>2</sub> emissions [1]. However, rising traffic volumes not only contribute significantly to climate change. Traffic noise leads to health impacts and generally reduces quality of life, especially in urban areas. Mobility services like car sharing or ride pooling are often seen as an opportunity to reduce transport related impacts within cities by reducing private car ownership and offering the possibility to introduce alternatively fueled vehicles [2]. Assessing sustainability impacts of mobility services is a lot more complex than assessing impacts of private car ownership, especially with regard to social sustainability. Particularly the use phase plays an important role as mobility services are used in a different way than cars in private ownership.

To be able to capture all impacts of mobility services during the use phase in a holistic way, Gompf et al. [3] suggested for the first time a holistic set of indicators to be used for the assessment

of mobility services. This set of indicators is clustered in five stakeholder groups, in line with the UNEP/SETAC Guidelines for social life cycle assessment (S-LCA) [4]: Local Community, User, Worker, Value Chain Actors and Society. The revised and updated version of the UNEP/SETAC Guidelines also include a sixth group, the stakeholder group Children. Due to the fact that children are not allowed to drive cars and are therefore only indirectly affected by mobility services such as car sharing, the stakeholder group children is not included in this study.

Within the mentioned stakeholder groups, trade-offs can occur, for example when improved air quality due to electric driving leads to a deterioration of working conditions or higher costs for mobility service users. Trade-off can occur between the stakeholder groups as well as among indicators for the same stakeholder group. Therefore, for decision makers, a clear communication of results is difficult and poses a multi-criteria decision issue. To better support decision makers, a transparent participatory process is needed with the involvement of experts to identify the preferable alternative in case of trade-offs [5,6]. One approach is introducing weights to the criteria in order to be able to come to an aggregated evaluation [7]. In order to implement an operationalized framework for the assessment of different mobility services, the identification of the optimal weighting of sustainability criteria would support the decision-making process.

The framework given for Life Cycle Assessment (LCA) [8] as well as the UNEP/SETAC Guidelines for S-LCA [4] leave decision makers with the challenge of appropriately integrating information into their decisions. Principally, the results are a list of environmental and social impacts that may be understood as performance indicators of the product system under analyses. Given the fact that especially for S-LCA, a huge variety of indicators exist, not only choosing the relevant indicators but also interpreting the results can be demanding. In the case of trade-offs between several alternative scenarios that fulfill the same function, interpreting the results becomes even more complicated [9]. Therefore, a remaining methodological challenge is the construction of a comprehensive judgment of social and environmental performance from the many indicators assessed in S-LCA and LCA. This challenge can be approached using multi-criteria decision-making (MCDM). Several authors suggested the MCDM methodology in the context of sustainability assessment and stated positive results [10–13]. Conceptually, MCDM is introduced in the LCA framework and standards as the ‘weighting’ step [9].

Many different MCDM methods exist to introduce and establish weights, as for example the critic method [14], Simon’s procedure [15], the data envelopment analysis [7] and the conjoint analysis [6]. The most frequently used and well known method for weighting of different criteria is the analytical hierarchy process method (AHP) [16,17]. The AHP method was introduced by Tomas Saaty [18] and is widely employed in different multi-criteria decision-making areas, with manufacturing being the most frequently used application area, followed by logistics and government [17]. Also within the field of sustainability assessment, the AHP method is the most frequently used weighting method [13] and was used in various studies in the last years to determine weighting of environmental and social aspects [19–21].

One of the main advantages of the AHP technique is that a complex problem is broken down to several simple problems. The conversion of a problem into a hierarchical structure is considered as the most important part of the analytical hierarchy process. In that way, AHP simplifies complex problems into partial elements, which are hierarchically related to each other. Following the hierarchy formation, the criteria are ranked via paired comparisons. The advantage of a paired comparison is that the decision maker deals with the prioritization of only two options under comparison, irrespective of the other options. In addition, the AHP technique is well equipped for dealing with numerous criteria of various types, e.g. quantitative measurable data as well as qualitative subjective assessments [21–24]. Due to these advantages, the AHP method was also chosen for this research to determine weights.

Thus, the goal of this research is to support decision-making by transparently identifying an accepted set of weighting chosen with a participatory process through the use of the AHP method. To do so, decision makers from mobility service providers, city authorities as well as research institutes

were questioned how they evaluate trade-offs between the various social criteria suggested by Gompf et al. [3] to evaluate the impacts of mobility services.

## 2. Method

### 2.1 Analytical hierarchy process method (AHP)

An AHP research is based on organizing the problem in a hierarchical structure, with the overall goal at the top level and the various criteria arranged in the subsequent level [25]. Figure 1 illustrates the hierarchy tree used for this study with the previously defined social indicators by Gompf et al. [3] for the assessment of mobility services.



Figure 1: Hierarchy tree including all social indicators to be weighted within each stakeholder group.

A ranking of all criteria is achieved by using a pairwise comparison system of the hierarchy elements. These pairwise comparisons are conducted to convert verbal judgements into numerical values on a scale from 1 to 9, where 1 means that two criteria are of equal importance and 9 means a very strong importance of one criterion over another. Mathematically, we have a set of criteria  $\{x_1, x_2, \dots, x_n\}$  and we want to associate each criterion  $x_i$  with a weight  $w_i$  based on  $n \times n$  comparisons gathered in a comparison matrix  $A$ . The principal eigenvector  $w$  is acquired by solving the system of equations:

$$(A - \lambda_{\max} I) w = 0 \quad (1)$$

where  $I$  is the unit matrix;  $\lambda_{\max}$  the largest or principal eigenvalue of  $A$ ; and  $w$  the principal eigenvector (vector of priority factors) [26]. For more information, see Saaty [27,28], Winston [29] or Handfield et al. [30].

### 2.2 Design of the study and study execution

The comparison of criteria was conducted by questioning experts in Germany in the field of sustainable urban mobility from three different groups: 1) mobility services providers, 2) city authorities 3) academic institutions. That way, different perspectives from experts of these three groups can be gathered and compared to expert judgements within one group as well as with expert judgements of the other two groups. In total, 48 experts completed the pairwise comparison, with 46% representing mobility service providers, 29% academic institutions and 25% city authorities, see Figure 2, which corresponds to a large enough sample to conduct hypothesis from, according to Saaty [25].

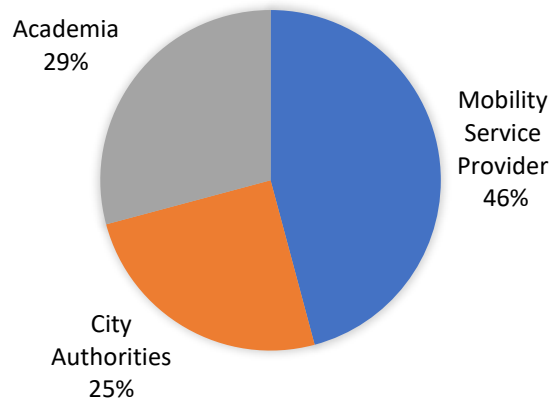


Figure 2: Distribution of experts that completed the pairwise comparisons.

For the experts to be able to evaluate each pair of criteria within the stakeholder groups in a systematic way, an online survey was set up. The online survey started with a short introduction to the study background and the goal of weighting different social indicators for the evaluation of mobility services. Then, the evaluation started with an example of how the pairwise comparison works. After the example, all social indicators of one stakeholder group were compared with each other. For a better understanding of the different indicators, a short explanation was given for every indicator. This was done for all five stakeholder groups. The question for every pair of indicators was always the same: With respect to improving sustainability performance of mobility services, which of the two criteria on each row is more important and how much more important is it? In Figure 3 an extract of the questionnaire can be seen for the stakeholder group Local Community.

	Extremely preferred				Strongly preferred				Equally preferred				Strongly preferred				Extremely preferred				
	↓				↓				↓				↓				↓				
Public Space	9	8	7	6	5	4	3	2	1	2	3	4	5	6	7	8	9	Air Quality			
Public Space	9	8	7	6	5	4	3	2	1	2	3	4	5	6	7	8	9	Employment			
Public Space	9	8	7	6	5	4	3	2	1	2	3	4	5	6	7	8	9	Noise Pollution			
Public Space	9	8	7	6	5	4	3	2	1	2	3	4	5	6	7	8	9	Community Engagement			
Public Space	9	8	7	6	5	4	3	2	1	2	3	4	5	6	7	8	9	Space Occupancy			
Air Quality	9	8	7	6	5	4	3	2	1	2	3	4	5	6	7	8	9	Employment			
Air Quality	9	8	7	6	5	4	3	2	1	2	3	4	5	6	7	8	9	Noise Pollution			
Air Quality	9	8	7	6	5	4	3	2	1	2	3	4	5	6	7	8	9	Community Engagement			
Air Quality	9	8	7	6	5	4	3	2	1	2	3	4	5	6	7	8	9	Space Occupancy			
Employment	9	8	7	6	5	4	3	2	1	2	3	4	5	6	7	8	9	Noise Pollution			
Employment	9	8	7	6	5	4	3	2	1	2	3	4	5	6	7	8	9	Community Engagement			
Employment	9	8	7	6	5	4	3	2	1	2	3	4	5	6	7	8	9	Space Occupancy			
Noise Pollution	9	8	7	6	5	4	3	2	1	2	3	4	5	6	7	8	9	Community Engagement			
Noise Pollution	9	8	7	6	5	4	3	2	1	2	3	4	5	6	7	8	9	Space Occupancy			
Community Engagement	9	8	7	6	5	4	3	2	1	2	3	4	5	6	7	8	9	Space Occupancy			

Figure 3: Extract of the questionnaire for the stakeholder group Local Community

In presenting the pairwise comparisons, there are three possible groups of answers [25,26]:

1. The two indicators are equally important for the evaluation of mobility services, meaning the ratio between the two criteria is 1:1 or the estimation is 1, situated in the middle of the assessment scale, see Figure 3.
2. The indicator on the left-hand side is more important for the evaluation of mobility services. This means that the ratio of the left criterion against the right criterion is from 2:1 to 9:1 or the estimation is from 2 to 9 on the left side of the scale.
3. The indicator on the right-hand is more important for the evaluation of mobility services than the one on the left-hand side. The ratios are reciprocal to the ratios in 2.

In order to reduce individual estimation subjectivity and potential personal bias, mean estimation values were used for the ratios and a consistency check was done. For the consistency check, Saaty [28] proposed the consistency index (CI) to verify the consistency of the comparison matrix. The CI

of the derived weights can be calculated by:  $CI = (\lambda_{max} - n)/n-1$ . If CI is less than 0.1, the set of judgments can be regarded as reliable.

## 2.3 Evaluation and presentation of results

From the mean values, the overall pairwise comparison matrices were conducted for all three groups of experts and for every stakeholder group. An example of the pairwise comparison matrix, based on the answers of the first group of experts (mobility service providers) for the stakeholder group Local Community, can be seen in the following:

$$A = \begin{bmatrix} & \text{Public space} & \text{Air quality} & \text{Local employment} & \text{Noise pollution} & \text{Community engagement} & \text{Space occupancy} \\ \text{Public space} & 1 & 1 & 5 & 1 & 5 & 3 \\ \text{Air quality} & 1 & 1 & 5 & 3 & 3 & 3 \\ \text{Local employment} & 1/5 & 1/5 & 1 & 1/5 & 1 & 1/3 \\ \text{Noise pollution} & 1 & 1/3 & 5 & 1 & 3 & 1/3 \\ \text{Community engagement} & 1/5 & 1/3 & 1 & 1/3 & 1 & 1/5 \\ \text{Space occupancy} & 1/3 & 1/3 & 3 & 3 & 5 & 1 \end{bmatrix}$$

With the help of the AHP Calculation software by CGI, the system of Eq. 1 was solved to get the vector of priority factors  $w$ :

$$w = \begin{bmatrix} \text{Public space} & 0.2696 \\ \text{Air quality} & 0.2990 \\ \text{Local employment} & 0.0463 \\ \text{Noise pollution} & 0.1476 \\ \text{Community engagement} & 0.0517 \\ \text{Space occupancy} & 0.1858 \end{bmatrix}$$

Using these results, the indicators within each stakeholder group were ranked for all three groups of experts. That way it can be evaluated which sustainability aspects are prioritized by which group and what are the similarities and differences.

## 3. Results and discussion

### 3.1 Results, discussion and implications

In Figure 4, an overview of the weighting results from all three groups of experts can be seen. All weighting results are presented on a scale from 0.0 to 0.7 for better comparability and the indicators are given a ranking according to their weights. The results clearly show that there are some obvious similarities between the three expert groups, however, also significant differences were identified. For the stakeholder group Local Community, the indicator air quality consistently received the highest ranking. This result gives a clear guidance and suggests to prioritize efforts and alternatives that improve air quality. In addition, the fact that local employment received low weighting by city authorities and mobility service providers can be regarded as tendency that should not be neglected, although academic institutions prioritized this aspect differently. For all the other indicators within this stakeholder group, however, it is very difficult to conclude a statement that is valid for all three groups, which clearly shows the different prioritization of aspects for academic institutions, city authorities and mobility service providers.

For the stakeholder group User, the safety of the user was ranked the highest by all three groups, which also clearly indicates that the focus of sustainability efforts within this stakeholder group should be on safety. Due to the fact that the possibility for users to give feedback was consistently ranked lowest, this aspect can be regarded as less important for all three groups compared to the other indicators. Except for the highest and lowest rank it is again difficult to draw overall valid conclusions, as weighting results differ too much between the groups.

The stakeholder group Worker showed a clear tendency towards high weighting of safety of the worker and fair salary, which suggests that in the case of having to choose between multiple alternatives, a focus on these two aspects is justified. Work-life balance and freedom of association, however, was given the lowest weighting by all three groups of experts. This of course does not mean that these two aspects are not important. The low weighting just gives additional information for decision makers in case of multi-criteria decision-making. Overall, the ranking by city authorities and mobility service providers for the stakeholder group Worker is almost identical. The prioritization by academic institutions, however, differs greatly, which is why no overall consistent ranking can be concluded.

The most inconsistent ranking among the three groups can be found for the indicators of the stakeholder group Value Chain Actors. Especially city authorities and mobility service providers, which showed similar or almost identical rankings for the previous stakeholder groups, now show partly opposing weighting. This makes it impossible to conclude an overall valid weighting in this case. Contrarily, the indicators of the stakeholder group Society received almost identical weighting and prioritization. Here, the prioritization of society's health is a very obvious result, as well as the low prioritization of tax income. This result, however, can be influenced by the fact that for this stakeholder group only three indicators needed to be weighted and therefore fewer prioritization options were possible which again leads to a higher chance of a consistent ranking of all three groups.

Overall, it should also be highlighted that each individual weighting within one group of experts differ from one another. Through the use of average weighting in the evaluation of indicators within one group, especially extreme weighting by single respondents was mitigated and weakened. Nevertheless, general tendencies as outlined above can be regarded as valuable input in case of multi-criteria decision-making. Should decision makers from academic institutions, city authorities or mobility service providers aim to implement a weighting for the mentioned indicators, there are two options:

1. implementation of the set of weighting from one of the three groups, depending on which group decision makers associate with.
2. implementation of the overall average weighting. This research suggests the first option, as clear differences among the three groups exist and that way a group specific weighting can be achieved.

### **3.2 Limitations and further research needs**

The main limitations of this research is the sample size, the geographical scope as well as the focus on only three groups representing decision makers in the field of sustainable urban mobility, namely academic institutions, city authorities and mobility service providers. Further research could look at expanding the sample size and the geographical scope, as it would be interesting to see if decision makers in the field of sustainable urban mobility in other countries outside Germany would come up with similar or different weighting. In addition, further research could be done on finding additional decision makers in relevant fields to further expand the group of respondents. It would also be interesting to see whether decision makers in similar geographic regions independent from the country would come up with similar weighting, for example decision makers in high density urban areas like Manhattan or Hong Kong, compared to decision makers in lower density urban areas like Copenhagen or Amsterdam. Having a large enough sample in different countries and different geographical regions would allow to draw respective conclusions and could lead to country specific or even city type specific weighting.



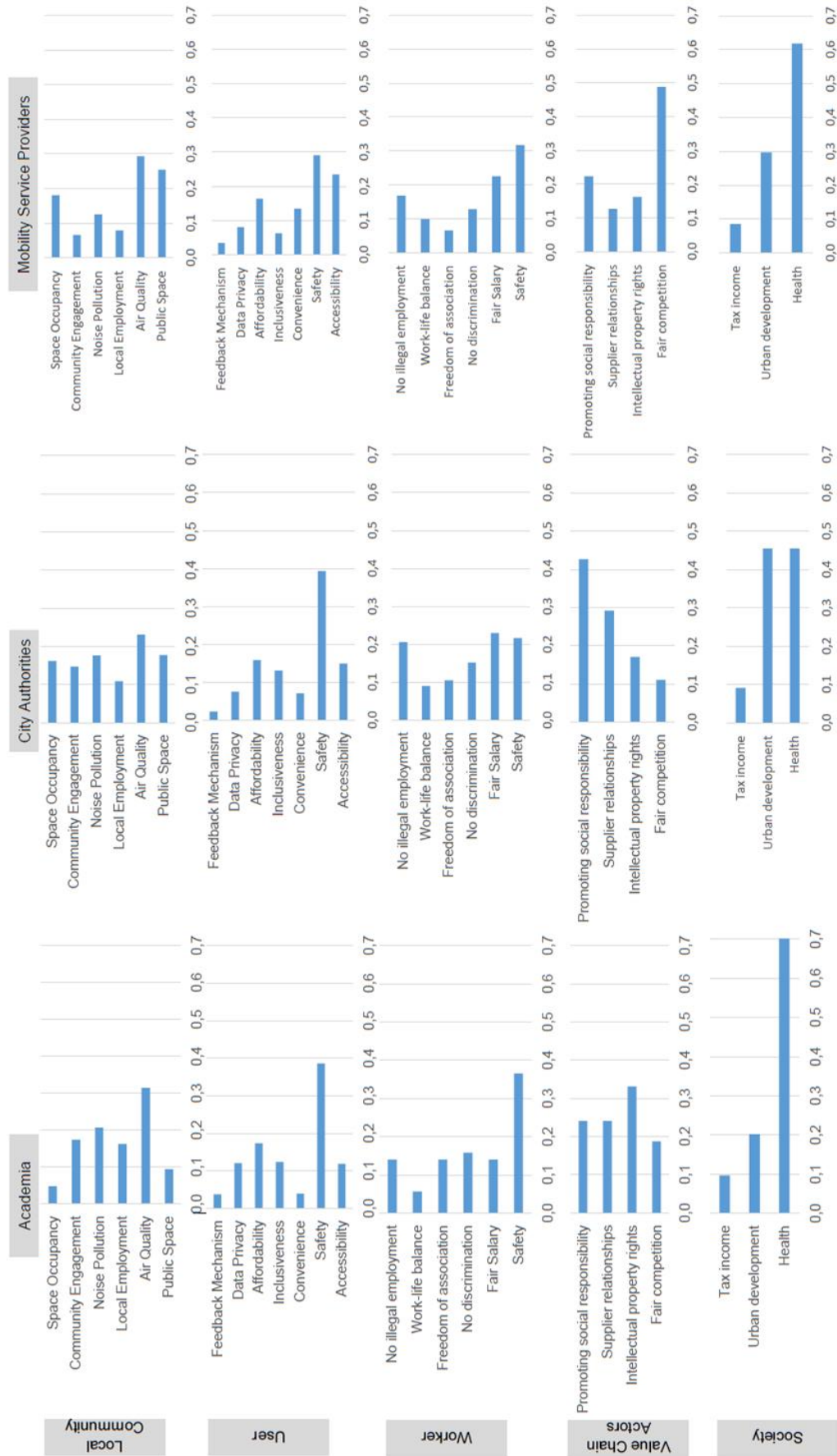


Figure 4: Overview of weighting results for the three expert groups



## 4. Conclusions

The goal of this paper was to support decision makers in the field of sustainable urban mobility by determining weights for different indicators within the five stakeholder groups defined by the UNEP/SETAC Guidelines [4]: Local Community, User, Worker, Value Chain Actors and Society. The selected indicators to be weighted were adopted from Gompf et al. [3], which conducted an intensive literature review and suggested for the first time a holistic set of indicators for the evaluation of mobility services. The method used to determine weights was the AHP method. For the weighting process, experts in the field of sustainable urban mobility were questioned. These experts were chosen from three different groups: academic institutions, city authorities and mobility service providers in order to be able to analyze differences as well as similarities between these groups. In total, 48 experts completed the weighting process.

The results showed clear similarities for some indicators but also significant differences for other indicators. For example, all three groups of experts consistently ranked indicators regarding air quality highest within the stakeholder group Local Community. For the stakeholder group User, all three groups of experts ranked indicators regarding safety highest. The stakeholder group Worker showed a clear tendency towards high weighting of safety of the workers and fair salary. For the stakeholder group Society, health indicators were clearly prioritized. However, for the stakeholder group Value Chain Actors, no consistent ranking could be concluded, as results partly differ greatly between the three groups of experts.

This result can give guidance for decision makers in the field of sustainable urban mobility, however it makes it difficult to suggest a weighting that represents the opinion of all three groups. Therefore, there are two options for weighting adoptions: 1. implementation of the set of weighting from one of the three groups or 2. implementation of the overall average weighting. As the research results makes it difficult to propose a weighting set that represents all three groups and average weighting would weaken group specific results, it is suggested that decision makers in the field of sustainable urban mobility adopt the results from one of the three groups that they associate with.

Further research should consider expanding the sample size, the geographic scope as well as investigate if further expert groups in the area of urban sustainable mobility should be included in the research.

## References

1. IPCC *Climate Change 2014: Mitigation of Climate Change. Contribution of Working Group III to the Fifth Assessment Report of the Intergovernmental Panel on Climate Change*; 2014;
2. Gould, E.; Wehrmeyer, W.; Leach, M.; Electric, S. Transition pathways of e-mobility services. *Trans. Ecol. Environ.* 2015, 194, 349?359, doi:10.2495/SC150311.
3. Gompf, K.; Traverso, M.; Hetterich, J. Towards social life cycle assessment of mobility services: systematic literature review and the way forward. *Int. J. Life Cycle Assess.* 2020, doi:10.1007/s11367-020-01788-8.
4. UNEP/SETAC Guidelines for Social Life Cycle Assessment of Products Available online: <http://wedocs.unep.org/handle/20.500.11822/7912> (accessed on Dec 30, 2019).

5. Bond, A.; Morrison-saunders, A.; Pope, J.; Bond, A.; Morrison-saunders, A.; Sustainability, J.P. Sustainability assessment: the state of the art. **2012**, *5517*, doi:10.1080/14615517.2012.661974.
6. Tarne, P. Introducing weights to life cycle sustainability assessment — how do decision-makers weight sustainability dimensions ? **2018**.
7. Yang, G.; Yang, J.; Xu, D.; Khoveyni, M. A three-stage hybrid approach for weight assignment in MADM \$. *Omega* **2017**, *71*, 93–105, doi:10.1016/j.omega.2016.09.011.
8. ISO 14040 Environmental management - life cycle assessment - principles and framework 2006.
9. Zanghelini, G.M.; Cherubini, E.; Soares, S.R. How Multi-Criteria Decision Analysis (MCDA) is aiding Life Cycle Assessment (LCA) in results interpretation. *J. Clean. Prod.* **2018**, *172*, 609–622, doi:10.1016/j.jclepro.2017.10.230.
10. Jeswani, H.K.; Azapagic, A.; Schepelmann, P.; Ritthoff, M. Options for broadening and deepening the LCA approaches. *J. Clean. Prod.* **2010**, *18*, 120–127, doi:10.1016/j.jclepro.2009.09.023.
11. Cinelli, M.; Coles, S.R.; Kirwan, K. Analysis of the potentials of multi criteria decision analysis methods to conduct sustainability assessment. *Ecol. Indic.* **2014**, *46*, 138–148, doi:10.1016/j.ecolind.2014.06.011.
12. Laurin, L.; Amor, B.; Bachmann, T.M.; Bare, J. Life cycle assessment capacity roadmap (section 1): decision-making support using LCA. *Int. J. Life Cycle Assess.* **2016**, *21*, 443–447.
13. Angelo, A.C.M.; Marujo, L.G. Life cycle sustainability assessment and decision-making under uncertainties. *Life Cycle Sustain. Assess. Decis.* **2020**, 253–268, doi:10.1016/b978-0-12-818355-7.00012-9.
14. Diakoulaki, D.; Mavrotas, G.; Papayannakis, L. Determining objective weights in multiple criteria problems: the critic method. **1995**, *22*, 763–770.
15. Figueira, J.; Roy, B. Determining the weights of criteria in the ELECTRE type methods with a revised Simos ' procedure Jos. *Eur. J. Oper. Res.* **2002**, *139*, 317–326.
16. Dos Santos, P.H.; Neves, S.M.; Sant'Anna, D.; Oliveira, C.H. De; De Carvalho, H.D.; Neves, S.M.; Ornaghi, D.; Anna, S.; Oliveira, C.H. De The analytical hierarchy process supporting decision making for sustainable development: an overview of applications. *J. Clean. Prod.* **2018**, doi:10.1016/j.jclepro.2018.11.270.
17. Ho, W. The state-of-the-art integrations and applications of the analytic hierarchy process William Ho. *Eur. J. Oper. Res.* **2018**, *267*, 399–414.
18. Saaty, T.L. *The analytic hierarchy process*; McGraw-Hill Book Co, N.Y, 1980;
19. Shapira, A.; Shoshany, M.; Nir-Goldenberg, S. Combining Analytical Hierarchy Process and Agglomerative Hierarchical Clustering in Search of Expert Consensus in Green Corridors Development Management. *Environ. Manage.* **2013**, *52*, 123–135.
20. Portman, M.E.; Shabtay-Yanai, A.; Zanzuri, A. Incorporation of socioeconomic features' ranking in multicriteria analysis based on ecosystem Services for Marine Protected Area

Planning. *PLoS One* **2016**, *11*, doi:<https://doi.org/10.1371/journal.pone.0154473>.

21. Opher, T.; Friedler, E.; Shapira, A. Comparative life cycle sustainability assessment of urban water reuse at various centralization scales. *Int. J. Life Cycle Assess.* **2019**, *24*, 1319–1332, doi:10.1007/s11367-018-1469-1.
22. Dekamin, M.; Barmaki, M.; kanooni, A. *Selecting the best environmental friendly oilseed crop by using Life Cycle Assessment, water footprint and analytic hierarchy process methods*; Elsevier B.V., 2018; Vol. 198; ISBN 9821770843.
23. Nikkhah, A.; Firouzi, S.; El Haj Assad, M.; Ghnimi, S. Application of analytic hierarchy process to develop a weighting scheme for life cycle assessment of agricultural production. *Sci. Total Environ.* **2019**, *665*, 538–545, doi:10.1016/j.scitotenv.2019.02.170.
24. Ong, M.S.; Chang, M.Y.; Foong, M.J.; Chiew, J.J.; Teh, K.C.; Tan, J.; Lim, S.S.; Foo, D.C.Y. An integrated approach for sustainability assessment with hybrid AHP-LCA-PI techniques for chitosan-based TiO<sub>2</sub> nanotubes production. *Sustain. Prod. Consum.* **2020**, *21*, 170–181, doi:10.1016/j.spc.2019.12.001.
25. Saaty, T.L. Decision making with the Analytic Hierarchy Process. *Int. J. Serv. Sci.* **2008**, *1*, 83–98, doi:10.1504/ijssci.2008.017590.
26. Lipušček, I.; Bohanec, M.; Oblak, L.; Zadnik Stirn, L. A multi-criteria decision-making model for classifying wood products with respect to their impact on environment. *Int. J. Life Cycle Assess.* **2010**, *15*, 359–367, doi:10.1007/s11367-010-0157-6.
27. Saaty, T.L. *Fundamentals of Decision Making and Priority Theory with the Analytic Hierarchy Process*; Pittsburg, 1994;
28. Saaty, T.L. Decision-making with the AHP: Why is the principal eigenvector necessary. *Eur. J. Oper. Res.* **2003**, *145*, 85–91, doi:10.1016/S0377-2217(02)00227-8.
29. Winston, W.L. *Operations Research: Applications and Algorithms*; Wadsworth Publishing Company: Belmont, CA, 1994;
30. Handfield, R.; Walton, S. V; Sroufe, R.; Melnyk, S.A. Applying environmental criteria to supplier assessment: A study in the application of the Analytical Hierarchy Process. *Eur. J. Oper. Res.* **2002**, *141*, 70–87.

# An initial exploration of measures of transport efficiency through optimising a simple truck model

Khashayar Shahrezaei<sup>1,\*</sup>, Ciarán J. O'Reilly<sup>1,2</sup>, Timo Lähivaara<sup>3</sup> and Peter Göransson<sup>1,2</sup>

<sup>1</sup>*KTH Royal Institute of Technology, Teknikringen 8, 100 44 Stockholm, Sweden*

<sup>2</sup>*The Centre for ECO<sup>2</sup> Vehicle Design, Teknikringen 8, 100 44 Stockholm, Sweden*

<sup>3</sup>*University of Eastern Finland, Yliopistonranta 1, 70210 Kuopio, Finland*

\* *Corresponding author. Email: khasha@kth.se*

---

Sustainability has become a very important research area in transportation where demands and associated environmental impacts have been increasing. An introductory exploration is established here, where transport efficiency is studied in two partial measures, mass efficiency and volume efficiency. An optimisation problem is then formulated here to find an acceptable design configuration that merely satisfies the transport constraints and maximising transport efficiency. It is observed that there are trade-offs between environmental impacts in terms of energy requirement and the optimised design configuration.

© 2021 by the authors. Published by the Resource Efficient Vehicles Conference.  
This is an open access article under the CC BY license (<http://creativecommons.org/licenses/by/4.0/>).

---

## 1. Introduction

The activity of transport sector shows significant growth driven by developments in the economy [1]. This growth increases the demands on road freight transportation together with associated emissions and environmental damages. Hence, the sector stresses the need for secure energy supplies, sustainable energy consumption, lower fossil fuel dependence, and improvements in transport efficiency. In order to fulfil these demands, optimisation methodology frameworks are required to find the optimum transportation solutions and simultaneously decrease the associated environmental impacts and damages [2].

Up to date, there is no standard definition of transport efficiency, whilst emerging consensus indicates that economy, environment, and social well-being have a great impact on transport efficiency or sustainable transport system [3, 4]. In other words, an efficient transport system not only involves economic measures, but also involves the usage of resources, and environmental impacts associated with the sector. Improvement in transportation requires improvement over the ability to deliver goods without wasting resources such as materials, time, and energy [5]. Finding new solutions for improvement requires balancing a large number of measures which can exhibit a conflicting interaction with each other. Hence, exploring and analysing efficiency of such a system is essential towards sustainable development of the freight transport system. The main question remaining is how can we design vehicles such as delivery trucks which are optimum from transport system perspective?

A major challenge in vehicle design is to simultaneously meet the transport demands while minimising energy use and its associated environmental impacts [6]. In order to meet this challenge optimum design methodologies are relevant to consider all aspects of a finished design to achieve an optimal trade-off design between economic, environmental and technical parameters. The main

focus of this paper is to formulate an optimisation problem to examine the merits of different vehicle designs from transport system perspective. Here, it is proposed to examine the goodness of the vehicle design by introducing two basic partial design efficiencies, mass and volume efficiency. The objective of this paper is to merge these two mentioned partial efficiency measures into a unified efficiency measure and integrate them into a multidisciplinary design optimisation methodology framework. This integration is used directly to explore transport efficiency. Furthermore, this paper aims to explore trade-offs between the conceptual model and its energy requirement. For instance, what are the trade-offs between energy requirement and the optimum design configuration when the optimiser increases the height of the truck to establish more aerodynamic truck? Therefore, trade-offs between the choice of structural and non-structural characteristics of trucks are directly integrated into an optimisation problem and been analysed in a static drive-cycle simulation.

## 2. Methodology outline

In this section the main building blocks of the exploration is presented and discussed.

### 2.1 Conceptual simple truck model

Vehicles may be described as a multi-functional system, and must fulfil both the physical requirements of transportation and the regulatory requirements to be approved for sale and use [6]. Vehicle's main function is usually specified as to carry and move payload from point A to B, i.e. to transport. Hence, an abstract model of a multi-functional truck has been developed here through functional decomposition approach to capture transport function. The decomposed functions are load-carrying and movement function. Load-carrying function examines the physical ability of the truck to carry payload, whilst, movement function examines the required energy to move the truck. These two decomposed sub-functions are cross-dependent with design configuration of the truck, which means, changes in design configuration may alter the performance of each decomposed function and essentially the main function.

To model the truck and capture the resulting concept and trade-offs in a conceptual model, the emerging computational model comprises a certain level of computational granularity. This means that the truck is functional decomposed according to transport function and multiple parallel computational models is required to create the overall conceptual model of the truck. The interdependency structure of the constituent computational models is illustrated in Fig. 1. Here models compute an intermediate result based on inputs. The level of granularity of the model may impact different model properties such as precision, accuracy, fidelity, and modularity of the model [7]. However, the fact that vehicles are multi-functional systems, a multidisciplinary and interdependent conceptual model can be established by functional decomposition where each function then performs a portion of the main function.

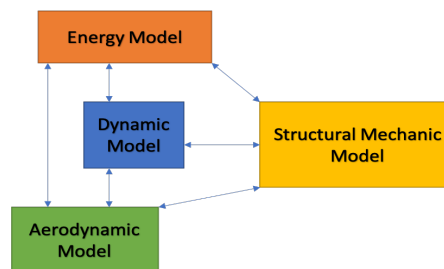


Figure 1: The decomposition of truck model according to transport function.

As the focus of this paper is on exploring transport efficiency, the complexity of the truck model, its functionalities, and the optimisation thereof, are purposely kept simple. In order to explicitly

couple all the computational models, a simplified chassis, a simplified suspension, and a payload with constant volume has been developed. The simplified chassis has a load-carrying function and it is modelled as a beam with certain second moment of area. The beam shown in Fig. 2 creates an explicit link between all computational models shown in Fig. 1, since the modelled beam has a certain mass which influence the overall energy consumption, a cross sectional area which influence the aerodynamic performance, and a certain bending stiffness which influence the dynamic and structural performance of the truck. Changing the design variable of the beam impacts the second moment of area, thereof overall performance of the truck. For example, an increase in second moment of area means an increase in mass, cross sectional area, bending stiffness and essentially give rise to energy consumption and better load-carrying performances, i.e a trade-off. Furthermore, the simplified suspension system has a hyphenate function and it is a simple assumption of wheel support points. Changing the location of these support points impacts the structural strength and thereof load-carrying function. The support points considered to be fixed at the distance of 0.1 and 0.8 length unit from left and respectively right end of the beam as it is illustrated in Fig. 2. Furthermore, there are two assumption regarding the payload, firstly, the volume is constant, and secondly, the length of the vehicle is equal with the length of the payload. These two assumption also creates an explicit link between all computational models shown in Fig. 1. For example, an increase of length will reduce the height of the payload and add more weight to the truck, thereof it will decrease the required energy to overcome aerodynamic resistance, increase the required energy to overcome rolling resistance and inertia resistance to accelerate, and also decrease the bending stiffness of the beam thereof load-carrying performances.

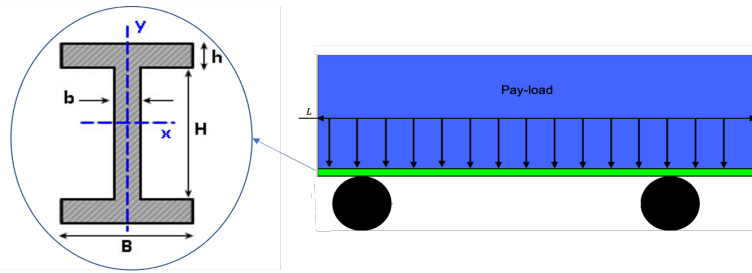


Figure 2: The simple truck model to be optimised with set of design variables.

Table 1: List of design variables and their minimum, maximum, and initial value.

Variable	Minimum value	Maximum value	Initial value
$K$	0.01	100	1
$L$ (m)	0.01	100	10

### 2.1.1 Design variables

The simplified chassis, i.e. the beam, has two design variables that ensures the truck model has an effectively acceptable configurations for the specified goals and simultaneously couple all the decomposed functions. These two variables are the cross-sectional area scale factor  $K$  and length of the beam  $L$  which essentially is the length of the truck and the payload. The cross-sectional area scale factor, essentially scales the second moment of area to ensure high enough bending stiffness. The cross section profile of the beam is selected to be I-shaped as it is illustrated in Fig. 2. Structure steel has been selected as the material which has Young's modulus of 210 GPa and a density of 7.80

$\text{kgm}^{-3}$ . The payload shown in Fig. 2 has a constant mass ( $m_p$ ) of 10 tonne and a constant density ( $\rho_p$ ) of  $500 \text{ kgm}^{-3}$ . These variables are kept constant to enable the optimiser to find the optimum length  $L$  for the payload which essentially influence the height of the payload where it allocates portions of the total height of the truck. The height of the payload ( $H_P$ ) may be expressed as

$$H_P = m_p / \rho_p L B. \quad (1)$$

The second moment of area may be expressed by parallel axis theorem as

$$I = \left[ \frac{H^3 b}{12} + 2 \left[ \frac{h^3 B}{12} + \frac{hb(H+h)^2}{4} \right] \right] K^4 \quad (2)$$

where  $A$  is the area of the cross-section,  $K$  denotes scale factor and the reset of the parameters are the variables which configure the cross section of the beam as it is shown in Fig. 2. The initial value selected for second moment of area is  $I_0 = 2 \times 10^{-3} \text{ m}^4$ . The minimum, maximum, and initial values of the design variables inserted into the optimiser are shown in Table. 1.

### 2.1.2 Energy Model

To determine the total energy required for transportation,  $W_T(X, s)$  is expressed as [8, 6]

$$W_T(X, s) = W_R(X, s) + W_A(X, s) + W_D(X, s) \quad (3)$$

where

$$W_R(X, s) = (1 - r) g c_R m(X) \int_{s_0}^{s_1} ds \quad (4a)$$

$$W_A(X, s) = m(X) \int_{s_0}^{s_1} a(s) ds \quad (4b)$$

$$W_D(X, s) = 0.5 \rho_a c_D A(X) \int_{s_0}^{s_1} v^2(s) ds, \quad (4c)$$

where  $W_R(X, s)$ ,  $W_A(X, s)$ , and  $W_D(X, s)$  refers to the energy to overcome rolling resistance, aerodynamic drag, and inertia resistance to acceleration respectively at distance  $s$ . Variable  $r$  is a fraction (in %) which is the kinetic energy regained during the deceleration,  $m$  is the total mass,  $c_R$  is the rolling resistance coefficient,  $\rho_a$  is the air density,  $c_D$  is the drag coefficient, and  $A$  is the frontal area of the vehicle. The rest of the remaining parameters,  $a$  (acceleration),  $v$  (velocity), and  $s$  (distance) are the characteristic value in which are depended on the profile of the drive cycle. Furthermore, the Worldwide Harmonized Light-Duty Vehicles Test Procedure class 3b (WLTP3) is employed as the prescribed drive-cycle and represents one delivery route.

## 2.2 Transport efficiency measures

Efficiency measures are often expressed by the ratio of useful output to total input and transport efficiency measures refers to the actual transportation output as a percentage of an ideal situation [9]. An efficiency of 100% means that the theoretical, ideal situation is attained. For instance, 100% time efficient vehicle means, the vehicle is utilised non-stop, 24-h a day. An efficiency measure below 100% means an insufficient actual transportation and depending on the dimension of the measurement whether the actual value should be the numerator and the ideal value denominator.

In an effort to explore trade-offs between transport function and design configuration and simultaneously merit transport efficiency, two efficiency measures were employed, mass efficiency and volume efficiency. These two efficiency measures were merged into a unified efficiency measure to

further evaluate transport efficiency and exploit trade-offs between functions and design configuration. The unified transport efficiency measure may be expressed as:

$$\eta_T(M, V) = \eta_M(X)\eta_V(X), \quad (5)$$

where  $\eta_T$  indicate the transport efficiency,  $M$  denotes mass,  $V$  volume, and  $X$  denotes a set of design variables. Further detail of each partial efficiency measure is provided in subsequent sections.

### 2.2.1 Mass efficiency

Mass efficiency is a qualitative measure of the ratio of required energy to move the payload to total mass of the truck. This is determined by mass dependent energy, i.e the energy consumed due to rolling resistance and inertia resistance to acceleration. An 100% mass efficiency means that the actual consumed energy during transportation is due to transportation of payload without any waste. In other words, the allocated energy to move the structural weight of the truck must be minimised to increase such efficiency. Mass efficiency is expressed as

$$\eta_m(X) = \frac{E_p(X)}{E_{tot}(X)}, \quad (6)$$

where  $E_p$  denotes the energy it requires to move the payload and  $E_{tot}$  denotes the required energy to move the total mass of the truck (payload + structural weight).

### 2.2.2 Volume efficiency

Volume efficiency refers to the capacity of the payload and it is measured in terms of space. It is defined as the percentage by which payload allocates space of the total volume of the truck. An optimum volume or 100% volume efficient truck may be the same as if the whole truck would be just the payload. Volume efficiency is expressed as

$$\eta_V(X) = \frac{V_p(X)}{V_{tot}(X)}, \quad (7)$$

where  $V_p$  denotes volume of the payload, and  $V_{tot}$  denotes the total volume of the truck (structural volume + payload volume).

## 2.3 Formulation of the optimisation problem

The importance of properly formulating a design optimisation problem must be stressed because the optimum solution will be only as good as the formulation [10]. The optimisation problem formulated here aims at finding an acceptable design that satisfies the transport constraints and maximising the unified transport efficiency. This is done numerically using computational resources which enables much larger designs to be explored. Even though in general there is more than one acceptable design, optimisation has the purpose of finding the best one of many acceptable designs available.

In the present multi-functional design optimisation, the unified transport efficiency measure is integrated and selected as the objective function to be optimised in a multidisciplinary design optimisation [10]. As mentioned before, two partial measures are considered as the main contributor factor to explore transport efficiency. The mathematical design optimisation problem to explore trade-offs in transport efficiency may be expressed as

$$\min(1 - \eta_T(M, V)) \quad (8)$$

subjected to constraints of the form:

$$T^E(X) \leq 0 \quad (9)$$



$$T^I(X) = 0 \quad (10)$$

$$X_{\min} \leq X \leq X_{\max} \quad (11)$$

Equations 9 and 10 are the set of transport-related functional equality and inequality constraints. Equality constraints arise quite often as a physical law, which must be solved as a sub-problem in order to assess an inequality constraint [6]. For instance, inequality could be that the maximum deflection is less than 1 cm, which might need to be assessed by solving the Euler-Bernoulli beam equation (an equality relation) before assessing the original constrain. An example of an inequality constraint could be that the design must carry at least a 100 kg load. Equation 11 is the set of design variable constraints. The variables are constrained by the minimum and maximum values as indicated by the indices.

Transport functions act as constraints on the design considering different properties: mechanical, i.e., bending stiffness, load capacity, and eventually other disciplinary fields. Although more functions and constraints may need to be considered in a realistic design, the constraints considered here are sufficient to fulfil the exploration as such. In this study two constraints were employed to examine trade-offs between functions and the optimum design configurations. Firstly, one linear elastic loading response is used to incorporate the load-carrying function of the beam. Secondly, maximum height constraints are set to evaluate the aerodynamic performance of the truck. Engaging these constraints, emphasis the trade-offs examination. For example, trade-offs between shorter lighter truck and longer heavier but more aerodynamic truck. These two constraints may be expressed as:

$$\frac{d}{d_{\max}} - 1 \leq 0 \quad (12a)$$

$$\frac{H}{H_{\max}} - 1 \leq 0, \quad (12b)$$

where  $d$  is the bending displacement of the beam and  $H$  is the total height of the truck inclusive wheels, beam height, and payload height. Verification that the bending displacement constraint is met is achieved by computing the linear elastic response via the Euler-Bernoulli equation. The maximum bending displacement selected for the first constraints is  $d_{\max} = 10 \times 10^{-3}$  m, and the maximum height for the truck is set to be  $H_{\max} = 4$  m.

## 2.4 Results

In this study, the optimisation is performed for the unified transport efficiency measure as the objective function. The optimum design variables are used to examine possible trade-offs between the conceptual truck model and energy demand. Table. 2 shows the optimum design variables, corresponding objective function value and the total mass of the I-Beam.

Table 2: Resulting optimal design variables, objective function value and total design mass.

Variables	K [-]	L [m]	$\eta_T$ [%]	m [kg]
Initial Values	1	10	0.024	4992
Optimum Values	0.21	3.23	1.06e-04	70.01

As been seen, the solution tends to a solution with minimum weight and it is achieved by reducing the length of the truck, which consequently reduce the scale factor for the beam too. This reduction of

values provides high enough bending stiffness for all functional constraints to be satisfied. However, reduction to initial beam length has increased the height of the truck. It is observed that the energy needed to overcome aerodynamic resistance has considerably increased due to increased height of the payload (Fig. 3) and consequently the height of the truck. From the result presented, it is clear that there is trade-off between energy consumption and design configurations of the conceptual truck model. Although the actual design configurations themselves might be inconsequential, the fact that trade-off is identified is of considerable significance.

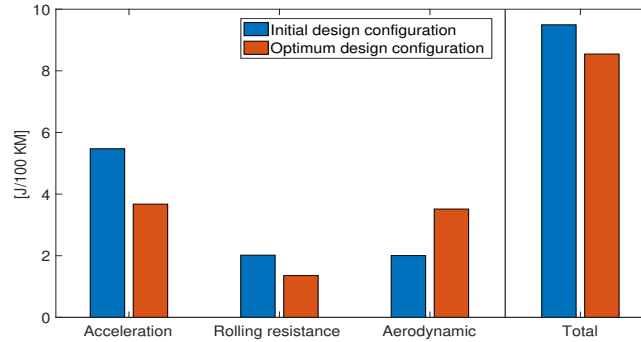


Figure 3: Normalised use phase energies, a direct comparison between initial and optimum design.

### 3. Discussion

An initial exploration of transport efficiency measures have been presented, where different partial transport efficiency measures have been merged into a unified transport efficiency measure. This was done through the optimisation of a simple truck model. The unified transport efficiency measure was used as the objective function and formally integrated into a design methodology. This may be an enabler to explore what measures have a considerable influence on the unified transport efficiency measure under predefined circumstances. The exploration has roughly identified the design parameters and partial measures with significant influence on the unified efficiency measure. The results indicate that mass efficiency measure has a significant influence on the unified efficiency measure where the length of the truck is reduced in order to reduce mass. This mass reduction increases the unified transport efficiency measure, and less energy is required to move the structural characteristics of the truck, i.e. chassis.

However, the optimum solution and its trade-offs must be carefully examined. The introduced scale factor  $K$  changes the moment of inertia by a power of 4 and indeed have a significant impact on the load-carrying function of the truck. The second moment of area is an important property is crucial for determine the beam's bending deflection which examines the load-carrying function. The energy profile modelled for the truck in this work is highly weight-dependent due to the energies relative to rolling-resistance and inertial resistance to acceleration; while the energy required to overcome aerodynamic resistance is attributed to the frontal area of the entire truck and it is not weight-dependent. Thus mass efficiency measure appears to be the measure with the most influence on the unified transport efficiency measure where the design formulation here become effectively a mass minimisation problem. Furthermore, the design of the truck is significantly affected by the mass efficiency measure where the length of the beam is reduced in order to save weight; And there are two trade-offs related to this observation. Firstly, the truck is shorter and lighter, and secondly, the truck is less aerodynamic efficient. In other words, the energy required to overcome the aerodynamic resistance is increased, whilst the energy to overcome rolling resistance and inertia resistance due to acceleration is decreased.

## 4. Conclusion

In this paper, an exploration of various measures of transport efficiency has been initiated through optimising a simple truck model. The design has been optimised for the unified transport efficiency measure. Although the purpose of the case study was not to perform a real design, it nevertheless serves to illustrate the trade-offs. The optimisation formulation is successful in achieving a design, which meets the functional constraints and maximises the transport efficiency measure. Continued research is needed to see the performance of the transport efficiency using the same simple truck model in a dynamic drive cycle. It is important to explore the total transport efficiency where several dimension such as traffic flow and economy aspects are included.

## 5. Acknowledgements

The authors would like to thank the Centre for ECO2 Vehicle Design, which is funded by the Swedish Innovation Agency Vinnova (Grant Number 2016-05195). Also, this research was supported by the Academy of Finland (the Finnish Centre of Excellence of Inverse Modeling and Imaging) project 321761.

## References

1. European Commission, *EU energy, transport and GHG emissions: trends to 2050 : reference scenario 2016*. Luxembourg: Office for official publications of the european communities, 2016. OCLC: 1140951516.
2. T. Ghandriz, J. Hellgren, M. Islam, L. Laine, and B. Jacobson, "Optimization based design of heterogeneous truck fleet and electric propulsion," in *2016 IEEE 19th International Conference on Intelligent Transportation Systems (ITSC)*, (Rio de Janeiro, Brazil), pp. 328–335, IEEE, Nov. 2016.
3. C. Mihyeon Jeon and A. Amekudzi, "Addressing Sustainability in Transportation Systems: Definitions, Indicators, and Metrics," *Journal of Infrastructure Systems*, vol. 11, pp. 31–50, Mar. 2005.
4. P. Maheshwari, R. Khaddar, P. Kachroo, and A. Paz, "Dynamic Modeling of Performance Indices for Planning of Sustainable Transportation Systems," *Networks and Spatial Economics*, vol. 16, pp. 371–393, Mar. 2016.
5. J. Fu and E. Jenelius, "Transport efficiency of off-peak urban goods deliveries: A Stockholm pilot study," *Case Studies on Transport Policy*, vol. 6, pp. 156–166, Mar. 2018.
6. C. J. O'Reilly, P. Göransson, A. Funazaki, T. Suzuki, S. Edlund, C. Gunnarsson, J.-O. Lundow, P. Cerin, C. J. Cameron, P. Wennhage, and J. Potting, "Life cycle energy optimisation: A proposed methodology for integrating environmental considerations early in the vehicle engineering design process," *Journal of Cleaner Production*, vol. 135, pp. 750–759, Nov. 2016.
7. J. F. Maier, C. M. Eckert, and P. John Clarkson, "Model granularity in engineering design-concepts and framework," *Design Science*, vol. 3, p. e1, 2017.
8. C. Koffler and K. Rohde-Brandenburger, "On the calculation of fuel savings through lightweight design in automotive life cycle assessments," *Int J Life Cycle Assess*, p. 8, 2010.
9. B. Tilanus and A. Samuelsson, "A framework efficiency model for goods transportation, with an application to regional less-than-truckload distribution," *Transport Logistics*, vol. 1, pp. 139–151, June 1997.
10. J. S. Arora, "Optimum design problem formulation," in *Introduction to Optimum Design (Second Edition)* (J. S. Arora, ed.), pp. 15–54, San Diego: Academic Press, second edition ed., 2004.

---

# Towards a multi-scale and multi-domain modelling of road cargo systems

Per-Olof Sturesson<sup>1\*</sup>, Stefan Edlund<sup>2</sup>

<sup>1</sup>*KTH Royal Institute of Technology, Teknikringen 8, 100 44 Stockholm, Sweden*

<sup>2</sup>*Volvo Group Trucks Technology, Gothenburg, Sweden*

\*Corresponding author. Email: [perplof@kth.se](mailto:perplof@kth.se)

---

The introduction of new technologies such as internet of things (IoT), autonomous driving (AD) and new propulsion system technologies, i.e. electrification, opens new perspectives of concept evaluation and selection. These challenge any form of optimization in the product development of future road cargo systems. In the early phase of product development data uncertainty, which is related to design degrees of freedom, is high. The difficulty in the mathematical modelling of road vehicle cargo systems in the concept phase lies in the definition of the principal parameters and their relations that captures the key questions to be answered in the product development decision process from i.e. a business and sustainability perspective. In a radical technological change and when introducing additional domains to the vehicle like general infrastructure and IoT services in the model, the outcome may be different as well as the engineering challenges. This paper focuses on the definition of a general framework for modelling of road vehicle cargo systems using a multi-scale and modelling approach and provides an outlook for future studies.

© 2021 by the authors. Published by the Resource Efficient Vehicles Conference.  
This is an open access article under the CC BY license (<http://creativecommons.org/licenses/by/4.0/>).

---

## 1. Introduction

The quest for means to mitigate the ongoing climate change has resulted in introduction of different new technologies, which may disrupt since long established business models for OEM:s, their supplier chain and also clients. Examples of new technology trends are the transition from internal combustion engines to more sustainable propulsion systems, connectivity, digitalization and advanced driver assistance system. The change in propulsion technology may also affect the society as a whole as the existing eco-system of energy supply and distribution (petrol & diesel) for road transportation will see a significant change in demand while alternative propulsion technologies, which need to have much less CO<sub>2</sub> footprint, will require investments in the transitioning energy system including generation, supply and distribution. As a consequence, the drivers for peak oil may change compared what has historically been put forward [1].

The development of road cargo systems featuring propulsion system(s) with low or zero CO<sub>2</sub> emission is evolving at current time. As product development in the heavy truck industry as well as the automotive industry in general is by its nature evolutionary, the introduction of new innovative and disruptive technologies like electrification of the propulsion system and autonomous driving, yields a high degree of uncertainty in the conceptual decision making process of i.e. a vehicle architecture. The systems, especially the energy buffer system, may dominate vehicle capabilities and characteristics like curb weight and maybe most important, cost. From a stakeholder perspective,

which may range from OEM over transport provider to society, it is therefore essential that the conceptual decisions taken are as optimal and robust as possible.

The conceptual decisions of a vehicle architecture for heavy truck applications, featuring electrical propulsion system and/or autonomous capabilities, depend on the operational context on the vehicle such as long distance hauling, distribution or construction but also on capabilities and characteristics of systems that are exogenous to the vehicle such as infrastructure (energy distribution, road and connectivity systems) and services, see Fig. 1.

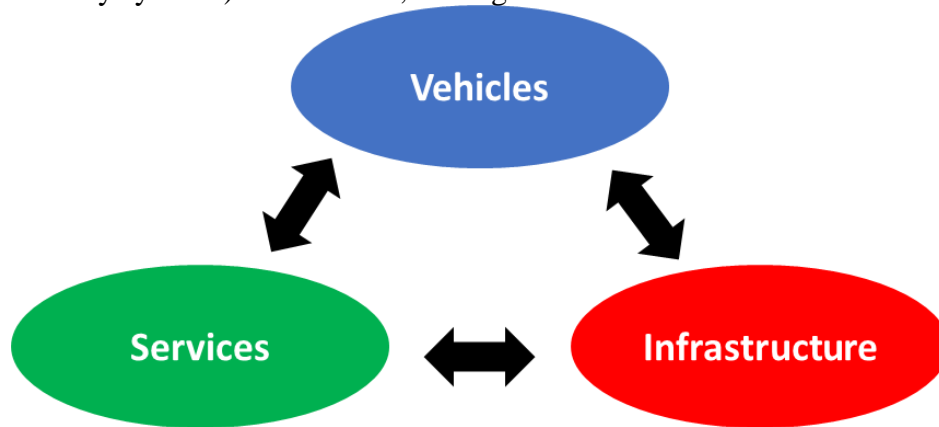


Figure 1: Transport scenario and solutions with domains.

Characteristics and capabilities of the different domains (vehicles, infrastructure and services) interacts dynamically and feature also different inertia or time lags. Additionally, stakeholders for each domain are different, varying from private (providers and clients) to federal (authorities and communities) and also the public (clients and opinion and values). The financial funding and transactions for realization of the product development and manufacturing of vehicles, the infrastructure and services are also complex in general and feature also different stakeholders, ranging from business to federal authorities as well as the public.

Disruptions by means of new technologies are not a new event, there are examples in consumer products to learn from like the transition from vacuum tubes to semiconductors, photographic film to digital technology and cell phones to smart phones. The driving factors behind the disruption are many. More advantageous price and product capabilities and performances for the customer are likely to create the tipping point towards new technologies from a consumer preference.

In case of transportation infrastructure and systems there are also examples to learn from like transition to railways from canals and river based conveyance of small size cargo carriers and then from railways to roads. The drivers behind these two transitions are technology based inventions; the steam locomotive and the combustion engine. These two inventions did not by themselves drive the two transitions alone. Funding and construction of railway and road systems by both federal and private means were important to realize the transition. The approaches applied in the transition phase to railway, mainly in the 19<sup>th</sup> century in Western Europe and United States, ranged from governmental bonds and grants to private companies as well as fully state implementation depending on country. In the case of road infrastructure investments several decades later the implementation relied mainly on public authorities, federal or state level.

The development of production and distribution systems for electrical power in Western Europe and United States is in general driven by a mixture of state and private implementations depending on country in contrast to petroleum based products where private enterprises have played the major role.

The transition to electrical propulsion system for road transportation requires substantial investments in additional electrical power generation independent of battery electric vehicles or hydrogen propelled fuel cell vehicle will dominate the future roads. Additionally, infrastructure investments in energy distribution for electricity to a network of charging stations or hydrogen stations may also be needed. The time lag and inertia of introducing new innovations in infrastructure may also be different from the product development rate in the heavy vehicle industry.

Standardisation of hardware components and software protocols for energy charging is another factor that may also be an important factor for transition rate of electrification of propulsion system. This may be an enabler for faster customer acceptance and purchase decision making.

The application of system dynamics modelling and simulation of transportation systems has been applied for several decades [2]. The system dynamics approach connects qualitative and quantitative models. The qualitative models incorporate input and output causal relationship between different entities and also feedback loops often displayed by causal loop diagrams (CLD). In case of the feedback loops, which either are positive (or reinforcing) or negative (or balancing) the system dynamics of a model can then feature dynamic equilibrium. Modelling complex systems in detail by causal loop diagrams may result in a model that is too difficult to understand. The benefit of using causal loop diagrams during conceptualization varies [3][4]. Most often quantitative results may be requested for decision making purposes resulting in the need models build on mathematical representation of input and output relationship including feedback loops with gain and time lag.

Transportation system simulations using system dynamics modelling is usually restricted to one of the domains viewed in Fig. 1 [6] or statically in the meaning that critical dynamic interaction or feedback between subsystems are not included. Efforts to optimise vehicle concepts with respect to mainly total cost of ownership have been done considering interaction to road infrastructure for different propulsion concepts and truck configurations [6]. One observation is that the optimisation problem quickly gets very large as the number of vehicle configurations is substantial. Optimality of the solution may then be an issue. Problem size could be reduced when introducing performance based constraints.

During the conceptual phase in vehicle engineering data uncertainty is high. A detailed model with many degrees of freedom may look credible at a glance but may feature many sources of critical errors. Such a model may therefore not be “useful” (quote by G.E.P Box “Essentially, all models are wrong but some are useful”). Understanding or exercising a model, by changing the model inputs and assess if response is reasonable, is important to find potential flaws. A simpler model will therefore be more advantageous.

Reduction of development time and cost while increasing or keeping quality is an intricate task that many automotive OEM is focusing on. A high performing and effective product development organization is a competitive advantage as more products can be put the market faster [6]. Adding high innovation rate as a feature in the product development system is an intriguing challenge where many automotive OEMs fail. The traditional engineering design practice, independent of concurrent or not, quickly converge, often early in development process, into a single solution, a point in the solution space, then tries to optimize the solution through several iterations or loop-backs. This might be a time and cost effective approach unless the starting point is wrong, which is not unusual [7].

Some companies, mainly in the software industry, have been successful with iterative and incremental approaches. This might be effective when feedback cycles are fast, often daily, and cost of rework is low but also when quality of initial starting point is high [7]. When cost of rework is high, feedback loops are long and quality initial starting point is low different approaches may be applied like set based concurrent engineering [7]. This situation may also hold for future

transportation systems. The main principle in set based concurrent engineering is to postpone the concept selection as late as possible when data uncertainty is significantly lower in the development process while keeping and assessing several design alternatives and in each iteration eliminating the weakest alternative. This may then yield into less iterations and costly rework.

The conceptualization of complex systems like road cargo system is of importance in the early phase of product development. The introduction of new technologies in transportation systems involve many different stakeholders. As data exhibits high levels of uncertainty the understanding of system dynamics response including architecture trade-offs is beneficial in the product decision making process. With introduction of new technologies like electrification of the propulsion system the analysis is crucial to support decision at hand. This paper focus on basic definition of the general framework for modelling of road cargo systems using a multi-scale and modelling approach.

## 2. General Framework for Road Cargo Systems Modelling

The general framework for modelling road cargo systems was developed from the domain model depicted in Fig. 1 where the framework followed the template shown in Fig. 2. For each domain the context, e.g. the boundary conditions, dynamic or static, are defined together with system interaction to other domains. With characteristics is here meant engineering data and interfaces like weight or propulsion system power in the case of vehicle domain. In case of infrastructure the characteristics

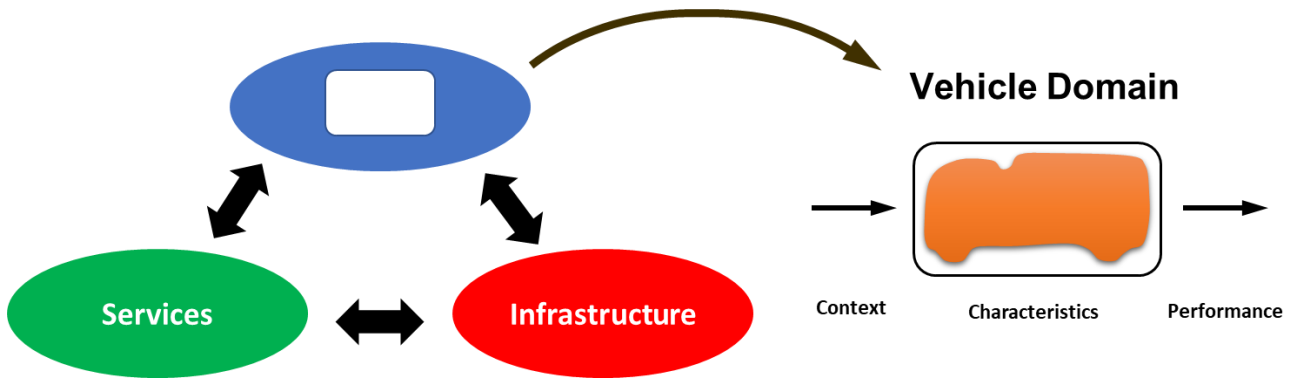


Figure 2: Domain template for road cargo system framework.

can be road width or length. Performance may be static or dynamic attributes that feature a domain like cost, safety or drivability in case of vehicle while in the case of infrastructure performance metrics can be traffic flow. The idea is to try to achieve symmetry and analogous metrics in the domains. The infrastructure domain may contain not only road infrastructure but also infrastructure for energy distribution and digital data (information). Further examples are provided in Table 1.

Table 1: Examples of key characteristics and performances.

Domain	Context	Characteristics	Performances
<b>Vehicles</b>	<ul style="list-style-type: none"> <li>• Transport Mission</li> <li>• Infrastructure</li> <li>• Service</li> </ul>	<ul style="list-style-type: none"> <li>• Structural (load carrying) weight</li> <li>• Non-structural weight <ul style="list-style-type: none"> <li>• Propulsion</li> <li>• Energy buffers</li> <li>• Other</li> </ul> </li> <li>• Propulsion characteristics</li> <li>• Energy buffers size</li> <li>• Charging capability</li> <li>• Digitalization level</li> </ul>	<ul style="list-style-type: none"> <li>• Load capacity</li> <li>• Range</li> <li>• Energy consumption</li> <li>• Drivability</li> <li>• Safety</li> <li>• Uptime</li> <li>• User Experience</li> <li>• Product Cost &amp; CO2 impact</li> <li>• Operational Cost &amp; CO2 impact</li> </ul>



<b>Infrastructure</b>	<ul style="list-style-type: none"> <li>• Transport Mission</li> <li>• Service</li> <li>• Vehicle</li> </ul>	<i>Road</i> <ul style="list-style-type: none"> <li>• Width / # of lanes</li> <li>• Length</li> <li>• Topography</li> <li>• Speed limits</li> <li>• Axle load limits</li> <li>• Road profile</li> <li>• Digitalization level</li> </ul>	<i>Road</i> <ul style="list-style-type: none"> <li>• Traffic flow</li> <li>• Uptime</li> <li>• Specific Safety</li> <li>• Specific Energy Consumption</li> <li>• Specific CO2 Emission</li> <li>• Specific Noise</li> <li>• User Experience</li> <li>• Construction Cost &amp; CO2 impact</li> <li>• Operational Cost &amp; CO2 impact</li> </ul>
		<i>Energy</i> <ul style="list-style-type: none"> <li>• Distance between fuel/charging</li> <li>• Charging limitations</li> <li>• Digitalization level</li> </ul>	<i>Energy</i> <ul style="list-style-type: none"> <li>• Fuel/charging time</li> <li>• Uptime</li> <li>• User Experience</li> <li>• Construction Cost &amp; CO2 impact</li> <li>• Operational Cost &amp; CO2 impact</li> </ul>
		<i>Digital</i> <ul style="list-style-type: none"> <li>• Availability</li> <li>• Functionality</li> <li>• Bandwidth</li> </ul>	<i>Digital</i> <ul style="list-style-type: none"> <li>• Latency</li> <li>• Uptime</li> <li>• User Experience</li> <li>• Construction Cost &amp; CO2 impact</li> <li>• Operational Cost &amp; CO2 impact</li> </ul>
<b>Services</b>	<ul style="list-style-type: none"> <li>• Transport Mission</li> <li>• Infrastructure</li> <li>• Vehicle</li> </ul>	<ul style="list-style-type: none"> <li>• Functionality</li> <li>• Processing capacity</li> <li>• Adaptability               <ul style="list-style-type: none"> <li>• Customers</li> <li>• Standards</li> </ul> </li> <li>• Cyber security</li> </ul>	<ul style="list-style-type: none"> <li>• Overall Equipment Effectiveness               <ul style="list-style-type: none"> <li>• Time utilization</li> <li>• Load Capacity utilization</li> <li>• Energy efficiency / utilization</li> </ul> </li> <li>• Uptime</li> <li>• Response time</li> <li>• User Experience</li> <li>• Product Cost &amp; CO2 impact</li> <li>• Operational Cost &amp; CO2 impact</li> </ul>

The general framework for modelling road cargo systems was developed from the domain model. Inclusion of financial transactions may be possible to include as well. In Fig. 3 the networks for goods, energy, information and financial flow is shown.

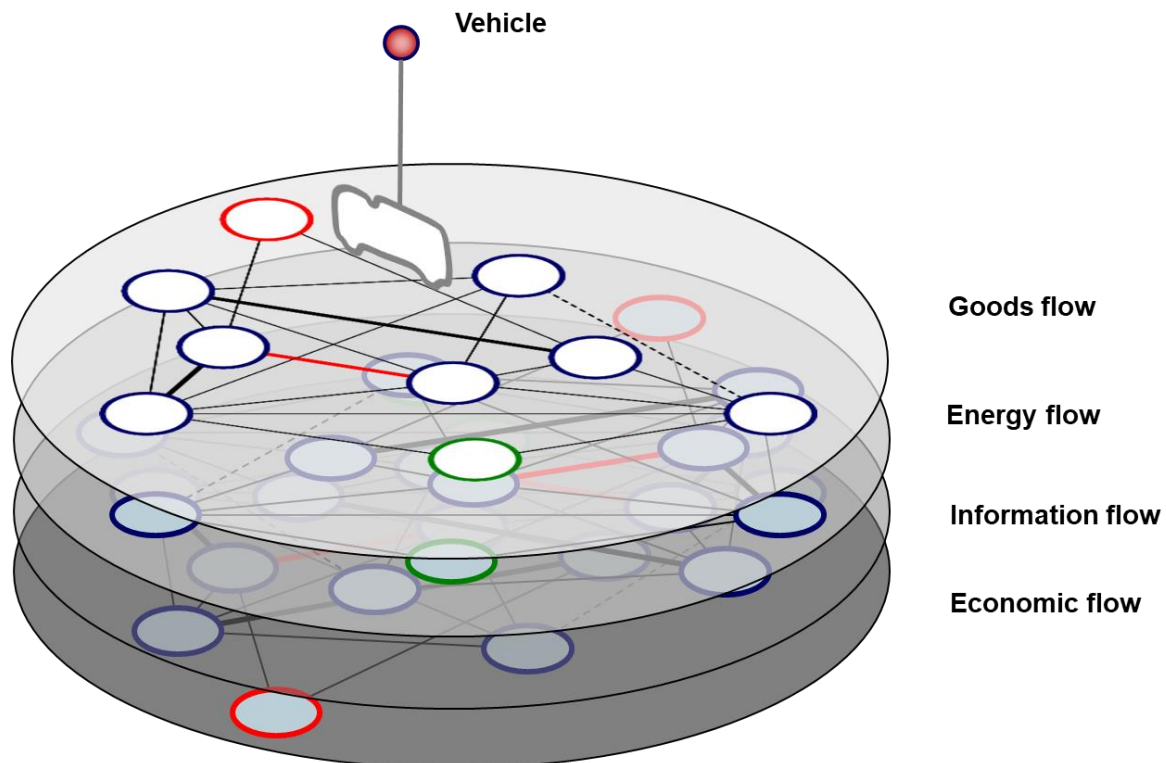


Figure 3: Domain networks including financial transactions.



### 3. Discussion

A general framework for modelling road cargo systems featuring interactions that in the next step may be modelled using system dynamics approach is suggested. The framework holds for each domain system context, characteristics and performance. The next step is to quantitatively model the interaction between the domains using as simple models as possible to understand system response and assess and reconcile data to other models and empirical data.

### Acknowledgment

The authors are grateful for all discussions, opinions and inputs by staff members at Volvo Group Technology and KTH Royal Institute of Technology, Centre for ECO2 Vehicle Design.

### References

1. T. Seba, Tony Seba: Clean Disruption - Energy & Transportation, <https://www.youtube.com/watch?v=2b3ttqYDwF0>, 2017.
2. S.P. Shepherd, A review of system dynamics models applied in transportation, *Transportmetrica B: Transport Dynamics*, 2:2, 83-105, DOI:10.1080/21680566.2014.916236, 2014.
3. G.P. Richardson, Problems with causal-loop diagrams. *System Dynamics Review*, 2(2), 158-170, 1986.
4. J. D. W. Morecroft, A Critical Review of Diagramming Tools for Conceptualizing Feedback System Models, *Dynamica* 8(1): 20-29, 1982.
5. T. Ghandriz, Transportation Mission Based Optimization of Heavy Vehicle Fleets including Propulsion Tailoring, Licentiate Thesis, Chalmers University of Technology, 2018.
6. D. P. Oosterwal, *The Lean Machine - How Harley-Davidson drove top-line growth and profitability with revolutionary lean product development*, ISBN 978-0-8144-3288-4, Amacom, 2010.
7. D. K. Sobek II, A.C. Ward and J.K. Liker, Toyota's Principles of Set-Based Concurrent Engineering, *MIT Sloan Management Review*, Vol 40, Issue #2, 1999.

---

# On the trade-off between noise exposure cost and resource efficiency in traffic

Johan Nygren<sup>1,2,3,\*</sup>, Susann Boij<sup>1,2,3</sup>, Romain Rumpler<sup>1,2,3</sup> and Ciarán J. O'Reilly<sup>1,2</sup>

<sup>1</sup>*KTH Royal Institute of Technology, Teknikringen 8, 100 44 Stockholm, Sweden*

<sup>2</sup>*The Centre for ECO<sup>2</sup> Vehicle Design, Teknikringen 8, 100 44 Stockholm, Sweden*

<sup>3</sup>*MWL, The Marcus Wallenberg Laboratory of Sound and Vibration Research, Teknikringen 8, 100 44 Stockholm, Sweden*

\*Corresponding author. Email: [johnygr@kth.se](mailto:johnygr@kth.se)

---

Achieving sustainable transport involves a trade-off between providing transportation while reducing traffic-related impact, such as improving resource efficiency and reducing the noise exposure. Previous studies showed that the trade-off between reducing the noise exposure cost and reducing the energy demand is dependent on other factors than the vehicle itself. Being part of traffic in a road network, the interactions between other vehicles will affect both the necessary mechanical work associated with the motion of the vehicle, the energy demand, and the resulting noise exposure cost due to the noise emissions from each vehicle in the traffic flow and the vehicles' locations with respect to the measurement points in the network at which the noise exposure is evaluated. While initial results of microscopic traffic simulations indicate that a vehicle's energy demand and noise exposure cost are positively correlated, it is also shown that the vehicle-specific noise exposure cost does not correlate with the increase in system-wide noise exposure costs under peak traffic conditions. For vehicles travelling in the network during peak hours, this means that a reduction in the vehicle-specific noise exposure cost may not necessarily correspond to a lower rate-of-change for the system-wide noise exposure cost. A different allocation strategy may improve the correlation between the vehicle-specific noise exposure cost and the system-wide effects. The study aims to analyse the correlation between different vehicle-specific effects and system-wide effects in a microscopic traffic simulation. It also aims to analyse how a weighting-based allocation strategy for the vehicle-specific noise exposure cost affects the correlation between the vehicle-specific noise exposure cost and the rate of change of the system-wide noise exposure cost, and how this allocation strategy in turn influences the correlation between the energy demand and the vehicle-specific noise exposure cost.

© 2021 by the authors. Published by the Resource Efficient Vehicles Conference.  
This is an open access article under the CC BY license (<http://creativecommons.org/licenses/by/4.0/>).

---

## 1. Introduction

For transport to be sustainable, it is important not only to consider the provision of transportation but also to make sure it remains efficient and reduces the traffic-related effects, such as the health-related effects from traffic noise exposure. In a previous study [1], it was observed that a reduction in the vehicle-specific noise exposure cost, meaning the impact of noise exposure evaluated in monetary units for an individual vehicle, occurred under peak hour traffic conditions - under which the system-wide noise exposure cost increased the most. It was concluded that the preferred behaviour for the individual vehicles to reduce their individual noise exposure cost may not be the preferred

behaviour in terms of reducing the system-wide noise exposure cost. Another strategy in terms of the allocation of noise exposure cost from a system perspective down to each individual vehicle, based on their respective noise contribution, may reflect the system-wide effects during peak hours. An original allocation strategy, denoted here as the weighting-based allocation strategy, was then proposed [1]. The present study extends this work by analysing the correlation between the vehicle-specific noise exposure cost to the system-wide noise exposure cost increase and how this is affected by the weighting-based allocation strategy.

However, by changing the allocation strategy of the noise exposure cost to improve the correlation between the vehicle-specific- and the system-wide noise exposure cost, the relation between a vehicle's energy demand and duration to the vehicle-specific noise exposure cost will be changed as well. As the energy demand, the noise exposure cost and the duration in the network for a specific vehicle are all dependent on the driving behaviour, it means that a change in the behaviour to reduce the noise exposure cost will also result in a different energy demand. A change to the allocation strategy results in a different noise exposure cost and a different relation between the driving behaviour and the corresponding noise exposure cost. The preferred behaviour in terms of reduced noise exposure cost with this weighting-based allocation strategy may then be less beneficial in terms of lower energy demand or shorter duration. Therefore, this study also considers the correlation between the vehicle-specific noise exposure cost and the vehicle's energy demand and duration, which are used as proxies for the resource efficiency evaluation associated with individual vehicles and their specific driving behaviour.

## **2. Case study**

The case study introduced here uses vehicle kinematics data obtained from the microscopic traffic simulation software SUMO [2] to calculate each individual vehicle's noise exposure cost, energy demand and duration in the network. The vehicle-specific noise exposure cost is a monetary impact assessment of the resulting noise exposure at measurement points in the network, evaluated by means of a willingness-to-pay model. The method of calculating the vehicle-specific noise exposure cost based on the actual behaviour was proposed in [1]. A vehicle's energy demand is a measure of the necessary mechanical work to overcome the work arising from frictional forces exerted on the vehicle during its motion in the network [3, 4].

The present contribution extends the work performed in [1], and the same configurations in terms of road network, vehicle type and traffic demand are used here. In addition, the present study introduces a stochastic behaviour and studies how the observed variation in energy demand, noise exposure cost and duration correlate with each other for each individual vehicle over 100 simulations, each with a total simulation time of 24 hours. Including a stochastic behaviour enables the analysis of the performance of the weighting-based allocation strategy and how it impacts the correlation between the vehicle-specific noise exposure cost and the noise exposure cost evaluated at a system level. Using a weighting-based allocation strategy may also impact the correlation between the vehicle-specific noise exposure cost and energy demand, which will be investigated as well.

### **2.1 Road network**

The layout of the road network affects how the vehicles are able to move from their starting position to their destination. In the present study, a road network consisting of a total of 2 two-lane roads is implemented, see Fig. 1. The two roads intersect at two locations, resulting in a three-way junction at each intersection where one route will have a lower priority as they will have to make a left turn. This results in a total of 4 possible routes in the network between two points. In addition, 24 measurement points are located along each road, totalling to 48 measurement points in the network. It is at these points that the noise exposure is evaluated, and an associated noise exposure cost is calculated.

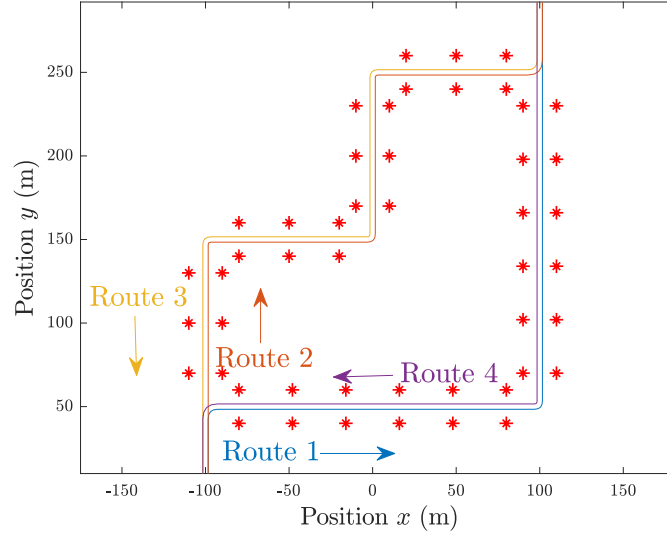


Figure 1: A map of the road network including the measurement points, marked as  $*$ , used for evaluating the impact of the noise exposure.

## 2.2 Traffic demand and vehicle properties

The traffic demand defines the amount of traffic on the network. It is represented here as how often a vehicle is entering the network. It is set up in such a way that there are two periods of high traffic demand, corresponding to peak traffic conditions where a large amount of vehicles are entering the network, with periods of low traffic demand in between with fewer vehicles entering the network per unit time. For more details on the specific traffic demand, see [1].

A vehicle's motion is modelled in SUMO using a vehicle follower model. The vehicle aims to drive at the speed of the lane it is currently driving on while keeping a certain safe distance to the leading vehicle in order to avoid collisions. In SUMO, a vehicle type is defined by certain parameters, see Table 1. The actual speed a particular vehicle will drive at will depend on the resulting speed factor, which is a normally distributed parameter defined by a mean, `speedFactor`, and a standard deviation, `speedDev`. Provided this target speed is below the maximum capable speed of that vehicle type, `maxSpeed`, the vehicle will try to maintain the target speed. A resulting speed factor value above 1 provides a target speed above the speed limit of the lane, meaning that the vehicle will inherently attempt to exceed the speed limit of the lane. In contrast, a value below 1 provides a target speed below the speed limit of the lane instead. Over the 100 simulations performed, the resulting speed factor of each vehicle will be a different value in each simulation.

In addition to the normal speed distributions, the vehicle's behaviour is altered by a driving imperfection parameter  $\sigma$ , which is a value between 0 and 1. For  $\sigma = 0$ , all vehicles of that type drive perfectly, whereas for  $\sigma > 0$  the driving quality will decay in the sense that they will have to continuously adjust their speed to keep distance to leading vehicles and to maintain their current target speed.

Table 1: Parameters defining the vehicle type in SUMO.

Parameter	Description	Value
length	Length of the vehicle	5.0 m
maxSpeed	Maximum capable speed	50.0 m/s
speedFactor	Mean of the normal speed factor distribution	1
speedDev	Standard deviation of the normal speed factor distribution	0.1
accel	Maximum acceleration	2.6 m/s <sup>2</sup>
decel	Maximum deceleration	4.5 m/s <sup>2</sup>
sigma	Driving imperfection parameter	0.5

In order to calculate a vehicle's energy demand, additional parameters related to the vehicle need to be defined, see [1, 3, 4]. The vehicle-related parameters, the rolling resistance, vehicle mass, drag coefficient and frontal area, that are used in the present study are defined in Table 2.

Table 2: Parameters used to define a typical light road vehicle.

Parameter	Description	Value
$f_R$	Rolling resistance	0.01
$m$	Vehicle mass	1500 kg
$c_D$	Drag coefficient	0.3
$A$	Frontal area	2 m <sup>2</sup>

Apart from the vehicle parameters in SUMO and to calculate the energy demand, the vehicle type is also defined in terms of its noise source characteristics. The noise source model IMAGINE [5] is used to model the noise emissions from each vehicle, together with an included correction factor for the source directivity from [6].

### 3. Methodology

#### 3.1 Calculating the noise exposure cost and resource efficiency

The noise exposure cost is based on a model by Andersson *et al.* of the willingness-to-pay associated with a certain noise exposure [7]. The resulting noise exposure cost  $C$  associated with a change in the noise exposure from  $L_1$  to  $L_2$ , given in A-weighted equivalent noise levels over a time  $T$ , is given by

$$C = \frac{T}{T_{1yr}} \frac{\max(L_2, L_{A,threshold}) - \max(L_1, L_{A,threshold})}{2} (\Pi(L_1) + \Pi(L_2)), \quad (1)$$

where  $T/T_{1yr}$  is the fraction of time  $T$  with respect to one year, and  $L_{A,threshold}$  is the A-weighted equivalent noise level threshold for the demand function  $\Pi(L)$ , given by

$$\Pi(L) = \begin{cases} 3859 - 173.4(75 - L), & L \geq L_{A,threshold} = 52.8 \text{ dB(A)}, \\ 0, & \text{otherwise.} \end{cases} \quad (2)$$

In [1], the resulting calculation of the vehicle-specific noise exposure cost  $C_{R,V_{ID}}(t_i)$ , at time  $t_i$  for vehicle  $V_{ID}$  associated with the measured noise exposure at measurement point  $R$ , uses the information of the individual vehicle's contribution to the noise, its estimated instantaneous mean-square pressure contribution  $\tilde{p}_{R,V_{ID}}^2(t_i)$ , and the information of the total traffic noise contribution,

$\tilde{p}_{R,traffic}^2(t_i)$ . The proposed weighting-based allocation strategy, shown in Eq. (3), uses weighting functions  $K(x)$  of the form  $K(x) = A_m x^m$ . The term  $A_m$  is used to normalize the results so that the sum of the vehicle-specific noise exposure costs over all time  $T$  and all vehicles is equal to the total traffic-related noise exposure cost  $C_{R,traffic}$ . In the present study, the vehicle-specific noise exposure cost was calculated with a linear weighting function for  $K_{VID}(x)$ , with  $m = 1$ , and  $K_{traffic}(x)$  was allowed to be either linear ( $m = 1$ ) or quadratic ( $m = 2$ ).

$$C_{R,VID}(t_i) = K_{VID} \left( \frac{\tilde{p}_{R,VID}^2(t_i)}{\tilde{p}_{R,traffic}^2(t_i)} \right) K_{traffic} \left( \frac{\tilde{p}_{R,traffic}^2(t_i)}{\sum_{t=0}^T \tilde{p}_{R,traffic}^2(t)} \right) C_{R,traffic}. \quad (3)$$

The energy demand is a measure of a vehicle's total necessary mechanical work  $W_T$ , to move as described by the vehicle kinematics data provided by the microscopic traffic simulation. The total work  $W_T$  is comprised of contributions related to the work to overcome rolling resistance  $W_R$ , inertial resistance  $W_a$ , and aerodynamic drag  $W_L$ , see Eq. (4). For more details on the calculations of the different contributions to the total necessary mechanical work, see [1, 3, 4].

$$W_T = W_R + W_a + W_L. \quad (4)$$

### 3.2 Correlation coefficient

To analyse how the observed fluctuations in noise exposure cost, energy demand and duration for each vehicle between the 100 simulations co-variate or correlate, the linear Pearson correlation coefficient  $r_{xy}$  is used. It may be considered a function of the covariance of the samples  $\{x_i\}$  and  $\{y_i\}$  of two stochastic variables  $X$  and  $Y$ , divided by the estimated standard deviation of each respective variable from the samples, and is given by

$$r_{xy} = \frac{\sum_{i=1}^N (x_i - \bar{x})(y_i - \bar{y})}{\sqrt{\sum_{i=1}^N (x_i - \bar{x})^2} \sqrt{\sum_{i=1}^N (y_i - \bar{y})^2}}. \quad (5)$$

The correlation coefficient  $r_{xy}$  is a value between -1 and 1. A value of 1 (-1) means that the observed data have a strong positive (negative) linear correlation. On the other hand, a value of 0 means that the variables appear not to be linearly correlated with each other in the data.

## 4. Results and analysis

The correlation analysis was performed on a subset of the vehicles. The correlation coefficients were calculated for all vehicles along routes 1 and 4 in Fig. 1. The correlation coefficient between the vehicle-specific noise exposure cost and the average rate of change of the system-wide noise exposure cost for all measurement points along the same road as the vehicle is presented in Fig. 2. The average rate of change of the system-wide noise exposure cost is estimated over the duration of each individual vehicle as the total noise exposure cost increase while the vehicle was in the system, divided by the duration of the vehicle. Each point in the figure represents an individual vehicle, entering the network at a given departure time.

A non-linear weighting function in the allocation strategy improves the correlation between vehicle-specific noise exposure costs and the system-wide increase of the noise exposure cost. However, the observed effects depend on the specific route that the vehicle drove on, indicating a system-dependency in the resulting effects of the non-linear allocation strategy. As can be seen in Fig. 2, the correlation coefficient for vehicles driving along route 4 during peak hours (departure times between 8h and 11h) is increased to slightly more positive when going from a linear allocation strategy, see a), to a non-linear allocation strategy, see b).

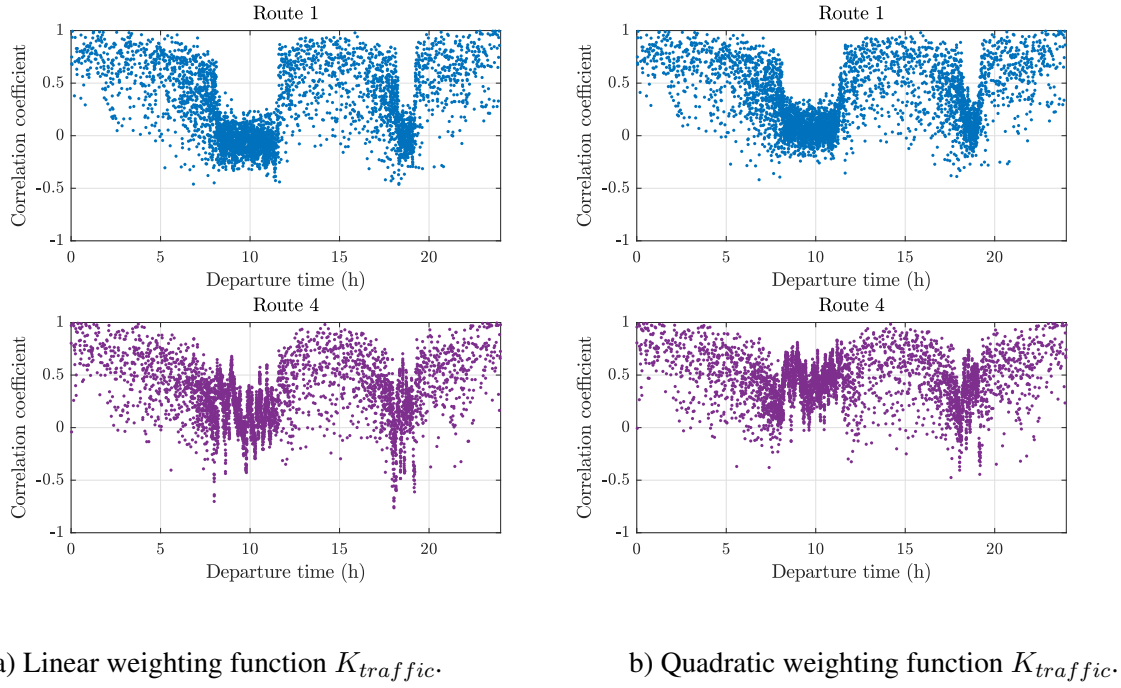


Figure 2: Correlation coefficient between linearly (a), or non-linearly (b), allocated vehicle-specific noise exposure cost and the average cost increase per second for the measurement points along the same road.

However, vehicles along route 1 do not observe as great an impact on the correlation coefficient during the same time period. The correlation coefficients for vehicles entering the network during peak hours are distributed around  $r_{xy} = 0$ , indicating a weak linear correlation or no linear correlation.

A change in the allocation strategy for the noise exposure cost also impacts the relation between observed variations in noise exposure cost and that of the duration and energy demand. Figure 3 presents the calculated correlation coefficient between each individual vehicle's noise exposure cost and duration in the network, for vehicles along routes 1 and 4.

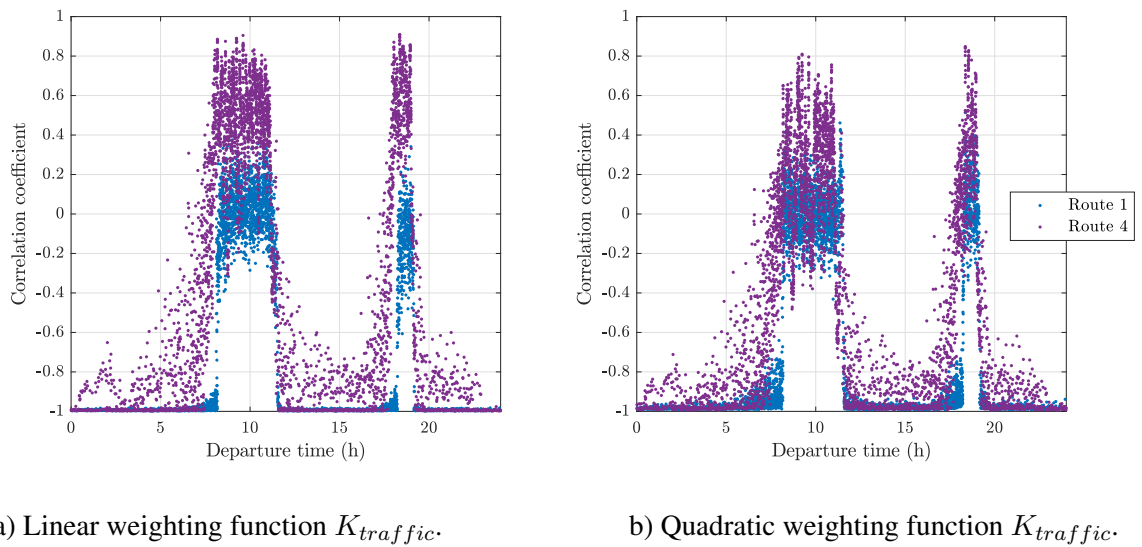


Figure 3: Correlation coefficient between linearly (a), or non-linearly (b), allocated vehicle-specific noise exposure cost and the duration.

By comparing the resulting correlation coefficient between the duration and the noise exposure

cost with either a linear- or non-linear allocation strategy, shown in Fig. 3, it is observed that the correlation is slightly weaker for vehicles along route 4 when a non-linear weighting function is used. The correlation coefficient is also more spread just before the peak hour traffic with a non-linear weighting function, indicating again a weaker correlation.

The different allocation strategies have a different effect on the correlation between energy demand and noise exposure cost. In Fig. 4, showing the correlation coefficient between energy demand and vehicle-specific noise exposure cost for vehicles along routes 1 and 4 at their departure time, the correlation coefficient for vehicles along route 4 is slightly increased in b) when using a non-linear weighting function compared to a).

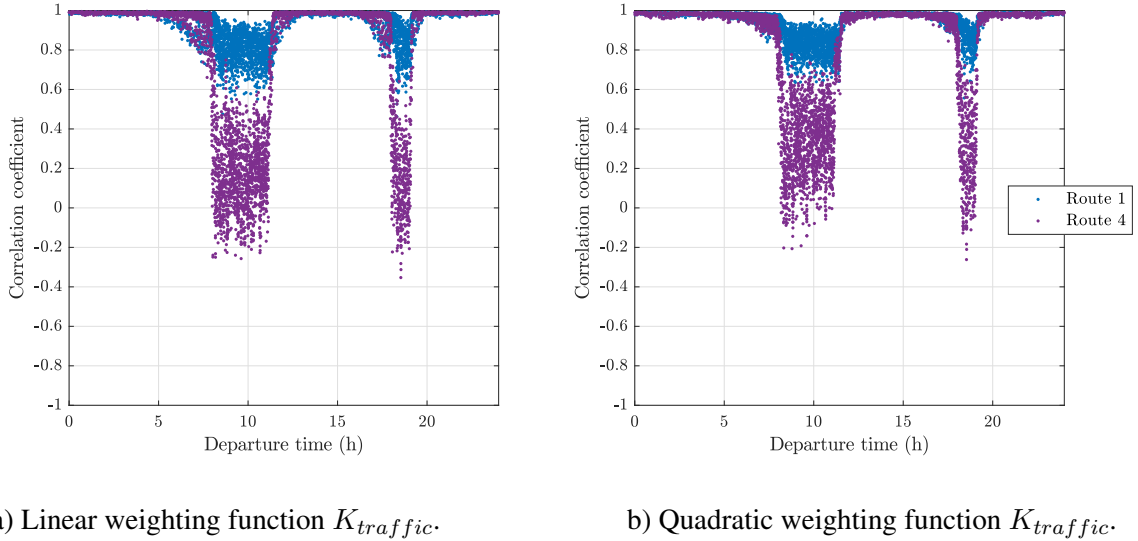


Figure 4: Correlation coefficient between linearly (a), or non-linearly (b), allocated vehicle-specific noise exposure cost and the energy demand.

There is a slight increased variation in the calculated correlation coefficient at off-peak traffic conditions when the noise exposure cost is calculated with the non-linear weighting function in b) compared to the linear weighting function in a).

## 5. Conclusions

The results are dependent on the road network, as it impacts the vehicle behaviour and dependencies. Analysing a microscopic traffic simulation and allocating the noise exposure cost down to individual vehicles is a computationally costly process. A city-scale network model would require more efficient modelling techniques, as developed in [8].

Allocating the noise exposure cost down to individual vehicles using non-linear weighting functions may improve the correlation between the observed variations in the vehicle-specific noise exposure cost and the overall increase in noise exposure cost in the system. However, by using a different allocation strategy the relation between the noise exposure cost and aspects of resource efficiency will be impacted as well. The allocation strategy therefore affects the trade-off between reducing noise exposure and achieving resource efficient transport, and should not be chosen in isolation. There may be an allocation strategy for the noise exposure cost that is less ideal in terms of noise exposure alone, but allows for a better comparison between the noise exposure cost and resource efficiency under different traffic conditions.



## Acknowledgements

The authors would like to thank the Centre for ECO<sup>2</sup> Vehicle Design at KTH, funded by the Swedish Innovation Agency Vinnova (Grant Number 2016-05195); and the strategic research area TRENoP for their financial contributions to this work.

## References

1. J. Nygren, et al., "An investigation of allocation strategies for internalizing the impact from traffic noise," ISMA2020 International Conference on Noise and Vibration Engineering, 2020. pp. 2395–2404.
2. P.A. Lopez, et al., 2018. "Microscopic Traffic Simulation using SUMO," 2018 21st International Conference on Intelligent Transportation Systems (ITSC), 2018, pp.2575–2582.
3. C. Koffler, K. Rohde-Brandenburger. "On the calculation of fuel savings through lightweight design in automotive life cycle assessments," The International Journal of Life Cycle Assessment, Vol 15 (1), 2010, pp. 128–135.
4. C. J. O'Reilly, et al. "Life cycle energy optimisation: A proposed methodology for integrating environmental considerations early in the vehicle engineering design process," Journal of Cleaner Production, Vol. 135 (C), 2016, pp. 750–759.
5. B. Peeters, G. J. van Blokland, 2007. "The Noise Emission Model For European Road Traffic. Improved Methods for the Assessment of the Generic Impact of Noise in the Environment," (IMAGINE), Deliverable 11 of the IMAGINE project.
6. H.G. Jonasson, "Acoustical Source Modelling of Road Vehicles," *Acta Acustica united with Acustica*, vol. 93, no. 2, pp. 173-184, 2007.
7. H. Andersson, J-E. Swärdh, M. Ögren, "Efterfrågan på tystnad: skattning av betalningsviljan för icke-marginella förändringar av vägtrafikbuller," *The Swedish Transport Administration (Trafikverket)*, pp. 1-20, 2013.
8. V. Le Bescond, A. Can, P. Aumond, and P. Gastineau. "Open-source modeling chain for the dynamic assessment of road traffic noise exposure," Transportation research. Part D, Transport and environment, vol. 94, p. 102793, 2021, doi: 10.1016/j.trd.2021.102793.